

Hartmut J.W. Haug
Antti-Pekka Jauho

SPRINGER SERIES IN SOLID-STATE SCIENCES 123

Quantum Kinetics in Transport and Optics of Semiconductors

Second, Substantially Revised Edition

Springer Series in SOLID-STATE SCIENCES

Series Editors:

M. Cardona P. Fulde K. von Klitzing R. Merlin H.-J. Queisser H. Störmer

The Springer Series in Solid-State Sciences consists of fundamental scientific books prepared by leading researchers in the field. They strive to communicate, in a systematic and comprehensive way, the basic principles as well as new developments in theoretical and experimental solid-state physics.

- 136 **Nanoscale Phase Separation and Colossal Magnetoresistance**
The Physics of Manganites and Related Compounds
By E. Dagotto
- 137 **Quantum Transport in Submicron Devices**
A Theoretical Introduction
By W. Magnus and W. Schoenmaker
- 138 **Phase Separation in Soft Matter Physics**
Micellar Solutions, Microemulsions, Critical Phenomena
By P.K. Khabibullaev and A.A. Saidov
- 139 **Optical Response of Nanostructures**
Microscopic Nonlocal Theory
By K. Cho
- 140 **Fractal Concepts in Condensed Matter Physics**
By T. Nakayama and K. Yakubo
- 141 **Excitons in Low-Dimensional Semiconductors**
Theory, Numerical Methods, Applications
By S. Glutsch
- 142 **Two-Dimensional Coulomb Liquids and Solids**
By Y. Monarkha and K. Kono
- 143 **X-Ray Multiple-Wave Diffraction**
Theory and Application
By S.-L. Chang
- 144 **Physics of Transition Metal Oxides**
By S. Maekawa, T. Tohyama, S.E. Barnes, S. Ishihara, W. Koshiba, and G. Khaliullin
- 145 **Point-Contact Spectroscopy**
By Y.G. Naidyuk and I.K. Yanson
- 146 **Optics of Semiconductors and Their Nanostructures**
Editors: H. Kalt and M. Hetterich
- 147 **Electron Scattering in Solid Matter**
A Theoretical and Computational Treatise
By J. Zabloudil, R. Hammerling, L. Szunyogh, and P. Weinberger
- 148 **Physical Acoustics in the Solid State**
By B. Lüthi
- 149 **Solitary Waves in Complex Dispersive Media**
Theory · Simulation · Applications
By V.Yu. Belashov and S.V. Vladimirov
- 150 **Topology in Condensed Matter**
Editor: M.I. Monastyrsky
- 151 **Particle Penetration and Radiation Effects**
By P. Sigmund
- 152 **Magnetism**
From Fundamentals to Nanoscale Dynamics
By J. Stöhr and H.C. Siegmann
- 153 **Quantum Chemistry of Solids**
The LCAO First Principles Treatment of Crystals
By R.A. Evarestov
- 154 **Low-Dimensional Molecular Metals**
By N. Toyota, M. Lang, and J. Müller
- 155 **Diffusion in Solids**
Fundamentals, Methods, Materials, Diffusion-Controlled Processes
By H. Mehrer

Volumes 90–135 are listed at the end of the book.

Hartmut Haug Antti-Pekka Jauho

Quantum Kinetics in Transport and Optics of Semiconductors

Second, Substantially Revised Edition

With 98 Figures



Springer

Professor Dr. Hartmut Haug
Institut für Theoretische Physik, J. W. Goethe Universität
Max-von-Laue-Str. 1, 60438 Frankfurt am Main, Germany

Professor Dr. Antti-Pekka Jauho
Department of Micro and Nanotechnology (MIC), Technical University of Denmark
Building 345 E, 2800 Kongens Lyngby, Denmark

Series Editors:

Professor Dr., Dres. h. c. Manuel Cardona
Professor Dr., Dres. h. c. Peter Fulde*
Professor Dr., Dres. h. c. Klaus von Klitzing
Professor Dr., Dres. h. c. Hans-Joachim Queisser
Max-Planck-Institut für Festkörperforschung, Heisenbergstrasse 1, 70569 Stuttgart, Germany
* Max-Planck-Institut für Physik komplexer Systeme, Nöthnitzer Strasse 38
01187 Dresden, Germany

Professor Dr. Roberto Merlin
Department of Physics, 5000 East University, University of Michigan
Ann Arbor, MI 48109-1120, USA

Professor Dr. Horst Störmer
Dept. Phys. and Dept. Appl. Physics, Columbia University, New York, NY 10027 and
Bell Labs., Lucent Technologies, Murray Hill, NJ 07974, USA

ISSN 0171-1873

ISBN 978-3-540-73561-8 2nd Edition Springer Berlin Heidelberg New York
ISBN 3-540-61602-0 1st Edition Springer Berlin Heidelberg New York

Library of Congress Control Number: 2007931202

This work is subject to copyright. All rights are reserved, whether the whole or part of the material is concerned, specifically the rights of translation, reprinting, reuse of illustrations, recitation, broadcasting, reproduction on microfilm or in any other way, and storage in data banks. Duplication of this publication or parts thereof is permitted only under the provisions of the German Copyright Law of September 9, 1965, in its current version, and permission for use must always be obtained from Springer. Violations are liable to prosecution under the German Copyright Law.

Springer is a part of Springer Science+Business Media.

© Springer-Verlag Berlin Heidelberg 1997, 2008

The use of general descriptive names, registered names, trademarks, etc. in this publication does not imply, even in the absence of a specific statement, that such names are exempt from the relevant protective laws and regulations and therefore free for general use.

Typesetting: Data prepared by SPI Kolam using a Springer L^AT_EX macro package
Cover: eStudio Calamar Steinen

Printed on acid-free paper SPIN: 12081660 57/3180/SPI - 5 4 3 2 1 0

To our families

Preface

During the 11 years since the first edition was published the field of quantum kinetics has experienced a great expansion, and the methods described in the first edition are now widely used in a large number of different subfields. Literally thousands of papers have been published in this area and an attempt to give an exhaustive review is clearly beyond the present scope. In this revised edition we have attempted to include some examples of modern topics, essentially from the research areas we have been active in. We are fully aware of the fact that this approach will leave many important topics untouched, and our hope is that the leading researchers in those areas write their own books!¹ More specifically, in our revision we have left the first nine chapters essentially unchanged, only supplying a few updated references, and correcting misprints. On the other hand, the last nine chapters have been substantially revised, reorganized, and expanded. In the sections describing transport phenomena we have included a number of new topics, such as transport in a superlattice, molecular electronics (and inelastic interactions), and noise calculations. We have added a new chapter, describing the dynamical Franz–Keldysh effect, which follows directly from the field-dependent Green functions, originally introduced to describe high-field transport in semiconductors. In the sections dealing with optical properties we emphasize that the concepts of quantum kinetics have proved to be extremely fruitful for the analysis of new experiments in ultrafast semiconductor spectroscopy. Some highlights included in the new edition are: The femtosecond build-up of screening and of polaron correlations, four-wave mixing studies of the plasma-density dependent dephasing, the femtosecond formation of phonon–plasmon mixed modes, detection of light-induced band gaps, and non-Markovian relaxation in the short femtosecond regime. None of these fascinating new observations can be understood in the framework of a semiclassical Markovian Boltzmann kinetics, but require for their description the theory of quantum kinetics as demonstrated

¹ Recent progress in research using nonequilibrium Green functions is reviewed in a very useful series of edited volumes due to M. Bonitz and co-workers [55–57].

VIII Preface

in the new edition. Even with these new topics we have attempted to keep the total page number essentially unchanged, which naturally has led to omission of some material which we no longer felt was necessary. Our hope is that the readers, new and old, will find the revised book useful in their research work.

We have worked with many colleagues on the new topics included here. We would particularly like to mention Mads Brandbyge, Thomas Frederiksen, Paul Gartner, Alfred Leitenstorfer, Bernhard Mieck, Tomáš Novotný, Gloria Platero, Arne Schmenkel, Oli Schmidt, Fabricio Souza, Alexandra Stein, and Tuyen Vu. Also, the many students who have found mistakes and misprints, and suggested improvements, deserve our sincere thanks.

Frankfurt and Copenhagen,
July 2007

*Hartmut Haug
Antti-Pekka Jauho*

Preface to the First Edition

New textbooks on various aspects of theoretical physics seem to overflow the market. A prospective author must be able to provide convincing answers to at least the following questions (posed by the publisher, colleagues, and last but not least, by him/herself and the associated family members). (1) Why bother writing the book? (2) Is there a sufficient audience for the text? (3) Is not the topic already covered by a number of books, and is not the author's best hope just to add a new wrinkle to the existing lore (and perhaps enhance his/her own publication record)? (4) Is there any practical need for the book? (5) Are there any important open problems that the book will contribute to finding solutions to (or, at least, be able to identify points where the present understanding is insufficient).

We have thought carefully about the above questions, and have become convinced (at least between ourselves), that indeed there is a purpose in writing the book that you are holding in your hands.

In what follows we will try to outline reasons why we feel that this book might be useful and define its scope and ultimate goals. First of all, this is a book on a *technique*. More precisely, this is a book on nonequilibrium Green functions (NEGF). Narrowing the definition down even more precisely, this is a book about how NEGF are applied in *semiconductor science*. To identify the final qualifier, we are mostly interested in systems where *extremely short* length scales ($\simeq 1 \text{ nm}$) and *extremely fast* time scales ($\simeq 1 \text{ fs}$) play a crucial role. In these short length and timescales the electrons exhibit their quantum mechanical wave nature: the quantum coherence of the electronic excitations becomes important. To properly describe phenomena of this kind, one needs a quantum theory of nonequilibrium phenomena and the NEGF provide such a technique. One of the purposes of this book is to show how deeply the quantum coherence modifies the physics in short time and length scales: the relaxation and dephasing dynamics differ radically from their semiclassical counterparts, and the collision terms of the quantum kinetic equations have a non-Markovian memory structure.

Equilibrium Green functions (EGF) have been one of the central items in the toolbox of a theoretical physicist for many years, and the interested student can find many excellent treatises on the topic (a brief bibliography is given in Chap. 3). Many of these books are written by the very people who invented the formalism, and obviously our ambitions must be set on a lower level. Nonequilibrium Green functions, on the other hand, are much less frequently mentioned in the canonical textbooks. An exception is, of course, the classic work by Kadanoff and Baym [191], where the whole topic was introduced, but this work is now more than 30 years old, and obviously should be followed by a more modern treatise.

One may wonder why the beautiful techniques developed by Kadanoff and Baym [191] (and, independently, by Keldysh [198]), have so far not acquired the same popularity as equilibrium Green functions. For some reason there seems to be a rather widespread prejudice to the effect that the nonequilibrium techniques are accessible to only a very small select group of experts. We strongly disagree with this standpoint; in fact one of the main goals of our work is to emphasize that NEGF are conceptually no more difficult (or easy) than normal Green functions are. In our opinion there are several factors that have contributed to this misconception. The first is that the physics of *degenerate Fermi systems* has defined the central topic of interest for the majority of many-body theorists. For this particular class of problems an extremely powerful formalism exists: *quasi-classical Green functions*, which take advantage of the fact that the electronic momenta are confined to the neighborhood of the Fermi surface, and thus allow the development of an essentially linear (in terms of the external driving field) theory. Consequently, the full potential power of the Kadanoff–Baym–Keldysh theory has not been called for. The second reason is that once the Fermi energy does not provide the overall largest energy scale, the all-important (in sense of the Landau school of theoretical physics) “small parameter” is not so easy to define. Thus applying rigorous many-body techniques to semiconductors under nonequilibrium conditions is, by definition, a topic that purists would be hesitant to touch. To quote a remark attributed to W. Pauli: “One should not work on semiconductors, that is a filthy mess; who knows whether they really exist,” and this remark was made long before highly nonequilibrium semiconductors were even considered. We are fully aware that some of the theories described in this book suffer from this lack of rigor; nevertheless we have taken the risks of writing down expressions that later developments may require to be modified. Our philosophy has consistently been that we try to expose our topic as it stands today, and not have any false pretense in that what we are saying would be the final truth. (Parenthetically, if everything was well-known and understood, would there be real challenge in writing the book?!)

Perhaps another reason for the not-so-widespread use of nonequilibrium Green functions is that there are relatively few texts available that offer a systematic treatment. In book form we, of course, have the classic work of Kadanoff and Baym [191], but in addition to that, it has been necessary to look

for journals. A few review articles exist; we have particularly benefitted from those by Langreth [231], Chou et al. [80], and Rammer and Smith [287], but these works are written for an experienced scientist and not for a (graduate) student. It is interesting to note that during the last few years several books addressing many-body physics in general have added sections on NEGF, (see, e.g., books by Datta [93], Enz [105], Ferry [109], or Mahan [254]), but always as a kind of side remark. Many authors still feel that it is necessary to add an appendix or two in their research papers explaining the basic notions of NEGF whenever they are needed in their research. If our book contributes towards a weakening of this feeling, one of our main goals has been achieved.

Semiconductor microscience has developed dramatically throughout the 1980s and 1990s. Many laboratories have access to samples and instruments that probe new and exciting effects in parameter ranges where standard theories, such as the Boltzmann equation or the Kubo formula, are not applicable. Hence there is a strong experimental motivation to search for theories that can applied in these new situations. We feel that nonequilibrium Green functions are a good candidate for such a theoretical framework. It was already mentioned that this is a book on a *technique*, and not on a *topic*. A highly respected approach among the theoretical community is to attack a *problem* and then use whatever technique is necessary to sort out the problem. This is at the same time the distinction between a monograph and a textbook (in our definition): we do not attempt to cover a single topic in all its variations; what we do attempt to do is to take a given technique (NEGF in our case) and use it in a number of carefully chosen topics. The textbook approach has dictated rather stringently the choice of topics: throughout the book we have chosen a level of presentation where a diligent student can follow all steps with a finite amount of pencils and paper. This may have occasionally led to rather trivial algebraic steps, at least for some of our sophisticated colleagues, but we have deliberately chosen this route. Our justification is based on the experience that students learn more from a text, and feel more secure about its essential contents, if they know that all the materials are carefully chosen so that no essential steps are hidden behind elusive statements like “it can be shown,” etc. Thus we are essentially providing an engineering approach: take our book, make sure that you can reproduce every single equation in it, and we will guarantee that you have acquired the weaponry to attack many as of yet unresolved issues in contemporary physics! Or, more modestly, after studying our book you should not be intimidated by a reference to NEGF, and will be prepared to continue the conversation on whatever *physics* that was discussed.

The pedagogical approach chosen in this book has necessarily had its price. We do not show many experimental curves and their best theoretical fits. Rather, we focus on different theoretical approaches, and compare their inter-relations. In particular this means that our “semiconductor” seldom has a real band structure with several (anisotropic) conduction and/or valence bands, or that we do not dwell in detail on various aspects of the self-consistent

calculations (where the dynamical quantities determine the effective parameters that define the structures under investigation), nor do we dwell in detail on the many possible different scattering mechanisms that take place in a real semiconductor (thus we consider only “impurities,” not worrying about their charge or internal degrees of freedom, and most of our “phonons” are of the dispersionless optical variety). We hope that this somewhat weakened connection to real materials is compensated for by the ability to carry out the calculations analytically, as far as it is possible, and that whenever the practical need arises, the general *structure* of the theory, as it is outlined here, can be applied to the real materials one is interested in.

We also need to comment about the prerequisites for the students approaching our text. A solid command of statistical physics and quantum mechanics is necessary. Some familiarity with second quantization would certainly be helpful, even though we give a brief summary on the topic. The hardest issue concerns the required background knowledge on equilibrium Green functions. This topic is viewed as a rather advanced issue in standard curricula, and we have no way of approaching the topics that lie at the core of our book without assuming some prior knowledge of EGF. However, we do provide a summary of EGF in Chap. 3, and since one of our most important messages is that NEGF are conceptually *no more difficult* than EGF, our hope is that even a reader with a slightly rusty command of EGF will not shun away from our book; rather our hope is that this reader will learn more about EGF’s as a by-product of studying our book!

There is yet another philosophical point that has contributed to the birth of this book. We are strong believers that different disciplines in science can learn and benefit from a forced contact with each other. In this day and age of ever increasing specialization, different physics communities find it ever more difficult to communicate with each other, even though the mathematical principles underlying their respective research topics can be (once stripped of the everyday jargon) actually quite similar. To make a point in case, one of the standard books in Green function theory, Fetter and Walecka [110], nicely talks about common themes in solid-state physics and nuclear physics. We have tried to follow the same route, but with a much more restrictive definition: we emphasize throughout our book that the *optical* and *transport* communities in semiconductor physics are actually tackling very similar problems. Thus we conceive as one of our main tasks the abolishment of any artificial barriers between these two groups of scientists.

The structure of this book is clear-cut: the text is divided into four parts, the first of which serves as a summary of some the concepts needed later, and also gives some Boltzmann-level results relevant to our topic; Part II develops the general theoretical framework; Part III applies it to transport in semiconductor microstructures, and, finally, Part IV discusses optical applications. Parts III and IV are independent of each other, but our belief is that a serious student will greatly benefit by comparing the similar theoretical structures arising from superficially different physical starting points.

Last, but not least, it is our great pleasure to thank the many colleagues we have worked together with, and without whose expertise and (at times) friendly criticism we would not have been able to complete the book. (Naturally, the responsibility for all errors and inaccuracies lies with us.) Our special thanks go to Laci Bánya, Rita Bertoncini, John Davies, Claudia Ell, Karim El Sayed, David Ferry, Karsten Flensberg, Klaus Henneberger, Ben Hu, Kristinn Johnsen, Leonid Keldysh, Stephan Koch, Tillman Kuhn, David Langreth, Pavel Lipavský, Gerry Mahan, Yigal Meir, Jørgen Rammer, Lino Reggiani, Ernst Reitsamer, Christian Remling, Wilfried Schäfer, Stefan Schuster, Henrik Smith, Bao Tran Thoai, Bedřich Velický, Andreas Wacker, Martin Wegener, John Wilkins, Ned Wingreen, and Roland Zimmermann.

Frankfurt and Copenhagen,
August 1996

*Hartmut Haug
Antti-Pekka Jauho*

Contents

Part I Introduction to Kinetics and Many-Body Theory

1	Boltzmann Equation	3
1.1	Heuristic Derivation of the Semiclassical Boltzmann Equation	3
1.2	Approach to Equilibrium: H-Theorem	5
1.3	Linearization: Eigenfunction Expansion	8
2	Numerical Solutions of the Boltzmann Equation	11
2.1	Introduction	11
2.2	Linearized Coulomb Boltzmann Kinetics of a 2D Electron Gas	12
2.3	Ensemble Monte Carlo Simulation	20
2.3.1	General Theory	20
2.3.2	Simulation of the Relaxation Kinetics of a 2D Electron Gas	23
2.4	$N^+N^-N^+$ Structure: Boltzmann Equation Analysis	29
3	Equilibrium Green Function Theory	35
3.1	Second Quantization	35
3.2	Density Matrix Equations: An Elementary Derivation of a Non-Markovian Quantum Kinetic Equation	38
3.3	Green Functions	41
3.3.1	Examples of Measurable Quantities	43
3.4	Fluctuation–Dissipation Theorem	45
3.5	Perturbation Expansion of the Green Function	47
3.6	Examples of Simple Solvable Models	50
3.6.1	Free-Particle Green Function	50
3.6.2	Resonant-Level Model	50

XVI Contents

3.7	Self-Energy	52
3.7.1	Electron–Phonon Interaction	52
3.7.2	Elastic Impurity System: Impurity Averaging	54
3.8	Finite Temperatures	58

Part II Nonequilibrium Many-Body Theory

4	Contour-Ordered Green Functions	63
4.1	General Remarks	63
4.2	Two Transformations	64
4.3	Analytic Continuation	69
5	Basic Quantum Kinetic Equations	75
5.1	Introductory Remarks	75
5.2	The Kadanoff–Baym Formulation	75
5.3	Keldysh Formulation	77
6	Boltzmann Limit	79
6.1	Gradient Expansion	79
6.2	Quasiparticle Approximation	81
6.3	Recovery of the Boltzmann Equation	82
7	Gauge Invariance	85
7.1	Choice of Variables	85
7.2	Gauge Invariant Quantum Kinetic Equation	87
7.2.1	Driving Term	87
7.2.2	Collision Term	90
7.3	Retarded Green Function	91
8	Quantum Distribution Functions	93
8.1	Relation to Observables, and the Wigner Function	93
8.2	Generalized Kadanoff–Baym Ansatz	94
8.3	Summary of the Main Formal Results	97

**Part III Quantum Transport
in Semiconductors**

9	Linear Transport	101
9.1	Quantum Boltzmann Equation	101
9.2	Linear Conductivity of Electron-Elastic Impurity Systems	104
9.2.1	Kubo Formula	105
9.2.2	Quantum Kinetic Formulation	109
9.3	Weak Localization Corrections to Electrical Conductivity ..	111

10 Field-Dependent Green Functions	115
10.1 Free Green Functions	
and Spectral Functions in an Electric Field	115
10.2 A Model for Dynamical Disorder:	
The Gaussian White Noise Model	121
10.2.1 Introduction	121
10.2.2 Determination of the Retarded Green Function	121
10.2.3 Kinetic Equation for the GWN	123
10.2.4 Other Transport Properties	127
10.3 Introduction to High-Field Transport in Semiconductors	129
10.4 Resonant-Level Model in High Electric Fields	131
10.4.1 Introduction	131
10.4.2 Retarded Green Function:	
Single Impurity Problem	131
10.4.3 Retarded Green Function:	
Dilute Concentration of Impurities	133
10.4.4 Analytic Continuation	140
10.4.5 Quantum Kinetic Equation	141
10.5 Quantum Kinetic Equation	
for Electron–Phonon Systems	144
10.6 An Application:	
Collision Broadening for a Model Semiconductor	148
10.6.1 Analytical Considerations	148
10.6.2 A Simple Model:	
Optical Phonon Emission at $T = 0$	150
10.7 Spatially Inhomogeneous Systems	151
11 Optical Absorption in Intense THz Fields	157
11.1 Introductory Remarks	157
11.2 Optical Absorption as a Response Function	158
11.3 Absorption Coefficient	162
11.4 Static Electric Field	163
11.5 Harmonically Varying External Electric Fields	164
11.5.1 Joint Density of States, 2D	167
11.5.2 Joint Density of States, 3D	169
11.6 Dynamical Franz–Keldysh Effect: Excitonic Effects	171
11.6.1 Matrix Truncation	172
11.6.2 Floquet Space Formulation	175
12 Transport in Mesoscopic Semiconductor Structures	181
12.1 Introduction	181
12.2 Nonequilibrium Techniques	
in Mesoscopic Tunneling Structures	184
12.3 Model Hamiltonian	185
12.4 General Expression for the Current	186

XVIII Contents

12.5	Current Conservation	191
12.6	Noninteracting Resonant-Level Model	192
12.7	Density Functional Theory and Modeling of Molecular Electronics	195
12.8	Resonant Tunneling with Electron–Phonon Interactions	196
12.9	Transport in a Semiconductor Superlattice	198
12.10	Transport in Atomic Gold Wires: Signature of Coupling to Vibrational Modes	202
12.11	Transport Through a Coulomb Island	205
13	Time-Dependent Phenomena	213
13.1	Introduction	213
13.2	Applicability to Experiments	214
13.3	Mathematical Formulation	215
13.4	Average Current	217
13.5	Time-Dependent Resonant-Level Model	218
13.5.1	Response to Harmonic Modulation	221
13.5.2	Response to Step-Like Modulation	224
13.6	Linear-Response	227
13.7	Fluctuating Energy Levels	229
13.8	Noise	230
13.8.1	The Disconnected Terms	235
13.8.2	The Connected Terms	236

**Part IV Theory of Ultrafast Kinetics
in Laser-Excited Semiconductors**

14	Optical Free-Carrier Interband Kinetics in Semiconductors	243
14.1	Interband Transitions in Direct-Gap Semiconductors	243
14.1.1	Reduced Density Matrices	243
14.1.2	Nonequilibrium Green Functions	245
14.1.3	Calculations of the Two-Time-Dependent Nonequilibrium Green Function	245
14.1.4	Replacement of Two-Time Propagators by a One-Time Density Matrix and a Two-Time Spectral Function	246
14.2	Free-Carrier Kinetics Under Laser-Pulse Excitation	251
14.3	The Optical Free-Carrier Bloch Equations	255
15	Interband Quantum Kinetics with LO-Phonon Scattering .	259
15.1	Derivation of the Interband Quantum Kinetic Equations . . .	259
15.2	The Spectral Green Functions $G_{\mu\nu}^r$ and $G_{\mu\nu}^a$	266

15.2.1	Free-Particle Retarded Green Function	266
15.2.2	Retarded GF in the Mean-Field Approximation	267
15.2.3	Spectra of Retarded Gfs	269
15.2.4	Dephasing of Retarded Green Functions	274
15.3	Intraband Relaxation	279
15.4	Interband-Polarization Dephasing	281
15.5	Numerical Strategies	283
16	Two-Pulse Spectroscopy	287
16.1	Introductory Remarks	287
16.2	Thin Samples	289
16.3	Low-Intensity Two-Beam Experiments	290
16.3.1	LO-Phonon Relaxation Cascades	291
16.3.2	LO-Phonon Quantum Beats in FWM	292
16.3.3	Two-Time Electron-Phonon Quantum Kinetics	294
17	Coulomb Quantum Kinetics in a Dense Electron-Hole Plasma	301
17.1	Introduction	301
17.2	Screening in the Nonequilibrium GF Theory	302
17.3	Coulomb Quantum Kinetics	306
17.4	Plasmon-Pole Approximation for the Two-Time-Dependent Potential	309
17.4.1	Parametric Plasma Oscillations	311
17.4.2	Instantaneous Static Potential Approximation	313
18	The Buildup of Screening	317
18.1	Screening of the Coulomb Interaction	317
18.1.1	Calculations of the Two-Time-Dependent Screened Potential	318
18.1.2	Femtosecond Optical Pump and THz Probe Spectroscopy	320
18.2	Time-Dependent Screening of Phonon-Mediated and Coulomb Interactions	320
18.2.1	Buildup of the Phonon-Plasmon Mixed Modes	324
19	Femtosecond Four-Wave Mixing with Dense Plasmas	331
19.1	Time-Resolved Four-Wave Mixing	331
19.2	Time-Integrated Four-Wave Mixing	334
19.3	Four-Wave Mixing with Coherent Control	335
References		341
Index		353

Part I

Introduction to Kinetics and Many-Body Theory

1

Boltzmann Equation

Summary. We review some of the general properties of the semiclassical Boltzmann equation - not necessarily restricting ourselves to the dilute electron gas - paying special attention to its irreversible properties.

1.1 Heuristic Derivation of the Semiclassical Boltzmann Equation

The kinetic theory of Boltzmann which connects the regime of dynamics with that of thermodynamics has been a milestone in the development of theoretical physics. In order to describe the kinetics of, e.g., an atomic gas, Boltzmann [51] introduced, with great intuition, more than half a century before the rise of quantum mechanics, a probabilistic description for the evolution of a single-particle distribution which anticipated atomistic scattering concepts. Boltzmann introduced a single-particle probability distribution in the phase space of the canonical variables \mathbf{r} and \mathbf{p} . This Boltzmann distribution function is usually denoted as $f(\mathbf{r}, \mathbf{p}, t)$. Obviously, this object is classical, because in quantum mechanics \mathbf{r} and \mathbf{p} are noncommuting operators so that they cannot be simultaneously measured with arbitrary precision. We will analyze in the following chapter how this conceptual difficulty affects the limits of validity of the Boltzmann equation. Here we will first present a heuristic derivation of the semiclassical Boltzmann equation. Later in this book we will pay special attention to the more detailed quantum mechanical justifications of the Boltzmann kinetics, present discussions of the limits of this semiclassical theory, and, most importantly, derive and study the quantum kinetics which has to be used instead of the Boltzmann kinetics on small length and/or short timescales. In the framework of the classical Hamilton theory the total change in time of this distribution function is

$$\begin{aligned}\frac{df(\mathbf{r}, \mathbf{p}, t)}{dt} &= \frac{\partial f}{\partial t} + \frac{d\mathbf{r}}{dt} \cdot \nabla_{\mathbf{r}} f + \frac{d\mathbf{p}}{dt} \cdot \nabla_{\mathbf{p}} f \\ &= \frac{\partial f}{\partial t} + \frac{\mathbf{p}}{m} \cdot \nabla_{\mathbf{r}} f - [\nabla_{\mathbf{r}} V(\mathbf{r})] \cdot \nabla_{\mathbf{p}} f = \frac{\partial f}{\partial t} \Big|_{\text{coll}},\end{aligned}\quad (1.1)$$

where $V(\mathbf{r})$ is a single-particle potential. The left-hand side of (1.1) describes the dynamics of a single particle. The influence of the other particles will give rise to a further change of the distribution function $\partial f / \partial t|_{\text{coll}}$ which describes the effect of the collisions in the gas. We will not proceed historically, but include directly the proper quantum statistics for quantum gases, so that we are not limited to nondegenerate gases. This extension is necessary for the application of the Boltzmann kinetics to electron gases in semiconductors which are often degenerate, whether they are produced by doping, injection, or optical excitation. Fermi's golden rule gives us the transition probability per unit time and thus the wanted change of f due to collisions. For an interacting Fermi gas we calculate this change by considering approximately free-particle collisions in which the particle is scattered from a momentum state \mathbf{p} to a momentum state \mathbf{p}' and simultaneously another particle is scattered from state \mathbf{p}_1 to \mathbf{p}'_1 , as well as the inverse process

$$\begin{aligned}\frac{\partial f(\mathbf{p})}{\partial t} \Big|_{\text{coll}} &= - \sum_{\mathbf{p}', \mathbf{p}_1, \mathbf{p}'_1} w(\mathbf{p}, \mathbf{p}_1; \mathbf{p}', \mathbf{p}'_1) \left\{ f(\mathbf{p})f(\mathbf{p}_1)[1 - f(\mathbf{p}')][1 - f(\mathbf{p}'_1)] \right. \\ &\quad \left. - [1 - f(\mathbf{p})][1 - f(\mathbf{p}_1)]f(\mathbf{p}')f(\mathbf{p}'_1) \right\},\end{aligned}\quad (1.2)$$

where the intrinsic transition probability per unit time is given by

$$\begin{aligned}w(\mathbf{p}, \mathbf{p}_1; \mathbf{p}', \mathbf{p}'_1) &= \frac{1}{2} |W_{\mathbf{p}, \mathbf{p}_1; \mathbf{p}', \mathbf{p}'_1} - W_{\mathbf{p}, \mathbf{p}_1; \mathbf{p}'_1, \mathbf{p}'}|^2 \\ &\times \delta_{\mathbf{p}+\mathbf{p}_1, \mathbf{p}'+\mathbf{p}'_1} \frac{2\pi}{\hbar} \delta(\varepsilon_p + \varepsilon_{p_1} - \varepsilon_{p'} - \varepsilon_{p'_1}).\end{aligned}\quad (1.3)$$

Here

$$W_{\mathbf{p}, \mathbf{p}_1; \mathbf{p}', \mathbf{p}'_1} = \langle \mathbf{p} \mathbf{p}_1 | W | \mathbf{p}' \mathbf{p}'_1 \rangle \quad (1.4)$$

is the interaction matrix element and ε_p is the energy of the particle. The second matrix element in (1.3) is the exchange term in which \mathbf{p}'_1 and \mathbf{p}' are interchanged. This form of the intrinsic transition probability is called the first Born approximation. The population factors take care that the initial states in the scattering event are populated and that the final states are empty in accordance with the Pauli principle. The scattering $\mathbf{p} + \mathbf{p}_1 \rightarrow \mathbf{p}' + \mathbf{p}'_1$ is a loss term which reduces $f(\mathbf{p})$, while the inverse process $\mathbf{p}' + \mathbf{p}'_1 \rightarrow \mathbf{p} + \mathbf{p}_1$ increases the distribution function. For shortness of notation, the parametric dependencies on the spatial coordinate \mathbf{r} and time t are not shown in the collision integral. The form of the collision integral leads to five conservation laws for: (a) the

number of particles, (b) the vector of the total momentum, and (c) the total energy. In a dilute, nondegenerate gas the final state population can be neglected, so that (1.2) can be simplified by the approximation $1 - f(\mathbf{p}) \simeq 1$.

A second important scattering rate for an electron gas in a perfect crystal is the scattering by emission or absorption of a phonon. Its form is

$$\begin{aligned} \frac{\partial f(\mathbf{p})}{\partial t} \Big|_{\text{coll}} = & - \sum_{\mathbf{p}', \mathbf{q}} w(\mathbf{p}, \mathbf{p}'; \pm \mathbf{q}) \times \left\{ f(\mathbf{p}) [1 - f(\mathbf{p}')] [\frac{1}{2} + n(\mathbf{q}) \pm \frac{1}{2}] \right. \\ & \left. - [1 - f(\mathbf{p})] f(\mathbf{p}') [\frac{1}{2} + n(\mathbf{q}) \mp \frac{1}{2}] \right\}, \end{aligned} \quad (1.5)$$

where the intrinsic transition probability per unit time is given by

$$w(\mathbf{p}, \mathbf{p}'; \pm \mathbf{q}) = |M_q|^2 \delta_{\mathbf{p}, \mathbf{p}' \pm \mathbf{q}} \frac{2\pi}{\hbar} \delta(\varepsilon_{p'} \pm \hbar\omega_q - \varepsilon_p). \quad (1.6)$$

Here, M_q is the electron–phonon interaction matrix element, and $n(\mathbf{q})$ and ω_q are the phonon distribution and frequency, respectively. Consider the upper sign first, then the first term in (1.5) describes a scattering of an electron from \mathbf{p} into the state \mathbf{p}' accompanied with an emission of a phonon. The final state boson population factor $[1 + n(\mathbf{q})]$ shows that the emission can be spontaneous or stimulated. The energy conservation also shows that the energy ε_p of the initially populated state is shared between the particle in the final state and the phonon. The contribution of the lower sign in (1.5) describes a scattering from \mathbf{p} to \mathbf{p}' via absorption of a phonon with an occupation factor $n(\mathbf{q})$. The form of (1.5) shows that for the electron–phonon scattering rate only the electron particle number is conserved, but no longer the total momentum and the total energy of the electron gas which both can be transferred to the phonon system. The phonon distribution in turn is also governed by a similar Boltzmann equation which we will not give explicitly here.

Obviously the semiclassical Boltzmann equation cannot be used on very short timescales because the assumption that the energy is conserved in an isolated collision (1.2), (1.5) breaks down. In a short time interval δt the energy remains undetermined due to the uncertainty relation $\delta t \delta E \geq \hbar$. Therefore the strict energy conservation in an individual collision is not an inherent property of the quantum kinetic description.

The mathematical properties of the Boltzmann kinetics contained in (1.1), (1.2), and (1.5) have been thoroughly investigated. Its full theory is a wide subject in its own; we will discuss only a few properties here. For a much more complete treatment and for studies of its applications we have to refer to such excellent books as Ziman [380], Cercignani [76], and Smith and Jensen [327].

1.2 Approach to Equilibrium: H-Theorem

It is easy to convince oneself that the semiclassical Boltzmann equation (1.2) describes indeed an evolution toward the thermal equilibrium in the absence

of external fields. We introduce first an arbitrary function $F(\mathbf{p}, f_{\mathbf{p}})$ which depends on the momentum and the distribution $f(\mathbf{r}, \mathbf{p}, t)$. Its local density is

$$\langle F(\mathbf{r}, t) \rangle = \sum_{\mathbf{p}} F(\mathbf{p}, f_{\mathbf{p}}) f_{\mathbf{p}} . \quad (1.7)$$

The change of this function due to the collisions is [here we consider explicitly the collision operator (1.2)]

$$\begin{aligned} \frac{\partial \langle F(\mathbf{r}, t) \rangle}{\partial t} \Big|_{\text{coll}} &= \sum_{\mathbf{p}} \left[\frac{\partial F(\mathbf{p})}{\partial f(\mathbf{p})} + F(\mathbf{p}) \right] \frac{\partial f(\mathbf{p})}{\partial t} \Big|_{\text{coll}} \\ &= - \sum_{\mathbf{p}\mathbf{p}', \mathbf{p}_1, \mathbf{p}'_1} w(\mathbf{p}, \mathbf{p}_1; \mathbf{p}' \mathbf{p}'_1) \frac{\partial [F(\mathbf{p}) f(\mathbf{p})]}{\partial f(\mathbf{p})} \\ &\quad \times \left\{ f(\mathbf{p}) f(\mathbf{p}_1) [1 - f(\mathbf{p}')][1 - f(\mathbf{p}'_1)] \right. \\ &\quad \left. - [1 - f(\mathbf{p})][1 - f(\mathbf{p}')][f(\mathbf{p}_1) f(\mathbf{p}'_1)] \right\} . \end{aligned} \quad (1.8)$$

Exploiting the symmetry of the intrinsic transition probability $w(\mathbf{p}, \mathbf{p}_1; \mathbf{p}' \mathbf{p}')$ with respect to the exchange of particle coordinates

$$\begin{aligned} w(\mathbf{p}, \mathbf{p}_1; \mathbf{p}', \mathbf{p}'_1) &= w(\mathbf{p}_1, \mathbf{p}; \mathbf{p}'_1, \mathbf{p}') \\ &= w(\mathbf{p}', \mathbf{p}'_1; \mathbf{p}, \mathbf{p}_1) = w(\mathbf{p}'_1, \mathbf{p}'; \mathbf{p}_1, \mathbf{p}) , \end{aligned} \quad (1.9)$$

one finds that

$$\begin{aligned} \frac{\partial \langle F(\mathbf{r}, t) \rangle}{\partial t} \Big|_{\text{coll}} &= -\frac{1}{4} \sum_{\mathbf{p}\mathbf{p}', \mathbf{p}_1, \mathbf{p}'_1} w(\mathbf{p}, \mathbf{p}_1; \mathbf{p}', \mathbf{p}'_1) \\ &\quad \times \left[\frac{\partial(Ff)}{\partial f} + \frac{\partial(Ff)}{\partial f_1} - \frac{\partial(Ff)}{\partial f'} - \frac{\partial(Ff)}{\partial f'_1} \right] \\ &\quad \times \left[ff_1(1 - f')(1 - f'_1) - (1 - f)(1 - f_1)f'f'_1 \right] . \end{aligned} \quad (1.10)$$

In (1.10) we have introduced a shorthand notation, for example in $\partial(Ff)/\partial f$ all involved functions are evaluated at the argument \mathbf{p} . Now consider the following choice for F :

$$f(\mathbf{p})F(\mathbf{p}, f_{\mathbf{p}}) = f(\mathbf{p}) \ln f(\mathbf{p}) + [1 - f(\mathbf{p})] \ln [1 - f(\mathbf{p})] . \quad (1.11)$$

The partial derivative with respect to f yields

$$\frac{\partial(Ff)}{\partial f(\mathbf{p})} = \ln \frac{f(\mathbf{p})}{1 - f(\mathbf{p})} . \quad (1.12)$$

Equation (1.10) becomes

$$\begin{aligned} \frac{\partial}{\partial t} \Big|_{\text{coll}} \sum_{\mathbf{p}} f(\mathbf{p}) \ln f(\mathbf{p}) + [1 - f(\mathbf{p})] \ln [1 - f(\mathbf{p})] &= \frac{\partial}{\partial t} H(\mathbf{r}, t) \Big|_{\text{coll}} \\ &= -\frac{1}{4} \sum_{\mathbf{pp}', \mathbf{p}_1, \mathbf{p}'_1} w(\mathbf{p}, \mathbf{p}_1; \mathbf{p}', \mathbf{p}'_1) \ln \left[\frac{f f_1 (1 - f') (1 - f'_1)}{(1 - f) (1 - f_1) f' f'_1} \right] \\ &\quad \times [f f_1 (1 - f') (1 - f'_1) - (1 - f) (1 - f_1) f' f'_1]. \end{aligned} \quad (1.13)$$

The integrand is of the form $(x - y) \ln(x/y)$, and hence nonnegative, because $x - y$ and $\ln(x/y)$ have the same sign. Thus the H -function (called “eta”-function, the capital greek eta looks like a latin H) always decreases in the approach to equilibrium. This is the content of Boltzmann’s famous eta-theorem, generalized to a Fermi gas.

The eta-theorem shows that the entropy density, which for a Fermi gas is given by [226]

$$\begin{aligned} s(\mathbf{r}, t) &= -k_B H(\mathbf{r}, t) \\ &= -k_B \sum_{\mathbf{p}} \{ f(\mathbf{p}) \ln f(\mathbf{p}) + [1 - f(\mathbf{p})] \ln [1 - f(\mathbf{p})] \}, \end{aligned} \quad (1.14)$$

reaches a maximum in the equilibrium. Here, k_B is Boltzmann’s constant.

Finally, we will show that the Boltzmann equation (1.2) describes indeed an approach to the well-known Fermi equilibrium function. For this purpose we formalize the already mentioned conservation laws. We define the functions $F_i(\mathbf{p})$ with $i = 1, \dots, 5$ as

$$F_1 = 1, \quad F_i = p_i, \quad i = 2, 3, 4, \quad F_5 = \varepsilon_p, \quad (1.15)$$

we see immediately from (1.10) that the corresponding $\langle F_i \rangle$ are not changed by the collisions. In equilibrium the term in curly brackets in (1.2) has to vanish:

$$[f^0 f_1^0 (1 - f^{0'}) (1 - f_1^{0'}) - (1 - f^0) (1 - f_1^0) f^{0'} f_1^{0'}] = 0. \quad (1.16)$$

From this relation one sees that

$$\ln \frac{f^0}{(1 - f^0)} + \ln \frac{f_1^0}{(1 - f_1^0)} = \ln \frac{f^{0'}}{(1 - f^{0'})} + \ln \frac{f_1^{0'}}{(1 - f_1^{0'})}. \quad (1.17)$$

In other words, $\ln[f^0/(1 - f^0)]$ is also a conserved quantity. Because we have only five basic conservation laws, this quantity can be expressed as a linear combination of 1, \mathbf{p} , and ε_p :

$$\ln \frac{f^0}{(1 - f^0)} = A + \mathbf{B} \cdot \mathbf{p} + C \varepsilon_p \quad (1.18)$$

with

$$A = \beta\mu, \quad \mathbf{B} = \beta\mathbf{u}, \quad C = -\beta, \quad (1.19)$$

where $\beta = 1/(k_B T)$, μ is the chemical potential and \mathbf{u} is the drift velocity. All the expressions in (1.19) can still be – slowly varying – functions of \mathbf{r} and t . Such a situation is called a local equilibrium. Equation (1.18) has the solution

$$f^0(\mathbf{p}) = \frac{1}{e^{\beta(\varepsilon_p - \mathbf{p} \cdot \mathbf{u} - \mu)} + 1}, \quad (1.20)$$

which is the Fermi distribution function. A similar derivation for the Boltzmann equation with electron–phonon scattering results in an equilibrium phonon distribution function of the form

$$n^0(\mathbf{p}) = \frac{1}{e^{\beta(\hbar\omega_p - \mathbf{p} \cdot \mathbf{u})} - 1}, \quad (1.21)$$

because the chemical potential of bosons, whose total number is not conserved, is identical to zero.

1.3 Linearization: Eigenfunction Expansion

Close to thermal equilibrium the nonlinear Boltzmann equation, e.g., (1.2), can be linearized with respect to the deviation $\delta f \equiv f - f^0$ from the thermal equilibrium solution (1.20). For simplicity we consider here a spatially homogeneous electron gas without drift. It turns out that it is advantageous to use a normalized deviation $\phi(\mathbf{p}, t)$ which is introduced by writing

$$f(\mathbf{p}, t) = \frac{1}{e^{\beta(\varepsilon_p - \mu) - \phi(\mathbf{p}, t)} + 1}. \quad (1.22)$$

Expanding this function with respect to $\phi(\mathbf{p}, t)$ yields

$$\delta f(\mathbf{p}, t) = f^0(\mathbf{p})[1 - f^0(\mathbf{p})]\phi(\mathbf{p}, t). \quad (1.23)$$

The linearized Boltzmann equation yields the following net scattering rate for the state \mathbf{p} :

$$\begin{aligned} \frac{\partial \phi(\mathbf{p}, t)}{\partial t} &= -\frac{2}{f^0(\mathbf{p})[1 - f^0(\mathbf{p})]} \sum_{\mathbf{p}_1, \mathbf{p}', \mathbf{p}'_1} w(\mathbf{p}, \mathbf{p}_1; \mathbf{p}', \mathbf{p}'_1) \\ &\times \left\{ \phi(\mathbf{p}, t) [f^0(1 - f^0)f_1^0(1 - f^{0'})f_1^{0'}] \right. \\ &\left. + f^0(1 - f^0)(1 - f_1^0)f^{0'}f_1^{0'} \right\} + \dots \end{aligned} \quad (1.24)$$

The dots indicate terms of similar structure proportional to $\phi(\mathbf{p}_1, t)$, $\phi(\mathbf{p}', t)$, and $\phi(\mathbf{p}'_1, t)$. In equilibrium

$$f^0 f_1^0 (1 - f^{0'}) (1 - f_1^{0'}) = (1 - f^0) (1 - f_1^0) f^{0'} f_1^{0'} . \quad (1.25)$$

Using relation (1.25), the linearized Boltzmann equation (1.24) reduces to

$$\frac{\partial \phi(\mathbf{p}, t)}{\partial t} = -\frac{2}{f^0(\mathbf{p})[1 - f^0(\mathbf{p})]} \sum_{\mathbf{p}_1, \mathbf{p}', \mathbf{p}'_1} \mathcal{W}(\mathbf{p}, \mathbf{p}_1; \mathbf{p}', \mathbf{p}'_1) \quad (1.26)$$

$$\times [\phi(\mathbf{p}, t) + \phi(\mathbf{p}_1, t) - \phi(\mathbf{p}', t) - \phi(\mathbf{p}'_1, t)] = -\mathcal{L} \phi(\mathbf{p}, t), \quad (1.27)$$

with

$$\mathcal{W}(\mathbf{p}, \mathbf{p}_1; \mathbf{p}', \mathbf{p}'_1) = w(\mathbf{p}, \mathbf{p}_1; \mathbf{p}', \mathbf{p}'_1) f^0 f_1^0 (1 - f^{0'}) (1 - f_1^{0'}) . \quad (1.28)$$

The transition matrix \mathcal{W} of the linearized Boltzmann equation has the following symmetry properties:

$$\begin{aligned} \mathcal{W}(\mathbf{p}, \mathbf{p}_1; \mathbf{p}', \mathbf{p}'_1) &= \mathcal{W}(\mathbf{p}_1, \mathbf{p}; \mathbf{p}', \mathbf{p}'_1) \\ &= \mathcal{W}(\mathbf{p}', \mathbf{p}'_1; \mathbf{p}, \mathbf{p}_1) = \mathcal{W}(\mathbf{p}, \mathbf{p}_1; \mathbf{p}'_1, \mathbf{p}') . \end{aligned} \quad (1.29)$$

The linearized Boltzmann equation also conserves the total particle number, the total momentum, and the total energy. If one chooses a $\phi(\mathbf{p}, t)$ which is proportional to either $1, \mathbf{p}$, or ε_p , the r.h.s of the Boltzmann equation (1.26) vanishes. Thus, these particular forms of $\phi(\mathbf{p})$ are eigenfunctions to the collision operator \mathcal{L} with a vanishing eigenvalue. The collision operator is an integral operator

$$\mathcal{L}\phi(\mathbf{p}) = \sum_{\mathbf{p}'} \mathcal{L}(\mathbf{p}, \mathbf{p}') \phi(\mathbf{p}') . \quad (1.30)$$

In general the eigenfunctions $\phi_\lambda(\mathbf{p})$ are solutions of the stationary equation

$$\mathcal{L}\phi_\lambda(\mathbf{p}) = \lambda\phi_\lambda(\mathbf{p}) . \quad (1.31)$$

One can define a scalar product $\langle \sigma | \phi \rangle$ and a norm $|\phi|$ by

$$\langle \sigma | \phi \rangle = \sum_{\mathbf{p}} f^0(\mathbf{p}) [1 - f^0(\mathbf{p})] \sigma^*(\mathbf{p}) \phi(\mathbf{p}) , \quad |\phi|^2 = \langle \phi | \phi \rangle , \quad (1.32)$$

and span a Hilbert space by the eigenfunctions of \mathcal{L} . Using the symmetry relations of \mathcal{W} , one shows that \mathcal{L} is a hermitian, real, and positive semidefinite operator in this Hilbert space, i.e.,

$$\langle \sigma | \mathcal{L}\phi \rangle = \langle \mathcal{L}\sigma | \phi \rangle ; \quad \langle \phi | \mathcal{L}\phi \rangle \geq 0 . \quad (1.33)$$

The equality sign holds, if ϕ is one of the five collision invariants. With these definitions the solution of the time-dependent linearized Boltzmann equation

with a given initial deviation $\phi(t = 0) = \phi_0$ can be found by expanding ϕ_0 in terms of the set of eigenfunctions ϕ_λ of \mathcal{L} . The solution is then of the form

$$\phi(\mathbf{p}, t) = \sum_{\lambda} A_{\lambda} e^{-\lambda t} \phi_{\lambda}(\mathbf{p}) . \quad (1.34)$$

The eigenvalues λ are true relaxation frequencies for deviations ϕ_{λ} . However, it is obvious from (1.34) that, in general, a description of the Boltzmann relaxation kinetics with only one relaxation time is not possible. Therefore the most frequently used linear approximation to the collision rate, the so-called relaxation-time approximation,

$$\frac{\partial f(\mathbf{p})}{\partial t} \Big|_{\text{coll}} \simeq -\frac{\delta f(\mathbf{p})}{\tau} \quad (1.35)$$

is only a very crude description of the relaxation kinetics toward equilibrium. The effective relaxation time τ in the resulting exponential decay of a deviation from the thermal equilibrium distribution has, in general, no well-defined meaning, and is known not to describe adequately the experimentally observed transport properties (e.g., viscosities and thermal conductivity of simple mono- and diatomic gases) [327]. Since the linearized collision operator commutes with the operator for the angular momentum in \mathbf{p} -space, the normalized deviation $\phi(\mathbf{p})$ can be factorized into a radial function and an angular part. Unfortunately, the eigenfunctions have to be evaluated numerically. Only for a nondegenerate system of Maxwell molecules with a repulsive interaction potential $\propto r^{-4}$ analytical eigenfunctions have been found. In the case of degenerate Fermi systems, where all momenta are confined to the neighborhood of p_F , the eigenfunction expansions have provided rapidly converging series for various transport coefficients [60, 190].

We will illustrate in Chap. 2 the use of the eigenfunction expansion for the numerical evaluation of the relaxation kinetics due to Coulomb scattering in a quasi-two-dimensional (2D) electron gas. Such a 2D electron gas can be, for example, realized in a semiconductor quantum well structure. This example simultaneously addresses an important relaxation process of hot electrons in semiconductors, because in a dense electron gas in semiconductors the Coulomb scattering provides the fastest relaxation process.

2

Numerical Solutions of the Boltzmann Equation

Summary. Various concepts for the numerical solution of the semiclassical Boltzmann equation are discussed, including an illustration of the use of a linearized Boltzmann equation and its eigenfunction expansion for a 2D electron gas. The numerical results for the linearized Boltzmann equation are compared with those of an ensemble Monte Carlo simulation of the Master equation. Finally the Boltzmann equation together with the Poisson equation is solved self-consistently for a spatially inhomogeneous electron gas in the relaxation time approximation.

2.1 Introduction

In general, the solution of the Boltzmann equation requires numerical methods. One possibility, which has been applied to the study of the Boltzmann kinetics for electron systems in semiconductors, is the direct numerical integration [85, 317, 329]. Several examples of such direct numerical integrations will be discussed in Part IV of this book as limiting cases of the treatment of the more general quantum kinetics, and we postpone the further discussion of this method up to that point.

If one studies only the relaxation of a small deviation from an equilibrium distribution, one can linearize the Boltzmann equation as discussed in Chap. 1. Powerful mathematical solution methods are available for linear integral equations. We will illustrate the use of the eigenfunction expansion by treating the relaxation kinetics due to Coulomb collisions in a dense electron gas in a quasi-two-dimensional quantum well structure in Sect. 2.2. If one can make, in addition to the linearization, an expansion in the small momentum change in the collision, the Boltzmann integral equation can be approximated by the Fokker–Planck equation [241, 295] which is a second-order differential equation and describes the relaxation in terms of a drift and a diffusion of the distribution in momentum space. The Fokker–Planck approximation is particularly useful for electron–phonon scattering, while the additional momentum and energy conservation laws of the Coulomb scattering lead to a more complicated integro-differential equation [144].

Finally, the collision kinetics can be simulated by stochastic methods, called Monte Carlo simulation [42]. Many simulations make use of the semiclassical concept of the population of small phase space volume elements $\Delta^3x\Delta^3p$ [109, 126, 168, 169, 188, 213, 277, 334]. These methods allow one to treat very naturally spatially inhomogeneous systems and they are very important in the simulation of actual semiconductor devices. Due to the semiclassical nature of the method, the treatment of degenerate electron gases is less accurate. In this respect the ensemble Monte Carlo simulations for homogeneous systems in \mathbf{k} -space [102] are more accurate because they simulate the underlying Master equation rather than the Boltzmann equation. For spatially homogeneous systems, one studies directly the stochastic time development of the occupation of momentum states, and obtains Boltzmann distribution probabilities from averaging over many microscopic realizations. The algorithm for the ensemble Monte Carlo simulation can be derived rather explicitly from the corresponding Master equation, and we will describe this method in Sect. 2.3, and demonstrate its use again in Sect. 2.4 in the case of Coulomb relaxation kinetics of a dense electron gas in a semiconductor quantum well structure.

2.2 Linearized Coulomb Boltzmann Kinetics of a 2D Electron Gas

The Boltzmann relaxation kinetics of an electron gas in semiconductors can be studied experimentally by time-resolved pump and probe spectroscopy. Therefore we will illustrate the eigenfunction expansion technique for the example of an electron gas in a quantum well structure following [102]. We assume that the quantum well is so narrow, that we can consider only the two-dimensional motion of the electrons in the lowest subband [31, 146]. The 2D electron momentum is $\mathbf{p} = \hbar\mathbf{k}$, where \mathbf{k} is the wavevector, the effective electron mass is m . The field lines of the Coulomb forces also enter the barrier material which often has very similar dielectric properties as the well material. Therefore, the Coulomb potential retains its three-dimensional $1/r$ form in these mesoscopic microstructures in real space. Its 2D Fourier transform is [146]

$$V_q = \frac{2\pi e^2}{\varepsilon_0 L^2 q}, \quad (2.1)$$

where q is the wavenumber, L^2 the 2D volume, and ε_0 is the background dielectric constant. In Coulomb systems the bare Coulomb potential in the collision integral has to be replaced by its screened counterpart [191, 380]. In the simplest approximation the statically screened 2D Coulomb potential $V_{s,q}$ is [146]

$$V_{s,q} = \frac{2\pi e^2}{\varepsilon_0 L^2 (q + \kappa)}, \quad (2.2)$$

where κ is the screening wavenumber [102],

$$\kappa = \frac{2mL^2}{\hbar^2} e^2 f_{k=0}. \quad (2.3)$$

Because, in general, the distribution of the lowest k -state changes in time during the relaxation process, the screening wavenumber will depend parametrically on the time. However, in the linearized Boltzmann equation this time dependence does not contribute because $f_0(t) \rightarrow f_0^0$.

In the following only isotropic distributions $f_k(t)$ will be considered, thus only the eigenfunctions with angular momentum $l = 0$ are needed. With this restriction only the particle number and the energy remain as collision invariants with eigenvalues $\lambda = 0$. For isotropic deviations an angular integration allows us to write the action of the collision operator (1.26) as that of a matrix with continuous wavenumber indices k :

$$\mathcal{L}\phi_k = \sum_{k'} \mathcal{L}_{k,k'} \phi_{k'}, \quad (2.4)$$

where the integral kernel follows from (1.3), (1.26), and (1.28) as

$$\begin{aligned} \mathcal{L}_{k,k'} &= \frac{me^4}{\pi\hbar^3\varepsilon_0^2} \int d^2p \int d^2q \frac{\delta[(\mathbf{p}-\mathbf{k})\cdot\mathbf{q}-q^2]}{(q+\kappa)^2} \frac{f_p^0(1-f_{|\mathbf{k}+\mathbf{q}|}^0)(1-f_{|\mathbf{p}-\mathbf{q}|}^0)}{(1-f_k^0)} \\ &\times [\delta(k'-k) + \delta(k'-p) - \delta(k'-|\mathbf{k}+\mathbf{q}|) - \delta(k'-|\mathbf{p}-\mathbf{q}|)]. \end{aligned} \quad (2.5)$$

Here the exchange term of (1.3) has been disregarded for simplicity. In order to determine the eigenfunctions numerically, the integral has to be approximated by a discrete sum on an equidistant grid $k_i = i\Delta k$ with $i = 0, 1, \dots, N$. Thus a cutoff wavenumber $k_N > k_F$ is introduced, which certainly has to be larger than the Fermi wavenumber, defined as $\hbar^2 k_F^2 / 2m = \mu$. The diagonal elements of the collision operator are usually called the collision frequencies ν_k . A further simplification of the calculation can be achieved by symmetrizing \mathcal{L} via a similarity transformation,

$$\tilde{\mathcal{L}} = g^{-1} \mathcal{L} g, \quad \tilde{\phi} = g^{-1} \phi \text{ with } \tilde{\mathcal{L}} \tilde{\phi}_\lambda = \lambda \tilde{\phi}_\lambda, \quad (2.6)$$

where g is a diagonal matrix with the elements

$$g_{k,k'} = \delta_{k,k'} \frac{1}{\sqrt{k f_k^0 (1 - f_k^0)}}. \quad (2.7)$$

As a first step, the matrix elements $\mathcal{L}_{k,k'}$ are computed for $k, k' \leq k_N$. Next the eigenfunctions and eigenvalues λ of the symmetric matrix $\tilde{\mathcal{L}}$ are evaluated. The eigenfunctions are finally transformed back by multiplication with the matrix g to get the desired eigenfunctions ϕ_λ . The step width for all calculations is taken to be $\Delta k = k_F/50$. A further reduction of the step width

does not change the results essentially. The dependence of the results on the cutoff wavenumber k_N will be discussed below.

The collision frequency ν_k is sometimes used [249] to get an estimate for the relaxation times due to inelastic carrier–carrier scattering. In Fig. 2.1 the collision frequency ν_k is shown for four different carrier densities. The material parameters are those of the conduction band of GaAs, i.e., $m = 0.0665m_0$ and $\varepsilon_0 = 13.71$. The collision frequency decreases with increasing density. This effect is caused by the Pauli-blocking of the final scattering states and the enhanced screening of the Coulomb potential. For increasing degeneracy a pronounced dip appears in the vicinity of the Fermi energy. This dip can be understood, if one recalls that ν_k is the sum of the equilibrium scattering rates in and out of the state with energy ε_k . These rates are related by detailed balance, i.e.,

$$\nu_k = \Gamma_k^{\text{in}} + \Gamma_k^{\text{out}}; \quad \Gamma_k^{\text{out}} = \frac{1 - f_k^0}{f_k^0} \Gamma_k^{\text{in}}. \quad (2.8)$$

At low temperatures these rates around k_F are very small. Consider, e.g., a state k , above but close to k_F ; its rate out is small because of the small number of empty final states between k and k_F . For $k \rightarrow \infty$ the collision frequency tends to 0. Generally one finds a dense spectrum of eigenvalues λ_n , $n = 1, 2, \dots, N$, therefore we define a density of eigenstates

$$\varrho(\lambda_n) = \frac{2\Delta k}{\lambda_{n+1} - \lambda_{n-1}}, \quad (2.9)$$

which becomes independent of the step width for small Δk . The density of eigenstates $\varrho(\lambda_n)$ is shown in Fig. 2.2 as a function of λ for two carrier densities

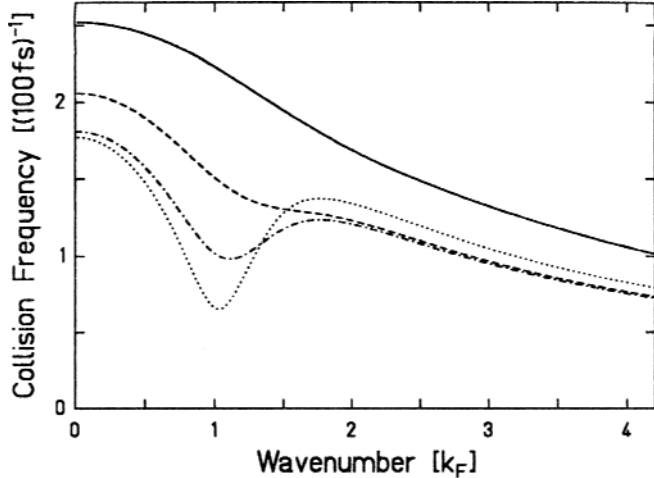


Fig. 2.1. Collision frequency ν_k vs. k/k_F for various 2D plasma densities in units of 10^{12} cm^{-2} : (Full line) $n = 0.64$; (dashed line) $n = 1.28$; (dashed-dotted line) $n = 2.56$; (dotted line) $n = 5.12$ according to [102]

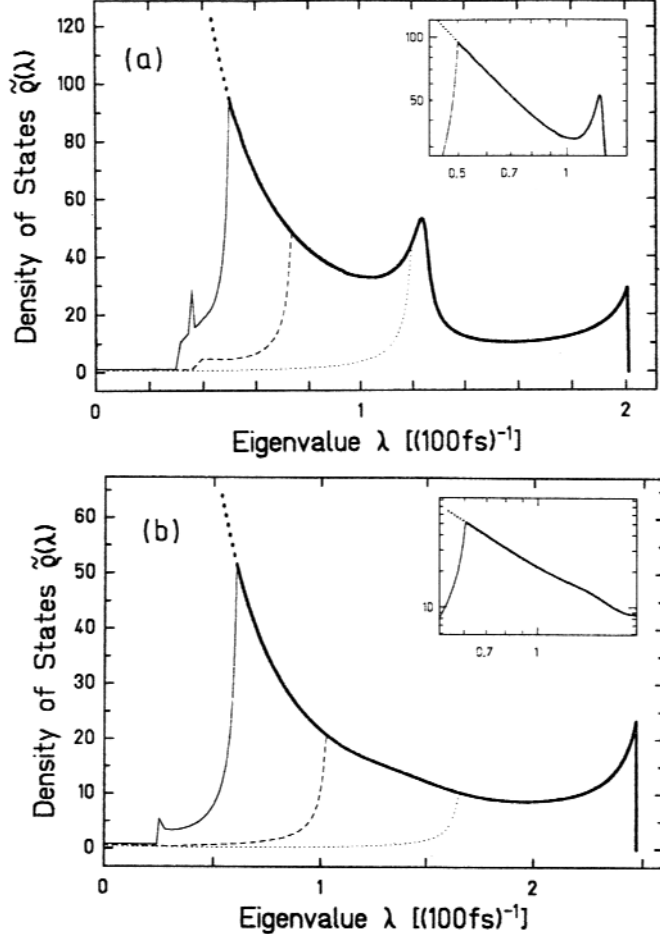


Fig. 2.2. Density of eigenstates $\rho(\lambda)$ of the collision eigenfrequencies for two plasma densities n and various values of the cutoff. (a) Top part: For $n = 1.28 \cdot 10^{12} \text{ cm}^{-2}$ and $k_N = 2k_F$ (dotted line); $k_N = 4k_F$ (dashed line); $k_N = 6k_F$ (full line). (b) Bottom part: For $n = 0.64 \cdot 10^{12} \text{ cm}^{-2}$ and $k_N = 2k_F$ (dotted line); $k_N = 4k_F$ (dashed line); $k_N = 7k_F$ (full line) according to [102]. The insets are double logarithmic plots

and three values of the cutoff wavenumber, respectively. The spectrum consists of two eigenvalues numerically close to zero (belonging to the collision invariants) and a continuous band. The upper bound of the spectrum is approximately given by the highest collision frequency. The peak in $\rho(\lambda_n)$ at the higher density of Fig. 2.2 is correlated with the structure in the collision frequency ν_k around k_F , and is therefore absent in the low-density case of Fig. 2.2b. The only effect of increasing the cutoff wavenumber is to add states below a k_N -dependent frequency, as the three curves for the various

cutoff values illustrate. Above this frequency, $\varrho(\lambda_n)$ remains unchanged if k_N is increased further. These unchanged parts of the curves are the thick line segments in Fig. 2.2.a, b. It is not clear whether a gap exists between the two zero-eigenvalues of the collision invariants and the continuous spectrum. The double-logarithmic insets in Fig. 2.2.a, b suggest that the density of eigenstates can be extrapolated to smaller λ -values by a power law $\varrho(\lambda_n) \propto \lambda^{-1.8}$ for both carrier densities (thick dotted parts of the curves). If this power law holds also for larger k_N , no gap exists in the complete spectrum for $k_N \rightarrow \infty$. For nondegenerate distributions, together with three-dimensional rigid spheres and power-law potentials, it has been shown with a scattering angular cutoff that the continuous spectrum of \mathcal{L} extends over the whole range of the collision frequencies [249]. It seems that degenerate 2D electron systems with a screened Coulomb potential have the same property.

The fundamental properties of the eigenfunctions ϕ_λ are the same for all densities, thus only the high-density case is discussed. In Fig. 2.3 the two first numerically obtained eigenfunctions $\phi_{0,1}$ and $\phi_{0,2}$ are compared with the exact orthonormalized collision invariants corresponding to 1 and ε_k ,

$$\phi_{0,1} = \alpha_1 \text{ and } \phi_{0,2} = \alpha_2 k^2 - \alpha_3 , \quad (2.10)$$

where the constants are determined by the orthonormalization conditions. The deviations on the high-energy side are caused by the cutoff.

Two typical eigenfunctions $\tilde{\phi}_{\lambda,k}$ of the continuous spectrum of the hermitian matrix are shown in Fig. 2.4, together with the corresponding distribution deviations $\delta f_{\lambda,k}$ for $\lambda = 0.8 \times 10^{-13}$ and $1.6 \times 10^{-13} \text{ s}^{-1}$, respectively. The eigenfunctions increase in amplitude and frequency with k until they reach their maxima at $k = k_\lambda$ for which the collision frequency ν_k equals the eigenfrequency λ , and vanish rapidly for still higher k values. Figure 2.4 shows

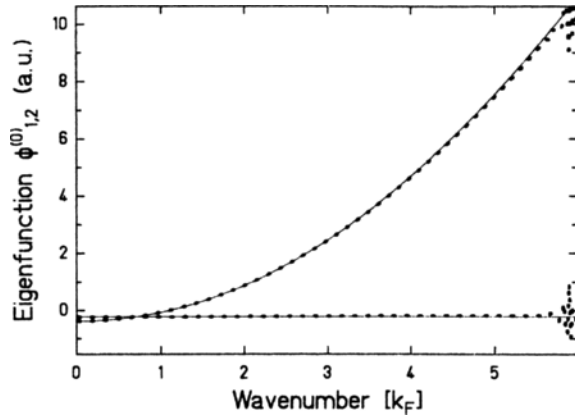


Fig. 2.3. The two eigenfunctions of the collision invariants $\phi_{0,1}(k)$ and $\phi_{0,2}(k)$ vs. k/k_F according to [102]. *Dots* numerical values, *lines* exact orthogonal eigenfunctions

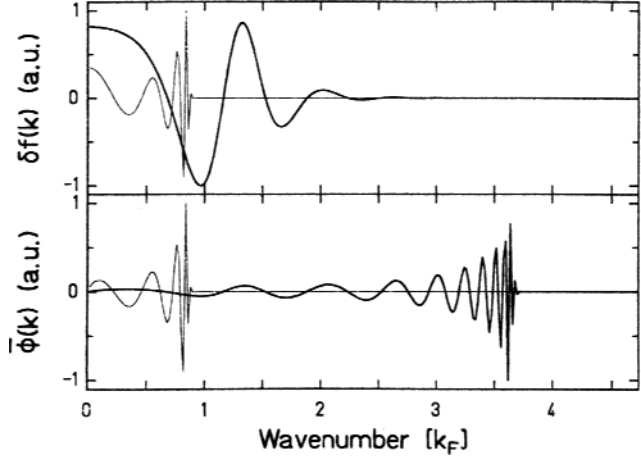


Fig. 2.4. Two eigenfunctions of the continuous spectrum $\tilde{\phi}_\lambda(k)$ vs. k/k_F for $\lambda = 0.8 \times 10^{-13} \text{ s}^{-1}$ (thick line) $\lambda = 1.6 \cdot 10^{-13} \text{ s}^{-1}$ (thin line) according to [102]. Above the corresponding distribution deviations $\delta f_{\lambda,k}$

that the eigenfunctions extend over the whole k -range below k_λ . The small wavenumber components of the distribution deviations $\delta f_{\lambda,k}$ are enhanced by the normalization factors as shown in the upper part of Fig. 2.4. Due to the extension of the distribution deviations $\delta f_{\lambda,k}$ it is not possible to define k -dependent relaxation times because, in general, many eigenfunctions are needed to represent a given narrow deviation from equilibrium.

The curves for the largest cutoff wavenumbers in Fig. 2.2a, b show that a peak in the density of eigenstates appears at low relaxation frequencies λ . This peak is due to one unique eigenfunction which extends over a wide range in k -space and, like the eigenfunctions belonging to higher eigenvalues, λ does not vanish at $k = 0$. The eigenfunctions which belong to the density of eigenstates below this peak are of different type and vanish rapidly for wavenumbers $k \leq 3k_F$. Thus for deviations below or up to the Fermi wavenumber, the eigenvalue of the unique eigenfunction determines the long-time relaxation behavior. However, due to the numerical incompleteness of the spectrum, no final conclusions can be made. Note that the maximum cutoff wavenumber is $6k_F$, which corresponds to an energy which is already 36 times the Fermi energy. Thus for a more detailed description of the long-time behavior, the detailed band structure has to be taken into account.

Next we study the relaxation kinetics with given initial deviations from the equilibrium distribution. The following form of the initial nonequilibrium distribution is considered

$$f_k(t=0) = f_k^{0,i} + C \exp \left[- \left(\frac{\varepsilon_k - \varepsilon^0}{\sigma} \right)^2 \right] = f_k^{0,f} + \delta f_k(t=0). \quad (2.11)$$

Here $f^{0,i}$ and $f^{0,f}$ are the initial background and the final equilibrium distributions, respectively. We have added a Gaussian nonequilibrium distribution to the initial background equilibrium distribution. The deviation $\delta f_k(t)$ from the final equilibrium distribution tends to zero for $t \rightarrow \infty$. Within the expansion method, the time development of the corresponding normalized deviation $\phi_k(t)$ is evaluated by an expansion in terms of the full set of eigenfunctions ϕ_{λ_n}

$$\phi_k(t) = \sum_{n=1}^N A_n \phi_{\lambda_n, k} e^{-\lambda_n t}. \quad (2.12)$$

The expansion coefficients A_n are evaluated with the discrete approximation of the scalar product:

$$A_n = \langle \phi(t=0) | \phi_{\lambda_n} \rangle = 2\pi \sum_k f_k^{0,f} (1 - f_k^{0,f}) \phi_k(t=0) \phi_{\lambda_n, k}. \quad (2.13)$$

Since we linearize around the final equilibrium distribution, the first two coefficients A_1 and A_2 vanish. The weight function $\alpha(\lambda)$ of an eigenvalue λ in the relaxation process given by

$$\alpha(\lambda_n) = \varrho(\lambda_n) A_n^2 \quad (2.14)$$

is shown in Fig. 2.5a–d for a carrier density $n = 1.28 \times 10^{12} \text{ cm}^{-2}$ with a temperature $T = 250 \text{ K}$ and a chemical potential $\mu = 43.6 \text{ meV}$ of the final

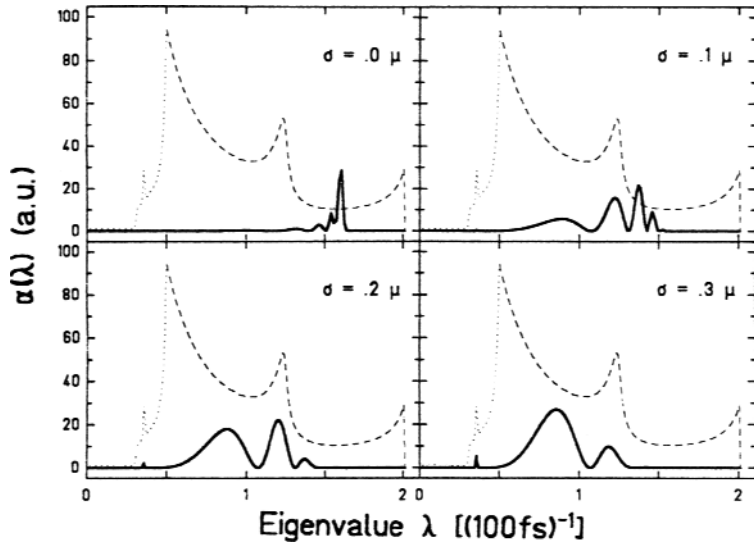


Fig. 2.5. Weight function α_λ of (2.4) vs. λ for four values of the peak width σ . The density of states is shown by the *dotted curves* for comparison according to [102]

equilibrium density. The central position of the initial deviation is $\varepsilon^0 = 0.8\mu$ and four different values of its width σ are used. For comparison the density of eigenstates is also shown. The first curve for $\sigma = 0$ is obtained for a deviation of the form $\delta f_i \propto \delta_{i,j}$ and has actually still a finite width given by the finite step width Δk . The spectral weight peaks at the collision frequency which belongs to the position of this delta-function-like deviation (Fig. 2.1). However, slower components do not vanish, explaining why the initially fast decay slows down. With increasing width σ , the slow components become more and more important, whereas the contribution of eigenvalues in the vicinity of the peak in the first curve vanishes. The eigenfunction which belongs to this peak oscillates very rapidly at the position of the perturbation. As a consequence, the scalar product vanishes if the perturbation is broad. On the other hand the eigenfunctions with lower eigenvalues oscillate more slowly in the vicinity of the deviation and gain spectral weight as the deviation becomes broader.

The relaxation kinetics will be characterized by the decay of the positive definite norm of the deviation from the final distribution determined by

$$|\phi(t)|^2 = \sum_{n=3}^N A_n^2 e^{-2\lambda_n t}. \quad (2.15)$$

Within the expansion method, a time-dependent relaxation rate $\gamma(t)$ is introduced by

$$|\phi(t)| = |\phi(0)| e^{-g(t)} \quad \text{with} \quad \frac{dg}{dt} = \gamma. \quad (2.16)$$

The relaxation rate $dg(t)/dt$ is shown in Fig. 2.6 for the parameters of Fig. 2.5. The relaxation rate decreases about 10% in one relaxation time. The dotted line, e.g., of Fig. 2.6 for a peak width $\sigma = 0.1\mu$, again shows that even a relatively narrow deviation decays appreciably slower than expected from

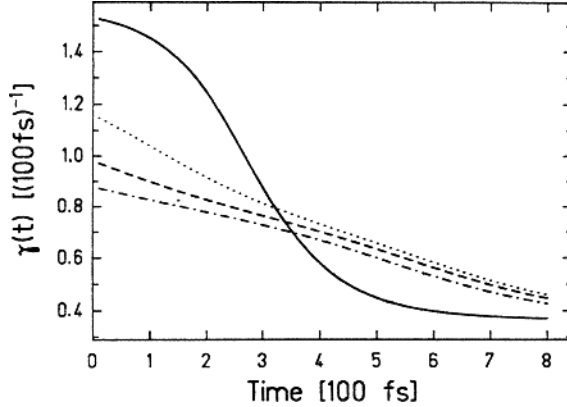


Fig. 2.6. Relaxation rate $\gamma(t)$ vs. t for the initial distributions with $\varepsilon^0 = 0.8\mu$ and various width values σ : $\sigma = 0$ (full line); $\sigma = 0.1\mu$ (dotted line); $\sigma = 0.2\mu$ (dashed line); $\sigma = 0.3\mu$ (dashed-dotted line) according to [102]

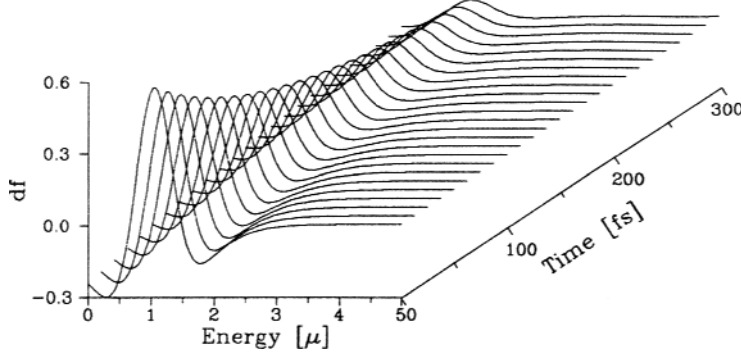


Fig. 2.7. Relaxation of a deviation from the final equilibrium distribution calculated by the eigenfunction expansion method according to [102]

the approximation in which the collision frequency ν_k is used for the relaxation rate.

Finally, the resulting relaxation kinetics of the expansion method is presented in Fig. 2.7. The temporal evolution of the deviation from the final distribution $\delta f_k(t) = f_k(t) - f_k^{0,f}$ is shown for an initial Gaussian deviation which is centered at $\varepsilon^0 = \mu$ and has a width $\sigma = 0.4\mu$, where the parameters of the final distribution are again $\mu = 43.6$ meV, $T = 250$ K and $n = 1.28 \times 10^{12} \text{ cm}^{-2}$. Because $\delta f_k(t)$ is the deviation from the final equilibrium distribution, $\delta f_k(0)$ in Fig. 2.7 differs at $t = 0$ from a simple Gaussian; it contains negative overshoots on both sides of the central peak. We observe that at these densities the relaxation process is completed in a few hundred femtoseconds. In this short timescale one may wonder whether the semiclassical Boltzmann equation with the statically screened Coulomb potential may be used. A detailed analysis of these concepts as well as their quantum kinetic extensions will be given in Part IV of this book.

2.3 Ensemble Monte Carlo Simulation

2.3.1 General Theory

In this chapter we want to discuss an important stochastic method for the solution of kinetic equations. We simulate concrete realizations of a system and have to average the result of the calculation over many ensembles. We consider a configuration or state α of the system. The probability for the state α is $P_\alpha \geq 0$ and $\sum_\alpha P_\alpha = 1$. The Master equation for time evolution of P_α is

$$\frac{dP_\alpha}{dt} = - \sum_{\alpha' \neq \alpha} \left[P_\alpha W_{\alpha,\alpha'} - P_{\alpha'} W_{\alpha',\alpha} \right], \quad (2.17)$$

where $W_{\alpha,\alpha'}$ is the transition probability per unit time from state α into state α' . It is given by Fermi's golden rule

$$W_{\alpha,\alpha'} = \frac{2\pi}{\hbar} |V_{\alpha,\alpha'}|^2 \delta(\varepsilon_\alpha - \varepsilon_{\alpha'}) , \quad (2.18)$$

where $V_{\alpha,\alpha'}$ are the matrix elements of a perturbation potential V . We notice that we could include an arbitrary diagonal transition probability $W_{\alpha,\alpha}$ to the Master equation without changing it. We do not consider here the interesting problem of how such an irreversible Master equation can be derived from the quantum mechanical Liouville equation of the statistical operator, see, for example, [132, 272, 296, 385].

If one describes a configuration in terms of the occupation numbers $n = \{n_{k_1}, n_{k_2}, n_{k_3}, \dots\}$ of the various single-particle states k_i , one gets the connection with the mean Boltzmann distribution functions f_k by

$$f_k(t) = \langle n_k(t) \rangle = \sum_n P_n(t) n_k . \quad (2.19)$$

For fermions $n_k = 0, 1$ and for bosons $n_k = 0, 1, 2, \dots$. A further assumption is that correlations are not important, so that, e.g.,

$$\langle n_k(t) n_{k'} \rangle \simeq f_k(t) f_{k'} . \quad (2.20)$$

As an example, for electrons scattering against impurities, one gets from the averaged Master equation (2.17) the Boltzmann equation

$$\frac{df_k}{dt} = - \sum_{k'} [f_k W_{k,k'} - f_{k'} W_{k',k}] , \quad (2.21)$$

with

$$W_{k,k'} = \frac{2\pi}{\hbar} n_i |V_{k,k'}|^2 \delta(\varepsilon_k - \varepsilon_{k'}) , \quad (2.22)$$

where n_i is the number of impurities and ε_k the kinetic energy of an electron with momentum \mathbf{k} .

An even simpler problem is the random walk of a single particle on a one-dimensional chain, on which only nearest-neighbor transitions with a transition probability W are allowed,

$$\frac{dP_n}{dt} = W [P_{n-1}(t) + P_{n+1}(t) - 2P_n(t)] , \quad (2.23)$$

where n denotes the site on the chain. This problem can be solved exactly. Nevertheless, we consider here an approximate method which will later be used in Monte Carlo simulations of more complicated problems. One approximates the differential equation by a difference equation with the discrete time steps $t_m = m\Delta t$ with $\Delta t = 1/2W$. With

$$\frac{dP_n(t)}{dt} \simeq \frac{P_n(m+1) - P_n(m)}{\Delta t} = 2W [P_n(m+1) - P_n(m)] , \quad (2.24)$$

we find

$$2P_n(m+1) = P_{n-1}(m) + P_{n+1}(m). \quad (2.25)$$

This equation can be solved analytically for a given initial condition $P_n(0)$. One gets by iteration

$$P_n(m) = \frac{1}{2^m} \sum_{l=0}^m \binom{m}{l} P_{n-m+2l}(0), \quad (2.26)$$

with the binomial coefficients

$$\binom{m}{l} = \frac{m!}{(m-l)!l!}.$$

Suppose that initially only one lattice point is occupied, i.e., $P_n(0) = \delta_{n,0}$. After m time steps the distribution has spread from $n = -m$ to $+m$, showing the diffusion of the probability by the random walk process on the chain. A comparison with the exact solution shows that the results of the discrete version rapidly approach the results of the differential equation for increasing time.

After this simple illustration we will treat the general Master equation using a similar discretization in time by choosing $(\Delta t)^{-1} = \tau_\alpha^{-1} = \sum_{\alpha' \neq \alpha} W_{\alpha,\alpha'}$ which yields

$$P_\alpha(t + \Delta t) = \sum_{\alpha' \neq \alpha} P_{\alpha'} \Pi_{\alpha',\alpha} \quad \text{with } \Pi_{\alpha,\alpha'} = \frac{W_{\alpha,\alpha'}}{\sum_{\alpha' \neq \alpha} W_{\alpha,\alpha'}}. \quad (2.27)$$

$\Pi_{\alpha,\alpha'}$ is obviously a probability with the properties $0 \leq \Pi_{\alpha,\alpha'} \leq 1$ and $\sum_{\alpha' \neq \alpha} \Pi_{\alpha,\alpha'} = 1$. The disadvantage in this formulation is that $\Delta t = \tau_\alpha$ depends on the actual configuration α and would thus have to be computed in each time step. To overcome this extremely time-consuming procedure, the concept of self-scattering is used by introducing a transition probability $W_{\alpha,\alpha}$ which, as noted below (2.18), does not change the Master equation. We choose the transition probability $W_{\alpha,\alpha} = W_\alpha$ for self-scattering in such a way that $\Delta t = \tau_s$ becomes a rather short, but α -independent self-scattering time:

$$P_\alpha(t + \Delta t) - P_\alpha(t) = -\Delta t \sum_{\alpha'} (P_\alpha W_{\alpha,\alpha'} - P_{\alpha'} W_{\alpha',\alpha}) \quad (2.28)$$

with

$$\frac{1}{\Delta t} = \sum_{\alpha'} W_{\alpha,\alpha'} \quad \text{where } \Delta t = \tau_s < \inf_\alpha \tau_\alpha, \quad (2.29)$$

so that

$$P_\alpha(t + \tau_s) = \sum_{\alpha'} P_{\alpha'}(t) \Pi_{\alpha',\alpha}(t). \quad (2.30)$$

If $P_{\alpha'}(t)$ is known, one can calculate $P_\alpha(t + \Delta t)$ with statistical methods. Suppose the probability $\Pi_{\alpha,\alpha'} = p$ with $0 \leq p \leq 1$. Next, one selects with a random number generator a random number ζ . If $\zeta \leq p$,

the transition from α' to α takes place, while it is not allowed if $\zeta > p$. With this rule one obtains the correct probability with many attempts, because

$$\frac{\text{number of cases with } \zeta \leq p}{\text{total number of attempts}} \rightarrow p .$$

Numerical number generators use the simple map

$$y_{n+1} = ay_n + b \bmod m \text{ and } \zeta_{n+1} = \frac{y_{n+1}}{m} . \quad (2.31)$$

The seed y_0 and the numbers a, b, m are large natural numbers, but their selection is crucial and has to be checked carefully, so that no cycles and obvious correlations exist in the numbers ζ_n .

2.3.2 Simulation of the Relaxation Kinetics of a 2D Electron Gas

In order to illustrate the use of the ensemble Monte Carlo simulation technique, we study again the relaxation of a 2D electron gas as in Sect. 2.2, with the important difference that we do not use a linear approximation. The general transition probability $W_{\alpha,\alpha'}$ in the Master equation is for the electron-electron interaction according to [102] given by [compare also with (1.3), (2.17), and (2.18)]

$$W_{\alpha,\alpha'} = \sum_{\mathbf{k}, \mathbf{k}_1, \mathbf{k}', \mathbf{k}'_1} w_{\mathbf{k}, \mathbf{k}_1; \mathbf{k}', \mathbf{k}'_1} n_{\mathbf{k}} n_{\mathbf{k}_1} (1 - n_{\mathbf{k}'}) (1 - n_{\mathbf{k}'_1}) D_{\mathbf{k}, \mathbf{k}_1; \mathbf{k}', \mathbf{k}'_1}^{\alpha; \alpha'} , \quad (2.32)$$

where

$$w_{\mathbf{k}, \mathbf{k}_1; \mathbf{k}', \mathbf{k}'_1} = \frac{2\pi}{\hbar} V_s^2 |\mathbf{k} - \mathbf{k}'| \delta_{\mathbf{k} + \mathbf{k}_1 - \mathbf{k}' - \mathbf{k}'_1} \delta(\varepsilon_k + \varepsilon_{k_1} - \varepsilon_{k'} - \varepsilon_{k'_1}) , \quad (2.33)$$

where V_s is the 2D screened Coulomb potential (2.2). The population $n_{\mathbf{k}}$ of the microscopic Fermi state \mathbf{k} is either 0 or 1. The microscopic populations are connected with the Boltzmann distribution via the ensemble average (2.19). The term $D_{\mathbf{k}, \mathbf{k}_1; \mathbf{k}', \mathbf{k}'_1}^{\alpha; \alpha'}$ contains all the δ -functions that connect the two configurations α and α' with the corresponding microscopic populations $n_{\mathbf{k}}$ and $n'_{\mathbf{k}}$

$$D_{\mathbf{k}, \mathbf{k}_1; \mathbf{k}', \mathbf{k}'_1}^{\alpha; \alpha'} = \delta_{n_{\mathbf{k}'}, n_{\mathbf{k}} - 1} \delta_{n_{\mathbf{k}'_1}, n_{\mathbf{k}_1} - 1} \delta_{n_{\mathbf{k}'}, n_{\mathbf{k}} + 1} \delta_{n_{\mathbf{k}'_1}, n_{\mathbf{k}'_1} + 1} , \quad (2.34)$$

because for transitions from the configuration α to α' the corresponding population of the \mathbf{k} state, e.g., has to be $n_{\mathbf{k}} = 1$, while after the transition the same state is empty: $n_{\mathbf{k}'} = 0$. Summing over α' implies just that the factor $D_{\mathbf{k}, \mathbf{k}_1; \mathbf{k}', \mathbf{k}'_1}^{\alpha; \alpha'}$ drops out:

$$\begin{aligned} \frac{1}{\tau_{\alpha}} = \sum_{\alpha'} W_{\alpha, \alpha'} &= \sum_{\mathbf{k}, \mathbf{k}_1, \mathbf{k}', \mathbf{k}'_1} w_{\mathbf{k}, \mathbf{k}_1; \mathbf{k}', \mathbf{k}'_1} n_{\mathbf{k}} n_{\mathbf{k}_1} (1 - n_{\mathbf{k}'}) (1 - n_{\mathbf{k}'_1}) \\ &\leq \sum_{\mathbf{k}, \mathbf{k}_1, \mathbf{k}', \mathbf{k}'_1} w_{\mathbf{k}, \mathbf{k}_1; \mathbf{k}', \mathbf{k}'_1} n_{\mathbf{k}} n_{\mathbf{k}_1} . \end{aligned} \quad (2.35)$$

Using the definitions

$$\gamma_{\mathbf{k}, \mathbf{k}_1} = \sum_{\mathbf{k}', \mathbf{k}'_1} w_{\mathbf{k}, \mathbf{k}_1; \mathbf{k}', \mathbf{k}'_1} n_{\mathbf{k}} n_{\mathbf{k}_1}, \text{ and } \gamma = \sup_{\mathbf{k}, \mathbf{k}_1} \gamma_{\mathbf{k}, \mathbf{k}_1}, \quad (2.36)$$

the right-hand side of (2.35) can be maximized further,

$$\frac{1}{\tau_\alpha} \leq \gamma \sum_{\mathbf{k}, \mathbf{k}_1} n_{\mathbf{k}} n_{\mathbf{k}_1} = \gamma N(N-1) = \frac{1}{\tau_s}, \quad (2.37)$$

where N is the number of electrons in the ensemble. By introducing $\pi_{\mathbf{k}, \mathbf{k}_1; \mathbf{k}', \mathbf{k}'_1}$, which is the normalized transition probability corresponding to $w_{\mathbf{k}, \mathbf{k}_1; \mathbf{k}', \mathbf{k}'_1}$

$$\pi_{\mathbf{k}, \mathbf{k}_1; \mathbf{k}', \mathbf{k}'_1} = \frac{w_{\mathbf{k}, \mathbf{k}_1; \mathbf{k}', \mathbf{k}'_1}}{\gamma_{\mathbf{k}, \mathbf{k}_1}} \text{ with } \sum_{\mathbf{k}', \mathbf{k}'_1} \pi_{\mathbf{k}, \mathbf{k}_1; \mathbf{k}', \mathbf{k}'_1} = 1, \quad (2.38)$$

W_α can be written as

$$W_\alpha = \sum_{\mathbf{k}, \mathbf{k}_1, \mathbf{k}', \mathbf{k}'_1} \pi_{\mathbf{k}, \mathbf{k}_1; \mathbf{k}', \mathbf{k}'_1} n_{\mathbf{k}} n_{\mathbf{k}_1} [\gamma - \gamma_{\mathbf{k}, \mathbf{k}_1}(1 - n_{\mathbf{k}'})(1 - n_{\mathbf{k}'_1})]. \quad (2.39)$$

The probability factors $\Pi_{\alpha, \alpha'}$ of (2.27) become

$$\begin{aligned} \Pi_{\alpha, \alpha'} &= \sum_{\mathbf{k}, \mathbf{k}_1, \mathbf{k}', \mathbf{k}'_1} \pi_{\mathbf{k}, \mathbf{k}_1; \mathbf{k}', \mathbf{k}'_1} \frac{n_{\mathbf{k}}}{N} \frac{n_{\mathbf{k}_1}}{N-1} \\ &\times \left\{ D_{\mathbf{k}, \mathbf{k}_1; \mathbf{k}', \mathbf{k}'_1}^{\alpha; \alpha'} \frac{\gamma_{\mathbf{k}, \mathbf{k}_1}}{\gamma} (1 - n_{\mathbf{k}'})(1 - n_{\mathbf{k}'_1}) \right. \\ &\left. + \delta_{\alpha, \alpha'} \left[1 - \frac{\gamma_{\mathbf{k}, \mathbf{k}_1}}{\gamma} (1 - n_{\mathbf{k}'})(1 - n_{\mathbf{k}'_1}) \right] \right\}. \end{aligned} \quad (2.40)$$

As discussed above, the probability to find at time $t + \tau_s$ a system in state α which was in the state α_0 at time t is given by $\Pi_{\alpha_0, \alpha}$.

Consider a specific state α_1 that differs from α_0 only in the occupation of the four momentum states \mathbf{k}, \mathbf{k}_1 and $\mathbf{k}', \mathbf{k}'_1$. Then Π_{α_0, α_1} and $\Pi_{\alpha_0, \alpha}$ are

$$\Pi_{\alpha_0, \alpha_1} = \pi_{\mathbf{k}, \mathbf{k}_1; \mathbf{k}', \mathbf{k}'_1} \frac{n_{\mathbf{k}}}{N} \frac{n_{\mathbf{k}_1}}{N-1} \frac{\gamma_{\mathbf{k}, \mathbf{k}_1}}{\gamma} (1 - n_{\mathbf{k}'})(1 - n_{\mathbf{k}'_1}), \quad (2.41)$$

$$\Pi_{\alpha_0, \alpha_0} = \pi_{\mathbf{k}, \mathbf{k}_1; \mathbf{k}', \mathbf{k}'_1} \frac{n_{\mathbf{k}}}{N} \frac{n_{\mathbf{k}_1}}{N-1} \left[1 - \frac{\gamma_{\mathbf{k}, \mathbf{k}_1}}{\gamma} (1 - n_{\mathbf{k}'})(1 - n_{\mathbf{k}'_1}) \right]. \quad (2.42)$$

This result shows that Π_{α_0, α_i} with $i = 0, 1$ is the product of three probabilities $P^{(1)}, P^{(2)}$, and $P^{(3)}$, where

$$P^{(1)}(\mathbf{k}, \mathbf{k}_1) = \frac{n_{\mathbf{k}}}{N} \frac{n_{\mathbf{k}_1}}{N-1} \text{ with } \sum_{\mathbf{k}, \mathbf{k}_1} P^{(1)}(\mathbf{k}, \mathbf{k}_1) = 1 \quad (2.43)$$

is the probability for the electrons with momentum \mathbf{k} and \mathbf{k}_1 to be the scatterers;

$$P_{\mathbf{k}, \mathbf{k}_1}^{(2)}(\mathbf{k}', \mathbf{k}'_1) = \pi_{\mathbf{k}, \mathbf{k}_1; \mathbf{k}', \mathbf{k}'_1} \text{ with } \sum_{\mathbf{k}', \mathbf{k}'_1} P_{\mathbf{k}, \mathbf{k}_1}^{(2)}(\mathbf{k}', \mathbf{k}'_1) = 1 \quad (2.44)$$

is the probability that these electrons are scattered into the states \mathbf{k} and \mathbf{k}_1 , and, finally

$$P_{\mathbf{k}, \mathbf{k}_1; \mathbf{k}', \mathbf{k}'_1}^{(3)}(\alpha_i) = \begin{cases} \frac{\gamma_{\mathbf{k}, \mathbf{k}_1}}{\gamma} (1 - n_{\mathbf{k}'}) (1 - n_{\mathbf{k}'_1}) & \text{if } i = 1 \\ 1 - \frac{\gamma_{\mathbf{k}, \mathbf{k}_1}}{\gamma} (1 - n_{\mathbf{k}'}) (1 - n_{\mathbf{k}'_1}) & \text{if } i = 0 \end{cases}, \quad (2.45)$$

with

$$\sum_{i=0,1} P_{\mathbf{k}, \mathbf{k}_1, \mathbf{k}', \mathbf{k}'_1}^{(3)}(\alpha_i) = 1, \quad (2.46)$$

is the probability that the four selected momentum states lead to a real or a self-scattering event: the factor $(1 - n_{\mathbf{k}'}) (1 - n_{\mathbf{k}'_1})$ ensures that a real scattering can occur only if the final states are empty. (Remember that this factor has been dropped in the definition (2.37) of the self-scattering time τ_s .)

$\gamma_{\mathbf{k}, \mathbf{k}_1}/\gamma$ can be understood as a correction factor. Using $P^{(1)}(\mathbf{k}, \mathbf{k}_1)$ to select the scatterers, all electron pairs have equal probability. But this is wrong, because the scattering cross section varies for different momentum states. For a large cross section $\gamma_{\mathbf{k}, \mathbf{k}_1} \simeq \gamma$ (i.e., $P^{(3)} \simeq 1$, if the final states are empty) the selection of \mathbf{k} and \mathbf{k}_1 is likely to produce a real scattering event. In the opposite case a self-scattering event is most probable. (Remember that $\gamma_{\mathbf{k}, \mathbf{k}_1}$ has been replaced by γ for τ_s .)

We conclude this section by showing some results for the relaxation kinetics of a 2D electron gas [102]. Such a 2D electron gas can be realized in optically excited quantum-well semiconductor structures. At the initial time $t = 0$ we assume that a Gaussian nonequilibrium distribution has been created. The initial distribution is centered at the energy $\varepsilon^0 = 60$ meV above the band edge and has a spread $\sigma = 60$ meV,

$$f_{\mathbf{k}}(t = 0) = C(n) \exp \left[- \left(\frac{\varepsilon_{\mathbf{k}} - \varepsilon^0}{\sigma} \right)^2 \right]. \quad (2.47)$$

In contrast to the initial condition (2.11) no background equilibrium distribution is assumed in (2.47). By varying the amplitude $C(n)$ between 0.22 and 1.0, one varies the density between 0.6×10^{12} and $2.7 \times 10^{12} \text{ cm}^{-2}$. We study the relaxation of the normalized distribution deviation (1.23) from equilibrium $\phi_{\mathbf{k}}(t)$. The equilibrium distribution $f_{\mathbf{k}}^0$ has the same particle and energy densities as the nonequilibrium distribution $f_{\mathbf{k}}(t)$. The relaxation of the norm $|\phi_{\mathbf{k}}(t)|$ is again expressed in terms of a time-dependent relaxation rate $\gamma(t)$ as in (2.31)

$$|\phi_{\mathbf{k}}(t)| = |\phi_{\mathbf{k}}(0)| e^{-\gamma(t)t}. \quad (2.48)$$

With Monte Carlo results a differentiation is not possible. One finds that the resulting $\gamma(t)$ varies up to 50% during the first 100 fs: an initially fast relaxation slows down. These results show that a unique relaxation time cannot be defined properly, because the nonexponential behavior shows up on the same timescale as the relaxation time itself. On the other hand, the density-dependence of the initial relaxation time can still be well defined. Averaging $\gamma(t)$ over the first 50 fs, the resulting relaxation times (i.e., $1/\gamma$) are shown in Fig. 2.8 for two different approximations of the screening. The statically screened potential depends, according to (2.2), in 2D on the distribution $f_{k=0}(t)$. If the actual distribution is used, one speaks about time-dependent static screening, if $f_{k=0}(t)$ is replaced by $f_{k=0}^0$ one speaks about equilibrium screening. The solid line in Fig. 2.8 is a power-law fit for Monte Carlo data obtained with time-dependent screening (solid squares) and the dashed line for those with equilibrium screening (open squares). The labels give the temperature of the final Fermi distribution f^0 , which cannot be fixed by the initial condition. The best fits are

$$\tau = \begin{cases} 185 \text{ fs} \left(\frac{n}{10^{11} \text{ cm}^{-2}} \right)^{-0.30} & \text{for time-dependent screening ,} \\ 242 \text{ fs} \left(\frac{n}{10^{11} \text{ cm}^{-2}} \right)^{-0.22} & \text{for equilibrium screening .} \end{cases} \quad (2.49)$$

The two different screening concepts yield nearly the same density dependence, but different absolute values. Time-dependent static screening leads to shorter relaxation times, because for the given initial condition the screening is less effective at the beginning. In a high-density system the distribution is

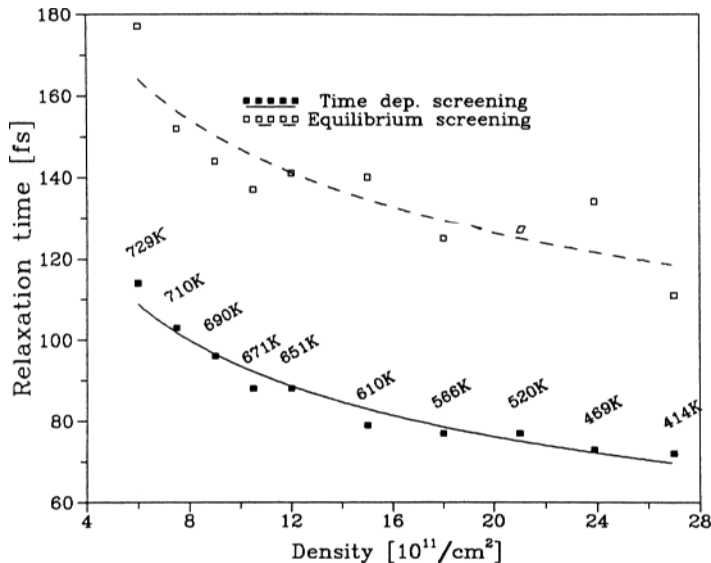


Fig. 2.8. Relaxation rate $\gamma(t)$ for two different screening models according to [102]

relaxed when the number of scattering events is comparable to the number of electrons. For a low-density system more scattering events are necessary, because in each collision less momentum and energy is transferred due to the smaller screening momentum. Becker et al. [34] measured for the density dependence of the polarization dephasing in bulk GaAs an exponent of -0.3 , but the agreement with our result is certainly fortuitous, as will be discussed in detail with the corresponding quantum kinetic treatment in Part IV.

If one adjusts the peak position, the width and the amplitude of the initial Gaussian distribution in order to keep the temperature of the final equilibrium distribution constant, the same density dependence but with different absolute values are found.

Figure 2.9 shows the evolution of an initial Gaussian distribution centered at $\varepsilon^0 = 30$ meV with a width $\sigma = 20$ meV and an amplitude of 1. The temperature of the final Fermi distribution is 236 K, the chemical potential is 30 meV and the density is 0.96×10^{12} cm $^{-2}$. The relaxation time is about 50 fs.

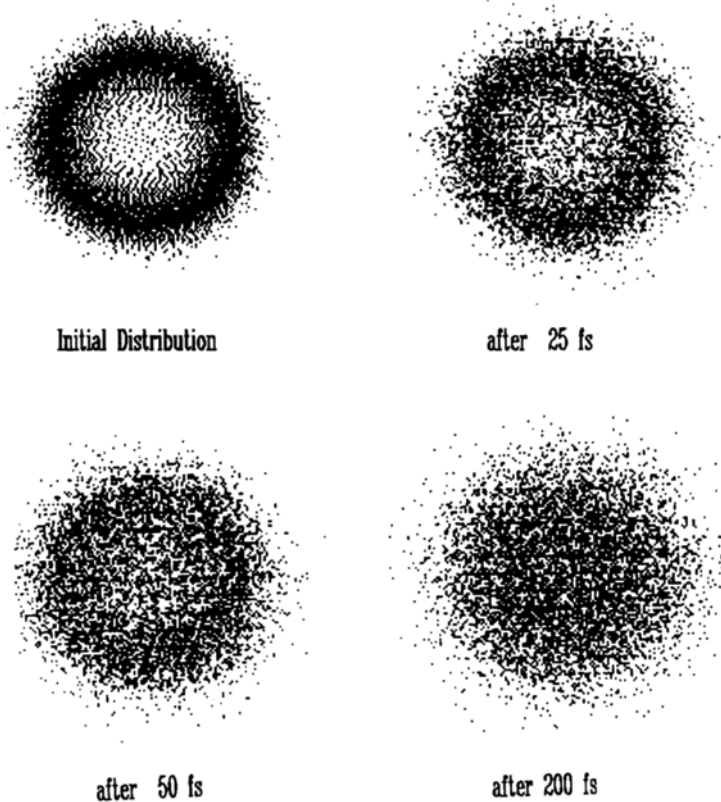


Fig. 2.9. Monte Carlo generated electron distribution in the 2D k-space after four times ($t=0, 25, 50, 200$ fs) according to [102]

In Fig. 2.9 an ensemble of about 5000 electrons is shown in the 2D k -space at four different times, as obtained from the screen of a personal computer. Each point corresponds to an electron. The initial distribution corresponds to an initial Gauss distribution centered at $\varepsilon^0 = 30$ meV above the band edge with a width of $\sigma = 20$ meV. In Fig. 2.10 the corresponding distribution functions are given averaged over five runs. It is seen that the relaxation consists in a small drift and a pronounced diffusion in k -space [144]. After 200 fs, i.e., four relaxation times, the deviation of the electron distribution from the equilibrium distribution reaches the noise level. The simulation shows that the relaxation is more or less completed if the number of collisions equals the number of electrons in the system. Thus one collision per particle is sufficient to relax the system.

Finally, we will use the Monte Carlo simulation to calculate also the decay of an initially given deviation from an equilibrium distribution. In order to make a quantitative comparison with the results of the eigenfunction expansion (shown in Fig. 2.7), we use the same conditions. The equilibrium screening which is inherent to the expansion method was also used in the simulations.

Figure 2.11 again shows the temporal evolution of the deviation from the final distribution $\delta f_k(t) = f_k(t) - f_k^{0,f}$ for an initial Gaussian deviation which

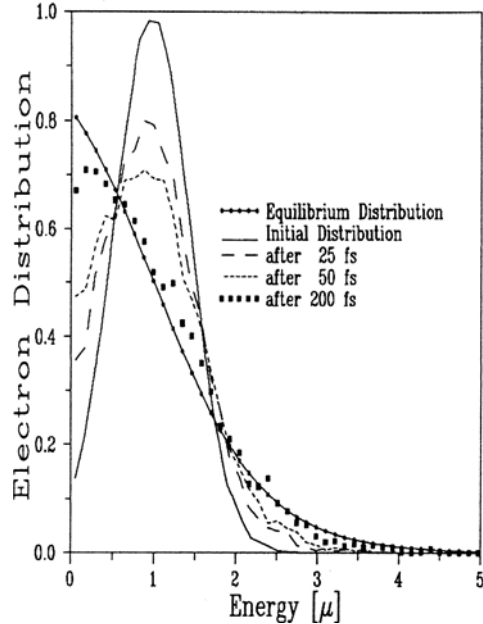


Fig. 2.10. Boltzmann distributions corresponding to the four snapshots of Fig. 2.9 after four times ($t=0, 25, 50, 200$ fs) obtained by averaging over five Monte Carlo simulations according to [102]

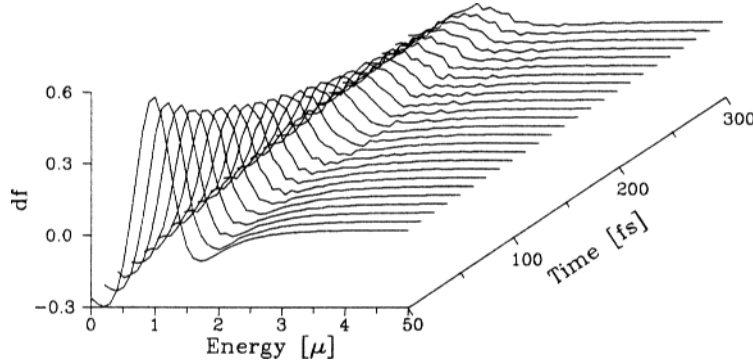


Fig. 2.11. Monte Carlo relaxation kinetics. Plotted is the deviation from the final equilibrium distribution as in Fig. 2.7 for identical parameters according to [102]

is centered at $\varepsilon^0 = \mu$ with a width $\sigma = 0.4\mu$. The Monte Carlo data were averaged over five runs. For the Monte Carlo method it is necessary to define an initial equilibrium background to ensure that the initial distribution, i.e., the Gaussian deviation plus background, has the same density and energy as the final one. While the results of the linearization method do not depend on the amplitude of the deviation, for the Monte Carlo simulation the amplitude has to be chosen (here $C = 0.8$ has been used) to be as small as possible, but big enough to give a good signal-to-noise ratio. The deviation has to fulfill the following constraints: (a) It must be possible to find a initial equilibrium background, so that the distribution relaxes to the final one given by the parameters of the linearization. (b) The distribution has to be a probability $0 \leq f_k(t) \leq 1$. For Figs. 2.7 and 2.11 the parameters of the initial equilibrium background distribution are $T^i = 235$ K, $\mu^i = 12.5$ meV.

Except for the noise in the Monte Carlo results of Fig. 2.11, the agreement with the results of the eigenfunction expansion method of Fig. 2.7 is extremely good, in spite of the fact we treated a relatively large deviation from equilibrium for which the validity of the linearization may be questioned.

2.4 $N^+N^-N^+$ Structure: Boltzmann Equation Analysis

We conclude our review on Boltzmann-level studies relevant to semiconductor microstructures by presenting results obtained by [25] for a $N^+N^-N^+$ -structure, i.e., a structure where a thin (“mesoscopic”) weakly doped region is sandwiched between two heavily doped metallic contacts. The key issue is the spatial inhomogeneity of the structure, which requires a self-consistent determination of the electric field. For simplicity, we shall consider a one-dimensional system. Thus, the task is to calculate the distribution function

(from which charge densities and current then follow) with the Boltzmann equation,

$$\left[v \frac{\partial}{\partial x} + \frac{(-e)E(x)}{m} \frac{\partial}{\partial v} \right] f(x, v) = -\frac{1}{\tau} [f(x, v) - f^{\text{l.e.}}(x, v)] . \quad (2.50)$$

For simplicity, the collision term is evaluated in a relaxation-time approximation. The important feature of (2.50) is that the nonequilibrium distribution function $f(x, v)$ relaxes toward a *local nondegenerate equilibrium distribution function*, discussed generally in connection with (1.20),

$$f^{\text{l.e.}}(x, v) = n(x) \sqrt{\frac{m}{2\pi k_B T_0}} \exp \left[-\frac{mv^2}{2k_B T_0} \right] . \quad (2.51)$$

Here T_0 is the lattice temperature, and the local density is determined from the nonequilibrium distribution function, $n(x) = \int dv f(x, v)$. The choice (2.51) guarantees that the current continuity equation is satisfied. To see this, integrate (2.50) over v :

$$\int dv \left[v \frac{\partial f}{\partial x} + \frac{(-e)E(x)}{m} \frac{\partial f}{\partial v} \right] = -\frac{1}{\tau} \int dv [f(x, v) - f^{\text{l.e.}}(x, v)] . \quad (2.52)$$

The right-hand side of (2.52) vanishes and so does the second term on the left-hand side. In the first term we can commute the velocity integration and the spatial differentiation, and find $\partial/\partial x \int dv f(x, v) = dJ(x)/dx = 0$, i.e., the steady-state continuity equation. One should note that the collision term in (2.50) is not energy conserving: It represents inelastic collisions which allow the energy fed in by the electric field to be dissipated to the lattice at temperature T_0 .

Finally, the electric field $E(x)$ is determined from the Poisson equation,

$$\frac{dE(x)}{dx} = \frac{4\pi e}{\varepsilon} [N_D(x) - n(x)] , \quad (2.53)$$

where $N_D(x)$ is the doping density,

$$N_D(x) = \begin{cases} N^+ & x \in \text{contacts} \\ N^- & x \in \text{central region} \end{cases} . \quad (2.54)$$

The experimental boundary condition is provided by the applied voltage: $V_{\text{app}} = V(x_{\max}) - V(x_{\min})$, where $x_{\max, \min}$ are suitably chosen points deep in the contact regions, where the electrical field is screened to zero. The potential $V(x)$ is linked to the electric field via $V(x) = - \int^x dx' E(x')$. The task is thus to solve the coupled equations (2.50) and (2.53). We observe that the problem is nonlinear, because the electric field $E(x)$ appearing in (2.50) involves the distribution function $f(x, v)$. Before discussing the general solution of (2.50) and (2.53), it is useful to consider some simple special cases.

In the case of zero applied voltage, $V_{\text{app}} = 0$, the distribution function reduces to the local equilibrium distribution function (2.51), and the collision term in the Boltzmann equation vanishes identically. We can derive an equation for the equilibrium charge density $n^0(x)$ by multiplying (2.50) by v and integrating over v . This results in

$$\frac{k_B T_0}{m} \frac{dn^0(x)}{dx} + \frac{(-e)E(x)}{m} n^0(x) = 0, \quad (2.55)$$

which can be integrated to

$$n^0(x) = N^+ \exp \left[\frac{e}{k_B T_0} \int_{x_{\min}}^x dx' E(x') \right]. \quad (2.56)$$

This relation combined with the Poisson equation (2.53) yields a closed equation for the electric field, and hence the other quantities of interest as well. The equilibrium results are displayed as a dotted line in Fig. 2.12.

Consider next spatially uniform electric fields. The results obtained for this case should approximate the inhomogeneous case quite accurately for geometries where the N^- region is long compared to other length scales (Debye screening length $\lambda_D = \sqrt{\varepsilon k_B T_0 / (4\pi e^2 N^-)}$ or thermal mean free path $\lambda_{\text{th}} = \tau v_{\text{th}}$, $v_{\text{th}} = \sqrt{k_B T_0 / m}$). The Boltzmann equation can now be solved exactly [16]:

$$f^{\text{hom}}(v) = \frac{1}{2} \frac{n}{v_d} \exp \left[-\frac{v}{v_d} + \frac{1}{2} \left(\frac{v_{\text{th}}}{v_d} \right)^2 \right] \text{erfc} \left[\frac{1}{\sqrt{2}} \left(-\frac{v}{v_{\text{th}}} + \frac{v_{\text{th}}}{v_d} \right) \right], \quad (2.57)$$

where erfc stands for the complement of the error function, and we introduced the drift velocity $v_d = -eE\tau/m$ (note that the electric field has a negative

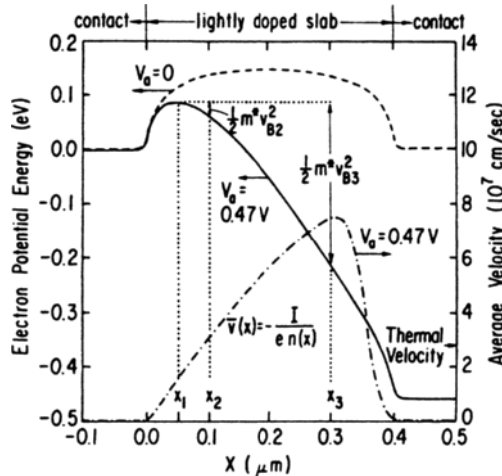


Fig. 2.12. Potential energy $U(x) = e \int dx' E(x')$ and electron velocity $v(x) = \int dv v f(x, v)$ for the $N^+N^-N^+$ -structure according to Baranger et al. [25]

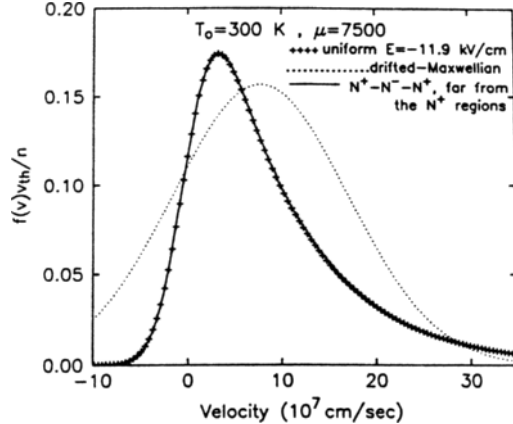


Fig. 2.13. Normalized electron velocity distribution function for a uniform field (pluses) compared to a drifted-Maxwellian distribution at the same average velocity and temperature (dotted line) and the distribution far away from the contacts for a $N^+ N^- N^+$ structure

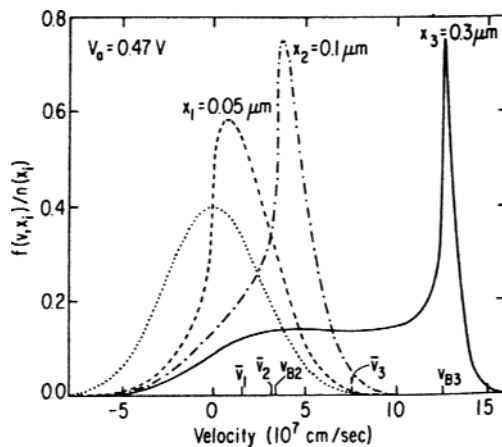


Fig. 2.14. Electron velocity distributions at the points $x = x_1, x_2, x_3$ defined in Fig. 2.12

numerical value so that the current flows from left to right). Solution (2.57) differs markedly from the drifted Maxwellian, which is an often used model for nonequilibrium distribution functions (Fig. 2.13), but agrees well with a distribution obtained from the full self-consistent solution. The results of Fig. 2.13 cast serious doubts on the applicability of drifted-Maxwellian (or drifted-Fermi) distributions to modeling of mesoscopic structures. For nonzero applied voltages the self-consistent equations (2.50) and (2.53) must be solved

numerically. It is advantageous to change variables in the Boltzmann equation from (x, v) to (x, w) , where $w = mv^2/2 + U(x)$ is the total energy:

$$v(w, x) \frac{df(x, w)}{dx} = -\frac{1}{\tau} [f(x, w) - f^{l.e.}(x, w)] . \quad (2.58)$$

w enters this equation simply as a parameter. A detailed description of the required (rather extensive) numerical work is given by Baranger [25], and we concentrate here on some representative examples. Figure 2.12 shows the calculated potential energy profile, and the local velocity, in equilibrium and at a finite applied voltage. The effect of the applied voltage is to lower and shift the effective potential energy barrier, which keeps the carriers in the highly doped contacts. Electrons with sufficiently high right moving velocities can be injected ballistically to the central region, and examples of the resulting highly non-Maxwellian distribution functions are shown in Fig. 2.14. These results once again underline the profound effects of the spatial inhomogeneity: Any attempt to model these nonequilibrium distribution functions with some effective temperatures is necessarily very crude.

3

Equilibrium Green Function Theory

Summary. The second quantization for many-body systems is introduced. Within this formalism an elementary derivation of a non-Markovian quantum kinetic equation is given for the reduced density matrix. Next we review the equilibrium Green functions, including the dissipation-fluctuation theorem, the self-energy concept, and the perturbation expansion.

3.1 Second Quantization

Equilibrium many-body theory and Green functions use a formalism called second quantization. In this formalism particles are represented by the field operators $\psi(x)$:

$$\psi(x) = \sum_k u_k(x) c_k , \quad \psi^\dagger(x) = \sum_k u_k^*(x) c_k^\dagger . \quad (3.1)$$

The operator c_k annihilates a particle in state k , and the operator c_k^\dagger creates a particle in state k , respectively. The field operators ψ and ψ^\dagger operate in the abstract occupation-number Hilbert space, since they are expressed in terms of c_k and c_k^\dagger , respectively. The system dimensionality has not yet been fixed, and for the moment we suppress the vector notation. In what follows we also suppress the spin labels; it is relatively straightforward to include them afterward [110]. The wavefunctions $u_k(x)$ form a complete set of single-particle eigenfunctions with quantum labels k . Consider now the action of the creation operator c_k^\dagger in the Fock space formed by the Hilbert spaces for all particle numbers $0, 1, 2, \dots$. For fermions the states with several particles have to be antisymmetric, and for bosons symmetric. We will limit ourselves here to Fermi systems:

$$\begin{aligned} c_k^\dagger = & |k\rangle\langle 0| + \sum_{k_1} |k, k_1\rangle_A \langle k_1| \\ & + \frac{1}{2!} \sum_{k_1, k_2} |k, k_1, k_2\rangle_A \langle k_1, k_2| + \dots \end{aligned} \quad (3.2)$$

$|0\rangle$ denotes the vacuum state with no particles. The antisymmetrical two-particle fermion state is

$$|k, k'\rangle_A = \frac{1}{\sqrt{2!}}(|1, k\rangle|2, k'\rangle - |2, k\rangle|1, k'\rangle), \quad (3.3)$$

where in the first term particle 1 is in state $|k\rangle$ and particle 2 is in state $|k'\rangle$. In general, an antisymmetric many-particle state is obtained by the following sum over all $N!$ permutations:

$$|k_1, k_2, \dots, k_N\rangle_A = \sum_{\nu=1}^{N!} \frac{(-1)^\nu}{\sqrt{N!}} P_\nu |1, k_1\rangle|2, k_2\rangle \dots |N, k_N\rangle, \quad (3.4)$$

where P_ν is the permutation operator, which generates ν successive permutations of two particles. The first term of (3.2) projects out of a given state the vacuum and replaces it by a one-particle state which occupies state k . Similarly, the second term looks for all one-particle states and replaces them by a two-particle state with the proper symmetry.

The annihilation operator c_k is the Hermitian conjugate of (3.2):

$$\begin{aligned} c_k = & |0\rangle\langle k| + \sum_{k_1} |k_1\rangle_A \langle k, k_1| \\ & + \frac{1}{2!} \sum_{k_1, k_2} |k_1, k_2\rangle_A \langle k, k_1, k_2| + \dots \end{aligned} \quad (3.5)$$

Combining (3.2) and (3.5) one gets the following product

$$\begin{aligned} c_k c_{k'}^\dagger = & |0\rangle\langle k|k'\rangle\langle 0| + \sum_{k_1, k_2} |k_1\rangle_A \langle k, k_1|k', k_2\rangle_A \langle k_2| + \dots \\ = & \delta_{kk'} |0\rangle\langle 0| + \sum_{k_1, k_2} (\delta_{k,k'} \delta_{k_1, k_2} - \delta_{k,k_2} \delta_{k_1, k'}) |k_1\rangle\langle k_2| + \dots, \end{aligned} \quad (3.6)$$

where we took into account that states with different particle numbers are orthogonal. Evaluating the sums yields

$$\begin{aligned} c_k c_{k'}^\dagger = & \delta_{k,k'} (|0\rangle\langle 0| + \sum_{k_1} |k_1\rangle\langle k_1| + \dots) - |k\rangle\langle k'| - \dots \\ = & \delta_{k,k'} - |k'\rangle\langle k| - \dots. \end{aligned} \quad (3.7)$$

Here we used the completeness relation in Fock space

$$1 = |0\rangle\langle 0| + \sum_{k_1} |k_1\rangle\langle k_1| + \frac{1}{2!} \sum_{k_1, k_2} |k_1, k_2\rangle_A \langle k_1, k_2| + \dots. \quad (3.8)$$

For the opposite order of the two operators we find

$$\begin{aligned} c_{k'}^\dagger c_k &= |k'\rangle\langle 0|0\rangle\langle k| + \sum_{k_1, k_2} |k', k_1\rangle_A \langle k_1|k_2\rangle_A \langle k, k_2| + \dots \\ &= |k'\rangle\langle k| + \sum_{k_1} |k', k_1\rangle_A \langle k, k_1| + \dots \end{aligned} \quad (3.9)$$

The sum of (3.7) and (3.9) yields

$$c_k c_{k'}^\dagger + c_{k'}^\dagger c_k = [c_k, c_{k'}^\dagger]_+ = \delta_{k, k'} . \quad (3.10)$$

This is the fermion anticommutator rule, which can also be written in the form $[a, b]_+ = \{a, b\}$. Similar analysis can be used to derive the corresponding commutator rule for bosons. Here one has to work with symmetrical many-particle states, and has to allow a multiple population of a given single particle state. We list here all resulting anticommutator and commutator relations for fermions and bosons:

$$\begin{aligned} [c_k, c_{k'}^\dagger]_\pm &= \delta_{k, k'} , \\ [c_k, c_{k'}]_\pm &= [c_k^\dagger, c_{k'}^\dagger]_\pm = 0 , \end{aligned} \quad (3.11)$$

and with (3.1) we get

$$\begin{aligned} [\psi(x), \psi^\dagger(x')]_\pm &= \delta(x - x') , \\ [\psi(x), \psi(x')]_\pm &= [\psi^\dagger(x), \psi(x')]_\pm = 0 . \end{aligned} \quad (3.12)$$

The following Hamiltonians are of interest: The single-particle Hamiltonian

$$\begin{aligned} H_0 &= \int d^3x \psi^\dagger(x) T(x) \psi(x) \\ &= \sum_k \epsilon_k c_k^\dagger c_k , \end{aligned} \quad (3.13)$$

where $T(x)$ is any one-body operator, e.g., the kinetic energy: $T(x) \rightarrow -(\hbar^2/2m)\nabla^2$, and ϵ_k is its matrix element in the basis $|k\rangle$ (in the case of plane waves, we have $\epsilon_k = \hbar^2 k^2/2m$). An interaction Hamiltonian for a two-particle interaction is of the form

$$H_{\text{int}} = \frac{1}{2} \int d^3x \int d^3x' \psi^\dagger(x) \psi^\dagger(x') V(x, x') \psi(x') \psi(x) . \quad (3.14)$$

Here, $V(x, x')$ is the interaction potential between particles. An important example is Coulomb interaction, for which $V(x-x') = e^2/|x-x'|$. We urge the

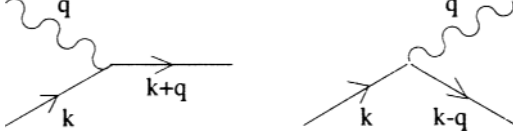


Fig. 3.1. Electron–phonon interaction. *Left:* A phonon (*wavy line*) is absorbed, while an electron (*solid line*) is scattered from state k to state $k + q$. *Right:* phonon emission

reader to work out (3.14) in the basis $|k\rangle$. Finally, electron–phonon interaction Hamiltonian is given by

$$H_{\text{el-ph}} = \sum_{q,k} M_q c_{k+q}^\dagger c_k (a_q + a_{-q}^\dagger) , \quad (3.15)$$

where M_q is the interaction matrix element. Here, c_k , c_k^\dagger are the fermion operators of the electrons, a_q , a_q^\dagger are the boson operators of the phonons, which have the free Hamiltonian $H_{\text{ph}}^0 = \sum_q \omega_q a_q^\dagger a_q$. Graphically the electron–phonon interaction is represented by a vertex (see Fig. 3.1).

3.2 Density Matrix Equations: An Elementary Derivation of a Non-Markovian Quantum Kinetic Equation

We present the derivation as a four-step procedure.

- (a) As a first application of the second quantization formalism we want to present a simple derivation of a quantum kinetic equation with a memory structure. We will use the hierarchy of density matrix equations of motion. This technique can be elaborated further and is an alternative [54,214] to the nonequilibrium Green function technique which will be used in this book. The single-particle electron density matrix of a spatially homogeneous system is defined by

$$\rho_{\mathbf{k}}(t) = \langle c_{\mathbf{k}}^\dagger(t) c_{\mathbf{k}}(t) \rangle = f_{\mathbf{k}}(t) , \quad (3.16)$$

which is nothing but the time-dependent single-particle distribution function $f_{\mathbf{k}}(t)$ in momentum space. The temporal evolution of the occupation probability is determined by the commutator of the interaction Hamiltonian $H_{\text{el-ph}}$ (3.15) with $c_{\mathbf{k}}^\dagger c_{\mathbf{k}}$ (note that H_0 commutes with $c_{\mathbf{k}}^\dagger c_{\mathbf{k}}$):

$$\begin{aligned} \frac{df_{\mathbf{k}}}{dt} &= \frac{i}{\hbar} \left\langle \left[H_{\text{el-ph}}(t), c_{\mathbf{k}}^\dagger(t) c_{\mathbf{k}}(t) \right] \right\rangle \\ &= \frac{i}{\hbar} \sum_{q,l} M_q \left\langle \left[\left(c_{l+q}^\dagger(t) c_l(t) a_q(t) + \text{h.c.} \right), c_{\mathbf{k}}^\dagger(t) c_{\mathbf{k}}(t) \right] \right\rangle . \end{aligned} \quad (3.17)$$

Working out the commutators leads to

$$\begin{aligned} \frac{df_k}{dt} = & -\frac{i}{\hbar} \sum_q M_q \langle (c_k^\dagger(t)c_{k-q}(t)a_q(t) - c_{k+q}^\dagger(t)c_k(t)a_q(t) \\ & + a_q^\dagger(t)c_k^\dagger(t)c_{k+q}(t) - a_q^\dagger(t)c_{k-q}^\dagger(t)c_k(t)) \rangle . \end{aligned} \quad (3.18)$$

- (b) As a next step, one has to evaluate the equations of motion of the expectation values of the four operator expressions in (3.18), also called the electron–phonon amplitudes, each of which consists of a product of three operators. Because these operators do not commute with the free Hamiltonian H_0 for the electrons and phonons, also this part of H has to be used. Consider, e.g., the first term on the right-hand side of (3.18):

$$\begin{aligned} \frac{d}{dt} \langle c_k^\dagger(t)c_{k-q}(t)a_q(t) \rangle = & i(\epsilon_k - \epsilon_{|k-q|} - \omega_q) \langle c_k^\dagger(t)c_{k-q}(t)a_q(t) \rangle \\ & - \frac{i}{\hbar} \sum_{p,l} M_p \langle [c_k^\dagger(t)c_{k-q}(t)a_q(t), a_p^\dagger(t)c_l^\dagger(t)c_{l+p}(t)] \rangle , \end{aligned} \quad (3.19)$$

where ϵ_k/\hbar and ω_q are the frequencies of the free electrons and phonons, respectively. As a rather simple approximation, we break the hierarchy at this level by factorizing the expectation values of the products of six operators into three single-particle density matrices of the electrons and phonons. Thus, a typical term is treated as

$$\begin{aligned} & \langle c_k^\dagger(t)c_{k-q}(t)a_q(t)a_p^\dagger(t)c_l^\dagger(t)c_{l+p} \rangle \\ & \simeq \langle a_q(t)a_p^\dagger(t) \rangle \langle c_k^\dagger(t)c_{k-q}(t)c_l^\dagger(t)c_{l+p} \rangle \\ & \simeq \delta_{q,p} (1 + g_q(t)) \delta_{k,l+p} f_k(t) \delta_{k-q,l} (1 - f_{k-q}(t)) . \end{aligned} \quad (3.20)$$

Here $g_q(t) = \langle a_q^\dagger(t)a_q(t) \rangle$ is the phonon distribution function which obeys its own kinetic equation. Note that only one of the two possible pairings in the electronic part leads to a nonzero contribution. For simplicity we assume here that the phonons can be treated as a thermal bath. Treating the other term in (3.19) similarly and performing a formal integration yields

$$\begin{aligned} \langle c_k^\dagger(t)c_{k-q}(t)a_q(t) \rangle = & \frac{i}{\hbar} M_q \int_0^t dt' e^{i(\epsilon_k - \epsilon_{|k-q|} - \omega_q)(t-t')} \\ & \times [f_k(t')(1 - f_{k-q}(t'))(1 + g_q(t')) \\ & - (1 - f_k(t'))f_{k-q}(t')g_q(t')] . \end{aligned} \quad (3.21)$$

Inserting the result (3.21), and the corresponding expressions for the three other three-particle correlation functions in (3.18) yields

$$\begin{aligned} \frac{df_k}{dt} = & -\frac{2}{\hbar^2} \sum_q \int_0^t dt' M_q^2 \{ \cos((\epsilon_k - \epsilon_{|k-q|} - \omega_q)(t - t')) \\ & \times [(f_k(t')(1 - f_{k-q}(t'))(1 + g_q(t')) \\ & - (1 - f_k(t'))f_{k-q}(t')g_q(t'))] \} - \{ k \rightarrow k + q \} . \end{aligned} \quad (3.22)$$

We have used the fact that in the first and the fourth term in (3.18) the creation and annihilation operators are exchanged, so that the initial and final states in the scattering process are also exchanged: $g_q(t') \leftrightarrow (1 + g_q(t'))$ and $f_{\mathbf{k}}(t) \leftrightarrow (1 - f_{\mathbf{k}}(t'))$. The same relationship exists between the terms two and three. Finally, one gets the second term from the first one, if one replaces the vector \mathbf{k} by $\mathbf{k} + \mathbf{q}$.

- (c) The result (3.22) is the quantum kinetic equation for the scattering of electrons through the interaction with phonons. The main difference in comparison with the semiclassical Boltzmann equation is that (3.22) contains no longer the energy conservation for the individual scattering processes, which cannot hold for short times due to the energy-time uncertainty relation. Thus the quantum kinetic equation extends the validity of the theory to the ultrashort time regime with time intervals shorter or comparable to characteristic inverse frequencies of the system. In comparison with the Boltzmann equation (1.5) one recognizes easily again the same population factors for the initial and final states of the scattering processes. However, in contrast to the Boltzmann equation all occupation function in the scattering integrals of (3.22) enter at the earlier time t' . Thus the quantum kinetic equation (3.22) contains in contrast to the semiclassical Boltzmann equation memory effects. One has to integrate over the past of the system. Instead of the energy conservation for the individual collisions, one gets the energy difference between the states before and after the collision as frequencies in the cosine function. These oscillating functions which depend on the time difference of the present time t and the remote time t' determine the integral kernel of the convolution integral and thus memory depth. The semiclassical Boltzmann equation is local in time, such equations are called Markov equations. The quantum kinetic equation (3.22) is a non-Markovian equation. The oscillating terms in (3.22) stem from the quantum mechanical wave nature of the particles. The coherence of the quantum mechanical waves decays due to the various interaction mechanisms, thus one can expect in a higher approximation next to the oscillating term a damping term of the form $\exp[-(\gamma_{\mathbf{k}} + \gamma_{\mathbf{k}-\mathbf{q}})(t - t')]$. This intuitive result can indeed be obtained in a simple approximation for the nonequilibrium Green functions. The damping constant $\gamma_{\mathbf{k}}$ – called collision damping – is also caused by the considered collisions. A more detailed discussion of a consistent description of the coherence decay will be discussed in several later chapters.
- (d) Finally we will discuss the connection between the quantum kinetic equation (3.22) and the semiclassical Boltzmann equation in the long-time limit. For a sufficiently short memory depth one can pull out of the integral the distribution functions at their value on the upper boundary, i.e., at time t . The remaining integral has the structure

$$2 \int_0^t dt' \cos(\Delta\omega(t - t')) e^{-\Gamma(t-t')} = \frac{1 - e^{(i\Delta\omega - \Gamma)t}}{-i\Delta\omega + \Gamma} + \frac{1 - e^{(-i\Delta\omega - \Gamma)t}}{i\Delta\omega + \Gamma}. \quad (3.23)$$

For $\Gamma t \gg 1$

$$2 \int_0^t dt' \cos(\Delta\omega(t-t')) e^{-\Gamma(t-t')} = \frac{2\Gamma}{(\Delta\omega)^2 + \Gamma^2} \rightarrow 2\pi\delta(\Delta\omega), \quad (3.24)$$

i.e., instead of an exact energy conservation one gets in the long-time limit of an exponentially decaying memory kernel a Lorentzian resonance curve which reduces only in the limit $\Gamma \rightarrow 0$ to the delta function. A broadened resonance however does not result in a stable long-time kinetics in which the particles would reach their thermal equilibrium value. This shows that a simple exponential damping does not result in a correct kinetics. In the long-term limit the damping should not be in conflict with the energy conservation [214].

On the other hand also for the case $\Gamma = 0$ formula (3.23) yields asymptotically a delta function:

$$\frac{1 - e^{i\Delta\omega t}}{i\Delta\omega} - \frac{1 - e^{-i\Delta\omega t}}{i\Delta\omega} = \frac{2\sin(\Delta\omega t)}{\Delta\omega} \rightarrow 2\pi\delta(\Delta\omega). \quad (3.25)$$

In this case however, the justification to pull the distribution functions out of the integral is missing. This discussion shows that it is not an easy task to connect the short-time quantum kinetics with the long-time Boltzmann kinetics.

3.3 Green Functions

In classical physics Green functions are used as a powerful method for solving inhomogeneous differential equations. There, the Green functions obey the differential equation with a singular inhomogeneity, i.e., a delta function in the variable(s). Similarly, one can introduce in many-body physics Green functions which, because of their construction, obey a wave equation with a singular inhomogeneity. These Green functions turn out to provide a very powerful technique for evaluating properties of many-body systems in both thermal equilibrium and nonequilibrium situations, which are the central topic of this book. As an introduction, we describe first the equilibrium Green functions. Our introduction has the nature of a summary, and the reader may find it useful to supplement it with a look at any of the standard textbooks on the topic (there are many excellent treatises available such as [2, 96, 105, 110, 251, 254]).

In equilibrium one needs in principle only one Green function, but even here it is advantageous to introduce various Green functions, which, however, can be expressed in terms of each other. We start by defining a time-ordered (also called causal) zero-temperature single-particle Green function

$$G(x, t; x', t') = \frac{-i}{\hbar} \frac{\langle \Psi_0 | T\{\psi_H(x, t)\psi_H^\dagger(x', t')\} | \Psi_0 \rangle}{\langle \Psi_0 | \Psi_0 \rangle}. \quad (3.26)$$

Here, $H|\Psi_0\rangle = E_0|\Psi_0\rangle$ is the ground state of the interacting system, $T\{\dots\}$ is the time-ordering operator: It always moves the operator with the earlier time argument to the right (or, equivalently, the mnemonic rule: late goes to left):

$$T\{A(t)B(t')\} = \theta(t-t')A(t)B(t') \mp \theta(t'-t)B(t')A(t), \quad (3.27)$$

where the upper sign refers again to fermions. This negative sign occurs because in the second term the two fermion operators have been interchanged by the time-ordering operator. The operators $\psi_H(x, t)$ are time dependent, i.e., they are in the Heisenberg picture, and evolve according to $\dot{\psi}_H(t) = i\hbar^{-1}\partial\psi_H/\partial t = i\hbar^{-1}\partial\psi_H/\partial t|_{t=0}e^{iHt/\hbar}\psi(t=0)e^{-iHt/\hbar}$.

If one differentiates the Green function (3.26) with respect to the time t one finds using (3.27), and recalling $\partial\theta(t-t')/\partial t = \delta(t-t')$ and $\partial\theta(t'-t)/\partial t = -\delta(t-t')$ the following equation of motion

$$\begin{aligned} i\hbar \frac{\partial G(x, t; x', t')}{\partial t} &= \delta(t-t') \frac{\langle \Psi_0 | [\psi_H(x, t), \psi_H^\dagger(x', t')]_\pm | \Psi_0 \rangle}{\langle \Psi_0 | \Psi_0 \rangle} \\ &\quad - \frac{i}{\hbar} \frac{\langle \Psi_0 | T\{i\hbar \frac{\partial \psi_H(x, t)}{\partial t} \psi_H^\dagger(x', t')\} | \Psi_0 \rangle}{\langle \Psi_0 | \Psi_0 \rangle}. \end{aligned} \quad (3.28)$$

Recalling (3.12) the first term in (3.28) is just a delta function in the spatial coordinates, i.e., we rediscover the singular inhomogeneous term in the differential equation which is generic for any Green function.

As an example consider free particles, for which the Heisenberg equation of motion is [$H = -\hbar^2/(2m) \int dx \psi^\dagger(x) \nabla^2 \psi(x)$]:

$$i\hbar \frac{\partial \psi_H(x, t)}{\partial t} = [\psi_H(x, t), H] = -\frac{\hbar^2 \nabla_x^2}{2m} \psi_H(x, t). \quad (3.29)$$

so that the differential equation for the free-particle Green function G_0 becomes the inhomogeneous Schrödinger equation:

$$\left(i\hbar \frac{\partial}{\partial t} + \frac{\hbar^2 \nabla_x^2}{2m} \right) G_0(x, t; x', t') = \hbar \delta(t-t') \delta(x-x'). \quad (3.30)$$

The definition of the Green function can be generalized to describe an equilibrium system at a finite temperature:

$$G(x, t; x', t') = \frac{-i}{\hbar} \text{Tr} \left\{ \varrho T \psi_H(x, t) \psi_H^\dagger(x', t') \right\}. \quad (3.31)$$

Here ϱ is the density matrix operator and the trace Tr is the sum over all diagonal elements of a complete set. One can also define in an analogous fashion two- and many-particle Green functions.

With all these abstract definitions, we must be prepared for a question from the student.

“What are the *physical* reasons for studying such an object?” There are (at least) two answers to this question:

- Experimentally relevant quantities can be extracted from the knowledge of the Green function.
- The definition (3.26) allows the construction of a systematic perturbation theory.

We elaborate upon these answers next.

3.3.1 Examples of Measurable Quantities

The particle density is given by $\langle n(x) \rangle = \langle \psi^\dagger(x)\psi(x) \rangle$. But this object is directly related to the Green function

$$\langle n(x) \rangle = -i\hbar G(x, t; x, t^+) , \quad (3.32)$$

where $t^+ = \lim_{\varepsilon \rightarrow 0} (t + \varepsilon)$ is infinitesimally larger than t , in order to get the correct time ordering. Consider next the expectation values for the kinetic energy and the total energy, respectively, which can be written as [110]

$$\langle T \rangle = -i\hbar \int d^3x \lim_{x' \rightarrow x} \frac{-\hbar^2 \nabla_x^2}{2m} G(x, t; x', t^+) , \quad (3.33)$$

$$\begin{aligned} E = \langle H \rangle &= -\frac{i}{2}\hbar \int d^3x \lim_{t' \rightarrow t^+} \lim_{x' \rightarrow x} \left(i\hbar \frac{\partial}{\partial t} - \frac{\hbar^2 \nabla^2}{2m} \right) G(x, t; x', t') \\ &= -\frac{i}{2}\hbar V \int \frac{d^3k}{(2\pi)^3} \int \frac{d\omega}{2\pi} e^{i\omega\epsilon} \left(\frac{\hbar^2 k^2}{2m} + \hbar\omega \right) G(k, \omega) . \end{aligned} \quad (3.34)$$

Note that in equilibrium, and for uniform systems Green functions depend only on differences of variables, $G(x, t; x', t') = G(x - x', t - t')$, and it is advantageous to work in Fourier space

$$G(k, \omega) = \int d^3x \int dt e^{i\omega(t-t')} e^{-ik \cdot (x-x')} G(x - x', t - t') . \quad (3.35)$$

From this on, we drop the \pm sign for Fermi or Bose particles, and work exclusively with fermions. For the fermion anticommutator we use the notation $[a, b]_+ = \{a, b\}$. Furthermore, to lighten the notation we set $\hbar = 1$. Naturally, in the final physical results one has to reintroduce Planck's constant, and we shall occasionally do so in chapters to follow.

For future use we also define retarded, advanced, and the “lesser than” (or just “lesser”) and “greater than” (or just “greater”) Green functions:

$$G^r(x, t; x', t') = -i\theta(t - t') \langle \{ \psi(x, t), \psi^\dagger(x', t') \} \rangle , \quad (3.36a)$$

$$G^a(x, t; x', t') = i\theta(t' - t) \langle \{ \psi(x, t), \psi^\dagger(x', t') \} \rangle , \quad (3.36b)$$

$$G^<(x, t; x', t') = i \langle \psi^\dagger(x', t') \psi(x, t) \rangle , \quad (3.36c)$$

$$G^>(x, t; x', t') = -i \langle \psi(x, t) \psi^\dagger(x', t') \rangle . \quad (3.36d)$$

The retarded Green function G^r differs from zero only for times $t \geq t'$, thus this function can be used to calculate the response at time t to an earlier perturbation of the system at time t' . The advanced Green function G^a is only finite for $t \leq t'$. Due to the (anti)commutator structure, these two functions again obey an inhomogeneous differential equation as the originally defined time-ordered Green function. The “lesser than” Green function is also called the particle propagator, while the “greater than” Green function, in which the order of the creation and annihilation operators are reversed, is called the hole propagator. Importantly, their differential equations do not have the singular inhomogeneous terms. This observation is the precursor of a more fundamental difference between the lesser/greater and retarded/advanced functions; this difference will be accentuated under nonequilibrium conditions. These various functions are not independent: they obey

$$G^r - G^a = G^> - G^<. \quad (3.37)$$

In (3.36a)–(3.36d) we have also simplified the notation: We dropped normalization factor $\langle \Psi_0 | \Psi_0 \rangle$,¹ and do not explicitly specify the Heisenberg representation. In equilibrium all four Green functions (3.36a)–(3.36d) can be expressed, e.g., in terms of the time-ordered Green function (Sect. 3.3). However, in nonequilibrium situations all functions become very important. We note that the time-ordered, the retarded, and the advanced Green functions can be expressed in terms of $G^>$ and $G^<$:

$$\begin{aligned} G(x, t; x', t') &= \theta(t - t')G^>(x, t; x', t') + \theta(t' - t)G^<(x, t; x', t'), \\ G^{r,a}(x, t; x', t') &= \pm\theta(\pm t \mp t')[G^>(x, t; x', t') - G^<(x, t; x', t')]. \end{aligned} \quad (3.38)$$

The observables can also be expressed in terms of $G^{>,<}$; for example

$$\langle n(x) \rangle = -iG^<(x, t; x, t). \quad (3.39)$$

Since all Green functions can be expressed in terms of each other, one may wonder, why does one take the trouble to introduce all these different Green functions? The answer is that each one of them has its own advantages:

- $G(x, t; x', t')$ has a systematic perturbation theory.
- $G^{r,a}(x, t; x', t')$ have a nice analytic structure (poles in one half-plane) and are well suited for calculating a physical response. Information about spectral properties, densities of states, and scattering rates is contained in $G^{r,a}(x, t; x', t')$.
- $G^{<,>}(x, t; x', t')$ are directly linked to observables and kinetic properties, such as particle densities or currents.

One of the most important properties of equilibrium theory is that all four functions $G, G^{r,a}, G^{>,<}$ are linked via the fluctuation–dissipation theorem. We will prove this theorem next.

¹ Strictly speaking, this is justified only in Sect. 3.5, where we discuss the interaction picture and the perturbation expansion for the Green function.

3.4 Fluctuation–Dissipation Theorem

In many applications one needs the spectral function, defined as

$$A(k, \omega) = i[G^r(k, \omega) - G^a(k, \omega)] = i[G^>(k, \omega) - G^<(k, \omega)]. \quad (3.40)$$

This function has the property

$$\begin{aligned} \int_{-\infty}^{+\infty} \frac{d\omega}{2\pi} A(k, \omega) &= \int d^3(x - x') e^{-ik(x-x')} \langle \{\psi(x, t), \psi^\dagger(x', t)\} \rangle \\ &= 1, \end{aligned} \quad (3.41)$$

because of the equal-time anticommutation rule. Furthermore, the density of states is conveniently computed with the spectral function $A(k, \omega)$:

$$\varrho(\omega) = \frac{1}{2\pi} \int \frac{d^3k}{(2\pi)^3} A(k, \omega). \quad (3.42)$$

The version of fluctuation–dissipation theorem that we need links the spectral function $A(k, \omega)$ to the particle propagator $G^<(k, \omega)$ (and hence also to $G(k, \omega)$ and $G^>(k, \omega)$). The proof is a direct calculation using the complete eigenstates of H and N . Of course these states are not explicitly known for an interacting many-body system, and hence we can use them only in formal derivations, but not in concrete calculations. In the following manipulations the wavevector argument k is not important and we suppress it. Inserting the set of complete states allows one to write

$$\begin{aligned} G^<(\omega) &= i \int_{-\infty}^{+\infty} dt e^{i\omega t} \langle \psi^\dagger(0) \psi(t) \rangle \\ &= i \int dt e^{i\omega t} \sum_{n,m} \langle n | \varrho \psi^\dagger(0) | m \rangle \langle m | e^{iHt} \psi(0) e^{-iHt} | n \rangle. \end{aligned} \quad (3.43)$$

We work here at a finite temperature T , because no extra effort is required. We use the density matrix for a grand-canonical ensemble

$$\varrho = e^{-\beta(H-\mu N)} / Z \quad (3.44)$$

with the partition function

$$Z = \text{Tr } e^{-\beta(H-\mu N)} = e^{-\beta\Omega}, \quad (3.45)$$

where $\beta = (k_B T)^{-1}$, μ is the chemical potential, N is the number operator, and Ω is the grand-canonical thermodynamic potential. Since the states $|m\rangle$ are eigenstates of both H and N , we can proceed as

$$\begin{aligned} G^<(\omega) &= \frac{i}{Z} \int dt e^{i\omega t} \sum_{n,m} e^{-\beta(E_n - \mu N_n)} e^{i(E_m - E_n)t} \langle n | \psi^\dagger(0) | m \rangle \langle m | \psi(0) | n \rangle \\ &= \frac{i}{Z} \sum_{n,m} 2\pi\delta(\omega + E_m - E_n) e^{-\beta(E_n - \mu N_n)} \langle n | \psi^\dagger(0) | m \rangle \langle m | \psi(0) | n \rangle. \end{aligned} \quad (3.46)$$

Note that state $|n\rangle$ contains one more particle than state $|m\rangle$, i.e., $N_n - N_m = 1$. Similarly,

$$\begin{aligned} G^>(\omega) &= -i \int dt e^{i\omega t} \langle \psi(t) \psi^\dagger(0) \rangle \\ &= -\frac{i}{Z} \int dt e^{i\omega t} \sum_{n,m} \langle n | \varrho e^{iHt} \psi(0) e^{-iHt} | m \rangle \langle m | \psi^\dagger(0) | n \rangle \\ &= -\frac{i}{Z} \sum_{n,m} 2\pi\delta(\omega + E_n - E_m) e^{-\beta(E_n - \mu N_n)} \langle n | \psi(0) | m \rangle \langle m | \psi^\dagger(0) | n \rangle. \end{aligned} \quad (3.47)$$

Comparing these two expressions for $G^<$ and $G^>$ we see that interchanging n and m in the summation brings them into close agreement. The only difference is in the thermal weight factor: $G^<$ has $\exp[-\beta(E_n - \mu N_n)]$, while $G^>$ has $\exp[-\beta(E_m - \mu N_m)]$. The delta-function allows us to substitute $E_m = E_n - \omega$, and we already know that $N_m = N_n - 1$. We thus obtain

$$G^>(\omega) = -e^{\beta(\omega-\mu)} G^<(\omega). \quad (3.48)$$

With (3.40) we can express the spectral density as

$$A(k, \omega) = -i(e^{\beta(\omega-\mu)} + 1) G^<(k, \omega) \quad (3.49)$$

or

$$G^<(k, \omega) = if(\omega) A(k, \omega), \quad (3.50)$$

where

$$f(\omega) = \frac{1}{e^{\beta(\omega-\mu)} + 1}. \quad (3.51)$$

Equation (3.50) is an extremely useful relation, which will be used several times later on. Its form also explains the name “fluctuation–dissipation” theorem: (3.50) tells us that the correlation function $G^<$ (which also carries information about fluctuations) is proportional to the dissipative part A ;² the proportionality factor is the Fermi function.

If the spectral function is a sharply peaked function, which is the case, for example, for noninteracting systems, $A(k, \omega) = 2\pi\delta(\varepsilon_k - \omega)$, one can replace the energy argument in the Fermi function by the single-particle energy ε_k . Even in the case of a weakly interacting system the spectral function may be peaked³ and progress can be made by the substitution $\omega \rightarrow e_k$. This replacement amounts to what is known as the “quasi-particle approximation.” Equation (3.50) has a companion relation:

² A is essentially the imaginary part of the retarded Green function, and it determines the decay in time domain, and, hence, also the dissipation.

³ The maximum of A may be shifted due to interactions, $\varepsilon_k \rightarrow e_k$, where e_k is the “renormalized energy,” and the peak may not carry the same weight as in the noninteracting case (“wavefunction renormalization”).

$$G^>(k, \omega) = -i[1 - f(\omega)]A(k, \omega). \quad (3.52)$$

The hole propagator is proportional to the probability of finding a hole, i.e., an unoccupied state times the spectral function.

The fluctuation–dissipation theorem is often expressed in an alternative form as a relation between the causal Green function and the spectral function. Using the integral representation of the Heaviside step function,

$$\theta(t) = \int \frac{d\omega}{2\pi i} \frac{e^{i\omega t}}{\omega - i\eta},$$

we get

$$\begin{aligned} G(\omega) &= \int dt e^{i\omega t} [\theta(t)G^>(t) + \theta(-t)G^<(t)] \\ &= \int \frac{d\omega_1}{2\pi} \int \frac{d\omega_2}{2\pi i} \int dt e^{i\omega t} \left[G^>(\omega_1) \frac{e^{-i(\omega_1 - \omega_2)t}}{\omega_2 - i\eta} + G^<(\omega_1) \frac{e^{-i(\omega_1 + \omega_2)t}}{\omega_2 - i\eta} \right] \\ &= \int \frac{d\omega_1}{2\pi i} \left[\frac{G^>(\omega_1)}{\omega_1 - \omega - i\eta} + \frac{G^<(\omega_1)}{\omega - \omega_1 - i\eta} \right] \\ &= \int \frac{d\omega_1}{2\pi} A(k, \omega_1) \left[\frac{f(\omega_1)}{\omega - \omega_1 - i\eta} - \frac{1 - f(\omega_1)}{\omega_1 - \omega - i\eta} \right], \end{aligned} \quad (3.53)$$

from which we identify

$$\begin{aligned} \text{Re } G(k, \omega) &= -\mathcal{P} \int \frac{d\omega_1}{2\pi} \frac{A(k, \omega_1)}{\omega_1 - \omega}, \\ \text{Im } G(k, \omega) &= -\frac{1}{2} \tanh \left[\frac{\beta(\omega - \mu)}{2} \right] A(k, \omega) \\ &= \tanh \left[\frac{\beta(\omega - \mu)}{2} \right] \text{Im} G^r(k, \omega). \end{aligned} \quad (3.54)$$

Here \mathcal{P} stands for the principal part. Similar relations can be derived for bosonic functions, and the reader is urged to carry out this calculation as an exercise.

3.5 Perturbation Expansion of the Green Function

Let us start by recalling the various representation pictures of quantum mechanics:

- *Schrödinger picture.* The wavefunctions are time-dependent: $i\frac{\partial}{\partial t}\psi(t) = H\psi(t)$; the operators are constant.
- *Heisenberg picture.* The wavefunctions are constant; the operators are time-dependent $\mathcal{O}(t) = e^{iHt}\mathcal{O}(0)e^{-iHt}$.

- *Interaction picture*. The wavefunctions develop under the influence of the “difficult” interaction part of the Hamiltonian $H = H_0 + V$: $\hat{\psi}(t) = e^{iH_0 t} e^{-iHt} \psi(0)$. The operators develop under the influence of the “easy” noninteracting Hamiltonian H_0 only: $\hat{O}(t) = e^{iH_0 t} \hat{O}(0) e^{-iH_0 t}$.⁴

The time development of the interaction picture is often expressed in terms of a U operator (or matrix):

$$\hat{\psi}(t) = U(t)\psi(0), \quad U(t) = e^{iH_0 t} e^{-iHt}. \quad (3.55)$$

We next introduce the S -matrix, which changes the wavefunction from $\hat{\psi}(t')$ to $\hat{\psi}(t)$:

$$\hat{\psi}(t) = S(t, t')\hat{\psi}(t'). \quad (3.56)$$

Thus,

$$S(t, t') = U(t)U^\dagger(t'). \quad (3.57)$$

The S -matrix obeys the group property $S(t, t') = S(t, t'')S(t'', t')$. Furthermore, the S -matrix can be expressed as a time-ordered product (for a derivation based on the equation of motion for S), see [251, 254]:

$$S(t, t') = T \exp \left\{ -i \int_{t'}^t dt_1 \hat{V}(t_1) \right\}. \quad (3.58)$$

Our definition for the Green function contains a problem: It involves the exact ground state of the system. But this is one of the things we want to compute with the Green function! To make any progress, we must express the exact ground state $|\Psi_0\rangle$ in terms of quantities we know, for example the noninteracting ground state $|\Phi_0\rangle$. This connection is formed by the Gell-Mann and Low theorem:

$$|\Psi_0\rangle = S(0, -\infty)|\Phi_0\rangle, \quad (3.59)$$

The proof for this relation is rather subtle (see [110], pp. 61–64) and we do not reproduce it here. In analogy with (3.59), we have

$$\langle\Psi_0| = \langle\Phi_0|S(\infty, 0). \quad (3.60)$$

The object $\langle\Phi_0|S(\infty, 0)S(0, -\infty)|\Phi_0\rangle$ may have an ill-defined phase, this is, however, canceled by a similar phase factor arising from the numerator of the definition of the time-ordered Green function:

$$G(x, t; x', t') = -i \frac{\langle\Phi_0|T\{S(\infty, -\infty)\hat{\psi}(x, t)\hat{\psi}^\dagger(x', t')\}|\Phi_0\rangle}{\langle\Phi_0|S(\infty, -\infty)|\Phi_0\rangle}. \quad (3.61)$$

This important result generates the systematic perturbation scheme for the Green function. The calculation proceeds by expanding the S -matrix (both in the numerator and in the denominator) in $\hat{V}(t)$:

⁴ In what follows we distinguish wavefunctions and operators in the interaction picture with a caret.

$$S(\infty, -\infty) = \sum_{n=0}^{\infty} \frac{(-i)^{n+1}}{n!} \int_{-\infty}^{+\infty} dt_1 \cdots dt_n T\{\hat{V}(t_1) \cdots \hat{V}(t_n)\}, \quad (3.62)$$

Since each \hat{V} contains three or four field operators (3.14) and (3.5), we need a device for evaluating expectation values such as

$$\langle \Phi_0 | T\{\hat{\psi}(t)\hat{\psi}^\dagger(t')\hat{\psi}^\dagger(t_1)\hat{\psi}^\dagger(t_2)\hat{\psi}(t_2)\hat{\psi}(t_1)\} | \Phi_0 \rangle \quad (3.63)$$

and higher order similar terms. These expressions are evaluated with Wick's theorem, which states that the result of (3.63) is the sum of all pairwise contractions. Thus (3.63) gives rise to six terms: for example, $\hat{\psi}(t)$ can be paired with $\hat{\psi}^\dagger(t')$, and the remaining four operators can be paired in two different ways. Thus one gets $3 \times 2 = 6$ terms. These terms are most easily expressed in terms of Feynman diagrams. The six diagrams resulting from (3.63) are shown in Fig. 3.2.

The six diagrams have quite distinct properties. (a) and (b) are disconnected diagrams. These are exactly canceled by the denominator in (3.63). This is good because disconnected diagrams often diverge! Terms (c) and (e) are equal, likewise (d) and (f). After some combinatorics, one finds that

$$G(x, t; x', t') = -i \sum_{n=0}^{\infty} (-i)^n \int_{-\infty}^{+\infty} dt_1 \cdots dt_n \times \langle \Phi_0 | T\hat{\psi}(x, t)\hat{\psi}^\dagger(x', t')\hat{V}(t_1) \cdots \hat{V}(t_n) | \Phi_0 \rangle_{\text{conn}}, \quad (3.64)$$

where the summation only includes topologically different connected diagrams. Equation (3.64) is the desired perturbation expansion for the Green function, and it forms the starting point for many calculations.

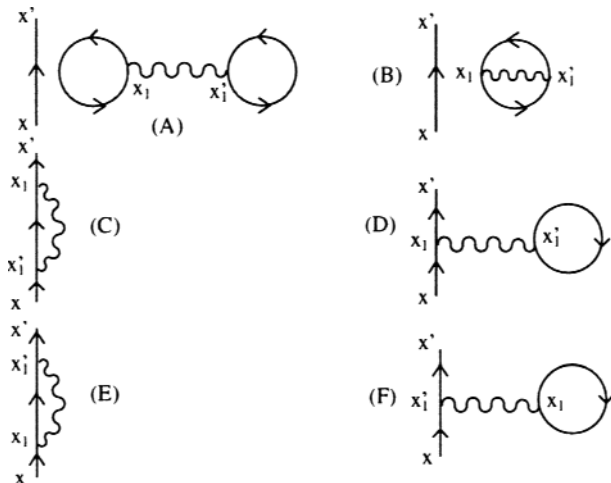


Fig. 3.2. The diagrams generated by (3.63)

3.6 Examples of Simple Solvable Models

We will give two examples of important exactly solvable models.

3.6.1 Free-Particle Green Function

Now we have $H_0 = \sum_p \varepsilon_p a_p^\dagger a_p$, and we call the free Green function as G_0 : $G_0(p, t) = -i\langle T\{a_p(t)a_p^\dagger(t')\}\rangle$. We can work out the time dependence explicitly:

$$\begin{aligned} i\dot{a}_p &= [a_p, H_0] = \sum_{p'} \varepsilon_{p'} [a_p, a_{p'}^\dagger a_{p'}] \\ &= \sum_{p'} \varepsilon_{p'} (a_p a_{p'}^\dagger a_{p'} - a_{p'}^\dagger a_{p'} a_p) = \sum_{p'} \varepsilon_{p'} (a_p a_{p'}^\dagger a_{p'} + a_{p'}^\dagger a_p a_{p'}) \\ &= \sum_{p'} \varepsilon_{p'} [(a_p a_{p'}^\dagger + (\delta_{p',p} - a_p a_{p'}^\dagger)) a_{p'}] = \varepsilon_p a_p , \end{aligned} \quad (3.65)$$

which can be integrated to

$$a_p(t) = e^{-i\varepsilon_p t} a_p(0) . \quad (3.66)$$

We thus obtain

$$G_0(p, t) = e^{-i\varepsilon_p(t-t')} (-i) [\theta(t-t') \langle a_p a_p^\dagger \rangle - \theta(t'-t) \langle a_p^\dagger a_p \rangle] , \quad (3.67)$$

or, in Fourier space,

$$\begin{aligned} G_0(p, \omega) &= -i \int_0^\infty d\tau e^{i(\omega-\varepsilon_p+i\eta)\tau} (1 - f_p) - \int_{-\infty}^0 d\tau e^{i(\omega-\varepsilon_p-i\eta)\tau} f_p \\ &= \frac{1-f_p}{\omega-\varepsilon_p+i\eta} + \frac{f_p}{\omega-\varepsilon_p-i\eta} . \end{aligned} \quad (3.68)$$

The free Green function is the basic building block for the perturbation series, and it will make frequent appearances in the subsequent development.

3.6.2 Resonant-Level Model

Consider the following Hamiltonian:

$$H = \sum_p \varepsilon_p a_p^\dagger a_p + \varepsilon_0 b^\dagger b + \sum_p V_p (a_p^\dagger b + b^\dagger a_p) . \quad (3.69)$$

This Hamiltonian describes a continuum of states (the a -operators) interacting with a discrete state (the b -operator). Physical realizations of this Hamiltonian include an impurity state interacting with conduction electrons, or a tunneling system, where electrons from a “contact” region are coupled to a state

in a quantum well. It is also closely related to the Fano model [108] which describes the line shape of an optical absorption spectrum in the presence of two interfering transition mechanisms. The evaluation of the Green function proceeds with the equation-of-motion technique. Just for fun, let us analyze the retarded Green function, $G^r(p, p', t) \equiv -i\theta(t - 0)\langle\{a_p(t), a_{p'}^\dagger(0)\}\rangle$:

$$i\frac{\partial}{\partial t}G^r(p, p', t) = \delta(t - 0)\delta_{p,p'} - i\theta(t - 0)\langle\{[a_p, H](t), a_{p'}^\dagger(0)\}\rangle. \quad (3.70)$$

The commutator in the second term is

$$[a_p, H] = \varepsilon_p a_p + V_p b. \quad (3.71)$$

The equation of motion thus involves a new Green function:

$$i\frac{\partial}{\partial t}G^r(p, p', t) = \delta(t)\delta_{p,p'} + \varepsilon_p G^r(p, p', t) + V_p \Gamma(p', t), \quad (3.72)$$

where

$$\Gamma(p', t) = -i\theta(t - 0)\langle\{b(t), a_{p'}^\dagger(0)\}\rangle. \quad (3.73)$$

This function obeys

$$i\frac{\partial}{\partial t}\Gamma(p', t) = \varepsilon_0 \Gamma(p', t) + \sum_{p''} V_{p''} G^r(p'', p', t). \quad (3.74)$$

It is useful to introduce the resonant-level free Green function $g_0(t)$, which obeys $(i\frac{\partial}{\partial t} - \varepsilon_0)g_0(t) = \delta(t)$. In terms of $g_0(t)$ (3.74) reads

$$\Gamma(p', t) = \int dt_1 g_0(t - t_1) \sum_{p''} V_{p''} G^r(p'', p', t_1). \quad (3.75)$$

In ω -space the coupled equations for G^r and Γ are

$$\begin{aligned} G^r(p, p', \omega) &= \delta_{p,p'} G_0^r(p, \omega) + G_0^r(p, \omega) V_p \Gamma(p', \omega), \\ \Gamma(p', \omega) &= g_0^r(\omega) \sum_{p''} V_{p''} G^r(p'', p', \omega), \end{aligned} \quad (3.76)$$

where the free Green functions are given by $G_0^r(p, \omega) = [\omega - \varepsilon_p + i\eta]^{-1}$ and $g_0^r(\omega) = [\omega - \varepsilon_0 + i\eta]^{-1}$, respectively. Multiplying the first equation with V_p and summing over p gives

$$\begin{aligned} \sum_p V_p G^r(p, p', \omega) &= \frac{\Gamma(p', \omega)}{g_0^r(\omega)} \\ &= V_{p'} G_0^r(p', \omega) + \sum_p V_p^2 G_0^r(p, \omega) \Gamma(p', \omega) \end{aligned} \quad (3.77)$$

or

$$\Gamma(p', \omega) = \frac{V_{p'} G_0^r(p', \omega)}{g_0^r(\omega)^{-1} - \sum_p V_p^2 G_0^r(p, \omega)} \quad (3.78)$$

and, finally,

$$\begin{aligned} G^r(p, p', \omega) &= G_0^r(p, \omega) \delta_{p,p'} \\ &+ G_0^r(p, \omega) \frac{V_p V_{p'}}{g_0^r(\omega)^{-1} - \sum_p V_p^2 G_0^r(p, \omega)} G_0^r(p', \omega) \\ &= G_0^r(p, \omega) \delta_{p,p'} + G_0^r(p, \omega) T_{p,p'} G_0^r(p', \omega). \end{aligned} \quad (3.79)$$

Here we have identified the retarded T -matrix,

$$T_{p,p'} = \frac{V_p V_{p'}}{\omega - \varepsilon_0 - \sum_p \frac{V_p^2}{\omega - \varepsilon_p + i\eta}}. \quad (3.80)$$

Chapter 10, which analyzes high-field transport, will make extensive use of the resonant-level model as a “testing ground” for quantum kinetics.

3.7 Self-Energy

One often needs to sum the perturbation expansion up to infinite order. This is done by identifying the most important subset of diagrams and including them in a self-energy. A warning is in place: the correct identification of the most important diagrams can be very tricky, even in the presence of a small parameter. The reason is that some high-order diagrams, which are not included in a particular model, even though formally smaller, may occur in such large numbers that they yield a contribution that must be included. Any perturbation theory may be just an asymptotic series and not converging in the strict mathematical sense. Finally, it is by no means clear that a “good” self-energy always even exists. Strongly interacting systems of this kind need a nonperturbative approach and are not addressed further in this book. Examples of these fascinating problems include the Kondo phenomenon, the fractional quantum Hall effect, Luttinger liquids in one-dimensional Fermi systems, and possibly even high temperature superconductors.

3.7.1 Electron–Phonon Interaction

In the case of electron–phonon interaction, the perturbation expansion generates the type of diagrams shown in Fig. 3.3. The self-energy can be evaluated in various levels of approximation. The simplest one is Born approximation:

$$\Sigma_B(k, \omega) = i \sum_q \int \frac{d\omega'}{2\pi} M_q^2 G_0(k - q, \omega - \omega') D_0(q, \omega'). \quad (3.81)$$

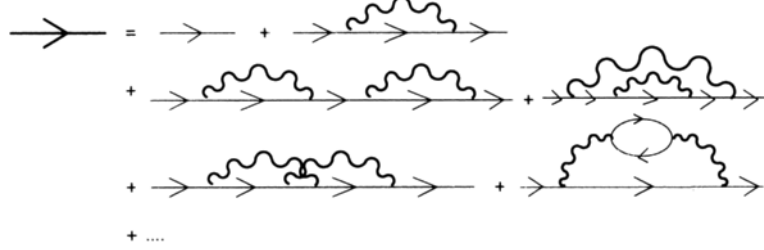


Fig. 3.3. Perturbation expansion for the electron Green function in an electron–phonon system. *Legend:* Free Green function: *thin line*; Full electron Green function: *thick line*; phonon-Green function: *wavy line*

$$\Sigma(\mathbf{k}, \omega) = \text{sum of diagrams} \quad \begin{matrix} \mathbf{q}, \omega' \\ \mathbf{k}-\mathbf{q}, \omega-\omega' \end{matrix}$$

Fig. 3.4. Born approximation for electron–phonon interaction

The Feynman rules are straightforward [2, 110, 251, 254]: one just has to conserve energy and momentum at each vertex, and multiply with the interaction matrix element M_q . All internal momenta and frequencies are integrated over. Finally, an extra factor i^m is added, where m is the number of four-dimensional momentum-frequency integrals. In our example $m = 1$. For each closed Fermi loop one has to multiply with an extra factor -1 . With the Born approximation (3.81) the Dyson equation reads

$$G(k, \omega) = G_0(k, \omega) + G_0(k, \omega)\Sigma_B(k, \omega)G(k, \omega) \quad (3.82)$$

or

$$G(k, \omega) = \frac{1}{\omega - \varepsilon_k - \Sigma_B(k, \omega)} . \quad (3.83)$$

The diagrams included in the (bare) Born approximation are shown in Fig. 3.4. The next level of approximation is the self-consistent Born approximation:

$$\Sigma_{SCB}(k, \omega) = i \sum_q \int \frac{d\omega'}{2\pi} M_q^2 G(k - q, \omega - \omega') D_0(q, \omega') , \quad (3.84)$$

which corresponds to the diagram shown in Fig. 3.5. One may need to evaluate a two-particle Green function in the analysis of, say, electrical conductivity. Some typical diagrams are shown in Fig. 3.6. In the case of electron–phonon interactions in metals, it is possible to prove a theorem named according to Migdal [267] (for a detailed discussion, see [110], pp. 406–410), which states that vertex corrections (an example of a diagram which contains vertex corrections is Fig. 3.6b) are of the order of $\sqrt{m/M} \simeq 10^{-2}$

$$\Sigma(\mathbf{k}, \omega) = \text{---} \xrightarrow{\qquad\qquad\qquad} \begin{matrix} \mathbf{q}, \omega' \\ \mathbf{k}-\mathbf{q}, \omega-\omega' \end{matrix}$$

Fig. 3.5. Self-consistent Born approximation for electron–phonon interaction

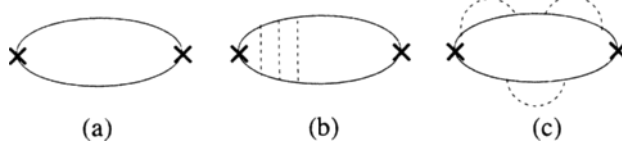


Fig. 3.6. Diagrams contributing to two-particle Green function. Diagram **b** contains vertex corrections in its left vertex

(here m is electron mass and M is ion mass) and hence can be neglected in many applications. It is an open question whether a similar theorem holds for semiconductors under highly nonequilibrium conditions.

3.7.2 Elastic Impurity System: Impurity Averaging

Consider an electron moving in a sample with impurities at random positions $\{\mathbf{R}_\alpha\}$. These give rise to a real-space potential $u(\mathbf{x}) = \sum_{\{\mathbf{R}_\alpha\}} v(\mathbf{x} - \mathbf{R}_\alpha)$.⁵ In second quantization the Hamiltonian becomes

$$H = \sum_{\mathbf{p}} \varepsilon_{\mathbf{p}} a_{\mathbf{p}}^\dagger a_{\mathbf{p}} + \sum_{\mathbf{p}, \mathbf{q}, \{\mathbf{R}_\alpha\}} \frac{v_{\mathbf{q}}}{\Omega} e^{-i\mathbf{q} \cdot \mathbf{R}_\alpha} a_{\mathbf{p}+\mathbf{q}}^\dagger a_{\mathbf{p}} , \quad (3.85)$$

where $v_{\mathbf{q}}$ is Fourier transform of $v(\mathbf{x})$, and Ω is the system volume. In bulk samples we do not expect that the sample’s macroscopic properties, such as electrical conductivity, depend on the actual locations of the impurities. However, since (3.85) does depend on these locations, we must devise a method which allows us to compute physical observables so that only the average properties of the impurity distribution matter. This technique is called impurity averaging [2], and it is based on the following construction. We suppose that the sample consists of many identical blocks, each one containing the same number of impurities, but at different positions. Each block is assumed to consist of many impurities. Let us assume that we can compute the object under consideration (Green function, density of states, etc.) for each individual block with a fixed impurity configuration, and denote the result of this calculation by $A(\{\mathbf{R}_\alpha\})$. The physical object corresponding to the whole sample, denoted by \bar{A} , is then computed as an ensemble average

⁵ For simplicity we assume that all impurities are alike, i.e., the impurity potential $v(x)$ does not depend on the impurity site α .

$$\bar{A} = \langle A(\{\mathbf{R}_\alpha\}) \rangle_{\text{imp}} = \prod_\alpha \int \frac{d\mathbf{R}_\alpha}{\Omega} A(\{\mathbf{R}_\alpha\}). \quad (3.86)$$

Before applying (3.86) to the elastic impurity problem a few comments are in place. First, (3.86) clearly assumes uncorrelated impurities, since the integral is extended over all space in an unrestricted manner. In principle it would be possible to allow for impurity correlations by including in (3.86) some appropriate impurity–impurity correlation function, which would have to be calculated separately. Second, one may inquire whether the impurity-averaging method works for arbitrarily small samples. The answer is clearly “no”: the above construction assumes that the sample can be constructed from an incoherent superposition of “blocks.” If the sample is so small that some coherence is maintained throughout it, one enters a “mesoscopic” regime, which will be a topic of many later sections. One of the striking properties of mesoscopic samples is that measured properties may depend on the individual impurity distributions. Summarizing, when we apply impurity averaging technique we are tacitly assuming the inequality sequence $l_{\text{imp}} \ll l_\phi \ll L$, where l_{imp} is the impurity mean free path, l_ϕ is the phase-coherence length (or phase-braking length), and L is the sample size.

We now outline how one computes the impurity-averaged retarded Green function $\langle G^r(\mathbf{p}, \mathbf{p}', \omega) \rangle_{\text{imp}}$. Note that before impurity averaging two momentum labels are needed, because the impurities have broken the translational invariance. The equation-of-motion method can be applied just like in case of the resonant-level model of Sect. 3.6.2. The details are left as an exercise, and one finds

$$\begin{aligned} G^r(\mathbf{p}, \mathbf{p}', \omega) &= \delta_{\mathbf{p}\mathbf{p}'} G_0^r(\mathbf{p}, \omega) \\ &+ G_0^r(\mathbf{p}, \omega) \frac{1}{\Omega} \sum_{\mathbf{q}, \{\mathbf{R}_\alpha\}} v_{\mathbf{q}} e^{-i\mathbf{q} \cdot \mathbf{R}_\alpha} G^r(\mathbf{p} - \mathbf{q}, \mathbf{p}', \omega). \end{aligned} \quad (3.87)$$

The strategy is clear-cut: One iterates (3.87), averages term-by-term using (3.86), and finally tries to identify repeating structures which perhaps can be summed up to infinite order. The zeroth-order term in the impurity potential is naturally unaffected by impurity averaging, and the first-order term reads

$$G^{r(1)}(\mathbf{p}, \mathbf{p}', \omega) = G_0^r(\mathbf{p}, \omega) \frac{1}{\Omega} \sum_{\{\mathbf{R}_\alpha\}} e^{-i(\mathbf{p}-\mathbf{p}') \cdot \mathbf{R}_\alpha} v_{\mathbf{p}-\mathbf{p}'} G_0^r(\mathbf{p}', \omega). \quad (3.88)$$

Applying (3.86) we evaluate the impurity average as

$$\begin{aligned} &\left[\int \frac{d\mathbf{R}_1}{\Omega} \int \frac{d\mathbf{R}_2}{\Omega} \cdots \int \frac{d\mathbf{R}_N}{\Omega} \cdots \int \frac{d\mathbf{R}_N}{\Omega} \right] \\ &\times \left[e^{-i(\mathbf{p}-\mathbf{p}') \cdot \mathbf{R}_1} + e^{-i(\mathbf{p}-\mathbf{p}') \cdot \mathbf{R}_2} + \dots \right. \\ &\quad \left. + e^{-i(\mathbf{p}-\mathbf{p}') \cdot \mathbf{R}_N} + \dots + e^{-i(\mathbf{p}-\mathbf{p}') \cdot \mathbf{R}_N} \right] \\ &= N \int \frac{d\mathbf{R}}{\Omega} e^{-i(\mathbf{p}-\mathbf{p}') \cdot \mathbf{R}} = \delta_{\mathbf{p}, \mathbf{p}'} N, \end{aligned} \quad (3.89)$$

where N is the number of impurities. Combining (3.89) with (3.88) and introducing the impurity concentration c , we have

$$\bar{G}^{r(1)}(\mathbf{p}, \mathbf{p}', \omega) = \delta_{\mathbf{p}, \mathbf{p}'} G_0^r(\mathbf{p}, \omega) cv(\mathbf{q} = 0) G_0^r(\mathbf{p}, \omega). \quad (3.90)$$

We observe that impurity averaging has reintroduced translational invariance, i.e., diagonality in the momentum labels. Let us next consider the second-order term, which is obtained by substituting (3.88) on right-hand side of (3.87). Instead of (3.89) we must now evaluate

$$\begin{aligned} & \prod_{\{\mathbf{R}_\gamma\}} \int \frac{d\mathbf{R}_\gamma}{\Omega} \sum_{\{\mathbf{R}_\beta\}} e^{-i\mathbf{q}\cdot\mathbf{R}_\beta} \sum_{\{\mathbf{R}_\alpha\}} e^{-i(\mathbf{p}-\mathbf{q}-\mathbf{p}')\cdot\mathbf{R}_\alpha} \\ &= N(N-1)\delta_{\mathbf{q}, 0}\delta_{\mathbf{p}, \mathbf{p}'} + N\delta_{\mathbf{p}, \mathbf{p}'}, \end{aligned} \quad (3.91)$$

which leads to the following expression for $\bar{G}^{r(2)}$:

$$\begin{aligned} \bar{G}^{r(2)}(\mathbf{p}, \mathbf{p}', \omega) &= \delta_{\mathbf{p}, \mathbf{p}'} [G_0^r(\mathbf{p}, \omega) cv(\mathbf{q} = 0) G_0^r(\mathbf{p}, \omega) cv(\mathbf{q} = 0) G_0^r(\mathbf{p}, \omega) \\ &\quad + G_0^r(\mathbf{p}, \omega) c \sum_{\mathbf{q}} |v(\mathbf{q})|^2 G_0^r(\mathbf{p} - \mathbf{q}, \omega) G_0^r(\mathbf{p}, \omega)]. \end{aligned} \quad (3.92)$$

Figure 3.7 shows the Feynman diagrams corresponding to (3.90) and (3.92), and some higher order diagrams. One often absorbs the structureless term $cv(\mathbf{q} = 0)$ in the single particle energy, and thus the free-standing impurity lines are not shown in many standard treatises. Just as in the phonon case, we can use Fig. 3.7 as a guideline in selecting an appropriate self-energy functional. An often used choice is the self-consistent Born approximation,

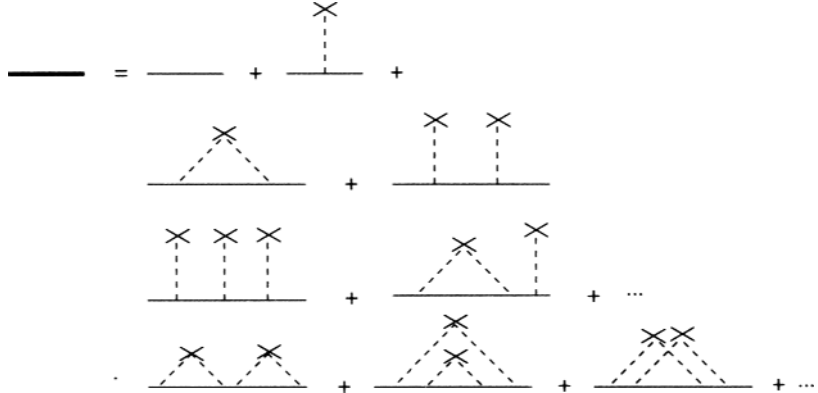


Fig. 3.7. Beginning of the diagrammatic expansion for the impurity-averaged Green function. Momentum is conserved at each vertex. *Thick line:* impurity averaged Green function; *thin line:* free Green function, *dotted line:* impurity potential. Only a few representative diagrams of third or fourth order in the impurity potential are shown on the third and fourth line, respectively

$$\Sigma_{\text{SCBA}}^r(\mathbf{p}, \omega) = c \sum_{\mathbf{q}} |v(\mathbf{p} - \mathbf{q})|^2 \bar{G}^r(\mathbf{q}, \omega). \quad (3.93)$$

This equation, and the Dyson equation $\bar{G}^r = \{\omega - \varepsilon_p - \Sigma_{\text{SCBA}}^r[\bar{G}^r]\}^{-1}$, define a self-consistent problem for the impurity-averaged Green function \bar{G}^r . The solution for this self-consistent problem is easy to find if one considers *s*-wave scatterers, i.e., suppresses the momentum dependence of the scattering potential. We make an Ansatz for the retarded self-energy, $\Sigma^r = -i/2\tau$, and determine the parameter τ . With this assumption we evaluate (3.93) as

$$\begin{aligned} -\frac{i}{2\tau} &= cv^2 \sum_{\mathbf{q}} \frac{1}{\omega - \varepsilon_q + i/2\tau} \\ &= cv^2 \int d\varepsilon_q N(\varepsilon_q) \frac{1}{\omega - \varepsilon_q + i/2\tau} \\ &\simeq cv^2 N(0) \int d\varepsilon_q \frac{-i/2\tau}{(\omega - \varepsilon_q)^2 + (1/2\tau)^2} \\ &= -icv^2 N(0)\pi. \end{aligned} \quad (3.94)$$

Equation (3.94) allows us to identify the impurity-limited life-time, $1/\tau = cv^2 N(0)2\pi$. It is worth commenting the main approximations used in the calculation leading to (3.94). First, we assume that the relevant energies are in the neighborhood of the Fermi energy, which allows us to replace the slowly varying density-of-states $N(\varepsilon)$ by its value at the Fermi surface. This approximation is good for degenerate Fermi systems, but it would require a modification for lightly doped semiconductors, where impurity scattering can have a significant energy dependence. Second, we ignored the real part of the self-energy. This quantity can be absorbed in the single-particle energies, just as we did with the Hartree-like term $cv(0)$ resulting from forward scattering from impurities. The retarded (advanced) Green function for impurity systems, $G^{r(a)} = [\omega - \varepsilon_p \pm i/2\tau]^{-1}$ will be used in many of the subsequent sections.

We finally wish to comment on the choice of diagrams contributing to the retarded Green function determined above. The self-consistent Born approximation does not include any *crossed diagrams* (an example is the last diagram on the fourth line of Fig. 3.7), even though other diagrams which are formally of the same order in the scattering potential (e.g., the two first diagrams on the last line of Fig. 3.7) are included. The justification for this procedure is as follows [2]. Using momentum conservation at vertices, one finds that the last two diagrams of Fig. 3.7 lead to self-energy contributions

$$\Sigma_{\text{rb}}(\mathbf{p}, \omega) = (cv^2)^2 \sum_{\mathbf{k}_1 \mathbf{k}_2} G(\mathbf{k}_1, \omega) G(\mathbf{k}_2, \omega) G(\mathbf{k}_1, \omega), \quad (3.95a)$$

$$\Sigma_{\text{cr}}(\mathbf{p}, \omega) = (cv^2)^2 \sum_{\mathbf{k}_1 \mathbf{k}_2} G(\mathbf{k}_1, \omega) G(\mathbf{k}_2, \omega) G(\mathbf{p} - \mathbf{k}_1 + \mathbf{k}_2, \omega), \quad (3.95b)$$

where the subscripts have their conventional meaning, rb = rain-bow, and cr = crossed. Following the arguments given above, all momenta and energies are confined to the neighborhood of the Fermi surface, and thus any difference in magnitude for diagrams of same order in perturbation theory must result from angular integrations. In evaluating Σ_{rb} no restrictions are placed for the angular variables in the two internal momentum integrations. Setting $\omega \simeq \varepsilon_F$ and $\varepsilon_k \simeq \varepsilon_F$, each of the three Green functions yields a contribution of the order of $[1/\tau]^{-1}$, and hence the total contribution can be estimated as $\propto (cv^2)^2 [1/\tau]^{-3}$. The situation is different for Σ_{cr} : only two Green functions can be estimated as $[1/\tau]^{-1}$, while the third one after angular integration gives a contribution of the order of ε_F^{-1} . Thus the ratio $\Sigma_{\text{cr}}/\Sigma_{\text{rb}}$ is of the order of $1/\tau\varepsilon_F \propto 1/k_F l \ll 1$ (here $l = v_F\tau$ is the mean free path), and the self-consistent Born approximation appears to include the most important diagrams. This is, however, not always the case: a more detailed analysis, which is sketched in Part III, shows that for two-particle Green function (which determines, among other things, the electrical conductivity) in two spatial dimensions corrections of the order of $1/k_F l$ must be included. In fact, it is possible to develop a systematic perturbation theory based on the smallness of this parameter, and the resulting theoretical predictions are in excellent agreement with experimental results (“weak localization”).

3.8 Finite Temperatures

We conclude by reviewing very briefly some of the considerations that enter the formulation of a finite temperature theory. The reader without prior familiarity with these ideas will probably find it useful to consult any of the texts quoted in Sect. 3.2. At finite temperatures the expectation value appearing in the definition of the Green function must include a thermal weighting factor, as already indicated in (3.31), (3.44), and (3.45). But now the interaction sits in two places: (1) in the thermal factors $\exp[-\beta(H - \mu N)]$, and in the S -matrix due to the Heisenberg picture time dependence of the operators $c_p(t), c_p^\dagger(t')$. This makes a straightforward expansion (which now becomes a double expansion) quite difficult. A way around this problem is the Matsubara technique, where one introduces a complex time $\tau = it$. Then the Green function, with the grand-canonical density matrix (3.44) and (3.45), becomes

$$\begin{aligned} \mathcal{G}(p, \tau - \tau') &= -\langle T_\tau c_p(\tau) c_p^\dagger(\tau') \rangle \quad (3.96) \\ &= -\text{Tr}\{e^{-\beta(H - \mu N - \Omega)} T_\tau e^{\tau(H - \mu N)} c_p e^{-(\tau - \tau')(H - \mu N)} c_p^\dagger e^{-\tau'(H - \mu N)}\}, \end{aligned}$$

where also for the time development the “grand-canonical” Hamiltonian $H - \mu N$ has been used. A function defined in this way obeys the boundary condition for $-\beta < \tau < 0$:

$$\mathcal{G}(p, \tau) = -\mathcal{G}(p, \tau + \beta). \quad (3.97)$$

This property suggests a Fourier series expansion in the strip $[0, \beta]$:

$$\begin{aligned}\mathcal{G}(p, i\omega_n) &= \int_0^\beta d\tau \mathcal{G}(p, \tau) e^{i\tau\omega_n} \\ \mathcal{G}(p, \tau) &= \frac{1}{\beta} \sum_n e^{-i\omega_n \tau} \mathcal{G}(p, i\omega_n) .\end{aligned}\quad (3.98)$$

The discrete frequencies are given by

$$\omega_n = \frac{2\pi(2n+1)}{\beta} . \quad (3.99)$$

For bosons the Green function is periodic, i.e., (3.97) has a plus sign on the right-hand side, and the discrete frequencies involve even integers.

One can derive a similar Feynman diagram technique for the finite temperature Green functions, as was done earlier for normal time-ordered Green functions. The S -matrix expansion, Wick's theorem, etc., are essentially unchanged. For further details we refer to Mahan [251,254] who gives a thorough account of these techniques. The final thing to note is that once the finite temperature function is known, the retarded and advanced functions follow with an analytic continuation:

$$\mathcal{G}(p, \varepsilon + i\delta) = G^r(p, \varepsilon) , \quad (3.100)$$

$$\mathcal{G}(p, \varepsilon - i\delta) = G^a(p, \varepsilon) . \quad (3.101)$$

In Part II a couple of examples are given which illustrate the interrelationship between the finite temperature formalism and the nonequilibrium formalism.

Part II

Nonequilibrium Many-Body Theory

Contour-Ordered Green Functions

Summary. We introduce the concept of nonequilibrium Green functions which are ordered on a time contour - also called Keldysh contour - running from the remote past where the system was in equilibrium to the highest relevant time and back to the remote past. The resulting four Green functions are shown to be interrelated, but two of them, e.g., a spectral Green function and a kinetic Green function contain in nonequilibrium separate information in sharp contrast to the equilibrium situation. Using analytic continuation useful relations for products of Green functions are derived.

4.1 General Remarks

We recall from Sect. 3.5 that the central quantity in constructing the perturbation theory for Green functions is the S -matrix $S(\infty, -\infty)$. In nonequilibrium there is no guarantee that the system returns to its initial state for asymptotically large times. In fact, often it does not. Consider, for example, an important problem in surface physics, where atoms or molecules impinging on a surface exchange charge with the surface, and hence the initial state at $t = -\infty$ is very different from the final state at $t = +\infty$. Thus, one should avoid any reference to the asymptotically large times in the nonequilibrium theory. The general formulation of the theory is slightly more complicated than in the equilibrium case. As we shall see, however, the abstract structure of the theory bears a close resemblance to the equilibrium theory.

The nonequilibrium problem is formulated as follows. We consider a system evolving under the Hamiltonian

$$H = h + H'(t) . \quad (4.1)$$

Here the time-independent part of the Hamiltonian h is split in two parts: $h = H_0 + H_i$, where H_0 is “simple” (in the sense that it can be diagonalized, and hence Wick’s theorem applies) and H_i is “complicated” (in the sense that it contains the many-body aspects of the problem, and hence requires a

special treatment). It is further assumed that the nonequilibrium part vanishes for times $t < t_0$. The nonequilibrium part could be, e.g., an electric field, a light excitation pulse, or a coupling to contacts at differing (electro) chemical potentials. All these cases will be treated in later chapters.

One often lets $t_0 \rightarrow -\infty$ at a suitable point. This procedure simplifies the treatment, and in order to display the structure of the nonequilibrium theory as concisely as possible, we will initially take this limit. However, in doing so the discussion of transient phenomena is excluded, and since transient phenomena are one of the central topics we wish to address, we shall return to this point below.

Before the perturbation is turned on, the system is described by the thermal equilibrium density matrix

$$\varrho(h) = \frac{\exp(-\beta h)}{\text{Tr}[\exp(-\beta h)]}. \quad (4.2)$$

The task is to calculate the expectation value of a given observable, to which one associates a quantum mechanical operator O , for times $t \geq t_0$:

$$\langle O(t) \rangle = \text{Tr}[\varrho(h)O_H(t)]. \quad (4.3)$$

The subscript H indicates that the time dependence is governed by the full Hamiltonian, i.e., O is written in the Heisenberg picture. Definition 4.3 can be generalized to two-time (or n -time) quantities (Green functions, correlation functions) in an obvious fashion.

One should note that we use an equilibrium density matrix $\varrho(h)$ in (4.3), and not some time dependent ϱ . Physically this means that the thermodynamic degrees of freedom, contained in h , do not follow instantaneously the rapid variations contained in $H'(t)$. Other choices may be possible, but we make this choice here because of the difficulties related to other choices (for example, see the discussion on pp. 214–216 in [254]). An alternative and potentially very promising approach consists of replacing the equilibrium density-matrix in the expectation value by some suitable generalization, such as suggested by Hershfield [153], and more recently elaborated in [50, 83, 97, 133]. We shall also address the possible limitations of this approach in Chap. 13, where we discuss time-dependent transport in semiconductor microstructures.

4.2 Two Transformations

The general plan of attack is similar to the equilibrium case. We transform the “hopelessly complicated” time dependence of O_H to a simpler form, namely to that of O_{H_0} . Since there are two operators to be eliminated, i.e., the time-dependent external perturbation $H'(t)$ and the “complicated” interaction term H_i , we expect to meet more complicated transformations than in



Fig. 4.1. Contour C_t

the equilibrium case. However, with suitable generalizations, it can be shown that the nonequilibrium and equilibrium formalisms can be made *structurally* equivalent.

The first step is to change the time dependence of O_H to that of O_h . This is achieved by the relation

$$O_H(t) = v_h^\dagger(t, t_0) O_h(t) v_h(t, t_0), \quad (4.4)$$

where

$$v_h(t, t_0) = T \left\{ \exp \left[-i \int_{t_0}^t dt''_h(t') \right] \right\} \quad (4.5)$$

and $H'_h(t)$ is the interaction representation of $H'(t)$:

$$H'_h(t) = \exp[ih(t - t_0)] H'(t) \exp[-ih(t - t_0)], \quad (4.6)$$

and T is the time-ordering operator which arranges the latest times to left.

We now introduce contour-ordered quantities. Expression (4.4) can be written in another, but equivalent, form:

$$O_H(t) = T_{C_t} \left\{ \exp \left[-i \int_{C_t} d\tau H'_h(\tau) \right] O_h(t) \right\}, \quad (4.7)$$

where the contour C_t is depicted in Fig. 4.1. Where possible, we shall employ the convention that time variables defined on a complex contour are denoted by greek letters, while roman letters are used for real time variables. The contour runs on the real axis (or slightly above it; if $H'(t)$ can be analytically continued no problems can arise) from t_0 to t , and back again. The meaning of the contour-ordering operator T_{C_t} is the following: The operators with time labels that occur later on the contour have to stand left to operators with earlier time labels. The next calculation illustrates some of the properties of functions defined on a contour.

Demonstration of Equivalence of (4.4) and (4.7)

In order to get some acquaintance with the functions defined on a contour we now explicitly demonstrate the equivalence of (4.4) and (4.7) [285]. We have

$$\begin{aligned} & T_{C_t} \left\{ \exp \left[-i \int_{C_t} d\tau H'_h(\tau) \right] O_h(t) \right\} \\ &= \sum_{n=0}^{\infty} \frac{(-i)^n}{n!} \int_{C_t} d\tau_1 \cdots \int_{C_t} d\tau_n T_{C_t} [H'_h(\tau_1) \cdots H'_h(\tau_n) O_h(t)]. \end{aligned} \quad (4.8)$$

Now divide the contour into two branches:

$$\int_{C_t} = \int_{\rightarrow} + \int_{\leftarrow}, \quad (4.9)$$

where \int_{\rightarrow} goes from t_0 to t , and \int_{\leftarrow} from t back to t_0 . Thus the n th order term in (4.8) generates 2^n terms. Let us consider one of them

$$\begin{aligned} & \int_{\rightarrow} d\tau_1 \int_{\rightarrow} d\tau_2 \int_{\leftarrow} d\tau_3 \cdots \int_{\leftarrow} d\tau_n T_{C_t} [H'_h(\tau_1) \cdots H'_h(\tau_n) O_h(t)] \\ &= \int_{\leftarrow} d\tau_3 \cdots \int_{\leftarrow} d\tau_n T_{\leftarrow} [H'_h(\tau_3) \cdots H'_h(\tau_n)] O_h(t) \\ & \times \int_{\rightarrow} d\tau_1 \int_{\rightarrow} d\tau_2 T_{\rightarrow} [H'_h(\tau_1) H'_h(\tau_2)]. \end{aligned} \quad (4.10)$$

We must do now some combinatorics. Out of the 2^n terms we have generated, there are $n!/[m!(n-m)!]$ terms with m integrals from t_0 to t ($m = 0, \dots, n$ and in the above example $m = 2$). All these terms give the same contribution. Thus we can write

$$\begin{aligned} & \int_{C_t} d\tau_1 \cdots \int_{C_t} d\tau_n T_{C_t} [H'_h(\tau_1) \cdots H'_h(\tau_n) O_h(t)] \\ &= \sum_{m=0}^n \frac{n!}{m!(n-m)!} \int_{\leftarrow} d\tau_{m+1} \cdots \int_{\leftarrow} d\tau_n T_{\leftarrow} [H'_h(\tau_{m+1}) \cdots H'_h(\tau_n)] O_h(t) \\ & \times \int_{\rightarrow} d\tau_1 \cdots \int_{\rightarrow} d\tau_m T_{\rightarrow} [H'_h(\tau_1) \cdots H'_h(\tau_m)]. \end{aligned} \quad (4.11)$$

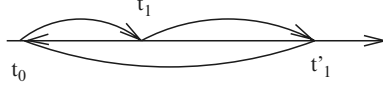
Now introduce a new variable $k = n - m$; we can sum both k and m from 0 to ∞ as long as their sum equals n , and this is achieved by inserting a Kronecker delta. Equation (4.11) yields

$$\begin{aligned} & \rightarrow \sum_{m,k=0}^{\infty} \frac{n!}{m!k!} \delta_{n,k+m} \left\{ \int_{\leftarrow} d\tau_1 \cdots \int_{\leftarrow} d\tau_k T_{\leftarrow} [H'_h(\tau_1) \cdots H'_h(\tau_k)] \right\} O_h(t) \\ & \times \left\{ \int_{\rightarrow} d\tau_1 \cdots \int_{\rightarrow} d\tau_m T_{\rightarrow} [H'_h(\tau_1) \cdots H'_h(\tau_m)] \right\}. \end{aligned} \quad (4.12)$$

We can now go back to (4.8). The n -sum is simple (due to the factor $\delta_{n,k+m}$), and we obtain

$$\begin{aligned} & T_{C_t} \left\{ \exp \left[-i \int_{C_t} d\tau H'_h(\tau) \right] O(t) \right\} \\ &= \sum_{k=0}^{\infty} \frac{(-i)^k}{k!} \int_{\leftarrow} d\tau_1 \cdots \int_{\leftarrow} d\tau_k T_{\leftarrow} [H'_h(\tau_1) \cdots H'_h(\tau_k)] O(t) \\ & \times \sum_{m=0}^{\infty} \frac{(-i)^m}{m!} \int_{\rightarrow} d\tau_1 \cdots \int_{\rightarrow} d\tau_m T_{\rightarrow} [H'_h(\tau_1) \cdots H'_h(\tau_m)]. \end{aligned} \quad (4.13)$$

But, comparing the factors multiplying $O(t)$ from left and right we can identify $v^\dagger(t, t_0)$ and $v(t, t_0)$, respectively. We have thus demonstrated the equivalence of (4.4) and (4.7).

**Fig. 4.2.** Contour C

The contour-ordering operator is a strong formal tool which will allow us to develop the nonequilibrium theory along lines parallel to the equilibrium theory.

We now define the contour-ordered Green function:

$$G(1, 1') \equiv -i\langle T_C[\psi_H(1)\psi_H^\dagger(1')]\rangle, \quad (4.14)$$

where the contour C starts and ends at t_0 ; it runs along the real axis and passes through t_1 and t'_1 once and just once (Fig. 4.2). Here, as in Part I, ψ_H and ψ_H^\dagger are the fermion field operators in the Heisenberg picture. Finally, we employ the shorthand notation $(1) \equiv (\mathbf{x}_1, t_1)$ (or $(1) \equiv (\mathbf{x}_1, \tau_1)$, when appropriate).

The contour-ordered Green function plays an analogous role in nonequilibrium theory as the causal Green function plays in equilibrium theory: as we shall see below, it possesses a perturbation expansion based on Wick's theorem. However, since the time labels lie on the contour with two branches, one must keep track of which branch is in question. With two time labels, which can be located on either of the two branches of the contour of Fig. 4.2, there are four distinct possibilities. Thus (4.14) contains four different functions:

$$G(1, 1') = \begin{cases} G_c(1, 1') & t_1, t_{1'} \in C_1 \\ G^>(1, 1') & t_1 \in C_2, t_{1'} \in C_1 \\ G^<(1, 1') & t_1 \in C_1, t_{1'} \in C_2 \\ G_{\bar{c}}(1, 1') & t_1, t_{1'} \in C_2 \end{cases}. \quad (4.15)$$

Here we have introduced the *causal*, or *time-ordered* Green function G_c ,

$$\begin{aligned} G_c(1, 1') &= -i\langle T[\psi_H(1)\psi_H^\dagger(1')]\rangle \\ &= -i\theta(t_1 - t_{1'})\langle\psi_H(1)\psi_H^\dagger(1')\rangle + i\theta(t_{1'} - t_1)\langle\psi_H^\dagger(1')\psi_H(1)\rangle, \end{aligned} \quad (4.16)$$

the “*greater*” function $G^>$,

$$G^>(1, 1') = -i\langle\psi_H(1)\psi_H^\dagger(1')\rangle, \quad (4.17)$$

the “*lesser*” function $G^<$,

$$G^<(1, 1') = +i\langle\psi_H^\dagger(1')\psi_H(1)\rangle, \quad (4.18)$$

and the *antitime-ordered* Green function $G_{\bar{c}}$,

$$\begin{aligned} G_{\bar{c}}(1, 1') &= -i\langle \tilde{T}[\psi_H(1)\psi_H^\dagger(1')]\rangle \\ &= -i\theta(t_{1'} - t_1)\langle\psi_H(1)\psi_H^\dagger(1')\rangle + i\theta(t_1 - t_{1'})\langle\psi_H^\dagger(1')\psi_H(1)\rangle. \end{aligned} \quad (4.19)$$

Since $G_c + G_{\bar{c}} = G^< + G^>$, there are only three linearly independent functions. This freedom of choice reflects itself in the literature, where a number of different conventions can be found. For our purposes the most suitable functions are the functions $G^{>,<}$ (which are often also denoted by a common name, “correlation function”), and the advanced and retarded functions defined as

$$\begin{aligned} G^a(1, 1') &= i\theta(t_{1'} - t_1)\langle\{\psi_H(1), \psi_H^\dagger(1')\}\rangle \\ &= \theta(t_{1'} - t_1)[G^<(1, 1') - G^>(1, 1')] , \end{aligned} \quad (4.20)$$

and

$$\begin{aligned} G^r(1, 1') &= -i\theta(t_1 - t_{1'})\langle\{\psi_H(1), \psi_H^\dagger(1')\}\rangle \\ &= \theta(t_1 - t_{1'})[G^>(1, 1') - G^<(1, 1')] . \end{aligned} \quad (4.21)$$

Here curly brackets denote an anticommutator. We observe that $G^r - G^a = G^> - G^<$. In later chapters we will discuss at length the physical interpretation of the functions $G^{<,>}$ and $G^{r,a}$.

After these definitions, we can return to the main task of this section: the transformation of the contour-ordered Green function (4.14) into a form, where Wick’s theorem can be applied. The first step is to repeat the analysis leading to (4.7), i.e., transformation from H -dependence to h -dependence. The result is

$$G(1, 1') = -i\langle T_C[S_C^H \psi_h(1) \psi_h^\dagger(1')]\rangle , \quad (4.22)$$

where

$$S_C^H = \exp\left[-i \int_C d\tau H'_h(\tau)\right] . \quad (4.23)$$

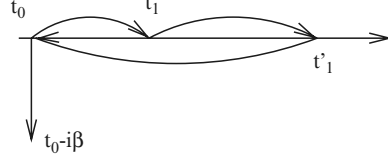
We still need one more transformation to show the existence of a diagrammatic perturbation theory. Recall that the operator h contains two terms, $h = H_0 + H_i$, and that Wick’s theorem only works for H_0 (i.e., quadratic Hamiltonians). Thus we must be able to replace the h -dependence by H_0 -dependence. Note also that the density matrix implicit in (4.22) also contains h , and h thus occurs in four different places in (4.22): $\varrho(h)$, S_C^H , and the field operators $\psi_h(1)$, and $\psi_h^\dagger(1')$, respectively.

The details of the transformations are somewhat tedious, but straightforward [287] and it is sufficient to state the final result:

$$G(1, 1') = -i \frac{\text{Tr}\left\{\varrho_0 T_{C_v}[S_{C_v}^i S'_C \psi_{H_0}(1) \psi_{H_0}^\dagger(1')]\right\}}{\text{Tr}[\varrho_0 T_{C_v}(S_{C_v}^i S'_C)]} , \quad (4.24)$$

where the density matrix ϱ_0 is given by

$$\varrho_0 = \frac{\exp(-\beta H_0)}{\text{Tr}[\exp(-\beta H_0)]} , \quad (4.25)$$

Fig. 4.3. Contour C_v

and

$$\begin{aligned} S'_C &= \exp \left[-i \int_C d\tau H'_{H_0}(\tau) \right], \\ S^i_{C_v} &= \exp \left[-i \int_{C_v} d\tau H^i_{H_0}(\tau) \right], \end{aligned} \quad (4.26)$$

where the time-dependence of the Hamiltonians is defined in analogy with (4.6). Further, the contour C was defined in Fig. 4.2 while the contour C_v is shown in Fig. 4.3.

Equation (4.24) is an important result. Despite its complicated appearance it has a number of attractive features. Firstly, it is exact. Next, all time dependence is governed by the ‘‘solvable’’ H_0 . In particular, the quadratic density matrix $\sim \exp(-\beta H_0)$ allows one to use Wick’s theorem. Thus, the Feynman diagrams can be constructed for the nonequilibrium problem. Just as in the equilibrium case, the denominator cancels the contribution arising from the disconnected diagrams.

We can summarize the main results of this section as follows. The equilibrium and nonequilibrium theories are structurally equivalent. The only difference is the replacement of real axis integrals by contour integrals.

4.3 Analytic Continuation

While the result (4.24) is a strong formal statement, it is rather impractical in calculations unless one can replace the contour integrals by real time integrals. This procedure is called the analytic continuation, and many different formulations exist in the literature. Here we analyze in some detail the generalization of the method of Kadanoff and Baym [191] due to Langreth [231].

As shown in Sect. 4.3, the contour-ordered Green function has the same perturbation expansion as the corresponding equilibrium time-ordered Green function. Consequently, given that a self-energy functional can be defined,¹

¹ In many problems one generates, either by the equation-of-motion technique or by functional differentiation, higher-order Green functions (or other objects with more than two time labels). While the formal theory can also be developed for these objects, we restrict ourselves presently to cases where a well-defined self-

the contour-ordered Green function has the same Dyson equation as the equilibrium function:

$$\begin{aligned} G(1, 1') = & G_0(1, 1') + \int d^3x_2 \int_{C_v} d\tau_2 G_0(1, 2) U(2) G(2, 1') \\ & + \int d^3x_2 \int d^3x_3 \int_{C_v} d\tau_2 \int_{C_v} d\tau_3 G_0(1, 2) \Sigma(2, 3) G(3, 1') , \end{aligned} \quad (4.27)$$

where we assume that the nonequilibrium term in the Hamiltonian can be represented by a one-body external potential U . The interactions are contained in the (irreducible) self-energy $\Sigma[G]$.

As mentioned in Sect. 4.1, a simplification occurs if we can set $t_0 \rightarrow -\infty$. If the interactions are coupled adiabatically, the contribution from the $[t_0, t_0 - i\beta]$ piece vanishes. The information lost by this procedure is related to initial correlations. In many physical situations, for example, in steady state transport, it appears plausible that the initial correlations have been washed out by the interactions when one reaches the steady state. On the contrary, if one studies transient response, the role of initial correlations can be important. This represents an interesting problem, which so far has received only limited attention [215, 363]. Also, more recently, important developments have appeared, which include the complex part of the contour in numerical implementations [89–91, 235]. – Here we consider the $t_0 \rightarrow -\infty$ limit. In this limit the contours C and C_v coincide, and we can consider only C .

Langreth Theorem. In considering the Dyson equation (4.27) we encounter terms with the structure $C = AB$, or, explicitly,

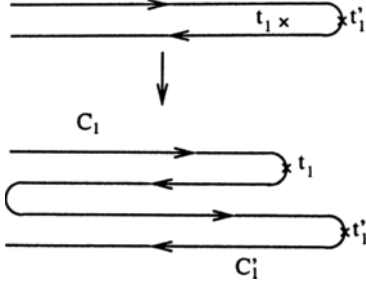
$$C(t_1, t_{1'}) = \int_C d\tau A(t_1, \tau) B(\tau, t_{1'}) , \quad (4.28)$$

and their generalizations involving products of three (or more) terms. Since we are presently only concerned with temporal variables, we suppress all other variables (spatial, spin, etc.), which have an obvious matrix structure. To evaluate (4.28) let us assume for definiteness that t_1 is on the first half of C , and that $t_{1'}$ is on the latter half (Fig. 4.2). In view of our discussion in connection with (4.16)–(4.21), we are thus analyzing a “lesser” function.

The next step is to deform the contour as indicated in Fig. 4.4. Thus (4.28) becomes

$$\begin{aligned} C^<(t_1, t_{1'}) = & \int_{C_1} d\tau A(t_1, \tau) B^<(\tau, t_{1'}) \\ & + \int_{C'_1} d\tau A^<(t_1, \tau) B(\tau, t_{1'}) . \end{aligned} \quad (4.29)$$

energy, expressed as a function of the one-particle Green function, exists. Further, for functions of more than two external variables, the intuitive notation (“lesser,” retarded, etc.) would have to be generalized.

**Fig. 4.4.** Deformation of contour C

Here, in appending the sign $<$ to the function B in the first term, we made use of the fact that as long as the integration variable τ is confined on the contour C_1 it is less than (in the contour sense) $t_{1'}$. A similar argument applies to the second term. Now consider the first term in (4.29) and split the integration into two parts:

$$\begin{aligned} \int_{C_1} d\tau A(t_1, \tau) B^<(\tau, t_{1'}) &= \int_{-\infty}^{t_1} dt A^>(t_1, t) B^<(t, t_{1'}) \\ &\quad + \int_{t_1}^{-\infty} dt A^<(t_1, t) B^<(t, t_{1'}) \\ &\equiv \int_{-\infty}^{\infty} dt A^r(t_1, t) B^<(t, t_{1'}) , \end{aligned} \quad (4.30)$$

where we used the definition of the retarded function (4.21). A similar analysis can be applied to the second term involving contour C'_1 ; this time the advanced function is generated. Putting the two terms together, we have the first of Langreth's results:

$$C^<(t_1, t_{1'}) = \int_{-\infty}^{\infty} dt [A^r(t_1, t) B^<(t, t_{1'}) + A^<(t_1, t) B^a(t, t_{1'})] . \quad (4.31)$$

The same result applies for the "greater" function: one just replaces all $<$'s by $>$'s.

It is easy to generalize the result (4.31) for a (matrix) product of three functions: If $D = ABC$ on the contour, then, on the real axis, one has

$$D^< = A^r B^r C^< + A^r B^< C^a + A^< B^a C^a . \quad (4.32)$$

Once again a similar equation holds for the "greater" functions.

One often needs the retarded (or advanced) component of a product of functions defined on the contour. The required expression is derived by repeated use of the definitions (4.16)–(4.21), and the result (4.31):

$$\begin{aligned} C^r(t_1, t_{1'}) &= \theta(t_1 - t_{1'}) [C^>(t_1, t_{1'}) - C^<(t_1, t_{1'})] \\ &= \theta(t_1 - t_{1'}) \int_{-\infty}^{\infty} dt [A^r(B^> - B^<) + (A^> - A^<)B^a] \end{aligned}$$

$$\begin{aligned}
&= \theta(t_1 - t_{1'}) \left[\int_{-\infty}^{t_1} dt (A^> - A^<) (B^> - B^<) \right. \\
&\quad \left. + \int_{-\infty}^{t_{1'}} dt (A^> - A^<) (B^< - B^>) \right] \\
&= \int_{t_{1'}}^{t_1} dt A^r(t_1, t) B^r(t, t_{1'}) . \tag{4.33}
\end{aligned}$$

In our compact notation this relation is expressed as $C^r = A^r B^r$.

When considering the various terms in the diagrammatic perturbation series one may also encounter terms where two Green function lines run (anti)parallel (this is the case, for example, of a polarization or electron–phonon self-energy (parallel fermion and boson Green functions). In this case one needs the “lesser” and/or retarded/advanced components of structures like

$$\begin{aligned}
C(\tau, \tau') &= A(\tau, \tau') B(\tau, \tau') , \\
D(\tau, \tau') &= A(\tau, \tau') B(\tau', \tau) , \tag{4.34}
\end{aligned}$$

where τ and τ' are contour variables. The derivation of the required formulae is similar to the analysis presented above, and is left for an exercise. One finds

$$\begin{aligned}
C^<(t, t') &= A^<(t, t') B^<(t, t') , \\
D^<(t, t') &= A^<(t, t') B^>(t', t) , \tag{4.35}
\end{aligned}$$

and

$$\begin{aligned}
C^r(t, t') &= A^<(t, t') B^r(t, t') + A^r(t, t') B^<(t, t') + A^r(t, t') B^r(t, t') , \\
D^r(t, t') &= A^r(t, t') B^<(t', t) + A^<(t, t') B^a(t', t) \\
&= A^<(t, t') B^a(t', t) + A^r(t, t') B^<(t', t) . \tag{4.36}
\end{aligned}$$

As earlier, the relations (4.35) can immediately be generalized to “greater” functions. For a quick reference, we have collected the rules provided by the Langreth theorem in Table 4.1.

Equilibrium Electron–Phonon Self-Energy

The retarded electron–phonon self-energy Σ_{ph}^r is a central object in the analysis of many physical properties of metals and semiconductors. At finite temperatures one conventionally uses the Matsubara technique to perform the analytic continuation (for an extended discussion, see [254]). The Langreth theorem can be used to give a very compact derivation of Σ_{ph}^r . In lowest order in the electron–phonon matrix element M_q we have

$$\Sigma_{ph}(k, \tau, \tau') = i \sum_q |M_q|^2 G(k - q, \tau, \tau') D(q, \tau, \tau') . \tag{4.37}$$

Table 4.1. Rules for analytic continuation

Contour	Real axis
$C = \int_C AB$	$C^< = \int_t [A^r B^< + A^< B^a]$ $C^r = \int_t A^r B^r$
$D = \int_C ABC$	$D^< = \int_t [A^r B^r C^< + A^r B^< C^a + A^< B^a C^a]$ $D^r = \int_t A^r B^r C^r$
$C(\tau, \tau') = A(\tau, \tau')B(\tau, \tau')$	$C^<(\tau, \tau') = A^<(\tau, \tau')B^<(\tau, \tau')$ $C^r(\tau, \tau') = A^<(\tau, \tau')B^r(\tau, \tau') + A^r(\tau, \tau')B^<(\tau, \tau')$ $+ A^r(\tau, \tau')B^r(\tau, \tau')$
$D(\tau, \tau') = A(\tau, \tau')B(\tau', \tau)$	$D^<(\tau, \tau') = A^<(\tau, \tau')B^>(\tau', \tau)$ $D^r(\tau, \tau') = A^<(\tau, \tau')B^a(\tau', \tau) + A^r(\tau, \tau')B^<(\tau', \tau)$

Here G is the free-electron Green function while D is the free-phonon Green function. Equation (4.37) is in a form where we can apply (4.36). In equilibrium all quantities depend on time only through the difference of the two time labels, and it is advantageous to work in frequency space. Performing the Fourier transform gives

$$\Sigma_{\text{ph}}^r(k, \omega) = i \int \frac{d\varepsilon}{2\pi} \sum_q |M_q|^2 [G^<(k - q, \omega - \varepsilon) D^r(q, \varepsilon) + G^r(k - q, \omega - \varepsilon) D^<(q, \varepsilon) + G^r(k - q, \omega - \varepsilon) D^r(q, \varepsilon)]. \quad (4.38)$$

The expressions for the free equilibrium Green functions are (the reader is urged to verify these relations!)

$$\begin{aligned} D^<(q, \omega) &= -2\pi i[(N_q + 1)\delta(\omega + \omega_q) + N_q\delta(\omega - \omega_q)], \\ D^r(q, \omega) &= \frac{1}{\omega - \omega_q + i\eta} - \frac{1}{\omega + \omega_q + i\eta}, \\ G^<(k, \omega) &= 2\pi i n_F(\omega)\delta(\omega - \varepsilon_k), \\ G^r(k, \omega) &= \frac{1}{\omega - \varepsilon_k + i\eta}. \end{aligned} \quad (4.39)$$

Substituting these expressions in (4.38), one finds after some straightforward algebra

$$\Sigma_{\text{ph}}^r(k, \omega) = \sum_q |M_q|^2 \left[\frac{N_q - n_F(\varepsilon_{k-q}) + 1}{\omega - \omega_q - \varepsilon_{k-q} + i\eta} + \frac{N_q + n_F(\varepsilon_{k-q})}{\omega + \omega_q - \varepsilon_{k-q} + i\eta} \right]. \quad (4.40)$$

The shortness of this derivation, as compared with the standard one, nicely illustrates the formal power embedded in the Langreth theorem.

Basic Quantum Kinetic Equations

Summary. The basic quantum kinetic equation which describes the time evolution of the particle propagator (or, the lesser Green function) $G^<$ is discussed in the formulations due to Kadanoff-Baym and due to Keldysh.

5.1 Introductory Remarks

The task of this chapter is to introduce the equations-of-motion (in real time) for the nonequilibrium Green functions (NEGF). These equations will form the basis of all subsequent developments. There are two different, but equivalent, formulations: The Kadanoff–Baym method, and the Keldysh method, and the final results are given by (5.7) and (5.11), respectively. Both of these approaches are treated in Sects. 5.1 and 5.2 separately. We have chosen not to retrace the original derivations but rather use the analytic continuation rules developed in the previous section, since this approach allows a concise and systematic derivation.

5.2 The Kadanoff–Baym Formulation

The starting point of the derivation is the differential form of the Dyson equation (4.27):

$$\begin{aligned} & \left\{ i \frac{\partial}{\partial \tau_1} - \left[-\frac{1}{2} \nabla_{x_1}^2 + U(\mathbf{x}_1, \tau_1) \right] \right\} G(\mathbf{x}_1, \tau_1, \mathbf{x}_{1'}, \tau_{1'}) \\ &= \delta(1 - 1') + \int_C d\sigma \int d^3y \Sigma(\mathbf{x}_1, \tau_1, \mathbf{y}, \sigma) G(\mathbf{y}, \sigma, \mathbf{x}_{1'}, \tau_{1'}) , \\ & \left\{ -i \frac{\partial}{\partial \tau_{1'}} - \left[-\frac{1}{2} \nabla_{x_{1'}}^2 + U(\mathbf{x}_{1'}, \tau_{1'}) \right] \right\} G(\mathbf{x}_1, \tau_1, \mathbf{x}_{1'}, \tau_{1'}) \\ &= \delta(1 - 1') + \int_C d\sigma \int d^3y G(\mathbf{x}_1, \tau_1, \mathbf{y}, \sigma) \Sigma(\mathbf{y}, \sigma, \mathbf{x}_{1'}, \tau_{1'}) . \quad (5.1) \end{aligned}$$

In what follows, it is more convenient to use a notation where a product of two terms is interpreted as a matrix product in the internal variables (space, time, spin, etc.). Quantities depending on only one variable (examples of such objects are G_0 and U) are diagonal in this representation. Hence, we write (5.1) as

$$\begin{aligned} (G_0^{-1} - U)G &= 1 + \Sigma G, \\ G(G_0^{-1} - U) &= 1 + G\Sigma. \end{aligned} \quad (5.2)$$

Our aim is to obtain an equation for the correlation functions $G^{<,>}$. Thus, applying the rule (4.31) we find

$$\begin{aligned} (G_0^{-1} - U)G^< &= \Sigma^r G^< + \Sigma^< G^a, \\ G^<(G_0^{-1} - U) &= G^r \Sigma^< + G^< \Sigma^a. \end{aligned} \quad (5.3)$$

One should note that the delta-function term in (5.2) vanishes identically, because the time-labels required in the construction of $G^<$ are, by definition, on different branches of the contour.

We next subtract these equations from each other:

$$[G_0^{-1} - U, G^<] = \Sigma^r G^< + \Sigma^< G^a - G^r \Sigma^< - G^< \Sigma^a. \quad (5.4)$$

We use the identities

$$\begin{aligned} A^r &\equiv \frac{1}{2}(A^r + A^a) + \frac{1}{2}(A^r - A^a), \\ A^a &\equiv \frac{1}{2}(A^a + A^r) + \frac{1}{2}(A^a - A^r) \end{aligned} \quad (5.5)$$

to symmetrize the terms involving the retarded or advanced functions on the right-hand side of (5.4). After some rearrangement of the various terms, we arrive at

$$\begin{aligned} [G_0^{-1} - U, G^<] - [\Sigma, G^<] - [\Sigma^<, G] \\ = \frac{1}{2}\{\Sigma^r - \Sigma^a, G^<\} - \frac{1}{2}\{G^r - G^a, \Sigma^<\}. \end{aligned} \quad (5.6)$$

Here we defined $\Sigma \equiv \frac{1}{2}(\Sigma^r + \Sigma^a)$ and $G \equiv \frac{1}{2}(G^r + G^a)$, and the curly brackets indicate an anticommutator. The right-hand side of (5.6) is not yet quite in the form we want to write it in. In equilibrium theory we have encountered the spectral function $a = -2\text{Im}g^r = i(g^r - g^a)$, and the imaginary part of the self-energy, $\gamma = -2\text{Im}\sigma^r = i(\sigma^r - \sigma^a)$. These objects can be generalized to nonequilibrium theory: $A \equiv i(G^r - G^a)$, and $\Gamma \equiv i(\Sigma^r - \Sigma^a)$. Using this notation we get

$$\begin{aligned} [G_0^{-1} - U, G^<] - [\Sigma, G^<] - [\Sigma^<, G] &= \frac{1}{2i}\{\Gamma, G^<\} - \frac{1}{2i}\{A, \Sigma^<\} \\ &= \frac{1}{2}\{\Sigma^>, G^<\} - \frac{1}{2}\{G^>, \Sigma^<\}. \end{aligned} \quad (5.7)$$

In the second line we used the relation $G^r - G^a = G^> - G^<$, and an analogous relation for the self-energy. Equation (5.7) is the (generalized) Kadanoff–Baym

equation (GKB), and it will form the basis of much of our subsequent discussion. One can also derive a GKB equation for the “greater” function $G^>$; it differs from (5.7) only on the left-hand side, where all $<$'s should be replaced with $>$ s, while the right-hand side coincides with the second line of (5.7). By subtracting the equations for $G^{<,>}$ one obtains an equation for the nonequilibrium spectral function A :

$$[G_0^{-1} - U - \Sigma, A] - [\Gamma, G] = 0. \quad (5.8)$$

This relation finds occasional use as a consistency check.

Before turning to specific applications, let us make a few comments of more a general nature. First, to have a closed set of equations, GKB must be supplemented with Dyson equations for $G^{r,a}$. The nonequilibrium Dyson equations are formally identical to the equilibrium Dyson equations; this follows from the analytical continuation rules of the previous chapter. Quite often the calculation splits into two stages; one first solves (or attempts to solve!) the Dyson equations for $G^{r,a}$, and uses the results as inputs for the GKB equation. There is a catch, however. One may encounter situations where the Dyson equations for $G^{r,a}$ also involve $G^{<,>}$; an example is the retarded electron–phonon self-energy, which, in addition to retarded functions, also involves the correlation function [e.g., (4.36)]. This leads to extreme complications, because in this case the Dyson equation and the GKB equation must be solved simultaneously.

The structure of the GKB is that of a transport equation, albeit in a somewhat disguised form. The correlation function $G^<$ corresponds in a sense to a generalized distribution function, even though one should avoid a literal interpretation; we elaborate this point further below. As we shall see, the first commutator on the left-hand side gives rise to a (generalized) driving term. The next two terms are renormalization terms. Finally, the terms on the right-hand side lead to a quantum collision term. As a side remark we may mention that the GKB equation is still exact and reversible. The irreversible behavior predicted by the Boltzmann equation is only introduced after certain approximations are made on the GKB.

In deriving the GKB equation we formed the difference of the two equations (5.1). One may wonder whether any information was lost in this process. The answer is positive: the GKB equation, as a transport equation, can determine the time evolution of a (generalized) distribution function, but it does not tell what are the consistent initial values for this distribution function. This information is contained in the original Dyson equations (5.1), and was lost in the derivation. Thus, in principle, the GKB equation should be supplemented with another equation, for example, the sum of the two equations (5.1). Below we shall see examples of how this works in practice.

5.3 Keldysh Formulation

For certain applications it is advantageous to write the Boltzmann equation as an integral equation, rather than an integro-differential equation (an

application is discussed in Chaps. 10 and 12). An analogous situation holds in quantum kinetics: instead of working with the GKB equation (5.7), it may be useful to consider its integral form. Historically, Keldysh [198] derived this alternative form almost simultaneously, and independently of Kadanoff and Baym. (Of course, both Kadanoff–Baym and Keldysh techniques have their roots in pioneering work of the Schwinger school, see [17, 18, 316].)

Keldysh and Kadanoff–Baym methods are equivalent, and for the sake of completeness we now derive the Keldysh integral equation. Rather than following Keldysh’s original treatment we apply the analytic continuation rules (Table 4.1) on the complex time Dyson equation, and after some rearrangement end up with a variation of the Keldysh equation. Thus, applying the rule (4.32) on (4.27)¹ yields

$$G^< = G_0^< + G_0^r \Sigma^r G^< + G_0^r \Sigma^< G^a + G_0^< \Sigma^a G^a . \quad (5.9)$$

We proceed by iteration with respect to $G^<$. Iterating once, and regrouping the terms we obtain

$$\begin{aligned} G^< = & (1 + G_0^r \Sigma^r) G_0^< (1 + \Sigma^a G^a) + (G_0^r + G_0^r \Sigma^r G_0^r) \Sigma^< G^a \\ & + G_0^r \Sigma^r G_0^r \Sigma^r G^< . \end{aligned} \quad (5.10)$$

The form of (5.10) is very suggestive, and it is easy to convince oneself that the infinite order iterate is

$$G^< = (1 + G^r \Sigma^r) G_0^< (1 + \Sigma^a G^a) + G^r \Sigma^< G^a . \quad (5.11)$$

Equation (5.11) is equivalent to Keldysh’s result. In the original work, however, it was written for another function, $G_K \equiv G^< + G^>$. This difference is only of minor significance.

The relation between the Keldysh equation and the GKB equation is analogous to the relation between an ordinary differential equation plus a boundary condition and the corresponding integral equation. It seems to be a matter of convenience which starting point one should choose.

¹ For simplicity we suppress the single-body potential: it can, with a suitable redefinition, be absorbed in the free Green function. The reader is urged to check how this works out in practice.

Boltzmann Limit

Summary. We demonstrate how one recovers the Boltzmann equation from the quantum kinetic equation by a gradient expansion which holds if the variation of the center-of-mass coordinates is slow compared to that of the relative coordinates. Furthermore, it is necessary for this recovery that the spectral functions are sufficiently sharp.

6.1 Gradient Expansion

The Boltzmann equation is expected to be valid for slow spatial and temporal variations. We thus need a device for separating the “fast” quantum variations from “slow” macroscopic variations. This separation is achieved by two steps: we first introduce so-called Wigner coordinates and then perform a systematic gradient expansion. The lowest order gradient approximation combined with the quasiparticle approximation, to be discussed below, leads then to the Boltzmann equation.

The natural question one faces in connection with all expansions is the query about the convergence, or domain of validity of such an expansion. In metal physics one can identify [287] small parameters, such as q/k_F (here q is the characteristic wavelength of the external potential, and k_F is the Fermi wavevector) and ω/ε_F (ω is the external frequency while ε_F is Fermi energy). A systematic theory, the so-called quasiclassical theory, based on these small parameters has been constructed and it has reached a high level of sophistication.

In the physics of semiconductor microstructures the situation is less clear. There is no “big” energy, such as the Fermi energy, because of the lower charge density. If one considers excitations from valence band to conduction band, the energy of the exciting photon is at least as big as the energy gap. One often considers room temperature situations, which implies that $k_B T \simeq 30$ meV, which is of the same order as typical Fermi energies. Thus all four (ε_F , $\hbar\omega$, $k_B T$, and E_g) easily identified energies are of the same

order of magnitude, and there is no obvious small energy parameter. A similar situation holds for spatial scales: If one considers tunneling structures, the characteristic length scale of the heterostructure potential is of the same order as the de Broglie wavelength of the charge carriers, and no small length parameter exists. In later chapters we shall discuss the conditions for the validity of the derived expressions, but here we adopt the philosophy that the physics is such that the first nonvanishing order in the gradient expansion is sufficient. This order of approximation is sufficient for a formal derivation of the Boltzmann equation, but it is important to keep in mind that the validity of the Boltzmann equation for semiconductor systems, despite its enormous success in the interpretation of experimental data, is not at all an obvious fact, as the analysis presented in [331, 332] reveals.

The transformation to Wigner coordinates proceeds as follows. First one transforms to center-of-mass and difference variables:

$$\begin{aligned} \mathbf{r} &= \mathbf{x}_1 - \mathbf{x}_{1'} , & \mathbf{R} &= \frac{1}{2}(\mathbf{x}_1 + \mathbf{x}_{1'}), \\ t &= t_1 - t_{1'} , & T &= \frac{1}{2}(t_1 + t_{1'}) . \end{aligned} \quad (6.1)$$

The variables \mathbf{r} and t vary on a fast, microscopic scale, and must be treated exactly (after Fourier transforms, $\mathbf{r} \leftrightarrow \mathbf{p}$, $t \leftrightarrow \omega$), while \mathbf{R} and T are macroscopic, slow variables with small gradients, and hence are treated approximately.

The systematic derivation of the gradient approximation is somewhat tedious, and is discussed as an example below. However, the final result can be summarized compactly. The various terms in the GKB have the following structure:

$$C(\mathbf{x}_1, t_1, \mathbf{x}_{1'}, t_{1'}) = \int d\mathbf{x} ds A(\mathbf{x}_1, t_1, \mathbf{x}, s) B(\mathbf{x}, s, \mathbf{x}_{1'}, t_{1'}) . \quad (6.2)$$

Expressed in terms of the new variables $(\mathbf{p}, \omega, \mathbf{R}, T)$, this becomes

$$C(\mathbf{p}, \omega, \mathbf{R}, T) = A(\mathbf{p}, \omega, \mathbf{R}, T) \mathcal{G}(\mathbf{p}, \omega, \mathbf{R}, T) B(\mathbf{p}, \omega, \mathbf{R}, T) , \quad (6.3)$$

where the gradient operator \mathcal{G} is defined as

$$\mathcal{G}(\mathbf{p}, \omega, \mathbf{R}, T) \equiv \exp\left(\frac{1}{2i}[\partial_T^A \partial_\omega^B - \partial_\omega^A \partial_T^B - \partial_R^A \cdot \partial_p^B + \partial_p^A \cdot \partial_R^B]\right) . \quad (6.4)$$

The superscripts (A, B) indicate which term in the product AGB is to be differentiated.

In the lowest nonvanishing order we get the following prescription for evaluating commutators and anticommutators:

$$\begin{aligned} [A, B]_{\mathbf{p}, \omega, \mathbf{R}, T} &= -i \left(\frac{\partial A}{\partial T} \frac{\partial B}{\partial \omega} - \frac{\partial A}{\partial \omega} \frac{\partial B}{\partial T} - \frac{\partial A}{\partial \mathbf{R}} \cdot \frac{\partial B}{\partial \mathbf{p}} + \frac{\partial A}{\partial \mathbf{p}} \cdot \frac{\partial B}{\partial \mathbf{R}} \right) , \\ \{A, B\}_{\mathbf{p}, \omega, \mathbf{R}, T} &= 2A(\mathbf{p}, \omega, \mathbf{R}, T)B(\mathbf{p}, \omega, \mathbf{R}, T) . \end{aligned} \quad (6.5)$$

Equations (6.5) constitute the gradient expansion.

Derivation of the Gradient Expansion

For simplicity we consider here only the temporal variables; the spatial variables can be treated identically. We need to evaluate the Fourier transform of

$$C(t, T) = \int ds A(t_1 - s, T + \frac{1}{2}[s - t_1']) B(s - t_1', T + \frac{1}{2}[s - t_1]) . \quad (6.6)$$

To do this we expand A and B in the (small) gradients of the center-of-mass variable:

$$\begin{aligned} A(t_1 - s, T + \frac{1}{2}[s - t_1']) &= \sum_{n=0}^{\infty} \frac{1}{n!} [\frac{1}{2}(s - t_1')]^n A^{(n)}(t_1 - s, T) , \\ B(s - t_1', T + \frac{1}{2}[s - t_1]) &= \sum_{m=0}^{\infty} \frac{1}{m!} [\frac{1}{2}(s - t_1)]^m B^{(m)}(s - t_1', T) , \end{aligned} \quad (6.7)$$

where $A^{(n)}$ stands for the n th derivative with respect to the center-of-mass variable. The Fourier transform is defined by

$$C(\omega, T) = \int d(t_1 - t_1') e^{i\omega(t_1 - t_1')} \int ds AB , \quad (6.8)$$

where the variable structure of $\int ds AB$ is the same as in (6.6). The integrand has a convolution structure, and hence its Fourier transform factorizes. By using (6.7), one can evaluate (6.6) term by term. The zeroth order term (no gradients) is simply $C_0(\omega, T) = A(\omega, T)B(\omega, T)$, and the first order term is

$$C_1(\omega, T) = \frac{1}{2i} \left(\frac{\partial A(\omega, T)}{\partial T} \frac{\partial B(\omega, T)}{\partial \omega} - \frac{\partial A(\omega, T)}{\partial \omega} \frac{\partial B(\omega, T)}{\partial T} \right) . \quad (6.9)$$

This result is easily generalized to n th order, and formally resummed to generate the gradient operator \mathcal{G} defined in the main text.

6.2 Quasiparticle Approximation

In Sect. 6.1 we considered the effects of a slowly varying (space and time) external perturbation. Here we make a further approximation: the interactions are assumed to be weak. As specific examples we may consider a weak electron–phonon coupling, or, as is done below, electrons scattering off a dilute concentration of impurities. From the smallness of the interaction it follows immediately that the second and third commutator on the left-hand side of Kadanoff–Baym equation (5.7) can be discarded: they are of second order in small quantities, because they involve a small gradient *and* a small interaction. Let us next evaluate the spectral function in the present level of approximation. From the Dyson equation for the retarded and advanced Green function, it follows, within the gradient approximation, that the spectral function $A = i(G^r - G^a)$ is given by

$$A(\mathbf{p}, \omega, \mathbf{R}, T) = -2\text{Im} \left[\frac{1}{\omega - \varepsilon(\mathbf{p}) - U(\mathbf{R}, T) - \Sigma^r(\mathbf{p}, \omega, \mathbf{R}, T)} \right] . \quad (6.10)$$

In the lowest order we must take $\Sigma^r \rightarrow -i\eta$, and thus

$$A_0(\mathbf{p}, \omega, \mathbf{R}, T) = 2\pi\delta[\omega - \varepsilon(\mathbf{p}) - U(\mathbf{R}, T)]. \quad (6.11)$$

We refer to this relation as the quasiparticle approximation. A more refined treatment based on (6.10) would lead to *renormalized* transport coefficients. Finally, it is instructive to note that the approximate solution (6.10) satisfies the exact consistency relation (5.8).

6.3 Recovery of the Boltzmann Equation

We now apply the gradient approximation (6.5) and the lowest order spectral function (6.11) to the GKB equation. To obtain explicit results, we must specify the scattering mechanism, and we choose electron-dilute impurity scattering. The interaction is treated on the level of a self-consistent Born approximation, which implies the following self-energy functional (Sect. 3.6.2)

$$\Sigma^{<,>}(\mathbf{p}, \omega, \mathbf{R}, T) = c \sum_{\mathbf{q}} |V(\mathbf{p} - \mathbf{q})|^2 G^{<,>}(\mathbf{q}, \omega, \mathbf{R}, T). \quad (6.12)$$

Instead of considering $G^{<,>}$ it is advantageous to introduce a new function $F(\mathbf{p}, \omega, \mathbf{R}, T)$ defined via

$$\begin{aligned} G^<(\mathbf{p}, \omega, \mathbf{R}, T) &= iA(\mathbf{p}, \omega, \mathbf{R}, T)F(\mathbf{p}, \omega, \mathbf{R}, T), \\ G^>(\mathbf{p}, \omega, \mathbf{R}, T) &= -iA(\mathbf{p}, \omega, \mathbf{R}, T)[1 - F(\mathbf{p}, \omega, \mathbf{R}, T)]. \end{aligned} \quad (6.13)$$

This relation is entirely general: it satisfies the exact relation $G^< - G^> = iA$, and it merely replaces one unknown function by another. However, within the quasiparticle approximation (6.11) it would be redundant to consider functions $F(\mathbf{p}, \omega, \mathbf{R}, T)$ that depend on both ω and \mathbf{p} , and it is sufficient to consider a three-variable function, $f(\mathbf{p}, \mathbf{R}, T)$, which will play the role of a distribution function.¹ We thus write

$$\begin{aligned} G^<(\mathbf{p}, \omega, \mathbf{R}, T) &= iA_0(\mathbf{p}, \omega, \mathbf{R}, T)f(\mathbf{p}, \mathbf{R}, T) \\ &= 2\pi i\delta[\omega - \varepsilon(\mathbf{p}) - U(\mathbf{R}, T)]f(\mathbf{p}, \mathbf{R}, T), \end{aligned} \quad (6.14)$$

and analogously for $G^>$. With these ingredients the GKB equation reduces to (we use $[G_0^{-1} - U, A_0] = 0$)

$$\begin{aligned} i(A_0[G_0^{-1} - U, f])_{\mathbf{p}, \omega, \mathbf{R}, T} &= -c \sum_{\mathbf{q}} A_0(\mathbf{p}, \omega, \mathbf{R}, T)A_0(\mathbf{q}, \omega, \mathbf{R}, T) \\ &\quad \times |V(\mathbf{p} - \mathbf{q})|^2 [f(\mathbf{q}, \mathbf{R}, T) - f(\mathbf{p}, \mathbf{R}, T)]. \end{aligned} \quad (6.15)$$

¹ Technically, at this stage, the function f is a mere mathematical object, however, as we shall discuss in later chapters, it can be interpreted as a (generalized) distribution function.

It still remains to evaluate the commutator on the left-hand side of (6.15). We recall that

$$(G_0^{-1} - U)_{\mathbf{p}, \omega, \mathbf{R}, T} = \omega - \varepsilon(\mathbf{p}) - U(\mathbf{R}, T). \quad (6.16)$$

Using (6.5), and integrating over ω , we finally arrive at

$$\begin{aligned} & \frac{\partial f}{\partial T} + \frac{\partial \varepsilon}{\partial \mathbf{p}} \cdot \frac{\partial f}{\partial \mathbf{R}} + \left(-\frac{\partial U(\mathbf{R}, T)}{\partial \mathbf{R}} \right) \cdot \frac{\partial f}{\partial \mathbf{p}} \\ &= c \sum_{\mathbf{q}} 2\pi |V(\mathbf{p} - \mathbf{q})|^2 \delta[\varepsilon(\mathbf{q}) - \varepsilon(\mathbf{p})] [f(\mathbf{q}, \mathbf{R}, T) - f(\mathbf{p}, \mathbf{R}, T)], \end{aligned} \quad (6.17)$$

which we recognize as the standard impurity Boltzmann equation. Quantum mechanical corrections to the Boltzmann equation can be evaluated by relaxing some of the approximations made in this section, and this will be the task of many chapters to follow.

Gauge Invariance

Summary. A formulation of the quantum kinetic equation is given which is independent of the particular choice of the electrodynamic scalar and vector potentials. Because the evaluation of the collision term also requires the knowledge of the spectral Green functions, the gauge invariant equation for the retarded Green function is given as well.

7.1 Choice of Variables

Since the lowest nonvanishing order gradient approximation to the GKB equation results in the Boltzmann equation, a natural approach to look for corrections to the Boltzmann equation would be to proceed to the next order. Performing gradient approximations on GKB, however, involves some pitfalls. For example, the external electric field can be introduced in a variety of ways (scalar potential, vector potential, or a combination thereof) and a direct application of the gradient approximation rules (6.5) leads to different transport equations for different choices of the potentials. This is clearly unacceptable, and one must find a way which avoids these problems. This is achieved by formulating the theory in a gauge invariant manner. The gauge invariant functions (denoted by a tilde) are constructed with¹

$$\tilde{g}(\mathbf{k}, \omega, \mathbf{R}, T) = \int d^3r \int d\tau \exp[iw(\omega, \tau, T, \mathbf{k}, \mathbf{r}, \mathbf{R})] g(\mathbf{r}, \tau, \mathbf{R}, T), \quad (7.1)$$

¹ The rule (7.1) can be written in a covariant form, thus making its gauge invariance rather obvious. Thus, defining $p \equiv (\omega, \mathbf{k})$, $x \equiv (\tau, \mathbf{r})$, $X \equiv (T, \mathbf{R})$, and $A \equiv (\phi, \mathbf{A})$, and using the Einstein summation convention $a_\mu b_\mu = a_0 b_0 - \mathbf{a} \cdot \mathbf{b}$, we can rewrite (7.1) as $\tilde{g}(p, X) = \int d^4x \exp\{ix_\mu [p_\mu + \int_{-1/2}^{1/2} d\lambda q A_\mu(X + \lambda x)]\} g(x, X)$.

where

$$w(\omega, \tau, T, \mathbf{k}, \mathbf{r}, \mathbf{R}) = \int_{-\frac{1}{2}}^{\frac{1}{2}} d\lambda \left\{ \tau [\omega + q\phi(\mathbf{R} + \lambda \mathbf{r}, T + \lambda\tau)] - \mathbf{r} \cdot [\mathbf{k} + q\mathbf{A}(\mathbf{R} + \lambda \mathbf{r}, T + \lambda\tau)] \right\}. \quad (7.2)$$

Here q is the charge of the particles, and $g(\mathbf{r}, \tau, \mathbf{R}, T) \propto \langle \psi(\mathbf{R} + \mathbf{r}/2, T + \tau/2) \psi^\dagger(\mathbf{R} - \mathbf{r}/2, T - \tau/2) \rangle$ is any of the one-particle Green functions discussed in previous sections. Further, we use the center-of-mass and difference variables introduced in (6.1). Further, $\phi(\mathbf{R}, T)$ and $\mathbf{A}(\mathbf{R}, T)$ are the scalar and vector potentials, respectively, and the electric and magnetic fields are computed according to (we set the velocity of light equal to unity, $c = 1$)

$$\begin{aligned} \mathbf{E}(\mathbf{R}, T) &= -\nabla\phi(\mathbf{R}, T) - \frac{\partial \mathbf{A}(\mathbf{R}, T)}{\partial T}, \\ \mathbf{B}(\mathbf{R}, T) &= \nabla \times \mathbf{A}(\mathbf{R}, T), \end{aligned} \quad (7.3)$$

as usual.

We shall now prove that functions transformed according to (7.1) and (7.2) are gauge invariant, i.e., they remain unchanged under the transformation

$$\begin{aligned} \mathbf{A}(\mathbf{x}, t) &\rightarrow \mathbf{A}'(\mathbf{x}, t) = \mathbf{A}(\mathbf{x}, t) + \nabla\chi(\mathbf{x}, t), \\ \phi(\mathbf{x}, t) &\rightarrow \phi'(\mathbf{x}, t) = \phi(\mathbf{x}, t) - \frac{\partial\chi(\mathbf{x}, t)}{\partial t}, \end{aligned} \quad (7.4)$$

where $\chi(\mathbf{x}, t)$ is an arbitrary scalar function. This transformation leaves the physical fields $\mathbf{E}(\mathbf{R}, T)$ and $\mathbf{B}(\mathbf{R}, T)$ unchanged, and is hence called a gauge transformation. From elementary quantum mechanics (see Sect. 12.4 in [225]) we recall that the wavefunction $\psi'(\mathbf{x}, t)$ in the new gauge is related to the wavefunction in the original gauge by

$$\psi'(\mathbf{x}, t) = \exp[iq\chi(\mathbf{x}, t)]\psi(\mathbf{x}, t),$$

where q is the charge of the particles. The same transformation rule holds for the second quantized field operators in the definition of the Green functions. The rule (7.1) then becomes:

$$\begin{aligned} \tilde{g}'(\mathbf{k}, \omega, \mathbf{R}, T) &= \int d^3r \int d\tau \exp[iw'(\omega, \tau, T, \mathbf{k}, \mathbf{r}, \mathbf{R})] g'(\mathbf{r}, \tau, \mathbf{R}, T) \\ &= \int d^3r \int d\tau \exp[i(w + \Delta w)] g(\mathbf{r}, \tau, \mathbf{R}, T) \\ &\quad \times \exp\left\{iq[\chi(\mathbf{R} + \mathbf{r}/2, T + \tau/2) - \chi(\mathbf{R} - \mathbf{r}/2, T - \tau/2)]\right\}, \end{aligned} \quad (7.5)$$

where Δw is given by

$$\begin{aligned}\Delta w(\mathbf{r}, \tau, \mathbf{R}, T) = -q \int_{-1/2}^{1/2} d\lambda & \left[\tau \frac{\partial \chi(\mathbf{R} + \lambda \mathbf{r}, T + \lambda \tau)}{\partial \tau} \right. \\ & \left. + \mathbf{r} \cdot \nabla \chi(\mathbf{R} + \lambda \mathbf{r}, T + \lambda \tau) \right].\end{aligned}\quad (7.6)$$

In order to maintain gauge invariance \tilde{g}' must equal \tilde{g} , and hence Δw must cancel the exponential factor in the third line of (7.5). This is indeed the case, because Δw can be expressed as a total derivative:

$$\begin{aligned}\Delta w = -q \int_{-1/2}^{1/2} d\lambda & \frac{d\chi(\mathbf{x}(\lambda), t(\lambda))}{d\lambda} \\ = -q[\chi(\mathbf{R} + \mathbf{r}/2, T + \tau/2) & - \chi(\mathbf{R} - \mathbf{r}/2, T - \tau/2)],\end{aligned}\quad (7.7)$$

and we see that the cancellation occurs.

7.2 Gauge Invariant Quantum Kinetic Equation

We shall next apply the transformation (7.1) to the Kadanoff–Baym transport equation. For simplicity, here we consider explicitly a static and spatially uniform electric field. In later sections we shall address time-varying and/or spatially inhomogeneous driving fields. One can choose to perform the calculation either in the scalar potential gauge, $\phi(\mathbf{R}, T) = -\mathbf{R} \cdot \mathbf{E}$, or in the vector potential gauge with $\mathbf{A}(\mathbf{R}, T) = -T\mathbf{E}$. For these potentials the general rule (7.1) reduces to

$$\tilde{g}(\mathbf{k}, \omega, \mathbf{R}, T) = \int d\tau d\mathbf{r} \exp[i(\omega - q\mathbf{E} \cdot \mathbf{R})\tau - i\mathbf{k} \cdot \mathbf{r}] g_\phi(\mathbf{r}, \tau, \mathbf{R}, T) \quad (7.8)$$

and

$$\tilde{g}(\mathbf{k}, \omega, \mathbf{R}, T) = \int d\tau d\mathbf{r} \exp[i\omega\tau - i(\mathbf{k} - q\mathbf{E}T) \cdot \mathbf{r}] g_A(\mathbf{r}, \tau, \mathbf{R}, T). \quad (7.9)$$

Here $g_{\phi(A)}$ is the Green function computed in the scalar (vector potential) gauge.

7.2.1 Driving Term

We first consider the calculation in the scalar potential gauge. The driving term $[G_0^{-1} - U, G^<]$ in terms of the $(\mathbf{x}, t, \mathbf{x}', t')$ variables is

$$\begin{aligned}[G_0^{-1} - U, G^<](\mathbf{x}, t, \mathbf{x}', t') = & \left\{ i \frac{\partial}{\partial t} + i \frac{\partial}{\partial t'} - \left[-\frac{1}{2}(\nabla^2 - \nabla'^2) \right. \right. \\ & \left. \left. + (U(\mathbf{x}) - U(\mathbf{x}')) \right] \right\} G^<(\mathbf{x}, t, \mathbf{x}', t').\end{aligned}\quad (7.10)$$

According to (7.1), we need to transform into the center-of-mass and relative variables $(\mathbf{r}, \tau, \mathbf{R}, T)$. The external potential corresponding to a steady and uniform electric field is $U(\mathbf{x}) = q\phi(\mathbf{x}) = -q\mathbf{x} \cdot \mathbf{E}$, and the driving term ($\equiv DT_\phi$) becomes

$$\begin{aligned} DT_\phi &= [G_0^{-1} - U, G_\phi^<](\mathbf{r}, \tau, \mathbf{R}, T) \\ &= \left[i \frac{\partial}{\partial T} + \frac{\partial}{\partial \mathbf{R}} \cdot \frac{\partial}{\partial \mathbf{r}} + q\mathbf{r} \cdot \mathbf{E} \right] G_\phi^<(\mathbf{r}, \tau, \mathbf{R}, T). \end{aligned} \quad (7.11)$$

The rest of the derivation is a direct calculation where, with the help of several partial integrations, one moves the various differentiations outside the integrals. Consider, for example, the term

$$\begin{aligned} &\int d\tau d\mathbf{r} \exp[i(\omega - q\mathbf{E} \cdot \mathbf{R})\tau - ik \cdot \mathbf{r}] \left[\frac{\partial}{\partial \mathbf{R}} \cdot \frac{\partial}{\partial \mathbf{r}} \right] G_\phi^<(\mathbf{r}, \tau, \mathbf{R}, T) \\ &= \int d\tau d\mathbf{r} \left[-\frac{\partial}{\partial \mathbf{r}} \exp[i(\omega - q\mathbf{E} \cdot \mathbf{R})\tau - ik \cdot \mathbf{r}] \right] \cdot \frac{\partial}{\partial \mathbf{R}} G_\phi^<(\mathbf{r}, \tau, \mathbf{R}, T) \\ &= ik \cdot \frac{\partial}{\partial \mathbf{R}} \tilde{G}^<(\mathbf{k}, \omega, \mathbf{R}, T) \\ &\quad - \int d\tau d\mathbf{r} \left\{ \left[ik \cdot \frac{\partial}{\partial \mathbf{R}} \right] \exp[i(\omega - q\mathbf{E} \cdot \mathbf{R})\tau - ik \cdot \mathbf{r}] \right\} G_\phi^<(\mathbf{r}, \tau, \mathbf{R}, T) \\ &= i \left[\mathbf{k} \cdot \frac{\partial}{\partial \mathbf{R}} + q\mathbf{E} \cdot \mathbf{k} \frac{\partial}{\partial \omega} \right] \tilde{G}^<(\mathbf{k}, \omega, \mathbf{R}, T). \end{aligned} \quad (7.12)$$

The other terms in (7.11) are treated similarly, and the final result for the gauge invariant driving term ($\equiv DT$) is

$$DT = i \left[\frac{\partial}{\partial T} + \mathbf{k} \cdot \frac{\partial}{\partial \mathbf{R}} + q\mathbf{E} \cdot \left(\frac{\partial}{\partial \mathbf{k}} + \mathbf{k} \frac{\partial}{\partial \omega} \right) \right] \tilde{G}^<(\mathbf{k}, \omega, \mathbf{R}, T). \quad (7.13)$$

It is also very instructive to consider the same calculation in the vector potential gauge. The driving term is now

$$\begin{aligned} DT_A &= \left[i \frac{\partial}{\partial T} + \frac{\partial}{\partial \mathbf{r}} \cdot \frac{\partial}{\partial \mathbf{R}} + iq\mathbf{E} \cdot \left(\tau \frac{\partial}{\partial \mathbf{r}} + T \frac{\partial}{\partial \mathbf{R}} \right) \right. \\ &\quad \left. - q^2 T \tau \mathbf{E}^2 \right] G_A^<(\mathbf{r}, \tau, \mathbf{R}, T). \end{aligned} \quad (7.14)$$

The required calculations are similar to the ones leading to (7.12), and we leave it to the reader to verify that (7.14) indeed leads to the gauge invariant driving term (7.13). The calculations presented above can be generalized to nonuniform and time-dependent electromagnetic fields [101, 237]. The details of the analysis in the general case are rather cumbersome and will not be

reproduced here. As an example, we give the result for a harmonically varying electric field $\mathbf{E}(T) = \mathbf{E} \exp[-i\Omega_0 T]$, and uniform magnetic field \mathbf{B} :

$$\begin{aligned}
DT &= i \left(\frac{\partial}{\partial T} + \mathbf{k} \cdot \nabla_{\mathbf{R}} \right) \tilde{G}^<(\mathbf{k}, \omega, \mathbf{R}, T) \\
&\quad + iq\mathbf{E}(T) \cdot \frac{\partial}{\partial \mathbf{k}} \int_{-1/2}^{1/2} ds \tilde{G}^<(\mathbf{k}, \omega - s\Omega_0, \mathbf{R}, T) \\
&\quad + q\mathbf{E}(T) \cdot \nabla_{\mathbf{R}} \frac{\partial}{\partial \omega} \int_{-1/2}^{1/2} ds s \tilde{G}^<(\mathbf{k}, \omega - s\Omega_0, \mathbf{R}, T) \\
&\quad + i \frac{q\mathbf{E}(T) \cdot \mathbf{k}}{\Omega_0} [\tilde{G}^<(\mathbf{k}, \omega + \Omega_0/2, \mathbf{R}, T) - \tilde{G}^<(\mathbf{k}, \omega - \Omega_0/2, \mathbf{R}, T)] \\
&\quad + i (\mathbf{k} \times q\mathbf{B}) \cdot \frac{\partial}{\partial \mathbf{k}} \tilde{G}^<(\mathbf{k}, \omega, \mathbf{R}, T) \\
&\quad + \frac{q^2 \mathbf{E}(T)^2}{\Omega_0} \frac{\partial}{\partial \omega} \int_{-1/2}^{1/2} ds s [\tilde{G}^<(\mathbf{k}, \omega - \Omega_0(s - 1/2), \mathbf{R}, T) \\
&\quad \quad - \tilde{G}^<(\mathbf{k}, \omega - \Omega_0(s + 1/2), \mathbf{R}, T)] \\
&\quad + q^2 \mathbf{E}(T) \cdot \left(\mathbf{B} \times \frac{\partial}{\partial \mathbf{k}} \right) \frac{\partial}{\partial \omega} \int_{-1/2}^{1/2} ds s \tilde{G}^<(\mathbf{k}, \omega - s\Omega_0, \mathbf{R}, T). \quad (7.15)
\end{aligned}$$

This rather formidable expression contains a number of interesting features. In the first line we recognize two standard terms, which we have already obtained when deriving (7.13). The second line reduces in the dc-limit to the normal Boltzmann electric field driving term; the present, more complicated form reflects the nonlocal form of quantum driving terms. The nonlocality is an essential feature of any nonuniform or time-dependent external potential. In Chap. 8 we shall see that the frequency integral of $\tilde{G}^<$ gives the Wigner distribution function. Thus, none of the terms in (7.15) that involve the operator $\partial/\partial\omega$ will contribute to the quantum kinetic equation for the Wigner function (which is obtained from (7.15) by integrating over ω). Since the Wigner distribution function in a sense represents the quantum mechanical generalization of the Boltzmann nonequilibrium distribution function, we infer that the terms with $\partial/\partial\omega$ are of quantum mechanical origin, and have no counterpart in the semiclassical Boltzmann language. The terms on the third, sixth, and the last line of (7.15) belong to this category. The term on the fourth line reduces in the dc-limit to the last term in (7.13). Finally, the term on the fifth line is the familiar driving term arising from the Lorentz force. Equation (7.15) should form the starting point for calculations of, say, high-frequency magneto-optical properties, and it would be very interesting to analyze the effect of the nonstandard terms of (7.13). To our knowledge, no such comparisons have yet been performed.

7.2.2 Collision Term

The collision integral for spatially inhomogeneous and time-dependent driving fields in its general form is very complicated. In order to gain some insight we continue to study the spatially homogeneous and time-independent case. We work in the vector potential gauge, and the reader is urged to repeat our analysis in the scalar potential gauge. All the terms in the collision integral (see, for example (5.4), or (5.7)) have the structure given in (6.2), which reduces in the spatially uniform case to

$$C(\mathbf{x}_1 - \mathbf{x}_{1'}, t_1, t_{1'}) = \int d\mathbf{x} ds A(\mathbf{x}_1 - \mathbf{x}, t_1, s) B(\mathbf{x} - \mathbf{x}_{1'}, s, t_{1'}) . \quad (7.16)$$

We analyze first the spatial variables and return to the temporal variables later. We also need the inverse of the transformation (7.9):

$$g_A(\mathbf{r}, \tau, T) = \int \frac{d\mathbf{k}}{(2\pi)^3} \exp[i(\mathbf{k} - q\mathbf{E}T) \cdot \mathbf{r}] \tilde{g}(\mathbf{k}, \tau, T) . \quad (7.17)$$

Substituting this in (7.16) leads to

$$\begin{aligned} C(\mathbf{x}_1 - \mathbf{x}_{1'}, t_1, t_{1'}) &= \int \frac{ds d\mathbf{k}_1}{(2\pi)^3} e^{i[\mathbf{k}_1 - (q/2)\mathbf{E}(t_1+s)] \cdot (\mathbf{x}_1 - \mathbf{x}_{1'})} \\ &\times \tilde{A}\left(\mathbf{k}_1, t_1 - s, \frac{t_1 + s}{2}\right) \tilde{B}\left(\mathbf{k}_1 - \frac{q}{2}\mathbf{E}(t_1 - t_{1'}), s - t_{1'}, \frac{s + t_{1'}}{2}\right) . \end{aligned} \quad (7.18)$$

The final step consists of applying the transformation (7.9), and we find

$$\begin{aligned} \tilde{C}(\mathbf{k}, \omega, T) &= \int d\tau d\tau' \tilde{A}\left[\mathbf{k} + \frac{q}{2}\mathbf{E}\left(\tau' + \frac{\tau}{2}\right), \frac{\tau}{2} - \tau', T + \frac{1}{2}\left(\tau' + \frac{\tau}{2}\right)\right] \\ &\times \tilde{B}\left[\mathbf{k} + \frac{q}{2}\mathbf{E}\left(\tau' - \frac{\tau}{2}\right), \frac{\tau}{2} + \tau', T + \frac{1}{2}\left(\tau' - \frac{\tau}{2}\right)\right] e^{i\omega\tau} . \end{aligned} \quad (7.19)$$

The intertwined momentum and time variables in (7.19) make its mathematical structure so complicated that it is difficult to make progress without some approximations. One can, for example, restrict the analysis to linear response [136, 254], when a gradient expansion of (7.19) can be developed, and in Chap. 9 we elaborate further on linear response. Another case where further simplification can be achieved is the analysis of a steady state system, when all dependence on the macroscopic time variable T can be ignored,² and all functions depend only on (\mathbf{k}, τ) (or, equivalently, on (\mathbf{k}, ω)). Here we give the

² One should note that even for time-independent fields the T -dependence may be important. This is the case, for example, if one studies the time-dependence of an initial nonequilibrium state under the influence of an external field.

gauge invariant transport equation for time-independent fields, but allowing the correlation functions to be time dependent:

$$\begin{aligned} i \left\{ \frac{\partial}{\partial T} + q \mathbf{E} \cdot \left[\frac{\partial}{\partial \mathbf{k}} + i\tau \mathbf{k} \right] \right\} \tilde{G}^<(\mathbf{k}, \tau, T) \\ = \int d\tau' \tilde{A}(\mathbf{k}_1, \tau_1, T_1) \tilde{B}(\mathbf{k}_2, \tau_2, T_2), \end{aligned} \quad (7.20)$$

where the shorthand $\tilde{A}\tilde{B}$ is defined by (see also (5.4))

$$\tilde{A}\tilde{B} = \tilde{\Sigma}^r \tilde{G}^< + \tilde{\Sigma}^< \tilde{G}^a - \tilde{G}^r \tilde{\Sigma}^< - \tilde{G}^< \tilde{\Sigma}^a, \quad (7.21)$$

with $\mathbf{k}_{1,2} \equiv \mathbf{k} + \frac{q}{2} \mathbf{E}(\tau' \pm \frac{\tau}{2})$, $\tau_{1,2} \equiv \frac{\tau}{2} \mp \tau'$, and $T_{1,2} \equiv T \pm \tau_{2,1}$. Equation (7.20) is our first encounter with a quantum kinetic equation. Special attention should be paid toward the complicated time dependence of the non-Markovian collision integral. This equation (and its subsequent generalizations) will play a central role in the rest of this book.

7.3 Retarded Green Function

The quantum kinetic equation must be supplemented with the nonequilibrium Dyson equation for the retarded Green function:

$$\begin{aligned} \left\{ i \frac{\partial}{\partial t} - \left[-\frac{1}{2} \nabla^2 + U(\mathbf{x}, t) \right] \right\} G^r(\mathbf{x}, t, \mathbf{x}', t') = \delta(t - t') \delta(\mathbf{x} - \mathbf{x}') \\ + \int d\mathbf{x}_1 dt_1 \Sigma^r(\mathbf{x}, t, \mathbf{x}_1, t_1) G^r(\mathbf{x}_1, t_1, \mathbf{x}', t') \end{aligned} \quad (7.22)$$

$$\begin{aligned} \left\{ -i \frac{\partial}{\partial t'} - \left[-\frac{1}{2} \nabla'^2 + U(\mathbf{x}', t') \right] \right\} G^r(\mathbf{x}, t, \mathbf{x}', t') = \delta(t - t') \delta(\mathbf{x} - \mathbf{x}') \\ + \int d\mathbf{x}_1 dt_1 G^r(\mathbf{x}, t, \mathbf{x}_1, t_1) \Sigma^r(\mathbf{x}_1, t_1, \mathbf{x}', t'). \end{aligned} \quad (7.23)$$

Instead of subtracting these equations from each other, as was done for the correlation function, it is now best to add them. The reason is that in the case of the retarded function it is important to keep the inhomogeneous term, i.e. the δ -function piece, because otherwise the necessary boundary condition cannot be properly accounted for. The boundary condition is provided by the equal-time anticommutation rule of the field operators, $G^r(\mathbf{x}, t, \mathbf{x}', t') \rightarrow -i\delta(\mathbf{x} - \mathbf{x}')$ as $t \rightarrow t^+$. In order to construct the gauge-invariant retarded Green function we follow the same procedure as the various driving terms are written in terms of the sum and difference variables, after which one applies the transformation (7.1). We leave the intermediate steps for an exercise, and give here the result for uniform and time-independent fields:

$$\left[\omega + \frac{q^2}{8} E^2 \frac{\partial^2}{\partial \omega^2} - \frac{k^2}{2} \right] \tilde{G}^r(\mathbf{k}, \omega) = 1 + \int d\tau d\tau' e^{i\omega\tau} \tilde{D}(\mathbf{k}_1, \tau_1) \tilde{E}(\mathbf{k}_2, \tau_2), \quad (7.24)$$

where

$$\tilde{D}\tilde{E} = \frac{1}{2}(\tilde{\Sigma}^r \tilde{G}^r + \tilde{G}^r \tilde{\Sigma}^r), \quad (7.25)$$

and, just as in the case of the quantum kinetic equation, $\mathbf{k}_{1,2} = \mathbf{k} + \frac{q}{2}\mathbf{E}(\tau' \pm \frac{\tau}{2})$, and $\tau_{1,2} = \frac{\tau}{2} \mp \tau'$. From (7.24) it follows that the *free* retarded field-dependent Green function ($\equiv \tilde{G}_E^r$) depends quadratically on the external field. To see this, consider (7.24) when interactions are turned off, $\Sigma^r \rightarrow 0$. Then the solution can be written as

$$\tilde{G}_E^r(\mathbf{k}, \omega) = \int d\tau e^{i\omega\tau} \tilde{G}_E^r(\mathbf{k}, \tau), \quad (7.26)$$

where

$$\tilde{G}_E^r(\mathbf{k}, \tau) = -i\theta(\tau) \exp[-i(k^2\tau/2 + q^2E^2\tau^3/24)]. \quad (7.27)$$

In Chap. 10, where we discuss high-field transport, we analyze further the consequences of (7.22)–(7.26).

Quantum Distribution Functions

Summary. The quantum kinetic equation is in the slowly-varying center-of-mass coordinate approximation expressed in terms of the Wigner function. The collision integral is simplified by means of the generalized Kadanoff–Baym ansatz formulated in a gauge invariant way which respects causality.

8.1 Relation to Observables, and the Wigner Function

The purpose of any useful formalism is to derive calculational methods for objects that can be related to measurable quantities. We will now establish a connection between the current density and the nonequilibrium Green functions. Similar derivations can be given to the observables encountered in later chapters. From elementary quantum mechanics we recall that the current density is calculated from Schrödinger wavefunctions $\psi(\mathbf{x}, t)$ with the prescription

$$\mathbf{j}(\mathbf{x}, t) = \frac{1}{2i} \lim_{\mathbf{x}' \rightarrow \mathbf{x}} (\nabla - \nabla') \psi^*(\mathbf{x}', t) \psi(\mathbf{x}, t). \quad (8.1)$$

In second quantization this relation becomes

$$\begin{aligned} \mathbf{j}(\mathbf{x}, t) &= \frac{1}{2i} \lim_{\mathbf{x}' \rightarrow \mathbf{x}} (\nabla - \nabla') \langle \psi^\dagger(\mathbf{x}', t) \psi(\mathbf{x}, t) \rangle \\ &= \frac{1}{2} \lim_{\mathbf{x}' \rightarrow \mathbf{x}} (\nabla' - \nabla) G^<(\mathbf{x}, t, \mathbf{x}', t). \end{aligned} \quad (8.2)$$

Thus the evaluation of the current requires the knowledge of the nonequilibrium lesser function $G^<$. In order to make a connection to the quantum kinetic equation derived in Chap. 7 we transform (8.2) in the center-of-mass and difference variables:

$$\begin{aligned} \mathbf{j}(\mathbf{R}, T) &= - \lim_{\mathbf{r} \rightarrow 0} \frac{\partial}{\partial \mathbf{r}} G^<(\mathbf{r}, \tau = 0, \mathbf{R}, T) \\ &= \int \frac{d\mathbf{k}}{(2\pi)^3} \int \frac{d\omega}{2\pi i} \mathbf{k} \tilde{G}^<(\mathbf{k}, \omega, \mathbf{R}, T). \end{aligned} \quad (8.3)$$

A similar analysis gives the relation between the number density $n(\mathbf{R}, T)$ and the lesser function:

$$n(\mathbf{R}, T) = \int \frac{d\mathbf{k}}{(2\pi)^3} \int \frac{d\omega}{2\pi i} \tilde{G}^<(\mathbf{k}, \omega, \mathbf{R}, T). \quad (8.4)$$

Examining (8.3) and (8.4) shows that they both relate an experimentally relevant object to the $\tau = 0$ component of $\tilde{G}^<(\mathbf{k}, \tau, \mathbf{R}, T)$. We note that

$$\begin{aligned} \tilde{G}^<(\mathbf{k}, \tau = 0, \mathbf{R}, T) &= \int \frac{d\omega}{2\pi} \tilde{G}^<(\mathbf{k}, \omega, \mathbf{R}, T) \\ &= i \int d\mathbf{r} e^{-i\mathbf{k}\cdot\mathbf{r}} \langle \psi^\dagger \left(\mathbf{R} - \frac{\mathbf{r}}{2}, T \right) \psi \left(\mathbf{R} + \frac{\mathbf{r}}{2}, T \right) \rangle \\ &\equiv i f^W(\mathbf{k}, \mathbf{R}, T), \end{aligned} \quad (8.5)$$

where $f^W(\mathbf{k}, \mathbf{R}, T)$ is the Wigner distribution function. A question then arises: Is it possible to develop a closed theory for the Wigner distribution alone? This would obviously be beneficial, since the f^W depends on one variable less than the lesser function $G^<$, and one might be able to avoid some complications. We can immediately find an equation for f^W by setting $\tau = 0$ in the quantum kinetic equation (7.20):

$$\begin{aligned} &\left[\frac{\partial}{\partial T} + q\mathbf{E} \cdot \frac{\partial}{\partial \mathbf{k}} \right] f^W(\mathbf{k}, T) \\ &= - \int d\tau' \tilde{A} \left(\mathbf{k} + \frac{q}{2} \mathbf{E} \tau', -\tau', T + \tau' \right) \tilde{B} \left(\mathbf{k} + \frac{q}{2} \mathbf{E} \tau', \tau', T + \tau' \right), \end{aligned} \quad (8.6)$$

where

$$\begin{aligned} &\tilde{A}(\mathbf{k}_1, \tau_1, T_1) \tilde{B}(\mathbf{k}_2, \tau_2, T_2) \\ &= [\tilde{\Sigma}^r \tilde{G}^< + \tilde{\Sigma}^< \tilde{G}^a - \tilde{G}^r \tilde{\Sigma}^< - \tilde{G}^< \tilde{\Sigma}^a](\mathbf{k}_1, \tau_1, T_1)(\mathbf{k}_2, \tau_2, T_2), \end{aligned} \quad (8.7)$$

and the variables $(\mathbf{k}_{1,2}, \tau_{1,2}, T_{1,2})$ can be identified from (8.6). Thus the collision integral depends on the full $\tilde{G}^<(\tau, T)$, and it is not possible to obtain a closed equation for f^W , unless one finds a way of “short-circuiting” the theory. This will be the task of Sect. 8.2.

8.2 Generalized Kadanoff–Baym Ansatz

The most obvious way to establish a link between the Wigner function and the correlation function would be to assume a relation between $G^<$ and f^W which has the same structure as (6.14), $G^< = iA f^W$, but where the spectral function is replaced by its nonequilibrium counterpart. This approach was used in early attempts to develop a nonequilibrium Green function theory for high electric field transport [178], where a *field-dependent* spectral function

was substituted in (6.14). While this approach may be useful to obtain some qualitative information, it was soon realized [170, 180] that there are some fundamental problems with it: when applied to problems which can be analyzed with other theoretical tools, such as linear response, it turned out that the results obtained with different methods did not always agree. A typical case was the linear electrical conductivity of electron–phonon systems: for this case extensive Kubo formula calculations had been performed by [157], and the nonequilibrium Green function formulae differed from the well-established Holstein formulae by certain factors of two. Likewise, the high-field transport equations obtained with density-matrix methods [238] and Green functions contained similar differences. Yet, the potential power of Green function formulations provided motivation for further research, and a few years later Lipavský et al. [246] found an expansion, whose first term removed the discrepancies between the different formulations. The first term in the expansion, which is called the Generalized Kadanoff–Baym ansatz (GKBA), has proven to be a fruitful starting point for further developments, and will be employed frequently in later chapters. It should be noted, however, that the precise range of validity of the GKBA, and its further improvements, are an active area of research (see, for example, [331, 332]).

We shall now derive the GKBA. Recall that the Wigner function is the time-diagonal part of the Green function: $f^W(T) = -iG^<(\tau = 0, T) = -iG^<(t = T, t' = T)$. The spatial variables do not play any role, and can be inserted after the analysis is completed. Thus the idea of the derivation is to isolate the time-diagonal part, and treat the rest as a perturbation. There is no small parameter at the outset, and one must address this issue after the completion of the derivation.

To begin with, we define the following auxiliary functions $G^{(r,a)(<,>)}$:

$$\begin{aligned} G^r(<,>)(t_1, t_2) &= \theta(t_1 - t_2)G^{<,>}(t_1, t_2), \\ G^a(<,>)(t_1, t_2) &= \theta(t_2 - t_1)G^{<,>}(t_1, t_2). \end{aligned} \quad (8.8)$$

Operate now by $(G^r)^{-1}$ from left on the first of equations (8.8):

$$\begin{aligned} (G^r)^{-1}G^{r<} &= \int d\bar{t} \left\{ \left[i\frac{\partial}{\partial t_1} - \varepsilon(\mathbf{p}) \right] \delta(t_1 - \bar{t}) - \Sigma^r(t_1, \bar{t}) \right\} G^{r<}(\bar{t}, t_2) \\ &= i\delta(t_1 - t_2)G^<(t_1, t_2) \\ &\quad + \theta(t_1 - t_2) \left\{ \left[i\frac{\partial}{\partial t_1} - \varepsilon(\mathbf{p}) \right] G^<(t_1, t_2) \right. \\ &\quad \left. - \int_{t_2}^{t_1} d\bar{t} \Sigma^r(t_1, \bar{t}) G^<(\bar{t}, t_2) \right\}. \end{aligned} \quad (8.9)$$

The first term on the right-hand side will lead to the Wigner function, since $i\delta(t_1 - t_2)G^<(t_1, t_2) = -\delta(t_1 - t_2)f^W(t_2)$. The term in curly brackets still

requires some work. Note first that it follows from the Keldysh equation (5.11) that $(G^r)^{-1}G^< = \Sigma^< G^a$, which reads explicitly

$$\begin{aligned} \left[i \frac{\partial}{\partial t_1} - \varepsilon(\mathbf{p}) \right] G^<(t_1, t_2) &- \int_{-\infty}^{t_1} d\bar{t} \Sigma^r(t_1, \bar{t}) G^<(\bar{t}, t_2) \\ &= \int_{-\infty}^{t_2} d\bar{t} \Sigma^<(t_1, \bar{t}) G^a(\bar{t}, t_2). \end{aligned} \quad (8.10)$$

We use this equation to eliminate the $G_0^{-1}G^<$ term from (8.9), and obtain

$$\begin{aligned} [(G^r)^{-1}G^r]^<(t_1, t_2) &= i\delta(t_1 - t_2)G^<(t_2, t_2) + \theta(t_1 - t_2) \\ &\times \int_{-\infty}^{t_2} d\bar{t} [\Sigma^r(t_1, \bar{t})G^<(\bar{t}, t_2) + \Sigma^<(t_1, \bar{t})G^a(\bar{t}, t_2)]. \end{aligned} \quad (8.11)$$

Finally, operating with G^r from the left, we arrive at

$$\begin{aligned} G^r^<(t_1, t_2) &= iG^r(t_1, t_2)G^<(t_2, t_2) \\ &+ \int_{t_2}^{t_1} d\bar{t} \int_{-\infty}^{t_2} d\bar{t}' G^r(t_1, \bar{t}) [\Sigma^r(\bar{t}, \bar{t}')G^<(\bar{t}', t_2) \\ &+ \Sigma^<(\bar{t}, \bar{t}')G^a(\bar{t}', t_2)]. \end{aligned} \quad (8.12)$$

The same analysis can be repeated for $(G^a)^<$ with the result

$$\begin{aligned} G^a^<(t_1, t_2) &= -iG^<(t_1, t_1)G^a(t_1, t_2) \\ &+ \int_{t_1}^{t_2} d\bar{t} \int_{-\infty}^{t_1} d\bar{t}' [G^<(t_1, \bar{t}')\Sigma^a(\bar{t}', \bar{t}) \\ &+ G^r(t_1, \bar{t}')\Sigma^<(\bar{t}', \bar{t})]G^a(\bar{t}, t_2). \end{aligned} \quad (8.13)$$

Since $G^< \equiv G^r^< + G^a^<$, these two equations allow, at least in principle, an iterative construction of $G^<(t_1, t_2)$ from its time-diagonal component, i.e., the Wigner function f^W . The first term gives the generalized Kadanoff–Baym ansatz, while the iterative corrections represent an expansion in terms of the various relaxation times in the system. For a further discussion of these matters we refer to [246]; here we concentrate on the first term. The two terms originating from (8.12) and (8.13) can be combined (we restrict ourselves to uniform fields, when it is convenient to work in the vector potential gauge, and insert the momentum label):

$$\begin{aligned} G^<(\mathbf{p}, t_1, t_2) &= iG^r(\mathbf{p}, t_1, t_2)G^<(\mathbf{p}, t_2, t_2) \\ &- iG^<(\mathbf{p}, t_1, t_1)G^a(\mathbf{p}, t_1, t_2). \end{aligned} \quad (8.14)$$

This equation is in a form which is suitable for further developments. For example, in Part III we analyze high-field transport using it, and in Part IV we generalize it to a two-band model. It is sometimes useful to express (8.14)

in terms of the gauge invariant variables discussed earlier in this section. The generalization of (7.9) to time-dependent fields, which follows immediately from the rule (7.1) and (7.2) says that

$$\tilde{g}(\mathbf{k}, \tau, T) = g_A \left(\mathbf{p} = \mathbf{k} + \int_{-1/2}^{1/2} d\lambda q \mathbf{A}[T + \lambda\tau], \tau, T \right). \quad (8.15)$$

The retarded and advanced functions in (8.14) are readily transformed according to (8.15), but the correlation functions, which have *equal* time labels require some care. Writing the time labels explicitly, we proceed as follows [consider, for example, the first term in (8.14)]:

$$\begin{aligned} G_A^<(\mathbf{p}, t_2, t_2) &= G_A^< \left(\mathbf{k} + \int d\lambda q \mathbf{A}(t_2 + \lambda(t_2 - t_2)), t_2 - t_2, t_2 \right) \\ &= G_A^< \left(\mathbf{k} + q \mathbf{A}(T - \tau/2), \tau = 0, T - \tau/2 \right) \\ &= i f^W \left(\mathbf{k} + q \mathbf{A}(T - \tau/2) - \int d\lambda q \mathbf{A}(T + \tau\lambda), T - \tau/2 \right) \\ &= i f^W(\mathbf{k}(\tau, T), T - \tau/2), \end{aligned} \quad (8.16)$$

where we defined

$$\mathbf{k}(\tau, T) \equiv \mathbf{k} + \int_{-1/2}^{1/2} d\lambda \int_{T-\tau/2}^{T+\lambda\tau} dt \mathbf{E}(t). \quad (8.17)$$

The $G^<(t_1, t_1)$ piece is treated analogously with the result

$$G_A^<(\mathbf{p}, t_1, t_1) = i f^W(\mathbf{k}(-\tau, T), T + \tau/2), \quad (8.18)$$

and combining (8.16) and (8.18) we finally get the GKB ansatz in gauge invariant form as

$$\tilde{G}^<(\mathbf{k}, \tau, T) = i A(\mathbf{k}, \tau, T) f^W(\mathbf{k}(|\tau|, T), T - |\tau|/2). \quad (8.19)$$

Here we recalled that $A(\mathbf{k}, \tau \gtrless 0, T) = \pm i G^{r,a}(\mathbf{k}, \tau, T)$. For time-independent fields, when T -dependence becomes irrelevant, (8.19) reduces to

$$\tilde{G}^<(\mathbf{k}, \tau) = i A(\mathbf{k}, \tau) f^W(\mathbf{k} + q \mathbf{E}|\tau|/2). \quad (8.20)$$

We observe that the Wigner distribution function occurs with a retarded time argument, and that the momentum and the time variables have become entangled; these properties of the GKBA will have far reaching consequences in many of the later developments.

8.3 Summary of the Main Formal Results

In Part II of this book we have developed the formal theory for nonequilibrium Green functions, and here we summarize the main results of our analysis.

1. Wick's theorem can be proven for nonequilibrium Green functions at the price of moving from the real-time-axis to complex contours. The diagrammatic structure of the perturbation theory is topologically equivalent to the equilibrium theory. Analytic continuation rules specify how Green functions defined on a complex-time contour can be expressed in terms of real-time quantities.
2. Complex-time Dyson equation leads to two (generally coupled) equations: (a) A quantum kinetic equation for the correlation function $G^<$ (Keldysh or Kadanoff–Baym equation) and (b) a nonequilibrium Dyson equation for the retarded Green function. The full analysis of the nonequilibrium problem requires that both of these equations are solved.
3. Both the quantum kinetic equation and the nonequilibrium Dyson equation should be expressed in a gauge invariant form before resorting to approximations.
4. Full correlation functions are often too complicated objects to be amenable for explicit analysis. On the other hand, it is not possible to close the equation-of-motion for the Wigner function, because for nontrivial interaction mechanisms it still involves the full correlation function. To close the gap an Ansatz is introduced, which allows significant simplification. The Ansatz (8.14) emerges as the leading order term in an integral equation, but the exact limits of its validity are still under active study [258, 315, 331, 332].

Part III

Quantum Transport in Semiconductors

Linear Transport

Summary. The quantum transport equation in the linear limit is derived. For the particularly transparent case of electron-elastic impurity scattering contact is made with the Kubo formalism. Finally the weak localization corrections to the electrical conductivity are derived from the linearized quantum transport equation.

9.1 Quantum Boltzmann Equation

Description of linear transport theory in Fermi systems has reached a very high level of sophistication, and a number of theoretical methods are available. The Kubo formula, which relates transport coefficients to current-current correlation functions, or, equivalently, to a two-particle Green function, is one of the cornerstones of the theoretical treatment. In the present chapter we shall work out the linear-response limit of the quantum kinetic equation derived in Chap. 7, and show that it leads to the same results as the Kubo formula. This is an important consistency check, since the basic formulation of the two theories appears to be quite different. In quantum kinetic theory one obtains an equation-of-motion for the lesser function $G^<$, which is formally a one-body object (it involves two field operators), while the Kubo formulation, as mentioned above, usually involves a two-particle Green function.¹ The choice of a number-conserving approximation is often quite obvious in a kinetic theory formulation: once a self-energy functional has been decided upon, the rest follows quite naturally. This will be illuminated later in connection with a calculation of linear conductivity for an electron-elastic impurity system. Finally, in many problems a quantum kinetic equation is a more convenient starting point for the calculation than the two-particle Green function.

¹ Of course the self-energies appearing in the kinetic equation may involve two-particle Green functions.

The theory underlying the quantum Boltzmann equation (QBE), which we now will derive, is due to Mahan and co-workers [136, 254], and our derivation, though different in detail, leads to the same final result.

The starting point is the kinetic equation (7.20), and the task is to linearize it with respect to the external electric field \mathbf{E} . For simplicity, we shall restrict ourselves to uniform and steady fields, when all reference to the variables \mathbf{R} and T can be ignored. We observe first that the left-hand side is already proportional to \mathbf{E} ; hence all that is required in linear theory is to replace the nonequilibrium Green function $\tilde{G}^<$ by its equilibrium counter part $g^<(\mathbf{k}, \tau)$. We recall from Part I that the fluctuation-dissipation theorem, valid for equilibrium Green functions, allows us to write $g^<(\mathbf{k}, \omega) = n_F(\omega)a(\mathbf{k}, \omega)$, where a is the full interacting spectral function and n_F is the Fermi function. Thus it is advantageous to Fourier-transform the kinetic equation, $\tau \rightarrow \omega$, which we shall also do after a few further steps. Now consider the collision integral, where the object $\tilde{A}\tilde{B} \equiv \Sigma^r G^< + \Sigma^< G^a - G^r \Sigma^< - G^< \Sigma^a$ is linearized as follows:

$$\begin{aligned} & \tilde{A} \left[\mathbf{k} + \frac{q}{2} \mathbf{E}(\tau' + \frac{\tau}{2}), \frac{\tau}{2} - \tau' \right] \tilde{B} \left[\mathbf{k} + \frac{q}{2} \mathbf{E}(\tau' - \frac{\tau}{2}), \frac{\tau}{2} + \tau' \right] \\ & \rightarrow A_{\text{eq}} \left(\mathbf{k}, \frac{\tau}{2} - \tau' \right) B_{\text{eq}} \left(\mathbf{k}, \frac{\tau}{2} + \tau' \right) \\ & + \frac{q}{2} \mathbf{E} \cdot \left\{ \left[\tau' - \frac{\tau}{2} \right] A_{\text{eq}} \left(\mathbf{k}, \frac{\tau}{2} - \tau' \right) \left[\frac{\partial}{\partial \mathbf{k}} B_{\text{eq}} \left(\mathbf{k}, \frac{\tau}{2} + \tau' \right) \right] \right. \\ & + \left[\frac{\partial}{\partial \mathbf{k}} A_{\text{eq}} \left(\mathbf{k}, \frac{\tau}{2} - \tau' \right) \right] \left[\frac{\tau}{2} + \tau' \right] B_{\text{eq}} \left(\mathbf{k}, \frac{\tau}{2} + \tau' \right) \Big\} \\ & + A_1 \left(\mathbf{k}, \frac{\tau}{2} - \tau \right) B_{\text{eq}} \left(\mathbf{k}, \frac{\tau}{2} + \tau' \right) \\ & + A_{\text{eq}} \left(\mathbf{k}, \frac{\tau}{2} - \tau' \right) B_1 \left(\mathbf{k}, \frac{\tau}{2} + \tau' \right). \end{aligned} \quad (9.1)$$

One should note the different origin of the various terms in (9.1). The first term, which is zeroth order in the external fields, yields a vanishing contribution, because the collision integral must vanish in equilibrium. This can be verified for each scattering mechanism separately, and the reader is urged to check this, say, for the electron–phonon scattering term when (4.37)–(4.39) can be applied. The next two terms arise from expanding the momentum argument of the $\tilde{A}\tilde{B}$ -terms. The last term, indicated by $A_{\text{eq}}B_1 + A_1B_{\text{eq}}$, is genuinely of a nonequilibrium nature in the sense that it involves nonequilibrium Green functions and self-energies (but only first-order in the field). They must be evaluated with field-independent momentum arguments to be consistent with the linear approximation. These terms are, in general, unknown, and must be found through a solution of the quantum kinetic equation. This procedure usually requires the solution of an integral equation, as we shall demonstrate later. We next Fourier-transform the kinetic equation [we repeatedly use the

identity $\int d\tau \exp(i\omega\tau) \tau f(\tau) = -i\partial f(\omega)/\partial\omega$, and using (9.1) for the collision integral results in

$$\begin{aligned} iq\mathbf{E} \cdot \left[\frac{\partial}{\partial\mathbf{k}} + \mathbf{k} \frac{\partial}{\partial\omega} \right] g^<(\mathbf{k}, \omega) \\ - i\frac{q}{2}\mathbf{E} \cdot \left\{ A_{\text{eq}}(\mathbf{k}, \omega) \left[\frac{\partial^A}{\partial\omega} \frac{\partial^B}{\partial\mathbf{k}} - \frac{\partial^A}{\partial\mathbf{k}} \frac{\partial^B}{\partial\omega} \right] B_{\text{eq}}(\mathbf{k}, \omega) \right\} \\ = A_{\text{eq}}(\mathbf{k}, \omega) B_1(\mathbf{k}, \omega) + A_1(\mathbf{k}, \omega) B_{\text{eq}}(\mathbf{k}, \omega). \end{aligned} \quad (9.2)$$

where the superscripts A and B indicate the direction of the differentiation, and we moved the terms originating from the expansion of the momentum arguments to the left-hand side; these terms give rise to a re-normalization of the driving term. Explicitly, one finds

$$\begin{aligned} A_{\text{eq}}(\mathbf{k}, \omega) \left[\frac{\partial^A}{\partial\omega} \frac{\partial^B}{\partial\mathbf{k}} - \frac{\partial^A}{\partial\mathbf{k}} \frac{\partial^B}{\partial\omega} \right] B_{\text{eq}}(\mathbf{k}, \omega) \\ = \frac{\partial\sigma^r}{\partial\omega} \frac{\partial g^<}{\partial\mathbf{k}} - \frac{\partial\sigma^r}{\partial\mathbf{k}} \frac{\partial g^<}{\partial\omega} + \frac{\partial\sigma^<}{\partial\omega} \frac{\partial g^a}{\partial\mathbf{k}} - \frac{\partial\sigma^<}{\partial\mathbf{k}} \frac{\partial g^a}{\partial\omega} \\ - \frac{\partial g^r}{\partial\omega} \frac{\partial\sigma^<}{\partial\mathbf{k}} + \frac{\partial g^r}{\partial\mathbf{k}} \frac{\partial\sigma^<}{\partial\omega} - \frac{\partial g^<}{\partial\omega} \frac{\partial\sigma^a}{\partial\mathbf{k}} + \frac{\partial g^<}{\partial\mathbf{k}} \frac{\partial\sigma^a}{\partial\omega}. \end{aligned} \quad (9.3)$$

Recalling the definitions $\sigma = \frac{1}{2}(\sigma^r + \sigma^a) = \text{Re}\sigma^r$ and $g = \frac{1}{2}(g^r + g^a) = \text{Re}g^r$, we write (9.2) as

$$\begin{aligned} iq\mathbf{E} \cdot \left\{ \left[1 - \frac{\partial\sigma}{\partial\omega} \right] \frac{\partial g^<}{\partial\mathbf{k}} + \left[\mathbf{k} + \frac{\partial\sigma}{\partial\mathbf{k}} \right] \frac{\partial g^<}{\partial\omega} + \frac{\partial g}{\partial\omega} \frac{\partial\sigma^<}{\partial\mathbf{k}} - \frac{\partial g}{\partial\mathbf{k}} \frac{\partial\sigma^<}{\partial\omega} \right\} \\ = \{-\Sigma^>(\mathbf{k}, \omega) G^<(\mathbf{k}, \omega) + G^>(\mathbf{k}, \omega) \Sigma^<(\mathbf{k}, \omega)\}_1, \end{aligned} \quad (9.4)$$

where the subscript “1” indicates that the quantity in curly brackets should be evaluated up to linear order in the electric field. The left-hand side allows considerable simplification. Let us recall the equilibrium relations $g^< = \text{in}_{\text{Fa}} = \text{in}_{\text{F}}(-2\text{Im}g^r)$ and $\sigma^< = \text{in}_{\text{F}}\gamma = \text{in}_{\text{F}}(-2\text{Im}\sigma^r)$, and introduce the notation $\Delta = \omega - \varepsilon_{\mathbf{k}} - \sigma$. Then

$$a = \frac{\gamma}{\Delta^2 + (\gamma/2)^2}; \quad g = \frac{\Delta}{\Delta^2 + (\gamma/2)^2}. \quad (9.5)$$

With this notation we can write the expression in curly brackets in the left-hand side of (9.4) as

$$\frac{\partial\Delta}{\partial\omega} \frac{\partial g^<}{\partial\mathbf{k}} - \frac{\partial\Delta}{\partial\mathbf{k}} \frac{\partial g^<}{\partial\omega} + \frac{\partial g}{\partial\omega} \frac{\partial\sigma^<}{\partial\mathbf{k}} - \frac{\partial g}{\partial\mathbf{k}} \frac{\partial\sigma^<}{\partial\omega}.$$

The differentiations result in two kinds of terms: terms proportional to n_F , and terms proportional to $\partial n_F / \partial \omega$. Straightforward manipulations using (9.5) show that the term involving n_F vanishes, and that the other term can be simplified to yield the following kinetic equation [136]:

$$\begin{aligned} & -\frac{1}{2}a^2(\mathbf{k}, \omega) \frac{\partial n_F(\omega)}{\partial \omega} q \mathbf{E} \cdot \left[\gamma \frac{\partial \Delta}{\partial \mathbf{k}} - \Delta \frac{\partial \gamma}{\partial \mathbf{k}} \right] \\ & = \left\{ -\Sigma^>(\mathbf{k}, \omega) G^<(\mathbf{k}, \omega) + G^>(\mathbf{k}, \omega) \Sigma^<(\mathbf{k}, \omega) \right\}_1 \\ & = i \left\{ \Gamma(\mathbf{k}, \omega) G^<(\mathbf{k}, \omega) - A(\mathbf{k}, \omega) \Sigma^<(\mathbf{k}, \omega) \right\}_1 . \end{aligned} \quad (9.6)$$

This equation is still exact, and it has served as a starting point for many transport calculations [252, 253].

At this point it is interesting to examine the relation between the Boltzmann equation and the quantum Boltzmann equation (9.6). We recall from Sect. 6.3 that one of the steps required to obtain the Boltzmann equation from the full kinetic equation was to let the spectral function approach a δ -function [qualitatively one should let $\gamma \rightarrow 0$ in (9.5)]; this procedure now appears to be ill-defined because of the *square* of the spectral function in (9.6). The limiting process can be regularized, however, by making the replacement:

$$\lim_{\gamma \rightarrow 0} a^2 \gamma = \lim_{\gamma \rightarrow 0} \frac{\gamma^3}{[\Delta^2 + (\gamma/2)^2]^2} = 4\pi \delta(\omega - \varepsilon_{\mathbf{k}}) . \quad (9.7)$$

The prefactor of the δ -function in (9.7) was determined by evaluating the integral $\int d\omega a^2 \gamma = 4\pi$. When (9.7) is used on the left-hand side of (9.6), and the ω -integral is performed, the singular behavior is removed, and one recovers the familiar (linearized) Boltzmann equation driving term, $\mathbf{E} \cdot \mathbf{k} \partial n_F(\varepsilon_{\mathbf{k}}) / \partial \varepsilon_{\mathbf{k}}$.

9.2 Linear Conductivity of Electron-Elastic Impurity Systems

Electrical conductivity of electrons in a (weakly) disordered system is a standard illustration of the use of many-body techniques in calculation of transport properties, and most textbooks have chapter(s) devoted to this problem [2, 96, 105, 254]. Most of these treatments are based on the Kubo formula, with the exception of [254], who also discusses the kinetic equation approach. In what follows, we shall outline the steps required in the Kubo formalism, and then discuss the kinetic equation method in detail. Our main emphasis will be on the differences of the two methods, and the reader should consult the above-mentioned references for additional technical details.

9.2.1 Kubo Formula

In the Kubo formalism the ac electrical conductivity is calculated from²

$$\sigma_{\alpha\beta}(\mathbf{q}, \omega) = \frac{i}{\omega} \left[\Pi_{\alpha\beta}^r(\mathbf{q}, \omega) + \frac{ne^2}{m} \delta_{\alpha\beta} \right], \quad (9.8)$$

where the retarded current-current correlation function Π^r is given by

$$\Pi_{\alpha\beta}^r(\mathbf{q}, \omega) = -i \int_{-\infty}^{\infty} dt(t-t') \theta(t-t') e^{i\omega(t-t')} \langle [j_{\alpha}(\mathbf{q}, t), j_{\beta}(-\mathbf{q}, t')] \rangle. \quad (9.9)$$

The angular brackets in (9.9) indicate a ground state average for $T = 0$, or an average over a suitable thermal ensemble for finite temperatures. The greek indices (α, β) denote cartesian components. In the case of a random impurity system, one must also average over the impurity configurations, and impurity-averaged quantities will be indicated henceforth with an overbar. The two current operators in (9.9) give rise to four creation or annihilation operators (recall that each current operator is of the form $j(\mathbf{q}) = (e/m) \sum_{\mathbf{p}} (\mathbf{p} + \frac{1}{2}\mathbf{q}) a_{\mathbf{p}+\mathbf{q}}^\dagger a_{\mathbf{p}}$) and hence, in general, the evaluation of (9.8) and (9.9) requires the knowledge of a two-particle Green function. In the present case, which consists of noninteracting electrons scattering off from impurities, the two-particle Green function can be exactly factorized into a product of two one-particle Green functions. This follows from the fact that for a fixed configuration of impurities the problem is diagonalizable (i.e., it is described by a bilinear Hamiltonian), and hence Wick's theorem can be applied directly. But Wick's theorem applies only to time-ordered quantities, and hence one must consider the time-ordered counterpart of (9.9):

$$\begin{aligned} \Pi_{\alpha\beta}^c(\mathbf{q}, \omega) &= -i \int_{-\infty}^{\infty} dt(t-t') e^{i\omega(t-t')} \langle T\{j_{\alpha}(\mathbf{q}, t) j_{\beta}(-\mathbf{q}, t')\} \rangle \\ &= -i \frac{e^2}{m^2} \int_{-\infty}^{\infty} dt(t-t') e^{i\omega(t-t')} \sum_{\mathbf{pp}'} (\mathbf{p} + \frac{1}{2}\mathbf{q})_{\alpha} (\mathbf{p}' - \frac{1}{2}\mathbf{q})_{\beta} \\ &\quad \times \langle T\{a_{\mathbf{p}+\mathbf{q}}^\dagger(t) a_{\mathbf{p}}(t) a_{\mathbf{p}'-\mathbf{q}}^\dagger(t') a_{\mathbf{p}'}(t')\} \rangle. \end{aligned} \quad (9.10)$$

Applying Wick's theorem to the four-operator expectation value yields

$$\begin{aligned} &\langle T\{a_{\mathbf{p}+\mathbf{q}}^\dagger(t) a_{\mathbf{p}}(t) a_{\mathbf{p}'-\mathbf{q}}^\dagger(t') a_{\mathbf{p}'}(t')\} \rangle \\ &= g^c(\mathbf{p}, \mathbf{p}' - \mathbf{q}, t - t') g^c(\mathbf{p}', \mathbf{p} + \mathbf{q}, t' - t), \end{aligned} \quad (9.11)$$

where the one-particle causal Green function has its conventional definition, $g^c(\mathbf{p}, \mathbf{p}' - \mathbf{q}, t - t') = -i \langle T\{a_{\mathbf{p}}(t) a_{\mathbf{p}'-\mathbf{q}}^\dagger(t')\} \rangle$. We note that the time-ordered correlation function is a product of two anti-parallel Green functions, and hence

² Note that in this section we set the charge of the particles equal to e in order to avoid confusion with the wavevector q .

the retarded correlation function can be constructed with a direct application of the results of Chap. 4 [in particular (4.36)].

The impurity averaging, however, must be done carefully, and it is essential to calculate the impurity average of the product of two Green functions \overline{gg} , which, in general, does not factorize into a product of two impurity-averaged one-particle Green functions, $\overline{gg} \neq \overline{g}\overline{g}$. The study of \overline{gg} leads to the study of vertex functions, and these must be chosen consistently with the self-energies used in the computation of \overline{g} . We have seen in Part I that the simplest, self-consistent approximation to the \overline{g} function leads to the (self-consistent) Born approximation to the self-energy, $\sigma_B(\mathbf{k}, \omega) = c \int d\mathbf{q}/(2\pi)^3 |V(\mathbf{k} - \mathbf{q})|^2 \overline{g}(\mathbf{q}, \omega)$.

A detailed analysis shows that the vertex function corresponding to σ_B consists of so-called ladder diagrams; this can be verified by studying Ward identities [2, 254], which are abstract statements of current conservation. Figure 9.1 gives a pictorial representation of the ladder diagrams. This step is by-passed in a quantum kinetic formulation: given a self-energy functional, the *structure* of the equations is such that conservation laws are guaranteed.³ This advantage becomes even larger in cases where the basic self-energy is more complicated, such as in the phenomenon called weak localization (for a review, see, for example, [5, 233], and Sect. 9.3).

The calculation of the conductivity proceeds by rewriting $\overline{\Pi}^c$ as [96]

$$\overline{\Pi}_{\alpha\beta}^c(\mathbf{q}, \omega) = -i \frac{e^2}{m^2} \sum_{\mathbf{p}} \int \frac{d\varepsilon}{2\pi} (\mathbf{p} + \frac{1}{2}\mathbf{q})_\alpha \overline{g}_\beta^{(2)}(\mathbf{p}, \mathbf{q}, \varepsilon, \omega), \quad (9.12)$$

where the impurity-averaged causal two-particle vector Green function is defined by

$$\overline{g}^{(2)}(\mathbf{p}, \mathbf{q}, \varepsilon, \omega) = \sum_{\mathbf{p}'} (\mathbf{p}' - \frac{1}{2}\mathbf{q}) \overline{g^c}(\mathbf{p}', \mathbf{p} + \mathbf{q}, \varepsilon) \overline{g^c}(\mathbf{p}, \mathbf{p}' - \mathbf{q}, \omega + \varepsilon). \quad (9.13)$$

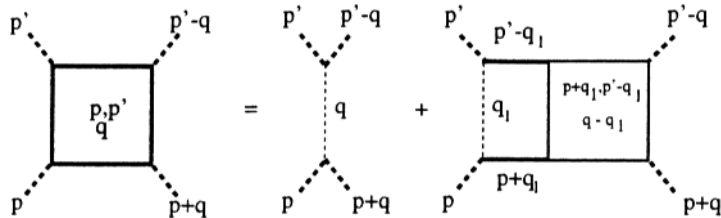


Fig. 9.1. Schematic representation of the integral equation satisfied by the vertex function in the ladder approximation. *Shaded box*: the vertex function; *dotted line*: the impurity potential; *solid line*: Green function; *short dashed line*: places where Green functions can be attached

³ One should note, however, that if approximations have been made on the quantum kinetic equation, the conservation laws must be checked separately [284, 287].

In Sect. 6.2 we showed that $g^c(\mathbf{p}, \mathbf{p}', \omega)$ satisfies the Dyson equation:

$$g^c(\mathbf{p}, \mathbf{p}', \omega) = \delta_{\mathbf{p}\mathbf{p}'} g_0^c(\mathbf{p}, \omega) + g_0^c(\mathbf{p}, \omega) \sum_{\mathbf{q}} v(\mathbf{p} - \mathbf{q}) g^c(\mathbf{q}, \mathbf{p}', \omega). \quad (9.14)$$

Here, $v(\mathbf{q}) = \sum_i \exp[-i\mathbf{q} \cdot \mathbf{R}_i] V(\mathbf{q})$, and the sum runs over the random impurity locations $\{\mathbf{R}_i\}$. The impurity averaging in (9.13) is performed with the method described in Part I: one substitutes the infinite series (9.14) in (9.13), and averages term-by-term. This procedure obviously results in a large number of terms. As explained above, one must choose an appropriate subset of these terms. Presently this consists of the above-mentioned ladder diagrams, in which case $\bar{g}^{(2)}$ satisfies the following integral equation:

$$\begin{aligned} \bar{g}^{(2)}(\mathbf{p}, \mathbf{q}, \varepsilon, \omega) &= g^c(\mathbf{p}, \varepsilon + \omega) g^c(\mathbf{p} + \mathbf{q}, \varepsilon) \\ &\times \left[\mathbf{p} + \frac{1}{2} \mathbf{q} + c \sum_{\mathbf{p}'} |V(\mathbf{p} - \mathbf{p}')|^2 \bar{g}^{(2)}(\mathbf{p}', \mathbf{q}, \varepsilon, \omega) \right], \end{aligned} \quad (9.15)$$

where g^c is the impurity-averaged one-particle Green function,⁴ and c denotes the impurity concentration.

We also wish to point out another slight technical complication in working with (9.8): The “diamagnetic” term $ine^2/\omega m$ diverges in the dc limit. Thus, in order to obtain a finite dc conductivity, the correlation function must contain a piece that cancels the diverging term. This is indeed the case, as we shall now proceed to show. In what follows we shall restrict ourselves to uniform systems, and hence work in the $\mathbf{q} \rightarrow 0$ limit. To isolate the terms that cancel the diamagnetic term, we must express the causal response function $\bar{\Pi}^c$ in terms of retarded and advanced Green functions. To do this, we apply the second rule (4.36) to $\bar{\Pi}^c$. This gives rise to $\bar{\Pi}^r(\omega) \propto \int d\varepsilon [g^r(\varepsilon) g^<(\varepsilon + \omega) + g^<(\varepsilon) g^a(\varepsilon + \omega)]$, and expressing the lesser functions in terms of retarded and advanced functions,⁵ leads to four terms. The $\bar{g}^r \bar{g}^a$ -terms give a finite contribution to the conductivity and read explicitly:

$$\begin{aligned} \sigma(\omega) &= \frac{2e^2}{3m^2} \int \frac{d\varepsilon}{2\pi} \sum_{\mathbf{p}\mathbf{p}'} \mathbf{p} \cdot \mathbf{p}' \frac{n_F(\varepsilon) - n_F(\varepsilon + \omega)}{\omega} \\ &\times \overline{g^a(\mathbf{p}, \mathbf{p}', \varepsilon + \omega) g^r(\mathbf{p}', \mathbf{p}, \varepsilon)}. \end{aligned} \quad (9.16)$$

⁴ Note that it is not necessary to use an overbar to indicate an impurity-averaged single-particle Green function, because the distinction is clear from the number of the momentum variables: unaveraged functions have two (9.14), while the averaged functions have one.

⁵ We recall that in equilibrium $g^<(\varepsilon) = -n_F(\varepsilon)[g^r(\varepsilon) - g^a(\varepsilon)]$.

In writing (9.16) we assume that the system is isotropic, i.e., $\sigma_{\alpha\beta}(\omega) = \sigma(\omega)\delta_{\alpha\beta}$, and thus made the replacement $\mathbf{p}_\alpha \mathbf{p}'_\alpha = \frac{1}{3}\mathbf{p} \cdot \mathbf{p}'$. The factor two accounts for the spin degeneracy.

To evaluate the contribution arising from the terms proportional to $\overline{g^r g^r}$ and $\overline{g^a g^a}$, it is sufficient to use the lowest order approximation for $\overline{\mathbf{g}}^{(2)}$, which follows directly from (9.15):

$$\overline{\mathbf{g}}_{rr}^{(2)}(\mathbf{p}, \mathbf{q} = 0, \varepsilon, \omega \rightarrow 0) \simeq \mathbf{p} g^r(\mathbf{p}, \varepsilon) g^r(\mathbf{p}, \varepsilon) \quad (9.17)$$

and similarly for $\overline{\mathbf{g}}_{aa}^{(2)}$. The contribution to $\sigma(\mathbf{q} = 0, \omega = 0)$ due to these terms can be calculated as

$$\begin{aligned} & -i \frac{2e^2}{3m^2} \sum_{\mathbf{p}} \int \frac{d\varepsilon}{2\pi} p^2 n_F(\varepsilon) \left\{ [g^a(\mathbf{p}, \varepsilon)]^2 - [g^r(\mathbf{p}, \varepsilon)]^2 \right\} \\ &= -i \frac{2e^2}{3m^2} \sum_{\mathbf{p}} \int \frac{d\varepsilon}{2\pi} p^2 \frac{\partial n_F}{\partial \varepsilon} [g^a(\mathbf{p}, \varepsilon) - g^r(\mathbf{p}, \varepsilon)] \\ &= -\frac{2e^2}{3m^2} p_F^2 N(\varepsilon_F) = -\frac{ne^2}{m}. \end{aligned} \quad (9.18)$$

In obtaining (9.18) we used the following observations: (1) $-\partial n_F / \partial \varepsilon \simeq \delta(\varepsilon - \varepsilon_F)$; (2) we integrated by parts to obtain the second line; (3) the difference of retarded and advanced Green functions is strongly peaked at $\varepsilon = \varepsilon(\mathbf{p})$, and since $\varepsilon \simeq \varepsilon_F$, we can replace p^2 by p_F^2 , and move it out of the integral; (4) the density of states at Fermi level is $N(\varepsilon_F) = 2 \sum_{\mathbf{p}} \delta(\varepsilon_F - \varepsilon_p) = m k_F / \pi^2 \hbar^2$; and, finally, (5) $n = k_F^3 / 3\pi^2$. Thus, this term exactly cancels the diamagnetic term in (9.8).

The origin of the formal divergence is the use of the vector potential to describe the electric field; the gauge-invariant variables discussed in Chap.7 lead to a description which involves only the physical \mathbf{E} -field, and thus the quantum kinetic equations do not suffer from this slight difficulty.

We conclude this section by outlining the calculation needed for the dc conductivity for the impurity system. In the dc limit the conductivity (9.16) becomes

$$\sigma_{dc} = \frac{2e^2}{3m^2} \int \frac{d\varepsilon}{2\pi} \left(-\frac{\partial n_F}{\partial \varepsilon} \right) \sum_{\mathbf{p}} \mathbf{p} \cdot \mathbf{g}_{ra}^{(2)}(\mathbf{p}, \mathbf{q} = 0, \varepsilon, \omega = 0). \quad (9.19)$$

The vertex equation that needs to be solved is

$$\gamma(\mathbf{p}, \varepsilon) \mathbf{p} \lambda(\mathbf{p}, \varepsilon) = a(\mathbf{p}, \varepsilon) \left[\mathbf{p} + c \sum_{\mathbf{p}'} |V(\mathbf{p} - \mathbf{p}')|^2 \mathbf{p}' \lambda(\mathbf{p}', \varepsilon) \right], \quad (9.20)$$

where we introduce a new function λ via $\mathbf{g}^{(2)}(\mathbf{p}, \varepsilon) = \mathbf{p} \lambda(\mathbf{p}, \varepsilon)$. In writing (9.20) we suppressed all \mathbf{q} and ω -dependence, since these variables do not play a role

in the solution. We also used the identity $g^r g^a \equiv (g^r - g^a)/(1/g^a - 1/g^r) = a/\gamma$. We postpone the solution of (9.20) until Sect. 9.2.2, where we derive an analogous result with the quantum kinetic formulation.

9.2.2 Quantum Kinetic Formulation

We now apply the linearized quantum kinetic equation (9.6) to the electron-impurity problem [254]. We do not consider contributions arising from high concentrations of impurities (this assumption was also used in the derivation of the self-energy functional), and hence the expression in brackets on the left-hand side of (9.6) can be simplified:

$$\left[\gamma \frac{\partial \Delta}{\partial \mathbf{k}} - \Delta \frac{\partial \gamma}{\partial \mathbf{k}} \right] = -\gamma \left(\mathbf{k} + \frac{\partial \sigma}{\partial \mathbf{k}} \right) - (\varepsilon - \varepsilon_k - \sigma) \frac{\partial \gamma}{\partial \mathbf{k}} \rightarrow -\gamma \mathbf{k}, \quad (9.21)$$

where we discarded all terms which are of the order c^2 . In evaluating the right-hand side of (9.6) we make the replacement $G^r \rightarrow g^r$; this procedure is justified by recalling from Sect. 7.3 that the free field-dependent retarded Green function depends quadratically on the electric field, $G_E^r = g_0^r + \mathcal{O}(E^2)$, and that the field-dependent corrections due to scattering (these can be calculated by expanding the right-hand side of (7.22) in powers of E) are small, because they involve momentum derivatives of equilibrium self-energies, which are small for impurity problems. Consequently, the same property can be used for A and Γ as well: $A \rightarrow a$ and $\Gamma \rightarrow \gamma$. Combining all these results we find:

$$\frac{1}{2} a^2(\mathbf{k}, \varepsilon) \gamma(\mathbf{k}, \varepsilon) \frac{\partial n_F}{\partial \varepsilon} \mathbf{E} \cdot \mathbf{k} = i [\gamma(\mathbf{k}, \varepsilon) G_1^<(\mathbf{k}, \varepsilon) - a(\mathbf{k}, \varepsilon) \Sigma_1^<(\mathbf{k}, \varepsilon)]. \quad (9.22)$$

It is next convenient to define a new function $\Lambda(\mathbf{k}, \varepsilon)$ in terms of the (as of yet unknown) nonequilibrium Green function:

$$G_1^<(\mathbf{k}, \varepsilon) = -ia(\mathbf{k}, \varepsilon) \frac{\partial n_F}{\partial \varepsilon} \mathbf{E} \cdot \mathbf{k} \Lambda(\mathbf{k}, \varepsilon). \quad (9.23)$$

We can also express $\Sigma_1^<$ in terms of $\Lambda(\mathbf{k}, \varepsilon)$:

$$\begin{aligned} \Sigma_1^<(\mathbf{k}, \varepsilon) &= c \sum_{\mathbf{q}} |V(\mathbf{k} - \mathbf{q})|^2 G_1^<(\mathbf{q}, \varepsilon) \\ &= c \sum_{\mathbf{q}} |V(\mathbf{k} - \mathbf{q})|^2 (-i)a(\mathbf{q}, \varepsilon) \frac{\partial n_F}{\partial \varepsilon} \mathbf{E} \cdot \mathbf{q} \Lambda(\mathbf{q}, \varepsilon). \end{aligned} \quad (9.24)$$

Further, using (9.23) in the expression for the current (8.3), we can identify the electrical conductivity:

$$\sigma_{dc} = \frac{2e^2}{3m^2} \int \frac{d\mathbf{k}}{(2\pi)^3} \int \frac{d\varepsilon}{2\pi} k^2 \left(-\frac{\partial n_F}{\partial \varepsilon} \right) a(\mathbf{k}, \varepsilon) \Lambda(\mathbf{k}, \varepsilon). \quad (9.25)$$

Thus it remains to solve for $\Lambda(\mathbf{k}, \varepsilon)$. By substituting (9.23), (9.24) in the kinetic equation, we find after some rearrangement:

$$\mathbf{k}\Lambda(\mathbf{k}, \varepsilon) = \frac{1}{2}\mathbf{k}a(\mathbf{k}, \varepsilon) + \frac{c}{\gamma(\mathbf{k}, \varepsilon)} \sum_{\mathbf{q}} |V(\mathbf{k} - \mathbf{q})|^2 \mathbf{q}a(\mathbf{q}, \varepsilon)\Lambda(\mathbf{q}, \varepsilon). \quad (9.26)$$

This equation can be brought to a close agreement with the Kubo formula result (9.23) by introducing a new function, $\hat{\lambda}(\mathbf{k}, \varepsilon) \equiv a(\mathbf{k}, \varepsilon)\Lambda(\mathbf{k}, \varepsilon)$:

$$\begin{aligned} \gamma(\mathbf{k}, \varepsilon)\mathbf{k}\hat{\lambda}(\mathbf{k}, \varepsilon) &= a(\mathbf{k}, \varepsilon) \left[\frac{1}{2}\mathbf{k}a(\mathbf{k}, \varepsilon)\gamma(\mathbf{k}, \varepsilon) \right. \\ &\quad \left. + c \sum_{\mathbf{k}'} |V(\mathbf{k} - \mathbf{k}')|^2 \mathbf{k}'\hat{\lambda}(\mathbf{k}', \varepsilon) \right]. \end{aligned} \quad (9.27)$$

The *only* difference between the two vertex equations is in the inhomogeneous term: the Kubo approach has a , while the quantum kinetic equation leads to $(1/2)\gamma a^2$. But this difference is immaterial: we have already shown in (9.7) that in the dilute limit these two expressions are completely equivalent, if they occur within an energy-integral, as they do in the conductivity formulae.

The solution for the vertex equation (9.20) [or (9.27)] can be found by multiplying both sides of the equation by \mathbf{p}/p^2 (the technical details can be found, e.g., in [251]). The resulting algebraic equation has the solution

$$\lambda(\varepsilon) = \frac{a(\mathbf{p}, \varepsilon)}{\gamma_{\text{tr}}(\mathbf{p}, \varepsilon)}, \quad (9.28)$$

where the “transport damping” γ_{tr} is given by

$$\gamma_{\text{tr}}(\mathbf{p}, \varepsilon) = \tau_{\text{tr}}^{-1} = 2\pi c \int \frac{d\Omega}{4\pi} |V(\theta)|^2 (1 - \cos \theta). \quad (9.29)$$

The above derivation used the fact that all momenta have magnitudes close to p_F . This can be verified by studying the iterative solution of the vertex equations: the strongly peaked nature of the spectral functions force ε and ε_p to be nearly equal, and the derivative of the Fermi function in (9.19) confines ε in the neighborhood of ε_F . When (9.29) is substituted in (9.19) [or (9.25)], we find the familiar dc conductivity

$$\sigma_{\text{dc}} = \frac{ne^2\tau_{\text{tr}}}{m}. \quad (9.30)$$

It may appear that much effort has been spent in recovering a Boltzmann equation result. This is, of course, true, but the real strength of the formalism is in problems, which are inherently beyond a Boltzmann description.

9.3 Weak Localization Corrections to Electrical Conductivity

In this section we demonstrate the use of the linearized quantum kinetic equation in a problem that cannot be addressed with Boltzmann formalism: an electron-impurity system where one considers the coherent back-scattering of electrons. This phenomenon, known as weak localization (WL), has received enormous attention during the last two decades, and the reader is referred to the literature for a full discussion [suitable review articles are [5,233,287]; here we use WL as an example of how to use the techniques developed above [323].

In order to simplify the forthcoming discussion, we will assume that the impurity potential is localized in space, and thus its Fourier component is momentum-independent; we also introduce the notation $cV^2 = u^2$. As a result, there is no distinction between the transport lifetime τ_{tr} and the scattering lifetime τ . We shall only evaluate the correction due to weak localization to normal impurity conductivity $\sigma = ne^2\tau/m$, and will therefore look for a perturbative solution.

As shown in Part I, any diagram which contains crossed impurity lines, is smaller by a factor $(lk_F)^{-1}$ than a diagram of the same order in the impurity potential, but without crossed impurity lines. (Here $l = v_F\tau$ is the impurity mean free path, and v_F is the Fermi velocity). However, all *maximally crossed* diagrams give a contribution which is of the same order of magnitude. Thus, in constructing the self-energy functional for the kinetic equation, it is necessary to sum over all these maximally crossed diagrams. Figure 9.2 shows the lowest order contribution to the weak localization self-energy Σ_{WL} . When inserting the momentum labels in the diagram of Fig. 9.2 we used the Feynman rules of Part I, which stipulate that momentum is conserved at each vertex. The mathematical expression for the nonequilibrium self-energy $\Sigma_{\text{WL}}^{(1)}$ is

$$\begin{aligned} \Sigma_{\text{WL}}^{(1)}(\mathbf{p}, t, t') = & u^4 \sum_{\mathbf{q}, \mathbf{q}_1} \int d\tau_1 d\tau_{1'} \\ & \times G(\mathbf{p} - \mathbf{q}_1, t, \tau_1) G(\mathbf{q}, \tau_1, \tau_{1'}) G(\mathbf{q} + \mathbf{q}_1, \tau_{1'}, t') . \end{aligned} \quad (9.31)$$

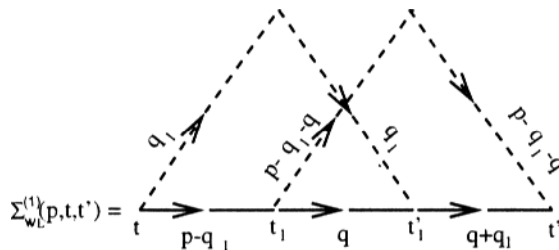


Fig. 9.2. Lowest order contribution to the weak localization self-energy $\Sigma_{\text{WL}}^{(1)}$

Similar structure prevails for the higher order maximally crossed diagrams, and the n th term in the series can be expressed as

$$\begin{aligned} \Sigma_{WL}^{(n)}(\mathbf{p}, t, t') &= u^{2(n+1)} \int d\tau_1 d\tau_{1'} \cdots d\tau_n d\tau_{n'} \sum_{\mathbf{q}_1 \cdots \mathbf{q}_n \mathbf{q}} G(\mathbf{q}, \tau_n, \tau_{n'}) \\ &\times \prod_{j=1}^n G \left(\mathbf{p} - \sum_{i=1}^j \mathbf{q}_i, \tau_{j-1}, \tau_j \right) \\ &\times \prod_{j'=1}^{n'} G \left(\mathbf{q} + \sum_{i'=1}^{j'} \mathbf{q}_{i'}, \tau_{n'-(j'-1)}, \tau_{n'-j'} \right). \end{aligned} \quad (9.32)$$

In writing (9.32) we used the notation $\tau_0 \equiv t$ (and $\tau_{0'} \equiv t'$). $\Sigma_{WL}^{(n)}$ is in a form for which the analytic continuation rule (4.27) can be applied (the generalization to a product of $2n + 1$ terms is obvious). This process leads to a sum of $(2n + 1)$ terms, and the self-energy has the structure

$$\begin{aligned} \Sigma_{WL}^{(n)<} &\propto G^< \underbrace{G^a \cdots G^a}_{2n \text{ terms}} + \cdots + \underbrace{G^r \cdots G^r}_{n \text{ terms}} G^< \underbrace{G^a \cdots G^a}_{n \text{ terms}} \\ &\quad + \cdots + \underbrace{G^r \cdots G^r}_{2n \text{ terms}} G^<. \end{aligned} \quad (9.33)$$

Let us next examine the variable structure of the momentum integrals in (9.33). Using (9.31) as a guideline, one can relabel the dummy integration variables, and rearrange the momentum integrations into pairs of the same type as the \mathbf{q}_1 -integration in (9.31). As argued above, we can replace the retarded and advanced Green functions by their equilibrium expressions. Further, integrals which involve two g^r 's (or two g^a 's) can be neglected in comparison to those which are of the form $g^r g^a$. Thus, only the term in (9.33) which has n g^r 's and g^a 's needs to be considered. All the n integrals involving the pairs $g^r g^a$ in $\Sigma_{WL}^{(n)<}$ give the same result, and it is sufficient to consider the contribution arising from $\Sigma_{WL}^{(1)<}$:

$$\begin{aligned} \Sigma_{WL}^{(1)<}(\mathbf{p}, \omega) &= u^2 \sum_{\mathbf{q}} \left[u^2 \sum_{\mathbf{q}_1} g^r(\mathbf{q}_1, \omega) g^a(\mathbf{p} + \mathbf{q} - \mathbf{q}_1, \omega) \right] G^<(\mathbf{q}, \omega) \\ &\equiv u^2 \sum_{\mathbf{q}} \zeta(\mathbf{p} + \mathbf{q}, \omega) G^<(\mathbf{q}, \omega). \end{aligned} \quad (9.34)$$

We evaluate the function $\zeta(\mathbf{q}, \omega)$ under the assumption $q \ll k_F$, and the calculation proceeds as follows:

$$\begin{aligned}
\zeta(\mathbf{q}, \omega) &= u^2 \int \frac{d^3 k}{(2\pi)^3} \frac{1}{\omega - \varepsilon(\mathbf{k} + \mathbf{q}/2) + i/2\tau} \frac{1}{\omega - \varepsilon(\mathbf{k} - \mathbf{q}/2) - i/2\tau} \\
&= u^2 N(0) \int \frac{d\Omega}{4\pi} \int d\varepsilon_k \frac{1}{\varepsilon_k + k_F q \cos \theta / 2m - \omega - i/2\tau} \\
&\quad \times \frac{1}{\varepsilon_k - k_F q \cos \theta / 2m - \omega + i/2\tau} \\
&= u^2 N(0) \pi i \int_{-1}^1 \frac{dx}{-k_F q x / m + i/\tau} = \frac{i}{2ql} \log \frac{lq + i}{lq - i}. \quad (9.35)
\end{aligned}$$

Here, we recalled the definition of the relaxation time $1/\tau = 2\pi u^2 N(0) = \gamma$, where $N(0)$ is the density of states at the Fermi level, and introduced the mean free path $l = v_F \tau$. We note that ω -dependence drops out from ζ . If one considers the ac conductance, the analysis presented above is essentially unchanged, and the final result for ζ is obtained from (9.35) by replacing the imaginary unit i in the log function by $i \rightarrow i + \omega_0 \tau$, where ω_0 is the external frequency. In what follows, we shall use this finite-frequency expression. In the limit $ql \ll 1, \omega_0 \tau \ll 1$ one finds $\zeta \simeq 1 + i\omega_0 \tau - D\tau q^2$, where $D = (1/3)v_F^2 \tau$ is the diffusion constant.

Summing up the series for the weak localization self-energy gives:

$$\begin{aligned}
\Sigma_{WL}^<(\mathbf{p}, \omega) &= \sum_n \Sigma_{WL}^{(n)<}(\mathbf{p}, \omega) \\
&= u^2 \sum_{\mathbf{p}'} \frac{\zeta(\mathbf{p} + \mathbf{p}', \omega)}{1 - \zeta(\mathbf{p} + \mathbf{p}', \omega)} G^<(\mathbf{p}', \omega) \\
&\simeq \frac{u^2}{\tau} \sum_{\mathbf{p}'} \frac{1}{-i\omega_0 + D(\mathbf{p} + \mathbf{p}')^2} G^<(\mathbf{p}', \omega) \\
&\simeq \frac{u^2}{\tau} G^<(-\mathbf{p}, \omega) F(\omega_0), \quad (9.36)
\end{aligned}$$

where

$$F(\omega_0) = \sum_{\mathbf{q}} \frac{1}{-i\omega_0 + D(\mathbf{q})^2}. \quad (9.37)$$

In obtaining the last line in (9.36) we used the fact that the integrand is strongly peaked at $\mathbf{p}' = -\mathbf{p}$, which allows one to move $G^<$ outside the integral.

We now return to the kinetic equation (9.22), and solve it with the weak localization self-energy (9.36) added to the normal Born approximation self-energy (9.24). Since we are looking for a perturbative solution, we write $G^< = G_1^< + \delta G^<$, where $G_1^<$ is the solution obtained for the “normal” impurity problem, $G_1^< = -i(\partial n_F / \partial \omega)(\mathbf{p} \cdot \mathbf{E})\tau a$. Thus, we write (9.22) as

$$\frac{1}{2} a^2 \gamma \frac{\partial n_F}{\partial \omega} (\mathbf{E} \cdot \mathbf{k}) = i[\gamma(G_1^< + \delta G^<) - a(\Sigma_1^< + \Sigma_{WL}^<)]. \quad (9.38)$$

Since $G_1^<$ is the solution to the kinetic equation without weak localization effects, we can immediately identify $\delta G^<$:

$$\begin{aligned}\delta G^<(\mathbf{p}, \omega) &= \frac{a(\mathbf{p}, \omega)}{\gamma(\mathbf{p}, \omega)} \Sigma_{\text{WL}}^<(\mathbf{p}, \omega) \\ &= a(\mathbf{p}, \omega) u^2 G_1^<(-\mathbf{p}, \omega) F(\omega_0),\end{aligned}\quad (9.39)$$

where we used $\gamma\tau = 1$. We recall that $G_1^<$ has a factor a in it, and hence combine some of the prefactors in (9.39) as $a^2 u^2 = a^2 \gamma / [2\pi N(0)] = a / [\pi N(0)]$, and substituting this back into the expression for $\delta G^<$ we finally obtain:

$$\begin{aligned}\delta G^<(\mathbf{p}, \omega) &= \frac{1}{\pi N(0)} F(\omega_0) G_1^<(-\mathbf{p}, \omega) \\ &= -\frac{i}{\pi N(0)} F(\omega_0) \frac{\partial n_F}{\partial \omega} (-\mathbf{p} \cdot \mathbf{E}) a \tau.\end{aligned}\quad (9.40)$$

We see that the correction to the conductivity, which is obtained from (9.40) by multiplying by \mathbf{p} and summing over \mathbf{p} , is proportional to the unperturbed conductivity, and, importantly, it is negative (weak localization!) because of the momentum argument in $G_1^<$:

$$\delta\sigma(\omega_0) = -\frac{1}{\pi N(0)} F(\omega_0) \sigma, \quad (9.41)$$

where $\sigma = ne^2\tau/m$ is the Drude dc conductivity. It remains to evaluate the integral in (9.37). Since we work all the time in the limit $ql \ll 1$, we must cutoff the upper limit at $q = 1/l$. In three dimensions one obtains a nonsingular contribution, while in two dimensions one finds a logarithmically singular result:

$$\begin{aligned}F(\omega_0) &= N(0) \int_0^{\hbar^2/(l^2 2m)} \frac{d\varepsilon_q}{-i\omega_0 + (2mD/\hbar^2)\varepsilon_q} \\ &\simeq \frac{N(0)\hbar^2}{2mD} \log(\omega_0\tau),\end{aligned}\quad (9.42)$$

where we omit nonsingular terms. Combining all the prefactors, we arrive at the first quantum correction to the conductivity [127]:

$$\delta\sigma/\sigma = (1/\pi k_F l) \log \omega_0 \tau. \quad (9.43)$$

This logarithmic frequency-dependence has been verified experimentally. It would go beyond the scope of this presentation to push the analysis further. However, we would like to point out the importance of magnetic fields: it turns out that the weak localization correction is intimately linked to time-reversal symmetry, and hence sensitive to magnetic fields. In general, theory and experiment are in good agreement, and weak localization has become an important tool in extracting material parameters, such as different scattering times. We refer the reader to the review articles mentioned in the beginning of this section for further details.

Field-Dependent Green Functions

Summary. As the device size shrinks, and the operating voltage is necessarily bounded from below, the electric fields inside the device must grow. In this chapter, we will address high-field transport phenomena in a systematic manner, and as a first step we study the general properties of free field-dependent Green functions which form the basic building blocks of the subsequent theory. In order to gain insight of how the general approach works, we next study a specific model of dynamical disorder, for which an analytic and exact theory can be developed. Finally, we give an extensive treatment of high-field transport in semiconductors, focusing in particular to the modifications one must make to the semiclassical Boltzmann equation.

10.1 Free Green Functions and Spectral Functions in an Electric Field

In order to address quantum phenomena occurring at strong electric fields, one should develop a quantum kinetic theory which is nonperturbative in the electric field. One way of achieving this goal is to use *field-dependent free* Green functions as the basic building block of the theory, and then develop a diagrammatic analysis, where the field-dependent Green functions replace the free Green functions of the equilibrium theory. We have actually already seen an example of a such a field-dependent Green function (7.26) in Chap. 7 and here we elaborate further these concepts. In this section we focus on retarded/advanced Green functions $G^{r/a}$ (and spectral densities $A = i(G^r - G^a)$); the correlation functions $G^<$ will be analyzed below in a discussion of quantum high-field kinetic equations.

The analysis can be carried out directly in terms of the gauge-invariant Green functions. However, sometimes additional insight can be obtained by working in a specific gauge, and in this section we first consider the scalar potential gauge. Thus we set $\phi(\mathbf{x}, t) = -\mathbf{x} \cdot \mathbf{E}$, where \mathbf{E} is the time-independent

uniform electric field. We will address time-dependent electric fields later in this chapter. The equation of motion for the retarded function is thus

$$\left[i \frac{\partial}{\partial t} - \left(-\frac{1}{2} \nabla^2 - q \mathbf{x} \cdot \mathbf{E} \right) \right] G_{\phi}^r(\mathbf{x}, t, \mathbf{x}', t') = \delta(\mathbf{x} - \mathbf{x}') \delta(t - t') . \quad (10.1)$$

The Fourier transform of (10.1) is

$$\left[i \frac{\partial}{\partial t} - \left(\frac{1}{2} k_{\parallel}^2 + \frac{1}{2} k_{\perp}^2 - iqE \frac{\partial}{\partial k_{\parallel}} \right) \right] G_{\phi}^r(\mathbf{k}, t, \mathbf{k}', t') = \delta(\mathbf{k} - \mathbf{k}') \delta(t - t') . \quad (10.2)$$

In writing (10.2) we used a coordinate system where the field defines a parallel direction and the other spatial directions are referred to as perpendicular directions. Since the translational invariance is still preserved in the perpendicular direction, it is sufficient to use just one perpendicular momentum to label the Green functions, and we write ($k_{\perp} \equiv |\mathbf{k}_{\perp}|$):

$$\left[i \frac{\partial}{\partial t} - \left(\frac{1}{2} k_{\parallel}^2 + \frac{1}{2} k_{\perp}^2 - iqE \frac{\partial}{\partial k_{\parallel}} \right) \right] G_{\phi}^r(k_{\parallel}, k'_{\parallel}, k_{\perp}, t - t') = \delta(k_{\parallel} - k'_{\parallel}) \delta(t - t') . \quad (10.3)$$

By defining a set of new variables,

$$u = t - \frac{1}{qE} k_{\parallel} , \quad v = \frac{1}{2} \left(t + \frac{1}{qE} k_{\parallel} \right) ,$$

we can cast (10.3) in the form

$$\left[\alpha(x) + \frac{d}{dx} \right] f(x) = g(x) ,$$

whose (particular) solution is

$$f(x) = \int_c^x dx'' \exp \left[\int_x^{x''} dx' \alpha(x') \right] g(x'') ,$$

where c is an integration constant. Making the appropriate identifications, choosing c to correspond to a retarded function, and returning to the original variables, we find G_{ϕ}^r :

$$\begin{aligned} G_{\phi}^r(k_{\parallel}, k'_{\parallel}, k_{\perp}, t - t') &= -i\delta \left[k_{\parallel} - k'_{\parallel} - qE(t - t') \right] \theta(t - t') \\ &\times \exp \left\{ i \frac{(qE)^2}{6} \left[\left(\frac{k'_{\parallel}}{qE} \right)^3 - \left(\frac{k_{\parallel}}{qE} \right)^3 \right] - \frac{i}{2} k_{\perp}^2 (t - t') \right\} . \end{aligned} \quad (10.4)$$

The argument in the exponential of (10.4) can be rearranged in a number of ways by making use of the δ -function. An instructive way is to write (10.4) as

$$\begin{aligned} G_{\phi}^r(k_{\parallel}, k'_{\parallel}, k_{\perp}, t - t') &= -i\delta[k_{\parallel} - k'_{\parallel} - qE(t - t')] \theta(t - t') \\ &\times \exp \left[-i \int_0^{t-t'} d\tau \varepsilon_{\mathbf{k}}(\tau) \right], \end{aligned} \quad (10.5)$$

where

$$\varepsilon_{\mathbf{k}}(\tau) = \frac{1}{2} [(k_{\parallel} - qE\tau)^2 + k_{\perp}^2] \quad (10.6)$$

is the time-dependent kinetic energy. We may understand (10.5) as a natural modification in an electric field of the zero-field Green function

$$G_0^r(\mathbf{k}, \mathbf{k}', t - t') = -i\delta(\mathbf{k} - \mathbf{k}')\theta(t - t') \exp[-i\varepsilon_{\mathbf{k}}(t - t')]. \quad (10.7)$$

The two changes are (a) the shift in the k_{\parallel} -momentum conservation law to account for the acceleration due to the electric field, and (b) the time evolution of the kinetic energy (10.6). For completeness, we also give the Fourier transform of (10.4):

$$\begin{aligned} G_{\phi}^r(k_{\parallel}, k'_{\parallel}, k_{\perp}, \omega) &= -\frac{i}{qE}\theta(k_{\parallel} - k'_{\parallel}) \\ &\times \exp \left[\frac{i}{qE} \left[\frac{k_{\parallel}^3 - k'^3_{\parallel}}{6} - (k_{\parallel} - k'_{\parallel}) \left(\frac{k_{\perp}^2}{2} - \omega \right) \right] \right]. \end{aligned} \quad (10.8)$$

This expression is formally singular in the $F \rightarrow 0$ limit, and it does not appear obvious how the zero-field limit is contained in it. Of course, one could go back to the time representation (10.4), where the zero-field limit is easy to work out. However, in many calculations the frequency representation is more convenient, and it is necessary to be able to verify in the various stages of calculation, that a correct zero-field limit can be recovered. The next example shows that, if one interprets (10.8) in the distribution sense, a consistent limiting procedure can be constructed.

Zero-Field Limit of Field-Dependent Green Functions

We demonstrate now how the correct zero-field limit can be obtained if the Green functions are interpreted in the distribution sense. To this effect, consider a generalized function $D(x)$ defined as

$$D(x) = \lim_{F \rightarrow 0} \left\{ \theta(x) \frac{1}{F} \exp[-\eta(x/F)] \exp[i(x/F)g(x)] \right\}, \quad (10.9)$$

where η is a positive infinitesimal. Identifying $x = k_{\parallel} - k'_{\parallel}$, we see that (10.8) is a special case of the function $D(x)$. We want to show that

$$D(x) = i \frac{\delta(x)}{g(x=0) + i\eta} . \quad (10.10)$$

Consider now the effect of $D(x)$ on a suitable test function $f(x)$,

$$d \equiv \int_{-\infty}^{\infty} dx D(x) f(x) . \quad (10.11)$$

If we can show that

$$d = i \frac{f(0)}{g(0) + i\eta} , \quad (10.12)$$

the proof is complete. The proof proceeds by a direct calculation:

$$\begin{aligned} d &= \lim_{F \rightarrow 0} \int_0^{\infty} dx \frac{1}{F} \exp[-\eta(x/F)] \exp[i(x/F)g(x)] f(x) \\ &= \lim_{F \rightarrow 0} \left\{ \left[\frac{\exp[-\eta t + itg(Ft)] f(Ft)}{-\eta + ig(Ft) + itFg'(Ft)} \right]_0^{\infty} \right. \\ &\quad \left. - \int_0^{\infty} dt \exp[-\eta t + itg(Ft)] \frac{\partial}{\partial t} \left[\frac{f(Ft)}{-\eta + ig(Ft) + itFg'(Ft)} \right] \right\} . \end{aligned} \quad (10.13)$$

On arriving at the second line of (10.13) we changed the variables via $x/F = t$, and integrated by parts. The first term in (10.13) leads to the desired final result (10.12) and the second term vanishes, which can be seen by the following reasoning: Consider the derivative of the term in the square brackets. The differentiation produces a multiplicative factor of F which can be moved outside the integral. The remaining integral is convergent [note the importance of the convergence factor $\exp(-\eta t)$], and hence a zero net result is obtained as the external field tends to zero. This completes the proof of (10.10).

We next show that the gauge-invariant form of (10.4) coincides with the result (7.26) found earlier. Following the prescription from Chap. 7 (see also [94]), we first transform G_{ϕ}^r in the difference and center-of-mass variables (we suppress the unessential k_{\perp} -dependence, and hence use one-dimensional variables r and R):

$$\begin{aligned} G_{\phi}^r(r, R, \tau) &= -i\theta(\tau) \sum_{k_{\parallel}, k'_{\parallel}} \exp[i k_{\parallel}(R + r/2) - i k'_{\parallel}(R - r/2)] \\ &\quad \times \delta(k_{\parallel} - k'_{\parallel} - qE\tau) \exp \left\{ \frac{i(qE)^3}{6} [k'^3_{\parallel} - k^3_{\parallel}] \right\} , \end{aligned} \quad (10.14)$$

and proceed with the help of the rule (7.8):

$$\tilde{G}^r(k, \tau) = \int dr \exp[-iqER\tau - ikr] G_{\phi}^r(r, R, \tau) .$$

We can immediately do the k_{\parallel} -sum with the help of the δ -function, the r -integral results in another δ -function, and the final k'_{\parallel} -sum is then also simple to do with the final result:

$$\tilde{G}^{r,a}(k, \tau) = \mp i\theta(\pm\tau) \exp[-i(\varepsilon_k \tau + (qE)^2 \tau^3 / 24)], \quad (10.15a)$$

$$\tilde{G}^{r,a}(k, \omega) = \sum_{n=0}^{\infty} \frac{(-1)^n}{n!} \left(\frac{(qE)^2}{24} \right)^n \left(\frac{\partial}{\partial \varepsilon_k} \right)^{3n} \frac{1}{\omega - \varepsilon_k \pm i\eta}. \quad (10.15b)$$

Here, the first equation coincides with (7.26) and we have also given the result for the advanced Green function; tracing back the analysis, the only difference is in the choice of the integration constant c . The Fourier representation, given in the second equation, can be obtained with a term-by-term expansion from the first equation. In spite of its highly singular character, it can be used if one needs to calculate power series expansions in the electric field. In addition, it explicitly displays the expected analytic structure of a retarded (advanced) Green function: the singularities in the complex ω -plane are in the lower (upper) half-plane.

We could have equally well started by considering the free field-dependent retarded Green function $G_A^r(\mathbf{p}, t, t')$ in the vector potential gauge, which satisfies the equation-of-motion:

$$\left\{ i \frac{\partial}{\partial t} - \varepsilon[\mathbf{p} - q\mathbf{A}(t)] \right\} G_A^r(\mathbf{p}, t, t') = \delta(t - t'). \quad (10.16)$$

This equation can be immediately integrated:

$$G_A^r(\mathbf{p}, t, t') = -i\theta(t - t') \exp \left\{ -i \int_{t'}^t dt_1 \varepsilon[\mathbf{p} - q\mathbf{A}(t_1)] \right\} \quad (10.17)$$

with the associated field-dependent spectral function,

$$A_A(\mathbf{p}, t, t') = \exp \left\{ -i \int_{t'}^t dt_1 \varepsilon[\mathbf{p} - q\mathbf{A}(t_1)] \right\}. \quad (10.18)$$

It is readily verified that in the dc-limit [$\mathbf{A} = -Et$], and after a transformation to the gauge invariant variables (10.17) coincides with the result (10.15a). We also quote the ω -representation of the gauge invariant spectral function \tilde{A} :

$$\begin{aligned} \tilde{A}(\mathbf{k}, \omega) &= 2 \int_0^\infty d\tau \cos[\omega\tau - (\varepsilon_k \tau + (qE)^2 \tau^3 / 24)] \\ &= \frac{2\pi}{\alpha} \text{Ai}\left(\frac{\varepsilon_k - \omega}{\alpha}\right), \end{aligned} \quad (10.19)$$

where $\text{Ai}(x)$ is the Airy function, and we introduced the field parameter $\alpha = (\hbar^2 q^2 E^2 / 8m)^{1/3}$. For a typical semiconductor, say GaAs with conduction band

effective mass $m_{\text{eff}} = 0.067m_e$, one can write $\alpha = 0.446 \text{ eV} \times E (\text{MV m}^{-1})$. It is important to notice that the spectral function satisfies the sum rule $\int d\omega/(2\pi) \tilde{A}(\mathbf{k}, \omega) = 1$, as it should. The field-dependent spectral function is plotted as a function of $\omega - \varepsilon_k$ in Fig. 10.1 for three different field strengths. The most important feature of Fig. 10.1 is that the *nonequilibrium* spectral function does not have to be positive. This property prohibits a straightforward interpretation of $\tilde{A}(\mathbf{k}, \omega)$ as some sort of “density,” as is customary in equilibrium theory. There the spectral function often has the structure:

$$a(\mathbf{k}, \omega) = Z(\mathbf{k})\delta[\omega - \varepsilon^*(\mathbf{k})] + \text{background}. \quad (10.20)$$

Comparing to the free spectral function $a_0(\mathbf{k}, \omega) = 2\pi\delta[\omega - \varepsilon(\mathbf{k})]$, one calls $\varepsilon^*(\mathbf{k})$ the “quasiparticle” dispersion, and $Z(\mathbf{k})$ is called the quasiparticle weight, or wavefunction renormalization. In view of the complicated structure displayed in Fig. 10.1, which clearly cannot be interpreted in terms of quasi-particles, the immediate conclusion is that the quasiparticle concept must be carefully reconsidered in nonequilibrium. However, one should bear in mind that Fig. 10.1 represents *free* particles in an electric field, and no interaction effects have been included. As later examples will reveal, interactions may smoothen, or effectively average A , and hence the rapid oscillations tend to be suppressed. Finally, it is clear from Fig. 10.1 that A does not approach its zero-field limit in any smooth fashion; this is another reflection of the singular character of the perturbing electric field.

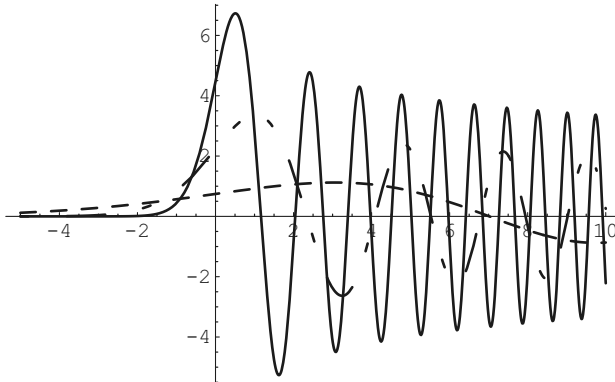


Fig. 10.1. The spectral function $\tilde{A}(\mathbf{k}, \omega)$ as a function of $(\omega - \varepsilon_k)$ for the field parameter $\alpha = 0.5, 1.0$, and 3.0 eV (*continuous line*, *dash-dotted line*, and *dashed line*, respectively), and effective mass $m = 0.067m_e$. The smaller the external field is, the more weight is located at $\omega - \varepsilon_k = 0$

10.2 A Model for Dynamical Disorder: The Gaussian White Noise Model

10.2.1 Introduction

In this section we apply the quantum kinetic equations to an *exactly solvable* model system: the Gaussian white noise model (GWN). Exactly solvable, but yet nontrivial, models are rare, and even though the GWN model has certain problems, to be discussed below, it provides an excellent “testing laboratory of the theory,” where we can analyze explicitly and analytically the quantum kinetic equations, which are very complicated for any realistic scattering mechanism. In particular, we shall evaluate the transient dynamics for the GWN model, following the work of [136, 172, 173].

The basic problem with the GWN model is that it possesses an inherent thermal instability: it does not maintain thermal equilibrium. The question is then: can one calculate the response of GWN to an external perturbation using a kinetic equation which contains this thermal instability, or does one have to modify the kinetic equation? We shall follow both of these lines, and contrast the different results obtained by each method. In our calculations we follow the general two-step strategy outlined in Chap. 5: one first determines the retarded Green function, and then uses this result as an input to the quantum kinetic equation.

10.2.2 Determination of the Retarded Green Function

Before turning to the kinetic equation, we must solve the dynamics, i.e., determine the disorder-averaged retarded Green function in an external field. We choose the following form of the Hamiltonian [124, 183]:

$$H = \int d\mathbf{x} \psi^\dagger(\mathbf{x}) \left[-\frac{1}{2} \nabla^2 + V(\mathbf{x}, t) \right] \psi(\mathbf{x}). \quad (10.21)$$

Here the ψ 's are anti-commuting fermion operators, $\{\psi(\mathbf{x}), \psi^\dagger(\mathbf{x}')\} = \delta(\mathbf{x} - \mathbf{x}')$, and the parametric time-dependence of the impurity potential reflects the random thermal fluctuations of the environment. Further, we set $\hbar = m = 1$. The average over disorder is performed with the prescription

$$\begin{aligned} \langle V(\mathbf{x}, t) \rangle &= 0, \\ \langle V(\mathbf{x}, t_x) V(\mathbf{y}, t_y) \rangle &= \gamma(\mathbf{x} - \mathbf{y}) \delta(t_x - t_y). \end{aligned} \quad (10.22)$$

All odd higher averages vanish, and higher even averages are given as a sum of all pair-wise averages. Just like in the elastic impurity problem discussed in Chap. 9, we use the self-consistent Born approximation for the self-energy:

$$\Sigma(\mathbf{x}, \mathbf{y}, t, t') = \gamma(\mathbf{x} - \mathbf{y}) G(\mathbf{x} - \mathbf{y}, t, t') \delta(t - t'), \quad (10.23)$$

where G is the impurity-averaged Green function.

Adding the external field does not change the diagrammatic structure of the theory. The only difference is that the free propagation between scattering events now takes place under the influence of the external field. Thus, one ends up with the following Dyson equation for the retarded Green function:

$$\begin{aligned} G^r(\mathbf{p}, t, t') = & G_A^r(\mathbf{p}, t, t') + \int dt_1 G_A^r(\mathbf{p}, t, t_1) \\ & \times \sum_{\mathbf{q}} \gamma(\mathbf{p} - \mathbf{q}) G^r(\mathbf{q}, t_1, t_1) G^r(\mathbf{p}, t_1, t') , \end{aligned} \quad (10.24)$$

where $G_A^r(\mathbf{p}, t, t')$ is given by (10.17). In (10.24) we also introduced $\gamma(\mathbf{p})$, which is the Fourier transform of $\gamma(\mathbf{x})$. Equation (10.24) is formally a nonlinear integral equation for G^r . However, it can be readily solved by using the equal-time anti-commutation rule for the field operators appearing in the definition of G^r .¹ Thus, we may write

$$\sum_{\mathbf{q}} \gamma(\mathbf{p} - \mathbf{q}) G^r(\mathbf{q}, t_1, t_1) = -\frac{i}{2} \sum_{\mathbf{q}} \gamma(\mathbf{p} - \mathbf{q}) \equiv -\frac{i}{2} \gamma_0 . \quad (10.25)$$

With (10.25) in (10.24), and converting the Dyson equation to a differential equation by multiplying with G_A^{-1} , one finds the solution:

$$G^r(\mathbf{p}, t, t') = -i\theta(t - t') \exp \left\{ -i \int_{t'}^t dt_1 \varepsilon[\mathbf{p} - q\mathbf{A}(t_1)] - \frac{\gamma_0}{2}(t - t') \right\} . \quad (10.26)$$

The gauge-invariant retarded (advanced) Green function is calculated with the techniques developed in Chap. 7. Explicitly, we have (here we consider static electric fields)

$$\begin{aligned} \tilde{G}^{r,a}(\mathbf{k}, \tau, T) &= \int d\mathbf{r} e^{-i(\mathbf{k}-q\mathbf{E}T)\cdot\mathbf{r}} G_A^{r,a}(\mathbf{r}, \tau, T) \\ &= \int d\mathbf{r} e^{-i(\mathbf{k}-q\mathbf{E}T)\cdot\mathbf{r}} \int \frac{d\mathbf{p}}{(2\pi)^3} e^{i\mathbf{p}\cdot\mathbf{r}} G_A^{r,a}(\mathbf{p}, T + \frac{\tau}{2}, T - \frac{\tau}{2}) \\ &= \mp i\theta(\pm\tau) \exp \left[-i \int_{-\tau/2}^{\tau/2} dt' \varepsilon(\mathbf{k} + q\mathbf{E}t') \mp \frac{\gamma_0}{2}\tau \right] . \end{aligned} \quad (10.27)$$

The result (10.27) is our first encounter with a field-dependent Green function with scattering, and we shall see several others in later sections. It is interesting to note that all T -dependence drops out from (10.27). This is what one expects on physical grounds: for time-independent external perturbations retarded Green functions should also be time-independent. This completes the first step of the calculation, and we now turn to the construction of the kinetic equation.

¹ It is necessary to assign a definite value to the somewhat ill-defined object $\theta(t \rightarrow t'^+)$. By considering the integral representation of the step-function, one sees that the proper choice corresponds to $\theta(t \rightarrow t'^+) = 1/2$.

10.2.3 Kinetic Equation for the GWN

There are two main methods for setting up the kinetic equation. One can use either the Keldysh formulation, which leads to an integral equation for the correlation function $G^<$, or the Kadanoff–Baym method, which leads to a differential equation for $G^<$. Here we give the details of the Kadanoff–Baym approach, and leave the details of the Keldysh method as an exercise.

Since many physical properties [density $N(\mathbf{R}, T)$, current density $\mathbf{J}(\mathbf{R}, T)$, etc.] are determined by the Wigner function f^W , which is a less complex object than the full correlation function $G^<$, it is often advantageous to inquire as to whether one can obtain a closed equation for f^W . In Chap. 8 we derived a kinetic equation for the Wigner function, and we reproduce it here for convenience:

$$\left[\frac{\partial}{\partial T} + q\mathbf{E} \cdot \frac{\partial}{\partial \mathbf{k}} \right] f^W(\mathbf{k}, T) = - \int d\tau' \tilde{A} \left(\mathbf{k} + \frac{q}{2}\mathbf{E}\tau', -\tau', T + \tau' \right) \\ \times \tilde{B} \left(\mathbf{k} + \frac{q}{2}\mathbf{E}\tau', \tau', T + \tau' \right), \quad (10.28)$$

where

$$\tilde{A}(\mathbf{k}_1, \tau_1, T_1) \tilde{B}(\mathbf{k}_2, \tau_2, T_2) = [\tilde{\Sigma}^r \tilde{G}^< + \tilde{\Sigma}^< \tilde{G}^a - \tilde{G}^r \tilde{\Sigma}^< - \tilde{G}^< \tilde{\Sigma}^a] \\ \times (\mathbf{k}_1, \tau_1, T_1)(\mathbf{k}_2, \tau_2, T_2). \quad (10.29)$$

Note that, in general, it is not possible to obtain a closed equation for the Wigner function, because the right-hand side of (10.28) involves the full correlation function. However, in the present case, the one-point nature of the GWN interaction [as evinced by the δ -function in time in (10.23)] allows one to obtain a closed equation for f^W .

In order to make further progress we must specify the various self-energies. The retarded and advanced self-energies we know already from the previous section:

$$\Sigma^r(\tau) = -\frac{i}{2}\gamma_0\delta(\tau) = -\Sigma^a(\tau). \quad (10.30)$$

There are two plausible choices for $\Sigma^<$. Following [136], one can choose:

$$\Sigma^<(t, t') = i\gamma_0 \int \frac{d\varepsilon}{2\pi} n_F(\varepsilon) \exp[-i\varepsilon(t - t')], \\ \Sigma^>(t, t') = -i\gamma_0 \int \frac{d\varepsilon}{2\pi} [1 - n_F(\varepsilon)] \exp[-i\varepsilon(t - t')]. \quad (10.31)$$

The first thing to note is that this choice satisfies the consistency check $\Sigma^r - \Sigma^a = \Sigma^> - \Sigma^<$. The physics behind this choice is that now GWN is “anchored” to thermal equilibrium: the scattering terms increasing the population of a given \mathbf{k} -state act as if the particles were emerging from an underlying thermal equilibrium state. In this way the thermal instability hidden in GWN (which will be made explicit below) is thus removed, and one can expect

to find a meaningful result in the long-time limit, which we plan to calculate. Using these expressions, and the retarded and advanced Green functions from (10.27), we can evaluate the collision term in (10.28):

$$\begin{aligned}\tilde{\Sigma}^r \tilde{G}^< - \tilde{G}^< \tilde{\Sigma}^a &\rightarrow \int d\tau' \left[\frac{-i}{2} \gamma_0 \delta(-\tau') \tilde{G}^< \left(\mathbf{k} + \frac{q}{2} \mathbf{E} \tau', \tau', T + \tau' \right) \right. \\ &\quad \left. - \tilde{G}^< \left(\mathbf{k} + \frac{q}{2} \mathbf{E} \tau', -\tau', T + \tau' \right) \frac{i}{2} \gamma_0 \delta(\tau') \right] \\ &= \gamma_0 f^W(\mathbf{k}, T)\end{aligned}$$

and

$$\begin{aligned}\tilde{\Sigma}^< \tilde{G}^a - \tilde{G}^r \tilde{\Sigma}^< &\rightarrow -\gamma_0 \int \frac{d\varepsilon}{2\pi} n_F(\varepsilon) \int_{-\infty}^0 d\tau' \\ &\times \left\{ e^{i\varepsilon\tau'} \exp \left[-i \int_{-\tau'/2}^{\tau'/2} dt' \varepsilon \left(\mathbf{k} + q\mathbf{E} \left[t' + \frac{\tau'}{2} \right] \right) + \frac{\gamma_0}{2} \tau' \right] \right. \\ &\quad \left. + \exp \left[-i \int_{\tau'/2}^{-\tau'/2} dt' \varepsilon \left(\mathbf{k} + q\mathbf{E} \left[t' + \frac{\tau'}{2} \right] \right) + \frac{\gamma_0}{2} \tau' \right] e^{-i\varepsilon\tau'} \right\} \\ &\equiv -\gamma_0 g(\mathbf{k}),\end{aligned}$$

where

$$g(\mathbf{k}) = \int \frac{d\varepsilon}{2\pi} n_F(\varepsilon) \int_0^\infty d\tau 2 \cos \left[\varepsilon\tau - \int_0^\tau d\tau' \varepsilon (\mathbf{k} - q\mathbf{E}\tau') \right] e^{-\gamma_0\tau/2}, \quad (10.32)$$

and the kinetic equation is thus:

$$\left[\frac{\partial}{\partial T} + q\mathbf{E} \cdot \frac{\partial}{\partial \mathbf{k}} \right] f^W(\mathbf{k}, T) = -\gamma_0 [f^W(\mathbf{k}, T) - g(\mathbf{k})]. \quad (10.33)$$

This equation has a relaxation-time form, where the nonequilibrium distribution function relaxes to the field-dependent function g . We observe that before the field is turned on, the equilibrium momentum distribution,

$$f^{\text{eq}}(\mathbf{k}) \equiv \int \frac{d\varepsilon}{2\pi i} g^<(\mathbf{k}, \varepsilon) = \int \frac{d\varepsilon}{2\pi} n_F(\varepsilon) a(\mathbf{k}, \varepsilon), \quad (10.34)$$

where the equilibrium spectral function is given by

$$a(\mathbf{k}, \varepsilon) = \frac{\gamma_0}{[\varepsilon - \varepsilon(\mathbf{k})]^2 + [\gamma_0/2]^2}, \quad (10.35)$$

satisfies (10.33) identically. This property confirms the statement made above that the self-energies (10.31) reintroduce thermal equilibrium in the problem.

We can now proceed to calculate the steady-state current, and we can set $\partial f^W / \partial T = 0$ in (10.33). We perform the calculation in two steps. First, sum over \mathbf{k} on both sides of (10.33). This gives, observing $\sum_{\mathbf{k}} \mathbf{E} \cdot [\partial / \partial \mathbf{k}] f^W(\mathbf{k}) = 0$,

$$0 = -\gamma_0 \left\{ \sum_{\mathbf{k}} f^W(\mathbf{k}) - \sum_{\mathbf{k}} \int \frac{d\varepsilon}{2\pi} n_F(\varepsilon) \right. \\ \left. \times \int_0^\infty d\tau 2 \cos[\varepsilon\tau - \int_0^\tau d\tau' \varepsilon(\mathbf{k} - q\mathbf{E}\tau')] e^{-\gamma_0\tau/2} \right\}. \quad (10.36)$$

Since $\sum_{\mathbf{k}} f^W(\mathbf{k}) = N$, we observe that the particle number depends on the applied field. Thus the assumed underlying thermal background acts as a source (or sink) of particles. This particle conservation violation can be viewed as being the price for introducing thermal equilibrium by hand.

The next step in the calculation consists of multiplying (10.33) by $q\mathbf{k}$, and summing over \mathbf{k} . Integrating the left-hand side by parts gives $-q^2 \mathbf{E}N$, and using (10.36) we obtain the following explicit result for the current [$\mathbf{J} = \sum_{\mathbf{k}} q\mathbf{k}f^W(\mathbf{k})$]:

$$\mathbf{J} = \sum_{\mathbf{k}} \left[q \left(\frac{q}{\gamma_0} \mathbf{E} + \mathbf{k} \right) \right] \int \frac{d\varepsilon}{2\pi} n_F(\varepsilon) \\ \times \int_0^\infty d\tau 2 \cos \left[\varepsilon\tau - \int_0^\tau d\tau' \varepsilon(\mathbf{k} - q\mathbf{E}\tau') e^{-\gamma_0\tau/2} \right]. \quad (10.37)$$

Equation (10.37) gives the full nonlinear current-field relationship for the GWN, in the special case of self-energies (10.31). It is interesting to explore the linear response limit of (10.37). To make the calculations as simple as possible, it is convenient to define a new integration variable in (10.37), $\mathbf{k} \rightarrow \mathbf{k}' = \frac{q}{\gamma_0} \mathbf{E} + \mathbf{k}$. Performing the linearization the linear current $\mathbf{J}^{(1)}$ is calculated as [we use shorthand notation $\Delta \equiv \varepsilon - \varepsilon(\mathbf{k})$]

$$\mathbf{J}^{(1)} = q^2 \sum_{\mathbf{k}} \mathbf{k}(\mathbf{k} \cdot \mathbf{E}) \int \frac{d\varepsilon}{2\pi} \int_0^\infty d\tau n_F(\varepsilon) \\ \times (-2 \sin \Delta\tau) \left(\frac{\tau^2}{2} + \frac{\tau}{\gamma_0} \right) e^{-\gamma_0\tau/2} \\ = q^2 \sum_{\mathbf{k}} \mathbf{k}(\mathbf{k} \cdot \mathbf{E}) \int \frac{d\varepsilon}{2\pi} [-n'_F(\varepsilon)] \left(\frac{1}{\gamma_0} - \frac{\partial}{\partial \gamma_0} \right) \\ \times \int_0^\infty d\tau 2 \cos \Delta\tau e^{-\gamma_0\tau/2},$$

where we integrated by parts with respect to ε . Finally, performing the τ -integration, we get

$$\mathbf{J}^{(1)} = q^2 \sum_{\mathbf{k}} \mathbf{k}(\mathbf{k} \cdot \mathbf{E}) \int \frac{d\varepsilon}{2\pi} [-n'_F(\varepsilon)] \frac{1}{2} a^2(\mathbf{k}, \varepsilon), \quad (10.38)$$

where a is the equilibrium spectral function (10.35). It is instructive to verify that this result can also be obtained with the linear quantum Boltzmann approach developed in Chap. 9; in particular, summing (9.22) over \mathbf{k} leads directly to (10.38).

We now turn to the other plausible choice for the self-energies $\Sigma^{<,>}$ [172, 173]. Here we use the form (10.23), which suggests using the following gauge-invariant self-energy:

$$\begin{aligned}\tilde{\Sigma}^<(\mathbf{k}, \tau, T) &= \sum_{\mathbf{k}'} \delta(\tau) \gamma(\mathbf{k} - \mathbf{k}') \tilde{G}^<(\mathbf{k}', \tau, T) \\ &= \delta(\tau) \sum_{\mathbf{k}'} \gamma(\mathbf{k} - \mathbf{k}') i f^W(\mathbf{k}', T).\end{aligned}\quad (10.39)$$

With this choice the kinetic equation becomes

$$\begin{aligned}\left[\frac{\partial}{\partial T} + q \mathbf{E} \cdot \frac{\partial}{\partial \mathbf{k}} \right] f^W(\mathbf{k}, T) \\ = - \left[\gamma_0 f^W(\mathbf{k}, T) - \sum_{\mathbf{k}'} \gamma(\mathbf{k} - \mathbf{k}') f^W(\mathbf{k}', T) \right].\end{aligned}\quad (10.40)$$

Ovchinnikov and Erikman [279] have given the lattice version of this equation, and its zero-field form appears also in [136, 183]. We observe that (10.39) is identical to the semiclassical Boltzmann equation which one would write for the GWN. It also resembles the conventional impurity Boltzmann equation. However, the normal energy-conserving δ -function is missing. This difference is crucial: the physics of GWN is quite different from normal elastic impurity systems. It is important to notice that (10.40) is actually more general than the Boltzmann equation: it was obtained with an exact sequence of transformations starting from the quantum kinetic equation for the correlation function $G^<$. As we showed in Chap. 6, the lowest-order gradient approximation to the quantum kinetic equation leads to the Boltzmann equation (we studied explicitly only the elastic impurity problem, but the same holds true for many other scattering mechanisms); the GWN is a special interaction in the sense that the quantum kinetic equation coincides with the Boltzmann equation. This property is a consequence of the one-point character of the GWN. It is also of interest to note that GWN does not display any *intracollisional field-effect*: i.e., the collision term in (10.40) does not depend on the applied field. In later sections, we shall see several other examples of scattering mechanisms, for which quantum kinetic considerations yield a field-dependent collision term.

We next evaluate the current using (10.40) as the starting point. As a preliminary, we sum both sides over \mathbf{k} , and find:

$$\frac{\partial}{\partial T} N = -\gamma_0 N + \sum_{\mathbf{k}, \mathbf{k}'} \gamma(\mathbf{k} - \mathbf{k}') f^W(\mathbf{k}', T) = 0,\quad (10.41)$$

where the second equality follows from the definition of γ_0 . Thus $N = \text{constant}$, and the continuity equation is identically satisfied. Here the two different self-energy models depart: we saw above that (10.31) leads to a field-dependent particle number. The next step in the evaluation of the current consists of multiplying (10.40) by $q\mathbf{k}$, and summing over \mathbf{k} , which leads to

$$\frac{\partial}{\partial T} \mathbf{J} - q^2 \mathbf{E} N = -\gamma_0 \mathbf{J} + \sum_{\mathbf{k}, \mathbf{k}'} \mathbf{k} \gamma(\mathbf{k} - \mathbf{k}') f^W(\mathbf{k}', T). \quad (10.42)$$

If we consider crystals with inversion symmetry, we must have $\sum_{\mathbf{k}} \mathbf{k} \gamma(\mathbf{k}) = 0$. Thus, making the replacement $\mathbf{k} = (\mathbf{k} - \mathbf{k}') + \mathbf{k}'$ on the right-hand side of (10.42), and performing the \mathbf{k} -summation, one finds that the right-hand side of (10.42) *vanishes*. Using the initial condition $\mathbf{J}(T = 0) = 0$, we obtain

$$\mathbf{J} = q^2 \mathbf{E} N T. \quad (10.43)$$

This is an interesting result: the interaction with the GWN potential has entirely dropped out from the current response! Thus, both of the considered models have somewhat peculiar properties: the first one, where thermal equilibrium was introduced by hand, does not conserve the particle number, while the second one is unable to relax momentum. We shall next examine other transport properties in the context of the second model.

10.2.4 Other Transport Properties

In Sect. 10.2.3, we found that the self-energy model (10.39) did not relax momentum in the conventional sense. From this it follows that its diffusion and energy relaxation properties are also unusual. Let us first consider energy relaxation by calculating the time-dependence of the average kinetic energy $\varepsilon(T) \equiv \sum_{\mathbf{k}} \frac{1}{2} k^2 f^W(\mathbf{k}, T)$. Multiply now (10.40) by $\frac{1}{2} k^2$, and sum over \mathbf{k} :

$$\begin{aligned} \frac{\partial \varepsilon(T)}{\partial T} + \sum_{\mathbf{k}} \frac{1}{2} k^2 q \mathbf{E} \cdot \frac{\partial}{\partial \mathbf{k}} f^W(\mathbf{k}, T) \\ = -\gamma_0 \varepsilon(T) + \sum_{\mathbf{k}, \mathbf{k}'} \frac{1}{2} k^2 \gamma(\mathbf{k} - \mathbf{k}') f^W(\mathbf{k}', T). \end{aligned} \quad (10.44)$$

The second term on the left-hand side can be integrated by parts to yield $-\mathbf{E} \cdot \mathbf{J} = -q^2 E^2 N T$, while the last term on the right-hand side is manipulated as follows:

$$\begin{aligned} & \sum_{\mathbf{k}, \mathbf{k}'} \frac{1}{2} k^2 \gamma(\mathbf{k} - \mathbf{k}') f^W(\mathbf{k}', T) \\ &= \sum_{\mathbf{k}, \mathbf{k}'} \frac{1}{2} (\mathbf{k} - \mathbf{k}' + \mathbf{k}')^2 \gamma(\mathbf{k} - \mathbf{k}') f^W(\mathbf{k}', T) \end{aligned}$$

$$\begin{aligned}
&= \sum_{\mathbf{k}, \mathbf{k}'} \left[\frac{1}{2}(\mathbf{k} - \mathbf{k}')^2 + (\mathbf{k} - \mathbf{k}') \cdot \mathbf{k}' + \frac{1}{2}k'^2 \right] \gamma(\mathbf{k} - \mathbf{k}') f^W(\mathbf{k}', T) \\
&= \gamma_2 N + 0 + \gamma_0 \varepsilon(T) .
\end{aligned}$$

The second term on the second line vanished upon \mathbf{k} -summation due to the assumed inversion symmetry, and we defined

$$\gamma_2 = \sum_{\mathbf{k}} \frac{1}{2} k^2 \gamma(\mathbf{k}) . \quad (10.45)$$

Collecting the terms, and integrating, we thus find:

$$\varepsilon(T) = \varepsilon(T=0) + \gamma_2 NT + \frac{1}{2} N q^2 E^2 T^2 . \quad (10.46)$$

The physical interpretation of this result is as follows. The last term corresponds to free particles accelerating under the influence of a uniform electric field. This is consistent with our previous results on lack of momentum relaxation. The second term describes heating due to the GWN interaction; it is a manifestation of the “self-heating” property of the GWN. As we shall see below, the second moment γ_2 of the interaction also affects the diffusion properties of the system.

We next wish to evaluate the diffusion constant of the GWN model with a zero applied field. There are a number of plausible definitions, and we choose to study the long-time behavior of test particle placed at the origin,

$$\langle x^2(T) \rangle = \int d\mathbf{R} R^2 \sum_{\mathbf{k}} f^W(\mathbf{k}, \mathbf{R}, T) . \quad (10.47)$$

If the system displays normal diffusion, one would expect that the long-time behavior of $\langle x^2(T) \rangle$ is linear in T , and the constant of proportionality could be identified as the diffusion constant.

In Chap. 7 we remarked that even in a system which is only influenced by uniform forces, spatial inhomogeneity must be considered, if the system starts its time-evolution from a spatially inhomogeneous initial state. In the present case this means that we must add an extra term to the left-hand side of the kinetic equation: $\mathbf{k} \cdot \partial/\partial\mathbf{R}$. An equation-of-motion for $\langle x^2(T) \rangle$ can be obtained by multiplying the kinetic equation (10.40) by R^2 , and integrating:

$$\frac{\partial}{\partial T} \langle x^2(T) \rangle + \sum_{\mathbf{k}} \int d\mathbf{R} R^2 \mathbf{k} \cdot \frac{\partial}{\partial \mathbf{R}} f^W(\mathbf{k}, \mathbf{R}, T) = 0 , \quad (10.48)$$

where the collision term can be shown to vanish by using similar manipulations as when deriving (10.46). The left-hand side involves an average of a new combination of variables. By integrating by parts, we see that this term can

be expressed as $\sum_{\mathbf{k}} \int d\mathbf{R} \mathbf{R} \cdot \mathbf{k} f^W(\mathbf{k}, \mathbf{R}, T) \equiv \langle xk(T) \rangle$. An equation-of-motion for $\langle xk(T) \rangle$ is obtained with the same method:

$$\frac{\partial}{\partial T} \langle xk(T) \rangle - \langle k^2(T) \rangle = 0 , \quad (10.49)$$

where we defined $\langle k^2(T) \rangle \equiv \sum_{\mathbf{k}} \int d\mathbf{R} k^2 f^W(\mathbf{k}, \mathbf{R}, T)$. Finally, the equation-of-motion for $\langle k^2(T) \rangle$ is

$$\frac{\partial}{\partial T} \langle k^2(T) \rangle = 2\gamma_2 N , \quad (10.50)$$

where we used (10.46). We can now combine (10.48)–(10.50) to get a closed equation for $\langle x^2(T) \rangle$; this equation is immediately integrated with the result:

$$\langle x^2(T) \rangle = \frac{1}{3}\gamma_2 NT^3 . \quad (10.51)$$

In writing (10.51) we made use of the initial conditions $[\partial^2 \langle x^2(T) \rangle / \partial T^2]_{T=0} = [\partial \langle x^2(T) \rangle / \partial T]_{T=0} = 0$. If one chooses a Gaussian matrix element, $\gamma(\mathbf{k}) = V_0^2 \exp(-\alpha^2 k^2/2)$, one can verify that (10.51) coincides with the result of [183], which was obtained with a different method. The T^3 -asymptotics further underline the nonstandard features of the GWN.

Summarizing this section, we have analyzed an explicitly solvable model for dynamical disorder. While the model has some pathological properties, it is nevertheless useful in illustrating the practical use of the quantum kinetic equations, because all calculations can be carried out explicitly and analytically. We shall next turn our attention to more realistic systems, where, however, approximations must be made in order to obtain explicit results.

10.3 Introduction to High-Field Transport in Semiconductors

Theoretical studies of high electric field transport in semiconductors is an old field, with a history dating back to 1930s (for a review of the early work, see [322]). In addition to the general theoretical interest in nonlinear nonequilibrium phenomena, there was also clear practical interest, such as developing an understanding of dielectric breakdown. The modern semiconductor industry has pushed the device size well below the $1 \mu\text{m}$ size, and high electric fields are commonplace in these devices. While a complete theoretical analysis of current–voltage characteristics in these devices requires a treatment of spatial inhomogeneities, the much simpler problem, transport in a uniform but arbitrarily strong electric field, remains as a topic of central importance. During the years a large variety of different theoretical analyses have been proposed to treat the problem. By far the most popular framework is based on the Boltzmann equation. The solution of the Boltzmann equation with

realistic scattering mechanisms is a difficult task, and a number of different methods have been proposed. The early analytical methods are described by Conwell [88], while several detailed accounts of the numerical Monte Carlo methods are available, such as [168, 290], or [169]. Despite of the obvious success of Boltzmann equation methods there remains a question: since the Boltzmann theory is semiclassical, is one perhaps overlooking some quantum mechanical effects? For example, the matrix elements required for the scattering terms in the collision integral are usually evaluated with plane waves (or Bloch waves), and not with some electric field-dependent wavefunctions. What then is the proper approach to take this field dependence into account? Answering this problem (and other related questions, such as what happens when the scattering rates are high, and the perturbative Boltzmann approach presumably breaks down) defines the topic of the remainder of this chapter: quantum high-field transport in uniform electric fields.

A large number of theoretical approaches for quantum high-field transport has emerged during the years. It would be impossible to give a detailed account for all these methods, and we will only briefly indicate a few central references, from which more information can be extracted. The methods can be divided in the following groups:

- (1) *Projection operator techniques.* This method was originally developed by Zwanzig [385], and applied to quantum transport in semiconductors by Barker [26, 27]; a review is available in [28].
- (2) *Feynman path integral methods.* The general formalism is described in [112], and its analytic applications to quantum transport are reviewed by Thornber [342–344]. A numerical approach was developed in [257].
- (3) *Density matrix methods.* A large body of literature is available, ranging from mainly analytical methods [319] to direct numerical integration of the Liouville equation, [63]. Many applications to semiconductor quantum transport can be found in [286], as well as in [165].
- (4) *Balance equation approach.* This method is also based on Green functions, but instead of setting up a quantum kinetic equation for the nonequilibrium distribution function, one parametrizes it with drift velocities, effective temperatures, etc., and derives equations for these quantities. The method is reviewed in [345].
- (5) *Nonequilibrium Green function techniques.* This is the topic of the present chapter, and it will be developed in detail. References to older literature can be found in reviews [35, 174–176]. One should also mention the very thorough work by Schoeller [315].

It seems reasonable to summarize all the above-mentioned methods by noting that convergence of opinion has not yet been reached: while occasionally, reasonable agreement with experiment can be obtained, the conclusions have not yet been so clear that a clearly preferred theoretical method has emerged. This “theoretical nonequilibrium” serves as a driving force for further research.

10.4 Resonant-Level Model in High Electric Fields

10.4.1 Introduction

We now apply the field-dependent Green functions of Sect. 10.3 to study the high electric field properties of a system consisting of electrons interacting with a dilute concentration of impurities. The main objectives are: (a) derivation of a (field-dependent) self-energy functional, (b) construction of the retarded Green function, which can be used in (c) setting up the quantum kinetic equation. When choosing the model interaction between electrons and impurities, we have kept the following considerations in mind. The main emphasis of this section is to illustrate the general structure of the nonlinear theory; however, we want to apply the techniques developed previously to a model, for which explicit and, if possible, analytic results can be obtained. We already encountered one such model earlier in this chapter: the Gaussian white noise model. We could solve it exactly, but this happened at high cost: the model contains a thermal instability. The next model one could consider would be the standard elastic impurity model, and we have discussed it in connection with the linearized quantum kinetic equations of Chap. 9. This model, however, has the slight complication that the single-site T -matrix satisfies an equation which is not analytically solvable (at least if one allows for a momentum-dependent scattering potential). The resonant-level model (RLM), which was studied in Sect. 3.6.2 as an example of an exactly solvable model, turns out to be a convenient yet rich model to study for nonequilibrium effects.

There are many physical situations, which can be modeled with the RLM. RLM can be viewed as describing a localized (in energy space) state in a continuum: the conduction electrons make transitions between the localized level and the continuum band, thus forming a scattering resonance. By varying the parameters of the model, one can adjust the position of the scattering resonance with respect to the Fermi level, thus displaying a variety of physical phenomena. Alternatively, we can view RLM as representing a tunneling process: electrons tunnel from one continuum (“source contact”) to the localized state, and then further to another continuum (“drain contact”). Physically, a system like this can be realized with semiconductor heterostructures, and we shall discuss them extensively in Chaps. 12 and 13. Here we treat RLM as a model, which leads to energy-dependent scattering with particularly convenient mathematics related to it. In particular, the energy dependence allows us to study the interplay of collisions and the driving field (the “intra-collisional field-effect”).

10.4.2 Retarded Green Function: Single Impurity Problem

We now generalize the RLM Hamiltonian (3.69) to include the electric field: $H_{\text{RLM}} \rightarrow H_{\text{RLM}} - i\mathbf{F} \cdot \nabla_{\mathbf{k}}$. The equation-of-motion analysis for the retarded Green function leading to (3.76) can be repeated, essentially unchanged,

with the result:

$$\begin{aligned} G^r(\mathbf{k}, \mathbf{k}', \omega) &= G_\phi^r(\mathbf{k}, \mathbf{k}', \omega) \\ &\quad + \sum_{\mathbf{q}_1, \mathbf{q}_2} G_\phi^r(\mathbf{k}, \mathbf{q}_1, \omega) T_{\mathbf{q}_1, \mathbf{q}_2}^\phi(\omega) G_\phi^r(\mathbf{q}_2, \mathbf{k}', \omega), \end{aligned} \quad (10.52)$$

where the field-dependent Green function is given by (10.8), and the field-dependent T -matrix is given by

$$T_{\mathbf{q}_1, \mathbf{q}_2}^\phi(\omega) = \frac{V(\mathbf{q}_1)V^*(\mathbf{q}_2)}{\omega - \varepsilon_0 - M^\phi(\omega)} \quad (10.53)$$

with

$$M^\phi(\omega) = \sum_{\mathbf{p}_1, \mathbf{p}_2} V^*(\mathbf{p}_1) G_\phi^r(\mathbf{p}_1, \mathbf{p}_2, \omega) V(\mathbf{p}_2). \quad (10.54)$$

To proceed further, we need an explicit form for $V(\mathbf{p})$. We choose $V(\mathbf{p}) = V_0 \exp(-\lambda^2 p^2/2)$, where the parameter λ describes the range of the interaction. With this choice we can calculate the field-dependent level width $\Gamma^\phi(\omega) \equiv \text{Im}M^\phi(\omega)$ as follows:

$$\begin{aligned} \Gamma^\phi(\omega) &= \text{Im} \left\{ -i \int_0^\infty dt e^{i\omega t} \sum_{\mathbf{p}} V\left(\mathbf{p} - \frac{1}{2}t\mathbf{F}\right) V\left(\mathbf{p} + \frac{1}{2}t\mathbf{F}\right) \right. \\ &\quad \times \exp \left[-i \left(\varepsilon_{\mathbf{p}} t + \frac{F^2 t^3}{24} \right) \right] \Big\} \\ &= -\frac{1}{2} V_0^2 \varrho \int_{-\infty}^\infty dt \int_0^\infty d\varepsilon_{\mathbf{p}} e^{-i(\varepsilon_{\mathbf{p}} - \omega)t} \\ &\quad \times \exp \left[-i \frac{F^2 t^3}{24} - \frac{\lambda^2 F^2 t^2}{4} - \lambda^2 p^2 \right] \\ &= \Gamma(\omega) \exp \left(\frac{2}{3} \lambda^6 F^2 \right) \int_{-\infty}^{\alpha(F)} dx \text{Ai}(-x). \end{aligned} \quad (10.55)$$

In the calculation leading to (10.55) several steps were taken. We converted the momentum integral to an energy integration with a constant weight factor ϱ . This implies that we are either considering a two-dimensional system, or that the energetics of the three-dimensional system are such that we can focus in the neighborhood of the Fermi surface, and thus replace the slowly varying square-root density of states by a constant. We have also introduced $\Gamma(\omega) = -\pi\varrho V_0^2 \exp(-2\lambda^2\omega)$, which is the negative of the zero-field level width. Finally, $\alpha(F) = 2\omega/F^{2/3} - \lambda^4 F^{4/3} = (m\hbar/q)^{1/3} [2\omega/E^{2/3} - q^2 m \lambda^4 E^{4/3}]$, where we have reintroduced all physical parameters into the latter expression. A numerical evaluation of (10.55) yields the results shown in Fig. 10.2. One can distinguish three regions: (a) low-field regime where the level width retains approximately its zero-field value, (b) transitional regime where the level width is a decreasing function of the electric field, and (c) high-field regime where the level width

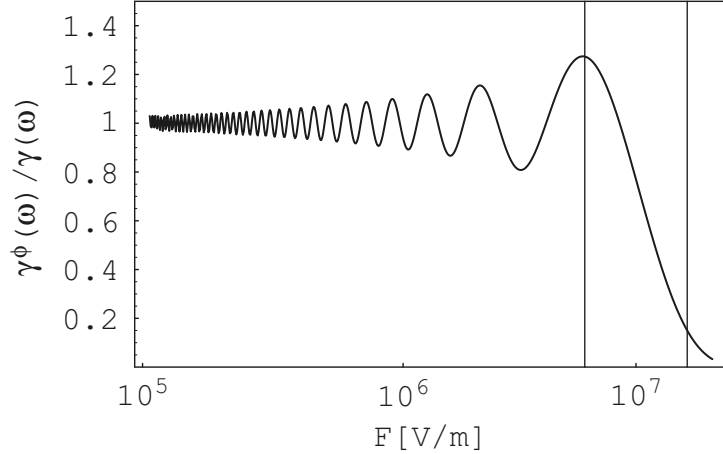


Fig. 10.2. Level width for a Gaussian model interaction for $\lambda = 20\text{\AA}$ and $\omega = 0.02\text{ eV}$. The two *vertical lines* mark the transitions between low-field, transitional, and high-field regimes discussed in the text

is very small, thus indicating decoupling of the conduction electrons from the resonant level. A detailed examination shows [180, 181] that $\Gamma^\phi(\omega)$ approaches its zero-field value for increasing energies. We will make use of these properties of $\Gamma^\phi(\omega)$ in Sect. 10.4.3, where we construct a field-dependent Green function including the effects of a finite concentration of impurities.

10.4.3 Retarded Green Function: Dilute Concentration of Impurities

We have discussed in Part I impurity averaging under equilibrium conditions. Now we must carry out the same procedure in the presence of an electric field. The basic approach is unchanged: the Dyson equation for a fixed configuration of impurities is iterated and averaged term-by-term, and, finally, a partial infinite resummation is carried out to construct a self-energy functional. Specifically, consider the Dyson equation:

$$G_{\{\mathbf{R}_\alpha\}}(\mathbf{k}, \mathbf{k}', \omega) = G_\phi(\mathbf{k}, \mathbf{k}', \omega) + \sum_{\mathbf{q}_1, \mathbf{q}_2, \{\mathbf{R}_\alpha\}} G_\phi(\mathbf{k}, \mathbf{q}_1, \omega) \exp[-i(\mathbf{q}_1 - \mathbf{q}_2) \cdot \mathbf{R}_\alpha] \times V(\mathbf{q}_1, \mathbf{q}_2; \omega) G_{\{\mathbf{R}_\alpha\}}(\mathbf{q}_2, \mathbf{k}', \omega), \quad (10.56)$$

where we explicitly indicate that the Green function depends on the particular impurity configuration. In (10.53) we have introduced a generalized scattering vertex $V(\mathbf{q}_1, \mathbf{q}_2, \omega)$ because this allows us to treat both the RLM and the elastic impurity problem on equal footing: for RLM we have

$$V^{\text{RLM}}(\mathbf{q}_1, \mathbf{q}_2; \omega) = V(\mathbf{q}_1) g_0(\omega) V(\mathbf{q}_2), \quad (10.57)$$

where $g_0(\omega) = [\omega - \varepsilon_0 + i\eta]^{-1}$ is the free localized state Green function. For the elastic impurity case we have

$$V^{\text{imp}}(\mathbf{q}_1, \mathbf{q}_2; \omega) = V(\mathbf{q}_1 - \mathbf{q}_2). \quad (10.58)$$

Just as in the equilibrium case, we ignore impurity–impurity correlations, and calculate the average nonequilibrium Green function \bar{G} with the prescription

$$\bar{G} = \langle G(\{\mathbf{R}\}) \rangle_{\text{imp}} = \prod_{\alpha} \int \frac{d\mathbf{R}_{\alpha}}{\Omega} G(\{\mathbf{R}_{\alpha}\}), \quad (10.59)$$

where Ω is the volume of the system.

The next step is to sum all scattering events at a given site \mathbf{R}_{α} . This procedure replaces the matrix element V in (10.56) by the single-site T -matrix

$$\begin{aligned} G_{\{\mathbf{R}_{\alpha}\}}(\mathbf{k}, \mathbf{k}', \omega) = & G_{\phi}(\mathbf{k}, \mathbf{k}', \omega) + \sum'_{\mathbf{q}_1, \mathbf{q}_2, \{\mathbf{R}_{\alpha}\}} G_{\phi}(\mathbf{k}, \mathbf{q}_1, \omega) \\ & \times T^{\mathbf{R}_{\alpha}}(\mathbf{q}_1, \mathbf{q}_2; \omega) G_{\{\mathbf{R}_{\alpha}\}}(\mathbf{q}_2, \mathbf{k}', \omega), \end{aligned} \quad (10.60)$$

The prime in the summation indicates that a given \mathbf{R}_{α} label is not allowed to be the same twice in succession when (10.60) is iterated because, by definition, the T -matrix contains all scattering events at a given site. The site-dependent T -matrix in (10.60) satisfies

$$\begin{aligned} T^{\mathbf{R}_{\alpha}}(\mathbf{q}_1, \mathbf{q}_2; \omega) = & e^{-i(\mathbf{q}_1 - \mathbf{q}_2) \cdot \mathbf{R}_{\alpha}} V(\mathbf{q}_1, \mathbf{q}_2, \omega) + \sum_{\mathbf{p}_1, \mathbf{p}_2} V(\mathbf{q}_1, \mathbf{p}_1, \omega) \\ & \times e^{-i(\mathbf{q}_1 - \mathbf{p}_1) \cdot \mathbf{R}_{\alpha}} G_{\phi}(\mathbf{p}_1, \mathbf{p}_2, \omega) T^{\mathbf{R}_{\alpha}}(\mathbf{p}_2, \mathbf{q}_2; \omega). \end{aligned} \quad (10.61)$$

Note that the T -matrix defined according to (10.61) is a functional of the free field-dependent Green function, $T^{\mathbf{R}_{\alpha}} = T^{\mathbf{R}_{\alpha}}[G_{\phi}]$.

We now iterate (10.60) and calculate the average term-by-term with (10.59). One obtains terms such as

$$\begin{aligned} \bar{G} = & \cdots + \langle G_{\phi} T^{\mathbf{R}_{\alpha}}[G_{\phi}] G_{\phi} T^{\mathbf{R}_{\beta}}[G_{\phi}] G_{\phi} T^{\mathbf{R}_{\alpha}}[G_{\phi}] G_{\phi} \rangle_{\text{imp}} \\ & + \cdots + \langle G_{\phi} T^{\mathbf{R}_{\alpha}}[G_{\phi}] G_{\phi} T^{\mathbf{R}_{\beta}}[G_{\phi}] G_{\phi} T^{\mathbf{R}_{\gamma}}[G_{\phi}] G_{\phi} T^{\mathbf{R}_{\alpha}}[G_{\phi}] G_{\phi} \rangle_{\text{imp}} \\ & + \cdots . \end{aligned} \quad (10.62)$$

When carrying out the impurity averaging, one can commute the \mathbf{R}_i integrals in such a way that the innermost integrals are always done first. For example, in (10.62) the \mathbf{R}_{β} (in the first term) and \mathbf{R}_{β} and \mathbf{R}_{γ} (in the second term) integrals are done first. The effect of this procedure is to build in parts of the impurity-averaged Green function as an *internal* line. It is easy to convince oneself that this part of the analysis is entirely equivalent to the standard one for vanishing external fields. The net result is that terms such as the ones in (10.62) can all be collected together by choosing a self-energy functional

which equals the single-site T-matrix averaged over its site label:

$$\Sigma[\bar{G}] = c \int \frac{d\mathbf{R}}{\Omega} T^{\mathbf{R}}[\bar{G}] , \quad (10.63)$$

where c is the impurity concentration. Note that the argument of the T -matrix is the full impurity-averaged Green function.

The choice (10.63) does not generate all the terms obtained by iterating (10.60): the crossed diagrams, discussed in Sect. 3.7.2 are left out. The equilibrium calculation of Part I, which showed that the crossed diagrams are smaller by $(lk_F)^{-1} \ll 1$ than noncrossed diagrams, is not necessarily valid in the nonequilibrium system. However, the crossed diagrams will always lead to a contribution to the self-energy which is of second or higher order in the concentration, and we use this as a formal justification for omitting them in subsequent calculations.

Our result (10.63) holds both for elastic impurity scattering and for the RLM. However, only in the RLM case is the T -matrix equation (10.61) explicitly solvable, and we find, following the analysis of Chap. 3,

$$\Sigma^{\text{RLM}}[\bar{G}] = c \int \frac{d\mathbf{R}}{\Omega} \frac{e^{-i(\mathbf{q}_1 - \mathbf{q}_2) \cdot \mathbf{R}} V(\mathbf{q}_1) V(\mathbf{q}_2)}{\omega - \varepsilon_0 - \bar{M}^{\mathbf{R}}(\omega)} , \quad (10.64)$$

where

$$\bar{M}^{\mathbf{R}}(\omega) = \sum_{\mathbf{p}_1, \mathbf{p}_2} e^{-i(\mathbf{p}_1 - \mathbf{p}_2) \cdot \mathbf{R}} V(\mathbf{p}_1) \bar{G}(\mathbf{p}_1, \mathbf{p}_2; \omega) V(\mathbf{p}_2) . \quad (10.65)$$

Let us now make a connection to the equilibrium case. For vanishing external fields the impurity-averaged Green function is diagonal in momentum labels, $\bar{G}(\mathbf{p}_1, \mathbf{p}_2) \rightarrow \delta_{\mathbf{p}_1, \mathbf{p}_2} \bar{g}(\mathbf{p}_1)$, and the \mathbf{R} integration in (10.64) is trivial with the result:

$$\sigma^{\text{RLM}}[\bar{g}] = \frac{c |V(\mathbf{q})|^2}{\omega - \varepsilon_0 - \bar{m}(\omega)} , \quad (10.66)$$

where

$$\bar{m}(\omega) = \sum_{\mathbf{k}} |V(\mathbf{k})|^2 \bar{g}(\mathbf{k}, \omega) . \quad (10.67)$$

The equilibrium results (10.66), (10.67), together with the Dyson equation, $\bar{g} = (\omega - \varepsilon_{\mathbf{k}} - \sigma^{\text{RLM}}[\bar{g}])^{-1}$, contain some interesting physics in their own right; this is discussed in the following example.

Equilibrium Density of States for the RLM

The standard technique for calculating electronic properties of disorder systems is the coherent potential approximation (CPA) [for a review, see [104]]. The self-consistent equations (10.66), (10.67) are closely related to the CPA self-energy functional (they lead to double counting of certain high order processes, which, however,

do not play a significant role in the present dilute impurity limit), and we shall use them now to determine the density of states for a system with a square-root free density of states, for example, a semiconductor close to a band edge. Defining $a(\omega) = \bar{m}(\omega)/\varepsilon_0$, we can cast the self-consistent problem in a dimensionless form:

$$a(\omega') = -\frac{2}{\pi} \sqrt{\gamma} \int_0^\infty dy \frac{y^{1/2} v^2(\varepsilon_0 y)}{y - (\omega' + 1) + \delta \frac{v^2(\varepsilon_0 y)}{\omega' - a(\omega')}} , \quad (10.68)$$

where the two parameters defining the system are given by $\gamma = [\pi N(\varepsilon_0) V_0^2 / (2\varepsilon_0)]^2$ and $\delta = cV_0^2/\varepsilon_0^2$, respectively. Further, we introduced $\omega' = \omega/\varepsilon_0 - 1$, and wrote the interaction as $V(\mathbf{k}) = V_0 v(\varepsilon_{\mathbf{k}})$, so that V_0 gives the strength of the interaction and $v(\varepsilon_{\mathbf{k}})$ gives its range. Once this equation is solved, we know the self-energy via $\sigma(\omega') = \delta/[\omega' - a(\omega')]$, and hence the Green function \bar{g} , and the density of states can be computed from $\varrho = -(1/\pi)\text{Im}\bar{g}$. One can proceed either with a direct numerical solution of (10.68) with a suitable model interaction (for example, the Gaussian-model discussed above), or proceed with an approximate analytical calculation. Some numerical work is described in [170]; here we apply an analytical technique due to Pankratov [280]. The analytic calculation is made possible by assuming that the interaction is essentially constant, except for providing a high-energy cutoff. Thus, we replace $v^2(\varepsilon_0 y)$ in (10.68) by a constant, and treat the now formally divergent integral as convergent. The y -integral can now be evaluated as a contour integral. Define

$$I_C = \int_C dz \frac{z^{1/2}}{z - A(\omega')} = I_R + I_- + I_\epsilon + I_+ , \quad (10.69)$$

where the contour C is shown in Fig. 10.3. In (10.68) we need I_+ ; since I_R and I_ϵ vanish and I_- equals I_+ , we get

$$I_+ = \pi i \sqrt{A(\omega')} \quad (10.70)$$

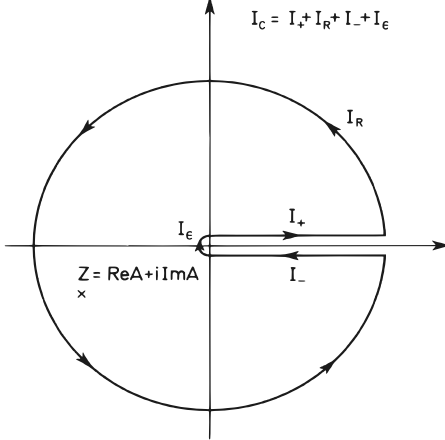


Fig. 10.3. Contour C in (10.69). Contribution from the *large circle* vanishes due to the implicit cutoff in the scattering interaction and the contribution from the small circle vanishes as $\epsilon \rightarrow 0$. Hence $I_C = I_+ + I_- = 2I_+ = 2\pi i \times (\text{sum of residues})$. The branch cut in (10.66) is placed on the positive x -axis. Pole at $z = \text{Re}A(\omega') + i\text{Im}A(\omega')$ is placed in the lower half-plane because we are dealing with the retarded function

or, going back to (10.68),

$$a(\omega') = -2i\sqrt{\gamma} \left[\omega' + 1 - \frac{\delta}{\omega' - a(\omega')} \right]^{1/2}. \quad (10.71)$$

We can rearrange this equation into a cubic polynomial in $a(\omega')$, the solutions of which are easy to write down explicitly. Rather than giving the rather complicated expressions, we now turn to the evaluation of the density of states. The momentum summation required for ϱ is again performed using the contour of Fig. 10.3, and the result is [170]

$$\begin{aligned} \varrho(\omega') = & \frac{1}{\sqrt{2}} \left(\omega' + 1 - \text{Re}\sigma(\omega') \right. \\ & \left. + \{[\omega' + 1 - \text{Re}\sigma(\omega')]^2 + [\text{Im}\sigma(\omega')]^2\}^{1/2} \right)^{1/2}. \end{aligned} \quad (10.72)$$

Similar techniques can be used to calculate the density of states for the localized electrons, and results are shown in Fig. 10.4. Also shown are results for a full numerical

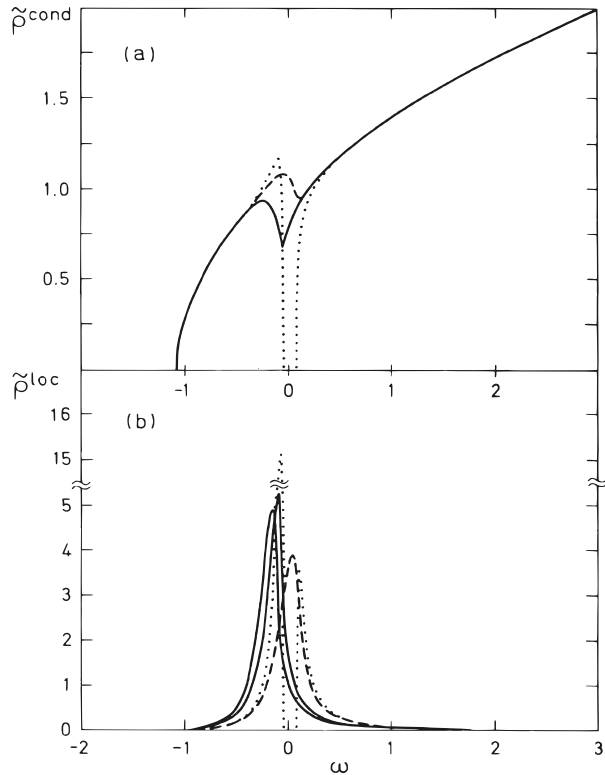


Fig. 10.4. Dashed line: (a) Conduction-electron density of states, and (b) the localized level density of states for parameters $\delta = 1/16$ and $\gamma = 1/256$, which corresponds to weak coupling. Solid lines give the results for a numerical calculation with energy cutoff $D = 5\varepsilon_0$, while dotted lines correspond to another related model [280]

solution of (10.68); even though only an approximate agreement is seen, the explicit analytic solution is useful because it can be used for a qualitative analysis, for example, the existence or nonexistence of separate impurity bands [179].

We now return to the nonequilibrium case, defined by (10.64), (10.65). The explicit \mathbf{R} -dependence in the denominator of (10.64) complicates the mathematical structure considerably, and we can only provide an approximate, but physically motivated, solution to the self-consistent problem defined by the Dyson equation and the self-energy (10.64). We use the results obtained for equilibrium (Sect. 39.2 in [2]) in constructing an approximate solution for the impurity-averaged field-dependent Green function. In equilibrium, and with the constant density of states approximation, which will be adopted heretofore, it is found that the self-consistent solution of (10.66), (10.67) is $\bar{m}(\omega) = -i\gamma$, where $\gamma = \pi\varrho V^2$. The crucial observation is that the *same* solution would have emerged even with the *free* Green function in (10.66); in other words the Born approximation and the self-consistent Born approximation yield identical results in the determination of the retarded Green function. We use this information in making the *first approximation*: It is assumed that $\bar{M}^{\mathbf{R}}$ in (10.65) can be evaluated with the *field-dependent free* Green function G_{ϕ} . The calculation is similar to the one performed in the evaluation of (10.55), and the result is:

$$\bar{M}^{\mathbf{R}}(\omega) = i\Gamma^{\phi}(\omega + \mathbf{F} \cdot \mathbf{R}), \quad (10.73)$$

where $\Gamma^{\phi}(\omega)$ is defined in (10.55) and we suppress the real part. Using (10.73) in the expression for the self-energy (10.64), we get the following equation for the Green function:

$$\begin{aligned} \bar{G}(k_{\parallel}, k'_{\parallel}, \mathbf{k}_{\perp}, \omega) &= G_{\phi}(k_{\parallel}, k'_{\parallel}, \mathbf{k}_{\perp}, \omega) + \int_0^L \frac{dR_{\parallel}}{L} \sum_{q_1^{\parallel}, q_2^{\parallel}} G_{\phi}(k_{\parallel}, q_1^{\parallel}, \mathbf{k}_{\perp}, \omega) \\ &\quad \times c \frac{e^{-i(q_1^{\parallel}-q_2^{\parallel})R_{\parallel}} V(q_1^{\parallel}, \mathbf{k}_{\perp}) V(q_2^{\parallel}, \mathbf{k}_{\perp})}{\omega - \varepsilon_0 - i\Gamma^{\phi}(\omega + FR_{\parallel})} \\ &\quad \times \bar{G}(q_2^{\parallel}, k'_{\parallel}, \mathbf{k}_{\perp}, \omega). \end{aligned} \quad (10.74)$$

The physical interpretation of (10.74) is the following. We imagine the charge carrier entering from a field-free region to a region of space $0 \leq R_{\parallel} \leq L$ where there is a uniform electric field. $\bar{G}(k_{\parallel}, k'_{\parallel}, \mathbf{k}_{\perp}, \omega)$ then describes the propagation of a charge carrier from a state $(k_{\parallel}, \mathbf{k}_{\perp}, \omega)$ to a state $(k'_{\parallel}, \mathbf{k}_{\perp}, \omega)$ under the influence of a constant electric field and the resonant interaction with impurities. Alternatively, in real space the Fourier transform of $\bar{G}(k_{\parallel}, k'_{\parallel}, \mathbf{k}_{\perp}, \omega)$ gives the propagation amplitude from one spatial point to another.

This interpretation implies that a *second approximation* has been made. In the calculation of G_{ϕ} it was not taken into account that the electric field extends over a finite region in space. Allowing this would complicate the analysis

significantly, and analytic progress would hardly be possible.² Thus, (10.74) assumes that the boundary effects do not play an important role and that the physics is run by the “bulk” properties. An experimentally realizable system could be a heterostructure, where charge carriers are injected into a region of space with a strong uniform electric field.

As it stands, (10.74) still seems impossible to solve analytically. However, a numerical solution may well be possible: one can evaluate the R_{\parallel} integral once and for all, and then proceed by some suitable iterative technique. Instead of pursuing this line further in the present context, we make a *third approximation*: motivated by our numerical study of the field-dependent level width [(10.55), also Fig.10.2] we replace the level width by its zero-field value. This is reasonable, since we found that for increasing energies Γ^{ϕ} approaches Γ ; for example, taking $F = 10^6 \text{ V m}^{-1}$ and $R_{\parallel} = 100 \text{ \AA}$, which can be viewed as representative numbers, the level width has essentially its zero-field value. Thus, only the first few scatterings have a width which significantly differs from the zero-field value. Since we are neglecting boundary effects anyway, we can safely assume that the important contribution to the integral (10.74) comes from the region where the level width has relaxed to its zero-field value. Setting $\Gamma^{\phi}(\omega + FR_{\parallel}) \simeq \Gamma(\omega)$ results in a major simplification: the R_{\parallel} -integral is trivial to perform, and we obtain

$$\begin{aligned} \bar{G}(k_{\parallel}, k'_{\parallel}, \mathbf{k}_{\perp}, \omega) &= G_{\phi}(k_{\parallel}, k'_{\parallel}, \mathbf{k}_{\perp}, \omega) + \sum_{q_{\parallel}} G_{\phi}(k_{\parallel}, q_{\parallel}, \mathbf{k}_{\perp}, \omega) \\ &\quad \times \frac{cV(q_{\parallel}, \mathbf{k}_{\perp})^2}{\omega - \varepsilon_0 - i\Gamma(\omega)} \bar{G}(q_{\parallel}, k'_{\parallel}, \mathbf{k}_{\perp}, \omega). \end{aligned} \quad (10.75)$$

This equation can be solved by iteration; the solution is made possible by the separability of the interaction. The result is:

$$\begin{aligned} \bar{G}(k_{\parallel}, k'_{\parallel}, \mathbf{k}_{\perp}, \omega) &= G_{\phi}(k_{\parallel}, k'_{\parallel}, \mathbf{k}_{\perp}, \omega) \\ &\quad \times \exp \left[\frac{-i}{F} \int_{k'_{\parallel}}^{k_{\parallel}} dq_{\parallel} \frac{cV(q_{\parallel}, \mathbf{k}_{\perp})^2}{\omega - \varepsilon_0 - i\Gamma(\omega)} \right]. \end{aligned} \quad (10.76)$$

This is an interesting result: it is an explicit solution to a field-dependent Dyson equation with an energy-dependent scattering mechanism. Further, we will need (10.76) as an input to the quantum kinetic equation constructed in the next section.

There are three important checks we must perform to ascertain that (10.76) is an acceptable solution. First of all, we must verify that it reduces to the correct zero-field Green function. This can be accomplished by a direct

² However, using the actual wavefunctions of the system as a basis set, certain progress can be made, at least on a formal level, and we shall illustrate this in Sect.10.7.

application of the method explained in the example in Sect. 10.1, and one finds that

$$\lim_{F \rightarrow 0} \bar{G}(k_{\parallel}, k'_{\parallel}, \mathbf{k}_{\perp}, \omega) = \frac{\delta(\mathbf{k} - \mathbf{k}')}{\omega - \varepsilon_{\mathbf{k}} - cV(\mathbf{k})^2 / (\omega - \varepsilon_0 - i\Gamma)} . \quad (10.77)$$

The second check concerns the frequency-sum rule, $\int d\omega/(2\pi)[-2\text{Im}\bar{G}] = 1$. An explicit calculation of the ω integral in (10.76) [or, actually, also for the equilibrium result (10.77)] is difficult. However, we may resort to the general analytic properties of the Green functions and self-energies: the free Green function (both with and without the field) exhausts the sum rule, while all higher order terms, obtained by expanding either (10.76) or (10.77), yield zero contribution when integrated over ω , because their poles always lie in either the upper or lower half-plane, and hence the contour can be closed in the opposite half-plane.

The final check concerns whether the found solution satisfies the self-consistency condition: Given the self-energy functional

$$\Sigma(\mathbf{q}, \omega) = \frac{cV(\mathbf{q})^2}{\omega - \varepsilon_0 - \bar{M}^{\mathbf{R}=\mathbf{0}}(\omega)} , \quad (10.78)$$

where

$$\bar{M}^{\mathbf{R}=\mathbf{0}}(\omega) = \sum_{\mathbf{p}_1, \mathbf{p}_2} V(\mathbf{p}_1)\bar{G}(\mathbf{p}_1, \mathbf{p}_2, \omega)V(\mathbf{p}_2) \quad (10.79)$$

and \bar{G} is given by (10.76), we must show that

$$\bar{M}^{\mathbf{R}=\mathbf{0}}(\omega) = i\Gamma(\omega) . \quad (10.80)$$

The proof is a direct calculation [180], and we urge the reader to check this.³ This concludes our discussion of the dynamics (single-particle properties) of the RLM in an external field; in the next section we discuss kinetic equations derived with the aid of the main results of this section.

10.4.4 Analytic Continuation

In the quantum kinetic equation one needs the analytic continuations $\Sigma^{><}$ of the self-energy functional (10.64) (with $\bar{M}^{\mathbf{R}=\mathbf{0}}$). This is achieved by repeated applications of the analytic continuation rules given in Table 4.1. In order to make the analysis as transparent as possible, we suppress all factors that do not affect the analytic continuation, and write the self-energy functional as $\Sigma = [g_0^{-1} - G]^{-1}$, and consider its series expansion:

$$\Sigma = g_0 + g_0 G g_0 + g_0 G g_0 G g_0 + \dots . \quad (10.81)$$

³ It is expedient to assume that the momentum-dependence of the matrix element $V(\mathbf{q})$ is so weak, that it can be neglected, $V(\mathbf{q}) \simeq V_0$.

Term-by-term analytic continuation results in

$$\begin{aligned}\Sigma^< = & g_0^< + g_0^r G^r g_0^< + g_0^r G^< g_0^a + g_0^< G^a g_0^a \\ & + g_0^r G^r g_0^r G^r g_0^< + g_0^r G^r g_0^r G^< g_0^a + g_0^r G^r g_0^< G^a g_0^a \\ & + g_0^r G^< g_0^a G^a g_0^a + g_0^< G^a g_0^a G^a g_0^a \dots .\end{aligned}\quad (10.82)$$

These terms can be regrouped

$$\begin{aligned}\Sigma^< = & (1 + g_0^r G^r) g_0^< (1 + G^a g_0^a) \\ & + (g_0^r + g_0^r G^r g_0^r) G^< (g_0^a + g_0^a G^a g_0^a) \dots .\end{aligned}\quad (10.83)$$

Continuing the process one finds that the final result is

$$\Sigma^< = \frac{1}{1 - g_0^r G^r} g_0^< \frac{1}{1 - g_0^a G^a} + \frac{1}{g_0^{-1} - G^r} G^< \frac{1}{g_0^{-1} - G^a} . \quad (10.84)$$

The first term in (10.84) vanishes because $g_0^{-1}(\omega) g_0^<(\omega) \equiv 0$. Reintroducing the momentum variables, we identify $T^R[\bar{G}^{r,a}]$ in (10.84), and have therefore obtained

$$\Sigma^<(\mathbf{q}_1, \mathbf{q}_2, \omega) = c \sum_{\mathbf{p}_1, \mathbf{p}_2} \int \frac{d\mathbf{R}}{\Omega} T_{\mathbf{q}_1, \mathbf{p}_1}^R [\bar{G}^r] \bar{G}^<(\mathbf{p}_1, \mathbf{p}_2, \omega) T_{\mathbf{p}_2, \mathbf{q}_2}^R [\bar{G}^a] \quad (10.85)$$

This is an important result: Among other things it can be used to derive a Boltzmann equation with the full T -matrix rather than the Born approximation for the scattering probability, which is what the standard derivations usually lead to. We also note that the above derivation is valid for cases where the T -matrix is not explicitly solvable (for example, for the elastic impurity case) and that it can be extended to the case where the Green functions depend separately on two time-labels, i.e., to the case of time-dependent external fields.

10.4.5 Quantum Kinetic Equation

We can now state the quantum kinetic equation for the RLM. Substituting the results of the previous section in the GKB equation (5.7), we obtain

$$\begin{aligned}& \left[G_\phi^{-1} - \frac{c}{2} \int \frac{d\mathbf{R}}{\Omega} (T^R[\bar{G}^r] + T^R[\bar{G}^a]), G^< \right] \\ & - \left[c \int \frac{d\mathbf{R}}{\Omega} (T^R[\bar{G}^r] G^< T^R[\bar{G}^a]), \frac{1}{2} (\bar{G}^a + \bar{G}^r) \right] \\ & = -\frac{c}{2} \int \frac{d\mathbf{R}}{\Omega} \{ T^R[\bar{G}^r] G^< T^R[\bar{G}^a], G^> \} \\ & + \frac{c}{2} \int \frac{d\mathbf{R}}{\Omega} \{ T^R[\bar{G}^r] G^> T^R[\bar{G}^a], G^< \} .\end{aligned}\quad (10.86)$$

In this equation, we have suppressed the intermediate position and time integrations. The extremely nonlinear character of these equations has been stressed by explicitly indicating how the various self-energy terms depend on the retarded and advanced Green functions. From (10.86) we also clearly see the two-step structure inherent in many nonequilibrium calculations: The expressions for the retarded and advanced Green functions $\bar{G}^{r/a}$ are needed as an input to the kinetic equation.

At this point it is useful to reiterate the different approximations that have been made so far. The choice of the self-energy functional picks a subset of all the different diagrams that are generated by the impurity averaging; in particular, crossed diagrams are not included in (10.86). The form of (10.86) implies no other approximations, however, the actual expressions found for $\bar{G}^{r/a}$ do involve additional approximations. In principle then, supposing one had the exact expressions for $\bar{G}^{r/a}$, (10.83) would give an exact prescription for determining the transport properties of a system consisting of noninteracting electrons coupled to a dilute concentration of resonant scatterers under the influence of an arbitrarily strong static electric field.

One should note, however, that in the electron-impurity system there is no mechanism to dissipate the energy fed in by the electric field. Thus if one were to use (10.86) to determine the nonlinear current, singularities may arise due to Joule heating. One should add terms to (10.86) which would allow the dissipation of the Joule heat. This could be done, for example, by coupling the system to a phonon bath. In later sections we will discuss the quantum kinetic equations for electron–phonon systems. The most important feature of (10.86) is that it allows an explicit study of how the conventional impurity Boltzmann equation is modified by an arbitrarily strong electric field.

To proceed with the analysis we use the approximate expressions for $\bar{G}^{r/a}$ found in Sect. 10.4.3. Explicitly, we have, using (10.84–10.85),

$$T_{\mathbf{q}_1, \mathbf{q}_2}^{\mathbf{R}} [\bar{G}^r] = \frac{V(\mathbf{q}_1)V(\mathbf{q}_2)\exp[-i(\mathbf{q}_1 - \mathbf{q}_2) \cdot \mathbf{R}]}{\omega - \varepsilon_0 + i\Gamma_0}. \quad (10.87)$$

$T^{\mathbf{R}}[\bar{G}^a]$ is obtained from (10.87) by setting $i\Gamma_0 \rightarrow -i\Gamma_0$. Use of these expressions in the self-energy part of the collision integral results in

$$\begin{aligned} \Sigma^<(\mathbf{k}, \mathbf{k}', \omega) &= c \sum_{\mathbf{q}_1, \mathbf{q}_2} \int \frac{d\mathbf{R}}{\Omega} \frac{\exp[-i(\mathbf{k} - \mathbf{q}_1 + \mathbf{q}_2 - \mathbf{k}') \cdot \mathbf{R}]}{(\omega - \varepsilon_o)^2 + \Gamma_0^2} \\ &\times V(\mathbf{k})V(\mathbf{q}_1)V(\mathbf{q}_2)V(\mathbf{k}')G^<(\mathbf{q}_1, \mathbf{q}_2, \omega). \end{aligned} \quad (10.88)$$

We recognize in (10.88) the resonant prefactor which is reminiscent of the energy-dependent relaxation time used in the Boltzmann equation for the RLM [328]. The energy-dependent prefactor will give rise to interesting additional structure even in the Boltzmann limit, which we shall study next. In order to apply the results of Chap. 6, where we developed tools to extract the Boltzmann limit from quantum kinetic equations, we must transform the

self-energy (10.88) into sum and difference variables, and perform a Fourier transformation for the difference variables. The temporal variables are actually in the desired form already, and we only need to consider the spatial coordinates. The transformation rules we need are:

$$\begin{aligned}\Sigma(\mathbf{p}, \mathbf{R}) &= \sum_{\mathbf{k}} \Sigma(\mathbf{p} - \mathbf{k}, \mathbf{p} + \mathbf{k}) e^{-2i\mathbf{k} \cdot \mathbf{R}}, \\ G(\mathbf{q}_1, \mathbf{q}_2) &= \int d\mathbf{R}' e^{-i\mathbf{R}' \cdot (\mathbf{q}_1 - \mathbf{q}_2)} G\left[\frac{1}{2}(\mathbf{q}_1 + \mathbf{q}_2), \mathbf{R}'\right]\end{aligned}\quad (10.89)$$

and after some simplification one finds

$$\begin{aligned}\Sigma^<(\mathbf{p}, \mathbf{R}, \omega) &= \frac{c}{(\omega - \varepsilon_0)^2 + \Gamma_0^2} \int d\mathbf{R}' \sum_{\mathbf{q}, \mathbf{p}'} \exp[i\mathbf{q} \cdot (\mathbf{R} - \mathbf{R}')] V(\mathbf{p} + \mathbf{q}/2) \\ &\quad \times V(\mathbf{p}' + \mathbf{q}/2) G^<(\mathbf{p}', \mathbf{R}', \omega) V(\mathbf{p}' - \mathbf{q}/2) V(\mathbf{p} - \mathbf{q}/2).\end{aligned}\quad (10.90)$$

In the Boltzmann limit we can use the lowest order gradient approximation, which is summarized in (6.5), and one finds that the collision integral $I^{\text{RLM}}[G]$ is given by

$$\begin{aligned}I^{\text{RLM}}[G] &= \frac{-c}{(\omega - \varepsilon_0)^2 + \Gamma_0^2} \int d\mathbf{R}' \sum_{\mathbf{q}, \mathbf{p}'} V(\mathbf{p} + \mathbf{q}/2) V(\mathbf{p}' + \mathbf{q}/2) \\ &\quad \times V(\mathbf{p}' - \mathbf{q}/2) V(\mathbf{p} - \mathbf{q}/2) [G^<(\mathbf{p}', \mathbf{R}', \omega) G^>(\mathbf{p}, \mathbf{R}, \omega) \\ &\quad - G^>(\mathbf{p}', \mathbf{R}', \omega) G^<(\mathbf{p}, \mathbf{R}, \omega)].\end{aligned}\quad (10.91)$$

In the Boltzmann limit we use the ansatz (6.14) to relate the particle propagator $G^<$ and the Wigner distribution function. Collecting all the terms and specializing to the Gaussian-model interaction used in previous sections, we obtain the final result:

$$\begin{aligned}[\nabla_{\mathbf{p}} \varepsilon_{\mathbf{p}} \cdot \nabla_{\mathbf{R}} + \mathbf{F} \cdot \nabla_{\mathbf{p}}] f(\mathbf{p}, \mathbf{R}) &= -\frac{c}{(\varepsilon_{\mathbf{p}} - \mathbf{F} \cdot \mathbf{R})^2 + \Gamma_0^2} \\ &\quad \times \sum_{\mathbf{p}} \int d\mathbf{R}' \frac{\exp[-(\mathbf{R} - \mathbf{R}')^2/2\lambda^2]}{(2\pi\lambda^2)^{3/2}} \\ &\quad \times V^2(\mathbf{p}) V^2(\mathbf{p}') \delta[\varepsilon_{\mathbf{p}} - \varepsilon_{\mathbf{p}'} - \mathbf{F} \cdot (\mathbf{R} - \mathbf{R}')] \\ &\quad \times [f(\mathbf{p}, \mathbf{R}) - f(\mathbf{p}', \mathbf{R}')].\end{aligned}\quad (10.92)$$

We want to emphasize the following central features of this result. (a) It is nonlocal in space. This is due to the finite range of the model interaction. (b) Field-dependence of the collision integral. This is a consequence of the energy-dependent prefactor characteristic of the RLM. For elastic impurity scattering no such field-dependence would occur. The field-dependent energy shifts in (10.92) are easily understood if one recalls that the potential energy is position dependent as a result of the applied field. (c) This transport equation cannot be reduced to a relaxation-time form, contrary to the

ordinary impurity Boltzmann equation. (d) The transport equation is consistent with the continuity equation only when coarse-grained over a distance several times the range of the Gaussian-model interaction. In the limit of a short-range interaction, we can simplify (10.92) to a “local” relaxation-time form:

$$\begin{aligned} & \left\{ \nabla_{\mathbf{p}} \varepsilon_{\mathbf{p}} \cdot \nabla_{\mathbf{R}} + F \left[\cos \theta \frac{\partial}{\partial p} - \frac{1}{p} \sin \theta \frac{\partial}{\partial \theta} \right] \right\} f(p, \theta, \mathbf{R}) \\ &= -\frac{1}{\tau(\varepsilon_{\mathbf{p}} - \mathbf{F} \cdot \mathbf{R})} [f(p, \theta, \mathbf{R}) - \bar{f}(\mathbf{p}, \mathbf{R})], \end{aligned} \quad (10.93)$$

where \bar{f} is the angular average of f ,

$$\bar{f}(\mathbf{p}, \mathbf{R}) = \int \frac{d\Omega}{4\pi} f(p, \theta, \mathbf{R}), \quad (10.94)$$

and

$$\frac{1}{\tau(\varepsilon)} = \frac{c \varrho V_0^4}{(\varepsilon - \varepsilon_0)^2 + \Gamma_0^2}. \quad (10.95)$$

In obtaining these results we have used the constant density of states approximation, and employed polar coordinates for momenta, $\mathbf{p} \rightarrow (p \equiv |\mathbf{p}|, \theta)$. We have remarked earlier about the lack of dissipation, which is common to all impurity models, and (10.93) makes this very explicit: while angular variations in f tend to be smoothed by scattering, there is nothing to prevent the angular average from heating due to the energy fed in by the electric field. Thus (10.93) is unsuitable for evaluation of the nonlinear current unless it is supplemented by some inelastic scattering mechanism. The main source for such inelasticity in semiconductors is due to phonons, and in Sect. 10.5 we develop the theory for electron–phonon quantum kinetics.

10.5 Quantum Kinetic Equation for Electron–Phonon Systems

The full quantum kinetic equation obeyed by the nonequilibrium Green function was derived in Part II [e.g. (7.20)–(7.25)]. In all their generality these equations appear prohibitively complicated, and for any realistic scattering mechanism, several approximations must be made if one wants to end up with equations that are amenable for an explicit evaluation. In this section we shall construct a quantum kinetic equation for a model electron–phonon system. The self-energy is treated in the self-consistent Born approximation given by the nonequilibrium generalization of (3.84), $\Sigma(\mathbf{k}, t, t') = i \sum_{\mathbf{q}} M_{\mathbf{q}}^2 G(\mathbf{k} - \mathbf{q}, t, t') D(\mathbf{q}, t, t')$. We will further assume that the phonon system will stay in equilibrium, and that phonon-life time effects are negligible, $D \rightarrow d \rightarrow d_0$. Further, we shall not attempt to analyze the full correlation function $G^<$, but rather concentrate on the Wigner function f^W . Finally, we

shall restrict ourselves to steady fields, even though a generalization to finite frequencies would be quite straightforward.

We have derived in Chap. 8 the quantum kinetic equation for the Wigner function, and we repeat it here for convenience:

$$\begin{aligned} & \left[\frac{\partial}{\partial T} + q\mathbf{E} \cdot \frac{\partial}{\partial \mathbf{k}} \right] f^W(\mathbf{k}, T) \\ &= - \int d\tau' \tilde{A}(\mathbf{k} + \frac{q}{2}\mathbf{E}\tau', -\tau', T + \tau') \tilde{B}(\mathbf{k} + \frac{q}{2}\mathbf{E}\tau', \tau', T + \tau') , \end{aligned} \quad (10.96)$$

where

$$\begin{aligned} & \tilde{A}(\mathbf{k}_1, \tau_1, T_1) \tilde{B}(\mathbf{k}_2, \tau_2, T_2) \\ &= \left[\tilde{\Sigma}^r \tilde{G}^< + \tilde{\Sigma}^< \tilde{G}^a - \tilde{G}^r \tilde{\Sigma}^< - \tilde{G}^< \tilde{\Sigma}^a \right] (\mathbf{k}_1, \tau_1, T_1) (\mathbf{k}_2, \tau_2, T_2) . \end{aligned}$$

In steady-state transport the third variable of \tilde{A} and \tilde{B} on the right-hand side of (10.96) can be ignored. Since the right-hand side still involves the full correlation function, we must supply additional information in order to get a closed set of equations. This is provided by the dc form of the GKB ansatz (8.19):

$$\begin{aligned} \tilde{G}^<(\mathbf{k}, \tau) &= -\tilde{G}^r(\mathbf{k}, \tau) f^W(\mathbf{k} + q\mathbf{E}\tau/2) + f^W(\mathbf{k} - q\mathbf{E}\tau/2) \tilde{G}^a(\mathbf{k}, \tau) \\ &= iA(\mathbf{k}, \tau) f^W(\mathbf{k} + q\mathbf{E}|\tau|/2) , \\ \tilde{G}^>(\mathbf{k}, \tau) &= -iA(\mathbf{k}, \tau) [1 - f^W(\mathbf{k} + q\mathbf{E}|\tau|/2)] . \end{aligned} \quad (10.97)$$

The analytic continuation for the self-energy is

$$\begin{aligned} \tilde{\Sigma}^<(\mathbf{k}, \tau) &= i \sum_{\mathbf{q}} M_{\mathbf{q}}^2 d_0^<(\mathbf{q}, \tau) \tilde{G}^<(\mathbf{k} - \mathbf{q}, \tau) , \\ \tilde{\Sigma}^>(\mathbf{k}, \tau) &= i \sum_{\mathbf{q}} M_{\mathbf{q}}^2 d_0^>(\mathbf{q}, \tau) \tilde{G}^>(\mathbf{k} - \mathbf{q}, \tau) , \end{aligned} \quad (10.98)$$

where

$$d_0^<(\mathbf{q}, \tau) = -i \sum_{\pm} N_q^{\pm} e^{\pm i\omega_q \tau} ; \quad d_0^>(\mathbf{q}, \tau) = -i \sum_{\pm} N_q^{\pm} e^{\mp i\omega_q \tau} , \quad (10.99)$$

with $N_q^{\pm} = N_q + \frac{1}{2} \pm \frac{1}{2}$, and N_q is the equilibrium Bose function. We now have all the ingredients needed for the construction of the kinetic equation. Recalling $G^r = \theta(\tau)(G^> - G^<)$, the collision integral becomes

$$\begin{aligned} \left(\frac{\partial f^W}{\partial T} \right)_{\text{coll}} &= i \int_{-\infty}^0 d\tau \sum_{\mathbf{q}} M_{\mathbf{q}}^2 \\ &\times \left\{ -\tilde{G}^> \left(\mathbf{k} + \frac{\tau}{2}\mathbf{E} - \mathbf{q}, -\tau \right) d_0^>(\mathbf{q}, -\tau) \tilde{G}^< \left(\mathbf{k} + \frac{\tau}{2}\mathbf{E}, \tau \right) \right. \\ &- \tilde{G}^< \left(\mathbf{k} + \frac{\tau}{2}\mathbf{E}, -\tau \right) d_0^>(\mathbf{q}, \tau) \tilde{G}^> \left(\mathbf{k} + \frac{\tau}{2}\mathbf{E} - \mathbf{q}, \tau \right) \\ &+ \tilde{G}^> \left(\mathbf{k} + \frac{\tau}{2}\mathbf{E}, -\tau \right) d_0^<(\mathbf{q}, \tau) \tilde{G}^< \left(\mathbf{k} + \frac{\tau}{2}\mathbf{E} - \mathbf{q}, \tau \right) \\ &\left. + \tilde{G}^< \left(\mathbf{k} + \frac{\tau}{2}\mathbf{E} - \mathbf{q}, -\tau \right) d_0^<(\mathbf{q}, -\tau) \tilde{G}^> \left(\mathbf{k} + \frac{\tau}{2}\mathbf{E}, \tau \right) \right\} . \end{aligned} \quad (10.100)$$

Using (10.98), (10.99) in the above equation brings us to the desired quantum kinetic equation for f^W :

$$\begin{aligned} \mathbf{E} \cdot \frac{\partial}{\partial \mathbf{k}} f^W(\mathbf{k}) = & \sum_{\mathbf{q}} M_{\mathbf{q}}^2 \int_{-\infty}^0 d\tau \left\{ -2\text{Re} \left[A \left(\mathbf{k} + \frac{\tau}{2} \mathbf{E} - \mathbf{q}, -\tau \right) \right. \right. \\ & \times A \left(\mathbf{k} + \frac{\tau}{2} \mathbf{E}, \tau \right) (N_q^+ e^{i\omega_q \tau} + N_q^- e^{-i\omega_q \tau}) \Big] \\ & \times [1 - f^W(\mathbf{k} + \tau \mathbf{E} - \mathbf{q})] f^W(\mathbf{k} + \mathbf{E}\tau) \\ & + 2\text{Re} \left[A \left(\mathbf{k} + \frac{\tau}{2} \mathbf{E}, -\tau \right) A \left(\mathbf{k} + \frac{\tau}{2} \mathbf{E} - \mathbf{q}, \tau \right) \right. \\ & \times (N_q^+ e^{i\omega_q \tau} + N_q^- e^{-i\omega_q \tau}) \Big] [1 - f^W(\mathbf{k} + \tau \mathbf{E})] \\ & \left. \left. \times f^W(\mathbf{k} + \mathbf{E}\tau - \mathbf{q}) \right\} . \right. \end{aligned} \quad (10.101)$$

This equation is central to studies of high-field quantum transport in semiconductors, and several comments are in order. Comparing to the semiclassical Boltzmann equation for electron–phonon systems, we observe the following differences. (a) The collision term is field-dependent: the arguments of the distribution function include field-dependent shifts, and the spectral functions may contain the electric field. This field-dependence leads to an effective broadening of the energy-conserving delta-functions. (b) The collision integral is non-Markovian: the time-integration introduces memory effects. (c) The Boltzmann equation is recovered, if the electric field is set to zero in the collision term, and if free spectral functions are used. Then the time-integration just reproduces the energy conserving delta-functions. (d) If all scattering is excluded from the spectral functions, i.e., one sets $A(\mathbf{k}, \tau) = \exp[-i(\varepsilon_{\mathbf{k}}\tau + \tau^3 F^2/24)]$, one recovers the quantum kinetic equation obtained by Levinson [238], and by Barker [27], who used density matrix techniques (see also Sect. 3.2, which gives an introduction to the density matrix method):

$$\begin{aligned} \mathbf{E} \cdot \frac{\partial}{\partial \mathbf{k}} f^W(\mathbf{k}) = & -2 \sum_{\mathbf{q}} M_{\mathbf{q}}^2 \sum_{\eta=\pm} N_q^\eta \int_{-\infty}^0 d\tau \\ & \times \left\{ \cos [(\varepsilon_{\mathbf{k}+\frac{\tau}{2}\mathbf{E}-\mathbf{q}} - \varepsilon_{\mathbf{k}+\frac{\tau}{2}\mathbf{E}} + \eta\omega_q)\tau] \right. \\ & \times [1 - f^W(\mathbf{k} + \tau \mathbf{E} - \mathbf{q})] f^W(\mathbf{k} + \mathbf{E}\tau) \\ & - \cos [(\varepsilon_{\mathbf{k}+\frac{\tau}{2}\mathbf{E}-\mathbf{q}} - \varepsilon_{\mathbf{k}+\frac{\tau}{2}\mathbf{E}} - \eta\omega_q)\tau] \\ & \left. \times [1 - f^W(\mathbf{k} + \tau \mathbf{E})] f^W(\mathbf{k} + \mathbf{E}\tau - \mathbf{q}) \right\} . \end{aligned} \quad (10.102)$$

This equation is also sometimes called the Barker–Ferry equation [29]. We can gain some qualitative information about the mathematical structure of (10.102) by analyzing the cos-prefactors alone, i.e., neglecting the field-dependence of the arguments (and hence τ -dependence) of the distribution

functions. The τ -integral then has the structure

$$I = 2 \int_{-\infty}^0 d\tau \cos[\tau(A\tau + 2B)] , \quad (10.103)$$

where the coefficients A and B are given by

$$\begin{aligned} A &= \mathbf{E} \cdot \mathbf{q}/2m \\ B &= [\mathbf{k} \cdot \mathbf{q}/m + q^2/2m \pm \omega_q]/2 , \end{aligned} \quad (10.104)$$

respectively. For vanishing electric fields (or if the phonon wavevector is perpendicular to the electric field) one finds $\lim_{E \rightarrow 0} I \rightarrow 2\pi\delta(B)$, and we have thus recovered the familiar energy-conserving δ -function due to the Fermi Golden rule used in the Boltzmann theory. For $A \neq 0$ one can express I in terms of Fresnel integrals $C(x)$ and $S(x)$ [1], Sect.7.3, and [292]:

$$I = \sqrt{2\pi/A} \{ \cos(B^2/A) [\frac{1}{2} - C(D)] + \sin(B^2/A) [\frac{1}{2} - S(D)] \} , \quad (10.105)$$

where $D = \sqrt{2/(\pi|A|^3)}AB$. A numerical example is shown in Fig. 10.5. Since I can be negative, it is not obvious how a standard Monte-Carlo simulation code could be applied to the numerical solution of (10.102), even within an approximation where the semiclassical δ -functions are replaced with I . A scheme, which is designed to overcome these difficulties, is presented in Sect. 10.6

It is important to remind ourselves of the approximations that have been employed in deriving (10.102): (a) the electron–phonon interaction is treated to lowest order, and (b) the GKB ansatz was used to relate the nonequilibrium Green function and the Wigner function. Since the GKB ansatz is known to have certain restrictions [331], these problems are inherently present in (10.101) as well. Nevertheless, it is interesting that (10.102) coincides exactly with the density matrix result, if free but field-dependent spectral

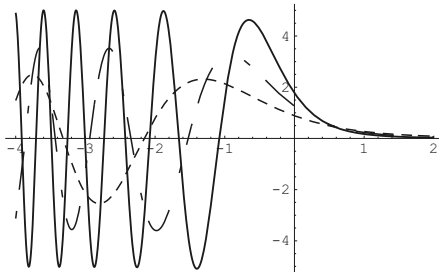


Fig. 10.5. The integral I defined in (10.103) for $A = 0.5, 1.0$, and 2.0 (solid, dashed, dot-dashed lines, respectively), as a function of B i.e., the energy transfer in an electron–phonon collision. The semiclassical limit corresponds to a δ -function at $B = 0$

functions are used. If one uses spectral functions which are computed from the nonequilibrium Dyson equation including collisions, an additional broadening is introduced; this broadening may lead to significant effects in high-field properties of materials with high scattering rates. Clearly our understanding has not yet reached a satisfactory stage, and results of future investigations may require some modifications in the quantum kinetic equation (10.101). We shall employ it in the following sections, because it offers a useful model quantum kinetic equation, which can be used to illustrate several intriguing effects.

10.6 An Application: Collision Broadening for a Model Semiconductor

10.6.1 Analytical Considerations

Here we describe how the quantum kinetic equation (10.101) can be transformed into a form that makes it amenable to a Monte Carlo solution. Explicitly, we shall consider nondegenerate electrons and dispersionless optical phonons, even though the generalization to more complicated scattering mechanisms is relatively straightforward. We write (10.101) as [199, 291]

$$\mathbf{E} \cdot \frac{\partial}{\partial \mathbf{k}} f^W(\mathbf{k}) = - \sum_{\mathbf{k}'} \int_0^\infty d\tau [P(\mathbf{k}' - \tau \mathbf{E}, \mathbf{k} - \tau \mathbf{E}, \tau) f^W(\mathbf{k} - \mathbf{E}\tau) - P(\mathbf{k} - \tau \mathbf{E}, \mathbf{k}' - \tau \mathbf{E}, \tau) f^W(\mathbf{k}' - \mathbf{E}\tau)], \quad (10.106)$$

where

$$P(\mathbf{k}, \mathbf{k}', \tau) = M_q^2 2 \text{Re} \left[A \left(\mathbf{k} + \frac{\tau}{2} \mathbf{E}, \tau \right) A \left(\mathbf{k}' + \frac{\tau}{2} \mathbf{E}, -\tau \right) \times (N_q^+ e^{-i\omega_q \tau} + N_q^- e^{i\omega_q \tau}) \right] \quad (10.107)$$

with $q = |\mathbf{k} - \mathbf{k}'|$. $P(\mathbf{k}, \mathbf{k}', \tau)$ represents in a certain sense a time-dependent quantum mechanical generalization of the transition probability used in the Boltzmann theory; the spectral functions account for the intra-collisional field-effect, and for the collision broadening. To make this analogue more quantitative, we next transform (10.106) into its integral form:

$$\begin{aligned} f^W(\mathbf{k}) &= \sum_{\mathbf{k}'} \int_0^\infty dt \int_0^\infty d\tau \{ P[\mathbf{k} - \mathbf{E}(t + \tau), \mathbf{k}' - \mathbf{E}(t + \tau), \tau] \\ &\quad \times f^W[\mathbf{k}' - \mathbf{E}(t + \tau)] - P f^W \} \\ &= \sum_{\mathbf{k}'} \int_0^\infty dt_1 \left[\widetilde{W}(\mathbf{k} - \mathbf{E}t_1, \mathbf{k}' - \mathbf{E}t_1, t_1) \right. \\ &\quad \left. \times f^W(\mathbf{k} - \mathbf{E}t_1) - \widetilde{W} f^W \right], \end{aligned} \quad (10.108)$$

where the notation Pf^W (and $\widetilde{W}f^W$) means a term identical with the preceding term but with momentum labels interchanged, $\mathbf{k} \rightleftharpoons \mathbf{k}'$, and

$$\widetilde{W}(\mathbf{K}, \mathbf{K}', t_1) = \int_0^{t_1} dt_2 P(\mathbf{K}, \mathbf{K}', t_2). \quad (10.109)$$

It is very instructive to compare (10.108) with the corresponding integral form of the Boltzmann equation:

$$f(\mathbf{k}) = \sum_{\mathbf{k}'} \int_0^\infty dt_1 [W(\mathbf{k} - \mathbf{E}t_1, \mathbf{k}' - \mathbf{E}t_1) f(\mathbf{k}' - \mathbf{E}t_1) - Wf], \quad (10.110)$$

where W is the Boltzmann scattering probability,

$$W(\mathbf{k}, \mathbf{k}') = 2\pi M_q^2 \sum_\eta \delta(\varepsilon_k - \varepsilon_{k'} + \eta\omega_q) N_q^\eta. \quad (10.111)$$

The *only* apparent mathematical difference between (10.108) and (10.110) is that the quantum transport equation has the time-dependent object \widetilde{W} instead of the static W probability found in semiclassical theory. The full analysis of (10.108) is still a matter of active research (see, for example, [243–245]) and it would go beyond the scope of the present analysis to enter this discussion. Instead, we proceed with two additional approximations, which allow further analytic progress.

First, we note that allowing the upper limit of the time-integration in (10.109) to approach infinity removes the mathematical differences between the quantum and Boltzmann theories. This is analogous to what is done in the derivation of the Fermi Golden Rule: there the energy conserving delta-functions emerge only in the infinite-time limit. The infinite-time limit is known as “completed collisions limit,” and it is usually expected to be valid for low collision rates [98]. This limit has an important implication for practical calculations: The mathematical equivalence⁴ allows one to draw from the vast number of techniques developed for the numerical solution of the Boltzmann equation, such as the Monte Carlo simulation techniques (see, for example, [168], or [169]).

The two quantum mechanical effects, intra-collisional field-effect and collisional broadening, which are contained in the quantum kinetic equation, are intertwined in a complicated way: the field shifts the momentum arguments of the spectral functions, which should be determined in the presence of both scattering and the electric field. The solution of the field-dependent Dyson equation for the retarded Green function, which yields the spectral function, represents itself a formidable task, and realistic analytic solutions, satisfying the necessary sum rules, scarcely exist. In what follows we shall focus on

⁴ One must still be cautious with the positive definiteness of \widetilde{W} ; for the model discussed in this section this turns out to be the case. We are not aware of general proofs of this important caveat.

collision broadening alone, since this will make further progress possible. This means that we can neglect the field-dependent shifts in the momenta, and consider only

$$\begin{aligned} W^{\text{QM}}(\mathbf{K}, \mathbf{K}') &\equiv \lim_{t \rightarrow \infty} \widetilde{W}(\mathbf{K}, \mathbf{K}', t) \\ &= \sum_{\eta} M_q^2 N_q^{\eta} K_{\eta}(\mathbf{K}, \mathbf{K}') , \end{aligned} \quad (10.112)$$

where the joint spectral function is defined via the convolution integral

$$K(\mathbf{K}, \mathbf{K}') = \int_{-\infty}^{\infty} \frac{d\omega}{2\pi} A(\mathbf{K}, \omega + \eta\omega_q) A(\mathbf{K}', \omega) . \quad (10.113)$$

As we shall see later, (10.112) can be readily used in a numerical scheme. (10.112) has an immediate physical interpretation: it states that collision broadening affects both the initial state \mathbf{K} , and the final state \mathbf{K}' . For example, if one uses a Lorentzian model for the spectral function, the joint spectral density has a width which equals the sum of the widths of the initial and the final state.

10.6.2 A Simple Model: Optical Phonon Emission at $T = 0$

We next consider a simple model, which allows one to work out the spectral function explicitly. The model uses a spherical and parabolic band, and only nonpolar optical processes at zero temperature are considered. In spite of its simplicity, this model has several interesting features. Within the standard semiclassical theory its properties are well understood [290]: (a) at intermediate field strengths it gives rise to the streaming-motion regime, and (b) at asymptotically high fields, it produces the quasielastic regime. Thus, the model provides a well-defined testing ground for contrasting the quantum kinetic and the semiclassical results.

In this model the line-width, or, equivalently, the imaginary part of the self-energy, is given by

$$\Gamma(\omega) = -2\text{Im}[\Sigma^r(\omega)] = 2\gamma(\omega - \omega_0)^{1/2}\theta(\omega - \omega_0) , \quad (10.114)$$

where ω_0 is the optical-phonon energy, and γ is the coupling strength [168]. With (10.114) the retarded Green function is $G^r(\mathbf{k}, \omega) = [\omega - \varepsilon_k + i\eta + i\Gamma(\omega)]^{-1}$, and the spectral density becomes

$$\begin{aligned} A(x_k, x) &= \frac{2}{\gamma^2} \left[\frac{(x - x_0)^{1/2}\theta(x_k - x_0)\theta(x - x_0)}{(x - x_k)^2 + (x - x_0)} \right. \\ &\quad \left. + \pi\delta(x - x_k)\theta(x_0 - x_k)\theta(x_0 - x) \right] , \end{aligned} \quad (10.115)$$

where we introduced dimensionless energies $x = \omega/\gamma^2$, $x_k = \varepsilon_k/\gamma^2$, and $x_0 = \omega_0/\gamma^2$. As always, it is important to verify the frequency sum-rule; presently

it reads $(\gamma^2/2\pi) \int_{-\infty}^{\infty} A dx = 1$, and using the contour integration techniques of Sect.10.4.3 one can verify that this is indeed the case. The joint spectral function corresponding to (10.115) can also be worked out explicitly [291,292]

$$\begin{aligned} K(x_k, x_{k'}) = & \frac{2}{\pi\gamma^2} \left[\pi \frac{\sqrt{x_{k'}} \theta(x_k - x_0) \theta(x_0 - x_{k'}) \theta(x_{k'})}{(x_0 + x_{k'} - x_k)^2 + x_{k'}} \right. \\ & + \int_{2x_0}^{\infty} dx \frac{\sqrt{(x - x_0)(x - 2x_0)} \theta(x - x_0) \theta(x_f - x_0)}{[(x - x_k)^2 + x - x_0][(x - x_0 - x_{k'})^2 + x - 2x_0]} \\ & \left. + \pi^2 \delta(x_0 + x_{k'} - x_k) \theta(x_0 - x_k) \theta(x_0 - x_{k'}) \right]. \end{aligned} \quad (10.116)$$

An important property of $K(x_k, x_{k'})$ is that it is possible to develop explicit analytical approximations to it, which is of crucial importance in Monte Carlo simulations. As compared to semiclassical simulations, where the final energy state is uniquely determined, in the quantum case one must use one additional random number generation: $K(x_k, x_{k'})$ is viewed as a probability distribution, which determines the final energy. A necessary prerequisite for this interpretation is that K obeys the sum rules

$$\frac{\gamma^2}{2\pi} \int_{-\infty}^{\infty} dx_k K(x_k, x_{k'}) = \frac{\gamma^2}{2\pi} \int_{-\infty}^{\infty} dx_{k'} K(x_k, x_{k'}) = 1, \quad (10.117)$$

which generalize the analogous relations found in the Boltzmann case

$$\int_{-\infty}^{\infty} dx_k \delta(x_k - x_{k'} \pm x_0) = \int_{-\infty}^{\infty} dx_{k'} \delta(x_k - x_{k'} \pm x_0) = 1. \quad (10.118)$$

A numerical evaluation of (10.117) with (10.116) confirms this consistency check. An unavoidable consequence of the probability distribution interpretation is an increase of the time needed for a convergent simulation, and the details of how this can be achieved in practice are described in [293]. Fig. 10.6 presents a numerical example; also a simulation corresponding to the intra-collisional field effect alone [for this case the joint spectral density is essentially given by (10.105)] is depicted. The important qualitative difference between the quantum mechanical and semiclassical results is the enhancement of charge carriers at high energies. This may lead to significant implications to phenomena such as field assisted run-away; however, the models employed in the simulations of Fig. 10.6 are still so oversimplified, that it is difficult to assess their practical implications. Clearly simulations with more realistic scattering mechanisms and band-structures would be desirable.

10.7 Spatially Inhomogeneous Systems

So far we have discussed only uniform external fields. However, all micro-devices are, almost by definition, extremely inhomogeneous, and it is important

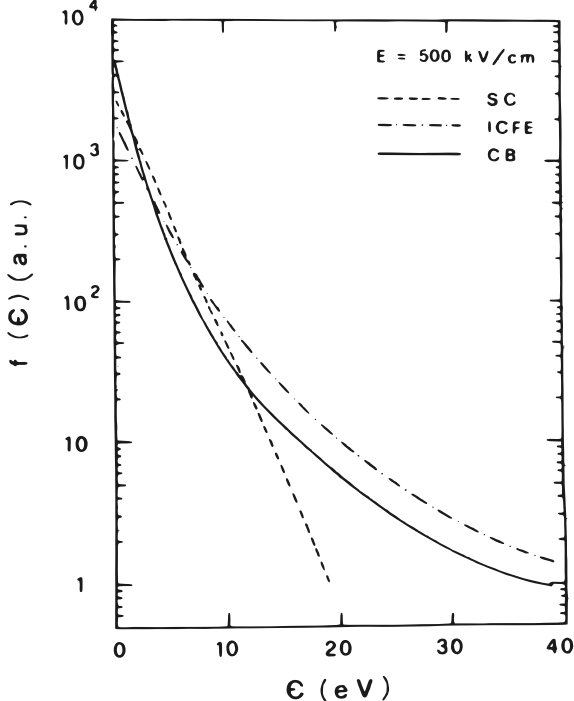


Fig. 10.6. Distribution function of the carrier kinetic energy at $E = 500 \text{ keV cm}^{-1}$. *Dashed curve* refers to the semiclassical (SC) simulation, *continuous curve* to a simulation which includes collisional broadening (CB) only, and *dot-dashed curve* to a simulation which includes intra-collisional field-effects (ICFE) only

to ask how much of the above can be generalized to spatially inhomogeneous systems. This is a very difficult task and only few results have been reported. To illustrate the difficulties we consider the Wigner function driving term for a general potential $U(x)$ (for simplicity we consider a one-dimensional system). The driving term is $[U(x) - U(x')]f^W(x, x')$, which after transformation to Wigner coordinates (6.1), gives rise to

$$\left[\frac{\partial}{\partial T} + \frac{p}{m} \frac{\partial}{\partial X} \right] f^W(p, X, T) - \int \frac{dp'}{2\pi i} M(p - p', X) f^W(p', X, T) = \left(\frac{\partial f^W}{\partial T} \right)_{\text{coll}} , \quad (10.119)$$

where

$$M(q, X) = \int dx e^{-iqx} [U(X + x/2) - U(X - x/2)] . \quad (10.120)$$

The spatial inhomogeneity has translated into nonlocality in momentum space, which implies considerable difficulties in numerical implementations.

A few applications to the resonant tunneling diode (which will be analyzed in some detail in Chap. 12 with a slightly different approach) have been reported [118, 205]; in these calculations the collision term has been treated in the relaxation-time approximation.

Driving Term for Harmonic Driving Forces

Harmonic forces play a central role in quantum mechanics. Thus, it is illustrative to consider the Wigner function transport equation if the external potential is of the form $U(x) = \frac{1}{2}kx^2$. The driving kernel $M(q, x)$ is then

$$\begin{aligned} M(q, X) &= \int dx e^{-iqx} \frac{1}{2} k [(X + x/2)^2 - (X - x/2)^2] \\ &= \int dx e^{-iqx} k X x = ik X \delta'(q), \end{aligned} \quad (10.121)$$

where δ' is the derivative of the Dirac delta-function. This form of M leads to a driving term $(-kX)(\partial/\partial p)f^W(p, X, T)$. Since $-kX$ is just the classical force acting on a particle in a harmonic potential, the Wigner function driving term is identical to the classical driving term! One may wonder what has happened to quantum mechanics: shouldn't the harmonic oscillator eigenstates reflect themselves somewhere? The answer to this paradox has actually been mentioned earlier (Sect. 5.2): There it was pointed out that the transport equation alone (which is obtained as a difference of two equations) does not contain the full description of the system, and that it must be supplied with other information which tells what states are “to be transported.”

Instead of attempting to solve the nonlocal transport equation, one may choose another strategy: one changes to a new basis defined by the eigenfunctions of the potential $U(x)$. The eigenfunctions are defined by

$$\left[-\frac{1}{2} \frac{d^2}{dx^2} + U(x) + \frac{1}{2} k_\perp^2 \right] \phi_n(x) = \varepsilon_n(k_\perp) \phi_n(x), \quad (10.122)$$

where we assumed translational invariance in the perpendicular direction. A physical realization could be the position dependent conduction band edge found in heterostructures. The transformed Green functions are defined by (the self-energies have analogous definitions)

$$G(k_\perp, x, x', \omega) = \sum_{n,n'} \phi_n(x) G_{nn'}(k_\perp, \omega) \phi_{n'}^*(x'), \quad (10.123)$$

and the transformed Dyson equation for the retarded Green function reads (the kinetic equation has a similar structure)

$$\begin{aligned} G_{mm'}^r(k_\perp, \omega) &= \delta_{mm'} g_m^r(k_\perp, \omega) \\ &+ \sum_n g_m^r(k_\perp, \omega) \Sigma_{mn}^r(k_\perp, \omega) G_{nm'}^r(k_\perp, \omega) \end{aligned} \quad (10.124)$$

with

$$g_m^r(k_\perp, \omega) = \frac{1}{\omega - \varepsilon_m(k_\perp) + i\eta} . \quad (10.125)$$

In the above equations the quantum numbers m, m' can also be continuous; in this case the sums must be replaced by integrations. The motivation behind these transformations is that the inhomogeneous potential has essentially been eliminated. If the self-energy is dominated by its diagonal components, $\Sigma_{mm'} \approx \delta_{mm'} \Sigma_m$, the Dyson equation is trivially solved, and one may expect analogous simplifications to take place in the kinetic equation.

This program has been carried through by Bertoni and co-workers [35–39] for the uniform field case, when the eigenfunctions are Airy functions. The technical details of these papers are quite involved and would be beyond the scope of our present goals. The end result, however, is both compact and intriguing, and we will discuss it at some length. The *only* approximation needed is that the self-energy can be approximated by an essentially diagonal quantity, and, as explained in the above references there are good reasons to believe that this is not a serious approximation. Given this, the fully nonlinear (in the external field) conductivity $\sigma(E)$ can be written as

$$\begin{aligned} \sigma(E) = & \frac{1}{2} \int \frac{d^2 k_\perp}{(2\pi)^2} \int d\Omega \left\{ \left[1 - \frac{\partial \text{Re}\Sigma^r}{\partial \Omega} \right] \right. \\ & \left. + [\Omega - \varepsilon(k_\perp) - \text{Re}\Sigma^r] \left[\frac{\partial \log \text{Im}\Sigma^r}{\partial \Omega} \right] \right\} A^2(k_\perp, \Omega) f(\Omega) , \end{aligned} \quad (10.126)$$

where Σ^r is the electron–phonon self-energy, which is assumed to be momentum independent (see Sect. 10.6), and $A(k_\perp, \Omega)$ is the spectral function obtained from the Dyson equation. The “distribution function” $f(\Omega)$ obeys a one-dimensional homogeneous integral equation,

$$f(\Omega) = \int d\Omega' F(\Omega, \Omega') f(\Omega') , \quad (10.127)$$

where the kernel F is a rather complicated function, but which can be expressed in terms of known functions [38, 39]. Finally, the homogeneous equation (10.127) requires a normalization condition; this is provided by

$$n = -i \int d\Omega \varrho_\perp(\Omega) f(\Omega) , \quad (10.128)$$

where n is the density and ϱ_\perp is the density of states for the motion in the plane perpendicular to the electric field. The set of equations (10.126) – (10.128) is well suited for a numerical evaluation, and an example will be given below. First, however, it is useful to comment some of the qualitative features of (10.126).

The result for the nonlinear conductivity bears formal similarities with the linear quantum kinetic theory of Mahan and co-workers, which was exposed in

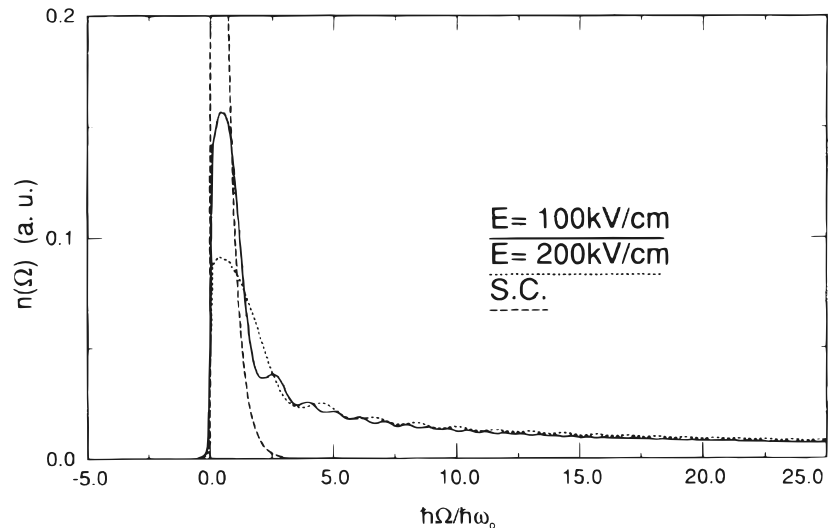


Fig. 10.7. The local density of particles as a function of the electron energy. Parameters applicable to Si are used

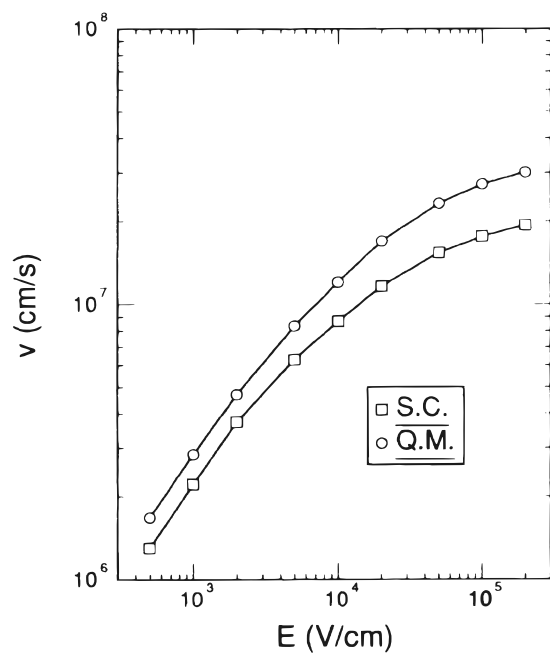


Fig. 10.8. The drift velocity vs. electric field. S.C. refers to a semiclassical simulation [The semiclassical result is courtesy of K. Komter (1991)]

Chap. 9. For example, some of the mass-renormalization factors have the same structure (but recall that here they are nonequilibrium quantities), and one also finds the square of the spectral density. It stays open whether a linearized version of (10.126) – (10.128) leads to the same conductivity as the quantum Boltzmann equation of Chap. 9, however, it is not difficult to demonstrate this equivalence in the quasiparticle limit [37].

We conclude by showing some numerical results: Figs. 10.7 and 10.8 display the nonequilibrium densities and drift velocities, respectively. We note that the nonequilibrium density has a significant high-energy tail; this is consistent with the results obtained in Sect. 10.6. As a consequence, the quantum drift velocity is significantly enhanced as compared to the semiclassical result, obtained with a standard Monte Carlo simulation. It remains to be seen how much of the above analysis can be carried over to less restrictive models of electron–phonon interaction and/or experimentally more interesting geometries, such as the biased resonant-tunneling diode.

Optical Absorption in Intense THz Fields

Summary. The optical absorption of intense THz radiation in a two-band semiconductor is calculated. For this end the two-time interband susceptibility is expressed in terms of nonequilibrium Green functions. A number of special cases are calculated explicitly. The approach is generalized to include excitonic effects. Finally the theoretical predictions are compared to measured spectra.

11.1 Introductory Remarks

Light absorption can be described in terms of a process where a polarization is induced in the medium. To linear order in the electric field component of the traversing light, \mathcal{E} , the induced polarizability, \mathcal{P} , can be expressed in terms of the dielectric susceptibility χ as

$$\mathcal{P}(t) = \int_{-\infty}^t dt' \chi(t, t') \mathcal{E}(t'). \quad (11.1)$$

If the absorbing medium is in a stationary state, the susceptibility tensor depends only on the difference of its time arguments, i.e., $\chi(t, t') = \chi(t - t')$. Under these conditions Maxwell's equation for \mathcal{E} is an algebraic equation in frequency space and one finds that the absorption is proportional to the imaginary part of $\chi(\omega)$. However, under nonequilibrium conditions, on which the present chapter focuses, the susceptibility is a two-time function, and Maxwell's equation remains an integral equation even in the frequency domain. Here we develop methods to calculate the nonequilibrium susceptibility function. Specifically, we consider an undoped semiconductor placed in an intense THz field; we assume that the THz field is not able to induce polarization, i.e., no carriers are excited in the conduction band. Properties of such systems have been investigated experimentally using the free electron laser (FEL) as a source for intense THz fields [77]; many interesting properties have been discovered, and others predicted, such as photon-assisted tunneling [130], dynamical localization and absolute negative conductivity [195],

ac Stark effect [158], and dynamical Franz–Keldysh effect and formation of sidebands [46, 177, 209, 288, 376]. Another situation where two-time susceptibilities are needed concerns ultra-fast transients, where the build-up of screening due to other carriers plays an important role; this situation is examined extensively in Chapters 17 and 18.

Thus, here we consider light absorption in mesoscopic systems subject to intense THz [or, equivalently, far infrared (FIR)] fields. Typical band-gaps are of the order of an electron volt, and hence frequency ω_l of the probe field \mathcal{E} is in the near infrared (NIR) part of the spectrum. This physical situation is conveniently treated with nonequilibrium Green function techniques. In particular, this NEGF method allows us to treat the intense FIR field nonperturbatively, and defines a framework in which screening can be treated systematically. Our analysis consists of the following steps. Starting from a two-band Hamiltonian we derive a formal expression for the interband susceptibility in terms of nonequilibrium Green functions. We use the general expression to derive the NIR absorption spectrum for noninteracting particles. We give explicit results for a number of special cases, and discuss the physical implications. Finally, we generalize our approach to include excitonic effects, and compare the theoretical predictions to experimentally measured spectra.

11.2 Optical Absorption as a Response Function

We shall now derive an expression for the dielectric interband susceptibility using nonequilibrium Green functions. The microscopic operator describing interband polarization is

$$\mathbf{P}(t) = \sum_{\mathbf{k}} \mathbf{d}_{\mathbf{k}} \left[a_{\mathbf{k}}^\dagger(t) b_{\mathbf{k}}(t) + b_{\mathbf{k}}^\dagger(t) a_{\mathbf{k}}(t) \right]. \quad (11.2)$$

Here $\mathbf{d}_{\mathbf{k}}$ is the dipole matrix-element, $a_{\mathbf{k}}^\dagger(t)$ [$a_{\mathbf{k}}(t)$] are the conduction band electron creation [annihilation] operators and $b_{\mathbf{k}}^\dagger(t)$ [$b_{\mathbf{k}}(t)$] are the valence band creation [annihilation] operators. The linearized Hamiltonian associated with a polarization $\mathbf{P}(t)$ induced by the external field $\mathcal{E}(t)$ is $H_P(t) = -\mathbf{P}(t) \cdot \mathcal{E}(t)$. Linear response theory (see, e.g., [254], or Sect. 9.2) yields the cartesian l -component of the induced interband polarization due to the probe field \mathcal{E} :

$$\mathcal{P}_l(t) = -i \int_{-\infty}^{\infty} dt' \theta(t-t') \langle [\mathbf{P}(t'), P_l(t)] \rangle \cdot \mathcal{E}(t'). \quad (11.3)$$

The retarded susceptibility tensor can be identified from (11.3)

$$\chi_{lm}^r(t, t') = -i \theta(t-t') \langle [P_m(t'), P_l(t)] \rangle. \quad (11.4)$$

Following the familiar line of attack in nonequilibrium theory, we first consider the contour-ordered response function:

$$\chi_{lm}^c(\tau, \tau') = -i\langle T_C[P_m(\tau')P_l(\tau)]\rangle \quad (11.5)$$

and use (11.2) to write the susceptibility as

$$\begin{aligned} \chi_{lm}^c(\tau, \tau') = & -i \sum_{\mathbf{q} \mathbf{k}} d_l(\mathbf{k}) d_m(\mathbf{q}) [\langle T_C[a_{\mathbf{q}}^\dagger(\tau') b_{\mathbf{q}}(\tau') a_{\mathbf{k}}^\dagger(\tau) b_{\mathbf{k}}(\tau)]\rangle \\ & + \langle T_C[a_{\mathbf{q}}^\dagger(\tau') b_{\mathbf{q}}(\tau') b_{\mathbf{k}}^\dagger(\tau) a_{\mathbf{k}}(\tau)]\rangle \\ & + \langle T_C[b_{\mathbf{q}}^\dagger(\tau') a_{\mathbf{q}}(\tau') a_{\mathbf{k}}^\dagger(\tau) b_{\mathbf{k}}(\tau)]\rangle \\ & + \langle T_C[b_{\mathbf{q}}^\dagger(\tau') a_{\mathbf{q}}(\tau') b_{\mathbf{k}}^\dagger(\tau) a_{\mathbf{k}}(\tau)]\rangle]. \end{aligned} \quad (11.6)$$

In equilibrium, a detailed theory for the two-particle correlation functions occurring in (11.6) has been developed in terms of the Bethe–Salpeter equation [142], which takes Coulomb interactions into account. A generalization of this approach to the nonequilibrium case will be discussed later, but we begin by considering a situation where interactions between the conduction and valence band can be neglected. This approach is motivated by the following considerations. The noninteracting limit will allow significant analytic progress, and the results form the basis for an interacting theory, to be discussed subsequently. Second, the noninteracting theory will provide some key elements towards the interpretation of the experimental findings of absorption in quantum wells subject to intense FIR [276].

For noninteracting particles we can use Wick’s theorem to factorize the two-particle correlation functions, and the nonequilibrium susceptibility can be expressed in terms of single-particle Green functions. A factorization of (11.6) leads to the following Green functions:

$$g_c(\mathbf{k}, \tau; \mathbf{q}, \tau') = -i\langle T_C[a_{\mathbf{k}}(\tau) a_{\mathbf{q}}^\dagger(\tau')]\rangle \quad (11.7)$$

$$g_v(\mathbf{k}, \tau; \mathbf{q}, \tau') = -i\langle T_C[b_{\mathbf{k}}(\tau) b_{\mathbf{q}}^\dagger(\tau')]\rangle \quad (11.8)$$

$$g_{ab}(\mathbf{k}, \tau; \mathbf{q}, \tau') = -i\langle T_C[a_{\mathbf{k}}(\tau) b_{\mathbf{q}}^\dagger(\tau')]\rangle \quad (11.9)$$

$$g_{ba}(\mathbf{k}, \tau; \mathbf{q}, \tau') = -i\langle T_C[b_{\mathbf{k}}(\tau) a_{\mathbf{q}}^\dagger(\tau')]\rangle. \quad (11.10)$$

We assume that the frequency Ω of the FIR field is such that $\hbar\Omega \ll \epsilon_g$. In typical experiments on III–V systems ϵ_g is of the order of eV, while $\hbar\Omega$ is a few meV, so this condition is satisfied. Consequently, interband transitions due to the FIR field can be ignored, and the Green functions related to Zener-effect, i.e., $g_{ab}(\mathbf{k}, \tau; \mathbf{q}, \tau')$ and $g_{ba}(\mathbf{k}, \tau; \mathbf{q}, \tau')$, are neglected from this on. The first order nonequilibrium susceptibility reads thus (assuming constant dipole matrix-elements, and suppressing the cartesian coordinate indices)

$$\begin{aligned} \chi^c(\tau, \tau') = & -id^2 \sum_{\mathbf{q} \mathbf{k}} [g_c(\mathbf{k}, \tau; \mathbf{q}, \tau') g_v(\mathbf{q}, \tau'; \mathbf{k}, \tau) \\ & + g_v(\mathbf{k}, \tau; \mathbf{q}, \tau') g_c(\mathbf{q}, \tau'; \mathbf{k}, \tau)]. \end{aligned} \quad (11.11)$$

The analytic continuation to real times is performed using the rules given in Table 4.1, and we find

$$\begin{aligned}\chi^r(t, t') = & -id^2 \sum_{\mathbf{k}} [g_c^<(\mathbf{k}, t, t') g_v^a(\mathbf{k}, t', t) + g_c^r(\mathbf{k}, t, t') g_v^<(\mathbf{k}, t', t) \\ & + g_v^<(\mathbf{k}, t, t') g_c^a(\mathbf{k}, t', t) + g_v^r(\mathbf{k}, t, t') g_c^<(\mathbf{k}, t', t)].\end{aligned}\quad (11.12)$$

The Fourier transform of the retarded susceptibility expressed in center-of-mass coordinates is

$$\begin{aligned}\chi^r(T, \omega_l) = & -id^2 \sum_{\mathbf{k}} \int_{-\infty}^{\infty} \frac{d\omega}{2\pi} \{ g_c^<(\mathbf{k}, T, \omega) \\ & \times [g_v^a(\mathbf{k}, T, \omega - \omega_l) + g_v^r(\mathbf{k}, T, \omega + \omega_l)] + g_v^<(\mathbf{k}, T, \omega) \\ & \times [g_c^a(\mathbf{k}, T, \omega - \omega_l) + g_c^r(\mathbf{k}, T, \omega + \omega_l)] \}.\end{aligned}\quad (11.13)$$

As shown later, the relevant quantity for continuous wave measurements at frequency ω_l is

$$\text{Im}\chi^r(T, \omega_l) = \text{Im} \left\{ \int_{-\infty}^{\infty} d\tau e^{i\omega_l \tau} \chi_{lm}^r(T, \tau) \right\} \quad (11.14)$$

to first-order in Ω/ω_l . Since $\chi^r(T, \tau)$ is real, the imaginary part of its Fourier transform is

$$\text{Im}\chi^r(T, \omega_l) = \frac{1}{2i} [\chi^r(T, \omega_l) - \chi^r(T, -\omega_l)].$$

Introducing the spectral functions

$$A_c(\mathbf{k}, T, \omega) = i[g_c^r(\mathbf{k}, T, \omega) - g_c^a(\mathbf{k}, T, \omega)]$$

and

$$A_v(\mathbf{k}, T, \omega) = i[g_v^r(\mathbf{k}, T, \omega) - g_v^a(\mathbf{k}, T, \omega)],$$

we find

$$\begin{aligned}\text{Im}\chi^r(T, \omega_l) = & \frac{i}{2} \sum_{\mathbf{k}} \int_{-\infty}^{\infty} \frac{d\omega}{2\pi} \{ g_c^<(\mathbf{k}, T, \omega) \\ & \times [A_v(\mathbf{k}, T, \omega - \omega_l) - A_v(\mathbf{k}, T, \omega + \omega_l)] + g_v^<(\mathbf{k}, T, \omega) \\ & \times [A_c(\mathbf{k}, T, \omega - \omega_l) - A_c(\mathbf{k}, T, \omega + \omega_l)] \}.\end{aligned}\quad (11.15)$$

The lesser functions can be expressed in the form

$$g_a^<(\mathbf{k}, T, \omega) = if_a(\mathbf{k}, T, \omega) A_a(\mathbf{k}, T, \omega)$$

where $f_a(\mathbf{k}, T, \omega)$ is a generalized particle distribution for particles of species a , and $A_a(\mathbf{k}, T, \omega)$ is the corresponding spectral function. In accordance with our assumption about no FIR field induced interband transitions, we can set $f_c(\mathbf{k}, T, \omega) = 0$ (zero occupation of conduction band), and $f_v(\mathbf{k}, T, \omega) = 1$

(all valence states are occupied). In the general case, e.g., when considering nonlinear effects in the *probing* light field, one would have to find $f_a(\mathbf{k}, T, \omega)$ via a direct integration of the quantum kinetic equations for $g_a^<(\mathbf{k}, T, \omega)$, as discussed in later chapters. With these assumptions the susceptibility reduces to

$$\begin{aligned} \text{Im}\chi_{lm}^r(T, \omega_l) &= -\frac{d^2}{2} \sum_{\mathbf{k}} \int_{-\infty}^{\infty} \frac{d\omega}{2\pi} A_v(\mathbf{k}, T, \omega) \\ &\quad \times \{A_c(\mathbf{k}, T, \omega - \omega_l) - A_c(\mathbf{k}, T, \omega + \omega_l)\} \\ &= \frac{d^2}{2} \sum_{\mathbf{k}} \int_{-\infty}^{\infty} \frac{d\omega}{2\pi} A_v(\mathbf{k}, T, \omega) A_c(\mathbf{k}, T, \omega + \omega_l) \\ &\equiv \frac{d^2}{2} \sum_{\mathbf{k}} A_{\text{joint}}(\mathbf{k}, T, \omega_l) = d^2 \pi \varrho_{\text{joint}}(\omega_l). \end{aligned} \quad (11.16)$$

Here we assumed momentum independent dipole matrix elements. The second equality comes about because we do not consider overlapping bands. Equation (11.16), which is the central result of this section, expresses the fact that the nonequilibrium interband susceptibility function can be calculated from a *joint spectral function*, which is a convolution of the individual band spectral functions. We also introduced another central concept: the joint density of states, defined in analog with (3.42). A similar result was found in our discussion of high-field quantum transport theory [see (10.113)]: there the field-dependent scattering rate is expressed as a joint spectral function for the initial and final states. We also emphasize that the spectral functions entering (11.16) may contain arbitrary *intra-band* interactions. Finally, as an additional illustration, let us consider the equilibrium limit of (11.16) for noninteracting particles. The conduction and valence band dispersion relations are

$$\epsilon_c(\mathbf{k}) = \frac{\hbar^2 k^2}{2m_e}, \quad \epsilon_v(\mathbf{k}) = -\frac{\hbar^2 k^2}{2m_h} - \epsilon_g, \quad (11.17)$$

and using the free equilibrium spectral functions $a_{c,v}^0(\omega, \mathbf{k}) = 2\pi\delta(\omega - \epsilon_{c,v}(\mathbf{k}))$ yields

$$\begin{aligned} \varrho_{\text{joint}}^0(\omega) &= \sum_{\mathbf{k}} \delta(\epsilon_c(\mathbf{k}) - \epsilon_v(\mathbf{k}) - \omega) \\ &= \sum_k \delta\left(\frac{\hbar^2 k^2}{2m_{\text{eff}}} + \epsilon_g - \omega\right). \end{aligned} \quad (11.18)$$

Here $m_{\text{eff}} = m_e m_h / (m_e + m_h)$. This is a familiar result discussed extensively in text-books, see, e.g. Chap. 5 in [146]. As we shall see below, a similar result holds also in nonequilibrium.

11.3 Absorption Coefficient in Terms of the Time-Dependent Dielectric Susceptibility

The wave equation for the light field in the absorbing medium is

$$\nabla^2 \mathcal{E}(t) - \frac{1}{c^2} \frac{\partial^2 \mathcal{D}(t)}{\partial t^2} = 0 \quad (11.19)$$

where $\mathcal{D}(t) = \mathcal{E}(t) + 4\pi\mathcal{P}(t)$, and \mathcal{P} is given by (11.2). The absorption coefficient $\alpha(\omega)$ is defined as the inverse of the length which light has to traverse in the medium at frequency ω in order for the intensity of the light to decrease by a factor of $1/e$. In equilibrium $\mathcal{D}(\omega) = [1 + 4\pi\chi(\omega)]\mathcal{E}(\omega) = \epsilon(\omega)\mathcal{E}(\omega)$ and the absorption coefficient becomes [146]

$$\alpha(\omega) = 4\pi\omega \frac{\text{Im}\chi(\omega)}{cn(\omega)}. \quad (11.20)$$

Here $n^2(\omega) = \frac{1}{2}[\text{Re}\epsilon(\omega) + |\epsilon(\omega)|]$ is the refraction coefficient which usually depends only weakly on ω . In nonequilibrium this analysis must be generalized slightly [185], and we proceed as follows. The probe field is

$$\mathcal{E}(\mathbf{r}, t) = \mathcal{E}_0 \exp[i(\mathbf{r} \cdot \mathbf{k} - \omega_l t)]. \quad (11.21)$$

and the polarization can therefore be expressed as

$$\mathcal{P}(t) = \mathcal{E}(\mathbf{r}, t) \int_{-\infty}^{\infty} dt' e^{i\omega_l(t-t')} \chi^r(t, t'). \quad (11.22)$$

This form explains why it is advantageous to express χ^r in terms of the center-of-mass and difference coordinates, as we did in Sect. 11.1. The characteristic time-scale for the center-of-mass time is set by the “slow” frequency Ω , while the difference-time varies on the scale of the “fast” frequency ω_l . Performing a gradient expansion as in Sect. 6.1 then yields

$$\mathcal{P}(\mathbf{r}, t) = \mathcal{E}(\mathbf{r}, t) \exp \left[\frac{i}{2} \frac{\partial^2}{\partial t \partial \omega_l} \right] \tilde{\chi}^r(t, \omega_l). \quad (11.23)$$

Equation (11.23) can now be used in Maxwell’s equation; note however that upon Fourier-transforming the dominant frequency comes from $\mathcal{E}(t)$ and we can keep t in $\tilde{\chi}^r(t, \omega_l)$ fixed. The slow time-variation will from this on be indicated by T . Proceeding as in deriving the static result (11.20), we identify the *time-dependent* absorption coefficient

$$\alpha_T(\omega) = 4\pi\omega \frac{\text{Im}\tilde{\chi}^r(T, \omega)}{cn_T(\omega)} + \mathcal{O}(\Omega/\omega). \quad (11.24)$$

If the driving force is periodic in T (the harmonic time-dependence due to a free-electron laser is an important special case), then the average absorption

coefficient is

$$\bar{\alpha}(\omega) = \frac{1}{T_{\text{period}}} \int_{\text{period}} dT \alpha_T(\omega) \\ = \frac{1}{T_{\text{period}}} \int_{\text{period}} dT 4\pi\omega \frac{\text{Im}\tilde{\chi}^r(T, \omega)}{cn_T(\omega)} \quad (11.25)$$

to *all* orders in Ω/ω . We stress that here $\tilde{\chi}^r(T, \omega)$ is Fourier transformed with respect to the difference variable τ . Below we shall represent numerical examples for the generalized absorption coefficient.

11.4 Static Electric Field

As a first illustration of the developed formalism we rederive the classic results of Franz [117] and Keldysh [197], who pointed out that static electric fields modify the linear optical properties of bulk semiconductors near the optical absorption edge: the absorption coefficient becomes finite (though small) for photon energies below the band gap, and the absorption coefficient shows oscillations for energies above the band gap. In terms of the joint density of states the absorption coefficient is

$$\alpha(\omega_l) = \frac{4\pi^2\omega_l|d|^2}{cn} \varrho_{\text{joint}}(\omega_l), \quad (11.26)$$

where joint density of states must be now evaluated with the field-dependent spectral functions (10.19). A short calculation yields (it is convenient to use the time-representation of the field-dependent spectral functions)

$$\varrho_{\text{joint}}(\omega_l) = \frac{1}{2\pi} \sum_{\mathbf{k}} \tilde{A}_{\text{eff}}(\mathbf{k}, \omega_l), \quad (11.27)$$

where \tilde{A}_{eff} is again given by (10.19) but now with the effective mass. In three spatial dimensions the momentum summation in (11.27) is converted to an energy integral via $\sum_{\mathbf{k}} \rightarrow \int d\varepsilon \varrho_0^{3D} \varepsilon^{1/2}$, which yields

$$\frac{\varrho_{\text{joint}}(\omega)}{\varrho_0^{3D}} = \int_{-\omega/\alpha}^{\infty} dt [\alpha t + \omega]^{1/2} \text{Ai}(t) \\ = \frac{1}{\sqrt{\pi}} \left[\text{Ai}'^2 \left(-\frac{\omega}{\Theta} \right) + \frac{\omega}{\Theta} \text{Ai}^2 \left(-\frac{\omega}{\Theta} \right) \right], \quad (11.28)$$

where we used various results for integrals involving Airy functions derived by Aspnes [10], and introduced $\Theta = (e^2 E^2 / 2m_{\text{eff}} \hbar)^{1/3} = 4^{1/3} \alpha / \hbar$. This result has been discussed in the literature several times, see, for example [196]. In two spatial dimensions we find

$$\frac{\varrho_{\text{joint}}(\omega)}{\varrho_0^{2D}} = 1/3 + \int_{-\omega/\alpha}^0 dt \text{Ai}(t). \quad (11.29)$$

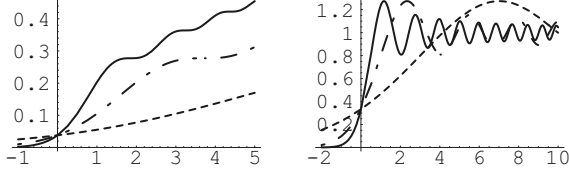


Fig. 11.1. Field dependent density of states for static electric fields (The Franz–Keldysh effect). *Left:* 3-dimensions; *right:* 2-dimensions. Field strengths are as in Fig. 10.1

The integral involving the Airy function cannot be expressed in terms of known functions, but it is easy to evaluate numerically.

The effective field-dependent density of states is shown in Fig. 11.1. We observe that the nonpositive semidefinite spectral functions always give rise to a positive density of states. The joint densities of states (11.28) and (11.29) can be used in (11.26) to compute the optical absorption coefficient, and subsequently compared to experiment. While the general trends are clearly confirmed, the experimental absorption spectra often display additional features attributed to excitons; these effects are discussed at length in several subsequent sections.

11.5 Harmonically Varying External Electric Fields

Using the results obtained earlier in this chapter we can go directly to the gauge-invariant spectral function:

$$\tilde{A}(\mathbf{k}, \omega, T) = \int d\mathbf{r} d\tau \exp(iw) A_A(\mathbf{r}, \tau, \mathbf{R}, T), \quad (11.30)$$

where $A_A(\mathbf{r}, \tau, \mathbf{R}, T)$ is (10.18) expressed in the center-of-mass and difference variables, and

$$w = \tau\omega - \mathbf{r} \cdot \mathbf{k} - \int_{T-\tau/2}^{T+\tau/2} \frac{dt_1}{\tau} \mathbf{r} \cdot \mathbf{A}(t_1). \quad (11.31)$$

After some calculation one finds

$$\begin{aligned} \tilde{A}(\mathbf{k}, \omega, T) &= \int d\tau \exp(i\omega\tau) \\ &\times \exp \left\{ -i \int_{T-\tau/2}^{T+\tau/2} dt_1 \varepsilon \left[\mathbf{k} + \int_{T-\tau/2}^{T+\tau/2} \frac{dt_2}{\tau} \mathbf{A}(t_2) - \mathbf{A}(t_1) \right] \right\} \\ &= \int d\tau \exp(i\omega\tau - i\varepsilon_k\tau) \\ &\times \exp \left\{ -\frac{i}{2} \left[\int_{T-\tau/2}^{T+\tau/2} dt_1 A^2(t_1) - \frac{1}{\tau} \left(\int_{T-\tau/2}^{T+\tau/2} dt_1 \mathbf{A}(t_1) \right)^2 \right] \right\}, \end{aligned} \quad (11.32)$$

where the second equality is valid for parabolic dispersion. We represent the harmonically varying electric field via

$$\mathbf{A}(t) = -\frac{\mathbf{F}}{\Omega} \sin(\Omega t) , \quad (11.33)$$

corresponding to $\mathbf{E}(t) = \mathbf{F} \cos(\Omega t)$. This particular choice for \mathbf{A} is useful, because throughout the calculation we can check that the correct zero-frequency limit is recovered. Substitution of (11.33) in (11.32) yields [177]

$$\tilde{A}(\mathbf{k}, \omega, T) = \int d\tau \cos[(\omega - \varepsilon_{\mathbf{k}} - \omega_F)\tau + X(\tau) + 2Y(\tau)] , \quad (11.34)$$

where we introduced the notation

$$X(\tau) = \frac{\omega_F}{\Omega} \sin \Omega\tau \cos 2\Omega T \quad (11.35)$$

$$Y(\tau) = \frac{\omega_F}{\Omega} \frac{4 \sin^2(\Omega\tau/2) \sin^2 \Omega T}{\Omega\tau} , \quad (11.36)$$

and defined the field parameter $\omega_F = e^2 F^2 / (4m\hbar\Omega^2)$. This parameter (which has been identified in the literature long time ago, see [288, 376]) has a simple physical interpretation: $\hbar\omega_F$ is the time-averaged kinetic energy of a free particle with charge e and mass m in a harmonic electric field of frequency Ω . $\hbar\omega_F \equiv \epsilon_f$ is called the ponderomotive energy in plasma physics. An explicit analytic evaluation of the integral in (11.34) is not possible, nor is a straightforward numerical calculation feasible, since it contains singularities, which must be isolated before attempting numerics. We proceed as follows. Use of the trigonometric identity $\cos(x+y) = \cos x - 2 \sin(x+y/2) \sin(y/2)$ allows us to write (11.34) as a sum of two terms, $\tilde{A} = \tilde{A}_1 + \tilde{A}_2$, where

$$\begin{aligned} \tilde{A}_1(\mathbf{k}, \omega, T) &= \int d\tau \cos[(\omega - \varepsilon_{\mathbf{k}} - \omega_F)\tau + X(\tau)] , \\ \tilde{A}_2(\mathbf{k}, \omega, T) &= -2 \int d\tau \sin[(\omega - \varepsilon_{\mathbf{k}} - \omega_F)\tau \\ &\quad + X(\tau) + Y(\tau)] \sin Y(\tau) . \end{aligned} \quad (11.37)$$

A numerical evaluation of \tilde{A}_2 is now straightforward, while analytic progress can be made with \tilde{A}_1 . Recalling the identity

$$\int_{-\infty}^{\infty} dx \cos(ax - b \sin x) = 2\pi \sum_{n=-\infty}^{\infty} J_n(b) \delta(n - a) ,$$

where J_n is the n th-order Bessel function, yields

$$\tilde{A}_1(\mathbf{k}, \omega, T) = 2\pi \sum_{n=-\infty}^{\infty} J_n \left[-\frac{\omega_F}{\Omega} \cos(2\Omega T) \right] \delta(\omega - \varepsilon_{\mathbf{k}} - n\Omega - \omega_F) . \quad (11.38)$$

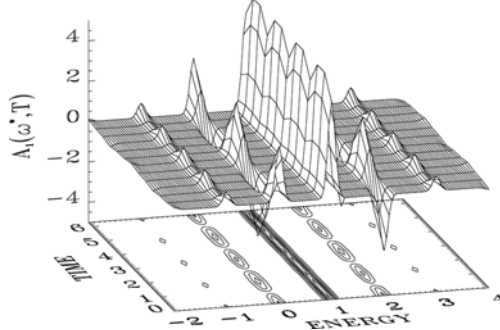


Fig. 11.2. The function \tilde{A}_1 as a function of the variable $\omega^* = (\omega - \varepsilon_k)/\Omega$. The field strength is given by $\omega_F/\Omega = 1$. The δ -function singularities have been broadened for illustrative purposes

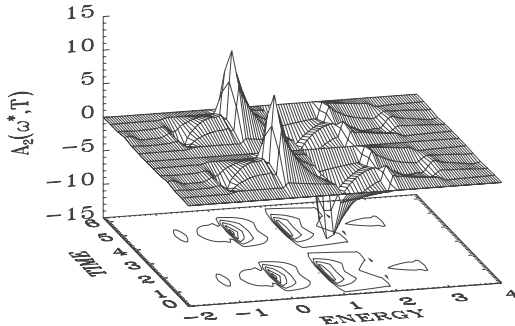


Fig. 11.3. The function \tilde{A}_2 as a function of the variable ω^*

These two components of the spectral function have quite distinct properties. The frequency sum rule is exhausted by \tilde{A}_1 alone,¹ i.e., $\int d\omega/2\pi \tilde{A}_1(\omega, T) = 1$, while $\int d\omega/2\pi \tilde{A}_2(\omega, T) = 0$. Further, the delta-function singularities of \tilde{A}_1 are reminiscent of *photonic side-bands*, however these features are shifted by the field- and frequency-dependent parameter ω_F . In the zero-field limit \tilde{A}_1 reduces to the field-free result $a_0(\mathbf{k}, \omega) = 2\pi\delta(\omega - \varepsilon_{\mathbf{k}})$, while \tilde{A}_2 vanishes. Note also that the spectral function depends *quadratically* on the electric field. This is confirmed by physical intuition: Since there is no preferred direction, it should not matter if the field is reversed, $\mathbf{F} \rightarrow -\mathbf{F}$, and thus we expect to find a spectral function that is even in the applied field. The functions \tilde{A}_1 and \tilde{A}_2 are displayed in Figs. 11.2 and 11.3, respectively.

¹ The proof is based on the properties of Bessel functions: (1) $J_{-n}(z) = (-1)^n J_n(z)$, and (2) $1 = J_0(z) + 2J_2(z) + 2J_4(z) + \dots$

The absorption coefficient is again evaluated with an integral analogous to (11.16) encountered earlier, but now using spectral functions for the time-dependent electric field. Rather than using the auxiliary functions \tilde{A}_1 and \tilde{A}_2 discussed above, it is advantageous to proceed slightly differently. The time-dependent density of states for a system of n spatial dimensions is

$$\varrho_{\text{joint}}^{nD}(T, \epsilon) = \int_{-\infty}^{\infty} d\tau e^{i\epsilon\tau/\hbar} \varrho_{\text{joint}}^{nD}(T, \tau), \quad (11.39)$$

where

$$\begin{aligned} \varrho_{\text{joint}}^{nD}(T, \tau) &= \int \frac{d^n k}{(2\pi)^n} \exp \left\{ -\frac{i}{\hbar} \int_{T-\tau/2}^{T+\tau/2} ds \epsilon [k + e\mathbf{A}(s)] \right\} \\ &= \int \frac{d^n k}{(2\pi)^n} \exp \left\{ -i \left[(\epsilon_k + \epsilon_f) \tau \right. \right. \\ &\quad \left. \left. + 2 \frac{e\hbar k \cdot \mathbf{F}}{m_{\text{eff}} \Omega^2} \sin(\Omega T) \sin\left(\frac{\Omega\tau}{2}\right) - \frac{\omega_f}{\Omega} \cos(2\Omega T) \sin(\Omega\tau) \right] \right\}. \end{aligned} \quad (11.40)$$

In order to perform the Fourier-transform (11.39) we utilize the identity

$$\exp(ix \sin \theta) = \sum_n J_n(x) \exp(in\theta); \quad (11.41)$$

we shall henceforth write $\sum_n \equiv \sum_{n=-\infty}^{\infty}$ to simplify the notation. The joint density of states becomes

$$\begin{aligned} \varrho_{\text{joint}}^{nD}(T, \epsilon) &= \sum_{l,j} \int \frac{d^n k}{(2\pi)^{n-1}} \delta(\epsilon - \epsilon_k - \epsilon_f + l\hbar\Omega) \\ &\quad \times J_{2j} \left[2 \frac{e\hbar k \cdot \mathbf{F}}{m_{\text{eff}} \Omega^2} \sin(\Omega T) \right] J_{l+j} \left[\frac{\omega_f}{\Omega} \cos(2\Omega T) \right]. \end{aligned} \quad (11.42)$$

The dimensionality is entirely contained in the remaining momentum integration $\int d^n k / (2\pi)^{n-1}$. We note that (11.42) implies a shift of the absorption edge by ϵ_f . The term $l\hbar\Omega$ in the Dirac-delta function gives rise to photonic side bands. Since $J_{2l}(x)$ is an even function, the density of states is invariant under the transformation $\mathbf{F} \rightarrow -\mathbf{F}$, as expected. In the following we give results for the 2D and 3D systems separately and show how the density of states smoothly evolves from a low field intensity regime into a high field intensity regime making the nonlinear effects of the THz-field apparent.

11.5.1 Joint Density of States, 2D

Several authors have considered fields perpendicular to the quantum well, see, e.g., [164, 366]; here we focus on the situation where the electric field is in the

plane of the two-dimensional electron gas. In such a system with no external field the density of states is constant

$$\rho_0^{2D}(\epsilon) = \frac{m}{\pi\hbar^2}\theta(\epsilon). \quad (11.43)$$

We thus arrive at

$$\begin{aligned} \varrho_{\text{joint}}^{2D}(T, \epsilon) &= \sum_{l,j} \int_0^\infty dk k \int_0^{2\pi} \frac{d\theta}{2\pi} \delta(\epsilon - \epsilon_k - \epsilon_f + l\hbar\Omega) \\ &\times J_{2j} \left[\frac{\sqrt{32\epsilon_f\epsilon_k}}{\hbar\Omega} \cos\theta \sin(\Omega T) \right] J_{l+j} \left[\frac{\epsilon_f}{\hbar\Omega} \cos(2\Omega T) \right]. \end{aligned} \quad (11.44)$$

The integrals in (11.44) are performed using

$$\int_0^{2\pi} d\theta J_{2l}(a \cos\theta) = 2\pi J_l^2(a) \quad (11.45)$$

and writing the result in the side-band picture we obtain

$$\varrho_{\text{joint}}^{2D}(T, \epsilon) = \sum_l r_l^{2D}(T, \epsilon - \epsilon_f + l\hbar\Omega) \rho_0^{2D}(\epsilon - \epsilon_f + l\hbar\Omega) \quad (11.46)$$

where the side-band weights are

$$r_l^{2D}(T, \epsilon) = \sum_j J_j^2 \left[\frac{\sqrt{32\epsilon_f\epsilon}}{\hbar\Omega} \sin(\Omega T) \right] J_{l+j} \left[\frac{\epsilon_f}{\hbar\Omega} \cos(2\Omega T) \right]. \quad (11.47)$$

A numerical example is given in Fig. 11.4.

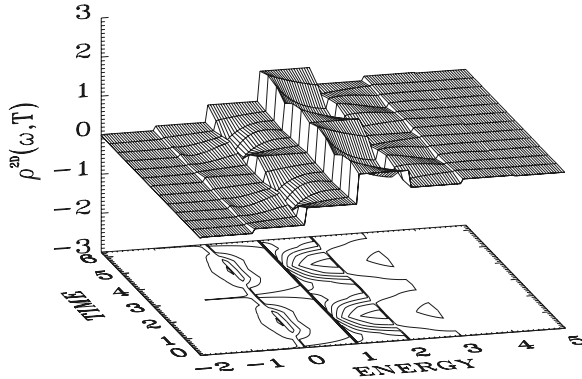


Fig. 11.4. Time-dependent joint density of states for free two-dimensional electrons in a harmonically varying electric field. The parameters are as in Fig. 11.2

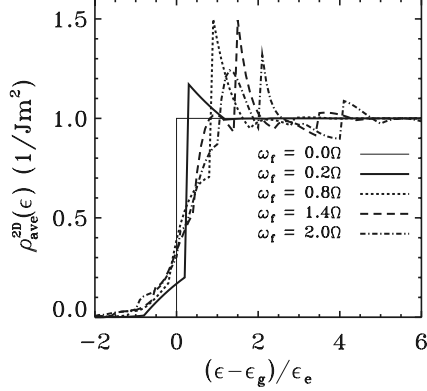


Fig. 11.5. The time averaged joint density of states for a 2D-system for a range of FIR-intensities, $\omega_F/\Omega = (0.0, 0.2, 0.8, 1.4, 2.0)$. At low intensities one observes a Stark-like blue-shift of the band edge as well as finite absorption within the band gap. With increasing intensity side bands emerge at $\epsilon = \epsilon_g + \epsilon_f \pm 2\hbar\Omega$

Many experiments are done under continuous illumination and subsequently time-averaged. Numerical results for the time averaged joint density of states

$$\rho_{\text{ave}}^{2D}(\epsilon) \equiv \frac{\Omega}{2\pi} \int_0^{2\pi/\Omega} dT \varrho_{\text{joint}}^{2D}(T, \epsilon) \quad (11.48)$$

are reported in Fig. 11.5. The figure clearly displays the characteristics of the Dynamical Franz–Keldysh effect [177]: (a) the Stark-like blueshift of the main absorption edge by ϵ_f , (b) the formation of sidebands at $\epsilon_g + \epsilon_f \pm n\hbar\Omega$, and (c) finite absorption within the band gap.

11.5.2 Joint Density of States, 3D

Absorption in bulk semiconductors subject to THz radiation was considered already long time ago by Yacoby [376] and later by Rebane [288]. These papers study transition rates between bands by investigating approximate solutions to the corresponding time-dependent Schrödinger equation. Yacoby [376] concluded that transitions occur in the gap and noted reduced rates above the gap, in agreement with the present work, while [288] pointed out that the absorption edge would be shifted, likewise in agreement with our work. The 3D field-free density of states is

$$\rho_0^{3D}(\epsilon) = \frac{1}{2\pi^2} \left(\frac{2m}{\hbar} \right)^{3/2} \theta(\epsilon) \epsilon^{1/2}.$$

With the external field the density of states becomes

$$\varrho_{\text{joint}}^{3D}(T, \epsilon) = \sum_l r_l^{3D}(T, \epsilon - \epsilon_f + l\hbar\Omega) \rho_0^{3D}(\epsilon - \epsilon_f + l\hbar\Omega) \quad (11.49)$$

with the side-band weights

$$\begin{aligned} r_l^{3D}(T, \epsilon) &= \sum_j J_{l+j} \left[\frac{\epsilon_f}{\hbar\Omega} \cos(2\Omega T) \right] \\ &\times \int_0^1 du J_{2j} \left[\frac{\sqrt{32\epsilon_f\epsilon}}{\hbar\Omega} \sin(\Omega T)u \right]. \end{aligned} \quad (11.50)$$

In Figs. 11.6 and 11.7 we illustrate the time-dependent joint density of states and its time average, respectively. Comparing the results for two and three dimensions, respectively, we observe that the quantum mechanical modifications are much more pronounced in two dimensions; this is a general trend seen in many physical situations, and also in later chapters. Many further applications of these techniques to other nanostructures can be found in [185].

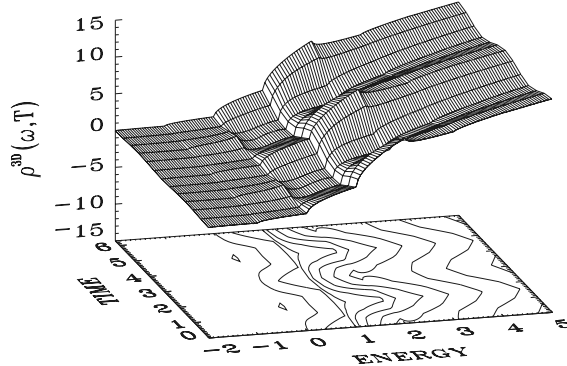


Fig. 11.6. Time-dependent joint density of states for free bulk electrons in a harmonically varying electric field. The parameters are as in Fig. 11.2

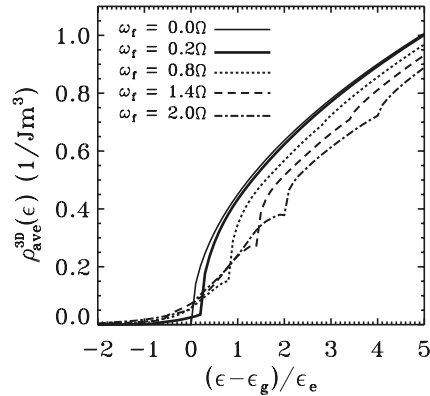


Fig. 11.7. The time averaged joint density of states for a 3D-system. The parameters are as in Fig. 11.5

11.6 Dynamical Franz–Keldysh Effect: Excitonic Effects

So far we have neglected Coulomb correlations, which is a drastic and often totally inadequate approximation. An electron excited in the conduction band by the probe field interacts strongly with the hole left behind in the valence band, forming an exciton. The presence of an exciton manifests itself as a strong enhancement of absorption (or reduced transmission) below the band edge, thus the features shown in Figs. 11.4–11.7 may be masked by the excitonic line(s). An example of a two-color² transmission measurement performed on a multi-quantum well sample using the USCB free-electron laser is shown in Fig. 11.8. One observes that the sharp band edge, characteristic for two-dimensional systems (see Fig. 11.5), is dominated by a strong resonance due to the exciton formed between the lowest electronic and hole sub-bands (e1h1 exciton). Excitons, being bound pairs of electrons and holes, have hydrogen-like quantized energy levels. If the energy difference of a pair of levels is close to the energy of the FEL photon, one expects a strong coupling between the exciton and the FEL photon [209], due to the ac Stark effect. The data in Fig. 11.8 shows how the exciton line both shifts in energy and changes its width as the intensity of the FEL is varied; the variation in the spectrum is qualitatively different depending on whether the FEL photon energy is larger or smaller than the energy-level splitting of the exciton. The energy shift can be quantified by computing the “center-of-mass” of the exciton resonance; this is indicated by arrows in Fig. 11.8. We will next construct a “minimal” theory for the energy shift, deferring the full theory of exciton quantum kinetics to later chapters.

We argue along the line familiar from many earlier chapters. Since the nonequilibrium theory is diagrammatically equivalent to the equilibrium theory, we can directly generalize any diagrammatic result obtained in equilibrium to nonequilibrium by replacing the equilibrium Green function lines by their nonequilibrium counterparts, and performing the appropriate analytic continuations by the rules summarized in Table 4.1. Specifically, we can include the Coulomb interaction in the *ladder approximation* of the Bethe–Salpeter equation [142] also in nonequilibrium simply by replacing the static susceptibility by its nonequilibrium counterpart. We thus know that the nonequilibrium susceptibility obeys (we consider here two-dimensional systems, relevant to the interpretation of the experimental data)

$$\begin{aligned} \chi^r(\mathbf{k}; t, t') = & \tilde{\chi}^r(\mathbf{k}; t, t') \\ & - \int \frac{d^2\mathbf{k}'}{(2\pi)^2} \int_{-\infty}^{\infty} dt'' \tilde{\chi}^r(\mathbf{k}; t, t'') V(|\mathbf{k} - \mathbf{k}'|) \chi^r(\mathbf{k}'; t'', t'), \end{aligned} \quad (11.51)$$

² Two-colors: strong far infrared light (due to the FEL) and weak near infrared light (due to Ti-sapphire laser)

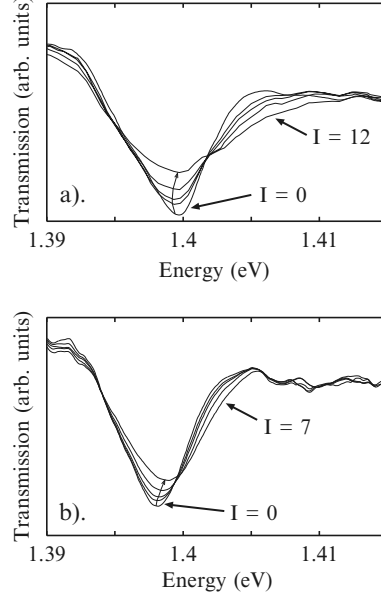


Fig. 11.8. Experimental transmission of multi-quantum well sample near e1h1 exciton with (a) $\hbar\Omega = 2.5$ meV at (relative) field intensities $I = 0, 1, 2, 4, 12$. (b) $\hbar\Omega = 14$ meV at $I = 0, 1, 2, 4, 7$. Arrows connect calculated centers of experimental peaks, and point in the direction of increasing intensity

where $V(|\mathbf{k} - \mathbf{k}'|)$ is the Coulomb interaction, and $\tilde{\chi}^r(\mathbf{k}; t, t')$ is the noninteracting nonequilibrium susceptibility discussed in Sect. 11.4:

$$\tilde{\chi}(\mathbf{k}, t, t') = id^2\theta(t - t') \exp \left\{ -i \int_{t'}^t \frac{d\bar{t}}{\hbar} \frac{[\hbar\mathbf{k} + e\mathbf{A}(\bar{t})]^2}{2m_{\text{eff}}} \right\}. \quad (11.52)$$

We next describe two different methods of solving (11.51).

11.6.1 Matrix Truncation

We first observe that the susceptibility is a periodic function when written in the Wigner coordinates, $\tilde{\chi}^r(\mathbf{k}, \tau, T) = \tilde{\chi}^r(\mathbf{k}, \tau, T + 2\pi/\Omega)$, and that it is therefore advantageous to introduce a Fourier expansion,

$$\begin{aligned} \tilde{\chi}^r(\mathbf{k}; \tau, T) &= \sum_n \tilde{\chi}_n^r(\mathbf{k}, \tau) e^{-in\Omega T} \\ &= \sum_n \int \frac{d\omega}{2\pi} \tilde{\chi}_n^r(\mathbf{k}, \omega) e^{-i\omega\tau - in\Omega T}. \end{aligned} \quad (11.53)$$

Using (11.53), the integral equation (11.51) becomes a matrix equation,

$$\begin{aligned}\chi_n^r(\mathbf{k}, \omega) &= \tilde{\chi}_n^r(\mathbf{k}, \omega) - \sum_{n'} \tilde{\chi}_{n-n'}^r[\mathbf{k}, \omega + n' \Omega/2] \\ &\quad \times \int \frac{d^2 q}{(2\pi)^2} V(|q|) \chi_{n'}^r(\mathbf{k} + \mathbf{q}, \omega + (n' - n)\Omega/2).\end{aligned}\quad (11.54)$$

For many practical purposes a truncation of n to small values ($n \simeq 2 \dots 4$) is sufficient. The angular integral appearing in (11.54) is treated by introducing angular expansions for the Coulomb interaction, and the n -resolved susceptibility:

$$V(|\mathbf{k} - \mathbf{k}'|) = \sum_{l=-\infty}^{\infty} v_l(k, k') e^{il\theta}, \quad (11.55)$$

and

$$\chi_n^r(\mathbf{k}, \omega) = \sum_{l=-\infty}^{\infty} \chi_n^{(l)}(k, \omega) e^{il\theta}, \quad (11.56)$$

respectively. Numerically, we solve the matrix equation including both s -wave and p -wave scattering; both are important, since, as mentioned above, the THz field will couple the s and p states of the exciton and influence the observed resonance, i.e. the ac Stark Effect. We solve the resulting equation by discretizing the integrals to yield a set of linear equations which we solve by standard methods [146]. Finally, the physically measurable quantities are obtained by expressing the macroscopic polarization as

$$\mathcal{P}(t) = \mathcal{E}_0 \sum_n \tilde{\chi}_n(\omega) e^{i(n\Omega - \omega)t}, \quad (11.57)$$

where $\tilde{\chi}_n(\omega) = \sum_{\mathbf{k}} \chi_n^r(\mathbf{k}, \omega) = \chi_n^r(\mathbf{r} = 0, \omega)$. The linear absorption is thus proportional to $\text{Im}\tilde{\chi}_0(\omega)$. The terms with $n \neq 0$ describe the nonlinear mixing of the NIR and THz field, resulting in optical sideband generation. The rich structure displayed by these side-bands is discussed in the next subsection.

Figure 11.9 presents results for calculated absorption spectra using the experimental parameters relevant for experiments shown in Fig. 11.8. If the energy difference between the $1s$ and $2p$ levels of the exciton is called $\hbar\omega_{12}$, two separate regimes can be distinguished. For $\Omega < \omega_{12}$, the numerics lead to a red-shift of the exciton absorption peak at low THz intensities. With increasing THz intensity, the shift saturates and then reverses, eventually becoming a net blue-shift. Theory also predicts a blue-shift for $\Omega > \omega_{12}$, which monotonically increases with THz intensity for experimentally accessible intensities. In both cases, the exciton peak is suppressed and inhomogeneously broadened with increasing intensity. Using the same method as for the measured spectra, we compute the center-of-mass of the calculated exciton lines. We plot the shift of the theoretical “center-of-mass” in Fig. 11.10 along with the experimental results. The theoretical and experimental peak shifts show identical qualitative behavior. We can understand the behavior seen in Fig. 11.10

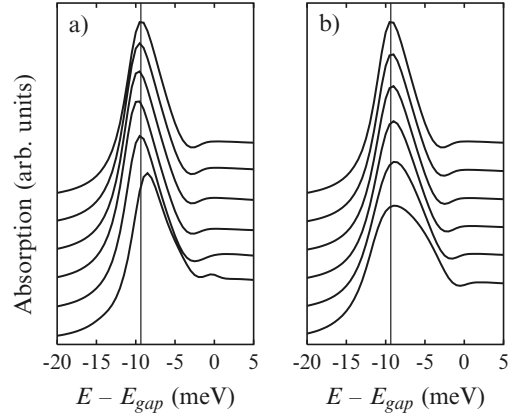


Fig. 11.9. Calculated absorption with (a) $\hbar\Omega = 2.5\text{meV} < \hbar\omega_{12}$ from top to down at $\omega_F/\Omega = 0, 0.03, 0.06, 0.1, 0.5$ and 1.5 , (b) $\hbar\Omega = 14\text{meV} > \hbar\omega_{12}$ from top to down at $\omega_F/\Omega = 0, 0.01, 0.04, 0.08$, and 0.15 .

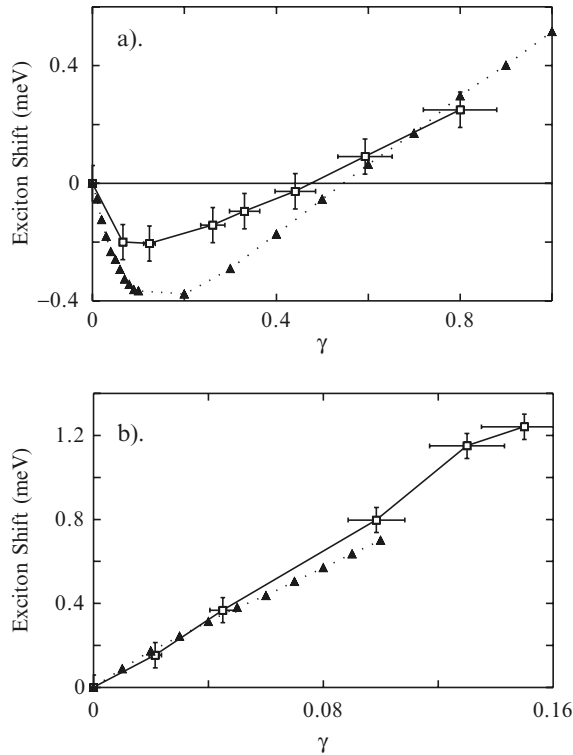


Fig. 11.10. Center of mass of measured (squares) and calculated (triangles) exciton transmission peak vs $\gamma \equiv e^2 E^2 / (4m_{\text{eff}} \hbar \Omega^3)$ for (a) $\hbar\Omega = 2.5\text{meV} < \hbar\omega_{12}$ and (b) $\hbar\Omega = 10.5\text{meV} > \hbar\omega_{12}$

as resulting from a competition between the ac Stark and DFKE shifts. The ac Stark effect results in a shift of the exciton level

$$\Delta \propto \frac{(\Omega - \omega_{12})E^2}{(\Omega - \omega_{12})^2 + \Gamma^2}, \quad (11.58)$$

where Γ is the width of the $1s \rightarrow 2p$ transition line [15]. The magnitude of Δ is dominated by broadening, and we expect little resonant enhancement of $|\Delta|$ for $\Omega \sim \omega_{12}$. It is also well known that Δ will saturate as E increases, going from quadratic to linear dependence on E [15]. The DFKE, however, always provides a blue-shift proportional to E^2 , given by ω_F .

Thus, for $\Omega < \omega_{12}$, one expects a red shift which saturates and reverses with increasing intensity, showing a roughly linear dependence on THz intensity at high fields (Fig. 11.10a). At low fields, Δ dominates, resulting in a net red shift. As Δ saturates with increasing field, ω_F begins to dominate, eventually overwhelming the red shift entirely and resulting in a net blue shift. For $\Omega > \omega_{12}$, we observe only an increasing blue-shift with increasing E (Fig. 11.10b). Here, Δ and ω_F cooperate to create a blue-shift. At low THz intensities, Δ and ω_F are both proportional to E^2 . At higher intensities, Δ saturates, which is suggested by the change in slope shown in the data.

11.6.2 Floquet Space Formulation

The method presented in Sect. 11.6.1 may suffer from numerical instabilities if one wants to study nonlinear mixing or generation of side-bands, i.e., one needs higher values of the index n . We present here an alternative approach, based on a Floquet space formulation, which avoids these difficulties [186]. We first convert the integral equation (11.51) into a real-space form. Specifically, Eq.(11.51) is equivalent to

$$\left\{ i\hbar \frac{\partial}{\partial t} - \frac{[-i\hbar \nabla_r + e\mathbf{A}(t)]^2}{2m_{\text{eff}}} + \frac{e^2}{4\pi\kappa r} \right\} \chi^r(\mathbf{r}, t, t') = \delta(\mathbf{r})\delta(t - t'), \quad (11.59)$$

where κ is the dielectric constant of the semiconductor. To prove (11.59), note that the noninteracting susceptibility obeys (here we drop the dipole matrix element d , and reintroduce it later in the induced polarization)

$$\left\{ i\hbar \frac{\partial}{\partial t} - \frac{[-i\hbar \nabla_r + e\mathbf{A}(t)]^2}{2m_{\text{eff}}} \right\} \tilde{\chi}^r(\mathbf{r}, t, t') = \delta(\mathbf{r})\delta(t - t') \quad (11.60)$$

and use the inverse of this expression to write (11.51) as $\tilde{\chi}^{-1}\chi^r = \delta - V\chi^r$, from which (11.59) follows. Consider now the homogeneous part of (11.59):

$$\left\{ -\frac{[-i\hbar \nabla_r + e\mathbf{A}(t)]^2}{2m_{\text{eff}}} + \frac{e^2}{4\pi\kappa r} \right\} \Psi(\mathbf{r}, t) = i\hbar \frac{\partial \Psi(\mathbf{r}, t)}{\partial t}. \quad (11.61)$$

This equation generalizes the Wannier equation (see, e.g., Chap. 10 of [146]) to ac-fields. A convenient method to solve this equation is to use the Floquet theory, which is a temporal analogue of the Bloch theory for spatially periodic systems.

Reminder of Floquet Theory

Here we briefly introduce the main concepts behind the Floquet theory; an extensive discussion with many applications can be found, e.g., in [208, 283]. Consider a system described by a time-periodic Hamiltonian $H(t) = H(t + T)$. The Floquet states are “steady states” of the system in the sense that if the system is prepared in a Floquet state, it stays there. Consider the time-evolution operator $U(t, t_0)$, which describes the time evolution of the states, i.e., $\psi(t) = U(t, t_0)\psi(t_0)$. It is unitary and has the properties $U(t, t) = 1$ and $U(t, t')U(t', t_0) = U(t, t_0)$, and obeys the Schrödinger equation,

$$i\hbar \frac{\partial U(t, t_0)}{\partial t} = H(t)U(t, t_0). \quad (11.62)$$

As seen in Chaps. 3 and 4, the formal solution of (11.62) is

$$U(t, t_0) = T \exp \left[-i \int_{t_0}^t \frac{ds}{\hbar} H(s) \right], \quad (11.63)$$

where T is the time-ordering operator. The time-periodic Floquet states $\phi_\alpha(\mathbf{r}, t)$ are the eigenstates of the operator evolving the system one period forward in time, and they obey

$$U(t + T, t)\phi_\alpha(\mathbf{r}, t) = e^{-i\tilde{\epsilon}_\alpha T/\hbar}\phi_\alpha(\mathbf{r}, t). \quad (11.64)$$

Here $\tilde{\epsilon}_\alpha$ is the *quasienergy* associated with the Floquet state $\phi_\alpha(\mathbf{r}, t)$. The Floquet states satisfy a closure relation

$$\sum_\alpha \phi_\alpha^*(\mathbf{r}, t)\phi_\alpha(\mathbf{r}', t) = \delta(\mathbf{r} - \mathbf{r}'). \quad (11.65)$$

The eigenvalue equation (11.64) is degenerate and determines the quasienergies only modulo $2\hbar\pi/T$. The Floquet states obey, in analogy with the Bloch theorem,

$$\left[H(t) - i\hbar \frac{\partial}{\partial t} \right] \phi_\alpha(\mathbf{r}, t) = \tilde{\epsilon}_\alpha \phi_\alpha(\mathbf{r}, t). \quad (11.66)$$

This equation separates the quasienergies into bands and allows for a selection of a complete set of states with quasienergies corresponding to a one-time Brillouin zone (TBZ). The first TBZ is $[-\hbar\pi/T, \hbar\pi/T]$. The central result of the Floquet theory is that any solution of the time-dependent Schrödinger equation

$$H(t)\Psi(\mathbf{r}, t) = i\hbar \frac{\partial}{\partial t} \Psi(\mathbf{r}, t) \quad (11.67)$$

can be expressed in terms of Floquet states from one TBZ as

$$\Psi(\mathbf{r}, t) = \sum_{\alpha \in \text{TBZ}} c_\alpha e^{-i\tilde{\epsilon}_\alpha t} \phi_\alpha(\mathbf{r}, t), \quad (11.68)$$

where the coefficients c_α are time-independent *c*-numbers.

The susceptibility has a compact form when expressed in terms of the Floquet states:

$$\chi^r(\mathbf{r}, t, t') = (i/\hbar)\theta(t - t') \sum_{\alpha} e^{i\tilde{\epsilon}_{\alpha}t/\hbar} \phi_{\alpha}^*(\mathbf{0}, t) \phi_{\alpha}(\mathbf{r}, t'). \quad (11.69)$$

The proof of (11.69) is a direct calculation: by working out its time-derivative, and using the closure relation (11.65) one immediately recovers (11.59). Introducing the expansion

$$\phi_{\alpha}(\mathbf{r}, t) = \sum_n \phi_{\alpha,n}(\mathbf{r}) e^{-in\Omega t}, \quad (11.70)$$

and reintroducing the dipole matrix element leads to the final expression for the optical susceptibility:

$$\chi_n^r(\omega_l) = -e^2 d^2 \sum_{n'} \frac{\phi_{\alpha,n+n'}^*(\mathbf{0}) \phi_{\alpha,n}(\mathbf{0})}{\hbar\omega_l - \tilde{\epsilon}_{\alpha} - n'\hbar\Omega + i0^+}. \quad (11.71)$$

Let us next examine what kind of experimental parameters are needed in order to reach a regime where interesting physics is expected to take place. The

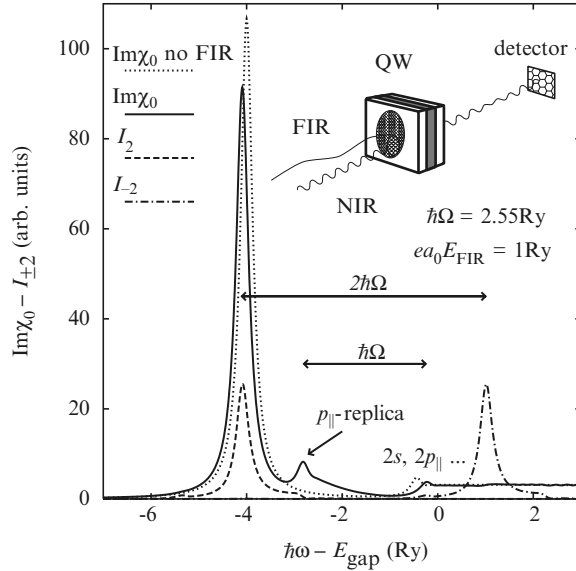


Fig. 11.11. Summary of effects due to intense FIR radiation, collinear with a weak NIR field. The linear optical absorption $\text{Im}\chi_0$ obtains: (a) an ac-Stark redshift of the $1s$ resonance, (b) Dynamical Franz–Keldysh blueshift of the $2s$ resonance, (c) a suppression of the oscillator strength, and (d) an emergence of a photon replica of the p_{\parallel} state. Nonlinear mixing $I_{\pm 2}$ leads to sideband emission at $\omega \pm n\Omega$. The insert illustrates the experimental geometry (Reproduced from [186].)

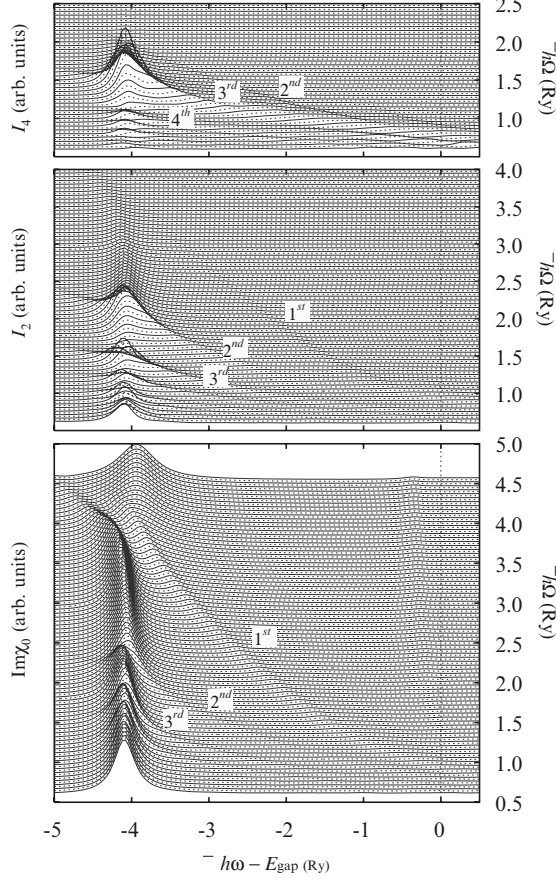


Fig. 11.12. The effect of the THz frequency at fixed field strength. From below; the absorption coefficient (proportional to $\text{Im}\chi_0$), two-, and four-photon sideband generation. Several avoided crossings in the quasienergy spectra can be distinguished, as splittings in the absorption and as resonant enhancement in the sideband generation (Reproduced from [186].)

strength of the FIR electric field should be such that the characteristic energy scale, $e a_0 E_{\text{FIR}}$, should be comparable to the effective Rydberg energy of the medium, $E_{\text{Ry}} = \hbar^2 / (2m_{\text{eff}}a_0^2)$, where $a_0 = \hbar^2 \kappa / (e^2 m_{\text{eff}})$ is the Bohr radius of the exciton. For InGaAs, for example, $E_{\text{Ry}} \simeq 2 - 3$ meV and $a_0 \simeq 200 \text{ \AA}$, which leads to $E_{\text{FIR}} \simeq 10^5 \text{ V m}^{-1}$, well within reach of free electron lasers. A two-dimensional exciton in equilibrium has the bound state spectrum $E_n = E_{\text{gap}} - E_{\text{Ry}} / (n - 0.5)^2$. The $n = 1$ state is a nondegenerate s state, while $n \neq 1$ are degenerate containing also p states, etc. [146] Since the FIR is linearly polarized, the doubly degenerate states can be decomposed into p_\perp and p_\parallel , and only p_\parallel couples to the field. The Floquet states and the corresponding

quasienergies can be found numerically by solving for the eigenstates of $U(t + 2\pi/\Omega, t)$.

Figure 11.11 shows characteristic numerical results for a fixed $\hbar\Omega = 2.55 E_{\text{Ry}}$ as a function of the NIR frequency. The THz frequency is below the $1s \rightarrow 2p_{\parallel}$ equilibrium transition frequency, $\hbar\omega_{12}^0 \simeq 3.56E_{\text{Ry}}$. As discussed above, the redshift of the $1s$ resonance is due to the ac-Stark effect. The $2s$ resonance, as well as the band-edge are blue-shifted due to the DFK effect. An interesting feature is the single photon replica of the dark p_{\parallel} state which under irradiation becomes optically active. Several other features of Fig. 11.11 are analyzed in [186].

Figure 11.12 shows results for a frequency sweep $\hbar\Omega = (0.5 \dots 5)E_{\text{Ry}}$. In $\text{Im}\chi_0$ one observes how the photon replicas form a fan as the THz frequency is increased; the fan blades are tagged with the order of the THz frequency involved. In view of (11.71), when the replicas reach the main resonance a strongly avoided crossing in the quasienergy spectrum results, which is clearly visible in the computed spectra. For the first-order process a splitting results (this effect is known as the Autler–Townes splitting). Also the side-bands, depicted in the upper panels, show clear evidence of the fan shape. In this case, however, the underlying avoided crossing in the quasienergy spectrum results in resonantly enhanced sideband generation. As discussed in [186], many other experimental predictions can be drawn from the theory discussed above.

12

Transport in Mesoscopic Semiconductor Structures

Summary. Stationary transport properties of tunneling structures such as double-barrier semiconductor heterostructures, superlattices, metallic nanowires, and Coulomb blockade structures are treated as examples for quantum transport through mesoscopic systems

12.1 Introduction

Study of mesoscopic phenomena is one of the most active areas of today's solid state physics. One can observe signatures of mesoscopics in a large number of different physical systems, and it would be impossible in the present context to cover all the possible variations of the mesoscopic theme. We restrict ourselves exclusively to the particular subclass which can be studied in semiconductors. Further, we do not consider quantizing magnetic fields; this enormously rich topic cannot be treated adequately in a book whose main goal is to illustrate in terms of a few simple examples how nonequilibrium Green functions can be applied to mesoscopic transport. Thus the generic system we have in mind is a semiconductor heterostructure where charge carriers are introduced either by modulation doping, or they flow in and out of the system through heavily doped (metallic) contacts. Transport physics in these systems can roughly be divided into two categories: perpendicular transport and parallel transport, according to whether the charge carriers' motion is perpendicular or parallel to the layers that form the heterostructures. A representative example of perpendicular transport is the resonant-tunneling diode (RTD), which consists of alternate layers of semiconductor materials with different band gaps; a schematic conduction band diagram is shown in Fig. 12.1. Charge carriers entering from left may, at a certain bias voltage, be tuned to the quasibound state in the quantum well, which results in a large enhancement of the transmitted current. At off-resonance conditions only a small current can flow, because transmission through the classically inaccessible regions is exponentially suppressed. This leads to a nonmonotonic current–voltage characteristic, and a

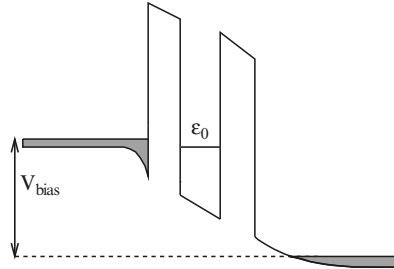


Fig. 12.1. Double-barrier semiconductor heterostructure biased close to resonance, where charge carriers emerging from the source contact are matched to the energy of the quasibound state ε_0 in the quantum well. Occupied contact states are shown as hatched, and the band bending is due to charge accumulation or depletion

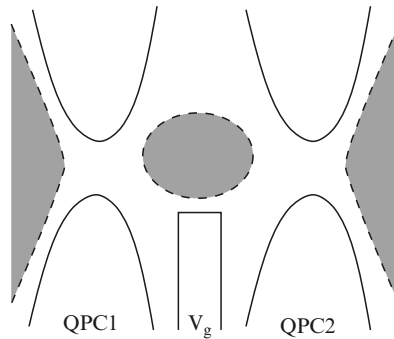


Fig. 12.2. Coulomb island, which consists of two tunable quantum point contacts QPC1 and QPC2, and a side gate which allows one to vary the chemical potential, and hence the charge density in the central region. The two-dimensional electron gas underlying the gate structure is depleted outside the hatched regions

number of device applications have been proposed, whose operating principles are based on this property. Below we shall discuss in some more detail the modeling of these structures. We note that the generic energy-level diagram shown in Fig. 12.1 also applies to the emerging field of molecular electronics: there the discrete level(s) in the central region correspond to molecular levels, the “barriers” could be the vacuum gap, and the “doped contacts” could be the metallic electrodes between which the molecule is placed. An introduction to this topic will also be given later.

In the case of parallel transport much attention has been devoted to quantum point contacts (QPC), see Fig. 12.2 for a typical experimental configuration, and other structures based on similar ideas. Here the key ingredient is metallic gates that are deposited on the heterostructure; by adjusting the gate potentials it is possible to deplete the underlying two-dimensional electron gas, and thus introduce spatial modulations of the two-dimensional charge density. Quantum point contacts are based on a split gate geometry: here,

at sufficiently high negative gate voltages, the effective connection between the two unmodulated electron gases (“source” and “drain”) is so narrow that perpendicular mode quantization becomes observable, and the measured conductance is an integer multiple of the quantum unit of conductance, e^2/h . In later sections, we describe simple models pertaining to structures like the one shown in Fig. 12.2.

The hallmark of mesoscopic phenomena is the phase coherence of the charge carriers, which is maintained over a significant part of the transport process. The interference effects resulting from this phase coherence are reflected in a number of experimentally measurable properties. We have already encountered weak localization in Chap. 9. Weak localization can be understood as an increased return probability (and hence increased resistance) due to *coherent* backscattering of charge carriers. Another example where phase coherence is central is the Aharonov–Bohm effect, where interference of two different transport paths in a ring geometry results in an oscillatory magnetoresistance. Yet another example is universal conductance fluctuations, where the conductance of a sample displays rapid changes on the scale of e^2/h (hence the “universality”) when an external control parameter is changed. The external parameter could be magnetic field, or thermal cycling, and the fluctuations reflect changes in the conducting channels either due to different impurity configurations (thermal cycling), or differences in the way the conduction channels are located in the sample (magnetic field). Extensive reviews of these phenomena can be found in [5, 210, 233]. Many of these phenomena can be observed in bulk samples; however, in what follows we shall concentrate on systems where the interesting physics takes place in a small region (either the tunneling region in an RTD, or the Coulomb island between the two QPC’s of Fig. 12.2).

It is natural to divide mesoscopic transport into stationary and time-dependent phenomena, and we shall take this route by first treating stationary transport and then later turn our attention to time-dependent phenomena. A central issue will be the treatment of interactions in the mesoscopic region, and, as we shall see, nonequilibrium Green function techniques are well suited for this purpose. First analyses of tunneling problems in nonequilibrium systems were performed already in the 1970s by Caroli and co-workers [73–75, 86]. In the beginning of 1990’s a number of authors studied the steady-state situation, including Refs. [6, 92, 95, 128, 154, 223, 240, 260, 262, 275, 339, 364, 365]. The modern reformulation of these ideas, due to Meir and Wingreen [260] has led to a veritable explosion in the number of papers addressing these issues (there are more than a thousand articles since 1992 which use the Keldysh approach to interacting mesoscopic transport). A full account of all of this work is obviously impossible, instead we will concentrate on a few central results. A key issue is that under certain conditions (to be discussed later) a Landauer-type conductance formula [228, 229] can be derived. The Landauer formula relates the conductance g of a mesoscopic sample [which is connected via “ideal” leads to two (or more) reservoirs] to its transmission properties, $g = (e^2/h)T$,

where T is the quantum mechanical transmission coefficient of the sample. Conductance formulae have played an important role in the analysis of many mesoscopic transport phenomena, and it is therefore of interest to investigate whether interactions and/or time-dependence can be treated in a similar fashion.

12.2 Nonequilibrium Techniques in Mesoscopic Tunneling Structures

Let us now examine how the techniques of Part II can be used to derive a perturbation scheme for mesoscopic systems far from equilibrium. We recall that the basic difference between construction of equilibrium and nonequilibrium perturbation schemes is that in nonequilibrium one cannot assume that the system returns to its ground state (or a thermodynamic equilibrium state at finite temperatures) as $t \rightarrow +\infty$. Irreversible effects break the symmetry between $t = -\infty$ and $t = +\infty$, and this symmetry was heavily exploited in the derivation of the equilibrium perturbation expansion. In nonequilibrium situations one can circumvent this problem by allowing the system to evolve from $-\infty$ to the moment of interest (for definiteness, let us call this instant t_0), and then continues the time evolvement from $t = t_0$ back to $t = -\infty$. The advantage of this procedure is that all expectation values are defined with respect to a well-defined state, i.e., the state in which the system was prepared in the remote past. The price is that one must treat the two time branches on an equal footing.

In the context of tunneling problems one can invoke the nonequilibrium formalism as follows. In the remote past the contacts (i.e., the left and right lead) and the central region are decoupled, and each region is in thermal equilibrium. The equilibrium distribution functions for the three regions are characterized by their respective chemical potentials; these do not have to coincide nor are the differences between the chemical potentials necessarily small. The couplings between the different regions are then established and treated as perturbations via the standard techniques of perturbation theory, albeit on the two-branch time contour. It is important to notice that the couplings do not have to be small, e.g., with respect level to spacings or $k_B T$, and typically must be treated to all orders.

While the above formulation is popular, and has worked in many situations exceedingly well, one should be aware of the fact that it is by no means unique. For example, Stefanucci and Almbladh [336] have presented a *partition-free* formulation: here the entire system (i.e., the leads and the central region) is in a spatially uniform thermodynamical equilibrium state before the nonequilibrium perturbation (e.g., the bias voltage) is switched on, and one then follows the temporal evolution of the system. In certain special cases it has been shown that the two approaches lead to the same asymptotic steady-state current, while the dynamic properties may well differ. The detailed relationship

of the two approaches is a topic of active current study. – A second point of concern is that dividing the system into an interacting central region and non-interacting leads is actually quite subtle: it is not necessarily obvious where the partition should take place, and in Sect. 12.10 we touch upon this issue.

12.3 Model Hamiltonian

We split the total Hamiltonian in three pieces: $H = H_c + H_T + H_{\text{cen}}$, where H_c describes the contacts, H_T is the tunneling coupling between contacts and the interacting region, and H_{cen} models the interacting central region, respectively. Below we discuss each of these terms.

Guided by the typical experimental geometry in which the leads rapidly broaden into metallic contacts, we view electrons in the leads as noninteracting except for an overall self-consistent potential. Thus, the contact Hamiltonian is

$$H_c = \sum_{k,\alpha \in L,R} \varepsilon_{k\alpha} \mathbf{c}_{k\alpha}^\dagger \mathbf{c}_{k\alpha} , \quad (12.1)$$

and the Green functions in the leads for the uncoupled system are:

$$\begin{aligned} g_{k\alpha}^<(t-t') &= i\langle \mathbf{c}_{k\alpha}^\dagger(t') \mathbf{c}_{k\alpha}(t) \rangle \\ &= i f(\varepsilon_{k\alpha}^0) \exp[-i\varepsilon_{k\alpha}(t-t')] , \end{aligned} \quad (12.2)$$

$$\begin{aligned} g_{k\alpha}^{r,a}(t-t') &= \mp i\theta(\pm t \mp t') \langle \{\mathbf{c}_{k\alpha}(t), \mathbf{c}_{k\alpha}^\dagger(t')\} \rangle \\ &= \mp i\theta(\pm t \mp t') \exp[-i\varepsilon_{k\alpha}(t-t')] . \end{aligned} \quad (12.3)$$

Here $f(\varepsilon_{k\alpha}) = [\exp[(\varepsilon_{k\alpha} - \mu_\alpha)/k_B T] + 1]^{-1}$ is the equilibrium distribution in a given lead.

The coupling constants between the leads and the central (interacting) region depend, in principle, on the actual charge densities (accumulation and depletion regions, charge build-up in the central region, etc.), and they should be determined via a self-consistent calculation. This program has been completed by combining the density functional theory (DFT) with the nonequilibrium Green function theory (see, e.g., [58]), and will be briefly addressed later. Here, however, we assume these parameters as known, and write

$$H_T = \sum_{k,\alpha \in L,R} \sum_n [V_{k\alpha,n} \mathbf{c}_{k\alpha}^\dagger \mathbf{d}_n + \text{h.c.}] . \quad (12.4)$$

Here, $\{\mathbf{d}_n^\dagger\}$ and $\{\mathbf{d}_n\}$ are the single-electron creation and annihilation operators for the complete and orthonormal set of the states $|n\rangle$ in the interacting region.

The form chosen for the central region Hamiltonian H_{cen} depends on geometry and on the physical behavior being investigated. We will discuss three

particular examples in detail. In the first, the central region is taken to consist of noninteracting levels,

$$H_{\text{cen}} = \sum_m \varepsilon_m \mathbf{d}_m^\dagger \mathbf{d}_m . \quad (12.5)$$

Here, \mathbf{d}_m^\dagger (\mathbf{d}_m) creates (destroys) an electron in state m . The choice (12.5) represents a simple model for resonant tunneling. Below we shall present general results for an arbitrary number of levels, and analyze the case of a single level, which is exactly solvable in detail.

The second example we will discuss is a situation where the states in the central region couple to phonons:

$$H_{\text{cen}}^{\text{el-ph}} = \varepsilon_0 \mathbf{d}^\dagger \mathbf{d} + \mathbf{d}^\dagger \mathbf{d} \sum_{\mathbf{q}} M_{\mathbf{q}} [\mathbf{a}_{\mathbf{q}}^\dagger + \mathbf{a}_{-\mathbf{q}}] . \quad (12.6)$$

Here, the first term represents a single electronic state, while the second term represents interaction of an electron in that level with phonons: $\mathbf{a}_{\mathbf{q}}^\dagger$ ($\mathbf{a}_{\mathbf{q}}$) creates (destroys) a phonon in mode \mathbf{q} , and $M_{\mathbf{q}}$ is the interaction matrix element. The full Hamiltonian of the system must also include the free-phonon contribution $H_{\text{ph}} = \sum_{\mathbf{q}} \hbar \omega_{\mathbf{q}} \mathbf{a}_{\mathbf{q}}^\dagger \mathbf{a}_{\mathbf{q}}$. This example, while not exactly solvable, is helpful to show how interactions influence the current.

The final example consists of an Anderson-type model [7] for electron-electron interactions in the central region:

$$H_{\text{cen}} = \sum_{\sigma} \varepsilon_0 \mathbf{d}_{\sigma}^\dagger \mathbf{d}_{\sigma} + U n_{\uparrow} n_{\downarrow} . \quad (12.7)$$

Here σ is a spin-label, n_{σ} is the occupation number operator of spin-state σ , and U describes the on-site Coulombic repulsion. This model has been the topic of intense study because of the very rich (and complicated) physics that it describes. For example, in the low temperature limit it exhibits Kondo behavior. In the high temperature limit the equation-of-motion technique allows a relatively simple analysis, which we will discuss in some detail.

12.4 General Expression for the Current

The current from the left contact through left barrier to the central region can be calculated from the time evolution of the occupation number operator of the left contact:

$$J_L = -e \langle \dot{N}_L \rangle = -\frac{ie}{\hbar} \langle [H, N_L] \rangle , \quad (12.8)$$

where $N_L = \sum_{k,\alpha \in L} \mathbf{c}_{k\alpha}^\dagger \mathbf{c}_{k\alpha}$ and $H = H_c + H_T + H_{\text{cen}}$. Since H_c and H_{cen} commute with N_L , one readily finds:

$$J_L = \frac{ie}{\hbar} \sum_{\substack{k,\alpha \in L \\ n}} [V_{k\alpha,n} \langle \mathbf{c}_{k\alpha}^\dagger \mathbf{d}_n \rangle - V_{k\alpha,n}^* \langle \mathbf{d}_n^\dagger \mathbf{c}_{k\alpha} \rangle]. \quad (12.9)$$

Now define two new Green functions (we set $\hbar = 1$, and reintroduce it in the final expression for the current):

$$\begin{aligned} G_{n,k\alpha}^<(t-t') &\equiv i\langle \mathbf{c}_{k\alpha}^\dagger(t') \mathbf{d}_n(t) \rangle, \\ G_{k\alpha,n}^<(t-t') &\equiv i\langle \mathbf{d}_n^\dagger(t') \mathbf{c}_{k\alpha}(t) \rangle. \end{aligned} \quad (12.10)$$

We see that the current is given by the time-diagonal components of the Green functions defined in (12.10). These functions have the property $G_{k\alpha,n}^<(t,t) = -[G_{n,k\alpha}^<(t,t)]^*$, and inserting the time-labels, the current can be expressed as

$$J_L = \frac{2e}{\hbar} \text{Re} \left[\sum_{\substack{k,\alpha \in L \\ n}} V_{k\alpha,n} G_{n,k\alpha}^<(t,t) \right]. \quad (12.11)$$

Next, one needs an expression for $G_{n,k\alpha}^<(t-t')$. For the present case, with noninteracting leads, a general relation for the contour-ordered Green function $G_{n,k\alpha}(\tau, \tau')$ can be derived rather easily with the equation-of-motion technique. Since the nonequilibrium theory is structurally equivalent to equilibrium theory, it is sufficient to consider the $T = 0$ equation-of-motion for the time-ordered Green function $G_{n,k\alpha}^t$:

$$-i\frac{\partial}{\partial t'} G_{n,k\alpha}^t(t-t') = \varepsilon_{k\alpha} G_{n,k\alpha}^t(t-t') + \sum_m G_{nm}^t(t-t') V_{k\alpha,m}^*, \quad (12.12)$$

where we defined the central region time-ordered Green function function $G_{nm}^t(t-t') = -i\langle T\{\mathbf{d}_n(t)\mathbf{d}_m^\dagger(t')\} \rangle$. Note that it is crucial that the leads be noninteracting; had we allowed interactions in the leads, the equation-of-motion technique would have generated higher order Green functions in (12.12), and we would not have a closed set of equations.

We can interpret the factor $(-i\partial_t' - \varepsilon_{k\alpha})$ multiplying $G_{n,k\alpha}^t(t-t')$ as the inverse of the contact Green function operator (working from right-hand side), and introduce a short-hand notation: $G_{n,k\alpha}^t g_{k\alpha}^{-1} = \sum_m G_{nm}^t V_{k\alpha,m}^*$. By operating with $g_{k\alpha}^t$ from right, we arrive at

$$G_{n,k\alpha}^t(t-t') = \sum_m \int dt_1 G_{nm}^t(t-t_1) V_{k\alpha,m}^* g_{k\alpha}^t(t_1-t'). \quad (12.13)$$

According to Part II, this equation has in nonequilibrium precisely the same form, except that the intermediate time integration runs on the complex contour:

$$G_{n,k\alpha}(\tau, \tau') = \sum_m \int d\tau_1 G_{nm}(\tau, \tau_1) V_{k\alpha,m}^* g_{k\alpha}(\tau_1, \tau'). \quad (12.14)$$

Here $G_{nm}(\tau, \tau_1)$ is the contour-ordered Green function for the central region.

An Alternative Derivation of (12.14)

The result (12.14) can be derived using the S -matrix expansion and interaction picture. The derivation is technically more complicated, but it gives a useful illustration of a general technique which can be applied systematically in more complex situations where the “by-hand” derivation given above becomes unwieldy. We write the contour-ordered Green function as

$$G_{n,k\alpha}(\tau, \tau') = -i\langle T_C S \tilde{d}_n(\tau) \tilde{c}_{k\alpha}^\dagger(\tau') \rangle, \quad (12.15)$$

where

$$S = \sum_{j=0}^{\infty} \frac{(-i)^j}{j!} \int_C d\tau_1 \cdots \int_C d\tau_j \langle T_C \tilde{H}_T(\tau_1) \cdots \tilde{H}_T(\tau_j) \rangle, \quad (12.16)$$

where $\tilde{H}(\tau)$ is the interaction representation of the tunneling Hamiltonian (12.4). The crux of the derivation is that in the interaction representation the coupling between the c - and d -operators is explicitly encoded in S : the Hamiltonian occurring in the thermal average contains no such coupling, and hence can be factorized in lead-averages and central region averages. Next one uses the fact that the leads are noninteracting, which allows one to use Wick’s Theorem for the c -operators. We manipulate the matrix element in the j th order term of the S -matrix expansion as follows:

$$\begin{aligned} & \langle T_C \tilde{d}_n(\tau) \tilde{c}_{k\alpha}^\dagger(\tau') [V_{k_1\alpha_1,m_1}^* \tilde{d}_{m_1}^\dagger(\tau_1) \tilde{c}_{k_1\alpha_1}(\tau_1) + \text{h.c.}] \\ & \quad \cdots \times [V_{k_j\alpha_j,m_j}^* \tilde{d}_{m_j}^\dagger(\tau_j) \tilde{c}_{k_j\alpha_j}(\tau_j) + \text{h.c.}] \rangle \\ &= \langle T_C \tilde{c}_{k_1\alpha_1}(\tau_1) \tilde{c}_{k\alpha}^\dagger(\tau') \rangle \\ & \quad \times V_{k_1\alpha_1,m_1}^* \langle T_C \tilde{d}_n(\tau) \tilde{d}_{m_1}^\dagger(\tau_1) [V_{k_2\alpha_2,m_2}^* \tilde{d}_{m_2}^\dagger(\tau_2) \tilde{c}_{k_2\alpha_2}(\tau_2) + \text{h.c.}] \times \cdots \\ & \quad + \langle T_C \tilde{c}_{k_2\alpha_2}(\tau_2) \tilde{c}_{k\alpha}^\dagger(\tau') \rangle \\ & \quad \times V_{k_2\alpha_2,m_2}^* \langle T_C \tilde{d}_n(\tau) \tilde{d}_{m_2}^\dagger(\tau_2) [V_{k_1\alpha_1,m_1}^* \tilde{d}_{m_1}^\dagger(\tau_1) \tilde{c}_{k_1\alpha_1}(\tau_1) + \text{h.c.}] \times \cdots \\ & \quad + \cdots (\text{remaining } j-2 \text{ terms}) \end{aligned} \quad (12.17)$$

That is, by Wick’s Theorem, we construct all the pairwise contractions of the c, c^\dagger pairs. Similar factorization cannot be applied to the d -operators, because their governing Hamiltonian may be nonquadratic. By relabelling dummy indices all the j terms in the above sum can be shown to be equal. The extra factor j can then be canceled against the factorial term $j!$ in (12.16), leaving just $(j-1)!$. This allows a reconstruction of the S -matrix, and identifying the lead Green function $g_{k\alpha}(\tau, \tau') = -i\langle T_C c_{k\alpha}(\tau) c_{k\alpha}^\dagger(\tau') \rangle$ [note that $\tilde{c}(\tau) = c(\tau)$] we have thus obtained

$$G_{n,k\alpha}(\tau, \tau') = \sum_m \int_C d\tau_1 G_{nm}(\tau, \tau_1) V_{k\alpha,m}^* g_{k\alpha}(\tau_1, \tau'), \quad (12.18)$$

in agreement with (12.14).

The analytic continuation rules of Table 4.1 can be applied to (12.14), and we find

$$\begin{aligned} G_{n,k\alpha}^<(t-t') &= \sum_m \int dt_1 V_{k\alpha,m}^*[G_{nm}^r(t-t_1)g_{k\alpha}^<(t_1-t')] \\ &\quad + G_{nm}^<(t-t_1)g_{k\alpha}^a(t_1-t') \end{aligned} \quad (12.19)$$

where the Green functions $g^{<,a}$ for the leads are defined in (12.2) and (12.3). The Fourier transform of (12.19) is

$$G_{n,k\alpha}^<(\varepsilon) = \sum_m V_{k\alpha,m}^*[G_{nm}^r(\varepsilon)g_{k\alpha}^<(\varepsilon) + G_{nm}^<(\varepsilon)g_{k\alpha}^a(\varepsilon)] \quad (12.20)$$

whereby the current (12.11) becomes

$$J_L = \frac{2e}{\hbar} \int \frac{d\varepsilon}{2\pi} \text{Re} \left\{ \sum_{\substack{k,\alpha \in L \\ n,m}} V_{k\alpha,n} V_{k\alpha,m}^* [G_{nm}^r(\varepsilon)g_{k\alpha}^<(\varepsilon) + G_{nm}^<(\varepsilon)g_{k\alpha}^a(\varepsilon)] \right\} \quad (12.21)$$

At this juncture, it is useful to convert the momentum summations to energy integration and define a level-width function:

$$[\Gamma^L(\varepsilon_k)]_{mn} = 2\pi \sum_{\alpha \in L} \varrho_\alpha(\varepsilon_k) V_{\alpha,n}(\varepsilon_k) V_{\alpha,m}^*(\varepsilon_k) \quad (12.22)$$

where $\varrho_\alpha(\varepsilon)$ is the density of states. There are two terms in the current expression (12.21). Consider, for example, the piece involving G_{mn}^r , which we evaluate as¹

$$\begin{aligned} &\frac{2e}{\hbar} \int \frac{d\varepsilon}{2\pi} \int d\varepsilon_k \Gamma^L(\varepsilon_k) \text{Re} [G^r(\varepsilon) i\delta(\varepsilon - \varepsilon_k) f_L(\varepsilon)] \\ &= \frac{2e}{\hbar} \int \frac{d\varepsilon}{2\pi} f_L(\varepsilon) \Gamma^L(\varepsilon) \text{Re} [iG^r(\varepsilon)] \\ &= -\frac{2e}{\hbar} \int \frac{d\varepsilon}{2\pi} f_L(\varepsilon) \Gamma^L(\varepsilon) \text{Im} [G^r(\varepsilon)] \\ &= \frac{ie}{\hbar} \int \frac{d\varepsilon}{2\pi} \Gamma^L(\varepsilon) f_L(\varepsilon) [G^r(\varepsilon) - G^a(\varepsilon)] \end{aligned} \quad (12.23)$$

Similar manipulations can be applied to the other term, and the current from left (right) contact to central region becomes

$$J_{L(R)} = \frac{ie}{\hbar} \int \frac{d\varepsilon}{2\pi} \text{Tr} \left(\boldsymbol{\Gamma}^{L(R)}(\varepsilon) \{ \mathbf{G}^<(\varepsilon) + f_{L(R)}(\varepsilon) [\mathbf{G}^r(\varepsilon) - \mathbf{G}^a(\varepsilon)] \} \right) \quad (12.24)$$

¹ In the calculation leading to (12.23) we treat $\Gamma_{mn}(\varepsilon)$ as real and suppressed the indices mn . The above result, however, carries over to the general case, and the reader is urged to check this.

Here, the boldface notation indicates that the level-width function $\mathbf{\Gamma}$ and the central-region Green functions $\mathbf{G}^{<,r}$ are matrices in the central-region indices m, n . In steady state, the current will be uniform, so that $J = J_L = -J_R$, and one can symmetrize the current: $J = (J_L + J_R)/2 = (J_L - J_R)/2$. Using (12.24) leads to the general expression for the dc-current [260]:

$$J = \frac{ie}{2\hbar} \int \frac{d\varepsilon}{2\pi} \text{Tr} \left\{ [\mathbf{\Gamma}^L(\varepsilon) - \mathbf{\Gamma}^R(\varepsilon)] \mathbf{G}^<(\varepsilon) \right. \\ \left. + [f_L(\varepsilon)\mathbf{\Gamma}^L(\varepsilon) - f_R(\varepsilon)\mathbf{\Gamma}^R(\varepsilon)] [\mathbf{G}^r(\varepsilon) - \mathbf{G}^a(\varepsilon)] \right\}. \quad (12.25)$$

Often the energy-dependence of the level-width function is not very important, and further simplification can be achieved by making assumptions on this energy-dependence. In particular, if the left and right line-width functions are proportional to each other, i.e., $\mathbf{\Gamma}^L(\varepsilon) = \lambda \mathbf{\Gamma}^R(\varepsilon)$, a very simple final result can be achieved. We observe that the current can be written as $J \equiv xJ_L - (1-x)J_R$, which gives, using (12.25):

$$J = \frac{ie}{\hbar} \int \frac{d\varepsilon}{2\pi} \text{Tr} (\mathbf{\Gamma}^R(\varepsilon) \{ [\lambda x - (1-x)] \mathbf{G}^<(\varepsilon) \\ + [\lambda x f_L - (1-x) f_R] [\mathbf{G}^r(\varepsilon) - \mathbf{G}^a(\varepsilon)] \}). \quad (12.26)$$

The arbitrary parameter x is now fixed so that the first term vanishes, i.e., $x = 1/(1+\lambda)$, which results in

$$J = \frac{ie}{\hbar} \int \frac{d\varepsilon}{2\pi} [f_L(\varepsilon) - f_R(\varepsilon)] \mathcal{T}(\varepsilon), \\ \mathcal{T}(\varepsilon) = \text{Tr} \left\{ \frac{\mathbf{\Gamma}^L(\varepsilon)\mathbf{\Gamma}^R(\varepsilon)}{\mathbf{\Gamma}^L(\varepsilon) + \mathbf{\Gamma}^R(\varepsilon)} [\mathbf{G}^r(\varepsilon) - \mathbf{G}^a(\varepsilon)] \right\}. \quad (12.27)$$

The ratio is well-defined because the $\mathbf{\Gamma}$ -matrices are proportional. The difference between the retarded and advanced Green functions is essentially the density of states. Despite the apparent similarity of (12.27) to the Landauer formula, it is important to bear in mind that, in general, there is no immediate connection between the quantity $\mathcal{T}(\varepsilon)$ and the transmission coefficient $T(\varepsilon)$. In particular, when inelastic scattering is present, there is no such connection. In later sections, where we analyze a noninteracting central region, a connection with the transmission coefficient *can* be established. Further, we shall see later how an analogous result can be derived for the average of the time-dependent current.

The results for the current derived in this section [(12.25) or (12.27)] form a starting point for many calculations. As such, they are powerful formal results, however, one must bear in mind that they involve both the full correlation function and the retarded Green functions *in the presence of tunneling*, and it is by no means obvious that these Green functions are easily calculable. The usefulness of (12.25), (12.27) depends on whether one is able to devise suitable calculation schemes for the Green functions. Below we shall see some examples of how this is done in practice.

12.5 Current Conservation

Any meaningful theory of transport must respect current conservation. Here we examine what implications this necessary requirement has on the derived expressions for the current flowing between the contacts and the central region. To this end, it is convenient to rewrite the current expressions (12.24), (12.25) in a slightly different form. Using the general relationship $\mathbf{G}^r - \mathbf{G}^a = \mathbf{G}^> - \mathbf{G}^<$, valid for both contact and central region Green functions, we re-express (12.21) as [113]

$$\begin{aligned} J_L &= \frac{e}{\hbar} \int \frac{d\varepsilon}{2\pi} \sum_{\substack{k,\alpha \in L \\ n,m}} V_{k\alpha,n} V_{k\alpha,m}^* [G_{nm}^>(\varepsilon) g_{k\alpha}^<(\varepsilon) - G_{nm}^<(\varepsilon) g_{k\alpha}^>(\varepsilon)] \\ &= \frac{e}{\hbar} \int \frac{d\varepsilon}{2\pi} \sum_{\substack{\alpha \in L \\ n,m}} [G_{nm}^>(\varepsilon) \Sigma_{\alpha,mn}^<(\varepsilon) - G_{nm}^<(\varepsilon) \Sigma_{\alpha,mn}^>(\varepsilon)] \\ &= \frac{e}{\hbar} \int \frac{d\varepsilon}{2\pi} \text{Tr} \{ \mathbf{G}^> \boldsymbol{\Sigma}_L^< - \mathbf{G}^< \boldsymbol{\Sigma}_L^> \}, \end{aligned} \quad (12.28)$$

where we have defined the tunneling self-energy $\boldsymbol{\Sigma} = \sum V^* g V$ with the components

$$\begin{aligned} \Sigma_{\alpha,mn}^{r,a}(\varepsilon) &= \sum_k V_{k\alpha,m}^* g_{k\alpha}^{r,a}(\varepsilon) V_{k\alpha,n} = \Lambda_{mn}^\alpha(\varepsilon) \mp \frac{i}{2} \Gamma_{mn}^\alpha(\varepsilon) \\ \Sigma_{\alpha,mn}^<(\varepsilon) &= \sum_k V_{k\alpha,m}^* g_{k\alpha}^<(\varepsilon) V_{k\alpha,n} = i \Gamma_{mn}^\alpha(\varepsilon) f_\alpha(\varepsilon) \\ \Sigma_{\alpha,mn}^>(\varepsilon) &= \sum_k V_{k\alpha,m}^* g_{k\alpha}^>(\varepsilon) V_{k\alpha,n} = -i \Gamma_{mn}^\alpha(\varepsilon) [1 - f_\alpha(\varepsilon)]. \end{aligned} \quad (12.29)$$

The current formula (12.28) has an obvious physical interpretation: the current flowing out of the left contact (first term) is proportional to $\boldsymbol{\Sigma}_L^<$, which gives the out-tunneling rate of the occupied states in the left contact, and to $\mathbf{G}^>$, which gives the number of available states in the central region. The second term, with opposite sign, gives then the current flowing from the central region to the left contact. We next define the total self-energy, which is the sum of tunneling contributions, and the interactions residing in the central region:

$$\boldsymbol{\Sigma}_{\text{tot}} = \boldsymbol{\Sigma}_{\text{int}} + \boldsymbol{\Sigma}_L + \boldsymbol{\Sigma}_R. \quad (12.30)$$

The condition for current conservation is $J_L + J_R = 0$, and we shall now show that this condition imposes a sum-rule for the interacting self-energy. To do this, we first note that the Keldysh equations for the lesser and greater Green functions, $\mathbf{G}^{<,>} = \mathbf{G}^r \boldsymbol{\Sigma}_{\text{tot}}^{<,>} \mathbf{G}^a$, can be combined to yield

$$(\mathbf{G}^r)^{-1} - (\mathbf{G}^a)^{-1} = \boldsymbol{\Sigma}_{\text{tot}}^< - \boldsymbol{\Sigma}_{\text{tot}}^>, \quad (12.31)$$

which allows us to do the following manipulation:

$$\begin{aligned}\text{Tr}\{\Sigma_{\text{tot}}^<\mathbf{G}^> - \Sigma_{\text{tot}}^>\mathbf{G}^<\}\ &= \text{Tr}\{\Sigma_{\text{tot}}^<\mathbf{G}^r\Sigma_{\text{tot}}^>\mathbf{G}^a - \Sigma_{\text{tot}}^>\mathbf{G}^r\Sigma_{\text{tot}}^<\mathbf{G}^a\} \\ &= \text{Tr}\{\Sigma_{\text{tot}}^<\mathbf{G}^r[\Sigma_{\text{tot}}^< - (\mathbf{G}^r)^{-1} + (\mathbf{G}^a)^{-1}]\mathbf{G}^a \\ &\quad - [\Sigma_{\text{tot}}^< - (\mathbf{G}^r)^{-1} + (\mathbf{G}^a)^{-1}]\mathbf{G}^r\Sigma_{\text{tot}}^<\mathbf{G}^a\} \\ &= 0,\end{aligned}\tag{12.32}$$

where we repeatedly used the cyclic property of Trace. The condition for current conservation thus becomes

$$\begin{aligned}J_L + J_R &= \frac{e}{\hbar} \int \frac{d\omega}{2\pi} \text{Tr}\{(\Sigma_{\text{tot}}^< - \Sigma_{\text{int}})\mathbf{G}^> - (\Sigma_{\text{tot}}^> - \Sigma_{\text{int}}^>)\mathbf{G}^<\} \\ &= 0\end{aligned}\tag{12.33}$$

which, using (12.32), implies a necessary condition that *any* model self-energy Σ_{int} must satisfy:

$$\int \frac{d\omega}{2\pi} \text{Tr}\{\Sigma_{\text{int}}^<\mathbf{G}^> - \Sigma_{\text{int}}^>\mathbf{G}^<\} = 0.\tag{12.34}$$

The self-consistent Born approximation (both for impurity scattering or electron–phonon interaction) is an example of a conserving approximation.

12.6 Noninteracting Resonant-Level Model

In the noninteracting case (or mean-field models), the Hamiltonian is $H = H_c + H_T + H_{\text{cen}}$, where $H_{\text{cen}} = \sum_n \varepsilon_n \mathbf{d}_n^\dagger \mathbf{d}_n$. The Dyson and the Keldysh equations are now

$$\begin{aligned}\mathbf{G}^r(\varepsilon) &= \mathbf{g}^r(\varepsilon) + \mathbf{g}^r(\varepsilon)\Sigma^r(\varepsilon)\mathbf{G}^r(\varepsilon) \\ \mathbf{G}^<(\varepsilon) &= \mathbf{G}^r(\varepsilon)\Sigma^<(\varepsilon)\mathbf{G}^a(\varepsilon),\end{aligned}\tag{12.35}$$

where the self-energy is given by (12.29), $\Sigma = \Sigma_L + \Sigma_R$. Upon substituting (12.35) in the expression for the tunneling current (12.28), one finds a very compact result:

$$J_L = \frac{e}{\hbar} \int \frac{d\varepsilon}{2\pi} T(\varepsilon) [f_L(\varepsilon) - f_R(\varepsilon)],\tag{12.36}$$

where the transmission probability $T(\varepsilon)$ is given by

$$T(\varepsilon) = \text{Tr}\{\boldsymbol{\Gamma}^L(\varepsilon)\mathbf{G}^r(\varepsilon)\boldsymbol{\Gamma}^R(\varepsilon)\mathbf{G}^a(\varepsilon)\}.\tag{12.37}$$

This equation has found many applications, but it should be recalled that it is valid only in the case when interactions can be modelled by one-body potentials, i.e., the interaction self-energies must be one-point functions with vanishing lesser and greater components.

In general, the solution of Eqs. (12.35) require matrix inversions. In the case of a single level, the scalar equations can be readily solved. Using the identity

$$G^r G^a = \frac{G^r - G^a}{G^{a-1} - G^{r-1}} = \frac{A(\varepsilon)}{\Gamma(\varepsilon)}, \quad (12.38)$$

where $A(\varepsilon) = i[G^r(\varepsilon) - G^a(\varepsilon)]$ is the spectral function, one can write $G^<$ in a “pseudoequilibrium” form:

$$G^<(\varepsilon) = iA(\varepsilon)\bar{f}(\varepsilon), \quad (12.39)$$

where

$$\begin{aligned} \bar{f}(\varepsilon) &= \frac{\Gamma^L(\varepsilon)f_L(\varepsilon) + \Gamma^R(\varepsilon)f_R(\varepsilon)}{\Gamma(\varepsilon)}, \\ A(\varepsilon) &= \frac{\Gamma(\varepsilon)}{[\varepsilon - \varepsilon_0 - A(\varepsilon)]^2 + [\Gamma(\varepsilon)/2]^2}. \end{aligned} \quad (12.40)$$

The current (12.28) becomes now

$$J = \frac{e}{\hbar} \int \frac{d\varepsilon}{2\pi} \frac{\Gamma^L(\varepsilon)\Gamma^R(\varepsilon)}{[\varepsilon - \varepsilon_0 - A(\varepsilon)]^2 + [\Gamma(\varepsilon)/2]^2} [f_L(\varepsilon) - f_R(\varepsilon)]. \quad (12.41)$$

Note that this derivation made no assumptions about proportionate coupling to the leads. The factor multiplying the difference of the Fermi functions is the familiar expression for elastic transmission coefficient $T(\varepsilon)$ through a resonant level. It is important to understand the difference between this result and the result obtained in Sect. 12.4 (despite the similarity of appearance): There, (12.27) gives the current for a fully interacting system, and the evaluation of the retarded and advanced Green functions requires a consideration of interactions (e.g., electron-electron, electron-phonon, and spin-flip) in addition to tunneling back and forth to the contacts. To further emphasize the difference, let us now suppose that the Green function for the interacting central region can be solved: $G^{r,a}(\varepsilon) = [\varepsilon - \varepsilon_0 - \lambda(\varepsilon) \pm i\gamma(\varepsilon)/2]^{-1}$, where λ and $\gamma/2$ are the real and imaginary parts of the self-energy (including interactions *and* tunneling). Then the interacting result for proportionate coupling (12.27) becomes

$$\begin{aligned} J &= \frac{e}{\hbar} \int \frac{d\varepsilon}{2\pi} [f_L(\varepsilon) - f_R(\varepsilon)] \frac{\Gamma^L(\varepsilon)\Gamma^R(\varepsilon)}{\Gamma^L(\varepsilon) + \Gamma^R(\varepsilon)} \\ &\times \frac{\gamma(\varepsilon)}{[\varepsilon - \varepsilon_0 - \lambda(\varepsilon)]^2 + [\gamma(\varepsilon)/2]^2}. \end{aligned} \quad (12.42)$$

This result coincides with the noninteracting current expression (12.41) if $\lambda(\varepsilon) \rightarrow A(\varepsilon)$ and $\gamma(\varepsilon) \rightarrow \Gamma(\varepsilon) = \Gamma^R(\varepsilon) + \Gamma^L(\varepsilon)$. In a phenomenological model, where the total level-width is expressed as a sum of elastic and inelastic widths, $\gamma = \gamma_e + \gamma_i$, one recovers the results of Jonson and Grincwajg [187],

and Weil and Vinter [369]. If the level-width and level-shift functions Γ and Λ are energy-independent, it is easy to evaluate the integral in (12.41), and get the current–voltage characteristic. However, the model still lacks two essential ingredients before the nonmonotonic IV-curve characteristic to RTD-devices can be obtained. The first missing item concerns the band-widths of the contacts: so far the band-width is essentially infinite. This failure can be remedied by considering a model where the contacts have a finite, occupied band-width; we introduce a low energy cutoff $D_{L/R}$, in addition to the upper cutoff provided by the electrochemical potential. Further, we must specify how the central-region energy ε_0 depends on the applied voltage $\mu_L - \mu_R = eV$. As we have remarked above, and as will be discussed in Sect. 12.7, in general this requires a self-consistent calculation. However, for present purposes it is sufficient to simply assume that the left chemical potential μ_L defines the zero-point for energy, and that the other two field-dependencies are given by $\mu_R(V) = \mu_R - eV$, and $\varepsilon_0(V) = \varepsilon_0 - eV/2$, respectively. The zero-temperature IV-characteristic is then (Fig. 12.3)

$$J_{dc}(V) = \frac{e}{\hbar} \frac{2\Gamma^L \Gamma^R}{\Gamma} \left[\tan^{-1} \frac{\mu_L - \varepsilon_0(V)}{\Gamma/2} - \tan^{-1} \frac{\mu_L - D_L - \varepsilon_0(V)}{\Gamma/2} \right. \\ \left. - \tan^{-1} \frac{\mu_R(V) - \varepsilon_0(V)}{\Gamma/2} + \tan^{-1} \frac{\mu_R(V) - D_R - \varepsilon_0(V)}{\Gamma/2} \right]. \quad (12.43)$$

We note that the strong increase in current, which is observed in experimental systems at very high voltages, is not present in our model: this is because we have ignored the bias-dependence of the barrier heights as well as any higher lying resonances. The present simple model, however, will be useful in later sections where we consider ac-response of a biased resonant tunneling diode.

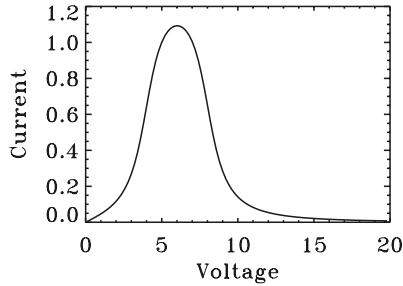


Fig. 12.3. IV-characteristic for a model resonant tunneling device. The system is defined by parameters $\varepsilon_0(V = 0) = 2$, $\mu_L = \mu_R(V = 0) = 0$, and $D_L = D_R = 2$. The energy parameters are in units of Γ , and the current is shown in units of $e\Gamma/\hbar$.

12.7 Density Functional Theory and Modeling of Molecular Electronics

In this section we give a brief introduction to the computational schemes that combine some ab initio electron structure theory and a nonequilibrium transport theory. In the rapidly growing literature one can find several implementations; here we use the code developed in [58] as an illustrative example. The present subsection assumes that the reader has some familiarity with the basic notions of the density functional theory (DFT) .

Most electronic structure calculations are restricted in the sense that the geometry must be finite, or periodic, and that the electronic system is in equilibrium. The present situation is very different: now a small subsystem lacking translational invariance couples to semi-infinite leads *and* the electronic subsystem can be far from equilibrium. Ideally one should describe the whole system (the central region and electrodes) on equal footing. As is well known, the density functional theory gives the exact electronic density and total energy, if the exact exchange-correlation functional was known. Since this is not the case, one must resort to approximate forms of the functional, such as the local-density approximation (LDA), or the generalized gradient approximation (GGA), or something else. There is no theory to say which (approximate) functional is the best, rather the choice is made based on painstaking tests, and comparisons in some limits where alternative methods, or experiments, can give benchmarks. In an attempt to extend DFT to nonequilibrium situations one must go one step further: the Kohn-Sham single-particle wave-functions $\psi_{\text{KS}}(x)$ are used when calculating the current. This implies a leap of faith: as is well-known, the ψ_{KS} are useful mathematical objects used in the construction for the ground-state density, but which have no immediate physical interpretation. Nonperturbative many-particle effects, such as the Kondo effect, are excluded from the treatment. On the other hand, inelastic effects can be included, as discussed in Sect. 12.10. A further development of the present approach could conceivably be reached by the current-density formalism [354], or time-dependent density-functional formalism [298].

At the core of the DFT-NEGF implementation described in [58] is the SIESTA code [302] for calculating the electronic properties for large numbers of atoms. This approach has been tested in a large number of applications with excellent results, and it has many technical advantages because of the employed finite range orbitals for the valence electrons: not only do the numerics get faster but also the system partitioning into leads and the central region becomes unambiguous. The SIESTA approach can be extended to nonequilibrium by using a nonequilibrium electron density as an input; as we recall the density readily follows from the lesser Green function,

$$n(x) = -iG^<(x = x', t = t') = \int \frac{d\epsilon}{2\pi i} G^<(x = x', \epsilon). \quad (12.44)$$

$G^<$ follows directly from the Keldysh equation, because the self-energy is a known function for mean-field theories, $\Sigma^< = i(\Gamma^L f_L + \Gamma^R f_R)$. Hence, all that one needs are the retarded and advanced Green functions, and these are obtained by evaluating

$$\mathbf{G}^{r,a}(E) = [E\mathbf{I} \pm i\eta - \mathbf{H}]^{-1}, \quad (12.45)$$

where

$$\mathbf{H} = \begin{pmatrix} \mathbf{H}_L + \boldsymbol{\Sigma}_L & \mathbf{V}_L & 0 \\ \mathbf{V}_L^\dagger & \mathbf{H}_C & \mathbf{V}_R \\ 0 & \mathbf{V}_R^\dagger & \mathbf{H}_R + \boldsymbol{\Sigma}_R \end{pmatrix} \quad (12.46)$$

with an obvious nomenclature. The semi-infinite left and right leads are accounted for by the self-energies $\boldsymbol{\Sigma}_{L/R}$, see, e.g., the book by Datta [93]. Importantly, to determine \mathbf{V}_R , \mathbf{V}_L , or \mathbf{H}_C one does not need to evaluate the density matrix outside the L - C - R region, if the L - C - R region is defined so large that all screening takes place inside it.

Summarizing, and somewhat simplifying, the iterative loop consists of the steps

$$\text{initial } n(x) \Rightarrow \text{SIESTA} \Rightarrow \psi_{\text{KS}}(x) \Rightarrow \text{NEGF} \Rightarrow \text{new } n(x) \quad (12.47)$$

and the iteration is repeated until convergence is achieved for the desired quantity, such as the current for a given voltage difference. For a detailed description of many of the technical details suppressed here we refer to the paper by Brandbyge [58]. The scheme outlined above has been applied by a large group of researchers to many specific physical systems. Occasionally the agreement with experiments reaches a quantitative level, which is indeed very satisfying, while sometimes the predicted current can be orders of magnitude too large. At present, there is no consensus of whether the discrepancies are due to poorly controlled experiments, bad implementations of the DFT-NEGF scheme, or due to an inadequacy of the entire concept. A possible cause for the discrepancy has very recently been identified by Toher et al. [351], who suggest that self-interaction corrections (which are not included in the GGA-LDA underlying most theoretical work) could remedy some of the problems. Nevertheless, a lot of research remains to be done.

12.8 Resonant Tunneling with Electron–Phonon Interactions

In addition to the main maximum in the IV-characteristic (see Fig. 12.3), resonant tunneling diodes occasionally show satellite peaks. A typical experiment is shown in Fig. 12.4. The secondary structure is due to interactions between the tunneling electrons and optical phonons.² The physical picture

² Some controversy remains whether one should consider optical phonons related to the barrier material, or whether phonons belonging to the quantum well are more appropriate. In our qualitative discussion these details are not relevant.

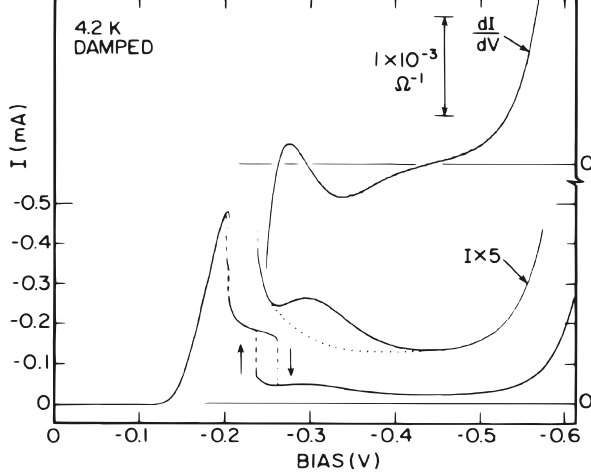


Fig. 12.4. Experimental IV-curve showing optical phonon-related additional structure [125]

is straightforward: an electron, which approaches the double-barrier structure with a nonresonant energy, can be tuned in the energy of the quasibound state in the quantum well by emitting (or absorbing) an optical phonon, and thus become resonant with an enhanced transmission probability, and increased current. The central-region Hamiltonian (12.6) is a mathematical formulation for this physical picture. For simplicity, we consider only energy-independent level-widths Γ_L and Γ_R , when the current (12.27) becomes

$$J = \frac{e}{\hbar} \frac{\Gamma^L \Gamma^R}{\Gamma^L + \Gamma^R} \int \frac{d\varepsilon}{2\pi} [f_L(\varepsilon) - f_R(\varepsilon)] \int_{-\infty}^{\infty} dt e^{i\varepsilon t} A(t), \quad (12.48)$$

where $A(t) = i[G^r(t) - G^a(t)]$ is the interacting spectral function. In general, an exact evaluation of $A(t)$ is not possible, however, if one *ignores the Fermi sea*, $G^r(t)$ [and hence $A(t)$] can be calculated exactly (pp. 285–324 in [254]; for recent work relaxing this approximation, see, e.g., [116]):

$$G^r(t) = -i\theta(t) \exp[-it(\varepsilon_0 - \Delta) - \Phi(t) - \Gamma t/2], \quad (12.49)$$

where

$$\begin{aligned} \Delta &= \sum_{\mathbf{q}} \frac{M_{\mathbf{q}}^2}{\omega_{\mathbf{q}}}, \\ \Phi(t) &= \sum_{\mathbf{q}} \frac{M_{\mathbf{q}}^2}{\omega_{\mathbf{q}}^2} [N_{\mathbf{q}}(1 - e^{i\omega_{\mathbf{q}}t}) + (N_{\mathbf{q}} + 1)(1 - e^{-i\omega_{\mathbf{q}}t})], \end{aligned} \quad (12.50)$$

and the electron–phonon interaction is given by (12.6). When substituted in the expression for current, one recovers the result of [370,371], which originally

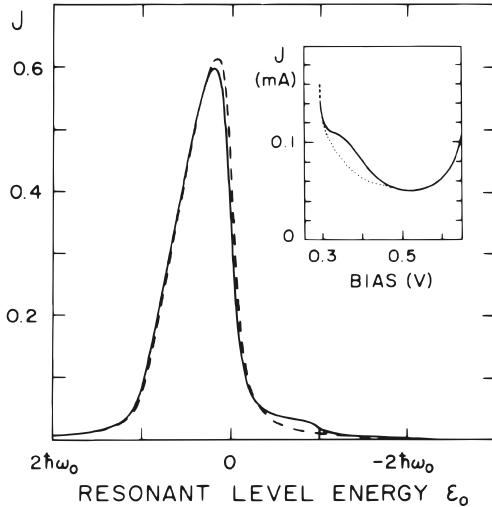


Fig. 12.5. Current as a function of the resonant-level energy (or, equivalently, voltage), as calculated in [372]. The dashed curve is for no electron–phonon coupling while the solid curve is for a coupling $g = 0.03$. The shoulder in the computed IV curve is quite similar to the one seen in experiments (*inset*), [125]

was derived by analyzing the much more complex two-particle Green function $G(\tau, s, t) = \theta(s)\theta(t)\langle d(\tau - s)d^\dagger(\tau)d(t)d^\dagger(0)\rangle$. The advantage of the method presented here is that one only needs the *single*-particle Green function to use the interacting current formula (12.27). Other systematic approaches to the single-particle Green function can therefore be directly applied to the current (e.g., perturbation theory in the tunneling Hamiltonian; [6, 163]; for further refinements needed in the description of vibrational effects in molecular electronics, see [59] or [268]). A numerical example is presented in Fig. 12.5. It is also interesting to note that the model considered in this section can be applied to other electron–boson interactions: the theoretical analysis in connection with plasmon-assisted resonant tunneling is essentially identical to the one presented above [379].

12.9 Transport in a Semiconductor Superlattice

In 1970 Esaki and Tsu [106] suggested that semiconductor superlattices, man-made structures which consist of alternating layers of different semiconductor materials, would have physical properties that could be used for a number of device applications. Very shortly, the periodic spatial variations in the band-gaps will lead to a spatially periodic conduction band edge, which in its turn gives rise to minibands, often modeled by a tight-binding expression

$$\epsilon(k) = \epsilon_0 - \Delta - 2t \cos(kd), \quad (12.51)$$

where ϵ_0 is the energy of a bound state in an isolated quantum-well, Δ is a shift due to overlap with the neighboring wells, t is the overlap integral which governs the width of the miniband, and d is the superlattice period. Minibands display very interesting transport properties, such as Bloch oscillations, or negative differential resistance. A well-known result, which can be easily derived by considering the Boltzmann equation in the relaxation-time approximation, and using the miniband dispersion (12.51) to compute the band velocity, is the Esaki–Tsu IV-characteristic,

$$I(V) = 2I_{\max}V_0 \frac{V}{V^2 + V_0^2}, \quad (12.52)$$

where I_{\max} and V_0 depend on the physical parameters of the system, such as the superlattice period, scattering rate, and temperature. To derive expressions like this, three main approaches have been used in the literature: (1) Miniband transport [106], (2) Wannier–Stark hopping [353], and (3) sequential tunneling [270]. The three different approaches have different domains of validity, and are all likely to fail if the three basic energy scales, i.e. scattering induced broadening, miniband width, and potential drop per period all have comparable values. The basic features of these three approaches are summarized in Fig. 12.6.

In order to map out the boundaries of the various domains of validity, and to access the region where the approaches (1)–(3) fail, a higher level theory is required. We shall next describe how nonequilibrium Green functions can be used for this task [360, 361].³ Here we can give only a qualitative discussion of the developed formalism; the reader is referred to recent review articles where a much fuller account can be found [52, 362].

One should note that the quantum theory has not yet been fully developed to the case when the electric field is inhomogeneous (domain formation), nor is it available for the time-dependent case (photo-assisted transport; progress is, however, being made see, *e.g.*, Appendix C in the review by Wacker [362]). For these important situations one has to apply one of the simpler approaches discussed above. As far as scattering is concerned, impurity scattering and phonon scattering have been discussed, but carrier–carrier interaction is still a future task.

As so many times before, the task is now to solve the coupled Keldysh and Dyson equations. We adopt the tight-binding representation of the single-particle Hamiltonian:

$$H_{n,m} = (\delta_{n,m-1} + \delta_{n,m+1})t + \delta_{n,m}(E_k - neEd), \quad (12.53)$$

³ There are other theoretical methods capable of including (some) quantum effects, such as the density-matrix method [64, 212], or the balance equation approach. [236]

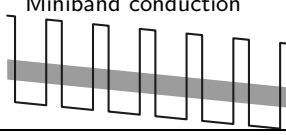
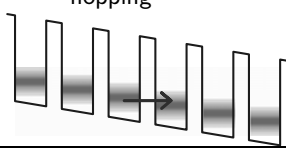
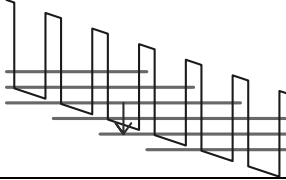
	coupling t	field drop eEd	scattering Γ
Miniband conduction 	exact miniband	acceleration	golden rule
Wannier Stark hopping 		exact: Wannier Stark states	golden rule
Sequential tunneling 	lowest order	energy match mis-	"exact" spectral function

Fig. 12.6. The three standard approaches to miniband transport, and the physical picture underlying them (Courtesy of A. Wacker)

where t is the nearest neighbor coupling, $E_k = \hbar^2 k^2 / (2m)$ the kinetic energy perpendicular to the growth direction, E the applied field, and d the superlattice period. In this basis the Keldysh and Dyson equations read [360]

$$G_{mn}^<(\omega) = \sum_{m_1} G_{mm_1}^r \left(\omega + eEd \frac{m_1 - n}{2} \right) \Sigma_{m_1}^< \left[\omega + eEd \left(m_1 - \frac{m+n}{2} \right) \right] \\ \times G_{m_1 n}^a \left(\omega + eEd \frac{m_1 - m}{2} \right) \quad (12.54)$$

$$G_{mn}^r(\omega) = g_m^r \left(\omega + eEd \frac{m - n}{2} \right) \left[\delta_{mn} + \sum_l \Sigma_{ml}^r \left(\omega + eEd \frac{l - n}{2} \right) \right. \\ \left. \times G_{ln}^r \left(\omega + eEd \frac{l - m}{2} \right) \right]. \quad (12.55)$$

Next one needs to specify the self-energies. Computations have been performed for impurity scattering, optical phonon scattering, and acoustic phonon scattering (by approximating acoustic phonons by very low-energy optical phonons), all in the self-consistent Born approximation [360, 361]. Note that the retarded self-energy is nondiagonal in the site indices, while the lesser self-energy is diagonal. This follows from the fact that we assume that the many-particle interactions (which determine $\Sigma^<$) are diagonal in the site index.

By numerically solving these coupled equations, computing the current, and comparing to the corresponding IV-curves found by the simpler approaches (1)–(3), one can construct a “phase-diagram” (see Fig. 12.7), which indicates where the simpler approaches hold, and where a quantum approach is necessary.

It is also of interest to compare the quantum mechanical drift–velocity vs. field relation to the results obtained with a semiclassical Monte Carlo simulation. This places a stringent bench-mark on the numerical calculations because the two methods are totally different, and both require computationally rather intensive calculations. Typical results are shown in Fig. 12.8. For the parameters considered here, the Monte Carlo simulation gives very good results, except that it misses the weak phonon replica seen in the quantum calculation.

The approach sketched here has been used in a number of practical device models. These include quantum cascade lasers [107], where the current injection occurs through a “funnel”: the superlattice is designed so that the miniband width varies with distance. Another recent calculation concerns the evaluation of gain in such structures [234].

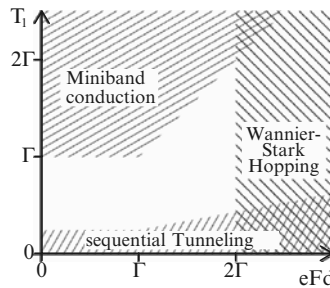


Fig. 12.7. The range of validity of various approaches to superlattice transport, in the parameter space spanned by the nearest-neighbor coupling T_1 , and the potential energy drop eFd per period, in units of the scattering width Γ

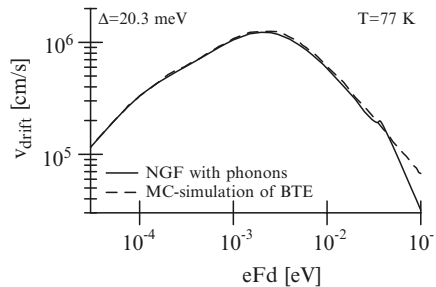


Fig. 12.8. Drift velocity vs. applied field

12.10 Transport in Atomic Gold Wires: Signature of Coupling to Vibrational Modes

The issue of vibrational effects in molecular electronics has recently drawn a lot of interest because inelastic scattering and energy dissipation inside atomic-scale conductors are of paramount importance for device characteristics, working conditions, and their stability [116, 216, 326, 367]. Inelastic effects are important, not only because of their potentially detrimental influence on device functioning, but also because they can open up new possibilities and operating modes. Vibrational effects are often visible in the measured conductances of nanoscopic objects; here we focus on recent experimental studies on free standing atomic gold wires [3]. Agraït and co-workers used a cryogenic STM tip to first create an atomic-scale gold wire (lengths up to seven gold atoms have been achieved), and then measured its conductance as a function of the displacement of tip, and the applied voltage. The data showed clear drops of conductance at a certain voltage, and the interpretation was that an excitation of an inelastic mode was taking place, leading to enhanced back-scattering, and hence drop in the conductance. It should be pointed out that opening a new vibrational mode in the atomic scale conductor does not necessarily lead to a decrease in conductance (one can envisage various assisted processes), and a proper theory should be able to predict conductance enhancement as well, whenever the physics dictates so.

Here we will briefly describe how the DFT-based computational techniques can be generalized to include inelastic effects in the kind of wires studied by Agraït et al. [3]. We will also address the issue of phonon heating, which turns out to play a crucial role. Further details can be found in [115].

The calculational method consists of three steps. (a) The mechanical normal modes and frequencies of the gold chain are evaluated. (b) The electronic structure and electron-vibration coupling elements are evaluated in a localized atomic-orbital basis set. (c) The inelastic transport is evaluated using nonequilibrium Green functions, with a self-consistent Born approximation self-energy in the Dyson and Keldysh equations for the respective Green functions. The electrical current and the power transfer are then evaluated with⁴

$$I_L = \frac{e}{h} \int d\epsilon t_L(\epsilon) \quad (12.56)$$

$$P_L = \int \frac{d\epsilon}{2\pi\hbar} \epsilon t_L(\epsilon), \quad (12.57)$$

$$t_L(\epsilon) = \text{Tr} \left\{ \Sigma_L^<(\epsilon) \mathbf{G}^>(\epsilon) - \Sigma_L^>(\epsilon) \mathbf{G}^<(\epsilon) \right\}, \quad (12.58)$$

⁴ The derivation of the expression for the power transfer is parallel to the one given for the electric current in Sect. 12.4; instead of considering the time-derivative of the lead occupation, one computes the time-derivative of the lead Hamiltonian. [113]

where the Hartree and Fock parts of self-energy components are

$$\Sigma^{H,r} = i \sum_{\lambda} \frac{2}{\Omega_{\lambda}} \int \frac{d\epsilon'}{2\pi} \mathbf{M}^{\lambda} \text{Tr}[\mathbf{G}^{<}(\epsilon') \mathbf{M}^{\lambda}], \quad (12.59)$$

$$\Sigma^{H,<} = 0, \quad (12.60)$$

$$\begin{aligned} \Sigma^{F,r}(\epsilon) &= i \sum_{\lambda} \int \frac{d\epsilon'}{2\pi} \mathbf{M}^{\lambda} [D_0^r(\epsilon - \epsilon') \mathbf{G}^{<}(\epsilon') \\ &\quad + D_0^r(\epsilon - \epsilon') \mathbf{G}^r(\epsilon') + D_0^{<}(\epsilon - \epsilon') \mathbf{G}^r(\epsilon')] \mathbf{M}^{\lambda} \end{aligned} \quad (12.61)$$

$$\Sigma^{F,<}(\epsilon) = i \sum_{\lambda} \int \frac{d\epsilon'}{2\pi} \mathbf{M}^{\lambda} D_0^{<}(\omega - \omega') \mathbf{G}^{<}(\epsilon') \mathbf{M}^{\lambda}. \quad (12.62)$$

Here the vibrational modes are labeled by λ , and Ω_{λ} is the corresponding eigenfrequency. It is worth noting that the lack of translational invariance makes the retarded Hartree term nonzero, and potentially important. Also, at this stage the phonon propagators are undamped – an approximation that merits further investigation. The coupled equations are iterated until convergence is achieved, and in the following we give some representative results. Let us consider a linear four-atom gold wire under two different states of strain, as shown in Fig. 12.9. We calculate the phonon signal in the nonlinear differential conductance vs. bias voltage for two extremal cases: the energy transferred

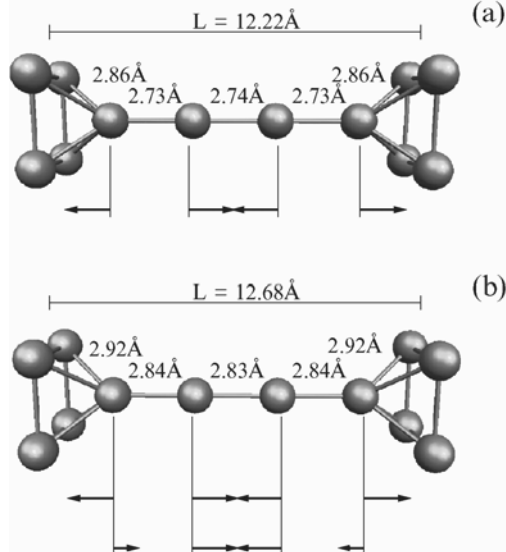


Fig. 12.9. Geometry of a four-atom gold wire under two different states of stress. The dominating alternating bond-length modes, which cause the inelastic scattering, are shown schematically with arrows. For the shorter wire only one mode is active, while the elongated wire has two active modes. (Reproduced from [114])

from the electrons to the vibrations is either (1) instantaneously absorbed into an external heat bath, or (2) accumulated and only allowed to leak via electron–hole pair excitations. These limits are referred to as the externally damped and externally undamped cases, respectively. Figures 12.10 and 12.11

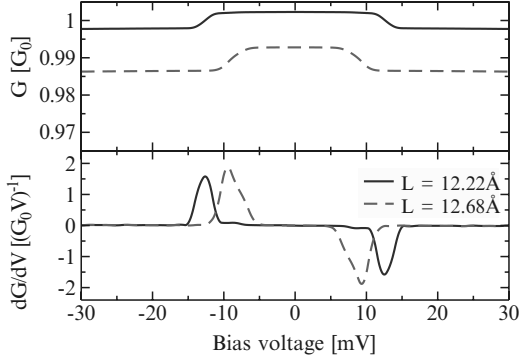


Fig. 12.10. Differential conductance and its derivative for the four-atom gold wire at two different tensions in the case where the oscillators are externally damped. Reproduced from [114]

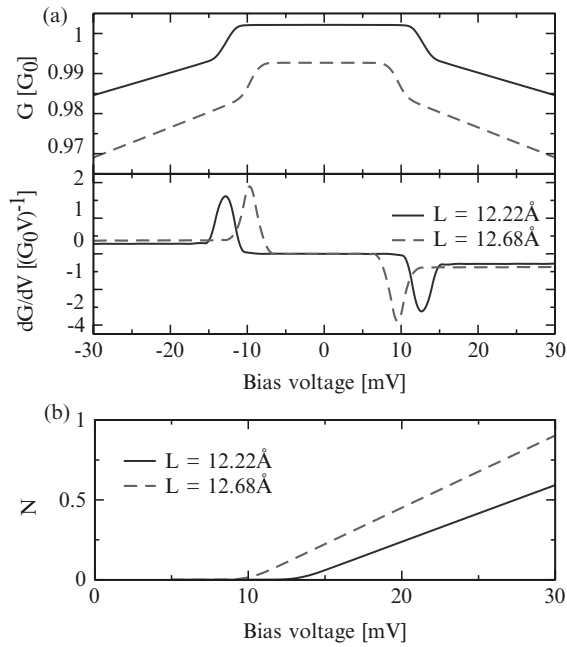


Fig. 12.11. (a) Differential conductance and its derivative for the four-atom gold wire at two different tensions in the externally undamped limit. Only the most important mode is included in this calculation. (b) Mode occupation vs. bias voltage. Reproduced from [114]

show the corresponding results. Since a typical experiment is done at low temperatures, the mode occupation in the externally damped case vanishes, $N_\lambda \approx 0$. In the externally undamped case the mode occupation N_λ is an unknown parameter entering the electron–phonon self-energy, and additional physical input is necessary to determine this parameter. We argue as follows. Since the system is in a steady state, the net power transferred from the electrons to the device must vanish, i.e., $P_L + P_R = 0$. Using (12.57) one then obtains the required constraint on N_λ . This procedure works in a straightforward way if there is only a single active mode, but if several modes are present, a more detailed theory of how the phonon modes equilibrate would be needed. The bottom panel of Fig. 12.11 shows how the occupation of the leading phonon mode, or, equivalently, the effective temperature, changes as a function of bias. When comparing to the experiments of Agraït et al. [3], one sees that the externally undamped model is in near quantitative agreement with the data: the conductance drop at the onset of inelastic scattering, and the slope after the drop are very well reproduced. We view this as strong evidence of the presence of heating in the experiment, but at the same time recognize the need for a detailed microscopic theory including phonon–phonon interactions.

12.11 Transport Through a Coulomb Island

As a final example, we analyze transport through a Coulomb island, i.e., the Hamiltonian is given by (12.7), and a typical experimental geometry is sketched in Fig. 12.2. We note first that *without* coupling to the contacts the Green function of the central region can be solved exactly. This is quite analogous to the electron–phonon case studied in Sect. 12.8. The analysis proceeds with the equation-of-motion technique. Thus, one obtains (we assume again that there is only one level in the central region, i.e., $G_{mn} \rightarrow G_{11} \rightarrow G$, and the equilibrium counterpart of G is denoted by $g^{\sigma\sigma}(t - t') = -i\langle T\{d_\sigma(t)d_\sigma^\dagger(t')\}\rangle$):

$$\begin{aligned} i\frac{\partial}{\partial t}g^{\sigma\sigma}(t - t') &= \delta(t - t') + \varepsilon_\sigma g^{\sigma\sigma}(t - t') + U g^{(2)}(t - t') , \\ (\omega - \varepsilon_\sigma)g^{\sigma\sigma}(\omega) &= 1 + U g^{(2)}(\omega) , \end{aligned} \quad (12.63)$$

where we used $i\dot{d}_\sigma = \varepsilon_\sigma d_\sigma + U d_\sigma n_{\bar{\sigma}}$, and defined $\bar{\sigma} = -\sigma$. The second term in the equation of motion for d_σ , which is due to the on-site interactions, generated the higher order Green function $g^{(2)}$:

$$g^{(2)}(t - t') \equiv -i\langle T\{d_\sigma(t)n_{\bar{\sigma}}(t)d_\sigma^\dagger(t')\}\rangle . \quad (12.64)$$

The next step is to consider the equation-of-motion for $g^{(2)}$. Since $[n_{\bar{\sigma}}, H] = 0$, one only has to consider the time-derivative of d_σ in (12.64). The result is

$$\begin{aligned} i\frac{\partial}{\partial t}g^{(2)}(t - t') &= \delta(t - t')\langle n_{\bar{\sigma}} \rangle + \varepsilon_\sigma g^{(2)}(t - t') + U g^{(2)}(t - t') , \\ (\omega - \varepsilon_\sigma - U)g^{(2)}(\omega) &= \langle n_{\bar{\sigma}} \rangle . \end{aligned} \quad (12.65)$$

Equation (12.65) can now be substituted in (12.63), and we have thus found an expression for $g^{\sigma\sigma}$ in terms of $\langle n_{\bar{\sigma}} \rangle$:

$$\begin{aligned} g^{\sigma\sigma}(\omega) &= \frac{\omega - \varepsilon_\sigma - (1 - \langle n_{\bar{\sigma}} \rangle)U}{(\omega - \varepsilon_\sigma - U)(\omega - \varepsilon_\sigma)} \\ &= \frac{\langle n_{\bar{\sigma}} \rangle}{\omega - \varepsilon_\sigma - U} + \frac{1 - \langle n_{\bar{\sigma}} \rangle}{\omega - \varepsilon_\sigma}, \end{aligned} \quad (12.66)$$

where the second line shows that the Green function has two resonances, at $\omega = \varepsilon_\sigma + U$ and $\omega = \varepsilon_\sigma$, with weights $\langle n_{\bar{\sigma}} \rangle$ and $(1 - \langle n_{\bar{\sigma}} \rangle)$, respectively.

Equation (12.66) can be used to determine $\langle n_{\bar{\sigma}} \rangle$ [and hence $g^{\sigma\sigma}(\omega)$] self-consistently. In equilibrium we can use the fluctuation-dissipation theorem:

$$\langle n_{\bar{\sigma}} \rangle = \int \frac{d\omega}{2\pi i} g^{\sigma\sigma,<}(\omega) = \int \frac{d\omega}{2\pi} [-2\text{Im}g^{\sigma\sigma,r}(\omega)] n_F(\omega), \quad (12.67)$$

where the retarded function is obtained from (12.66) with the replacement $\omega \rightarrow \omega + i\eta$, where η is an infinitesimal. This is as much as we can get from the equilibrium analysis, and next, the coupling to the leads must be considered.⁵ In a phenomenological approach one can model the coupling to the leads by replacing the infinitesimal η by a finite self-energy [129]: $G^{-1} = g^{-1} - \Sigma$. A suitable model for the self-energy could be the *noninteracting* tunneling self-energy (12.29):

$$\Sigma_0(\omega) = \sum_{k\alpha} |V_{k\alpha}|^2 g_{k\alpha}(\omega), \quad (12.68)$$

and the retarded Green function becomes

$$\begin{aligned} G^{\sigma\sigma,r}(\omega) &= \frac{g^{\sigma\sigma}(\omega)}{1 - g^{\sigma\sigma}(\omega)\Sigma^r(\omega)} \\ &= \frac{\omega - \varepsilon_\sigma - (1 - \langle n_{\bar{\sigma}} \rangle)U}{(\omega - \varepsilon_\sigma - U)(\omega - \varepsilon_\sigma) - \Sigma_0^r(\omega)[\omega - \varepsilon_\sigma - (1 - \langle n_{\bar{\sigma}} \rangle)U]} \\ &\simeq \frac{1 - \langle n_{\bar{\sigma}} \rangle}{\omega - \varepsilon_\sigma - \Sigma_0^r} + \frac{\langle n_{\bar{\sigma}} \rangle}{\omega - \varepsilon_\sigma - U - \Sigma_0^r}, \end{aligned} \quad (12.69)$$

where the final line shows how the tunneling broadens the isolated site-levels ε_σ . Since the self-energy is given explicitly, we can use the Keldysh equation (which is now an explicit relation, and not an integral equation for $G^{<}$), and immediately write down the correlation function:

$$G^{\sigma\sigma,<}(\omega) = G^{\sigma\sigma,r}(\omega)\Sigma_0^{<}(\omega)G^{\sigma\sigma,a}(\omega), \quad (12.70)$$

where

$$\Sigma_0^{<}(\omega) = \sum_{k\alpha} |V_{k\alpha}|^2 g_{k\alpha}^{<}(\omega) \quad (12.71)$$

⁵ Recall that the current formula requires the central-region Green function in the presence of the contacts.

and the noninteracting contact Green functions are given by (12.2). These equations have precisely the same structure as was found in Sect. 12.6, where we treated the noninteracting resonant-level model. In particular, the correlation function $G^<$ again has the “pseudoequilibrium form” (12.39). The only difference is that (12.70) needs to be integrated over energy to find the self-consistent solution for $\langle n_{\bar{\sigma}} \rangle$. Once this is done, the current again follows from (12.27).

Unfortunately, this appealingly simple approach actually misses a lot of interesting physics: Kondo-like correlations, which are caused by multiple transitions from contacts to the central site require a much more careful treatment [154, 155, 261, 262]. The analysis gets quite complicated because the most natural approach, which is to do perturbation theory in the coupling to the leads, is not applicable. The reason is that the unperturbed Hamiltonian is nonquadratic in the field operators, and hence does not possess Wick’s theorem, and consequently, no standard perturbation expansion. Special techniques have been developed to tackle this situation (for example, the slave-boson technique due to [81, 82]), but a detailed exposition of these methods would be beyond our present purposes. However, at temperatures much higher than the Kondo temperature one can develop a perturbation scheme [222], and we shall next illustrate how the calculation proceeds.

When we consider coupling to the leads, we must also take into account the terms generated by the tunneling Hamiltonian (12.4):

$$H_T = \sum_{k\alpha\sigma} [V_{k\alpha} c_{k\alpha\sigma}^\dagger d_\sigma + \text{h.c.}] , \quad (12.72)$$

where we now must also include the spin index (but we assume that the coupling matrix element is independent of spin). This innocent looking extra term changes the physics entirely, and we must proceed with caution. In addition to the operator d_σ , we also need the time-evolution for a number of other operators, and we list them here for later use:

$$\dot{id}_\sigma = \varepsilon_\sigma d_\sigma + U d_\sigma n_{\bar{\sigma}} + \sum_{q\beta} V_{q\beta}^* c_{q\beta\sigma} , \quad (12.73a)$$

$$\dot{id}_{\bar{\sigma}}^\dagger = -\varepsilon_{\bar{\sigma}} d_{\bar{\sigma}}^\dagger - U n_\sigma d_{\bar{\sigma}}^\dagger - \sum_{q\beta} V_{q\beta} c_{q\beta,\bar{\sigma}}^\dagger , \quad (12.73b)$$

$$\dot{ic}_{k\alpha\sigma} = \varepsilon_{k\alpha} c_{k\alpha\sigma} + V_{k\alpha} d_\sigma , \quad (12.73c)$$

$$\dot{ic}_{k\alpha,\bar{\sigma}}^\dagger = -\varepsilon_{k\alpha} c_{k\alpha,\bar{\sigma}}^\dagger - V_{k\alpha}^* d_{\bar{\sigma}}^\dagger , \quad (12.73d)$$

$$\dot{in}_{\bar{\sigma}} = \sum_{q\beta} [-V_{q\beta} c_{q\beta,\bar{\sigma}}^\dagger d_{\bar{\sigma}} + V_{q\beta}^* d_{\bar{\sigma}}^\dagger c_{q\beta,\bar{\sigma}}] . \quad (12.73e)$$

Using (12.73a) we find that $G^{\sigma\sigma}$ satisfies (we also carry out the Fourier transform)

$$(\omega - \varepsilon_\sigma)G^{\sigma\sigma}(\omega) = 1 + UG^{(2)}(\omega) + \sum_{q\beta} V_{q\beta}^* \Gamma_{q\beta}^{\sigma\sigma}(\omega), \quad (12.74)$$

where $\Gamma_{q\beta}^{\sigma\sigma}(\omega)$ is the Fourier transform of

$$\Gamma_{q\beta}^{\sigma\sigma}(t - t') = -i\langle T\{c_{q\beta\sigma}(t)d_\sigma^\dagger(t')\}\rangle, \quad (12.75)$$

and $G^{(2)}(\omega)$ is the nonequilibrium generalization of (12.64). The equation-of-motion for $\Gamma_{q\beta}^{\sigma\sigma}$ is readily written down with the aid of (12.73c)

$$(\omega - \varepsilon_{q\beta})\Gamma_{q\beta}^{\sigma\sigma} = V_{q\beta}G^{\sigma\sigma}(\omega), \quad (12.76)$$

and (12.74) becomes

$$[\omega - \varepsilon_\sigma - \Sigma_0(\omega)]G^{\sigma\sigma}(\omega) = 1 + UG^{(2)}(\omega). \quad (12.77)$$

The equation-of-motion for $G^{(2)}$ can be constructed using (12.73a) – (12.73e), and we write it as

$$\begin{aligned} & (\omega - \varepsilon_\sigma - U)G^{(2)}(\omega) \\ &= \langle n_{\bar{\sigma}} \rangle + \sum_{q\beta} [V_{q\beta}^* \Gamma_{1,q\beta}^{(2)}(\omega) + V_{q\beta} \Gamma_{2,q\beta}^{(2)}(\omega) - V_{q\beta}^* \Gamma_{3,q\beta}^{(2)}(\omega)], \end{aligned} \quad (12.78)$$

where the new correlation functions are defined as

$$\begin{aligned} \Gamma_{1,q\beta}^{(2)}(t - t') &= -i\langle T\{c_{q\beta\sigma}(t)n_{\bar{\sigma}}(t)d_\sigma^\dagger(t')\}\rangle, \\ \Gamma_{2,q\beta}^{(2)}(t - t') &= -i\langle T\{c_{q\beta,\bar{\sigma}}^\dagger(t)d_\sigma(t)d_{\bar{\sigma}}(t)d_\sigma^\dagger(t')\}\rangle, \\ \Gamma_{3,q\beta}^{(2)}(t - t') &= -i\langle T\{c_{q\beta,\bar{\sigma}}(t)d_{\bar{\sigma}}^\dagger(t)d_\sigma(t)d_\sigma^\dagger(t')\}\rangle. \end{aligned} \quad (12.79)$$

These expressions allow us to quantify the phenomenological approach leading to (12.69). Specifically, let us make the Hartree–Fock approximation, i.e.,

$$\Gamma_{1,q\beta}^{(2)}(\omega) \simeq \langle n_{\bar{\sigma}} \rangle \Gamma_{q\beta}^{\sigma\sigma}(\omega), \quad (12.80)$$

and set $\Gamma_2 = \Gamma_3 = 0$. Substituting these approximations in (12.77) we then find:

$$(\omega - \varepsilon_\sigma - U)G^{(2)}(\omega) = \langle n_{\bar{\sigma}} \rangle [1 + \Sigma_0(\omega)G^{\sigma\sigma}(\omega)]. \quad (12.81)$$

Equations (12.77) and (12.81) can now be solved to yield

$$G^{\sigma\sigma}(\omega) = \frac{\omega - \varepsilon_\sigma - U(1 - \langle n_{\bar{\sigma}} \rangle)}{(\omega - \varepsilon_\sigma)(\omega - \varepsilon_\sigma - U) - \Sigma_0(\omega)[\omega - \varepsilon_\sigma - U(1 - \langle n_{\bar{\sigma}} \rangle)]} \quad (12.82)$$

which is identical to the earlier result (12.69). We have thus shown that “adding-by-hand” of the noninteracting self-energy corresponds to making a Hartree–Fock approximation to the higher order correlation function [222].

The intricate spin-structure of (12.79) serves as a hint of the complicated spin-flip correlations generated by the tunneling term. The analysis proceeds by considering the equations-of-motion for the Γ_i 's. By repeated application of the relations (12.73a)–(12.73e) one finds

$$\begin{aligned}
& (\omega - \varepsilon_{q\beta}) \Gamma_{1,q\beta}^{(2)}(\omega) \\
&= V_{q\beta} G^{(2)}(\omega) + \sum_{k\alpha} [-V_{k\alpha} \Gamma_{1,k\alpha q\beta}^{(3)}(\omega) + V_{k\alpha}^* \Gamma_{2,k\alpha q\beta}^{(3)}(\omega)] , \\
& (\omega + \varepsilon_{q\beta} - \varepsilon_\sigma - \varepsilon_{\bar{\sigma}} - U) \Gamma_{2,q\beta}^{(2)}(\omega) \\
&= V_{q\beta}^* G^{(2)}(\omega) + \sum_{k\alpha} V_{k\alpha}^* [\Gamma_{3,k\alpha q\beta}^{(3)}(\omega) + \Gamma_{4,k\alpha q\beta}^{(3)}(\omega)] , \\
& (\omega - \varepsilon_{q\beta} + \varepsilon_{\bar{\sigma}} - \varepsilon_\sigma) \Gamma_{3,q\beta}^{(2)}(\omega) \\
&= V_{q\beta} [G^{\sigma\sigma}(\omega) - G^{(2)}(\omega)] + \sum_{k\alpha} [-V_{q\beta} \Gamma_{5,k\alpha q\beta}^{(3)}(\omega) \\
&\quad + V_{q\beta}^* \Gamma_{6,k\alpha q\beta}^{(3)}(\omega)] , \tag{12.83}
\end{aligned}$$

where the third-order correlation functions $\Gamma_i^{(3)}$ are defined by

$$\begin{aligned}
\Gamma_{1,q\beta k\alpha}^{(3)}(t-t') &= -i\langle T\{c_{q\beta\sigma}(t)c_{k\alpha\bar{\sigma}}^\dagger(t)d_{\bar{\sigma}}(t)d_\sigma^\dagger(t')\}\rangle \\
\Gamma_{2,q\beta k\alpha}^{(3)}(t-t') &= -i\langle T\{c_{q\beta\sigma}(t)d_\sigma^\dagger(t)c_{k\alpha\bar{\sigma}}(t)d_\sigma^\dagger(t')\}\rangle \\
\Gamma_{3,q\beta k\alpha}^{(3)}(t-t') &= -i\langle T\{c_{q\beta\bar{\sigma}}^\dagger(t)c_{k\alpha\sigma}(t)d_{\bar{\sigma}}(t)d_\sigma^\dagger(t')\}\rangle \\
\Gamma_{4,q\beta k\alpha}^{(3)}(t-t') &= -i\langle T\{c_{q\beta\bar{\sigma}}^\dagger(t)d_\sigma(t)c_{k\alpha\bar{\sigma}}(t)d_\sigma^\dagger(t')\}\rangle \\
\Gamma_{5,q\beta k\alpha}^{(3)}(t-t') &= -i\langle T\{c_{q\beta\bar{\sigma}}(t)c_{k\alpha\bar{\sigma}}^\dagger(t)d_\sigma(t)d_\sigma^\dagger(t')\}\rangle \\
\Gamma_{6,q\beta k\alpha}^{(3)}(t-t') &= -i\langle T\{c_{q\beta\bar{\sigma}}(t)d_{\bar{\sigma}}^\dagger(t)c_{k\alpha\sigma}(t)d_\sigma^\dagger(t')\}\rangle . \tag{12.84}
\end{aligned}$$

One can proceed by considering the equations-of-motion of these functions, but it is clear that the analysis gets quite complicated. Instead, we resort to physical approximations. We shall assume that higher-order spin-correlations in the leads can be neglected. In practice this means that in (12.84) we set correlation functions that involve *unlike* lead spin-indices equal to zero (i.e., we approximate $\Gamma_1^{(3)} = \Gamma_2^{(3)} = \Gamma_3^{(3)} = \Gamma_6^{(3)} = 0$), and factorize the correlation functions with like spin:

$$\begin{aligned}
\Gamma_{4,q\beta k\alpha}^{(3)}(\omega) &\approx -\delta_{k\alpha,q\beta} f(\varepsilon_{k\alpha}) G^{\sigma\sigma}(\omega) , \\
\Gamma_{5,q\beta k\alpha}^{(3)}(\omega) &\approx \delta_{k\alpha,q\beta} [1 - f(\varepsilon_{k\alpha})] G^{\sigma\sigma}(\omega) , \tag{12.85}
\end{aligned}$$

where $f(\varepsilon_{k\alpha})$ is the equilibrium occupation of lead α . These approximations imply that we restrict the analysis to the high-temperature regime, $T \gg T_K$ [here $T_K \simeq \sqrt{U\Gamma} \exp(-\pi|\mu - \varepsilon_\sigma|/\Gamma)$ is the Kondo temperature

with $\Gamma \propto \text{Im}\Sigma_0$. If $T < T_K$, the correlation functions of the type $\langle c_{k\sigma}^\dagger c_{q\sigma} \rangle$ develop logarithmic singularities, and the above approximation scheme breaks down [222].

With (12.85) the second-order correlation functions $\Gamma_i^{(2)}$, $i = 1, 2, 3$, become

$$\begin{aligned}\Gamma_{1,q\beta}^{(2)}(\omega) &= \frac{V_{q\beta}}{\omega - \varepsilon_{q\beta}}, \\ \Gamma_{2,q\beta}^{(2)}(\omega) &= \frac{V_{q\beta}^*}{\omega + \varepsilon_{q\beta} - \varepsilon_{\bar{\sigma}} - \varepsilon_{\bar{\sigma}} - U} [G^{(2)}(\omega) - f(\varepsilon_{q\beta})G^{\sigma\sigma}(\omega)], \\ \Gamma_{3,q\beta}^{(2)}(\omega) &= \frac{-V_{q\beta}}{\omega - \varepsilon_{q\beta} + \varepsilon_{\bar{\sigma}} - \varepsilon_{\sigma}} [G^{(2)}(\omega) - f(\varepsilon_{q\beta})G^{\sigma\sigma}(\omega)].\end{aligned}\quad (12.86)$$

The self-consistent equations for $G^{\sigma\sigma}$ and $G^{(2)}$ are now

$$\begin{aligned}\Sigma_1(\omega)G^{\sigma\sigma}(\omega) + [\omega - \varepsilon_\sigma - U - \Sigma_0(\omega) - \Sigma_3(\omega)]G^{(2)}(\omega) &= \langle n_{\bar{\sigma}} \rangle, \\ [\omega - \varepsilon_\sigma - \Sigma_0(\omega)]G^{(\sigma\sigma)}(\omega) &= 1 + UG^{(2)}(\omega),\end{aligned}\quad (12.87)$$

where Σ_0 is given by (12.42), and we defined, following [259], two new self-energies $\Sigma_{1,3}$:

$$\Sigma_i(\omega) = \sum_{q\beta} A_{k\alpha}^{(i)} |V_{k\alpha}|^2 \left[\frac{1}{\omega + \varepsilon_{q\beta} - \varepsilon_{\bar{\sigma}} - \varepsilon_{\sigma} - U} + \frac{1}{\omega - \varepsilon_{q\beta} + \varepsilon_{\bar{\sigma}} - \varepsilon_{\sigma}} \right], \quad (12.88)$$

where $A_{k\alpha}^{(1)} = f(\varepsilon_{k\alpha})$ and $A_{k\alpha}^{(3)} = 1$, respectively. Finally, the solution for $G^{\sigma\sigma}$ is:

$$\begin{aligned}G^{\sigma\sigma}(\omega) &= \frac{\omega - \varepsilon_\sigma - U(1 - \langle n_{\bar{\sigma}} \rangle) - \Sigma_0(\omega) - \Sigma_3(\omega)}{[\omega - \varepsilon_\sigma - \Sigma_0(\omega)][\omega - \varepsilon_\sigma - U - \Sigma_0(\omega) - \Sigma_3(\omega)] + U\Sigma_1(\omega)} \\ &= \frac{1 - \langle n_{\bar{\sigma}} \rangle}{\omega - \varepsilon_\sigma - \Sigma_0(\omega) + U\Sigma_1(\omega)[\omega - \varepsilon_\sigma - U - \Sigma_0(\omega) - \Sigma_3(\omega)]^{-1}} \\ &\quad + \frac{\langle n_{\bar{\sigma}} \rangle}{\omega - \varepsilon_\sigma - U - \Sigma_0(\omega) - U\Sigma_2(\omega)[\omega - \varepsilon_\sigma - \Sigma_0(\omega) - \Sigma_3(\omega)]^{-1}}\end{aligned}\quad (12.89)$$

where Σ_2 is defined with (12.88), but with $A_{k\alpha}^{(2)} = 1 - f(\varepsilon_{k\alpha})$. It is interesting to compare (12.89) to the Green function obtained for the isolated site, given by (12.66). Again, there are two resonances, located in the vicinity of $\omega = \varepsilon_\sigma$ and $\omega = \varepsilon_\sigma + U$, respectively, with corresponding weights $(1 - \langle n_{\bar{\sigma}} \rangle)$ and $\langle n_{\bar{\sigma}} \rangle$. However, the tunneling processes back and forth to the contacts have modified the widths and caused shifts; these are determined by the self-energies Σ_i , $i = 1, 2, 3$. (12.89) also shows that the modification of the isolated site resonances is much more complicated than caused by the noninteracting tunneling self-energy Σ_0 alone.

The retarded Green function can be extracted from (12.89) by setting $\omega \rightarrow \omega + i0^+$. If one is interested in zero-bias conductance, which is an equilibrium quantity, it is permissible to use the fluctuation dissipation theorem, $G^< = \inf_F(-2\text{Im}G^r)$, to obtain a closed equation for the occupation $\langle n_\sigma \rangle$, and hence determine the retarded Green function. Then, finally, the current can be computed with (12.27). At finite bias, however, the situation is more complicated, and one should consider the analytic continuation of (12.77), (12.78). We are not aware of any works where this has been carried out in detail, and hence leave it as an exercise, which may lead to publishable results!

In order to model experiments, such as those of [263], one should generalize (12.89) to include several levels in the central region. This has been done in [259], and we conclude this section by a brief introduction to this work. The different levels may have different couplings to the leads, and it is reasonable to assume that the higher the energy of a given level is, the more strongly it couples to the leads. The experimentally measured conductance shows periodic peaks as a function of gate voltage V_g (see Figs. 12.2, 12.13) which moves the energy levels of the central region with respect to the lead energy levels, or, equivalently, moves the chemical potential of the leads. The periodicity of the conductance oscillations is explained quite readily with the charging energy U of the central region; however, more interesting is the experimental observation that the individual conductance peaks show a complicated temperature dependence. Another important observation is that the conductance peaks remain resolved in temperatures much higher than the bare-energy-level spacing $\Delta\varepsilon$, which is of the order of 0.05 meV in the samples studied in [263]. This clearly shows that interaction effects are important (because in the non-interacting case all resonance features would be washed out if $k_B T > \Delta\varepsilon$); one may estimate that the charging energy U is of the order of 0.5 meV. Thus, in the temperature range $\Delta\varepsilon < k_B T < U$ an anomalous temperature dependence can be expected.

Figure 12.12 [259] shows the conductance, in units of e^2/\hbar , for a two-level system, as a function of the chemical potential. The energy difference between the single-particle levels is $\Delta\varepsilon = \varepsilon_\downarrow - \varepsilon_\uparrow = 0.1U$, and the respective tunneling couplings are $\Gamma_\downarrow = 10\Gamma_\uparrow = 0.01U$. The following features of Fig. 12.12 are noteworthy: (a) Only two peaks in the conductance are seen, even though the interacting density-of-states, following from (12.89), in principle contains four resonances. The suppression of peaks is caused by the dependence of the density-of-states of a given level on the occupancy of the other level, e.g., the weight of the resonance at $\omega = \varepsilon_\sigma$ is given by $(1 - \langle n_\sigma \rangle)$. Thus, when the chemical potential passes the lower energy level ε_\uparrow , the occupancy of this level approaches unity, and (12.89) implies that all the weight of the down-spin level is moved to $\omega = \varepsilon_\downarrow + U$. (b) The temperature dependence of the two conductance resonances is quite different. While the resonance at higher chemical potential shows typical noninteracting behavior (height $\propto 1/T$, width $\propto T$), the lower resonance actually shows a nonmonotonic temperature dependence. This is caused by the contribution originating from

the upper level ε_\downarrow , which becomes significant at temperatures approaching the bare-level splitting.

Figure 12.13 compares experimentally measured and theoretical curves. The simulations are performed for ten nondegenerate levels. As in the example of Fig. 12.12, the coupling to leads increases with increasing single-particle energy; however, one of the couplings is further increased to simulate impurity effects. Again, the complicated temperature dependence is due to several contributing levels. It can be concluded that the phenomenology of the experiment is reproduced very well with the theoretical model.

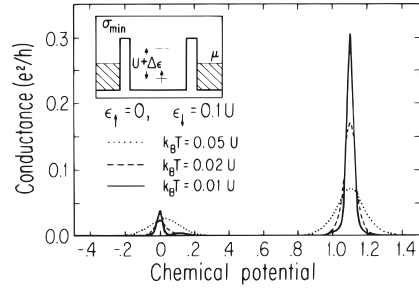


Fig. 12.12. Conductance vs. chemical potential (in units of U), for three temperatures, following from (12.89) and (12.27). Inset: Schematic band-edge diagram corresponding to the conductance valley at $\mu \simeq (U + \varepsilon_\downarrow)/2$

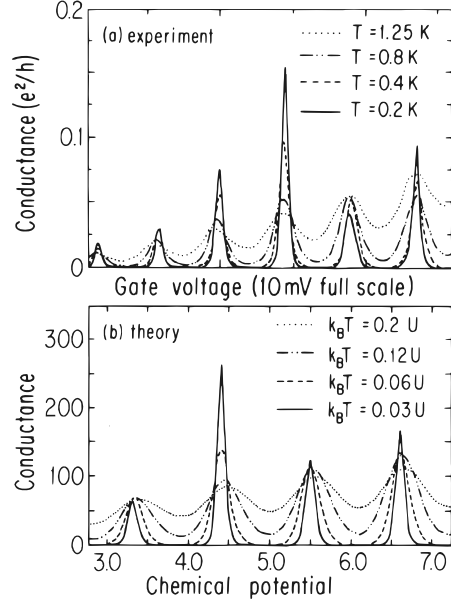


Fig. 12.13. (a) Experimental conductance [263] of a device of the type shown in Fig. 12.2, as a function of gate voltage. (b) Theoretical conductance [259], as a function of chemical potential

13

Time-Dependent Phenomena

Summary. The theory of time-dependent transport phenomena in mesoscopic structures is formulated. Results are presented for a periodically modulated and a fluctuating resonant level model. A theory of noise is also developed.

13.1 Introduction

We have learnt from previous chapters that the phase of the wavefunction of charge carriers lies at the heart of many mesoscopic phenomena. In stationary transport this phase can be affected by, e.g., magnetic fields or temperature. In this chapter we focus on an alternative way of affecting the phase coherence: external *time-dependent* perturbations. The interplay of external time dependence and phase coherence can be phenomenologically understood as follows. If the single-particle energies acquire a time dependence, then the wavefunctions have an extra phase factor, $\psi \sim \exp[-i \int^t dt' \varepsilon(t')]$. For a uniform system such an overall phase factor is of no consequence. However, if the external time dependence is different in different parts of the system and if the particles can move between these regions (without being “dephased” by inelastic collisions), the phase difference becomes important.

The interest in time-dependent mesoscopic phenomena stems from recent progress in several experimental techniques (descriptions of recent experimental advances can be found in [202], or [184]). Time dependence is a central ingredient in many different experiments, of which we mention the following:

1. *Single-electron pumps and turnstiles.* Here, time-modified gate signals move electrons one by one through a quantum dot, leading to a current which is proportional to the frequency of the external signal. These structures have considerable importance as current standards. The Coulombic repulsion of the carriers in the central region is crucial to the operational principle of these devices, and underlines the fact that extra care must be paid to interactions when considering time-dependent transport in mesoscopic systems.

2. *AC response and transients in resonant-tunneling devices.* Resonant tunneling devices (RTD) have a number of applications as high-frequency amplifiers or detectors. For the device engineer, a natural approach would be to model these circuit elements with resistors, capacitors, and inductors. The question then arises as to what, if any, are the appropriate “quantum” capacitances and inductances one should ascribe to these devices. Answering this question requires the use of time-dependent quantum-transport theory.

The literature on time-dependent nonequilibrium transport treated with Green functions is much more restricted than in the stationary case. We are aware of an early paper in surface physics [48], but only in the beginning of the 90s groups working in mesoscopic physics began to address these issues, for example in [62, 78, 156, 162, 166, 167, 182, 232, 247, 274, 281, 299, 300, 333, 373]. The field is presently experiencing rapid growth, and good reviews have recently become available [208, 283].

Below we shall derive an expression for the time-dependent current flowing from noninteracting leads to the central (interacting) region. This result will bear a close analogue to the stationary result analyzed in the previous section. The time dependence enters through the self-consistent parameters defining the model. We will show that under certain restrictions, to be specified below, a Landauer-like formula can be obtained for the *time-averaged* current. We will also present a number of explicit results, both analytical and numerical, for several model systems.

13.2 Applicability to Experiments

A central question one must address is: Under which conditions are the nonequilibrium techniques transferable to time-dependent situations, such as the experiments mentioned above?

The time-dependent problem has to be formulated carefully, particularly with respect to the leads. It is essential to a Landauer-type of approach that the electrons in the leads be noninteracting. In practice, however, the electrons in the leads near the mesoscopic region contribute to the self-consistent potential. We approach this problem by dividing the transport physics into two steps [68, 230]: (1) the self-consistent determination of charge pileup and depletion in the contacts, the resulting barrier heights, and single-particle energies in the interacting region and (2) transport in a system defined by these self-consistent parameters. Step (1) requires a capacitance calculation for each specific geometry (pioneering work in this area can be found in [65, 68, 69]) and we do not address it in the present context. Instead, we assume the results of (1) as time-dependent input parameters and give a full treatment of the transport through the mesoscopic region (2). In practice, the interactions in the leads are absorbed into a time-dependent potential and from then on the electrons in the leads are treated as noninteracting. This means that when relating

our results to actual experiments some care must be exercised. Specifically, we calculate only the current flowing into the mesoscopic region, while the total time-dependent current measured in the contacts includes contributions from charge flowing in and out of accumulation and depletion regions in the leads. In the *time-averaged* (DC) current, however, these capacitive contributions vanish and the corresponding time-averaged theoretical formulae are directly relevant to experiment. It should be noted, though, that these capacitive currents may influence the effective time-dependent parameters in step (1).

Let us next estimate the frequency limits that restrict the validity of our approach. Two criteria must be satisfied. First, the driving frequency must be sufficiently slow so that the applied bias is dropped entirely across the tunneling structure. When a bias is applied to a sample, the electric field in the leads can only be screened if the driving frequency is smaller than the plasma frequency, which is tens of THz in typical doped semiconductor samples. For signals slower than this, the bias is established entirely across the tunneling structure by accumulation and depletion of charge near the barriers. The unscreened Coulomb interaction between net excess charge is quite strong, and hence the bias across a tunneling structure is caused by a relatively small excess of charge in accumulation and depletion layers. The formation of these layers then causes a rigid shift of the bottom of the conduction band deeper in the leads, which is the origin of the rigid shift of energy levels in our treatment of a time-dependent bias.

The second frequency limit on our approach is that the buildup of electrons required for the formation of the accumulation and depletion layers must not significantly disrupt the coherent transport of electrons incident from the leads. One way to quantify this is to ask: What is the probability that an electron incident from the leads participates in the buildup of charge associated with a time-dependent bias? This probability will be the ratio of the net current density flowing into the accumulation region to the total incident flux of electrons. For a three-dimensional double-barrier resonant tunneling structure, the AC-current charging the accumulation layer is $I_{\text{acc}}^{\text{rms}} = 2\pi\nu CV^{\text{rms}}/A$, where ν is the driving frequency, C is the capacitance, V^{rms} is the applied bias, and A is the area. In comparison, the total incident flux is $I_{\text{inc}} = 3/8 e n v_F$. Using the parameters appropriate for a typical experiment (we use that of [61]), we find that up to 10 THz the probability of an electron participating in the charge buildup is only 1%. Summarizing, these estimates indicate that our approach should be accurate up to frequencies of tens of THz, which are large by present experimental standards, and consequently, the analysis presented in what follows should be valid for most experimental situations.

13.3 Mathematical Formulation

We now reexamine the formulation of the stationary situation to see what difference is caused by the external time dependence. Before the couplings

between the various regions are turned on, the single-particle energies acquire rigid time-dependent shifts, which – in the case of the noninteracting contacts – translate into extra phase factors for the propagators (but not in changes in occupations). The perturbation theory with respect to the couplings has the same diagrammatic structure as in the stationary case. The calculations, of course, become more complicated because of the broken time translational invariance. Physically, applying a time-dependent bias (electrostatic potential difference) between the source and drain contacts means that the single-particle energies become time dependent: $\varepsilon_{k\alpha}^0 \rightarrow \varepsilon_{k\alpha}(t) = \varepsilon_{k\alpha}^0 + \Delta_\alpha(t)$. The occupation of each state $k\alpha$, however, remains unchanged. The occupation, for each contact, is determined by an equilibrium distribution function established in the distant past, before the time dependence or tunneling matrix elements are turned on.

The contact Green functions are now given by:

$$\begin{aligned} g_{k\alpha}^<(t, t') &\equiv i\langle \mathbf{c}_{k\alpha}^\dagger(t') \mathbf{c}_{k\alpha}(t) \rangle \\ &= if(\varepsilon_{k\alpha}^0) \exp \left[-i \int_{t'}^t dt_1 \varepsilon_{k\alpha}(t_1) \right], \end{aligned} \quad (13.1)$$

$$\begin{aligned} g_{k\alpha}^{r,a}(t, t') &\equiv \mp i\theta(\pm t \mp t') \langle \{\mathbf{c}_{k\alpha}(t), \mathbf{c}_{k\alpha}^\dagger(t')\} \rangle \\ &= \mp i\theta(\pm t \mp t') \exp \left[-i \int_{t'}^t dt_1 \varepsilon_{k\alpha}(t_1) \right]. \end{aligned} \quad (13.2)$$

In order to derive an expression for the time-dependent current through the left barrier, we can follow essentially unchanged the analysis given in Sect. 12.4. The expression for current given in (12.11) is still valid, and the Green function $G_{n,k\alpha}^<$ is given by an expression like (12.19), with the exception that all functions now depend on the two time labels separately, and not only on their difference, $(t - t') \rightarrow (t, t')$. Thus there is no advantage in Fourier transforms, and we must stay in the time domain. Instead of (12.21) we now get

$$\begin{aligned} J_L &= -\frac{2e}{\hbar} \text{Im} \left\{ \sum_{\substack{k,\alpha \in L \\ n,m}} V_{k\alpha,n} \int_{-\infty}^t dt_1 e^{i \int_{t_1}^t dt_2 \varepsilon_{k\alpha}(t_2)} V_{k\alpha,m}^*(t_1) \right. \\ &\quad \times \left. [G_{nm}^r(t, t_1) f_L(\varepsilon_{k\alpha}) + G_{nm}^<(t, t_1)] \right\}. \end{aligned} \quad (13.3)$$

The expression for the level-width function must be generalized and we find

$$\begin{aligned} [\Gamma^L(\varepsilon, t_1, t)]_{mn} &= 2\pi \sum_{\alpha \in L} \varrho_\alpha(\varepsilon) V_{\alpha,n}(\varepsilon, t) V_{\alpha,m}^*(\varepsilon, t_1) \\ &\quad \times \exp \left[i \int_{t_1}^t dt_2 \Delta_\alpha(\varepsilon, t_2) \right]. \end{aligned} \quad (13.4)$$

In terms of this generalized level-width function (13.4), the general expression for the current is

$$J_L(t) = -\frac{2e}{\hbar} \int_{-\infty}^t dt_1 \int \frac{d\varepsilon}{2\pi} \text{ImTr} \left\{ e^{-i\varepsilon(t_1-t)} \boldsymbol{\Gamma}^L(\varepsilon, t_1, t) \right. \\ \times \left. [\mathbf{G}^<(t, t_1) + f_L(\varepsilon) \mathbf{G}^r(t, t_1)] \right\}. \quad (13.5)$$

An analogous formula applies for $J_R(t)$, the current flowing into the central region through the right barrier. One should note, that due to the time dependence, the left and right currents do not have to be equal.

Result (13.5) is the central formal result of this section, and in what follows we evaluate in several different special cases. Before turning to the applications a few remarks of a more general nature are in order. Just as in the stationary case, the time-dependent current is expressed in terms of local quantities: Green functions of the central region. The first term in (13.5), which is proportional to the lesser function $G^<$, suggests an interpretation as the out-tunneling rate (recalling $\text{Im } G^<(t, t) = N(t)$). Likewise, the second term, which is proportional to the occupation in the leads and to the density of states in the central region, can be associated to the in-tunneling rate. However, one should bear in mind that all Green functions in (13.5) are to be calculated in the presence of tunneling. Thus, $G^<$ may depend on the occupation in the leads. Furthermore, in the presence of interactions, G^r may depend on the central-region occupation. Consequently, the current can be a nonlinear function of the occupation factors [224]. Finally, it is a useful exercise to verify that the time-dependent current (13.5) reduces to the stationary result (12.24), if the time dependence is turned off, $\Delta_\alpha \rightarrow 0$.

13.4 Average Current

In analogy with the stationary case, where we found a compact expression for the current for the case of proportionate coupling, the time-dependent case allows further simplification, if assumptions are made on the line-width functions. In this case, we assume a generalized proportionality condition:

$$\boldsymbol{\Gamma}^L(\varepsilon, t_1, t) = \lambda \boldsymbol{\Gamma}^R(\varepsilon, t_1, t). \quad (13.6)$$

One should note that, in general, this condition can be satisfied only if $\Delta_\alpha^L(t) = \Delta_\alpha^R(t) = \Delta(t)$. However, in the wide-band limit (WBL), to be considered in detail below, the time variations of the energies in the leads do not have to be equal.

We next consider the occupation of the central region $N(t) = \sum_m \langle \mathbf{d}_m^\dagger(t) \mathbf{d}_m(t) \rangle$ and apply the continuity equation:

$$e \frac{dN(t)}{dt} = J_R(t) + J_L(t), \quad (13.7)$$

which allows one to write for arbitrary x :

$$J_L(t) = xJ_L(t) + (1-x) \left[e \frac{dN(t)}{dt} - J_R(t) \right]. \quad (13.8)$$

Choosing $x \equiv 1/(1+\lambda)$ leads to

$$\begin{aligned} J_L(t) = & \left(\frac{\lambda}{1+\lambda} \right) \left[e \frac{dN}{dt} - \frac{2e}{\hbar} \text{ImTr} \left\{ \int_{-\infty}^t dt_1 \int \frac{d\varepsilon}{2\pi} \right. \right. \\ & \times e^{-i\varepsilon(t_1-t)} \boldsymbol{\Gamma}^R(\varepsilon, t_1, t) \mathbf{G}^r(t, t_1) [f_L(\varepsilon) - f_R(\varepsilon)] \left. \right\} \right]. \end{aligned} \quad (13.9)$$

The time average of a time-dependent object $F(t)$ is defined by

$$\langle F(t) \rangle = \lim_{T \rightarrow \infty} \frac{1}{T} \int_{-T/2}^{T/2} dt F(t). \quad (13.10)$$

If $F(t)$ is a periodic function of time, it is sufficient to average over the period. Upon time averaging, the first term in (13.9) vanishes, $\langle dN/dt \rangle \rightarrow 0$, because the occupation $N(t)$ is finite for all T . The expression for the time-averaged current further simplifies if one can factorize the energy and time dependence of the tunneling coupling, $V_{k\alpha,n}(t) \equiv u(t)V_{\alpha,n}(\varepsilon_k)$. We then obtain

$$\begin{aligned} \langle J_L(t) \rangle = & -\frac{2e}{\hbar} \int \frac{d\varepsilon}{2\pi} [f_L(\varepsilon) - f_R(\varepsilon)] \\ & \times \text{ImTr} \left\{ \frac{\boldsymbol{\Gamma}^L(\varepsilon)\boldsymbol{\Gamma}^R(\varepsilon)}{\boldsymbol{\Gamma}^L(\varepsilon) + \boldsymbol{\Gamma}^R(\varepsilon)} \langle u(t)\mathbf{A}(\varepsilon, t) \rangle \right\}, \end{aligned} \quad (13.11)$$

where

$$\mathbf{A}(\varepsilon, t) = \int dt_1 u(t_1) \mathbf{G}^r(t, t_1) \exp[i\varepsilon(t-t_1) + i \int_{t_1}^t dt_2 \Delta(t_2)]. \quad (13.12)$$

Due to (13.6) we do not have to distinguish between L/R in the definition of $\mathbf{A}(\varepsilon, t)$; below we shall encounter situations where this distinction is necessary.

The expression (13.11) is of the Landauer-type: It expresses the current as an integral over a weighted density of states, times the difference of the two contact occupation factors. It is valid for arbitrary interactions in the central region, but it was derived with the somewhat restrictive assumption of proportional couplings to the leads.

13.5 Time-Dependent Resonant-Level Model

The analysis from Sect. 12.5 carries over again without essential changes, and we can just state the final results. The Dyson equation for the retarded Green function is

$$\mathbf{G}^r(t, t') = \mathbf{g}^r(t, t') + \int dt_1 \int dt_2 \mathbf{g}^r(t, t_1) \boldsymbol{\Sigma}^r(t_1, t_2) \mathbf{G}^r(t_2, t') , \quad (13.13)$$

where

$$\boldsymbol{\Sigma}_{nn'}^r(t_1, t_2) = \sum_{k\alpha \in L, R} V_{k\alpha, n}^*(t_1) g_{k\alpha}^r(t_1, t_2) V_{k\alpha, n'}(t_2) , \quad (13.14)$$

and $g_{k\alpha}^r$ is given by (13.2). The correlation function $\mathbf{G}^<$ is given by the Keldysh equation:

$$\mathbf{G}^<(t, t') = \int dt_1 \int dt_2 \mathbf{G}^r(t, t_1) \boldsymbol{\Sigma}^<(t_1, t_2) \mathbf{G}^a(t_2, t') , \quad (13.15)$$

where

$$\boldsymbol{\Sigma}^<(t_1, t_2) = i \sum_{L, R} \int \frac{d\varepsilon}{2\pi} e^{-i\varepsilon(t_1 - t_2)} f_{L/R}(\varepsilon) \boldsymbol{\Gamma}^{L/R}(\varepsilon, t_1, t_2) . \quad (13.16)$$

For simplicity, we continue to consider only a single level in the central region. As in the previous section, we assume that one can factorize the momentum and time dependence of the tunneling coupling, but allow for different time dependence for each barrier: $V_{k\alpha}(t) \equiv u_{L/R}(t)V_{\alpha, n}(\varepsilon_k)$. Referring to (12.29), the wide-band limit (WBL) consists of (1) neglecting the level shift $\Lambda(\varepsilon)$, (2) assuming that the line widths are energy independent constants, $\sum_{\alpha \in L, R} \Gamma_\alpha = \Gamma^{L/R}$, and (3) allowing a single time dependence, $\Delta_{L/R}(t)$, for the energies in each lead. The retarded self-energy in (13.13) thus becomes:

$$\begin{aligned} \boldsymbol{\Sigma}^r(t_1, t_2) &= \sum_{\alpha \in L, R} u_\alpha^*(t_1) u_\alpha(t_2) e^{-i \int_{t_2}^{t_1} dt_3 \Delta_\alpha(t_3)} \\ &\times \int \frac{d\varepsilon}{2\pi} e^{-i\varepsilon(t_1 - t_2)} \theta(t_1 - t_2) [-i\Gamma_\alpha] \\ &= -\frac{i}{2} [\Gamma^L(t_1) + \Gamma^R(t_1)] \delta(t_1 - t_2) . \end{aligned} \quad (13.17)$$

(Here we have introduced the notation $\Gamma^{L/R}(t_1) \equiv \Gamma^{L/R}(t_1, t_1) = \Gamma^{L/R} |u_{L/R}(t_1)|^2$.) With this self-energy, the retarded (advanced) Green function becomes

$$G^{r,a}(t, t') = g^{r,a}(t, t') \exp \left\{ \mp \int_{t'}^t dt_1 \frac{1}{2} [\Gamma^L(t_1) + \Gamma^R(t_1)] \right\} \quad (13.18)$$

with

$$g^{r,a}(t, t') = \mp i\theta(\pm t \mp t') \exp \left[-i \int_{t'}^t dt_1 \varepsilon_0(t_1) \right] . \quad (13.19)$$

This solution can now be used to evaluate the lesser function (13.15), and further in (13.5), to obtain the time-dependent current. In the WBL the ε - and t_1 -integrals in the term involving $G^<$ are readily evaluated, and we

write the current as (using $\text{Im}\{G^<(t,t)\} = N(t)$, where $N(t)$ is the occupation of the resonant-level)

$$\begin{aligned} J_L(t) &= -\frac{e}{\hbar} \left[\Gamma^L(t)N(t) + \int \frac{d\varepsilon}{\pi} f_L(\varepsilon) \right. \\ &\quad \times \left. \int_{-\infty}^t dt_1 \Gamma^L(t_1, t) \text{Im}\{e^{-i\varepsilon(t_1-t)} G^r(t, t_1)\} \right]. \end{aligned} \quad (13.20)$$

For a compact notation we introduce

$$\begin{aligned} A_{L/R}(\varepsilon, t) &= \int dt_1 u_{L/R}(t_1) G^r(t, t_1) \\ &\quad \times \exp \left[i\varepsilon(t - t_1) - i \int_t^{t_1} dt_2 \Delta_{L/R}(t_2) \right]. \end{aligned} \quad (13.21)$$

Obviously, in the time-independent case $A(\varepsilon)$ is just the Fourier transform of the retarded Green function $G^r(\varepsilon)$. In terms of $A(\varepsilon, t)$ the occupation $N(t)$ (using (13.15) for $G^<$) is given by

$$N(t) = \sum_{L,R} \Gamma^{L/R} \int \frac{d\varepsilon}{2\pi} f_{L/R}(\varepsilon) |A_{L/R}(\varepsilon, t)|^2. \quad (13.22)$$

We write the current as a sum of currents flowing out from the central region into the left (right) contact, and currents flowing into the central region from the left (right) contact, $J_{L/R}(t) = J_{L/R}^{\text{out}}(t) + J_{L/R}^{\text{in}}(t)$ ¹:

$$\begin{aligned} J_{L/R}^{\text{out}}(t) &= -\frac{e}{\hbar} \Gamma^{L/R}(t) N(t), \\ J_{L/R}^{\text{in}}(t) &= -\frac{e}{\hbar} \Gamma^{L/R} u_{L/R}(t) \int \frac{d\varepsilon}{\pi} f_{L/R}(\varepsilon) \text{Im}\{A_{L/R}(\varepsilon, t)\}. \end{aligned} \quad (13.23)$$

It is readily verified that these expressions coincide with earlier steady state results if all time-dependent quantities are replaced by constants.

Employing the same approach as in Sect. 13.4 and provided that $u_L(t) = u_R(t) = u(t)$, we find that the time-averaged current in the WBL is given by

$$\begin{aligned} \langle J \rangle &= -\frac{2e}{\hbar} \frac{\Gamma^L \Gamma^R}{\Gamma^L + \Gamma^R} \int \frac{d\varepsilon}{2\pi} \text{Im}\{f_L(\varepsilon) \langle u(t) A_L(\varepsilon, t) \rangle \\ &\quad - f_R(\varepsilon) \langle u(t) A_R(\varepsilon, t) \rangle\}. \end{aligned} \quad (13.24)$$

Unlike the general case of (13.11), there is no restriction in the WBL that the energy dependence be the same in the two leads. The expression (13.24) can therefore be used for the case of a time-dependent bias, where $\Delta_L(t)$ and

¹ The reader may worry about the direction of the in and out currents, because both terms in (13.23) apparently have the same sign. However, one can prove that $\langle \text{Im } A \rangle < 0$, and the in and out currents flow in opposite directions, as expected.

$\Delta_R(t)$ will be different. It is interesting to note that the function of energy appearing in the time-averaged current is positive definite. In particular, it can be shown [182] that

$$-\langle \text{Im}\{u_{L/R}(t)A_{L/R}(\varepsilon, t)\} \rangle = \frac{\Gamma}{2} \langle |A_{L/R}(\varepsilon, t)|^2 \rangle. \quad (13.25)$$

One consequence of (13.25) is that if only the level is time dependent, the average current cannot flow against the bias.

We shall next consider two specific examples for the time variation, which are relevant for experimental situations.

13.5.1 Response to Harmonic Modulation

Harmonic time modulation is probably the most commonly encountered example of time dependence. Here, we treat the case when the contact and site energy levels vary as

$$\Delta_{L/R,0}(t) = \Delta_{L/R,0} \cos(\omega t). \quad (13.26)$$

It is easy to generalize the treatment to situations where the modulation frequencies and/or phases are different in different parts of the device. Assuming that the barrier heights do not depend on time ($u_{L/R} = 1$), and substituting (13.26) in the expression (13.21) for $A(\varepsilon, t)$, one finds

$$\begin{aligned} A_{L/R}(\varepsilon, t) &= \exp \left[-i \frac{\Delta_0 - \Delta_{L/R}}{\omega} \sin(\omega t) \right] \\ &\times \sum_{k=-\infty}^{\infty} J_k \left(\frac{\Delta_0 - \Delta_{L/R}}{\omega} \right) \frac{e^{ik\omega t}}{\varepsilon - \varepsilon_0 - k\omega + i\Gamma/2}, \end{aligned} \quad (13.27)$$

where $J_{-k}(x) = (-1)^k J_k(x)$ is the k th order Bessel function.

Figures 13.1 and 13.2 show $|A(\varepsilon, t)|^2$ and $\text{Im}A(\varepsilon, t)$ as a function of time, respectively. We recall from (13.23) that the current at a given time is determined by integrating $|A(\varepsilon, t)|^2$ and $\text{Im}A(\varepsilon, t)$ over energy, and thus an examination of Fig. 13.1 helps one to understand the complicated time dependence discussed below.² The physical parameters used to generate these plots are given in the figure caption. The three-dimensional plot (top part of figure) is projected down on a plane to yield a contour plot in order to help to visualize the time dependence. As expected, the time variation is periodic with period $T = 2\pi/\omega$. The time dependence is strikingly complex. The most easily recognized features are the maxima in the plot for $|A|^2$; these are related to photonic side bands occurring at $\varepsilon = \varepsilon_0 \pm k\omega$ (also (13.28) below) [66, 67].

The current is computed using the methods described in [182], and is shown in Fig. 13.3. We also display the drive voltage as a broken line. Bearing

² We show only A_L ; similar results hold for A_R .

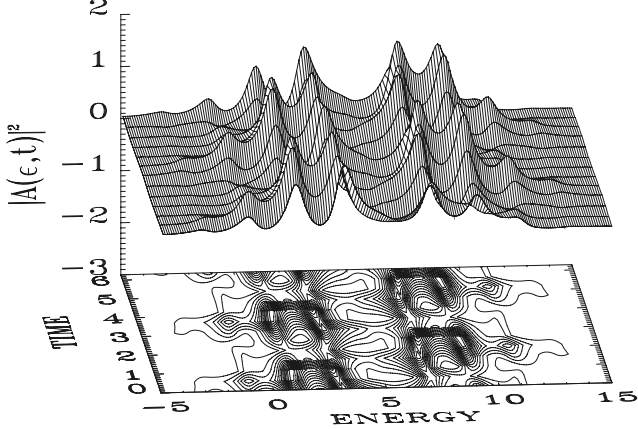


Fig. 13.1. $|A(\varepsilon, t)|^2$ as a function of time for harmonic modulation for a symmetric structure, $\Gamma_L = \Gamma_R = \Gamma/2$. The unit for the time axis is \hbar/Γ , and all energies are measured in units of Γ , with the values $\mu_L = 10$, $\mu_R = 0$, $\varepsilon_0 = 5$, $\Delta = 5$, $\Delta_L = 10$, and $\Delta_R = 0$. The modulation frequency is $\omega = 2\Gamma/\hbar$

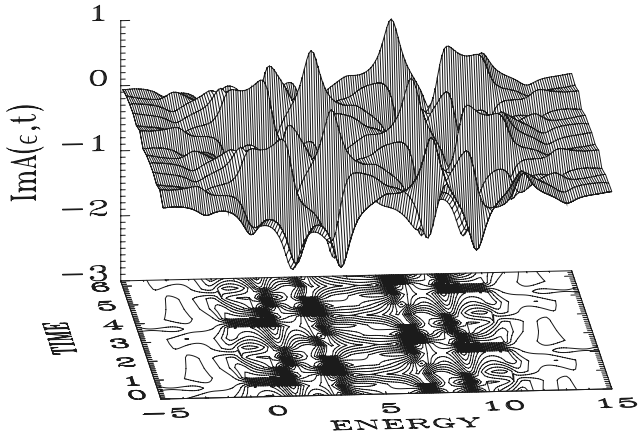


Fig. 13.2. The time dependence of $\text{Im}A(\varepsilon, t)$ for the case shown in Fig. 13.1

in mind the complex time dependence of $|A|^2$ and $\text{Im}A$, which determine the out and in currents, respectively, it is not surprising that the current displays a nonadiabatic time dependence. The basic physical mechanism underlying the secondary maxima and minima in the current is the lineup of a photon-assisted resonant tunneling peak with the contact chemical potentials. The rapid time variations are due to J^{in} (or, equivalently, due to $\text{Im}A$): the out current J^{out} is determined by the occupation $N(t)$, and hence varies only on a timescale Γ/\hbar , which is the time scale for charge density changes.

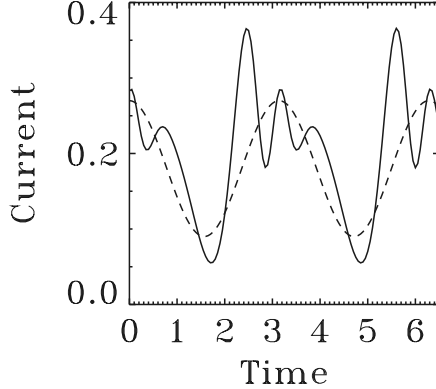


Fig. 13.3. The time-dependent current $J(t)$ for harmonic modulation corresponding to the parameters of Figs. 13.1 and 13.2. The DC bias is defined via $\mu_L = 10$ and $\mu_R = 0$, respectively. The *dotted line* shows (not drawn to scale) the time dependence of the drive signal. The temperature is $k_B T = 0.1\Gamma$

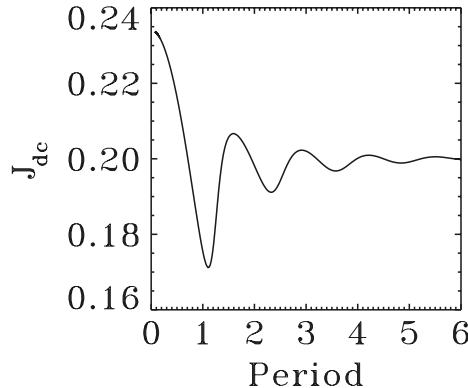


Fig. 13.4. Time-averaged current J_{DC} as function of the AC oscillation period $2\pi/\omega$. The DC amplitudes are the same as those in Fig. 13.3

We next consider the time average of the current. For the case of harmonic time dependence, we find³

$$\langle \text{Im}A_{L/R}(\varepsilon, t) \rangle = -\frac{\Gamma}{2} \sum_{k=-\infty}^{\infty} \frac{J_k^2[(\Delta_0 - \Delta_{L/R})/\omega]}{(\varepsilon - \varepsilon_0 - k\omega)^2 + (\Gamma/2)^2}. \quad (13.28)$$

Figure 13.4 shows the resulting time-averaged current J_{DC} . A consequence of the complex harmonic structure of the time-dependent current is that for temperatures $k_B T < \hbar\omega$, the average current oscillates as a function of period

³ It is useful to recall the identity $\exp[i\alpha \sin(\omega t)] = \sum_{k=-\infty}^{k=\infty} e^{i\omega t k} J_k(\alpha)$, where J_k is the k th order Bessel function.

$2\pi/\omega$. The oscillation can be understood by examining the general expression for average current (13.11) together with (13.28): whenever a photon-assisted peak in the effective density of states, occurring at $\varepsilon = \varepsilon_0 \pm k\omega$ in the time-averaged density of states $\langle \text{Im}A_{L/R} \rangle$, moves in or out of the allowed energy range, determined by the difference of the contact occupation factors, a maximum (or minimum) in the average current results.

13.5.2 Response to Step-Like Modulation

We give results for the case when the central site level changes abruptly at $t = t_0$: $\varepsilon_0 \rightarrow \varepsilon_0 + \Delta$. If the contacts also change at the same time, the corresponding results are obtained by letting $\Delta \rightarrow \Delta - \Delta_{L/R}$. Thus, simultaneous and equal shifts in the central region and the contacts have no effect. Assuming that the barrier heights do not depend on time ($u_{L/R} \equiv 1$), one finds for $t > t_0$ (from (13.21)

$$A(\varepsilon, t) = \frac{1}{\varepsilon - \varepsilon_0 + i\Gamma/2} \times \left\{ 1 + \Delta \frac{[1 - \exp[i(\varepsilon - (\varepsilon_0 + \Delta) + i\Gamma/2)(t - t_0)]]}{\varepsilon - (\varepsilon_0 + \Delta) + i\Gamma/2} \right\}. \quad (13.29)$$

This result is easily generalized [373] to a pulse of duration s , and numerical results are discussed below.

It is instructive to study analytically the long- and short-time behavior of $A(\varepsilon, t)$. It is easily verified that $A(\varepsilon, t)$ has the expected limiting behavior:

$$A(\varepsilon, t \rightarrow \infty) = [\varepsilon - (\varepsilon_0 + \Delta) + i\Gamma/2]^{-1}. \quad (13.30)$$

Thus, when the transients have died away, $A(\varepsilon, t)$ settles to its new steady-state value.

Consider next the change in current at short times after the pulse, $t - t_0 \equiv \delta t \ll \hbar/\Gamma, \hbar/\varepsilon$. Note that the second inequality provides an effective cutoff for the energy integration required for the current. In this limit we may write

$$A(\varepsilon, t) \simeq \frac{1 - i\Delta\delta t}{\varepsilon - \varepsilon_0 + i\Gamma/2}. \quad (13.31)$$

Since $\delta J^{\text{out}}(t) \propto |A(\varepsilon, t)|^2 \propto (\delta t)^2$, the leading contribution comes from $J^{\text{in}}(t)$. For low temperatures we find

$$\begin{aligned} \delta J_{L/R}(t) &\simeq \frac{e\Gamma^{L/R}}{\pi\hbar} \int_{-\hbar/\delta t}^{\mu_{L/R}} d\varepsilon \text{Im} \delta A(\varepsilon, t) \\ &\simeq \frac{e\Gamma^{L/R}}{\pi\hbar} \Delta\delta t \log \delta t. \end{aligned} \quad (13.32)$$

We next discuss the numerical results for a step-like modulation. Just like in the case of harmonic modulation, it is instructive to study the time dependence of $|A|^2$ and $\text{Im}A$; these are shown in Figs. 13.5 and 13.6, respectively.

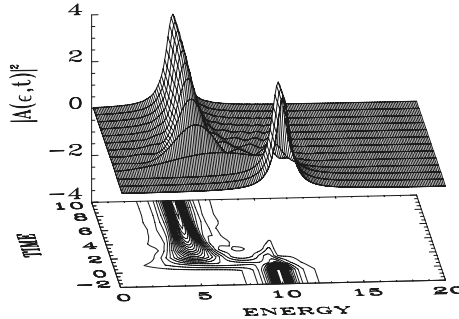


Fig. 13.5. $|A(\varepsilon, t)|^2$ as a function of time for step-like modulation. At $t = 0$ the resonant-level energy ε_0 suddenly decreases by 5Γ

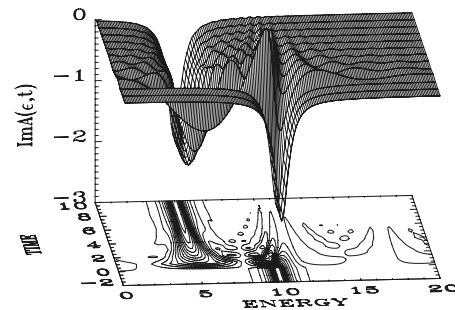


Fig. 13.6. The time dependence of $\text{Im}A(\varepsilon, t)$ for the case shown in Fig.13.5

The observed time dependence is less complex than in the harmonic case. Nevertheless, the resulting current, which we have computed for a pulse of duration s and displayed in Fig. 13.7, shows an interesting ringing behavior. The ringing is again due to the movement of the side bands of $\text{Im}A_{L/R}$ through the contact Fermi energies.

Due to the experimental caveats discussed in Sect. 13.2, the ringing showed in Fig. 13.7 may be masked by capacitive effects not included in the present work. However, the ringing should be observable in the time-averaged current by applying a series of pulses such as that of Fig. 13.6, and then varying the pulse duration. In Fig. 13.8 the derivative of the DC-current with respect to pulse length is plotted, normalized by the repeat time τ between pulses. For pulse lengths s of the order of the resonance lifetime \hbar/Γ , the derivative of the DC-current closely mimics the time-dependent current following the pulse and, likewise, asymptotes to the steady-state current at the new voltage.

The examples discussed in this section are all for noninteracting electrons. In Chap. 12 we developed methods and approximation schemes for including the Coulomb interaction for stationary transport phenomena. These approximations can be generalized to the time-dependent case, usually, however, the expressions become so complicated that progress can only be made with

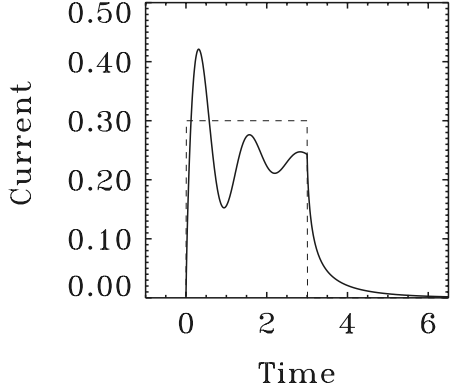


Fig. 13.7. Time-dependent current $J(t)$ through a symmetric double-barrier tunneling structure in response to a rectangular bias pulse. Initially, the chemical potentials μ_L and μ_R and the resonant-level energy ε_0 are all zero. At $t = 0$, a bias pulse (*dashed curve*) suddenly increases energies in the left lead by $\Delta_L = 10$ and increases the resonant-level energy by $\Delta = 5$. At $t = 3$, before the current has settled to a new steady value, the pulse ends and the current decays back to zero. The temperature is $k_B T = 0.1\Gamma$

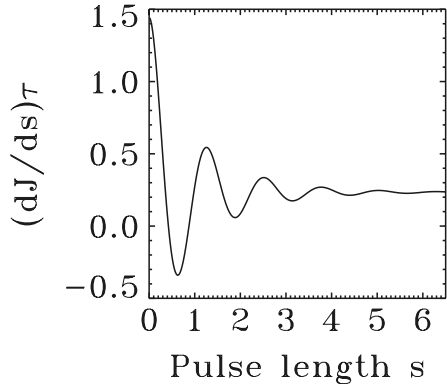


Fig. 13.8. Derivative of the integrated DC-current J_{DC} with respect to pulse duration s , normalized by the interval between pulses τ . For pulse durations much longer than the resonance lifetime \hbar/Γ , the derivative is just the steady state current at the bias voltage, but for shorter pulses the ringing response of the current is evident

numerical methods. We do not pursue this approach further, and refer the interested reader to the literature, e.g., [248, 340, 378]. Another recent development is to relax the wide-band limit, and perform the analysis directly in the two-time domain, see [256].

13.6 Linear-Response

For circuit modeling purposes it would often be desirable to replace the mesoscopic device with a conventional circuit element, with an associated complex impedance $Z(\omega)$, or admittance $Y(\omega)$. Our results for the nonlinear time-dependent current form a very practical starting point for such a calculation. For the noninteracting case, the current is determined by $A(\varepsilon, t)$, and all one has to do is linearize A (13.21) with respect to the amplitude of the drive signal, i.e., $\Delta - \Delta_{L/R}$. It is important to note that we do not linearize with respect to the chemical potential difference: the results given below apply to an arbitrary static bias voltage.

Performing the linearization, one finds

$$\begin{aligned} |A_{L/R}^{(1)}(\varepsilon, t)|^2 &= \frac{\Delta - \Delta_{L/R}}{\omega} \operatorname{Re} \left\{ \frac{1}{\varepsilon - \varepsilon_0 + i\Gamma/2} \right. \\ &\quad \times \left. \left[\frac{e^{-i\omega t}}{\varepsilon - \varepsilon_0 - \omega - i\Gamma/2} - \frac{e^{i\omega t}}{\varepsilon - \varepsilon_0 + \omega - i\Gamma/2} \right] \right\} \end{aligned} \quad (13.33)$$

and

$$\begin{aligned} \operatorname{Im} A_{L/R}^{(1)}(\varepsilon, t) &= \frac{\Delta - \Delta_{L/R}}{2\omega} \operatorname{Im} \left\{ \frac{e^{i\omega t}}{\varepsilon - \varepsilon_0 - \omega + i\Gamma/2} \right. \\ &\quad \left. - \frac{e^{-i\omega t}}{\varepsilon - \varepsilon_0 + \omega + i\Gamma/2} + \frac{e^{-i\omega t} - e^{i\omega t}}{\varepsilon - \varepsilon_0 + i\Gamma/2} \right\}. \end{aligned} \quad (13.34)$$

At finite temperature the energy integration must be done numerically [182], while at $T = 0$ they can be done analytically. In the latter case, all the integrals can be cast into the form

$$\begin{aligned} &\int_{-\infty}^{\mu} \frac{d\varepsilon}{(\varepsilon - \varepsilon_1 + i\Gamma_1/2)(\varepsilon - \varepsilon_2 + i\Gamma_2/2)} \\ &= \frac{1}{\varepsilon_1 - \varepsilon_2 + i(\Gamma_2 - \Gamma_1)/2} \log \frac{\mu - \varepsilon_1 + i\Gamma_1/2}{\mu - \varepsilon_2 + i\Gamma_2/2}. \end{aligned} \quad (13.35)$$

Using $\log(x + iy) = 1/2 \log(x^2 + y^2) + i \tan^{-1}(y/x)$ yields

$$J_{L/R}^{(1),\text{in}} = \frac{e}{\hbar} \Gamma^{L/R} \frac{\Delta - \Delta_{L/R}}{2\pi\omega} [\cos(\omega t) F_{L/R}(\omega) + \sin(\omega t) G_{L/R}(\omega)] \quad (13.36)$$

and

$$\begin{aligned} J_{L/R}^{(1),\text{out}} &= \frac{e}{\hbar} \Gamma^{L/R} \sum_{L,R} \Gamma^{L/R} \frac{\Delta - \Delta_{L/R}}{2\pi\omega} \\ &\quad \times \left\{ \cos(\omega t) \left[\frac{\omega}{\omega^2 + \Gamma^2} G_{L/R}(\omega) - \frac{\Gamma}{\omega^2 + \Gamma^2} F_{L/R}(\omega) \right] \right. \\ &\quad \left. - \sin(\omega t) \left[\frac{\Gamma}{\omega^2 + \Gamma^2} G_{L/R}(\omega) + \frac{\omega}{\omega^2 + \Gamma^2} F_{L/R}(\omega) \right] \right\}, \end{aligned} \quad (13.37)$$

where we defined

$$G_{L/R}(\omega) = \log \frac{|\mu_{L/R} - \varepsilon_0 + i\Gamma/2|^2}{|(\mu_{L/R} - \varepsilon_0 + i\Gamma/2)^2 - \omega^2|} \quad (13.38)$$

and

$$F_{L/R}(\omega) = \tan^{-1} \left[\frac{\mu_{L/R} - \varepsilon_0 - \omega}{\Gamma/2} \right] - \tan^{-1} \left[\frac{\mu_{L/R} - \varepsilon_0 + \omega}{\Gamma/2} \right]. \quad (13.39)$$

These expressions give the linear AC-current for an arbitrarily biased double-barrier structure, where both contacts and the central-region energies are allowed to vary harmonically.

Considerable simplification occurs, if one considers a symmetric structure at zero bias: $\Gamma^L = \Gamma^R = \Gamma/2$, and $\mu_L = \mu_R \equiv \mu$, respectively. The net current from left to right is $J^{(1)} = 1/2[J_L^{(1),\text{in}} + J_R^{(1),\text{out}} - J_L^{(1),\text{out}} - J_R^{(1),\text{in}}]$. Using (13.36) and (13.37), one finds that the “out” contributions cancel, and that the “in” currents combine to give the net current:

$$J^{(1)}(t) = -\frac{e}{\hbar} \frac{\Gamma}{4} \frac{\Delta_L - \Delta_R}{2\pi\omega} [\cos(\omega t)F(\omega) + \sin(\omega t)G(\omega)]. \quad (13.40)$$

Here, the functions $F(\omega)$ and $G(\omega)$ are given by (13.38) and (13.39), but using μ and $\Gamma/2$ as parameters. It is possible to obtain this result directly from a linear-response formalism [119] (Fig. 13.9).

We now wish to apply the formal results derived in this section to an experimentally relevant system. The key feature of a resonant tunneling diode

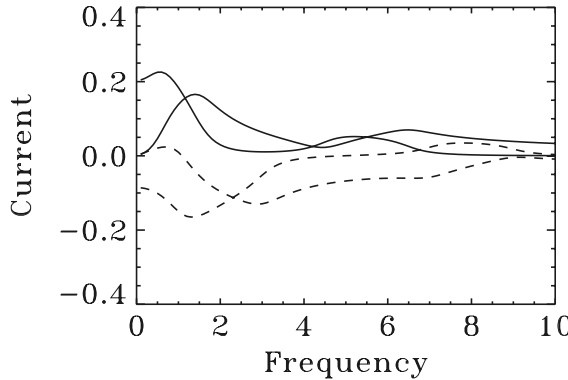


Fig. 13.9. In-phase and out-of-phase components of the linear-response current (in units of $e\Gamma/h$ and normalized with the amplitude of the drive signal Δ_L to yield admittance) for two bias points, $eV = 5$ (continuous line) and $eV = 10$ (dashed line). Other parameters are as in Fig.12.3. The out-of-phase components always tend to zero for vanishing frequency, while the in-phase component can have either a positive or negative zero-frequency limit depending on the dc bias

is its ability to show negative differential resistance (NDR). In Sect. 12.5 we introduced a simple model which has this property (Fig. 12.3). We need to generalize the F and G functions to take into account the finite bandwidth; this is, however, easy to do with the replacements $F_\mu \rightarrow \tilde{F} = F_\mu - F_{\mu-D}$, and analogously for G_μ . We show in Fig. 13.6 the resulting linear-response admittance $Y(\omega)$ for a symmetric structure ($\Gamma_L = \Gamma_R$). Several points are worth noting. For DC bias $eV = 5$ (energies are given in units of Γ) the calculated admittance resembles qualitatively zero external bias results [119]. More interestingly, for DC bias in the NDR regime, the real part is negative for small frequencies. This simply reflects the fact that the device is operating under NDR bias conditions. At higher frequencies the real part becomes positive, thus indicating that further modeling along the lines sketched here may lead to important implications on the high-frequency response of resonant tunneling structures.

13.7 Fluctuating Energy Levels

As a final example, we analyze how the techniques developed in the previous sections can be used in connection with a fluctuating time dependence. In particular, we wish to evaluate the average current using (13.11). We consider a very simple model, where the central-region energy level $\varepsilon_0(t)$ is a Gaussian random variable [297]. The time average is defined by specifying the correlators

$$\begin{aligned}\langle \varepsilon_0(t) \rangle &= 0, \\ \langle \varepsilon_0(t_1) \varepsilon_0(t_2) \rangle &= f(t_1 - t_2).\end{aligned}\quad (13.41)$$

All higher odd correlators vanish, while all even correlators are given as a sum of products of all pairwise correlators. In the calculation of $\langle \text{Im}A_{L/R}(\varepsilon, t) \rangle$ in (13.11) for $\langle J \rangle$ we need $\langle \exp[-i \int_{t-\tau}^t dt_1 \varepsilon_0(t_1)] \rangle$; this is evaluated by expanding the exponential functions and averaging term by term using (13.41). Consider, for example,

$$\begin{aligned}\left\langle \exp \left[-i \int_{t-\tau}^t dt_1 \varepsilon_0(t_1) \right] \right\rangle &= 1 - i \int_{t-\tau}^t dt_1 \langle \varepsilon_0(t_1) \rangle \\ &\quad + \frac{1}{2} (-i)^2 \int_{t-\tau}^t dt_1 \int_{t-\tau}^t dt_2 \langle \varepsilon_0(t_1) \varepsilon_0(t_2) \rangle + \dots \\ &= 1 - \frac{1}{2} \int \frac{d\omega}{2\pi} f(\omega) \left| \int_{t-\tau}^t dt_1 e^{-i\omega t_1} \right|^2 + \dots \\ &= 1 - \frac{1}{2} \int \frac{d\omega}{2\pi} \frac{f(\omega)}{\omega^2} \sin^2 \left(\frac{\omega\tau}{2} \right) + \dots,\end{aligned}\quad (13.42)$$

where $f(\omega)$ is the Fourier transform of $f(t - t')$. By using some simple combinatorics it is easy to convince oneself that the higher order averages generate

the $1/n!$ factors that occur in the series expansion of the exponential function. Thus the series can be resummed with the result

$$\begin{aligned} \langle \text{Im}A_{L/R}(\varepsilon, t) \rangle &= \frac{1}{2} \int_{-\infty}^{\infty} d\tau e^{i\varepsilon\tau - \Gamma|\tau|/2} \\ &\times \exp \left[-\frac{1}{2} \int \frac{d\omega}{2\pi} \frac{f(\omega)}{\omega^2} 4 \sin^2 \left(\frac{\omega\tau}{2} \right) \right]. \end{aligned} \quad (13.43)$$

A particularly simple result emerges if one assumes a white-noise spectrum: $f(\omega) = F$; then the only effect of the fluctuations is to enhance the line width: $\Gamma/2 \rightarrow \Gamma/2 + F$. This is consistent with the phenomenological model used in [187] and [369] in connection with inelastic scattering mechanisms in resonant tunneling: There the resonance width of the transmission coefficient is given an extra contribution due to inelastic processes. A more complicated spectrum would change the Lorentzian line shape to some other functional form.

13.8 Noise

In Sect. 13.7 we considered a very simple example of the effect of the fluctuations on the transmission properties of a mesoscopic system. Here we develop a more systematic approach to the calculation of noise. Studies of noise have in recent years become a very important subfield in nanoscience. There are several reasons for this trend. The noise spectrum gives additional and complementary information to the current–voltage characteristic. In particular, noise reflects the interactions in a subtle way. Noise, as we shall see below, is the second moment of the current operator, but one may also wish to study higher correlation functions. Here the theory has been advanced quite significantly, and many beautiful results have been obtained for the full counting statistics (FCS) (see, e.g., [239, 273], or [282]). Measurement of FCS is a very challenging task, and the first results are just beginning to emerge (see, e.g., [289] or [70]). Finally, many promising research areas, such as nanoelectromechanical systems (NEMS), spintronics, or quantum information processing involve noise in a fundamental way, underlying the importance of a solid theory for noise.

A very thorough review of noise calculations, focusing on the scattering matrix approach, has been given by Blanter and Büttiker [47]. Here we illustrate how the noise calculation can be performed with the nonequilibrium Green function approach. Several authors have used this approach, starting from the early work of Khlus on microcontacts between metallic structures [200], and the work on noninteracting resonant tunneling diodes by Chen and Ting [79]; here we follow the notation used by Souza and co-workers [330] in their work on spin-dependent noise. We recall from Chap. 12 the expression for the current operator (through the left barrier)

$$I_L = \frac{e\text{i}}{\hbar} \sum_k [t_k c_k^\dagger d - t_k^* d^\dagger c_k], \quad (13.44)$$

where we simplify the notation somewhat by suppressing indices which are not relevant to the structure of the theory. We define $\delta I_L(t) = I_L(t) - \langle I_L \rangle$, and plan to evaluate the correlation function

$$\begin{aligned} S(t, t') &= \langle \{\delta I_L(t), \delta I_L(t')\} \rangle = \langle \{I_L(t), I_L(t')\} \rangle - 2\langle I_L \rangle^2 \\ &= \left(\frac{ie}{\hbar}\right)^2 \sum_{k,k'} \left[t_k t_{k'} \langle c_k^\dagger(t) d(t) c_{k'}^\dagger(t') d(t') \rangle - t_k t_{k'}^* \langle c_k^\dagger(t) d(t) d^\dagger(t') c_{k'}(t') \rangle \right. \\ &\quad \left. - t_k^* t_{k'} \langle d^\dagger(t) c_k(t) c_{k'}^\dagger(t') d(t') \rangle + t_k^* t_{k'}^* \langle d^\dagger(t) c_k(t) d^\dagger(t') c_{k'}(t') \rangle \right] \\ &\quad + \text{h.c.} - 2\langle I_L \rangle^2. \end{aligned} \quad (13.45)$$

The Fourier transform of S is called the noise spectrum; in what follows we shall be particularly concerned with its zero-frequency component, $S(0) = \int d(t-t')S(t-t')$. In order to evaluate the (nonequilibrium) expectation values occurring in (13.45) in a systematic way, we first define the following causal two-particle Green functions

$$\begin{aligned} g_1^{cd}(t, t') &= i^2 \langle T c_k^\dagger(t) d(t) c_{k'}^\dagger(t') d(t') \rangle, \\ g_2^{cd}(t, t') &= i^2 \langle T c_k^\dagger(t) d(t) d^\dagger(t') c_{k'}(t') \rangle, \\ g_3^{cd}(t, t') &= i^2 \langle T d^\dagger(t) c_k(t) c_{k'}^\dagger(t') d(t') \rangle, \\ g_4^{cd}(t, t') &= i^2 \langle T d^\dagger(t) c_k(t) d^\dagger(t') c_{k'}(t') \rangle. \end{aligned} \quad (13.46)$$

The nonequilibrium noise correlator is then given by

$$\begin{aligned} S(t, t') &= \left(\frac{e}{\hbar}\right)^2 \sum_{k,k'} \left[t_k t_{k'} G_1^{cd,>}(t, t') - t_k t_{k'}^* G_2^{cd,>}(t, t') \right. \\ &\quad \left. - t_k^* t_{k'} G_3^{cd,>}(t, t') + t_k^* t_{k'}^* G_4^{cd,>}(t, t') \right] + \text{h.c.} - 2\langle I_L \rangle^2, \end{aligned} \quad (13.47)$$

where $G_i^{cd,>}(t, t')$ are the greater than components of the contour-ordered counterparts $G_i^{cd}(\tau, \tau')$ of the two-particle Green functions of (13.46). Since we are now dealing with two-particle Green functions, the analytic continuation rules of Chap. 4 are not immediately applicable, and a certain amount of formal work is needed before we have explicit expressions from which physical consequences can be extracted.

As the first step we express the Green functions (13.46) in terms of two-particle Green functions which only involve the central region operators. This step is fully analogous with our derivation of the current formula in Chap. 12: there we eliminated the c -operators from the hybrid function $G_{n,k\alpha}^<(t-t') = i\langle c_{k\alpha}(t') d_n(t) \rangle$, and thereby expressed it in terms of the central region Green function G_{nm} and the lead Green function $g_{k\alpha}$ (see (12.14)). Now there are

two c -operators in G_i^{cd} to be eliminated; therefore the algebra is slightly more complex. Both methods for eliminating the c -operators discussed in Chap. 12 can be used, and here we use the S -matrix expansion because it appears more systematic. Consider then, as an example, the nonequilibrium counter part of g_2^{cd} , which we treat as follows (the other components are similar, or simpler than the chosen example)

$$\begin{aligned} G_2^{cd}(\tau, \tau') &= i^2 \langle T_C c_k^\dagger(\tau) d(\tau) d^\dagger(\tau') c_{k'}(\tau') \rangle \\ &= i^2 \langle T_C \tilde{c}_k^\dagger(\tau) \tilde{d}(\tau) \tilde{d}^\dagger(\tau') \tilde{c}_{k'}(\tau') S \rangle, \end{aligned} \quad (13.48)$$

where tildes denote interaction picture with respect to the tunneling coupling, and the S -matrix is

$$S = \sum_{j=0}^{\infty} \frac{(-i)^j}{j!} \int_C d\tau_1 \cdots \int_C d\tau_j \langle T_C \tilde{H}_T(\tau_1) \cdots \tilde{H}_T(\tau_j) \rangle, \quad (13.49)$$

with the tunneling Hamiltonian

$$H_T = \sum_k [t_k c_k^\dagger d + t_k^* d^\dagger c_k]. \quad (13.50)$$

Up to second order in H_T the Green function becomes

$$\begin{aligned} G_2^{cd}(\tau, \tau') &= i^2 \langle T_C \tilde{c}_k^\dagger(\tau) \tilde{d}(\tau) \tilde{d}^\dagger(\tau') \tilde{c}_{k'}(\tau') \rangle \\ &\quad + i^2 \frac{(-i)^2}{2!} \left\langle T_C \tilde{c}_k^\dagger(\tau) \tilde{d}(\tau) \tilde{d}^\dagger(\tau') \tilde{c}_{k'}(\tau') \right. \\ &\quad \times \int d\tau_1 \int d\tau_2 \sum_{k_1, k_2} [t_{k_1} \tilde{c}_{k_1}^\dagger(\tau_1) \tilde{d}(\tau_1) + t_{k_1}^* \tilde{d}^\dagger(\tau_1) \tilde{c}(\tau_1)_{k_1}] \\ &\quad \left. \times [t_{k_2} \tilde{c}_{k_2}^\dagger(\tau_2) \tilde{d}(\tau_2) + t_{k_2}^* \tilde{d}^\dagger(\tau_2) \tilde{c}_{k_2}(\tau_2)] \right\rangle + \dots, \end{aligned} \quad (13.51)$$

where the dots represent higher order terms. The expectation values in (13.51) can now be factorized, because in the interaction picture the \tilde{c} and \tilde{d} operators are independent. We find (by a change of dummy variables, we see that (13.51) gives rise to two identical terms, thereby canceling the factor $1/2$)⁴

$$\begin{aligned} G_2^{cd}(\tau, \tau') &= -\delta_{kk'} g_k^0(\tau', \tau) G^0(\tau, \tau') - \int d\tau_1 \int d\tau_2 \sum_{k_1 k_2} t_{k_1} t_{k_2}^* \\ &\quad \times \langle T_C \tilde{c}_k^\dagger(\tau) \tilde{c}_{k'}(\tau') \tilde{c}_{k_1}^\dagger(\tau_1) \tilde{c}_{k_2}(\tau_2) \rangle i^2 \langle T_C \tilde{d}(\tau) \tilde{d}^\dagger(\tau') \tilde{d}(\tau_1) \tilde{d}^\dagger(\tau_2) \rangle. \end{aligned} \quad (13.52)$$

⁴ The overall sign of the second term in (13.52) is determined as follows. One requires an even number of permutations (in fact, eight) to bring all \tilde{c} 's and \tilde{d} 's adjacent to each other. The minus sign comes from the $(-i)^2$ of the second-order expansion.

We must next consider the expectation values involving four \tilde{c} 's and four \tilde{d} 's. Since the central region may contain interactions, the \tilde{d} -terms cannot be simplified, while the noninteracting nature of the contacts allows a further factorization:

$$\begin{aligned} \langle T_C \tilde{c}_k^\dagger(\tau) \tilde{c}_{k'}(\tau') \tilde{c}_{k_1}^\dagger(\tau_1) \tilde{c}_{k_2}(\tau_2) \rangle &= \langle T_C \tilde{c}_k^\dagger(\tau) \tilde{c}_{k'}(\tau') \rangle \langle T_C \tilde{c}_{k_1}^\dagger(\tau_1) \tilde{c}_{k_2}(\tau_2) \rangle \\ &\quad + \langle T_C \tilde{c}_k^\dagger(\tau) \tilde{c}_{k_2}(\tau_2) \rangle \langle T_C \tilde{c}_{k'}(\tau') \tilde{c}_{k_1}^\dagger(\tau_1) \rangle \\ &= -\delta_{kk'} \delta_{k_1 k_2} g_k^0(\tau', \tau) g_{k_1}^0(\tau_2, \tau_1) \\ &\quad + \delta_{k_2 k_1} g_k^0(\tau_2, \tau) g_{k'}(\tau', \tau_1). \end{aligned} \quad (13.53)$$

The first term of (13.52) and the first line of (13.53) can be combined:

$$-\delta_{kk'} g_k^0(\tau', \tau) \left[G_0(\tau, \tau') + \sum_{k_1} \int d\tau_1 \int d\tau_2 |t_{k_1}|^2 g_{k_1}^0(\tau_2, \tau_1) \right. \\ \left. \times i^2 \langle T_C \tilde{d}(\tau) \tilde{d}^\dagger(\tau') \tilde{d}(\tau_1) \tilde{d}^\dagger(\tau_2) \rangle \right]. \quad (13.54)$$

The quantity in square brackets is recognized as the beginning of the series expansion of the *full* central region Green function, $G(\tau, \tau') = -i \langle T_C d(\tau) d^\dagger(\tau') \rangle = -i \langle T_C \tilde{d}(\tau) \tilde{d}^\dagger(\tau') S \rangle$. It is straightforward to see that the higher order terms in H_T which have $g_k^0(\tau', \tau)$ as a common factor term by term reproduce the series expansion for $G(\tau, \tau')$.⁵ We thus conclude that all these terms sum up to $-\delta_{kk'} g_k^0(\tau, \tau') G(\tau, \tau')$. A similar analysis can be applied to the second line in (13.53). Qualitatively, the term obtained thus far can be written as (suppressing all variables) $tt^*(g^0)^2 \langle \tilde{d} \tilde{d}^\dagger \tilde{d} \tilde{d}^\dagger \rangle$, which is nothing but the zeroth order term of the series expansion of an interacting two-particle Green function for the central region. Higher order terms in the S -matrix expansion generate the full series for the interacting two-particle Green function, in full analogy of what was found in (13.54) (though with slightly more involved combinatorics). Combining the results we have thus obtained

$$G_2^{cd}(\tau, \tau') = -\delta_{kk'} g_k^0(\tau, \tau') G(\tau, \tau') - \int d\tau_1 \int d\tau_2 t_k^* t_{k'}^* \\ \times g_k^0(\tau_2, \tau) g_{k'}^0(\tau', \tau_1) G_2^{dd}(\tau, \tau', \tau_1, \tau_2), \quad (13.55)$$

where

$$G_2^{dd}(\tau, \tau', \tau_1, \tau_2) = i^2 \langle T_C d(\tau) d^\dagger(\tau') d(\tau_1) d^\dagger(\tau_2) \rangle. \quad (13.56)$$

Similar calculations for the remaining Green functions yield

$$G_1^{cd}(\tau, \tau') = -t_k^* t_{k'}^* \int d\tau_1 \int d\tau_2 g_k^0(\tau_1, \tau) g_{k'}^0(\tau_2, \tau') G_1^{dd}(\tau, \tau', \tau_1, \tau_2), \quad (13.57)$$

⁵ It is left as an exercise to check that the combinatorial factors combine correctly.

$$G_3^{cd}(\tau, \tau') = -\delta_{kk'} g_k^0(\tau, \tau') G(\tau', \tau) - t_k t_{k'}^* \int d\tau_1 \int d\tau_2 \\ \times g_k^0(\tau, \tau_1) g_{k'}(\tau_2, \tau') G_3^{dd}(\tau, \tau', \tau_1, \tau_2), \quad (13.58)$$

$$G_4^{cd}(\tau, \tau') = -t_k t_{k'} \int d\tau_1 \int d\tau_2 g_k^0(\tau, \tau_1) g_{k'}^0(\tau', \tau_2) G_4^{dd}(\tau, \tau', \tau_1, \tau_2), \quad (13.59)$$

where

$$G_1^{dd}(\tau, \tau', \tau_1, \tau_2) = i^2 \langle T_C d(\tau) d(\tau') d^\dagger(\tau_1) d^\dagger(\tau_2) \rangle, \quad (13.60)$$

$$G_3^{dd}(\tau, \tau', \tau_1, \tau_2) = i^2 \langle T_C d^\dagger(\tau) d(\tau') d(\tau_1) d^\dagger(\tau_2) \rangle, \quad (13.61)$$

$$G_4^{dd}(\tau, \tau', \tau_1, \tau_2) = i^2 \langle T_C d^\dagger(\tau) d^\dagger(\tau') d(\tau_1) d(\tau_2) \rangle, \quad (13.62)$$

respectively. We have thus far obtained

$$S(\tau, \tau') = \left(\frac{e}{\hbar} \right)^2 \left\{ \sum_k |t_k|^2 [g_k^0(\tau', \tau) G(\tau, \tau') + g_k^0(\tau, \tau') G(\tau', \tau)] \right. \\ + \sum_{kk'} |t_k|^2 |t_{k'}|^2 \int d\tau_1 \int d\tau_2 \\ \times [-g_k^0(\tau_1, \tau) g_{k'}^0(\tau_2, \tau') G_1^{dd}(\tau, \tau', \tau_1, \tau_2) \\ + g_k^0(\tau_2, \tau) g_{k'}^0(\tau', \tau_1) G_2^{dd}(\tau, \tau', \tau_1, \tau_2) \\ - g_k^0(\tau, \tau_1) g_{k'}^0(\tau_2, \tau') G_3^{dd}(\tau, \tau', \tau_1, \tau_2) \\ - g_k^0(\tau, \tau_1) g_{k'}^0(\tau', \tau_2) G_4^{dd}(\tau, \tau', \tau_1, \tau_2)] \Big\} + \text{h.c.} - 2 \langle I_L \rangle^2. \quad (13.63)$$

No approximations have been employed in arriving at (13.63), and it forms an entirely general starting point for noise calculations for a large variety of systems.

The next task in the general program is to extract the $\tau > \tau'$ part from (13.63). This is straightforward for the first line, but appears complicated for the remaining terms because of the two-particle Green functions. We have not discussed in this book how the analytic continuation rules for two-time functions can be generalized to objects involving four time labels, as is the case with (13.63). We do not embark on this ambitious project here. Instead, we make a Hartree–Fock level approximation to the two-particle Green functions in a fashion quite analogous to our discussion of transport through the Coulomb Island in Chap. 12. Specifically, we approximate

$$G_1^{dd}(\tau, \tau', \tau_1, \tau_2) \approx G(\tau, \tau_2) G(\tau', \tau_1) - G(\tau, \tau_1) G(\tau', \tau_2), \\ G_2^{dd}(\tau, \tau', \tau_1, \tau_2) \approx G(\tau, \tau') G(\tau_1, \tau_2) - G(\tau, \tau_2) G(\tau_1, \tau'), \\ G_3^{dd}(\tau, \tau', \tau_1, \tau_2) \approx G(\tau_1, \tau) G(\tau', \tau_2) - G(\tau', \tau) G(\tau_1, \tau_2), \\ G_4^{dd}(\tau, \tau', \tau_1, \tau_2) \approx G(\tau_2, \tau) G(\tau_1, \tau') - G(\tau_1, \tau) G(\tau_2, \tau'). \quad (13.64)$$

When substituting these expressions to (13.63), we observe that the two kinds of terms are generated: terms where the τ_1 - and τ_2 -integrals can be done separately, and terms where the two integrals are intertwined. We begin by considering the terms of the first kind, which we call “disconnected” terms.

13.8.1 The Disconnected Terms

The disconnected part of the noise is

$$\begin{aligned} S_{\text{dis}}(\tau, \tau') = & \left(\frac{e}{\hbar} \right)^2 \left\{ \sum_{kk'} |t_k|^2 |t_{k'}|^2 \int d\tau_1 \int d\tau_2 \right. \\ & \times [g_k^0(\tau_1, \tau) g_{k'}^0(\tau_2, \tau') G(\tau, \tau_1) G(\tau', \tau_2) \\ & - g_k^0(\tau_2, \tau) g_{k'}^0(\tau', \tau_1) G(\tau, \tau_2) G(\tau_1, \tau')] \\ & - g_k^0(\tau, \tau_1) g_{k'}^0(\tau_2, \tau') G(\tau_1, \tau) G(\tau', \tau_2) \\ & \left. + g_k^0(\tau, \tau_1) g_{k'}^0(\tau', \tau_2) G(\tau_1, \tau) G(\tau_2, \tau') \right\} + \text{h.c.} \quad (13.65) \end{aligned}$$

Since the τ_i -integrals are factorized, we can consider them one at a time. Let us examine, say, the first τ_1 -integral in (13.65): $\int d\tau_1 g_k^0(\tau_1, \tau) G(\tau, \tau_1)$. But at first sight the analytic continuation of this term seems ambiguous: there is just one time label, and a lesser/greater part does not seem to have any meaning. However, going back to the origin of this term, the first line in (13.46), we see that that the time τ in g_k^0 must be greater than the time τ in G (because otherwise $c^\dagger(\tau)$ would not be left of $d(\tau)$), and therefore what we really need is

$$\int d\tau_1 g_k^0(\tau_1, \tau^+) t_k^* G(\tau, \tau_1), \quad (13.66)$$

i.e., the *lesser* component of $\int d\tau_1 G(\tau, \tau_1) g_k^0(\tau_1, \tau)$, which is (we reintroduce the central region quantum number n)

$$\begin{aligned} \left[\int d\tau_1 G_n(\tau, \tau_1) t_k^* g_k^0(\tau_1, \tau) \right]^- &= \int dt_1 [G^r(t, t_1) t_k^* g_k^{0,-}(t_1, t) \\ &+ G^<(t, t_1) t_k^* g_k^{0,a}(t_1, t)] \\ &\equiv G_{nk}^<(t, t), \quad (13.67) \end{aligned}$$

i.e., the very same hybrid Green function (12.10) we encountered in Chap. 12 when deriving the expression for current. On the second line of (13.65) we encounter a term with a reverse order of the time labels, which is evaluated as

$$\left[\int d\tau_1 g_{k'}^0(\tau', \tau_1) t_{k'} G_n(\tau_1, \tau') \right]^- = G_{k'n}^<(t', t'). \quad (13.68)$$

The remaining terms in (13.65) can be treated similarly, and we end up with

$$\begin{aligned} S_{\text{dis}}(t, t') &= \left(\frac{e}{\hbar}\right)^2 \sum_{kk'} [t_k t_{k'} G_{nk}^<(t, t) G_{nk'}^<(t', t') - t_k t_{k'}^* G_{nk}^<(t, t) G_{k'n}^<(t', t')] \\ &\quad - t_k^* t_{k'} G_{kn}^<(t, t) G_{nk'}^<(t', t') + t_k^* t_{k'}^* G_{kn}^<(t, t) G_{k'n}^<(t', t')] + \text{h.c.} \\ &= 2 \left(\frac{e}{\hbar}\right)^2 \sum_{kk'} [t_k G_{nk}^<(t, t) - t_k^* G_{kn}^<(t, t)] \\ &\quad \times [t_{k'} G_{nk'}^<(t', t') - t_{k'}^* G_{k'n}^<(t', t')] \equiv 2\langle I_L \rangle^2, \end{aligned} \quad (13.69)$$

thereby exactly canceling the $-2\langle I_L \rangle^2$ term appearing in (13.45). This cancellation was desirable, because otherwise the zero-frequency component $S(\omega = 0)$ would acquire an anomalous zero-frequency delta-peak. We also note that an analogous cancellation occurred in the calculation of electrical conductivity (Chap. 9), where the disconnected part of the current-current correlation function canceled the diamagnetic term which diverges at zero frequency, see (9.18).

13.8.2 The Connected Terms

The remaining terms, which give the noise spectrum within Hartree–Fock approximation (or in any other mean-field approximation), read

$$\begin{aligned} S(\tau, \tau') &= \left(\frac{e}{\hbar}\right)^2 \left\{ \sum_k |t_k|^2 [g_k^0(\tau', \tau)G(\tau, \tau') + g_k^0(\tau, \tau')G(\tau', \tau)] \right. \\ &\quad + \sum_{kk'} |t_k|^2 |t_{k'}|^2 \int d\tau_1 \int d\tau_2 \\ &\quad \times [-g_k^0(\tau_1, \tau)g_{k'}^0(\tau_2, \tau')G(\tau, \tau_2)G(\tau', \tau_1) \\ &\quad + g_k^0(\tau_2, \tau)g_{k'}^0(\tau', \tau_1)G(\tau, \tau')G(\tau_1, \tau_2) \\ &\quad + g_k^0(\tau, \tau_1)g_{k'}^0(\tau_2, \tau')G(\tau', \tau)G(\tau_1, \tau_2) \\ &\quad \left. - g_k^0(\tau, \tau_1)g_{k'}^0(\tau', \tau_2)G(\tau_2, \tau)G(\tau_1, \tau')] \right\} + \text{h.c.} \end{aligned} \quad (13.70)$$

The various terms in (13.70) can be expressed in terms of ring diagrams (see, e.g., [301], or [49]), which also may be used to find ways of going beyond the present level of approximation. We do not pursue this line here, and consider next the analytic continuation of (13.70) and its $\tau > \tau'$ component. For the first two terms the result is obtained readily:

$$\begin{aligned} &[g_k^0(\tau', \tau)G(\tau, \tau') + g_k^0(\tau, \tau')G(\tau', \tau)]_{\tau > \tau'} \\ &= g_k^{0,<}(t', t)G^>(t, t') + g_k^{0,>}(t, t')G^<(t', t). \end{aligned} \quad (13.71)$$

The terms with the double integrations come in two different types. The first one is, which we rearrange slightly,

$$\begin{aligned}
& \left[\int d\tau_1 G(\tau', \tau_1) g_k^0(\tau_1, \tau) \int d\tau_2 G(\tau, \tau_2) g_{k'}^0(\tau_2, \tau') \right]_{\tau > \tau'} \\
&= \int dt_1 [G^r(t', t_1) g_k^{0,r}(t_1, t) + G^<(t', t_1) g_k^{0,a}(t_1, t)] \\
&\quad \times \int dt_2 [G^r(t, t_2) g_{k'}^{0,>}(t_2, t') + G^>(t, t_2) g_{k'}^{0,a}(t_2, t')]. \quad (13.72)
\end{aligned}$$

Analogously, the second type of term is written as

$$\begin{aligned}
& \left[G(\tau, \tau') \int d\tau_1 g_{k'}^0(\tau', \tau_1) G(\tau_1, \tau_2) g_k^0(\tau_2, \tau) \right]_{\tau > \tau'} \\
&= G^>(t, t') \int dt_1 \int dt_2 [g_{k'}^{0,r}(t', t_1) G^r(t_1, t_2) g_k^{0,<}(t_2, t) \\
&\quad + g_{k'}^{0,r}(t', t_1) G^<(t_1, t_2) g_k^{0,a}(t_2, t) \\
&\quad + g_{k'}^{0,<}(t', t_1) G^a(t_1, t_2) g_k^{0,a}(t_2, t)]. \quad (13.73)
\end{aligned}$$

The remaining terms in (13.70) are treated in the same way. The resulting expression contains thirty terms, and there is no need to present it here, because its structure is obvious from the terms discussed above. We note that the results obtained so far would allow a discussion of noise also in a situation where the external fields are time dependent, as has been the case in most examples discussed in this chapter. Alternatively, we could analyze the full frequency dependence of the noise. We do not wish to enter these interesting but rather complicated issues here, and simply consider the zero-frequency component of the noise under stationary conditions. Then, all the time integrals are convolutions, and the zero-frequency noise is simply the frequency integral: $S(0) = \int d(t - t') S(t - t') = \int d\epsilon/(2\pi) [S_1(\epsilon) + S_2(\epsilon)] \equiv S_1 + S_2$, where $S_{1,2}$ are the expressions arising from the $g^0 G$ and $g^0 g^0 GG$ terms, respectively. Explicitly, let us consider S_1 :

$$\begin{aligned}
S_1 &= 2 \left(\frac{e}{\hbar} \right)^2 \int \frac{d\epsilon}{2\pi} \sum_k |t_k|^2 [g_k^{0,<}(\epsilon) G^>(\epsilon) + g_k^{0,>}(\epsilon) G^<(\epsilon)] \\
&= 2 \left(\frac{e}{\hbar} \right)^2 \int \frac{d\epsilon}{2\pi} [i\Gamma_L(\epsilon) n_L(\epsilon) (G^r(\epsilon) - G^a(\epsilon)) \\
&\quad + i\Gamma_L(\epsilon) (2n_L(\epsilon) - 1) G^<(\epsilon)], \quad (13.74)
\end{aligned}$$

where we recalled the definition of the level-width function,

$$\Gamma_L(\epsilon) = 2\pi \sum_k |t_k|^2 \delta(\epsilon - \epsilon_k), \quad (13.75)$$

and eliminated $G^>$ using the relation $G^> - G^< = G^r - G^a$. The factor two comes from the hermitean conjugate. The 28 terms constituting S_2 are treated

in the same way, and we just state the final result:

$$\begin{aligned}
S = & 2 \left(\frac{e}{\hbar} \right)^2 \int \frac{d\epsilon}{2\pi} \left\{ i n_L(\epsilon) \Gamma^L(\epsilon) [G^r(\epsilon) - G^a(\epsilon)] \right. \\
& + i[2n_L(\epsilon) - 1] \Gamma^L(\epsilon) G^<(\epsilon) \\
& + [G^r(\epsilon) - G^a(\epsilon)] n_L(\epsilon) \Gamma^L(\epsilon) [G^r(\epsilon) - G^a(\epsilon)] \Gamma^L(\epsilon) \\
& + [G^r(\epsilon) - G^a(\epsilon)] [2n_L(\epsilon) - 1] \Gamma^L(\epsilon) G^<(\epsilon) \Gamma^L(\epsilon) \\
& - n_L(\epsilon) [1 - n_L(\epsilon)] [G^a(\epsilon) \Gamma^L(\epsilon) G^a(\epsilon) \Gamma^L(\epsilon) + G^r(\epsilon) \Gamma^L(\epsilon) G^r(\epsilon) \Gamma^L(\epsilon)] \\
& + G^<(\epsilon) \Gamma^L(\epsilon) [G^r(\epsilon) - G^a(\epsilon)] \Gamma^L(\epsilon) \\
& \left. + G^<(\epsilon) \Gamma^L(\epsilon) G^<(\epsilon) \Gamma^L(\epsilon) \right\}. \tag{13.76}
\end{aligned}$$

We next make use of the relations derived in Chap. 12:

$$\begin{aligned}
G^<(\epsilon) &= i G^r(\epsilon) [n_L(\epsilon) \Gamma^L(\epsilon) + n_R(\epsilon) \Gamma^R(\epsilon)] G^a(\epsilon), \\
G^r(\epsilon) - G^a(\epsilon) &= -i G^r(\epsilon) [\Gamma^L(\epsilon) + \Gamma^R(\epsilon)] G^a(\epsilon), \\
G^a(\epsilon) \Gamma^L(\epsilon) G^a(\epsilon) \Gamma^L(\epsilon) &+ G^r(\epsilon) \Gamma^L(\epsilon) G^r(\epsilon) \Gamma^L(\epsilon) \\
&= [G^a(\epsilon) - G^r(\epsilon)] \Gamma^L(\epsilon) [G^a(\epsilon) - G^r(\epsilon)] \Gamma^L(\epsilon) \\
&\quad + 2 G^r(\epsilon) \Gamma^L(\epsilon) G^a(\epsilon) \Gamma^L(\epsilon), \\
T(\epsilon) &= \Gamma^L(\epsilon) G^a(\epsilon) \Gamma^R(\epsilon) G^r(\epsilon). \tag{13.77}
\end{aligned}$$

A substitution of these in (13.76) leads to a rather formidable expression:

$$\begin{aligned}
S = & 2 \left(\frac{e}{\hbar} \right)^2 \int \frac{d\epsilon}{2\pi} \left\{ n_L(\epsilon) \Gamma^L(\epsilon) G^r(\epsilon) [\Gamma^L(\epsilon) + \Gamma^R(\epsilon)] G^a(\epsilon) \right. \\
& - [2n_L(\epsilon) - 1] \Gamma^L(\epsilon) G^r(\epsilon) [n_L(\epsilon) \Gamma^L(\epsilon) + n_R(\epsilon) \Gamma^R(\epsilon)] G^a(\epsilon) \\
& - G^r(\epsilon) [\Gamma^L(\epsilon) + \Gamma^R(\epsilon)] G^a(\epsilon) n_L(\epsilon) \Gamma^L(\epsilon) G^r(\epsilon) [\Gamma^L(\epsilon) + \Gamma^R(\epsilon)] \\
& \times G^a(\epsilon) \Gamma^L(\epsilon) + G^r(\epsilon) [\Gamma^L(\epsilon) + \Gamma^R(\epsilon)] G^a(\epsilon) [2n_L(\epsilon) - 1] \Gamma^L(\epsilon) G^r(\epsilon) \\
& \times [n_L(\epsilon) \Gamma^L(\epsilon) + n_R(\epsilon) \Gamma^R(\epsilon)] G^a(\epsilon) \Gamma^L(\epsilon) \\
& - n_L(\epsilon) [1 - n_L(\epsilon)] \{-G^r(\epsilon) [\Gamma^L(\epsilon) + \Gamma^R(\epsilon)] G^a(\epsilon) \\
& \times \Gamma^L(\epsilon) G^r(\epsilon) [\Gamma^L(\epsilon) + \Gamma^R(\epsilon)] G^a(\epsilon) \Gamma^L(\epsilon) + 2 G^r(\epsilon) \Gamma^L(\epsilon) G^a(\epsilon) \Gamma^L(\epsilon)\} \\
& + G^r(\epsilon) [n_L(\epsilon) \Gamma^L(\epsilon) + n_R(\epsilon) \Gamma^R(\epsilon)] G^a(\epsilon) \Gamma^L(\epsilon) G^r(\epsilon) [\Gamma^L(\epsilon) + \Gamma^R(\epsilon)] \\
& \times G^a(\epsilon) \Gamma^L(\epsilon) - G^r(\epsilon) [n_L(\epsilon) \Gamma^L(\epsilon) + n_R(\epsilon) \Gamma^R(\epsilon)] G^a(\epsilon) \\
& \times \Gamma^L(\epsilon) G^r(\epsilon) [n_L(\epsilon) \Gamma^L(\epsilon) + n_R(\epsilon) \Gamma^R(\epsilon)] G^a(\epsilon) \Gamma^L(\epsilon) \Big\}. \tag{13.78}
\end{aligned}$$

Since we expect the final result to be symmetric with respect to $\Gamma^L(\epsilon)$ and $\Gamma^R(\epsilon)$, we know that the coefficients of $\Gamma^L(\epsilon)^4$, $\Gamma^L(\epsilon)^3 \Gamma^R(\epsilon)$, and $\Gamma^L(\epsilon)^2 \Gamma^R(\epsilon)^0$ must vanish. Let us check this:

$$\begin{aligned}
&\Gamma^L(\epsilon)^4 \Gamma^R(\epsilon)^0 : \\
&- n_L(\epsilon) + n_L(\epsilon) [2n_L(\epsilon) - 1] + n_L(\epsilon) [1 - n_L(\epsilon)] + n_L(\epsilon) - n_L(\epsilon)^2 = 0
\end{aligned}$$

$$\begin{aligned}
& \Gamma^L(\epsilon)^3 \Gamma^R(\epsilon) : \\
& -2n_L(\epsilon) + [2n_L(\epsilon) - 1][n_L(\epsilon) + n_R(\epsilon)] \\
& + 2n_L(\epsilon)[1 - n_L(\epsilon)] + n_L(\epsilon) + n_R(\epsilon) - 2n_L(\epsilon)n_R(\epsilon) = 0 \\
& \Gamma^L(\epsilon)^2 \Gamma^R(\epsilon)^0 : \\
& n_L(\epsilon) - [2n_L(\epsilon) - 1]n_L(\epsilon) - 2n_L(\epsilon)[1 - n_L(\epsilon)] = 0
\end{aligned}$$

Thus everything is indeed homogeneous with respect to L/R , and it is easy to identify the transmission coefficient (or its square), and we find

$$\begin{aligned}
S &= 2 \left(\frac{e}{\hbar} \right)^2 \int \frac{d\epsilon}{2\pi} \left\{ n_L(\epsilon)T(\epsilon) - [2n_L(\epsilon) - 1]n_R(\epsilon)T(\epsilon) - n_L(\epsilon)T(\epsilon)^2 \right. \\
&\quad + [2n_L(\epsilon) - 1]n_R(\epsilon)T(\epsilon)^2 + n_L(\epsilon)[1 - n_L(\epsilon)]T(\epsilon)^2 \\
&\quad \left. + n_R(\epsilon)T(\epsilon)^2 - n_R(\epsilon)^2T(\epsilon)^2 \right\} \\
&= 2 \left(\frac{e}{\hbar} \right)^2 \int \frac{d\epsilon}{2\pi} \left\{ \{n_L(\epsilon)[1 - n_L(\epsilon)] + n_R(\epsilon)[1 - n_R(\epsilon)]\}T(\epsilon) \right. \\
&\quad \left. + [n_L(\epsilon) - n_R(\epsilon)]^2T(\epsilon)[1 - T(\epsilon)] \right\}. \tag{13.79}
\end{aligned}$$

Equation (13.79) is a well-known, and important result. The first term accounts for thermal noise (i.e., it vanishes at zero temperature), while the second term is a nonequilibrium term, which vanishes at zero bias. We refer to the review of Blanter and Büttiker [47] for an extended analysis of the various physical consequences; our motivation for presenting its detailed derivation with the nonequilibrium Green function technique is methodological: the expressions presented here can be applied in many situations, for example in connection with ab initio calculations of noise in molecular electronics. Further, with the general approach outlined here, one can use systematic methods to derive noise formulas which apply beyond the effective mean field theories, such as the Hartree–Fock factorization used here.

Part IV

Theory of Ultrafast Kinetics in Laser-Excited Semiconductors

Optical Free-Carrier Interband Kinetics in Semiconductors

Summary. The kinetics of the interband transitions in optically excited semiconductors is discussed and a brief historic review of this field is given. As an introductory example the free-carrier kinetics is formulated in terms of nonequilibrium Green functions, resulting in the semiconductor optical Bloch equations.

14.1 Interband Transitions in Direct-Gap Semiconductors

In Part IV of this book, we want to extend the quantum kinetic theory to the treatment of optical interband kinetics in laser-excited semiconductors. Such a quantum kinetic treatment is particularly relevant for the understanding of the ultrafast time-resolved spectroscopy with semiconductors which has been developed in the last two decades [321]. Laser pulses with a duration of only a few femtoseconds are available, so that one can study experimentally the kinetics of the excited carriers on a femtosecond or picosecond timescale. On these timescales the excited carriers behave, at least to some extent, like coherent quantum-mechanical waves. Another important recent progress in semiconductor physics, namely the development of microstructures with quantum confinement for the carriers on nanometer length scales, further enhances the need for a quantum kinetic description. In these low-dimensional structures, the phase space for phase destroying scattering processes is considerably reduced, so that the coherent behavior of the electronic excitations is more long lived than in bulk materials. For the description of the partially coherent behavior of the optically excited carriers, quantum kinetics is required.

14.1.1 Reduced Density Matrices

For the treatment of the interband quantum kinetics, two methods exist. The first method uses *reduced density matrices* which depend only on one time.

Starting with an equation of motion for the single-particle density matrix, one gets a whole hierarchy of equations of higher and higher density matrices. This hierarchy is truncated on a certain level by factorizing higher-order density matrices into lower ones [335]. Taking a formal integration of the highest considered equation and inserting the resulting density matrix on the next lower level, one gets necessarily integrals over the past of the system. Thus the kinetics becomes non-Markovian with memory integrals. Early applications of this method to ultrafast semiconductor spectroscopy are due to Zimmermann [382, 383], Mukamel [269, 271], Stahl et al. [311], and Kuhn et al. [211, 213, 308, 309]. For the low-excitation regime, a dynamics-controlled truncation scheme for the hierarchy of the density matrix equations has been developed by Axt and Stahl [12]. This method allows to include systematically all contributions up to a certain order in the laser light fields. In recent years, the number of publications in which the density matrix method has been used has increased so strongly that we can quote only some representative investigations which treated the following problems: quantum kinetics of the coupled carrier–phonon system [310], quantum kinetics of dephasing in an exactly solvable two-level model with diagonal electron–phonon interaction [151], coherent control with phase-locked double pulses [13, 148, 151, 338], heavy hole–light hole quantum beats [189, 214], quantum kinetics in spatially inhomogeneous situations [152], quantum kinetics of excitons including exciton–molecule correlations [30, 306, 324], and quantum kinetics for pump–probe as well as hyper-Raman experiments [134, 135].

Only recently Kuhn et al. [374] have pointed out the possibility to treat the screening of the Coulomb interactions also with the density matrix theory. For this end the four-point correlation functions have to be taken into account. This fact was known in plasma physics already as early as 1963 [375]. The advantage of this method is that also screened Coulomb exchange interactions can be included. However the method is so involved that it has not been used for the analysis of femtosecond experiments. The only application has been the study of carrier relaxation in a one-dimensional quantum wire with only one band [374]. The equation of motion technique for the density matrices has recently been used also for interacting bosonic excitons coupled to a cold thermal bath of acoustic phonons [313]. For a sufficiently low bath temperature and a sufficiently high exciton density, the system undergoes a Bose–Einstein condensation. Because the particle spectrum changes from a quadratic one in the normal phase to a phonon-like spectrum in the condensed phase, it is important to use a quantum kinetic description. Only quantum kinetics allows to incorporate the actual particle energies in the scattering integrals self-consistently. Starting with an uncondensed system, the quantum kinetics for the uncondensed and the condensed particles describe the kinetics of condensation. The solutions approach the self-consistent thermal equilibrium Hartree–Fock–Bogoliubov solutions with a finite condensate amplitude asymptotically.

14.1.2 Nonequilibrium Green Functions

Nonequilibrium Green functions – which will be mainly used here – provide an alternative method, as recognized in the eighties, e.g., by Schäfer and Treusch [304]. For femtosecond spectroscopy, a separation in fast and slow temporal variables is no longer possible.

14.1.3 Calculations

of the Two-Time-Dependent Nonequilibrium Green Function

Without further approximations particle propagators which depend on two-time arguments have to be calculated directly from their quantum kinetic equations. Already very early such an ambitious approach has been followed up by Hartmann and Schäfer [137] for a one-pulse excitation and scattering of the excited carriers by longitudinal optical (LO) phonons. In this work [137] $G^<(t, t')$ and $G^>(t, t')$ were calculated as the two independent Green functions (GF), starting with an equilibrium free-particle $G^{0,>}(t - t')$ long before the optical pulse arrived. It is hoped that the error introduced by the approximate initial conditions is cured by integration from a sufficiently remote initial time. Because such a numerical approach is very time consuming, neither a systematic variation of parameters nor an analysis of actual two-pulse experiments was performed at that time. Only later with faster computers, this direct numerical solution of the Kadanoff–Baym equations for the phonon scattering has been picked up again [341] and applied to calculate the four-wave mixing (FWM) signal [305]. The calculations of optical properties of semiconductor with the nonequilibrium Green function theory is described in a textbook by Schäfer and Wegener [307].

Gartner et al. [121, 122] used a different method by calculating $G^<(t, t')$ and $G^r(t, t')$. Because the retarded electron and hole polaron Green functions depend in equilibrium – long before the optical pulses arrived – again only on the time difference, while the particle propagators are zero, i.e., $G_{ee}^< = 0$ and $G_{hh}^< = 0$, it is easy to calculate $G^r(t - t')$ from the Dyson equation for the retarded Green function. These functions serve as initial condition for the calculation of the nonequilibrium Green functions. This initial condition is at least in principle exact. In particular it has been shown that the generalized Kadanoff–Baym ansatz (GKBA) (see Sect. 8.2, and also below) is fulfilled quite well for small polaron coupling constants, while for larger Fröhlich coupling constants $O(\alpha) = 1$ deviations occur. Recent time-resolved differential transmission experiments on CdTe with $\alpha = 0.31$ have therefore been analyzed successfully by directly computing the two-time nonequilibrium Green functions as described above [40]. Meden et al. [258] studied a one-dimensional electron–phonon model, in which, after linearization of the spectrum, the electrons can be described as bosons. This model allows to solve

the electron–phonon quantum kinetics exactly. This model has been incorporated by Zimmermann in the quantum kinetic calculations of a differential transmission spectrum [120]. The above-mentioned dynamic-controlled truncation has also been formulated [221] for the nonequilibrium GF formalism.

Considerable work also went into the direct solution of the Kadanoff–Baym equation for electron–electron scattering [45, 53, 218–220], however only with the use of an equilibrium random-phase approximation (RPA) screening which has even been taken in the static approximation. At least in the femtosecond regime such an approach is not consistent, because as it has been shown by early work of El Sayed et al. [99] and more rigorously by Bányai et al. [22], that the buildup of screening after the pulse needs some time which is of the order of an inverse plasma frequency in the system of excited carriers. In Bányai et al. [22], the two-time-dependent RPA-screened Coulomb interaction potential has been calculated self-consistently together with the quantum kinetics of the carriers which have been treated by one-time density matrices as will be discussed below in more detail.

A complete calculation within two-time electron Green functions and two-time screened interaction potentials is still missing. Because RPA is not a conserving approximation [32, 33], one obtains in the full two-time quantum kinetics a $q \rightarrow 0$ divergence in the RPA intraband-polarization loop. Gartner et al. [123] showed that this divergence can be eliminated by a vertex correction in the polarization loop. The vertex has to be calculated from a Bethe–Salpeter equation in the screened ladder approximation. Because of the complexity of these equations, numerical solutions have not yet been obtained.

A different attempt to solve the quantum kinetic equation without the use of the GKBA (see Sect. 14.1.4) is due to Kalvová and Velický [192–194], at least for a simple semiconductor model with impurity scattering only.

14.1.4 Replacement of Two-Time Propagators by a One-Time Density Matrix and a Two-Time Spectral Function

The majority of calculations for actual two-beam femtosecond experiments used a different approach. They treated only the quantum kinetic equation for the equal-time particle propagator $G^<(t, t)$ which is up to a factor i the single-particle density matrix. However, the self-energy of this Kadanoff–Baym equation introduces a coupling to off-diagonal Green functions in the time arguments. In a pioneering paper, Lipavsky et al. [246] have generalized the Kadanoff–Baym ansatz for Green functions from frequency space to its real-time representation in nonequilibrium: According to this GKBA, the two-time particle propagator is given approximately by the density matrix at the earlier time (say t') times a retarded Green function $G^r(t, t')$, which describes the correlation between different times. The idea of this approach is that at least in the weak-coupling case, one can then use relatively simple approximations for the retarded Green functions after the causality is built in correctly. Later the GKBA has been proven by explicit calculations [121] to hold very well for

small electron-LO-phonon coupling constants α_e . Thus for the model semiconductor, GaAs with $\alpha_e = 0.06$, on which most of the femtosecond pulse spectroscopy experiments have been performed, the GKBA is a very good approximation [121]. With the use of the GKBA one gets a closed quantum kinetic equation for the single-particle density matrix which contains scattering integrals, showing that quantum kinetics on short timescales is non-Markovian. This one-time approach for the Green function quantum kinetics has first been used for the cases in which the interaction with LO-phonons dominates the relaxation and dephasing kinetics [20,140,217]. Successively the Coulomb Hartree–Fock interaction has been taken into account [346]. In these early theories, the retarded (and advanced) Green functions have been taken in a free-particle Wigner–Weisskopf approximation, i.e., using a free-particle equilibrium GF with an additional exponential damping. Successively, it has been recognized that much better results can be obtained if the retarded Green function is calculated from its Dyson equation under the influence of the mean-field interactions, i.e., the Coulomb Hartree–Fock interaction and the self-consistent interaction with the coherent optical pulses [347,349].

This self-consistent theory has been applied to the calculation of FWM experiments on GaAs with 15 fs pulses [21,294,337,368]. Due to the partially coherent dynamics in the scattering integrals, the theory predicts oscillations on top of the decaying time-integrated FWM signal due to the interference of interband-polarization components which are coupled by the exchange of a LO-phonon in the conduction band. The observation of these oscillations [21] was the first direct evidence of the real-time quantum kinetics, a striking effect which cannot be understood using the semiclassical Boltzmann-type scattering rates. The exponential Wigner–Weisskopf damping of the retarded Green functions has also been recognized to be an oversimplification. The retardations typical for quantum kinetics on timescales smaller than the period of a lattice oscillation imply that the damping starts in a Gaussian form which only at later times approaches an exponential decay. As an analytical approximation a hyperbolic secant law has been shown to reproduce this scenario rather well [147], justifications have been obtained by numerical calculations of the polaron-retarded Green function [23,121]. Differential transmission spectroscopy (DTS) with the time-resolved buildup of phonon cascades of Leitnerstorfer et al. [120] have been analyzed in Schmenkel et al. [312]. It has been shown that the experiment can only be explained by the retarded quantum kinetical scattering integrals and not by the instantaneous Boltzmann scattering rates. Furthermore, coherence effects between the pump and probe beam – both taken from a two-color laser – had to be taken into account in a quantitative analysis.

The quantum kinetics in the high-density regime is governed by electron–electron scattering. Because many-body effects such as screening can be treated best in the Green function formalism, this approach has been used intensively to describe the high-density resonant femtosecond experiments. A review by Binder and Koch [44] emphasizes the use of the second Born

approximation so far applied mainly in the Markovian limit of the electron quantum kinetics. The general quantum kinetics with a two-time-dependent screened Coulomb potential and one-time density matrices has been formulated in Haug and Ell [145]. These studies of the ultrashort-time regime of the Coulomb quantum kinetics have all been done in the so-called GW-approximation for the scattering self-energies, because of the complexity of the momentum integrations of the vertex contribution. Early attempts to calculate, e.g., the time-integrated FWM signal treated only the initial time interval by using a bare Coulomb potential, assuming that the considered times were too short to have already a substantial screening [99]. In fact the predictions of that model, particularly a polarization decay according to $\exp(-(t/t_0)^3)$, coincided well with the semiclassical treatment of the dephasing of an electron–hole pair function in a random potential [131]. However, this law has never been observed experimentally indicating that the regime of a bare Coulomb interaction is not accessible by experiments even with pulses as short as 10 fs, because with short intensive femtosecond pulses the buildup times for screening get very short, too. Only for relatively low densities and short delay times, the bare Coulomb potential quantum kinetics resulted for DTS experiments [72] in a qualitatively good description of the experiment.

As mentioned above, the buildup kinetics of a screened Coulomb potential was calculated by El Sayed et al. [100] using mean-field semiconductor Bloch equations to determine the density and distribution of the excited carriers which cause the screening. It has been shown that a plasmon pole is formed in the effective screened potential in roughly an inverse plasma frequency. However this building up of the screening is a rather continuous process. Bányai et al. [22] finally calculated both the two-time-dependent screened Coulomb potential and the resulting quantum kinetics of electron relaxation and interband-polarization dephasing self-consistently. Applications of this theory to femtosecond DTS experiments for larger density and delay regimes [355] resulted in a generally good agreement, applications to the 11 fs FWM experiments of Wegener et al. in bulk GaAs [159] and quantum well GaAs [266] yielded an excellent agreement with the time-resolved FWM signals. They changed from a photon echo at earlier delay times to an induced polarization decay at longer delay times. This change of the time-resolved FWM signals is a direct manifestation of the buildup of a collective plasma from a gas of individual, uncorrelated carriers. The time-integrated signal both in three-dimensional and two-dimensional decayed according to theory and experiment with an inverse dephasing time which varies as $n^{1/3}$. Recently Vu et al. [356] applied the time-dependent screening to both the LO-phonon mediated interaction and to the Coulomb interaction and calculated self-consistently a two-time-dependent potential which shows two resonances corresponding to mixed phonon–plasmon modes. Applying coherent control to the resonant 11 fs FWM experiment, Wegener et al. have been able to observe these predicted oscillations superimposed on the decay of the time-integrated FWM signal [357]. The observed oscillation frequency follows for

varying excitation density the upper branch of the mixed phonon–plasmon mode, for which the calculated effective potential is strongest.

Femtosecond experiments with an optical pump and a delayed THz probe beam [160] in GaAs have confirmed this screening scenario by measuring directly the spectrum of the inverse dielectric function as a function of the delay time. The plasmon resonance is seen indeed to build up in the order of 100 fs. This experiment can be seen also as a direct observation of the buildup of a correlated plasma or of the dressing of particles with a polarization cloud [141]. Recent optical pump and THz probe experiments in InP [161] and their quantum kinetical analysis showed the evolution of the whole phonon–plasmon mixed-mode spectrum in time. In particular the observed vanishing of the optical phonon resonance at the LO frequency as the plasma resonance is formed and the reappearance at later delay times at the TO frequency is well reproduced by improved quantum kinetical calculations in which polaron effects are incorporated and in which the numerical accuracy of the time and frequency-dependent retarded interaction potential is increased by calculating it directly and not via the scattering components $V^<$ and $V^>$.

Recently, several applications of quantum kinetics to the transient optical properties of quantum dots embedded in a two-dimensional wetting layer or quantum well have been published. For the coupling of the quantum dot carriers to optical phonons, the detailed phonon side mode spectra have been calculated by Jahnke et al. [318], while the trapping and dephasing kinetics by phonon-assisted processes and by Auger processes with a two-time-dependent Coulomb potential has been studied for neutral quantum dots by Vu et al. [359]. In the scattering kinetics between continuum states and localized dot states, one has to orthogonalize the involved states [24].

With this short and certainly not complete historical review over the rather active field of quantum kinetics for ultrafast semiconductor spectroscopy, we conclude this introductory section. This review shows that the field, although not much more than one decade old, has already reached a certain level of maturity and is able to provide a good understanding of most of the presently performed ultrafast spectroscopic studies on semiconductors. Particularly, as far as the calculations of the two-time electron quantum kinetics are concerned, the field is still waiting for further progress.

In the following we will limit ourselves, for simplicity, to a classical description of the laser light field, but the photon kinetics can, in principle, also be included in a full quantum kinetic theory of the photons and the electrons in a semiconductor (see, e.g., the work of Henneberger and Koch [150]). The quantization of the light field is needed in all situations where spontaneous emission of photons has to be considered, e.g., in the theory of semiconductor luminescence in the form developed by Kira and Koch [201]. The basic interaction of the electric field $E(t)$ of laser light with the valence electrons of a semiconductor is a dipole interaction. The spatial variation of the light field can often be neglected because the wavelength is usually much larger than other relevant length scales, e.g., the crystal cell. In second

quantization for the electrons, the dipole interaction with a classical light field is given by

$$H_I = \int d^3x \psi^\dagger(\mathbf{x}) e \mathbf{x} \cdot \mathbf{E}(t) \psi(\mathbf{x}), \quad (14.1)$$

where $\psi(\mathbf{x})$ is the electron field operator. This operator is expanded into the single-particle eigenfunctions of the electrons (introductory text books are [9, 203, 250]). For bulk material one has

$$\psi(\mathbf{x}) = \frac{1}{\sqrt{L^3}} \sum_{\mu, \mathbf{k}} a_{\mu, \mathbf{k}} e^{i\mathbf{k} \cdot \mathbf{x}} u_{\mu, \mathbf{k}}(\mathbf{x}), \quad (14.2)$$

where $e^{i\mathbf{k} \cdot \mathbf{x}}$ is the slowly varying envelope plane wave of a freely propagating electron, and $u_{\mu, \mathbf{k}}(\mathbf{x})$ is the lattice periodic Bloch function of the band μ and the crystal momentum \mathbf{k} . In a mesoscopic semiconductor microstructure, the plane wave factor is replaced by the eigenfunctions of the electrons in the confinement potential, while the Bloch function remains essentially unchanged [31, 146]. For a quantum well layer perpendicular to the z -direction, e.g., the electron field operator is therefore

$$\psi(\mathbf{x}) = \frac{1}{\sqrt{L^2}} \sum_{n\mu, \mathbf{k}_\parallel} a_{n\mu, \mathbf{k}_\parallel} \phi_{n\mu}(z) e^{i\mathbf{k}_\parallel \cdot \mathbf{x}} u_{\mu, \mathbf{k}}(\mathbf{x}), \quad (14.3)$$

where $\phi_{n\mu}(z)$ is the n th envelope function of an electron belonging to band μ in the well potential. The momentum vector is given by $\mathbf{k} = \mathbf{k}_\parallel + k_n \mathbf{e}_z$, where k_n is the expectation value of the z -component of the momentum in state n . If all electrons are within one subband, say with $n = 1$, one speaks about a quasi-two-dimensional system. In the element semiconductor of group IV, and the isoelectronic compound semiconductors of the groups III–V, II–VI, and I–VII, the valence electrons are described by the sp^3 orbitals. Close to the center of the Brillouin zone, the conduction band is built from s -states, while the p -states form the top of three valence bands. Between these states the optical transitions are dipole allowed. As far as optics is concerned the direct-gap semiconductors, in which the extrema of the empty conduction band and of the filled valence bands are both at the Γ point, are of particular interest. These materials are in zeroth approximation transparent for light with a frequency smaller than the fundamental gap E_g of the semiconductor, but strongly absorbing for light with a frequency above the gap. For simplicity, here we treat only a two-band model of a semiconductor with a conduction band c and only one valence band v . We refer to the literature [9, 71, 203] for all problems connected with the presence of three valence bands, which are partly degenerated at the Γ point.

The interaction with the electric field $\mathbf{E}(t)$ of a light pulse introduces optical transitions between the valence band v and the conduction band c . The time-dependent dipole interaction Hamiltonian, e.g., in a bulk semiconductor, is in this simple situation:

$$H_I(t) = - \sum_{\mathbf{k}} E(t) \left(d_{\mathbf{k}} a_{c,k}^\dagger a_{v,k} + \text{h.c.} \right). \quad (14.4)$$

Here, h.c. denotes the hermitian conjugate of the preceding term and $d_{\mathbf{k}}$ is the projection of the dipole matrix element in the field direction \mathbf{e}_E between the Bloch states:

$$d_{\mathbf{k}} = e \int d^3x u_{c,k}^* \mathbf{e}_E \cdot \mathbf{x} u_{v,k} \simeq d. \quad (14.5)$$

As indicated, one can disregard the k -dependence of the dipole matrix element in the vicinity of the Γ point. In order to simplify the notation we will suppress the vector notation, wherever not absolutely necessary. For the laser light field we will assume the form

$$E(t) = E_0(t) \cos(\omega t), \quad (14.6)$$

where ω is the central frequency of the pulse. The time-dependent amplitude $E_0(t)$ describes a laser pulse with a width δt and a peak amplitude E_0 . Typically the pulses have the form of a Gaussian or of a hyperbolic secant

$$E_0(t) = E_0 e^{-((t-t_0)/\delta t)^2} \quad \text{or} \quad E_0(t) = \frac{E_0}{\cosh((t-t_0)/\delta t)}. \quad (14.7)$$

Often we take into account only the resonant terms of the interaction, namely

$$H_I(t) \simeq -\frac{1}{2} \sum_{\mathbf{k}} E_0(t) \left(d_{\mathbf{k}} a_{c,k}^\dagger a_{v,k} e^{-i\omega t} + \text{h.c.} \right). \quad (14.8)$$

This is the so-called *rotating-wave approximation*. Sometimes the interaction Hamiltonian is used without the factor 1/2, so that the effective field amplitudes differ by this factor in the two conventions.

The energies of the electrons can, in the vicinity of the Γ point, be described by the effective mass m_e of the electrons in the conduction band and m_h of the holes in the valence band:

$$e_{c,k} = \frac{E_g}{2} + \frac{k^2}{2m_e} = \frac{E_g}{2} + \varepsilon_{e,k} \quad (14.9)$$

and

$$e_{v,k} = -\frac{E_g}{2} - \frac{k^2}{2m_h} = \frac{E_g}{2} - \varepsilon_{h,k}. \quad (14.10)$$

14.2 Free-Carrier Kinetics Under Laser-Pulse Excitation

As an introductory example we will disregard all interactions of the excited electrons and holes and treat the free-carrier interband kinetics of a two-band direct-gap semiconductor. This simple model will be shown to lead to the optical Bloch equations of a semiconductor which will serve as an important

paradigm in the whole field of the ultrafast kinetics of laser-pulse excited semiconductors. The relevant nonequilibrium electron Green functions in a spatially homogeneous crystal are now 2×2 matrices in the band index

$$G_{\mu\nu,k}(t_1, t_2) = -i \left\langle T_C \left\{ a_{\mu,k}(t_1) a_{\nu,k}^\dagger(t_2) \right\} \right\rangle, \quad (14.11)$$

with $\{\mu, \nu\} = \{c, v\}$. The time arguments and the time-ordering operator T_C are defined on the contour C . The self-energy of this nonequilibrium electron Green function can be written as

$$\begin{aligned} \Sigma_{\mu\nu,k}(t_1, t_2) = & \Sigma_{\mu\nu,k}^\delta(t_1, t_2) + \theta(t_1 - t_2) \Sigma_{\mu\nu,k}^>(t_1, t_2) \\ & + \theta(t_2 - t_1) \Sigma_{\mu\nu,k}^<(t_1, t_2). \end{aligned} \quad (14.12)$$

The singular part of the self-energy Σ^δ has to be treated separately, as discussed, e.g., by Danielewicz [90]. It is given by

$$\Sigma_{\mu\nu,k}^\delta(t_1, t_2) = \Sigma_{\mu\nu,k}^s(t_1) \delta(t_1 - t_2). \quad (14.13)$$

With the self-energy (14.12), the two Dyson equations for the particle propagator become according to (5.3), where the potential U plays the role of the singular self-energy,

$$G_0^{-1} G^< = \Sigma^\delta G^< + \Sigma^r G^< + \Sigma^< G^a \quad (14.14)$$

and

$$G^< G_0^{-1} = G^< \Sigma^\delta + G^r \Sigma^< + G^< \Sigma^a. \quad (14.15)$$

Subtracting the two equations of motion and putting $t_1 = t_2 = t$ yields (5.4):

$$\begin{aligned} [G_0^{-1}, G^<]_{t_1=t_2=t} = & [\Sigma^\delta, G^<] + \Sigma^r G^< - G^< \Sigma^a \\ & + \Sigma^< G^a - G^r \Sigma^<. \end{aligned} \quad (14.16)$$

As an introductory example we treat free carriers only. Naturally many-body techniques are not required for such a simple case, elementary equation of motion techniques are sufficient. In order to get some practice with the many-body techniques in the multiband situation, we also treat this case with the nonequilibrium Green function method. The only remaining interaction in this problem is that of the electrons with the light pulse. It gives rise to a singular self-energy in the form

$$\Sigma_{\mu\nu,k}^s(t) = -dE(t) \sigma_\mu^x, \quad (14.17)$$

with the Pauli matrix $\sigma^x = \begin{pmatrix} 0 & 1 \\ 1 & 0 \end{pmatrix}$, while the nonsingular parts of Σ are zero. Here, $E(t)$ is the real electric light field (14.4). With (14.17) the equation of motion for $G_{\mu\nu,k}^<(t, t)$ becomes explicitly

$$\left(i \frac{\partial}{\partial t} - (e_{\mu,k} - e_{\nu,k}) \right) G_{\mu\nu,k}^<(t, t)$$

$$= -dE(t) \sum_{\varrho} (\sigma_{\mu\varrho}^x G_{\varrho\nu,k}^<(t,t) - G_{\mu\varrho,k}^<(t,t) \sigma_{\varrho\nu}^x). \quad (14.18)$$

First, we see that in this simple case a closed equation for the reduced density matrices $G_{\mu\nu,k}^<(t,t)$ results. The diagonal elements of the density matrix simply define the electron distribution for μ, k

$$G_{\mu\mu,k}^<(t,t) = i \langle a_{\mu,k}^\dagger(t) a_{\mu,k}(t) \rangle = i \varrho_{\mu\mu,k}(t) = i n_{\mu,k}(t), \quad (14.19)$$

where $\varrho_{\mu\mu,k}$ is the diagonal element of the density matrix:

$$\varrho_{\mu\nu,k}(t) = \langle a_{\nu,k}^\dagger(t) a_{\mu,k}(t) \rangle. \quad (14.20)$$

Electron distributions can be measured optically, e.g., with linear gain and absorption spectroscopy or with luminescence spectroscopy. However, in order to obtain the electron distributions from such spectra, one always needs some theoretical analysis in terms of a line shape theory. The off-diagonal elements ($\mu \neq \nu$)

$$G_{\mu\nu,k}^<(t,t) = i \langle a_{\nu,k}^\dagger(t) a_{\mu,k}(t) \rangle = i \varrho_{\mu\nu,k}(t) \quad (14.21)$$

are the interband-polarization components. $\varrho_{cv,k}$, e.g., describes the annihilation of a conduction band electron and the creation of a valence band electron. The relation

$$\varrho_{\nu\mu,k}(t) = \langle a_{\mu,k}^\dagger(t) a_{\nu,k}(t) \rangle = \varrho_{\mu\nu,k}^*(t) \quad (14.22)$$

holds. The physical polarization of the medium by a light beam can be obtained from (14.1) and (14.2). One gets in the two-band model for a real dipole moment d_k :

$$P(t) = \sum_k d_k [\varrho_{vc,k}(t) + \varrho_{cv,k}(t)]. \quad (14.23)$$

The measurement of the coherent polarization requires techniques of nonlinear optical spectroscopy, e.g., time-resolved FWM. In such an experiment the incoming beams create a laser-induced lattice. The light which is diffracted from this lattice is determined by a certain component of the polarization. Therefore, transient FWM experiments provide relatively direct means to observe the time development of the polarization.

In terms of the polarization and the densities, we get the optical interband kinetic equations:

$$\left(\frac{\partial}{\partial t} + i(e_{c,k} - e_{v,k}) \right) \varrho_{cv,k}(t) = -i dE(t) (\varrho_{cc,k}(t) - \varrho_{vv,k}(t)), \quad (14.24a)$$

$$\frac{\partial}{\partial t} \varrho_{cc,k}(t) = -\frac{\partial}{\partial t} \varrho_{vv,k}(t) = -i dE(t) (\varrho_{cv,k}(t) - \varrho_{vc,k}(t)). \quad (14.24b)$$

The complex conjugate of (14.24a) yields the equation for $\varrho_{vc,k}$. According to (14.6), the light field is of the form $E = (1/2)E_0(t)[\exp(i\omega t) + \exp(-i\omega t)]$.

Note that often the field is defined without the factor $1/2$ in front, then the resulting field-dependent terms in the Bloch equations also differ by such a factor. Introducing the electron–hole pair energy

$$e_{c,k} - e_{v,k} = e_k \quad (14.25)$$

with

$$e_k = E_g + \varepsilon_k \quad \text{and} \quad \varepsilon_k = \varepsilon_{e,k} + \varepsilon_{h,k} = \frac{k^2}{2\mu}; \quad \frac{1}{\mu} = \frac{1}{m_e} + \frac{1}{m_h}, \quad (14.26)$$

where μ is the reduced electron–hole mass, and taking only the resonant terms into account (rotating-wave approximation) we get, e.g.,

$$\begin{aligned} e^{i\omega t} \left(\frac{\partial}{\partial t} + ie_k \right) \varrho_{cv,k}(t) &= \left(\frac{\partial}{\partial t} - i(\omega - e_k) \right) \varrho_{cv,k}(t) e^{i\omega t} \\ &= -\frac{i}{2} \omega_R(t) (\varrho_{cc,k}(t) - \varrho_{vv,k}(t)). \end{aligned} \quad (14.27)$$

Introducing the slowly varying interband-polarization component P_k , the detuning δ_k , and the Rabi frequency ω_R by

$$P_k(t) = \varrho_{cv,k}(t) e^{i\omega t}, \quad \delta_k = e_k - \omega, \quad \omega_R(t) = dE_0(t), \quad (14.28)$$

the equations of motion with additional phenomenological damping terms become for the interband-polarization component and for the electron distribution

$$\frac{\partial}{\partial t} P_k = \frac{\partial P_k}{\partial t} \Big|_{coh} - \frac{P_k}{T_2}, \quad (14.29a)$$

$$\frac{\partial}{\partial t} \varrho_{cc,k}(t) = \frac{\partial \rho_{cc,k}}{\partial t} \Big|_{coh} - \frac{\varrho_{cc,k}(t)}{T_1}. \quad (14.29b)$$

The coherent unitary time evolution under the action of the coherent light pulse is according to (14.24a), (14.24b), and (14.27) given by

$$\frac{\partial P_k}{\partial t} \Big|_{coh} = -i\delta\omega_k P_k - \frac{i}{2} \omega_R(t) (\varrho_{cc,k}(t) - \varrho_{vv,k}(t)), \quad (14.30a)$$

$$\frac{\partial \rho_{cc,k}}{\partial t} \Big|_{coh} = \omega_R(t) \text{Im} P_k(t). \quad (14.30b)$$

In order to get a first understanding of the influence of relaxation processes, we included the relaxation times T_1 for the densities and T_2 for the polarization simply by hand. T_1 and T_2 are called the longitudinal and transversal relaxation times, respectively. The relaxation term for the electron density of the valence band is $-(\varrho_{vv,k} - 1)/T_1$, because this density relaxes toward the full valence band. Naturally, it will be the major task of quantum kinetics to replace these simple phenomenological relaxation terms by a more appropriate description of the relaxation processes.

14.3 The Optical Free-Carrier Bloch Equations

Now one can introduce the three real components of the Bloch vector \mathbf{U}_k

$$U_{1k} = 2\text{Re}P_k(t), \quad U_{2k} = 2\text{Im}P_k(t), \quad U_{3k} = \varrho_{cc,k}(t) - \varrho_{vv,k}(t). \quad (14.31)$$

The first two components refer to the real and imaginary part of the interband-polarization components. The third component is the inversion.

One gets the following equations of motion:

$$\frac{\partial U_{1k}}{\partial t} = -\Gamma_{11}U_{1k} + \delta_k U_{2k}, \quad (14.32a)$$

$$\frac{\partial U_{2k}}{\partial t} = -\Gamma_{22}U_{2k} - \delta_k U_{1k} - \omega_R(t)U_{3k}, \quad (14.32b)$$

$$\frac{\partial U_{3k}}{\partial t} = -\Gamma_{33}(U_{3k} + 1) + \omega_R(t)U_{2k}, \quad (14.32c)$$

with the phenomenological damping constants:

$$\Gamma_{11} = \Gamma_{22} = \frac{1}{T_2}, \quad \Gamma_{33} = \frac{1}{T_1}. \quad (14.33)$$

These equations are the optical Bloch equations, which have been used intensively in the optics of two-level atoms [4, 265, 325]. Note that the inversion relaxes to the full valence band, i.e., $U_{3k} \rightarrow -1$. The Bloch equations can be put into a simple vector equation

$$\frac{\partial \mathbf{U}_k}{\partial t} = -\boldsymbol{\Gamma} \cdot (\mathbf{U}_k + \mathbf{e}_3) + \boldsymbol{\Omega} \times \mathbf{U}_k, \quad (14.34)$$

where the vector of the rotation frequency is

$$\boldsymbol{\Omega} = \omega_R(t)\mathbf{e}_1 - \delta_k \mathbf{e}_3 \quad (14.35)$$

and the diagonal damping matrix is

$$\Gamma_{ij} = \Gamma_{ii}\delta_{ij}. \quad (14.36)$$

From classical mechanics we know that

$$\frac{\partial \mathbf{r}}{\partial t} = \boldsymbol{\Omega} \times \mathbf{r} \quad (14.37)$$

describes the rotation of the vector \mathbf{r} around the vector of the angular velocity $\boldsymbol{\Omega}$. Disregarding damping for a moment, the rotation alone does not change the length of the Bloch vector. In the ground state the Bloch vector is $\mathbf{U}_k = -\mathbf{e}_3$, i.e., its length is 1. The light field and the detuning cause a rotation of this unit vector. The field-induced rotations around the \mathbf{e}_1 -axis are called *Rabi flops*. A rectangular pulse of width $\omega_R\Delta t = \pi/2$, e.g., turns the Bloch vector from the ground state to an angle of $\pi/2$ around the \mathbf{e}_1 -axis to $\mathbf{U}_k = \mathbf{e}_2$.

A $\pi/2$ pulse thus generates from the ground state a maximum polarization. For a finite detuning δ_k , the polarization will then start to rotate around the $-\mathbf{e}_3$ -axis. The dispersion of the electron energies in the bands automatically introduces a spread of energies. In atomic systems the spread in energies is due to an inhomogeneous broadening. The facts that a finite pulse can turn the Bloch vector through a certain angle and that the detuning causes a further rotation are the basic ideas for photon echo experiments. Suppose a $\pi/2$ pulse has induced an initial polarization $U_{1k}(0) = 0, U_{2k}(0) = 1$. How does it decay after the pulse? Assuming for simplicity that $T_2 \ll T_1$, the equations with $\omega_R = 0$ which describe this free induction decay are

$$\frac{\partial}{\partial t} U_{2k} = -\delta_k U_{1k} - \frac{U_{2k}}{T_2}, \quad \frac{\partial}{\partial t} U_{1k} = +\delta_k U_{2k} - \frac{U_{1k}}{T_2} \quad (14.38)$$

with the solutions

$$\begin{pmatrix} U_{1k}(t) \\ U_{2k}(t) \end{pmatrix} = \begin{pmatrix} \cos \delta_k t & \sin \delta_k t \\ -\sin \delta_k t & \cos \delta_k t \end{pmatrix} \begin{pmatrix} U_{1k}(0) \\ U_{2k}(0) \end{pmatrix} e^{-t/T_2}. \quad (14.39)$$

Figure 14.1 shows schematically how the polarization spirals for a finite detuning δ_k according to (14.39) around the z -axis after the excitation with a $\pi/2$ pulse. Because of the dispersion in detuning, $\delta_k = e_k - \omega$, the polarization of electron-hole pairs with different k -values will rotate with different rotation frequencies. If we apply after the time t_1 a light pulse which causes a rotation of the Bloch vector around the \mathbf{e}_1 -axis through an angle π , we keep the Bloch vector in the $x - y$ plane. A polarization component which rotated in the time t_1 through the angle α will find itself after the π pulse at the angle $-\alpha$. As all polarization components continue to rotate around $-\mathbf{e}_3$ with δ_k , they will all return to the origin after the time $2t_1$. The coherent superposition of

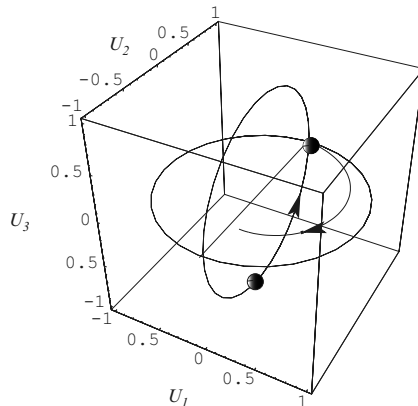


Fig. 14.1. Schematic plot of the rotation of the Bloch vector under a rectangular $\pi/2$ pulse and a finite detuning for $T_2 \ll T_1$

all polarization components will cause the emission of a light pulse, the so-called *photon echo*. Naturally, the intensity of the photon echo will decrease with time as $[\exp(-2t_1/T_2)]^2 = \exp(-4t_1/T_2)$. By varying the time delay t_1 between the two pulses, one can measure the transverse relaxation time T_2 with a photon echo experiment.

Interband Quantum Kinetics with LO-Phonon Scattering

Summary. The interband quantum kinetics is formulated for the scattering of the excited electrons and holes by a thermal bath of optical phonons. A series of approximations is developed for the required retarded functions, including a discussion of the band splitting introduced by a resonant intense laser beam. It is shown that the damping by LO-phonons can be described well with a hyperbolic secant. Finally strategies for the numerical solutions of the quantum kinetic equations are discussed.

15.1 Derivation of the Interband Quantum Kinetic Equations

We extend the treatment of the interband kinetics of Chap. 14 by taking additionally into account the scattering of the carriers by longitudinal optical (LO) phonons following Haug [140]. In polar semiconductors this interaction is responsible for the first rapid stage of the cooling of hot carriers on a subpicosecond timescale. The final stage of the cooling process due to the scattering with acoustic phonons occurs on a nanosecond timescale. The influence of the LO-phonon scattering on the line shape of emission and absorption spectra of polar semiconductors is correspondingly large. We assume that the density of the carriers which are excited by the light pulse is low enough so that carrier–carrier scattering as well as the screening of the electron–phonon interaction can be neglected. Because even in the low-density limit Coulomb interactions modify the band edge spectra of semiconductors strongly, we take the Coulomb mean-field interactions in form of the Hartree–Fock (HF) self-energy into account. This self-energy describes excitonic effects and the leading part of the density-dependent band gap renormalization. The bare Coulomb potential is an instantaneous interaction of the form $V_q(t, t') = V_q \delta(t - t') = \frac{4\pi e^2}{\varepsilon_0 q^2} \delta(t - t')$, where ε_0 is the background dielectric constant of the unexcited crystal. Note

that we are using cgs units. The contribution of the bare Coulomb potential to the singular HF self-energy $\Sigma_k^s(t)$ introduced in Chap. 14 is

$$\Sigma_{\mu\nu,k}^{\text{HF}}(t) = - \sum_q V_q (\rho_{\mu\nu,k-q} - \delta_{\mu,\nu} \delta_{\mu,q}). \quad (15.1)$$

This is the exchange or Fock interaction energy which can be obtained most directly from the Hamiltonian of the Coulomb interaction

$$H^C = \frac{1}{2} \sum_{\mu\nu,k,k',q} V_q a_{\mu,k+q}^\dagger a_{\nu,k'-q}^\dagger a_{\nu,k'} a_{\mu,k} \quad (15.2)$$

by taking all finite expectation values for pairs of operators. In a spatially homogeneous situation, the direct Coulomb terms (Hartree self-energy) with $q = 0$ do not contribute because of charge neutrality, i.e., $N_e = \sum_k n_{e,k} = \sum_k n_{h,k} = N_h$. Thus one gets from (15.2)

$$H^{C,\text{HF}} = - \sum_{\mu\nu,k,q} V_q (\rho_{\mu\nu,k-q} - \delta_{\mu,\nu} \delta_{\nu,q}) a_{\nu,k}^\dagger a_{\mu,k}. \quad (15.3)$$

The exchange contributions give just the Fock self-energy (15.1), where additionally the exchange interaction with the full valence band is subtracted, because it has already been taken into account in the band structure calculation. The diagonal parts of the HF self-energy are for the conduction band the electron exchange energy $\Sigma_{cc,k}^{\text{HF}}(t) = - \sum_q V_q \rho_{cc,k-q}(t)$ and for the valence band the hole exchange energy $\Sigma_{vv,k}^{\text{HF}}(t) = + \sum_q V_q \rho_{hh,k-q}(t)$, with the hole distribution function $\rho_{hh,k}(t) = 1 - \rho_{vv,k}(t)$. The off-diagonal parts of the HF self-energy $\Sigma_{cv,k}^{\text{HF}}(t) = - \sum_q V_q \rho_{cv,k-q}(t)$ describe the attractive electron–hole interaction. This term in the interband-polarization equation introduces the exciton resonances in the spectrum.

The generalized Kadanoff–Baym equation (14.16) for the two-band particle propagator $G_{\mu\nu,k}^<(t, t') = i \langle a_{\nu,k}^\dagger(t') a_{\mu,k}(t) \rangle$ is in the equal-time limit given by

$$\begin{aligned} & \left(i \frac{\partial}{\partial t} - e_{\mu,k} + e_{\nu,k} \right) G_{\mu\nu,k}^<(t, t) \\ &= -dE(t) \sum_\varrho \left(\sigma_{\mu\varrho}^x G_{\varrho\nu,k}^<(t, t) - G_{\mu\varrho,k}^<(t, t) \sigma_{\varrho\nu}^x \right) \\ &+ \sum_\rho \left(\Sigma_{\mu\rho,k}^{\text{HF}}(t) G_{\varrho\nu,k}^<(t, t) - G_{\mu\rho,k}^<(t, t) \Sigma_{\varrho\nu,k}^{\text{HF}}(t) \right) \\ &+ \sum_\varrho \int_{-\infty}^t dt' \left(\Sigma_{\mu\varrho,k}^>(t, t') G_{\varrho\nu,k}^<(t', t) - \Sigma_{\mu\varrho,k}^<(t, t') G_{\varrho\nu,k}^>(t', t) \right. \\ &\quad \left. - G_{\mu\varrho,k}^>(t, t') \Sigma_{\varrho\nu,k}^<(t', t) + G_{\mu\varrho,k}^<(t, t') \Sigma_{\varrho\nu,k}^>(t', t) \right), \end{aligned} \quad (15.4)$$

where we used the relations (4.20) and (4.21) to express the advanced and retarded Green functions in terms of the particle propagators. Splitting the time development again in a coherent part and in a scattering part

$$\frac{\partial}{\partial t} = \left. \frac{\partial}{\partial t} \right|_{\text{coh}} + \left. \frac{\partial}{\partial t} \right|_{\text{scatt}}, \quad (15.5)$$

we find the coherent evolution of the density matrix from the first three lines of (15.4) as

$$\begin{aligned} \left. \frac{\partial \rho_{\mu\nu,k}}{\partial t} \right|_{\text{coh}} &= -i(\varepsilon_{\mu,k} - \varepsilon_{\nu,k}) \rho_{\sigma\nu,k} \\ &\quad - i \sum_{\sigma} (\sigma_{\mu\sigma}^x (d_k E(t) - \Sigma_{\mu\sigma,k}^{\text{HF}}) \rho_{\sigma\nu,k} \\ &\quad - \rho_{\mu\sigma,k} (d_k E(t) - \Sigma_{\sigma\nu,k}^{\text{HF}}) \sigma_{\sigma\nu}^x), \end{aligned} \quad (15.6)$$

where we used the decomposition of the unit matrix $1_{\mu\nu} = \delta_{\mu\nu} + \sigma_{\mu\nu}^x$ in order to separate the terms which are renormalizing the energy

$$\varepsilon_{\mu,k} = e_{\mu,k} + \Sigma_{\mu\mu,k}^{\text{HF}} \quad (15.7)$$

from those which renormalize the Rabi frequency

$$\Omega_{R,k} = d_k E_0(t) - \Sigma_{\mu\sigma \neq \mu,k}^{\text{HF}}. \quad (15.8)$$

For the electron distribution and the slowly varying interband-polarization component $P_k(t) = \rho_{cv,k}(t)e^{i\omega t}$, the coherent mean-field equation can be put into the form for free carrier with renormalized energies $\varepsilon_{\mu,k}$ and a renormalized Rabi frequency $\Omega_R(t)$

$$\left. \frac{\partial \rho_{cc,k}}{\partial t} \right|_{\text{coh}} = +\text{Im}(\Omega_{R,k}^*(t) P_k(t)), \quad (15.9a)$$

$$\left. \frac{\partial P_k}{\partial t} \right|_{\text{coh}} = -i\delta\omega_k(t) P_k - \frac{i}{2} \Omega_{R,k}(t) (\varrho_{cc,k}(t) - \varrho_{vv,k}(t)), \quad (15.9b)$$

where the HF energies are explicitly given by

$$\begin{aligned} \varepsilon_{c,k}(t) &= e_{c,k} - \sum_q V_q \rho_{cc,k}(t), \\ \varepsilon_{v,k}(t) &= e_{v,k} - \sum_q V_q (\rho_{vv,k}(t) - 1), \end{aligned} \quad (15.10)$$

which results in the time-dependent detuning

$$\delta\omega_k(t) = \varepsilon_{c,k}(t) - \varepsilon_{v,k}(t) - \omega. \quad (15.11)$$

The Rabi frequency is modified by the inner field due to the attractive electron-hole interaction, which for low excitation causes the exciton resonances

$$\Omega_{R,k}(t) = d_k E_0(t) + 2 \sum_q V_q P_{k-q}(t). \quad (15.12)$$

Equations (15.9a) and (15.9b) are also called the semiconductor Bloch equations. The last two lines of (15.4) describe the influence of scattering processes. The only new feature of the scattering terms in (15.4) compared to those of Part III is that now both $G^<$ and $\Sigma^<$ are matrices with respect to the band index. For the scattering self-energies, we will take into account only the self-consistent, time-dependent Hartree–Fock contribution due to carrier scattering with a thermal bath of LO-phonons. Under these simplifications the scattering with the LO-phonons is a particularly simple model, mainly because the LO frequency $\omega_q \simeq \omega_0$ can be taken to be constant. By considering the phonons as a given thermal bath, we neglect the changes of the population, the dispersion and the interaction matrix element of the phonons. If these effects – which are known to be important in the relaxation of hot carriers [320] – have to be included, an equation for the kinetics of the phonons has to be added, and the self-energies have to be calculated more accurately. In the self-consistent generalized Hartree–Fock approximation, the scattering self-energy matrix is given by the left diagram of Fig. 15.1. The vertex corrections, shown in the right diagram of Fig. 15.1, are not included in the theory for the following reasons: The semiconductor GaAs for which most of the femtosecond experiments and calculations have been performed is a material with weak electron–phonon coupling. The dimensionless polaron interaction constant is small, i.e., $\alpha \ll 1$. Thus their contribution of the order $O(\alpha^2)$ is small. In general, however, vertex corrections can become important for larger coupling constants. The scattering self-energy therefore is

$$\Sigma_{\mu_\varrho, k}^<(t_1, t_2) = i \sum_q g_q^2 D_q^<(t_1, t_2) G_{\mu_\varrho, k-q}^<(t_1, t_2), \quad (15.13)$$

where only the unperturbed phonon propagators are considered

$$D_q^{0<}(t_1, t_2) = -i \sum_{\pm} N_q^{\pm} e^{\pm i\omega_0(t_1-t_2)}, \quad D_q^{0>}(t_1, t_2) = -D_q^{0<}(t_1, t_2)^*, \quad (15.14)$$

with $N_q^{\pm} = N + \frac{1}{2} \pm \frac{1}{2} = \binom{N+1}{N}$. $N = 1/(e^{\omega_0/k_B T} - 1)$ is the thermal phonon distribution and g_q is the Fröhlich interaction matrix element which is given by

$$g_q^2 = \frac{\omega_0 V_q}{2} \left(\frac{1}{\varepsilon_{\infty}} - \frac{1}{\varepsilon_0} \right), \quad (15.15)$$



Fig. 15.1. (a) Self-consistent Hartree–Fock diagram. (b) Leading vertex correction. *Full lines:* electron propagators, *dashed lines:* phonon propagators

where $V_q = 4\pi e^2/q^2V$ is the Coulomb potential. It is convenient to express the interaction matrix element in terms of the dimensionless polaron constant α

$$g_q^2 = \alpha \frac{4\pi(\omega_0)^{3/2}}{(2\mu)^{1/2}q^2V}, \quad \alpha = e^2 \left(\frac{\mu}{2\omega_0} \right)^{1/2} \left(\frac{1}{\varepsilon_\infty} - \frac{1}{\varepsilon_0} \right). \quad (15.16)$$

Here μ is, again, the reduced electron-hole mass. Inserting these expressions into the two-band quantum kinetic equation (15.4), we find with $i\varrho_{\mu\nu,k}(t) = G_{\mu\nu,k}^<(t,t)$ the scattering rate:

$$\frac{\partial \varrho_{\mu\nu,k}}{\partial t} \Big|_{\text{scatt}} = - \sum_{q,\varrho,\pm} g_q^2 N_q^\pm \int_{-\infty}^t dt' \quad (15.17)$$

$$\begin{aligned} & \times \left(e^{\mp i\omega_0(t-t')} \left(G_{\mu\varrho,k-q}^>(t,t') G_{\varrho\nu,k}^<(t',t) - G_{\mu\varrho,k}^>(t,t') G_{\varrho\nu,k-q}^<(t',t) \right) \right. \\ & \left. - e^{\pm i\omega_0(t-t')} \left(G_{\mu\varrho,k-q}^<(t,t') G_{\varrho\nu,k}^>(t',t) - G_{\mu\varrho,k}^<(t,t') G_{\varrho\nu,k-q}^>(t',t) \right) \right). \end{aligned}$$

We see that the last scattering terms in the second and third line are obtained from the preceding terms by interchanging $\mathbf{k} \leftrightarrow \mathbf{k} - \mathbf{q}$, so that (15.17) can be written more concisely as

$$\begin{aligned} \frac{\partial \varrho_{\mu\nu,k}}{\partial t} \Big|_{\text{scatt}} = & - \sum_{q,\varrho,\pm} g_q^2 N_q^\pm \int_{-\infty}^t dt' \left[\left(e^{\mp i\omega_0(t-t')} \right. \right. \\ & \times G_{\mu\varrho,k-q}^>(t,t') G_{\varrho\nu,k}^<(t',t) \\ & \left. \left. - e^{\pm i\omega_0(t-t')} G_{\mu\varrho,k-q}^<(t,t') G_{\varrho\nu,k}^>(t',t) \right) \right. \\ & \left. - (\mathbf{k} \leftrightarrow \mathbf{k} - \mathbf{q}) \right]. \quad (15.18) \end{aligned}$$

In order to reduce the two-time propagators on the RHS of (15.18), we use the GKBA (8.13) of Lipavský et al. [246] which reads in its multiband extension [140]:

$$\begin{aligned} & -iG_{\mu\nu,k}^<(t_1, t_2) \\ & = \sum_{\sigma} \left(G_{\mu\sigma,k}^r(t_1, t_2) G_{\sigma\nu,k}^>(t_2, t_2) - G_{\mu\sigma,k}^>(t_1, t_1) G_{\sigma\nu,k}^a(t_1, t_2) \right) \\ & = \pm i \sum_{\sigma} \left(G_{\mu\sigma,k}^r(t_1, t_2) \varrho_{\sigma\nu,k}^>(t_2) - \varrho_{\mu\sigma,k}^>(t_1) G_{\sigma\nu,k}^a(t_1, t_2) \right), \quad (15.19) \end{aligned}$$

where $\varrho^>$ are given by

$$\varrho_{\mu\nu,k}^<(t) = \langle a_{\nu,k}^\dagger(t) a_{\mu,k}(t) \rangle = \varrho_{\mu\nu,k}(t),$$

$$\varrho_{\mu\nu,k}^>(t) = \left\langle a_{\mu,k}(t) a_{\nu,k}^\dagger(t) \right\rangle = \delta_{\mu\nu} - \varrho_{\mu\nu,k}(t). \quad (15.20)$$

The retarded (advanced) functions $G^{r(a)}$ are given by

$$\begin{aligned} G_{\mu\nu,k}^r(t, t') &= -i\theta(t - t') \left\langle \left\{ a_{\mu,k}(t), a_{\nu,k}^\dagger(t') \right\} \right\rangle, \\ G_{\mu\nu,k}^a(t, t') &= i\theta(t' - t) \left\langle \left\{ a_{\mu,k}(t), a_{\nu,k}^\dagger(t') \right\} \right\rangle, \end{aligned} \quad (15.21)$$

and obey the relation

$$G_{\mu\nu,k}^a(t, t') = (G_{\nu\mu,k}^r(t', t))^*. \quad (15.22)$$

The connection between the two-point particle propagators and the reduced density matrix, therefore, is according to (15.19)

$$G_{\mu\nu,k}^<(t_1, t_2) = - \sum_{\sigma} (G_{\mu\sigma,k}^r(t_1, t_2) \varrho_{\sigma\nu,k}(t_2) - \varrho_{\mu\sigma,k}(t_1) G_{\sigma\nu,k}^a(t_1, t_2)) \quad (15.23)$$

and

$$\begin{aligned} G_{\mu\nu,k}^>(t_1, t_2) &= \sum_{\sigma} (G_{\mu\sigma,k}^r(t_1, t_2) (\delta_{\sigma\nu} - \varrho_{\sigma\nu,k}(t_2)) \\ &\quad - (\delta_{\mu\sigma} - \varrho_{\mu\sigma,k}(t_1)) G_{\sigma\nu,k}^a(t_1, t_2)). \end{aligned} \quad (15.24)$$

In contrast to the usual Kadanoff–Baym ansatz, the relations (15.23) and (15.24) take the causality correctly into account in the sense that the two-time particle propagator develops from its equal-time limit at the earlier time, according to the appropriate Green function. For $t_1 > t_2$ the time development is given by the retarded Green function $G^r(t_1, t_2)$, while for $t_2 > t_1$ it is governed by the advanced function $G^a(t_1, t_2)$. These relations are exact for noninteracting particles. In fact GKBA (15.19) is also exact for systems which are described by a mean-field Hamiltonian. The self-energy of such systems is singular (i.e., proportional to $\delta(t - t')$); their scattering, or, equivalently, in the Keldysh index off-diagonal, self-energies vanish. As Lipavský et al. [246] have shown, the correction term to (15.19) is proportional to the scattering self-energies, therefore (15.19) is also exact for the mean-field part of any Hamiltonian which does not produce any scattering. Note that, in the equal-time limit, the off-diagonal (in band index) Green functions $G^r(t_1, t_2)$ and $G^a(t_1, t_2)$ vanish, because the equal-time anticommutators vanish for these functions. Therefore, the equal-time limit of the GKBA also remains exact in the matrix extension.

The validity of the GKBA has been checked by comparing the numerical results for the two-time-dependent nonequilibrium Green functions with and without this approximation [121]. It has been found that the GKBA holds excellently for weak polar coupling, but becomes increasingly inaccurate as the polar coupling constant α increases to the intermediate coupling regime with values of $\alpha \simeq 1$.

Naturally, this ansatz still contains the two-time retarded and advanced Green functions. The philosophy of the further development is that, after the causality has been built in properly, one can now use relatively simple approximations for the two-time retarded/advanced Green functions. Using the generalized GKBA in the form (15.23) and (15.24), one can cast the resulting scattering integrals in the following form:

$$\begin{aligned} \frac{\partial \varrho_{\mu\nu,k}}{\partial t} \Big|_{\text{scatt}} &= - \sum_{q,\sigma\tau,\pm} g_q^2 \int_{-\infty}^t dt' \left(\left\{ G_{\mu\sigma,k-q}^r(t,t') G_{\tau\nu,k}^a(t',t) e^{\pm i\omega_0(t-t')} \right. \right. \\ &\quad \times (N_q^\mp (\delta_{\sigma\varrho} - \varrho_{\sigma\varrho,k-q}(t')) \varrho_{\varrho\tau,k}(t') \\ &\quad \left. \left. - N_q^\pm \varrho_{\sigma\varrho,k-q}(t') (\delta_{\varrho\tau} - \varrho_{\varrho\tau,k}(t')) \right\} - \{\mathbf{k} \leftrightarrow \mathbf{k} - \mathbf{q}\} \right) \quad (15.25) \end{aligned}$$

$$\begin{aligned} &= - \sum_{q,\sigma\tau,\pm} g_q^2 \int_{-\infty}^t dt' \left(\left\{ G_{\mu\sigma,k-q}^r(t,t') G_{\tau\nu,k}^a(t',t) e^{\pm i\omega_0(t-t')} \right. \right. \\ &\quad \times \left. \left. \left(N_q^\mp \varrho_{\sigma\tau,k}(t') - N_q^\pm \varrho_{\sigma\tau,k-q}(t') \pm \sum_\varrho \varrho_{\sigma\varrho,k-q}(t') \varrho_{\varrho\tau,k}(t') \right) \right\} \right. \\ &\quad \left. - \{\mathbf{k} \leftrightarrow \mathbf{k} - \mathbf{q}\} \right). \quad (15.26) \end{aligned}$$

In (15.26) the non-Markovian structure of the quantum kinetic collision terms becomes clear. The memory kernel of these equations is given by

$$G_{\mu\sigma,k-q}^r(t,t') G_{\tau\nu,k}^a(t',t) e^{\pm i\omega_0(t-t')}, \quad (15.27)$$

all density matrices enter only at the earlier time t' . The quantum mechanical correlations and the quantum coherence contained in the spectral functions are the origin of the memory of the system.

The non-Markovian nature of these equations is important not only in ultrashort pulse spectroscopy but also in stationary spectroscopy, provided the short-time correlations are involved. One example is the theory of the linear absorption tail – the so-called *Urbach tail* – below the band gap of a semiconductor. In linear spectroscopy, the densities may be approximated by $\varrho_{cc,k} = 0$ and $\varrho_{vv,k} = 1$ so that one is left with the equation for the polarization. The nearly universally observed exponential decay of the absorption below the exciton with decreasing light frequency cannot be explained using a Markovian damping for the polarization $\varrho_{cv,k}$, because it gives rise to a power law $\propto \omega^{-2}$ in the low-energy wing of the exciton resonance. The description of the exponential Urbach tail needs (even in a phenomenological theory) a non-Markovian damping term of the form

$$\int_{-\infty}^t dt' \sum_{k'} \gamma_{k,k'}(t-t') \varrho_{cv,k'}(t'), \quad (15.28)$$

as has been noted by Bánya et al. [19] and Haug et al. [143] in connection with the nonresonant optical Stark effect in the Urbach tail region. The quantum kinetics of the polarization (15.26) provides the formal derivation of such damping terms with memory structure which result in an exponential absorption tail due to phonon-assisted transitions, as will be demonstrated later. Because the exponential Urbach tail extends over a broad frequency range, it tests the short-time correlations and explains why quantum kinetics is even necessary in this classical problem of stationary, linear spectroscopy! The characteristic reaction time of the phonon system is given by the inverse phonon frequency $t_{\text{ph}} = 2\pi/\omega_0$. For times shorter than the phonon reaction time t_{ph} , the dissipation due to phonons becomes very small. This rapid decrease of the damping is taken into account in the delayed quantum kinetic description.

In order to proceed further, we have to evaluate the Green functions $G_{\mu\sigma,k-q}^{\text{r}}(t, t')$ and $G_{\tau\nu,k}^{\text{a}}(t', t)$ at least approximately.

15.2 The Spectral Green Functions $G_{\mu\nu}^{\text{r}}$ and $G_{\mu\nu}^{\text{a}}$

The retarded and advanced Green functions defined in (15.21) obey the relation (15.22), therefore only one of the two spectral functions has to be calculated. The retarded Green function, e.g., obeys a nonequilibrium Dyson equation. With $G_{\mu,k}^{0,-1}(t) = i\frac{\partial}{\partial t} - e_{\mu,k}$, the differential form of the Dyson equation for the retarded Green function is (we use the times t_1, t_2 , and $t_{12} = t_1 - t_2$)

$$\begin{aligned} G_{\mu,k}^{0,-1}(t_1)G_{\mu\nu,k}^{\text{r}}(t_1, t_2) &= \delta_{\mu,\nu}\delta(t_{12}) - dE(t_1) \sum_{\sigma} \sigma_{\mu\sigma}^x G_{\sigma\nu,k}^{\text{r}}(t_1, t_2) \\ &\quad + \sum_{\sigma} \Sigma_{\mu\sigma,k}^{\text{HF}}(t_1)G_{\sigma\nu,k}^{\text{r}}(t_1, t_2) \\ &\quad + \sum_{\sigma} \int_{t_2}^{t_1} dt_3 \Sigma_{\mu\sigma,k}^{\text{r}}(t_1, t_3)G_{\sigma\nu,k}^{\text{r}}(t_3, t_2), \end{aligned} \quad (15.29)$$

with the initial condition $G_{\mu\nu,k}^{\text{r}}(t_2, t_2) = \delta_{\mu,\nu}$. In the following we will discuss some increasingly sophisticated approximations for the retarded Green function.

15.2.1 Free-Particle Retarded Green Function

Neglecting the field term, the Hartree–Fock term, and the retarded electron–phonon self-energy in (15.29), we find the free-particle solution

$$G_{\mu\nu,k}^{\text{r}}(t_1, t_2) = -i\delta_{\mu,\nu}\theta(t_{12})e^{-ie_{\mu,k}t_{12}}. \quad (15.30)$$

This approximation is diagonal in the band index, oscillates with the free electron energies, and does not contain any dissipative decay.

In the quantum kinetics for femtosecond pulse spectroscopy, this free-particle approximation is often insufficient. The coherent laser pulse will mix the valence and conduction band states and induce off-diagonal elements in G^r . This coupling will renormalize further the particle spectra by light-intensity-dependent optical Stark shifts. The Coulomb interaction between the excited carriers will result in electron-density-dependent shifts of the single-particle energies and will introduce excitonic effects. Furthermore, often one has to include the dephasing of the coherence by the considered collisions, as will be discussed further below.

15.2.2 Time-Dependent Retarded GF in Mean-Field Approximation

In order to include the time-dependent band mixing due to the coherent laser pulse, i.e., the optical Stark effect, and the mean-field Coulomb effects (15.1), we neglect the scattering processes and treat only the mean-field Hamiltonian

$$H = \sum_{\mu\nu,k} H_{\mu\nu,k} a_{\mu,k}^\dagger a_{\nu,k}, \quad (15.31)$$

with

$$H_{\mu\nu,k} = e_{\mu,k} \delta_{\mu\nu} - dE(t) \sigma_{\mu\nu}^x + \Sigma_{\mu\nu,k}^{\text{HF}}(t), \quad (15.32)$$

or in the rotating-wave approximation

$$H_{\mu\nu,k} = \varepsilon_{\mu,k}(t) \delta_{\mu\nu} - \frac{1}{2} \sigma_{\mu\nu}^+ (\Omega_R(t) e^{-i\omega t} + \text{h.c.}), \quad (15.33)$$

with the HF-renormalized energies $\varepsilon_{\mu,k}(t)$ of (15.10) and Rabi frequency $\Omega_R(t)$ of (15.12). Here we use the Pauli matrices

$$\sigma^x = \begin{pmatrix} 0 & 1 \\ 1 & 0 \end{pmatrix}, \quad \sigma^y = \begin{pmatrix} 0 & -i \\ i & 0 \end{pmatrix}, \quad \sigma^z = \begin{pmatrix} 1 & 0 \\ 0 & -1 \end{pmatrix}, \quad (15.34)$$

and $\sigma^+ = \frac{1}{2}(\sigma^x + i\sigma^y) = \begin{pmatrix} 0 & 1 \\ 0 & 0 \end{pmatrix}$. The Heisenberg equation for the operator $a_{\mu,k}(t)$ yields

$$\dot{a}_{\mu,k} = -i \sum_{\rho} H_{\mu\rho,k}(t) a_{\rho,k}(t). \quad (15.35)$$

We eliminate the rapid oscillations with the transformation

$$a_{\mu,k}(t) = e^{-i\Delta_{\mu,k}(t)} \tilde{a}_{\mu,k}(t), \quad (15.36)$$

where the transformation phase function $\Delta_{\mu,k}(t)$ has still to be determined. The transformed equations are

$$\dot{\tilde{a}}_{\mu,k} = -i \sum_{\nu} \left[(\varepsilon_{\nu,k} - \dot{\Delta}_{\nu,k}) \delta_{\mu\nu} \right]$$

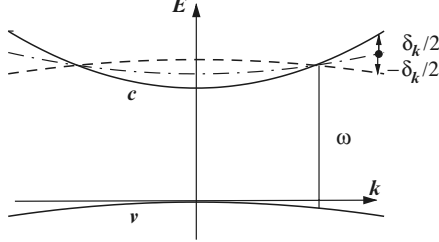


Fig. 15.2. Under coherent resonant excitation, the HF-renormalized valence band plus one photon energy ω (dashed line) is resonant with the HF-renormalized conduction band. From the dashed-dotted reference line the transformed conduction and valence band electrons have the symmetrical energies $\pm \frac{1}{2}\delta_k$, where δ_k is the detuning (15.39) for a given k value

$$+ \frac{1}{2} \left(\Omega_R \sigma_{\mu\nu}^+ e^{i(\Delta_{\mu,k} - \Delta_{\nu,k} - \omega t)} + \text{h.c.} \right) \tilde{a}_{\nu,k}. \quad (15.37)$$

We require that the oscillations of the field term in (15.37) vanish:

$$\Delta_{c,k}(t) - \Delta_{v,k}(t) - \omega t = 0. \quad (15.38)$$

Furthermore we demand that, after the transformation, the renormalized conduction and valence band energies in (15.37) are symmetrically given by one half of the detuning $\delta_k(t)$ (see Fig. 15.2)

$$\delta_k(t) = (\varepsilon_{c,k}(t) - \varepsilon_{v,k}(t) - \omega), \quad (15.39)$$

i.e.,

$$\varepsilon_{c,k} - \dot{\Delta}_{c,k} = \frac{1}{2}\delta\omega_k, \quad \varepsilon_{v,k} - \dot{\Delta}_{v,k} = -\frac{1}{2}\delta\omega_k. \quad (15.40)$$

From (15.38) to (15.40), one gets the phase functions as

$$\Delta_{c,k}(t) = \frac{1}{2} \left(\int_{-\infty}^t dt' (\varepsilon_{c,k}(t') + \varepsilon_{v,k}(t')) - \omega t \right), \quad (15.41a)$$

$$\Delta_{v,k}(t) = \frac{1}{2} \left(\int_{-\infty}^t dt' (\varepsilon_{c,k}(t') + \varepsilon_{v,k}(t')) + \omega t \right). \quad (15.41b)$$

The transformed unitary equation of motion is

$$\dot{\tilde{a}}_{\mu,k} = -\frac{i}{2} \sum_{\nu} \left(\sigma_{\mu\nu}^z \delta\omega_k(t) - (\Omega_R(t) \sigma_{\mu\nu}^+ + \text{h.c.}) \right) \tilde{a}_{\nu,k}(t). \quad (15.42)$$

We solve the linear equation (15.42) with the unitary time-development matrix $U_{\mu\nu,k}(t, t_0)$

$$\tilde{a}_{\mu,k}(t) = \sum_{\nu} U_{\mu\nu,k}(t, t_0) \tilde{a}_{\nu,k}(t_0), \quad (15.43)$$

where $t_0 \rightarrow -\infty$ is a remote initial time before the crystal is excited by the light pulse. Thus $U_{\mu\nu,k}(t_0, t_0) = \delta_{\mu\nu}$. The unitary matrix obeys the orthogonality relations

$$\sum_{\rho} U_{\mu\rho,k}(t, t') U_{\nu\rho,k}^*(t, t') = \delta_{\mu\nu}. \quad (15.44)$$

The matrix $U_k(t)$ obeys the equation-of-motion

$$\dot{U}_{\mu\nu,k}(t, t_0) = -\frac{i}{2} \sum_{\rho} (\sigma_{\mu\rho}^z \delta\omega_k(t) - (\Omega_R(t) \sigma_{\mu\rho}^+ + \text{h.c.})) U_{\rho\nu,k}(t, t_0). \quad (15.45)$$

The orthogonality relation can be fulfilled with the following coherence coefficients

$$\begin{aligned} U_{cc,k}(t) &= u_k(t), & U_{vv,k}(t) &= u_k^*(t), \\ U_{cv,k}(t) &= v_k(t), & U_{vc,k}(t) &= v_k^*(t), \end{aligned} \quad (15.46)$$

where we dropped for simplicity the time $t_0 \rightarrow -\infty$. The coefficients obey the Fermion relation

$$|u_k(t)|^2 + |v_k(t)|^2 = 1. \quad (15.47)$$

For $t \rightarrow t_0 \rightarrow -\infty$, the normal coefficients $u_k \rightarrow 1$ and the anomalous coefficients $v_k \rightarrow 0$. The coefficients $u_k(t)$ and $v_k(t)$ which result from the integration of (15.45) still contain rapid oscillations. One can get slowly varying variables by introducing the angles ϕ, ψ , and α :

$$u_k(t) = e^{i\phi_k(t)} \cos(\alpha_k(t)), \quad v_k(t) = e^{i\psi_k(t)} \sin(\alpha_k(t)). \quad (15.48)$$

The retarded Green function is finally given in terms of the unitary matrix $U_k(t, t_0)$ by the relation

$$G_{\mu\nu,k}^r(t_1, t_2) = -i\Theta(t_{12}) \sum_{\rho} U_{\mu\rho,k}(t_1, t_0) U_{\nu\rho,k}^*(t_2, t_0) e^{-i\Delta_{\mu,k} t_{10} + i\Delta_{\nu,k} t_{20}}. \quad (15.49)$$

The result (15.49) contains the time-dependent optical Stark effect, band gap renormalizations, and excitonic correlations [347]. An explicit numerical solution can only be obtained from a simultaneous self-consistent solution of the mean-field Dyson equation for the retarded GFs and the quantum kinetic equation for the density matrix.

15.2.3 Spectra of Retarded Gfs for Stationary Resonant Excitation: Light-Induced Gaps, Two-Band Mollow Triplet

Before we proceed to analyze the time dependence of the retarded GFs, we will calculate their spectra under intense stationary light fields, because the knowledge of these spectra is important to guide our intuition even for ultrashort

pulse spectroscopy. Furthermore, for this problem the two-time retarded Green function can be calculated analytically. We start with the left- and right-hand version of the Dyson equation for the retarded Green function of Sect. 7.3. Adding these two equations yields (we drop the momentum index k because it is not altered under the considered light-matter interaction)

$$\left(i \frac{\partial}{\partial t_1} - e_\mu \right) G_{\mu,\nu}^r(t_1, t_2) + \left(-i \frac{\partial}{\partial t_2} - e_\nu \right) G_{\mu,\nu}^r(t_1, t_2) \quad (15.50)$$

$$= 2\delta_{mu,\nu}\delta(t_1 - t_2) + \Sigma_{\mu,\rho}^r(t_1)G_{\rho,\nu}^r(t_1, t_2) + G_{\mu,\rho}^r(t_1, t_2)\Sigma_{\rho,\nu}^r(t_2). \quad (15.51)$$

The singular self-energy due to the interaction with the stationary light field $E(t) = E_0 \cos(\omega_0 t)$ is

$$\Sigma_{\mu,\nu}^r(t) = -d_{\mu,\nu}E(t)\sigma_{\mu,\nu}^x. \quad (15.52)$$

Introducing relative and center-of-mass coordinates $\sigma = t_1 - t_2$ and $\tau = (t_1 + t_2)/2$ with $t_{1,2} = \tau \pm \frac{\sigma}{2}$ and $\frac{\partial}{\partial t_{1,2}} = \frac{1}{2}\frac{\partial}{\partial \tau} \pm \frac{\partial}{\partial \sigma}$, we find

$$\left(i \frac{\partial}{\partial \sigma} - e_\mu \right) G_{\mu,\nu}^r(\sigma, \tau) + \left(i \frac{\partial}{\partial \tau} - e_\nu \right) G_{\mu,\nu}^r(\sigma, \tau) \quad (15.53)$$

$$= 2\delta_{mu,\nu}\delta(\sigma) + \Sigma_{\mu,\rho}^r\left(\tau + \frac{\sigma}{2}\right)G_{\rho,\nu}^r(\sigma, \tau) + G_{\mu,\rho}^r(\sigma, \tau)\Sigma_{\rho,\nu}^r\left(\tau - \frac{\sigma}{2}\right). \quad (15.54)$$

One can easily select the terms which are resonant with $\omega_0 = e_c - e_v$. Next we take the Fourier transform with respect to the relative coordinate $G^r(\tau, \omega) = \int_{-\infty}^0 d\sigma e^{i\omega\sigma} G^r(\tau, \sigma)$ and find

$$\begin{aligned} & (\omega - e_\mu)G_{\mu,\nu}^r(\omega, \tau) + (\omega - e_\nu)G_{\mu,\nu}^r(\omega, \tau) \\ &= 2\delta_{mu,\nu} - \frac{1}{2}d_{\mu,\rho}E_0 \left(G_{\rho,\nu}^r\left(\omega + \frac{\omega_0}{2}, \tau\right) e^{i\omega_0\tau} + G_{\rho,\nu}^r\left(\omega - \frac{\omega_0}{2}, \tau\right) e^{-i\omega_0\tau} \right) \\ & \quad - \left(G_{\mu,\rho}^r\left(\omega - \frac{\omega_0}{2}, \tau\right) e^{i\omega_0\tau} + G_{\mu,\rho}^r\left(\omega + \frac{\omega_0}{2}, \tau\right) e^{-i\omega_0\tau} \right) \frac{1}{2}d_{\rho,\nu}E_0. \end{aligned} \quad (15.55)$$

We pick out only the resonant terms and get

$$\begin{aligned} 2(\omega - e_c)G_{cc}^r(\omega, \tau) &= 2 - \frac{1}{2}d_{cv}E_0G_{vc}^r\left(\omega - \frac{\omega_0}{2}, \tau\right) e^{-i\omega_0\tau} \\ & \quad - G_{cv}^r\left(\omega - \frac{\omega_0}{2}, \tau\right) e^{i\omega_0\tau} \frac{1}{2}d_{vc}E_0, \end{aligned} \quad (15.56)$$

$$\begin{aligned} (\omega - e_c)G_{cv}^r(\omega, \tau) + (\omega - e_v)G_{cv}^r(\omega, \tau) &= -\frac{1}{2}d_{cv}E_0G_{vv}^r\left(\omega - \frac{\omega_0}{2}, \tau\right) e^{-i\omega_0\tau} \\ & \quad - G_{cc}^r\left(\omega + \frac{\omega_0}{2}, \tau\right) e^{-i\omega_0\tau} \frac{1}{2}d_{vc}E_0, \end{aligned} \quad (15.57)$$

and

$$\begin{aligned} 2(\omega - e_v)G_{vv}^r(\omega, \tau) &= 2 - \frac{1}{2}d_{vc}E_0G_{vc}^r\left(\omega + \frac{\omega_0}{2}, \tau\right)e^{i\omega_0\tau} \\ &\quad - G_{vc}^r\left(\omega + \frac{\omega_0}{2}, \tau\right)e^{-i\omega_0\tau}\frac{1}{2}d_{vc}E_0. \end{aligned} \quad (15.58)$$

We see that the only remaining time dependence is connected with the interband elements G_{cv}^r and G_{vc}^r . They are driven by the coherent light field, so that the expressions

$$g_{cv}^r(\omega) = G_{cv}^r(\omega, \tau)e^{i\omega_0\tau}, \quad g_{vc}^r(\omega) = G_{vc}^r(\omega, \tau)e^{-i\omega_0\tau} \quad (15.59)$$

are independent of time. One can get a closed system of equations if one shifts the conduction band down by the amount $\frac{\omega_0}{2}$ and the valence band up by the same amount. The resulting equations are (with $d_{cv} = d_{vc} = d$ and $G_\rho^{-1}(\omega) = \omega - e_\rho$)

$$G_c^{-1}\left(\omega + \frac{\omega_0}{2}\right)G_{cc,k}^r\left(\omega + \frac{\omega_0}{2}\right) + \frac{dE_0}{4}(g_{cv}(\omega) + g_{vc}(\omega)) = 1, \quad (15.60)$$

$$G_v^{-1}\left(\omega - \frac{\omega_0}{2}\right)G_{vv,k}^r\left(\omega - \frac{\omega_0}{2}\right) + \frac{dE_0}{4}(g_{cv}(\omega) + g_{vc}(\omega)) = 1, \quad (15.61)$$

$$\begin{aligned} &\left(G_c^{-1}\left(\omega + \frac{\omega_0}{2}\right) + G_v^{-1}\left(\omega - \frac{\omega_0}{2}\right)\right)g_{cv,k}^r(\omega) \\ &+ \frac{dE_0}{4}\left(G_{vv}\left(\omega - \frac{\omega_0}{2}\right) + G_{cc}^r\left(\omega + \frac{\omega_0}{2}\right)\right) = 0, \end{aligned} \quad (15.62)$$

$$\begin{aligned} &\left(G_c^{-1}\left(\omega + \frac{\omega_0}{2}\right) + G_v^{-1}\left(\omega - \frac{\omega_0}{2}\right)\right)g_{vc,k}^r(\omega) \\ &+ \frac{dE_0}{4}\left(G_{vv}\left(\omega - \frac{\omega_0}{2}\right) + G_{cc}^r\left(\omega + \frac{\omega_0}{2}\right)\right) = 0. \end{aligned} \quad (15.63)$$

The solutions of this inhomogeneous system of equations can be put into the form (see also [139])

$$\begin{aligned} G_{cc,k}^r\left(\omega + \frac{\omega_0}{2}\right) &= \frac{G_{v,k}^{-1}\left(\omega - \frac{\omega_0}{2}\right)}{Z_k(\omega)}, \quad G_{vv,k}^r\left(\omega + \frac{\omega_0}{2}\right) = \frac{G_{c,k}^{-1}\left(\omega - \frac{\omega_0}{2}\right)}{Z_k(\omega)}, \\ g_{cv,k}^r(\omega) &= g_{vc,k}^r(\omega) = \frac{dE_0}{2}\frac{1}{Z_k(\omega)}, \end{aligned} \quad (15.64)$$

with

$$Z_k(\omega) = G_{c,k}^{-1}\left(\omega + \frac{\omega_0}{2}\right)G_{v,k}^{-1}\left(\omega - \frac{\omega_0}{2}\right) - \left(\frac{dE_0}{4}\right)^2. \quad (15.65)$$

The two eigenvalues are given by the zeros of the denominator $Z_k(\omega)$. Expressed in terms of the shifted energies

$$\epsilon_{c,k} = e_{c,k} - \frac{\omega_0}{2} \quad \text{and} \quad \epsilon_{v,k} = e_{v,k} + \frac{\omega_0}{2}, \quad (15.66)$$

they are

$$\omega_{1,2,k} = \frac{1}{2} \left(\epsilon_{c,k} + \epsilon_{v,k} \pm \sqrt{(\epsilon_{c,k} - \epsilon_{v,k})^2 + 4\left(\frac{dE_0}{2}\right)^2} \right). \quad (15.67)$$

This is the standard result of perturbation theory for degenerate levels, showing that a gap is formed where the two shifted unperturbed bands become degenerate. The gap which is formed due to avoided level crossing is determined by the Rabi frequency dE_0 . This light-induced gap has been predicted first by Elesin [103] and rederived including Coulomb effects in the frame of a pair formalism by Comte and Mahler [87], and in the framework of nonequilibrium Green functions [139, 314]. By spectral decomposition, the diagonal elements with the original frequency ω can be written as (with $\rho = c, v$ and $\nu \neq \rho$)

$$G_{\rho\rho,k}^r(\omega) = \frac{u_{\rho,k}^2}{\omega - \sigma_{\rho\rho}^z \frac{\omega_0}{2} - \omega_{1,k}} + \frac{v_{\rho,k}^2}{\omega - \sigma_{\rho\rho}^z \frac{\omega_0}{2} - \omega_{2,k}}, \quad (15.68)$$

$$\begin{aligned} G_{cv,k}^r(\omega, \tau) &= \frac{dE_0 e^{-i\omega_0 \tau}}{2(\omega_{1,k} - \omega_{2,k})} \left(\frac{1}{\omega - \omega_{1,k}} - \frac{1}{\omega - \omega_{2,k}} \right) \\ &= u_{c,k} v_{c,k} e^{-i\omega_0 \tau} \left(\frac{1}{\omega - \omega_{1,k}} - \frac{1}{\omega - \omega_{2,k}} \right). \end{aligned} \quad (15.69)$$

The Hopfield coefficients are also expressed in terms of the shifted energies

$$\begin{aligned} u_{c,k}^2 = v_{v,k}^2 = u_k^2 &= \frac{\omega_{1,k} - \epsilon_{v,k}}{\omega_{1,k} - \omega_{2,k}} \\ &= \frac{1}{2} \left(1 + \frac{\epsilon_{c,k} - \epsilon_{v,k}}{\sqrt{(\epsilon_{c,k} - \epsilon_{v,k})^2 + 4 \left(\frac{dE_0}{2} \right)^2}} \right) \end{aligned} \quad (15.70)$$

and

$$u_{\rho,k}^2 + v_{\rho,k}^2 = u_k^2 + v_k^2 = 1. \quad (15.71)$$

The expression $u_k v_k$ can be written as

$$u_k v_k = \frac{1}{2} \frac{dE_0}{\sqrt{(\epsilon_{c,k} - \epsilon_{v,k})^2 + 4 \left(\frac{dE_0}{2} \right)^2}}. \quad (15.72)$$

The difference of the two eigenfrequencies which define the light-induced gap is

$$\omega_{1,k} - \omega_{2,k} = \sqrt{(\epsilon_{c,k} - \epsilon_{v,k})^2 + 4 \left(\frac{dE_0}{2} \right)^2}. \quad (15.73)$$

The square of the Hopfield coefficient $u_{c,k}^2$ describes to which extend the upper branch of the split conduction band is built by conduction band states. $v_{\rho,k}^2$ gives the probability for conduction band states in the lower conduction band branch. In Fig. 15.3, we see the split band structure. The discussed probabilities are encoded in a gray scale, in the dark parts the original band states dominate. In the lower branch of the conduction band, e.g., one sees that the intermixing of conduction band states is lost as one departs far from the

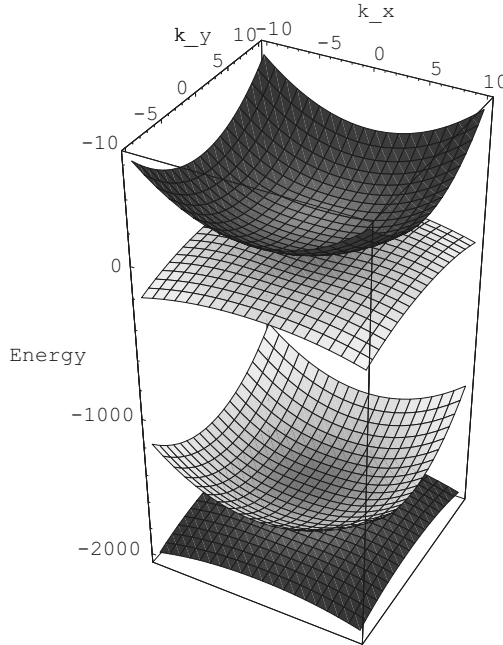


Fig. 15.3. Schematic band structure for a resonantly excited semiconductor shows the energy vs. the momentum components k_x and k_y . The probability that the states of the split bands are due to the original band is encoded in a gray scale

resonance region. Optical transitions in this split band structure will form a triplet of transition bands due to transitions between, e.g., the lower valence band and the upper conduction band, (l, v) to (u, c) and (u, v) to (l, c) , and a third band due to the degenerate transitions, (l, v) to (l, c) and (u, v) to (u, c) . This triplet of bands is the band version of the well-known Mollow triplet observed in atomic two-level systems under coherent excitation. Naturally the light intensity has to be so high that the induced gap is larger than the broadening of the states. On the other hand, the broadening due to carrier–carrier scattering increases as $n^{1/3}$ with the density of the excited electrons, as will be discussed later. Therefore this basic effect could not be observed in semiconductors until recently when it has been detected with an excitation of ultrashort laser pulses of a width of 5 femtosecond [359]. In the emitted spectrum around the third harmonics of the exciting laser frequency ω_0 , the two-band Mollow triplet has been seen and confirmed by fully dynamical calculations in the framework of semiconductor Bloch equations. Only on such a short timescale the coherent band mixing in semiconductors becomes observable.

15.2.4 Dephasing of Retarded Green Functions

As a next step we will incorporate the dissipative effects due to the scattering processes [147]. For this purpose we neglect in (15.29) the laser field and the Coulomb effects and treat only the self-energy correction. We will consider two asymptotic regimes: (A) a long-time regime in which one gets the weak-coupling equilibrium result, which leads to an exponential Wigner–Weisskopf damping, and (B) a short-time regime where one finds a Gaussian damping which corresponds to the strong-coupling result of the equilibrium theory. By means of an interpolation, we get a damping law in form of a hyperbolic secant which connects smoothly both asymptotic regimes [147]. Finally we will show that the hyperbolic secant is in qualitative agreement with the decay of the retarded Green function which one gets from direct numerical time integration of the corresponding Dyson equation [23].

Wigner–Weisskopf Damping for Retarded GFs

The collision processes cause a dissipative decay of the coherence described by the retarded Green function. Without field term the retarded Green function has only diagonal elements. For electrons, e.g., the Dyson equation (15.29) is

$$\left(i \frac{\partial}{\partial t_1} - e_k \right) G_k^r(t_1, t_2) = \delta(t_{12}) + \int_{t_2}^{t_1} dt_3 \Sigma_k^r(t_1, t_3) G_k^r(t_3, t_2). \quad (15.74)$$

We concentrate in the following only on the dissipative part of the self-energy (polaron energy corrections due the real part of the self-energy are assumed to be absorbed in the free-particle energy e_k). With the ansatz

$$G_k^r(t_1, t_2) = -i\theta(t_{12})e^{-ie_k t_{12}} g_k(t_1, t_2), \quad (15.75)$$

(15.74) becomes

$$\frac{\partial}{\partial t_1} g_k(t_1, t_2) = -i \int_{t_2}^{t_1} dt_3 \Sigma_k^r(t_1, t_3) e^{ie_k t_{13}} g_k(t_3, t_2). \quad (15.76)$$

If the time interval t_{12} is much larger than the correlation time, the function $g(t_1, t_2)$ can be pulled out of the integral on the right-hand side of (15.76), and one gets asymptotically

$$\begin{aligned} -i \int_{t_2}^{t_1} dt_3 \Sigma_k^r(t_1, t_3) e^{ie_k t_{13}} g_k(t_3, t_2) &\simeq \text{Im } \Sigma_k^r(\omega = e_k) g_k(t_1, t_2) \\ &\simeq -\alpha \omega_0 g_k(t_1, t_2), \end{aligned} \quad (15.77)$$

where α and ω_0 are the Fröhlich coupling constant (15.16) and the LO-phonon frequency. Equation (15.77) results in an exponential Wigner–Weisskopf damping of the retarded Green function

$$G_k^r(t_1, t_2) = -i\theta(t_{12})e^{(-ie_k - \gamma_k)t_{12}}, \quad (15.78)$$

with $\gamma_k \simeq \alpha\omega_0$.

A full evaluation of the imaginary part of the polaron self-energy for zero temperature yields

$$\gamma_k = \alpha\omega_0 \frac{\theta(e_k - \omega_0)}{\sqrt{e_k\omega_0}} \ln \left| \frac{\sqrt{\frac{e_k}{\omega_0} - 1} + \sqrt{\frac{e_k}{\omega_0}}}{\sqrt{\frac{e_k}{\omega_0} - 1} - \sqrt{\frac{e_k}{\omega_0}}} \right|. \quad (15.79)$$

It can be easily seen that the polaron damping (15.79) at $T = 0$ vanishes below the threshold for LO-phonon emission and remains approximately constant above that threshold $\gamma_k \simeq 1.2\alpha\omega_0$ in a wide range of energies. The approximation of a constant damping thus is reasonable for pumping above the LO-threshold during the early stages of the population evolution and at elevated temperatures where the thresholds are smeared out due to the presence of LO-phonon emission and absorption processes. One should contrast the situation to the low-temperature regime, considered in connection with high-field transport in Sect. 11.6.2, where the approximation $\gamma(\varepsilon) \propto \sqrt{\varepsilon - \omega_0}$ was used.

The exponentially damped retarded Green function leads to a Lorentzian line shape with the linewidth $\gamma \simeq \alpha\omega_0$. This weak-coupling line shape can be obtained under stationary conditions if the mean kinetic energy is much larger than the interaction energy $\alpha\omega_0$ [352].

Damping of Retarded GFs in the Initial Time Regime

If the time interval t_{12} is much shorter than the characteristic response time of the phonons ω_0^{-1} , the integral becomes proportional to the time interval t_{12} . This can be seen by considering the simple perturbation form of the self-energy explicitly. For a single electron one can write the retarded self-energy as (the vector notation is not given explicitly)

$$\Sigma_k^r(t_1, t_3) = i \sum_q g_q^2 D_q^<(t_1, t_3) G_{k-q}^r(t_1, t_3), \quad (15.80)$$

where $g_q^2 \propto \alpha\omega_0^2$ and varies with the phonon momentum q as $1/q^2$. The phonon particle propagator $D_q^<(t_1, t_3)$ is given by (15.14). The retarded electron Green function is in zeroth order $G_{k-q}^r(t_1, t_3) = -i\theta(t_{13})e^{-ie_{k-q}t_{13}}$. For the initial time interval all variations due to the exponential terms can be neglected and one finds asymptotically

$$-i \int_{t_2}^{t_1} dt_3 \Sigma_k^r(t_1, t_3) e^{ie_k t_{13}} g_k(t_3, t_2) = - \sum_{q,\pm}^{q_D} g_q^2 N_q^\pm t_{12} \simeq -C\alpha\omega_0^2 t_{12}, \quad (15.81)$$

where C is a dimensionless constant. Note that the momentum sum has to be truncated by a cutoff wavenumber q_D . The result (15.81) shows how the

damping builds up linearly in the initial time regime. Alternatively one can express the result (15.81) in the form

$$-C\alpha\omega_0^2 t_{12} g_k(t_1, t_2), \quad (15.82)$$

because the retarded function $g(t)$ is in this time interval still approximately equal to its initial value 1. From (15.82) together with (15.76), one gets for the initial time regime a Gaussian damping

$$G_k^r(t_1, t_2) = -i\theta(t_{12}) e^{-ie_k t_{12}} e^{-(\sqrt{(1/2)C\alpha}\omega_0 t_{12})^2}. \quad (15.83)$$

From this retarded Green function with Gaussian damping, one gets by a Fourier transform a Gaussian line shape with a half-width of $\sqrt{\alpha}\omega_0$. This result is well known, e.g., in the exciton line shape theory as the strong-coupling limit. Toyozawa [352] has shown that one obtains in the equilibrium theory this nonperturbational result under the condition that the kinetic energy of the exciton can be neglected in comparison with the LO-phonon energy. In exciton physics, it is known that one can make a smooth transition from the strong-coupling case to the weak-coupling case by motional narrowing. This transition has been observed recently on Si oligomers by increasing the chain length and thus increasing the mean kinetic energy of the exciton [204].

Hyperbolic Secant Damping for the Retarded GFs

A simple appropriate interpolation formula, which connects the short-time asymptote (15.82) and long-time asymptote (15.77), is

$$-i \int_{t_2}^{t_1} dt_3 \Sigma_k^r(t_1, t_3) e^{ie_k t_{13}} g_k(t_3, t_2) = -\alpha\omega_0 \tanh(\omega_0 t_{12}) g_k(t_1, t_2) \quad (15.84)$$

as illustrated in Fig. 15.4.

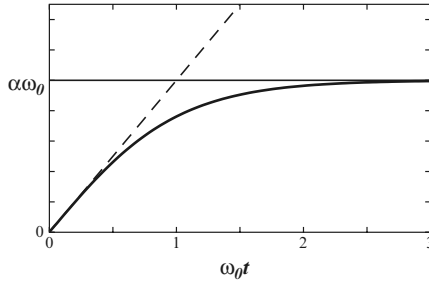


Fig. 15.4. Interpolation by $\alpha\omega_0 \tanh(\omega_0 t)$ between the short-time damping $\alpha\omega_0^2 t$ and the constant long-time damping $\alpha\omega_0$

Inserting this time-dependent interpolation formula (15.84) into the Dyson equation (15.76) yields

$$\frac{\partial g_k(t_1, t_2)}{\partial t_1} = -\alpha \omega_0 \tanh(\omega_0 t_{12}) g_k(t_1, t_2), \quad (15.85)$$

with the solution

$$g_k(t_1, t_2) = \frac{1}{\cosh^\alpha(\omega_0 t_{12})}, \quad (15.86)$$

so that the retarded Green function is finally

$$G_k^r(t_1, t_2) = -i\theta(t_{12}) e^{-ie_k t_{12}} \frac{1}{\cosh^\alpha(\omega_0 t_{12})}. \quad (15.87)$$

A mechanical analog may be helpful. The Newton equation for the velocity of a particle with a time-dependent Stokes damping is

$$\dot{v} = -\gamma(t)v(t). \quad (15.88)$$

For constant damping γ one gets an exponential decrease of the velocity. For a time-dependent damping $\gamma(t) = \gamma \tanh(at/\gamma)$, one finds

$$v(t) = \frac{v_0}{\cosh^{\gamma^2/a}(at/\gamma)}. \quad (15.89)$$

The hyperbolic secant envelope form (i.e., the inverse hyperbolic cosine function) is well known in soliton physics. The decay starts in the form of a Gaussian curve due to the inherent delay on small timescales, while it becomes exponential for long times as illustrated in Fig. 15.5.

While the pure exponential decay leads in the long-time limit of the quantum kinetics to a Markovian kinetics in which the energy conserving delta-function is replaced by a Lorentzian resonance line, the retarded hyperbolic secant decay law leads automatically to a broadening, which decreases in the

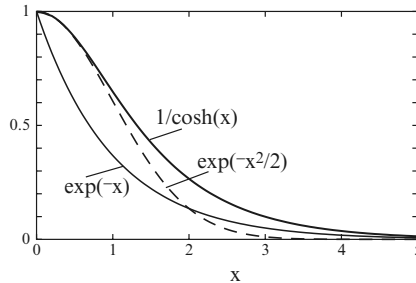


Fig. 15.5. Comparison of the exponential, the Gaussian, and the hyperbolic secant damping

wings faster than any inverse power of the energy. The slowly decreasing wings of a Lorentzian broadening of the energy conservation cause a heating in the resulting asymptotic distributions. This effect is particularly strong for carrier–carrier scattering where the Lorentzian broadening causes a runaway effect of the resulting carrier distributions [23]. This defect is not completely cured by the hyperbolic secant broadening (at least for $\alpha = 1$ the Fourier transform of a hyperbolic secant is again a hyperbolic secant) but the deviations of the resulting distributions from thermal ones occur at much later times [23].

Retarded Polaron Green Functions

In Fig. 15.6, we show the retarded Green function which has been calculated directly from solving the Dyson equation (15.76) numerically [23] at room temperature and for a coupling strength $\alpha = 1$. The value $\alpha = 1$ was chosen for better visibility of the functional form of the decay, although this intermediate coupling with $\alpha = 1$ is – strictly speaking – already out of the validity of the generalized Kadanoff–Baym ansatz. The slower decay at low energies is a remainder of the one-LO-phonon threshold at $T = 0$. On the high-energy side one sees clearly a decay which can be described qualitatively with a hyperbolic secant law. In a later chapter we will present full numerical calculations of the quantum kinetic Green functions $G_{\mu\nu,k}^<(t,t')$ and $G_{\mu\nu,k}^r(t,t')$ under the influence of a light pulse and with LO-phonon scattering according to [121]. These results will show that the polaron decay of the retarded Green function is rather robust and is changed only little by the light field. This provides a further justification for using a fixed polaron decay for the retarded Green function in the framework of the quantum kinetics for the particle propagator $G_{\mu\nu,k}^<(t,t')$. The light-induced off-diagonal elements of the retarded Green function, e.g., $G_{cv,k}^r(t,t')$, decay similarly.

For weak coupling it is therefore a very good approximation to use for the unitary time evolution the mean-field Green function $G_{\mu\nu,k}^r(t,t')$

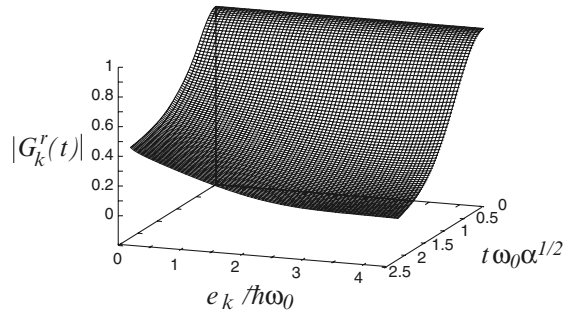


Fig. 15.6. Absolute value of the calculated retarded Green function for room temperature and a coupling strength of $\alpha = 1$ according to [23] vs. energy and time

according to (15.49), multiplied with a hyperbolic secant damping factor (15.86). A much simpler – but less accurate – approximation consists in the use of the free-particle retarded Green function with a Wigner–Weisskopf damping (15.78).

15.3 Intraband Relaxation

With the knowledge of the spectral functions $G_{\mu\nu,k}^r(t, t')$ and $G_{\mu\nu,k}^a(t', t)$, we can now evaluate how the electrons, e.g., in the conduction band relax toward a quasiequilibrium due to LO-phonon scattering.

In order to get a truly irreversible behavior, it is important that one integrates over at least one continuous spectrum which is obtained only in the limit of an infinitely large volume. Strictly speaking in any finite volume the energy spectra are discrete. In such a situation true irreversibility is not possible and recurrency occurs, even if the recurrency times may be extremely large for real systems.

The relaxation due to the coupling to LO-phonons will last several 100 fs. On this timescale the recombination of the electrons and holes can still be neglected. For $\nu = \mu = c$ the scattering integral (15.26) becomes

$$\begin{aligned} -\frac{\partial \varrho_{cc,k}}{\partial t} \Big|_{\text{scatt}} = & - \sum_{q,\sigma\tau,\pm} g_q^2 \int_{-\infty}^t dt' \left(\left\{ G_{c\sigma,k-q}^r(t, t') G_{\tau c,k}^a(t', t) e^{\pm i\omega_0(t-t')} \right. \right. \\ & \times \left(N_q^\mp \varrho_{\sigma\tau,k}(t') - N_q^\pm \varrho_{\sigma\tau,k-q}(t') \pm \sum_\rho \varrho_{\sigma\rho,k-q}(t') \varrho_{\rho\tau,k}(t') \right) \left. \right\} \\ & \left. - \{k \leftrightarrow k - q\} \right). \end{aligned} \quad (15.90)$$

Diagonal Contributions

Let us first consider only the diagonal elements of the density matrix and of the spectral functions, because all off-diagonal elements are induced by the coherent light pulses

$$\begin{aligned} -\frac{\partial \varrho_{cc,k}}{\partial t} \Big|_{\text{scatt}}^d = & - \sum_{q,\pm} g_q^2 \int_{-\infty}^t dt' \left(\left\{ G_{cc,k-q}^r(t, t') G_{cc,k}^a(t', t) e^{\pm i\omega_0(t-t')} \right. \right. \\ & \times \left(N_q^\mp \varrho_{cc,k}(t') - N_q^\pm \varrho_{cc,k-q}(t') \pm \varrho_{cc,k-q}(t') \varrho_{cc,k}(t') \right) \left. \right\} \\ & \left. - \{k \leftrightarrow k - q\} \right). \end{aligned} \quad (15.91)$$

Using the relation $G_{cc,k}^r(t, t') = G_{cc,k}^a(t', t)^*$, one finds the following structure

$$-\frac{\partial \varrho_{cc,k}}{\partial t}\Big|_{\text{scatt}}^d = -\sum_{q,\pm} g_q^2 \int_{-\infty}^t dt' \left\{ K_{cc,k,q}^+(t, t') \right. \quad (15.92)$$

$$\begin{aligned} & \times [n_q \varrho_{cc,k}(t') (1 - \varrho_{cc,k-q}(t')) \\ & - (n_q + 1) (1 - \varrho_{cc,k}(t')) \varrho_{cc,k-q}(t')] + K_{cc,k,q}^-(t, t') \\ & \times [(n_q + 1) \varrho_{cc,k}(t') (1 - \varrho_{cc,k-q}(t')) \\ & - n_q (1 - \varrho_{cc,k}(t')) \varrho_{cc,k-q}(t')] \end{aligned} \quad (15.93)$$

The integral kernel becomes real and is

$$K_{cc,k,q}^\pm(t, t') = 2G_{cc,k-q}^r(t, t') G_{cc,k}^a(t', t) e^{\pm i\omega_0(t-t')} + \text{c.c.} \quad (15.94)$$

The population factors in the square brackets of (15.92) are easily recognizable as those for a transition from state k to state $k - q$ under absorption of a phonon (first term in the first square bracket) and under emission of a phonon (first term in the second square bracket) minus the factors for the inverse processes. Note that the terms with three population factors cancel, so that only the bilinear terms of (15.91) remain. All these population factors are taken at the earlier time t' , exactly as we found it already in the introductory Chap. 3 by equation of motion techniques. Remember in our thermal phonon bath model, the population factors n_q do not depend on time. In the free-particle approximations the integral kernel is simply

$$K_{cc,k,q}^\pm(t, t') = 4 \cos((e_{c,k-q} - e_{c,k} \mp \omega_0)(t - t')), \quad (15.95)$$

again in complete agreement with the equation of motion technique of Chap. 3. Without repeating the still open subtle points of the transition to the Markov limit, we recognize that in the long-time limit these oscillations lead to the energy conservation for the individual scattering processes. The intraband scattering quantum kinetics thus reduces in the absence of a light pulse to the non-Markovian extension of the usual Boltzmann kinetics.

Off-Diagonal Contributions

Next we consider the contributions of the off-diagonal elements of the density matrix, still considering only diagonal spectral functions, i.e., $\sigma = \tau = c$ in (15.90). The sum over the index ρ yields the additional terms

$$\begin{aligned}
-\frac{\partial \varrho_{cc,k}}{\partial t} \Big|_{\text{scatt}}^{\text{od}} = & - \sum_{q,\pm} g_q^2 \int_{-\infty}^t dt' \\
& \times \left\{ G_{cc,k-q}^r(t,t') G_{cc,k}^a(t',t) e^{i\omega_0(t-t')} P_{k-q}(t') P_k^*(t') + \text{c.c.} \right. \\
& \left. - G_{cc,k}^r(t,t') G_{cc,k-q}^a(t',t) e^{i\omega_0(t-t')} P_k(t') P_{k-q}^*(t') + \text{c.c.} \right\}.
\end{aligned} \tag{15.96}$$

These so-called P^2 terms can be understood as follows: The light-induced interband polarization is the probability amplitude for finding a coherent admixture of conduction and valence band states. If an exchange of a phonon links the polarization components at momentum k and $k - q$ (pair scattering), the incoherent density at momentum k can change. Consider, e.g., the term $P_{k-q} P_k^* = \langle a_{v,k-q}^\dagger a_{c,k-q} \rangle \langle a_{c,k}^\dagger a_{v,k} \rangle$ which appears in (15.96). In detail an electron in state $c, k - q$ is coherently de-excited into the state $v, k - q$, coupled by the exchange of a phonon, simultaneously an electron of state v, k is coherently excited into state c, k . This process can result in a change of the electron density in state c, k . We will see later in the discussion of two-pulse experiments that the coupling of two-polarization components by a resonant phonon exchange leads to experimentally observable interference oscillations in the four-wave mixing signal.

In general also the off-diagonal elements of the spectral functions $G_{\mu\nu}^r$ and $G_{\mu\nu}^a$ according to (15.90) have to be taken into account, although the explicitly discussed terms are the leading terms in the lowest powers of the light field. The presented full theory with light-field-dependent spectral functions and the full quantum kinetic equation for the density matrix is, however, not a consistent expansion in powers of the light field. The expansion parameter in this theory is the polaron coupling constant α . An alternative construction of the theory in which up to a given order in the field all terms are contained has been developed in the so-called *controlled truncation method* [12].

15.4 Interband-Polarization Dephasing

Next we will examine the quantum kinetic scattering integral for the interband polarization $P_k(t) = \varrho_{cv,k} e^{i\omega t}$. From (15.26) we find

$$\begin{aligned}
-\frac{\partial \varrho_{cv,k}}{\partial t} \Big|_{\text{scatt}} = & - \sum_{q,\sigma\tau,\pm} g_q^2 \int_{-\infty}^t dt' \left(\left\{ G_{c\sigma,k-q}^r(t,t') G_{\tau v,k}^a(t',t) e^{\pm i\omega_0(t-t')} \right. \right. \\
& \times \left(N_q^\mp \varrho_{\sigma\tau,k}(t') - N_q^\pm \varrho_{\sigma\tau,k-q}(t') \pm \sum_\varrho \varrho_{\sigma\varrho,k-q}(t') \varrho_{\varrho\tau,k}(t') \right) \left. \right\} \\
& - \{ \mathbf{k} \leftrightarrow \mathbf{k} - \mathbf{q} \}).
\end{aligned} \tag{15.97}$$

We start again by taking only diagonal spectral functions $\sigma = c$ and $\tau = v$

$$\begin{aligned} -\frac{\partial P_k}{\partial t}\Big|_{\text{scatt}} &= -\sum_{q,\pm} g_q^2 \int_{-\infty}^t dt' \left(\left\{ G_{cc,k-q}^r(t,t') G_{vv,k}^a(t',t) e^{i(\omega \pm \omega_0)(t-t')} \right. \right. \\ &\times ((N_q^\mp \pm \varrho_{cc,k-q}(t')) P_k(t') - (N_q^\pm \mp \varrho_{vv,k}(t')) P_{k-q}(t')) \Big\} \\ &\quad \left. - \{\mathbf{k} \leftrightarrow \mathbf{k} - \mathbf{q}\} \right). \end{aligned} \quad (15.98)$$

From the exponents we see directly that the quantum kinetic dephasing integral contains also the phonon sidebands. In the free-particle approximation for the spectral functions, one finds contributions which are resonant at $\omega = e_{c,k-q} - e_{v,k} \mp \omega_0$. These terms describe the phonon-assisted interband transitions from the state v, k to the state $c, k - q$ under the absorption of a photon accompanied by the absorption or emission of a phonon.

The damping terms of the polarization P_k , e.g., are determined by the sum of scattering rates of two processes. The first one is the scattering out of the occupied state c, k with $\varrho_{cc,k} = 1$ accompanied by the absorption of a phonon. The corresponding probability is $\propto N(1 - \varrho_{cc,k-q})$. The second damping process is the scattering into the empty state $\varrho_{cc,k} = 0$ accompanied by the emission of a phonon with the probability $\propto (N+1)(\varrho_{cc,k-q})$. The sum is

$$N_q(1 - \varrho_{cc,k-q}) + (N_q + 1)(\varrho_{cc,k-q}) = (N_q + \varrho_{cc,k-q}). \quad (15.99)$$

Adding also the processes where emission and absorption are interchanged, one obtains the term

$$(N_q^\mp \pm \varrho_{cc,k-q}), \quad (15.100)$$

which is just the total scattering rate in the first term of (15.98). In the hole picture $\rho_{hh,k} = 1 - \rho_{vv,k}$, the next term has the same structure for scattering processes in and out of the state $v, k - q$.

In general again the full scattering rate (15.97) has to be used together with the off-diagonal spectral functions.

The coupled equations for the density matrix elements $\rho_{cc,k}$, $\rho_{vv,k}$, and $\rho_{cv,k}$ with both the coherent mean-field part and the scattering integrals can now be solved numerically for a given light pulse. For a femtosecond pulse the results show a relaxation of the excited carriers. If the carriers are excited sufficiently high above the band gap, one obtains a relaxation scenario in which one sees a cascade of phonon emission processes. In general the dispersion-less LO-phonons alone do not lead to a completely smooth Fermi distribution, because some areas in energy space cannot relax by phonon emission. The interband polarization is seen to decay smoothly in several hundred femtoseconds due to the phonon dephasing. Because the resulting density matrices after a single pulse excitation do not give results which are directly measurable,

we will present numerical results only for various two-pulse excitations. The first femtosecond pulse, often called *pump pulse*, excites carriers and induces a coherent interband polarization. With a delayed second pulse one can test the particle distributions and their relaxation, the coherent interband polarization, and its dephasing.

15.5 Numerical Strategies

For the numerical evaluation of the above-derived quantum kinetic equations, it is often convenient to change from the conduction–valence band picture to the electron–hole picture with parabolic one-particle energies measured from the edge of their bands (1.26):

$$\varepsilon_{j,k} = \frac{k^2}{2m_j} = \frac{\mu}{m_j} \varepsilon_k \quad \text{with } j = e, h. \quad (15.101)$$

The electron–hole pairs are resonantly excited by a strong coherent light field which can be described in the classical approximation. We are assuming that the excitation is isotropic, i.e., the induced polarization and the generated electron and hole densities depend only on $k = |\mathbf{k}|$. For shortness we denote often

$$\varrho_{cc,k}(t) = f_{e,k}(t) \quad \text{and} \quad 1 - \varrho_{vv,k}(t) = f_{h,k}(t). \quad (15.102)$$

For the assumed isotropic excitation, one can use instead of the momentum q the energy $\varepsilon_{k'} = (k - q)^2/(2\mu)$ as an integration variable. Because this transition in the integration variable is an important simplification in all isotropic kinetic problems, we describe this “trick” briefly in a form in which it can also be applied, e.g., to Coulomb scattering.

Change of Integration Variable from Momentum to Energy

With $g_q^2 \propto 1/q^2$, the scattering integrals have the structure

$$\sum_q \frac{1}{q^2} F[\varepsilon_k, \varepsilon_{k-q}] = \int d\varepsilon_{k'} \int \frac{d^3 q}{(2\pi)^3} \frac{1}{q^2} \delta(\varepsilon_{k'} - \varepsilon_{k-q}) F[\varepsilon_k, \varepsilon_{k'}], \quad (15.103)$$

where $F[\varepsilon_k, \varepsilon_{k'}]$ is some functional of the two energies. Now the q -integration can be evaluated:

$$\int_0^\infty d\varepsilon_{k'} F[\varepsilon_k, \varepsilon_{k'}] \int_0^\infty \frac{dq}{(2\pi)^2} \int_{-1}^{+1} d\cos\theta \delta\left(\varepsilon_{k'} - \varepsilon_k - \frac{q^2}{2\mu} + \frac{kq}{\mu} \cos\theta\right). \quad (15.104)$$

The integration over $\cos \theta$ results in

$$\frac{\mu}{k(2\pi)^2} \int_0^\infty d\varepsilon_{k'} F[\varepsilon_k, \varepsilon_{k'}] \int_{\sqrt{\varepsilon_{k'}} - \sqrt{\varepsilon_k}}^{\sqrt{\varepsilon_{k'}} + \sqrt{\varepsilon_k}} d\left(\frac{q}{\sqrt{2\mu}}\right) \frac{\sqrt{2\mu}}{q} \quad (15.105)$$

$$= \frac{\mu}{k(2\pi)^2} \int_0^\infty d\varepsilon_{k'} F[\varepsilon_k, \varepsilon_{k'}] \ln \left| \frac{\sqrt{\varepsilon_{k'}} + \sqrt{\varepsilon_k}}{\sqrt{\varepsilon_{k'}} - \sqrt{\varepsilon_k}} \right|. \quad (15.106)$$

With this transformation the quantum kinetic scattering integrals can be simplified. If one uses, e.g., a free-particle Wigner–Weisskopf retarded and advanced Green function, the memory kernel $K(t - t')$ can be written as a sum of factorized kernels.

Factorizing Integral Kernel

The exponential form of our integral kernels allows to write them in the form

$$K(t - t') = \sum_i \kappa_i(t) \kappa'_i(t'). \quad (15.107)$$

The set of differential equations symbolically has the structure

$$\frac{df}{dt} = \int_{-\infty}^t dt' \sum_i \kappa_i(t) \kappa'_i(t') F(t') = \sum_i \kappa_i(t) G_i(t) \quad (15.108)$$

with the supplementary variables

$$G_i(t) = \int_{-\infty}^t dt' \kappa'_i(t') F(t'), \quad (15.109)$$

for which one gets a set of local differential equations

$$\frac{dG_i(t)}{dt} = \kappa'_i(t) F(t). \quad (15.110)$$

This reformulation transforms the original set of integrodifferential equations into a larger set of local differential equations which can be solved, e.g., by a fourth-order Runge–Kutta integration procedure very efficiently. More generally this reduction is not possible, and one has to solve the integrodifferential equations on a time grid whose discretization time has to be adjusted and checked carefully to obtain the desired accuracy. In this situation an Adams–Bashforth–Moulton (ABM) procedure is used [11], which requires the functional values only on the time grid.

Because most of our calculations will be given for the semiconductor GaAs, we will list its material parameters: $m_e = 0.069m_0$, $m_h = 0.5m_0$, where m_0 is the free electron mass, $E_g(T = 0) = 1.517 \text{ eV}$, $E_g(T = 300 \text{ K}) = 1.425 \text{ meV}$, $\epsilon_0 = 12.9$, $\epsilon_\infty = 10.9$, $\alpha = 0.069$, $E_0 = 4.2 \text{ meV}$, $\omega_0 = 36 \text{ meV}$.

So far we have considered only one excitation pulse. However, much more information can be obtained by ultrafast spectroscopy with two pulses. The variation of delay time which separates the 2 femtosecond pulses allows to obtain valuable information on the dynamics of the excited electrons. Before we present any numerical results, we will formulate the semiconductor Bloch equations for the most important two versions of the two-pulse excitation, namely for pump and probe spectroscopy, which allows to study carrier relaxation, and for four-wave mixing, which allows to analyze the dephasing of the interband polarization. The numerical results for the semiconductor Bloch equations with two pulses and quantum kinetic scattering terms can be compared directly to a wealth of corresponding femtosecond experimental results.

Two-Pulse Spectroscopy

Summary. The full wealth of quantum kinetics can be tested by time-resolved femtosecond two-pulse spectroscopy either in the form of pump-probe spectroscopy or in the form of four-wave mixing. It is shown that pump-probe spectroscopy is amenable to follow the temporal evolution of the particle distributions. This is illustrated by calculations and experiments on the buildup of phonon cascades and on non-Markovian relaxation scenarios. Four-wave mixing, on the other hand, is shown to be well-suited for the study of quantum coherence and its dephasing illustrated by LO-phonon quantum beats.

16.1 Introductory Remarks

Time-resolved information about the relaxation of excited carriers, about the decay of the optically induced quantum coherence, but also about the buildup of correlations can be obtained from experiments with two pulses. The basic configuration for two-pulse experiments is shown schematically in Fig. 16.1.

In the pump–probe configuration one measures the transmission spectrum of the probe pulse after the sample has been excited by a pump pulse as a function of the delay time τ between the two pulses. To enhance the sensitivity of the pump–probe measurement one measures often the difference of the transmitted probe beam intensity with and without a preceding pump pulse, respectively. This differential transmission spectroscopy (DTS) is best suited to get time-resolved information about the relaxation of the distribution of carriers excited by the pump pulse, because the absorption of a light beam is mainly determined by the number of carriers which interact with the laser photons.

The four-wave mixing (FWM) signal has the big advantage to be background-free. One measures the beam diffracted from the optical lattice formed by the optical polarization fields induced by the two pulsed coherent beams. Because the optical lattice lasts only as long as the coherent optically induced polarizations still exist, this method is ideally suited to detect the dynamics and the dephasing of the optical polarization.

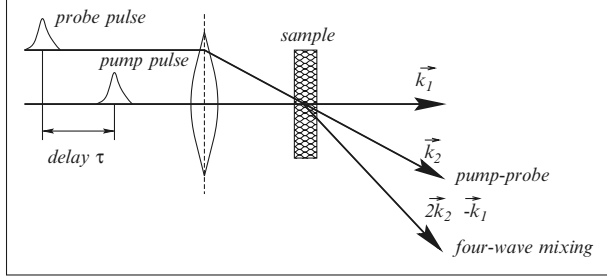


Fig. 16.1. Schematics of two-pulse experiments: Two successive pulses called pump and probe (or test) pulse with a delay time τ propagate in the directions \mathbf{k}_1 and \mathbf{k}_2 through the sample. In the pump and probe configuration the signal is measured in the direction \mathbf{k}_2 of the test pulse, in the four-wave mixing configuration the signal is measured in the direction $2\mathbf{k}_1 - \mathbf{k}_2$ of the beam diffracted from the lattice induced by the two pulses

The name *four-wave mixing* originates from the fact that one generally has to consider a total of four different \mathcal{E} -fields, three incident, and one diffracted field. Here, we discuss only the so-called degenerate case where one of the incident fields helps to form the optical lattice and will be diffracted at the same time from the lattice. Hence, this beam counts twice whereas the other incident beam and the diffracted beam count only once.

So far the semiconductor Bloch equations with their quantum kinetic scattering terms have been formulated for a spatially homogeneous system. In general one cannot consider an optically excited system as spatially homogeneous, because the light fields will be absorbed most strongly at the crystal surface where the beams enter and the two beams will in general propagate in different directions. The induced polarization will act as a spatially inhomogeneous source term in the Maxwell equations governing the propagation of the fields. Thus in general one has to determine a two-point density matrix of the form

$$\rho_{ij}(\mathbf{r}_1, \mathbf{r}_2, t) = \langle \psi_j^\dagger(\mathbf{r}_2, t) \psi_i(\mathbf{r}_1, t) \rangle. \quad (16.1)$$

Introducing the center-of-mass coordinate $\mathbf{R} = (m_i \mathbf{r}_1 + m_j \mathbf{r}_2)/(m_i + m_j)$, the relative coordinate $\mathbf{r} = \mathbf{r}_1 - \mathbf{r}_2$ and a Fourier transformation with respect to the relative coordinate \mathbf{r} one gets the Wigner distribution

$$\rho_{ij}(\mathbf{R}, \mathbf{k}, t) = \frac{1}{V} \int d\mathbf{r}^3 r e^{i\mathbf{k} \cdot \mathbf{r}} \rho_{ij}(\mathbf{R}, \mathbf{r}, t). \quad (16.2)$$

With these distributions one can calculate, e.g., the optically induced polarization as a function of space and time

$$P(\mathbf{R}, t) = \sum_{\mathbf{k}} d_{vc} \rho_{cv}(\mathbf{R}, \mathbf{k}, t) + \text{c.c.} \quad (16.3)$$

This polarization enters into the Maxwell equations describing the dynamics of the light field as it propagates through the sample. Obviously the determination of the Wigner functions and the resulting electromagnetic fields is considerably more involved in comparison with calculations of the density matrices in spatially homogeneous situations. As an alternative to the Wigner functions, one can use also density matrices which depend on two momenta [152]

$$\rho_{ij}(\mathbf{k}_1, \mathbf{k}_2, t) = \langle a_{j,\mathbf{k}_2}^\dagger(t) a_{i,\mathbf{k}_1}(t) \rangle \quad (16.4)$$

from which the information about the spatial variation can be obtained. In a single band, e.g., the distribution function at the spatial coordinate \mathbf{R} is

$$\rho(\mathbf{R}, \mathbf{k}, t) = \sum_{\mathbf{K}} \rho\left(\frac{1}{2}\mathbf{K} + \mathbf{k}, -\frac{1}{2}\mathbf{K} + \mathbf{k}, t\right) e^{i\mathbf{R}\cdot\mathbf{K}}, \quad (16.5)$$

which has again the form of (16.2). The advantage is that it is much easier to formulate the equations of motion in momentum space than in real space. So far these off-diagonal density matrices in K -space have been used successfully mainly for quantum wires, where the complications due to the angles between the two momenta do not exist.

In thin samples, however, where propagation effects and spatial inhomogeneities are of minor importance, one can calculate the resulting electromagnetic field which propagates in a certain direction by adiabatic approximations from the calculations for spatially homogeneous fields.

16.2 Thin Samples

In order to understand why the transmitted light in thin samples is proportional to the polarization field we consider Maxwell's wave equation for the electric field \mathcal{E} :

$$\frac{\partial^2 \mathcal{E}}{\partial t^2} - \frac{c^2}{n_0^2} \Delta \mathcal{E} = -4\pi \frac{\partial^2 P}{\partial t^2} \simeq 4\pi\omega^2 P, \quad (16.6)$$

where n_0 is the refractive index of the unexcited crystal. The polarization is formally an inhomogeneous term. The field \mathcal{E} can be calculated by a solution of the homogeneous equation plus an integral over the Green function of the homogeneous field equation folded with the inhomogeneous polarization term. As for the calculations of the retarded Liénard–Wiechert potentials in electrodynamics, this term reduces to the retarded polarization integral, in which the actual time is replaced by the retarded time $t - Rn/c$, where R is the distance between the coordinate of the polarization and that of the resulting field. In thin samples these retardation effects are very small, the integral reduces to a weighted spatial average of the polarization term over the sample. In other words, the field caused by the polarization in the medium is

in very thin samples proportional to the spatially homogeneous polarization. For optically thin samples we generalize the considered two-pulse laser light field which excites the sample by introducing the two propagation directions by means of two wave vectors \mathbf{k}_1 and \mathbf{k}_2 . A spatial variation of the amplitudes is not considered. This way, we can write

$$\begin{aligned}\mathcal{E}(t) &= \mathcal{E}_1(t)e^{-i(\omega_1 t - \mathbf{k}_1 \cdot \mathbf{r})} + \mathcal{E}_2(t - \tau)e^{-i(\omega_2(t - \tau) - \mathbf{k}_2 \cdot \mathbf{r})} \\ &= e^{i\mathbf{k}_1 \cdot \mathbf{r}} \left(\mathcal{E}_1(t)e^{-i\omega_1 t} + \mathcal{E}_2(t - \tau)e^{-i\omega_2(t - \tau)}e^{i\phi} \right),\end{aligned}\quad (16.7)$$

where we introduced the directional phase $\phi = (\mathbf{k}_2 - \mathbf{k}_1) \cdot \mathbf{r}$. With such an exciting field the calculated induced polarization will also depend on the directional phase

$$P(t, \tau, \phi) = \sum_{\mathbf{k}} d_{vc} \rho_{cv,k}(\phi) + \text{c.c.} \propto E_{\text{transm}}. \quad (16.8)$$

The polarizations induced by the two delayed parts of the field (16.7) form a transient lattice with the lattice vector $\mathbf{k}_1 - \mathbf{k}_2$. The field will be diffracted from this lattice into multiple orders determined by the factor $e^{i\mathbf{k}_1 \cdot \mathbf{r}} e^{in\phi}$. For $n = 1$ one gets the propagation vector \mathbf{k}_2 , that is the direction of the delayed test pulse (see Fig. 16.1). For $n = 2$ one gets the propagation vector $2\mathbf{k}_2 - \mathbf{k}_1$, etc. This is the direction of the first diffracted order in a degenerate *FWM* configuration.

We numerically evaluate the resulting polarization for various values of the directional phase. In actual calculations the polarization has to be obtained for only a few phase values. Because of the periodicity in ϕ , we extract from this knowledge the n th-order Fourier transform of the polarization

$$P_n(t, \tau) = \int_0^{2\pi} \frac{d\phi}{2\pi} P(t, \tau, \phi) e^{in\phi}. \quad (16.9)$$

This evaluation of the polarization in various directions without treating the spatial inhomogeneity explicitly is called an adiabatic approximation. Alternatively, one can expand the density matrix $\rho = \sum_n \rho_n e^{i\phi n}$ and calculate the equations of motion for the various components successively [207]. To discuss pump-probe experiments we have to calculate $P_1(t, \tau)$. The spectrum of the transmitted light is given by $|P_1(\omega, \tau)|^2$. Because the transmitted field in the test pulse direction \mathbf{k}_1 is not background-free, one often measures a differential signal by subtracting the spectrum for the test field alone $|P_1^0(\omega)|^2$.

16.3 Low-Intensity Two-Beam Experiments

In the following section we will limit us to the analysis of low-intensity measurements, where the relaxation and dephasing kinetics in polar semiconductors such as GaAs or CdS is determined by the interaction with LO-phonons.

We remind the reader that compound semiconductors of the groups III–V possess only a weak polar interaction with a small dimensionless polaron coupling constant (11.26) $\alpha \ll 1$, while the more polar semiconductors of the groups II–VI can approach the intermediate coupling range with $\alpha \simeq 1$. The latter case requires to go beyond the lowest order perturbation approximation in the carrier phonon coupling as discussed already for the retarded GF in Chap. 15.

16.3.1 LO-Phonon Relaxation Cascades

We discuss first a case where the modifications of the interband continuum due to excited carriers and their relaxation are studied [312]. Specifically, we discuss the results of a low-intensity experiment due to Leitenstorfer et al. on GaAs [120] with a two color titanium sapphire laser. The pump pulse was tuned to 150 meV above the band edge and had a duration of 120 fs. The pump pulse had a rather low intensity and excited only $8 \times 10^{14} \text{ cm}^{-3}$ electron–hole pairs. For these low carrier concentrations the relaxation kinetics was dominated by LO-phonon scattering as treated in the preceding chapter. The delayed probe pulse with a duration of 25 fs was tuned 120 meV above the gap. The intensity of the probe pulse was five times smaller than that of the pump pulse. In the scattering terms we used therefore a simple damped free-particle approximation for the spectral carrier Green functions. From the calculated interband polarization in the direction of the probe pulse, we calculated the absorption coefficient

$$\alpha(\omega) \propto \Im \frac{P(\omega)}{E_t(\omega)} . \quad (16.10)$$

In Fig. 16.2 we show in the top figure the measured DTS according to Fürst et al. [120] for various delay times. One sees at negative time delays (in the two curves with the lowest peak heights) an increased transition probability around the spectral position of the pump pulse due to Pauli blocking. Due to excitonic enhancement above the populated states and to a minor degree due to bandgap shrinkage, an induced absorption (negative signal) is observed above the spectral position of the pump pulse. A remarkably sharp feature is present in the region of induced absorption around 1.675 meV in the earliest probe spectrum which seems to contradict the time–energy uncertainty relation. Above a delay of 100 fs the buildup of the first LO-phonon cascade structure is seen clearly, followed by a structure due to two successive phonon emission processes at still later times.

In the three lower figures the calculated DTS are shown for various levels of the theory: In the first calculated spectrum (a) (second figure from the top) we present the results which have been calculated in the Markovian limit of the LO-phonon relaxation kinetics by inserting the population distributions calculated for the pump pulse into the Bloch equations for the test pulse. That means the spectra (a) have not been calculated by the discussed coherent projection technique, but from linearized semiconductor Bloch equations.

In comparison with the experimental spectra we see first that the phonon cascade structure due to LO-phonon emission builds up too fast with the instantaneous Boltzmann scattering rates. Furthermore, we see that the incoherent analysis fails to explain the sharp spectral features at the high energy cross-over from reduced to induced absorption at early time delays.

If one replaces the incoherent analysis by a coherent one, i.e., one treats only one set of Bloch equations for the two pulses together and determines at the end the polarization in the \mathbf{k}_1 direction, one sees that the sharp spectral features at the cross-over point and at earliest delays are now present as in the experimental spectra (see Fig. 16.2b, third figure from the top).

If one uses finally the delayed non-Markovian quantum kinetics of the phonon scattering (see Fig. 16.2c, lowest figure), the timescale of the buildup of the phonon peaks agrees now also with the experiment. Thus the analysis of this experiment shows clearly the need for the coherent determination of the test beam polarization and for the non-Markovian quantum relaxation kinetics.

16.3.2 LO-Phonon Quantum Beats in FWM

Next we discuss the femtosecond FWM experiment of Wegener et al. [21] on GaAs in which for the first time the LO-phonon quantum beats have been seen superimposed on the exponentially decaying time-integrated FWM signal. The time-integrated FWM signal is theoretically determined by $\int_{-\infty}^{+\infty} dt |P_2(t, \tau)|^2$. There is also the possibility to measure instead the time-resolved signal $|P_2(t, \tau)|^2$, both as a function of the real time t and the delay time τ , or the frequency-resolved signal $|P_2(\omega, \tau)|^2$. Examples for all three types of FWM measurements will be given in the following chapters.

In order to eliminate surface effects the GaAs bulk layer had a width of only $0.6\text{ }\mu\text{m}$ and was sandwiched in an $\text{Al}_{0.3}\text{Ga}_{0.7}\text{As}$ heterostructure. The sample was glued on a sapphire substrate and the top surface was antireflection coated. The lattice temperature was kept at 77 K. The excited carrier density was in the range of several 10^{16} cm^{-3} . The spectral carrier Green functions have been calculated in the time-dependent mean-field approximation combined with a Wigner–Weisskopf damping.

The quantum beats which are clearly seen in the experimental and theoretical time-integrated FWM signals of Fig. 16.3 are due to the phonon oscillations in the integral kernel of the non-Markovian scattering integrals. The two pulses had a duration of 14 fs and had the form of a hyperbolic secant

$$\mathcal{E}_0(t) = E_0 \frac{1}{\cosh(t/\Delta t)} . \quad (16.11)$$

Because a residual Coulomb scattering was also present under the experimental conditions we use in addition to the dephasing by phonon scattering an excitation induced phenomenological damping in the form $\gamma = \gamma_0 + \gamma_1 n(t)$,

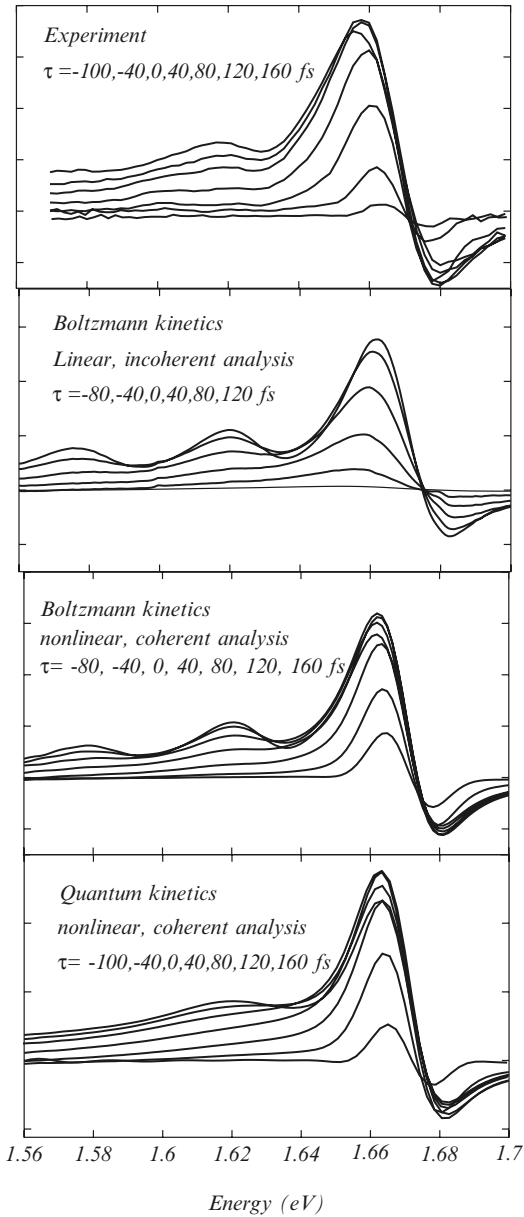


Fig. 16.2. Measured (top) [120] and calculated DTS spectra [312] in various approximations for delay times ranging from -100 to 160 fs. Generally speaking, the amplitudes of the curves increase with increasing delay time. (a) Incoherent analysis with Markovian scattering kinetics, (b) Coherent analysis with Markovian scattering kinetics, (c) Coherent analysis with non-Markovian quantum kinetics

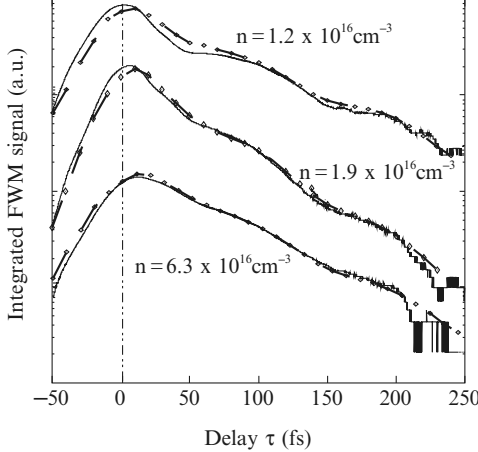


Fig. 16.3. Measured (solid lines) and calculated (dashed lines) time-integrated FWM signals for three excitation densities (from top to bottom $n = 1.2, 1.9, 6.3 \times 10^{16} \text{ cm}^{-3}$) according to Bányai et al. [21]. The curves are displaced vertically for clarity

where $n(t)$ is the number of carriers at time t . The carrier frequency of the two pulses was degenerate and was tuned to the exciton resonance.

As Fig. 16.3 shows one gets a nearly perfect agreement between the experiment and the quantum kinetic calculations. Naturally the oscillations are only present in a non-Markovian version of the dephasing kinetics. The oscillations superimposed on the exponential decay of the time-integrated FWM signals have a frequency of $(1 + m_e/m_h)\omega_0$, which can be understood as the beating frequency of two interband polarization components coupled by the coherent exchange of an LO-phonon between conduction band states: Suppose the light frequency is resonant at momentum k with $e_{k,e} + e_{k,h} + E_g = \omega$ (again \hbar is put to equal one). The electron state k' reached by picking up one phonon is: $e_{k',e} = e_{k,e} + \omega_0$ or $k'^2 = k^2 + 2m_e\omega_0$. Thus the resulting beat frequency is $(e_{k',e} + e_{k',h} + E_g) - (e_{k,e} + e_{k,h} + E_g) = (1 + m_e/m_h)\omega_0$. For a flat valence band (i.e., $m_h \rightarrow \infty$) the energy difference between the beating polarization components would be exactly ω_0 . But due to the negative curvature of the valence band this energy is increased to $(1 + m_e/m_h)\omega_0$. These observed phonon beats are a clear manifestation of the delayed quantum kinetics.

16.3.3 Two-Time Electron–LO-Phonon Quantum Kinetics: Formation of the Polaron

Finally we want to discuss a DTS experiment and its analysis [40] in the polar semiconductor CdTe where the Fröhlich coupling constant particularly for the heavy holes $\alpha_h = \sqrt{m_h/\mu}\alpha = 0.96 \simeq 1$ is relatively large. Here μ is again the reduced e–h mass. In this experiment [40] the detuning of the pump pulse was

chosen such that the excess energy of the excited heavy holes was less than the energy of an optical phonon. While in such a situation the relaxation of the holes by LO-phonon emission is suppressed in a weak coupling semiconductor (e.g. GaAs), in the intermediate coupling material of CdTe surprisingly a heavy-hole relaxation has been observed. The result of our quantum kinetic analysis is that this seeming violation of the energy conservation is connected with the formation of polaron states for the holes.

In the intermediate polaron coupling range perturbative approaches should not be used. In particular we do not want to use the generalized Kadanoff–Baym ansatz (GKBA) which relates the two-time particle propagator to the one-time density matrix, because this relation can only be justified for weak coupling. Therefore the original Dyson equation for the two-time Green functions $G^<(t_1, t_2)$ and $G^r(t_1, t_2)$ has to be calculated directly following the approach of Gartner et al. [121]. We choose the kinetic GF $G^<$ and the spectral function G^r rather than the pair $G^<, G^>$ chosen, e.g., by Schäfer et al. [137]. The reason is that one can formulate the initial values of the pair $G^<, G^r$ of two-time functions exactly for times long before the pulses arrive in terms of the equilibrium polaron GF $G^r(t_1 - t_2)$ which depends only on the relative time coordinate. Note that the kinetic equations for the nonequilibrium GF are integro-differential equations which need a whole function of the time argument and not constants as initial values. In the optical excitation problem the initial value can be chosen rather naturally at times long before the first pulse arrives, where the system still was in thermal equilibrium.

It is convenient to use [137] instead of the time arguments t_1, t_2 the arguments $t = t_1$ and the relative time $\tau = t_1 - t_2$. The time derivatives transform as $\frac{\partial}{\partial t_1} = \frac{\partial}{\partial t} + \frac{\partial}{\partial \tau}$ and $\frac{\partial}{\partial t_2} = -\frac{\partial}{\partial \tau}$. The calculations can be limited to the regime $t_2 \leq t_1$ or $\tau \geq 0$ because the following symmetries

$$G_{\mu\nu,k}^<(t_1, t_2)^* = -G_{\nu\mu,k}^<(t_2, t_1) \text{ and } G_{\mu\nu,k}^r(t_1, t_2)^* = G_{\nu\mu,k}^a(t_2, t_1) \quad (16.12)$$

allow to get the two-time functions also in the region above the $t_2 = t_1$ diagonal in the t_1, t_2 plane. From the original Kadanoff–Baym equation (5.4) in general matrix notation

$$[G_0^{-1} - U, G^<] = \Sigma^r G^< + \Sigma^< G^a - G^r \Sigma^< - G^< \Sigma^a, \quad (16.13)$$

we get with the form

$$i \frac{\partial G^<}{\partial t} = i \left. \frac{\partial G^<}{\partial t} \right|_{coh} + i \left. \frac{\partial G^<}{\partial t} \right|_{coll} \quad (16.14)$$

the collision term written with explicit time integrations

$$\begin{aligned} i \left. \frac{\partial G^<(t, t - \tau)}{\partial t} \right|_{coll} &= \int_{-\infty}^{t - \tau} dt' (-\Sigma^r(t, t') G^<(t - \tau, t')^+ \\ &+ \Sigma^<(t, t') G^r(t - \tau, t')^+ + G^r(t, t') \Sigma^<(t - \tau, t')^+ - G^<(t, t') \Sigma^r(t - \tau, t')^+) \end{aligned}$$

$$+ \int_{t-\tau}^t dt' (\Sigma^r(t,t')G^<(t',t-\tau) - G^r(t,t')\Sigma^<(t',t-\tau)) . \quad (16.15)$$

Here the crosses denote the hermitian conjugate with respect to the band indices and they arise when the symmetry properties (16.12) are used to bring the $t_1 < t_2$ quantities into the $t_1 \geq t_2$ half plane.

The corresponding scattering terms for the retarded GF have a much simpler structure and are given by

$$i \frac{\partial G^r(t,t-\tau)}{\partial t} \Big|_{\text{coll}} = \int_{t-\tau}^t dt' (\Sigma^r(t,t')G^r(t',t-\tau) - G^r(t,t')\Sigma^r(t',t-\tau)) . \quad (16.16)$$

As before the scattering self-energy is taken with free propagators for the thermal phonon bath $D_q(t-t')$ and with the full carrier propagators. Vertex corrections have not been included because of their complexity. At least in equilibrium we checked by explicit calculation that the vertex correction still can be neglected for intermediate coupling.

The scattering self-energies are in matrix notation for the band index

$$\Sigma_k^r(t,t-\tau) = i \sum_{\mathbf{q}} g_q^2 \left(D_q^>(\tau) G_{\mathbf{k}-\mathbf{q}}^r(t,t-\tau) + D_q^r(\tau) G_{\mathbf{k}-\mathbf{q}}^<(t,t-\tau) \right) \quad (16.17)$$

and

$$\Sigma_k^<(t,t-\tau) = i \sum_{\mathbf{q}} g_q^2 D_q^<(\tau) G_{\mathbf{k}-\mathbf{q}}^<(t,t-\tau) . \quad (16.18)$$

The phonon propagators are

$$D_q^>(\tau) = \frac{1}{i} \sum_{\zeta=\pm 1} N_{\zeta} e^{\mp i \zeta \omega_0 \tau}, \quad D_q^r(\tau) = \frac{1}{i} \sum_{\zeta=\pm 1} \zeta e^{-i \zeta \omega_0 \tau}, \quad (16.19)$$

where $N_{-1} = N$ is the Bose function, and $N_{+1} = N + 1$. The coherent time development is the same for both types of nonequilibrium GFs and is

$$i \frac{\partial G^{r,<}(t,t-\tau)}{\partial t} \Big|_{\text{coh}} = \Sigma^{\delta}(t) G^{r,<}(t,t-\tau) - G^{r,<}(t,t-\tau) \Sigma^{\delta}(t-\tau), \quad (16.20)$$

where $\Sigma^{\delta}(t)$ is the singular mean field self-energy due to the interaction with the coherent laser pulse and due to the Coulomb exchange interaction.

Concerning the initial conditions the knowledge of the equilibrium retarded GF is indeed sufficient, since $G_{cc,k}^<$ vanishes because the conduction band is empty and $G_{vv,k}^< = -G_{vv,k}^r$ for the full valence band. In equilibrium the equation for the retarded GF can be written, e.g., for the conduction band with

$$G_k^r(\tau) = \frac{1}{i} \mathcal{G}_k(\tau) e^{-i e_k \tau} \quad (16.21)$$

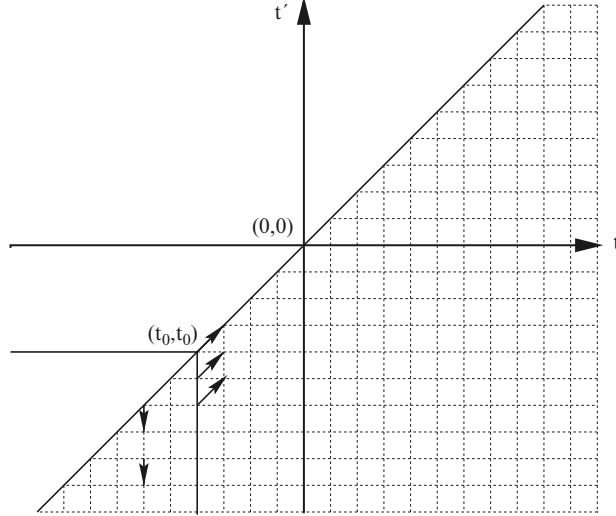


Fig. 16.4. Strategy for the solution of the Kadanoff–Baym equation for $G^<$ and G^r [121]. The time t_0 marks an initial time well before the first light pulse arrives. Before t_0 the system is in thermal equilibrium where the retarded GF is obtained from a $\tau = t_1 - t_2$ integration with fixed $t = t_1$

$$i \frac{\partial G_k(\tau)}{\partial \tau} = \int_0^\tau dt' \sigma_k^r(\tau - \tau') G_k(\tau') e^{ie_k(\tau - \tau')} \quad (16.22)$$

with the initial condition $G_k(0) = 1$. As always, the self-energies have the same symmetry properties (16.12) as the GFs. The interaction representation of the retarded self-energy is

$$\sigma_k^r(\tau) = \frac{1}{i} \sum_{q,\zeta} g_q^2 N_\zeta G_{k-q}(\tau) e^{-i(e_{k-q} + \zeta\omega_0)\tau}. \quad (16.23)$$

The solution of this equilibrium retarded GF is the polaron GF. Note that this function cannot be obtained from the Kadanoff–Baym equation for G^r with its derivative with respect to t . If the τ -dependence is not introduced in the kinetics as an initial condition, it will be missing for the whole kinetics.

Now the two-time GF can be calculated numerically by energy and time discretization. In Fig. 16.4 the discretized (t, t') plane is shown. The equilibrium polaron retarded GF can first be calculated for times before t_0 where the action of the light pulses is not yet felt. One integrates with fixed time $t = t_1$ by integrating over τ starting with the initial value $G^r(\tau = 0) = 1$ on the diagonal of the t_1, t_2 plane. At t_0, t_0 this function of τ is taken to give the initial value for the integration of the Kadanoff–Baym equations over t as shown in Fig. 16.4. We choose as in the experiment the material parameters of CdTe: The low-temperature bandgap $E_g = 160$ eV from which one gets the bare bandgap by subtracting the equilibrium polaron shift. The LO-phonon

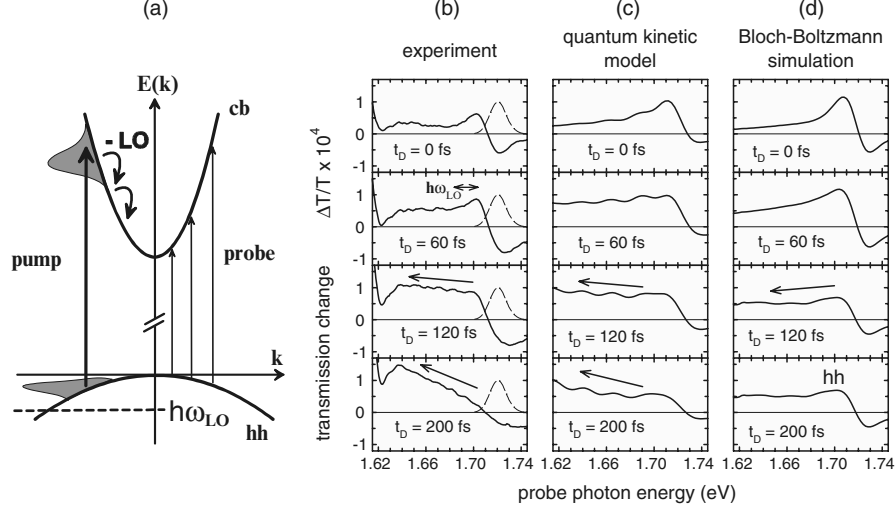


Fig. 16.5. DTS experiment in CdTe [40]: (a) Schematics of the excitation, (b) measured DTS for various delay times t_D , (c) calculated DTS with a two-time quantum kinetics of the LO-phonon scattering, (d) calculated DTS with a semi-classical Markovian Boltzmann kinetics

energy $\hbar\omega_0 = 36$ meV, the effective masses $m_e = 0.09 m_0$ and $m_{hh} = 10 m_e$, the polaron coupling constants $\alpha_e = 0.33$ and $\alpha_{hh} \simeq 1$. The light pulses have a Gaussian shape. The test pulse had a duration of 15 fs and a bandwidth of 100 meV. The pump pulse had a peak photon energy of $\hbar\omega_p = 1.72$ eV and a duration of 100 fs corresponding to a bandwidth of 13 meV. The excited carrier density $n = 1.3 \times 10^{15} \text{ cm}^{-3}$ was kept low in order to avoid Coulomb scattering. The excess energy of the excited electrons was 107 meV while for the heavy holes it was only 13 meV, so that a one-phonon emission process for the holes was forbidden. The optically induced polarization is calculated by $P(t) = d \sum_k G_{cv,k}^<(t,t)$ and the test pulse polarization by the projection technique described above. Finally the absorption coefficient of the weak test pulse is calculated from $\alpha(\omega) = \frac{4\pi\omega_t}{c} \text{Im} \frac{P_t(\omega)}{E_t(\omega)}$. The resulting DTS spectra for CdTe are shown in Fig. 16.5 as well as the schematics of the chosen excitation (a). The DTS spectra for various delay times are: (b) as measured, (c) as calculated by the described two-time quantum kinetics, and (d) for comparison as calculated with the semiconductor Bloch equations and the semi-classical scattering kinetics of the Boltzmann type.

We see both in experiment and in the calculated spectra at the delay time 0 the increased transition due to the Pauli blocking of the excited carriers. The reduced transmission above the filled states is caused mainly by excitonic enhancement and to a minor degree by bandgap reduction. While in the semi-classical Boltzmann kinetics which conserves the free-particle energies the hole contribution to the increased transmission does not relax (the maximum stays

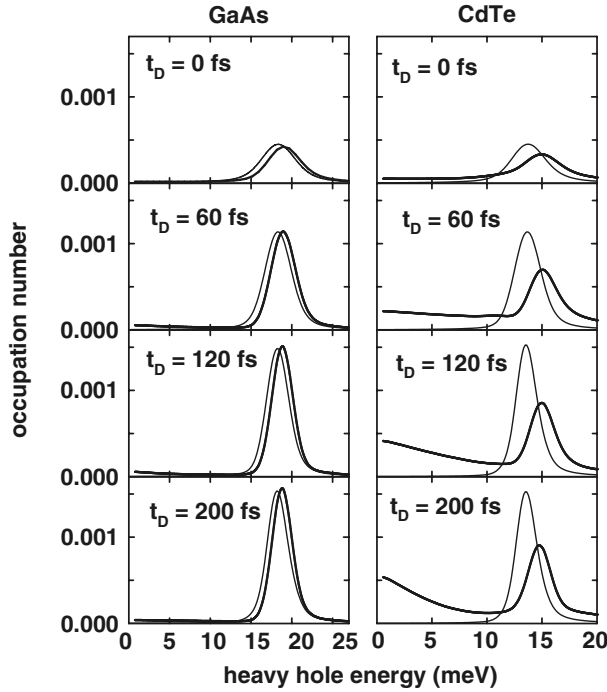


Fig. 16.6. Comparison of the relaxation of the heavy holes which have not sufficient energies to emit a LO-phonon in the weak coupling material GaAs and in the intermediate coupling material CdTe [40]. The *full lines* represent the results of the two-time quantum kinetics, the *thin lines* for comparison the results of the semiclassical Boltzmann kinetics

around 1.70 eV), the experiment and the two-time quantum kinetics show that both the electrons and the heavy holes relax at the latest delay times towards the band edge, resulting in an increasing transmission towards the band edge as indicated by the arrows. At the large delay times of 200 fs this is not due to the energy–time uncertainty which is encoded in the quantum kinetic scattering integrals, but due to the fact that not the free-carrier energies but their renormalized carrier energies enter into the quantum kinetic scattering terms. The experiment can thus be understood as a direct observation of the temporal buildup of the polaron correlation here in particular for the heavy holes. It can be shown that in a corresponding pump–probe experiment [40] on the weak coupling material GaAs (see Fig. 16.6) the corresponding hole relaxation does not take place, again demonstrating that it is the intermediate polaron correlation of the heavy holes which causes this rather surprising result. Figure 16.6 further shows that this effect is absent in the semiclassical kinetics in which the free-carrier energies together with the phonon energy enter in the energy conservation. In contrast the quantum kinetic scattering

integrals are in the long-time limit determined by the energies of the dressed particles, i.e., the polarons. Both the polaron shift and the broadening inherent in the polaron GF (see e.g., Fig. 15.6) open this surprising new relaxation channel.

At higher excitation intensities the density of optically excited carriers becomes so large that the interaction between the carriers determines the femtosecond relaxation and dephasing kinetics. In a dense e–h plasma the screening of the Coulomb interaction between two carriers by other optically excited carriers has to be included. On a femtosecond time scale screening is not instantaneous because it takes a certain time of the order of an inverse plasmon frequency until the carriers arrange themselves in order to provide full screening. We will see that with a related optical pump – THz probe experiment, one can follow the buildup of plasma correlations in the gas of excited carriers and the buildup of the resulting collective plasmon mode and of screening. Because of the time-dependent screening process the interaction potential becomes a function of two times. This two-time-dependent effective interaction has to be calculated self-consistently with the evolving carrier Coulomb quantum kinetics for the analysis of ultrafast high-intensity two-beam experiments. These problems will be dealt with in Chaps. 17 and 18.

Coulomb Quantum Kinetics in a Dense Electron–Hole Plasma

Summary. The quantum kinetics for Coulomb interactions is derived. It is shown that the screened scattering potential depends on two time arguments, because screening is built up only after the carriers have been excited and begin to rearrange. The nonequilibrium screened Coulomb potential obeys an integral equation with a polarization due to carrier–carrier scattering. By a generalization of the equilibrium theory, a time-dependent plasmon-pole approximation is derived in order to illustrate the physical content of the complex formalism.

17.1 Introduction

In a dense electron–hole plasma which has been excited by resonant optical pumping, the scattering between the charged carriers provides the fastest relaxation process. This Coulomb scattering is due to two-particle collisions, the corresponding scattering rates therefore increase roughly with the square of the plasma density, while the LO-phonon scattering increases only linearly, disregarding at the moment Pauli blocking effects. In comparison with the phonon scattering which has been studied so far, the Coulomb scattering has several new features. Coulomb scattering conserves the total momentum and energy of the plasma. Therefore it yields a fast relaxation of the originally excited nonequilibrium plasma into a thermal one, whose temperature is determined by the total energy of the plasma. The relaxation of the plasma temperature to that of the lattice will then take place due to the scattering of electrons with phonons, in polar semiconductors predominantly optical phonons. Furthermore, if we calculate as for the phonon scattering the Boltzmann transition rates by first-order perturbation theory – called the *first Born approximation* – one gets for the long-range bare Coulomb interaction a divergent result:

$$\begin{aligned} \frac{\partial n_{k_1}}{\partial t} \Big|_{\text{scatt}} &= -\frac{2\pi}{\hbar} \sum_{k_2, q} \delta(e_{k_1} + e_{k_2} - e_{k_1+q} - e_{k_2+q}) |W_q|^2 \\ &\times (n_{k_1} n_{k_2} (1 - n_{k_1+q}) (1 - n_{k_2-q}) - n_{k_1+q} n_{k_2-q} (1 - n_{k_1}) (1 - n_{k_2})). \end{aligned} \quad (17.1)$$

Here and in the following the vector notation for the momenta has been suppressed in order to slim the formulae. For the bare Coulomb potential $W_q \rightarrow V_q = \frac{4\pi e^2}{\epsilon_0 q^2}$, the q -integral results in $\int_0^\infty \frac{q^2 dq}{q^4} \delta(e_{k_1} + e_{k_2} - e_{k_1+q} - e_{k_2+q})$ which diverges at the lower boundary.

In the equilibrium many-body theory, one overcomes this difficulty by using a partial summation of higher-order diagrams for the effective two-particle Coulomb interaction. In this way the screening of the Coulomb potential by the surrounding carriers is taken into account. The bare Coulomb potential V_q is then replaced by the screened one: $W_q(\omega) = \frac{V_q}{\varepsilon(q, \omega)}$, where $\varepsilon(\mathbf{q}, \omega)$ is the retarded dielectric function, which depends on momentum and frequency. In the static limit $\omega = 0$, the dielectric function would replace in the potential the singular q^{-2} by the analytical $(q^2 + k_{TF}^2)^{-2}$, where k_{TF} is the Thomas–Fermi screening wave number. Thus at least in the static limit, one can use the screened Coulomb potential in the Boltzmann equation. Note that already the use of a frequency-dependent screened Coulomb potential requires a rederivation of the generalized Boltzmann equation starting from quantum kinetics (see, e.g., the textbook of Kadanoff and Baym [191]).

17.2 Screening in the Nonequilibrium GF Theory

In an equilibrium high-density plasma, the random phase approximation (RPA) which will be described below yields a relatively good description of the screening of the Coulomb potential although it does not conserve the total charge. The momentum- and frequency-dependent dielectric function $\varepsilon(\mathbf{q}, \omega)$ in the equilibrium theory originates from the dependences of the screened potential on the differences of the space and time coordinates, $\mathbf{r}_1 - \mathbf{r}_2, t_1 - t_2$, between the two interacting particles. However, in nonequilibrium many-body theory the screened Coulomb potential depends as any other Green function separately on all coordinates $\mathbf{r}_1, \mathbf{r}_2, t_1, t_2$ of the two interacting particles. Screening between two newly created carriers, e.g., builds up as the surrounding particles rearrange themselves by scattering, a process which is not instantaneous but needs some time. The description of this buildup of screening on a femtosecond timescale needs a screened potential $W_q(t_1, t_2)$ which depends on two times and the momentum if we consider for simplicity only spatially homogeneous systems. Because the buildup of screening takes place on a timescale given by the inverse plasmon frequency $\omega_{pl} = \sqrt{\frac{4\pi e^2 n}{\epsilon_0 m}}$, where n is the plasma density and m an effective carrier mass, this two-time dependence of the screened potential is important for the analysis of femtosecond experiments with pulses shorter than or equal to the inverse plasma frequency of the excited plasma. For GaAs, e.g., a plasma density of 10^{18} cm^{-3} corresponds to a plasma frequency of about 30 meV. The corresponding plasma oscillation period is around 100 fs. Under these conditions the screened Coulomb potential W_q has to be treated as a two-time-dependent function $W_q(t_1, t_2)$.

$$\begin{array}{c} W_q(t,t') \\ \text{---} \end{array} = \begin{array}{c} V_q \delta(t,t') \\ \text{---} \end{array} + \begin{array}{c} V_q \delta(t,t_1) \\ \text{---} \end{array} \begin{array}{c} L_q(t_1,t_2) \\ \text{---} \end{array} \begin{array}{c} W_q(t_2,t') \\ \text{---} \end{array}$$

$t \quad t' \quad t \quad t' \quad t \quad t_1 \quad t_2 \quad t' \quad t \quad t_2 \quad t'$

Fig. 17.1. Equation for the screened two-time Coulomb potential W given by a bold dashed line. The thin dashed line is the bare Coulomb potential V , L is the polarization function

for time intervals shorter than or comparable to 100 fs. The nonequilibrium Dyson equation for the effective potential $W_q(t_1, t_2)$ – which can be seen also as the plasmon GF – is

$$W_q(t_1, t_2) = V_q + V_q L_q(t_1, t_3) W_q(t_3, t_2), \quad (17.2)$$

where again the times are defined on the Keldysh contour and a matrix notation is implied, i.e., repeated time arguments have to be integrated. $L_q(t_1, t_2)$ is the intraband polarization function. The diagrammatic representation is given in Fig. 17.1.

So far practically all numerical work applied to the analysis of femtosecond spectroscopy is limited to RPA. In RPA the polarization function is simply given by a loop of two self-consistent particle Green functions

$$L_q(t_1, t_2) = -2i \sum_{k, \lambda, \lambda'} G_{k+q, \lambda, \lambda'}(t_1, t_2) G_{k, \lambda', \lambda}(t_2, t_1). \quad (17.3)$$

Vertex corrections are neglected in RPA. As analyzed by Gartner et al. [123], the general two-time kinetics with this RPA polarization function does not eliminate the $q \rightarrow 0$ divergency from the Coulomb quantum kinetics. Only if one includes a vertex function which has to be determined at least in the screened ladder approximation, the long-wavelength divergence is eliminated in the full two-time nonequilibrium GF theory. However, the complexity of this approach has so far prevented its implementation in numerical evaluations of the femtosecond semiconductor quantum kinetics.

For the application of the Coulomb quantum kinetics, it was therefore a lucky chance that the nonequilibrium RPA is free of divergencies if it is evaluated in the framework of the one-time-dependent density matrices by using the generalized Kadanoff–Baym ansatz

$$\begin{aligned} \overset{\geq}{G}_{k, \lambda, \lambda'}(t, t') &= i \sum_{\mu} G_{k, \lambda, \mu}^r(t, t') \overset{\geq}{G}_{k, \mu, \lambda'}(t', t') \\ &- i \sum_{\mu} \overset{\leq}{G}_{k, \lambda, \mu}^<(t, t) G_{k, \mu, \lambda'}^a(t, t'). \end{aligned} \quad (17.4)$$

We will describe in the following the proof given by Gartner et al. [123].

With the approximation (17.4) the retarded and advanced polarization loops vanish for $q \rightarrow 0$

$$\begin{aligned} L_0^r(t, t') &= \theta(t - t') (L_0^>(t, t') - L_0^<(t, t')) \\ &= -2i\theta(t - t') \sum_{k, \lambda, \lambda'} \left(G_{k, \lambda, \lambda'}^>(t, t') G_{k, \lambda', \lambda}^<(t', t) \right. \\ &\quad \left. - G_{k, \lambda, \lambda'}^<(t, t') G_{k, \lambda', \lambda}^>(t', t) \right) \\ &= -2i\theta(t, t') \sum_{k, \lambda, \lambda', \mu} G_{k, \lambda, \mu}^r(t, t') \left(G_{k, \mu, \lambda'}^>(t', t') G_{k, \lambda', \nu}^<(t', t') \right. \\ &\quad \left. - G_{k, \mu, \lambda'}^<(t', t') G_{k, \lambda', \nu}^>(t', t') \right) G_{k, \nu, \lambda}^a(t', t) = 0, \end{aligned} \quad (17.5)$$

because the equal-time commutator of $G^<$ and $G^>$ vanishes. A similar argument holds for L^a . The effective potential W_q has thus no higher singularity than the bare potential $V_q \propto \frac{1}{q^2}$. One sees that the difference $L_q^>(t, t') - L_q^<(t, t')$ is well behaved for $q \rightarrow 0$, but not $L_q^>(t, t')$ and $L_q^<(t, t')$ separately.

Next we have to consider the scattering self-energies $\Sigma^<$ and $\Sigma^>$ because the long-wavelength divergence of W_q is still dangerous. Taking the scattering self-energies in the so-called GW approximation (i.e., again neglecting vertex corrections), we have

$$\Sigma_{k, \lambda, \lambda'}^>(t, t') = -i \sum_q G_{k-q, \lambda, \lambda'}^>(t, t') W_q^>(t, t'). \quad (17.6)$$

At first sight this approximation looks insufficient, because the kinetics should be governed by the square of the interaction matrix element. However, the scattering interaction potentials can be reexpressed in terms of retarded and advanced potentials as follows.

Relation Between $W_q^<(t_1, t_2)$ and $L_q^<(t_1, t_2)$

The nonequilibrium screened Coulomb potential obeys the following equation

$$W = V + VLW, \quad (17.7)$$

where L is the intraband polarization function and V is the bare, instantaneous Coulomb potential. The “lesser” part of the screened Coulomb potential is obtained from (17.7) by using the relation (4.31):

$$W^< = VL^r W^< + VL^< W^a. \quad (17.8)$$

The retarded potential obeys the Dyson-like equation

$$W^r = V + VL^r W^r. \quad (17.9)$$

Multiplying (17.9) with the inverse potential V^{-1} from the left, this equation can also be written as $(W^r)^{-1}W^r = 1$, with $(W^r)^{-1} = V^{-1} - L^r$. Similarly, (17.8) can be written as

$$(W^r)^{-1}W^< = L^< W^a. \quad (17.10)$$

Multiplying (17.10) from the left with W^r yields the final result:

$$W^< = W^r L^< W^a. \quad (17.11)$$

The above analysis should appear familiar: it is quite analogous to our derivation of the Keldysh equation in Sect. 5.3. The reader is urged to reflect on the similarities and differences!

In extended notation the result (17.11) is

$$W_q^< (t, t') = \int_{-\infty}^t d\tau \int_{-\infty}^{t'} d\tau' W_q^r(t, \tau) L_q^< (\tau, \tau') W_q^a(\tau', t'). \quad (17.12)$$

This result (see also [145]) means that the two-time particle-like potential can be expressed exactly in terms of a convolution of the retarded potential, the particle-like polarization $L_q^<$, and the advanced potential. This result is a generalization of the corresponding equilibrium result given by Kadanoff and Baym [191].

Next we want to convince ourselves that the RPA screened Coulomb potential yields – in spite of the divergent self-energies – a well-defined one-time quantum kinetics. We use the quantum kinetic scattering rate (15.4) for the equal-time particle propagators

$$\begin{aligned} \left. \frac{\partial G_{k,\lambda,\lambda'}^<(t,t)}{\partial t} \right|_{\text{scatt}} &= -i \int_{-\infty}^t dt' \sum_{\mu} \\ &\times \left(\Sigma_{k,\lambda,\mu}^>(t,t') G_{k,\mu,\lambda'}^<(t',t) - \Sigma_{k,\lambda,\mu}^<(t,t') G_{k,\mu,\lambda'}^>(t',t) \right. \\ &\quad \left. - G_{k,\lambda,\mu}^>(t,t') \Sigma_{k,\mu,\lambda'}^<(t',t) + G_{k,\lambda,\mu}^<(t,t') \Sigma_{k,\mu,\lambda'}^>(t',t) \right) \\ &= - \sum_{q,\mu} \int_{-\infty}^t dt' \left(G_{k-q,\lambda,\mu}^>(t,t') W_q^>(t,t') G_{k,\mu,\lambda'}^<(t',t) \right. \\ &\quad \left. - G_{k-q,\lambda,\mu}^<(t,t') W_q^<(t,t') G_{k,\mu,\lambda'}^>(t',t) \right. \\ &\quad \left. - G_{k,\lambda,\mu}^>(t,t') W_q^<(t',t) G_{k-q,\mu,\lambda'}^<(t',t) \right. \\ &\quad \left. + G_{k,\lambda,\mu}^<(t,t') W_q^>(t',t) G_{k-q,\mu,\lambda'}^>(t',t) \right). \end{aligned} \quad (17.13)$$

With the first of the symmetry relations

$$W_q^<(t,t') = W_{-q}^>(t',t), \quad \left(W_q^>(t,t') \right)^* = -W_{-q}^<(t',t), \quad (17.14)$$

we see that in the limit $q \rightarrow 0$ the first two terms are canceled by the last two terms. Thus the equal-time scattering integral has no long-wavelength divergence in the RPA in contrast to the two-time scattering integral, where the discussed compensation does not take place.

Before we proceed with the derivation of the Coulomb scattering quantum kinetics, we want to demonstrate that our form of the RPA nonequilibrium intraband polarization function yields in equilibrium indeed the well-known Lindhard formula.

Equilibrium Form of the Polarization Function

With the equilibrium free-particle Green functions for a single band

$$\begin{aligned} G_{k+q}^r(t_1, t_2) &= -i\theta(t_1 - t_2)e^{-ie_{k+q}(t_1 - t_2)}, \\ G_k^a(t_2, t_1) &= i\theta(t_1 - t_2)e^{ie_k(t_1 - t_2)}, \end{aligned} \quad (17.15)$$

and with $t = t_1 - t_2$ we get the polarization function

$$L_q^r(t_1, t_2) = -2i\theta(t) \sum_k e^{i(e_k - e_{k+q})t} [f_k(t_2) - f_{k+q}(t_2)]. \quad (17.16)$$

In equilibrium where the distribution functions are time independent, a Fourier transform with respect to t yields the Lindhard formula:

$$L_q^r(\omega) = 2 \sum_k \frac{f_k - f_{k+q}}{\omega + i\delta + e_k - e_{k+q}}. \quad (17.17)$$

17.3 Coulomb Quantum Kinetics

Now we want to formulate the RPA Coulomb scattering integral for the one-time quantum kinetics in detail. Inserting the RPA polarization (17.3) and the relation (17.12) for the scattering potential, we find the one-time RPA scattering integral:

$$\begin{aligned} \left. \frac{\partial G_{k\lambda,\lambda'}^<(t, t)}{\partial t} \right|_{\text{scatt}} &= 2i \sum_{q,\mu} \int_{-\infty}^t dt' \int_{-\infty}^t d\tau \int_{-\infty}^{t'} d\tau' \\ &\times \left(G_{k-q,\lambda,\mu}^>(t, t') W_q^r(t, \tau) \sum_{k',\nu,\nu'} \left(G_{k'+q,\nu,\nu'}^>(\tau, \tau') G_{k',\nu',\nu}^<(\tau', \tau) \right) \right. \\ &\quad \times W_q^a(\tau', t') G_{k,\mu,\lambda'}^<(t', t) \\ &- G_{k-q,\lambda,\mu}^<(t, t') W_q^r(t, \tau) \sum_{k',\nu,\nu'} \left(G_{k'+q,\nu,\nu'}^<(\tau, \tau') G_{k',\nu',\nu}^>(\tau', \tau) \right) \\ &\quad \left. \times W_q^a(\tau', t') G_{k,\mu,\lambda'}^>(t', t) \right) \end{aligned} \quad (17.18)$$

$$\begin{aligned}
& - G_{k,\lambda,\mu}^>(t,t') W_q^r(t',\tau') \sum_{k',\nu,\nu'} \left(G_{k'+q,\nu,\nu'}^<(\tau',\tau) G_{k',\nu',\nu}^>(\tau,\tau') \right) \\
& \quad \times W_q^a(\tau,t) G_{k-q,\mu,\lambda'}^<(t',t) \\
& + G_{k,\lambda,\mu}^<(t,t') W_q^r(t',\tau') \sum_{k',\nu,\nu'} \left(G_{k'+q,\nu,\nu'}^>(\tau',\tau) G_{k',\nu',\nu}^<(\tau,\tau') \right) \\
& \quad \times W_q^a(\tau,t) G_{k-q,\mu,\lambda'}^>(t',t) .
\end{aligned}$$

The third and fourth scattering terms can be obtained from the first two terms by the following interchange of arguments:

$$k \leftrightarrow k - q, \quad k' \leftrightarrow k' + q, \quad W_q^r \leftrightarrow \left(W_q^a \right)^*. \quad (17.19)$$

For the spectral functions of the potential, one has to take into account that, e.g., $(W_q^r(t,t'))^* = W_q^a(t',t)$. Before we can make use of the generalized Kadanoff–Baym ansatz to express the two-time propagators in terms of density matrices and the spectral GFs, we have to establish a definite time order between the two intermediate times τ and τ' by splitting the τ' as follows:

$$\int_{-\infty}^t d\tau \int_{-\infty}^{t'} d\tau' = \int_{-\infty}^t d\tau \left(\int_{-\infty}^\tau d\tau' + \int_\tau^{t'} d\tau' \right). \quad (17.20)$$

Now we know that $\tau \leq t$, $\tau' \leq t'$, and $\tau' \leq \tau$ in the first τ' integral, and $\tau \leq \tau'$ in the second integral. With (17.4) the final form of the Coulomb scattering integrals becomes:

$$\begin{aligned}
& \frac{\partial G_{k\lambda,\lambda'}^<(t,t)}{\partial t} \Big|_{\text{scatt}} = 2i \sum_{q,k',\mu,\mu',\nu,\nu',\rho,\rho',\sigma} \int_{-\infty}^t dt' \int_{-\infty}^t d\tau \\
& \quad \times \left(G_{k-q,\lambda,\mu'}^r(t,t') G_{k-q,\mu',\mu}^>(t',t') W_q^r(t,\tau) \right. \\
& \quad \times \left(\int_{-\infty}^\tau d\tau' G_{k'+q,\nu,\rho}^r(\tau,\tau') G_{k'+q,\rho,\nu'}^>(\tau',\tau') G_{k',\nu',\rho'}^a(\tau',\tau) G_{k',\rho',\nu}^<(\tau',\tau) \right. \\
& \quad + \int_\tau^{t'} d\tau' G_{k'+q,\nu,\rho}^>(\tau',\tau') G_{k'+q,\rho,\nu'}^a(\tau,\tau') G_{k',\nu',\rho'}^r(\tau',\tau) G_{k',\rho',\nu}^<(\tau,\tau) \Big) \\
& \quad \times W_q^a(\tau',t') G_{k,\mu,\sigma}^<(t',t') G_{k,\sigma,\lambda'}^a(t',t) \\
& - G_{k-q,\lambda,\mu'}^r(t,t') G_{k-q,\mu',\lambda}^<(t',t') W_q^r(t,\tau) \\
& \quad \times \left(\int_{-\infty}^\tau d\tau' G_{k'+q,\nu,\rho}^r(\tau,\tau') G_{k'+q,\rho,\nu'}^<(\tau',\tau') G_{k',\nu',\rho}^>(\tau',\tau') G_{k',\rho,\nu}^a(\tau',\tau) \right. \\
& \quad + \int_\tau^{t'} d\tau' G_{k'+q,\nu,\rho}^<(\tau,\tau') G_{k'+q,\rho,\nu'}^a(\tau,\tau') G_{k',\nu',\rho'}^r(\tau',\tau) G_{k',\rho',\nu}^>(\tau,\tau) \Big)
\end{aligned} \quad (17.21)$$

$$\begin{aligned} & \times W_q^a(\tau', t') G_{k,\mu,\sigma}^>(t', t) G_{k,\sigma,\lambda'}^a(t', t) \\ & - \left\{ k \leftrightarrow k - q, k' \leftrightarrow k' + q, W_q^r \leftrightarrow \left(W_q^r \right)^* \right\}. \end{aligned}$$

Again the last line accounts for the scattering terms 3 and 4 which are generated from the explicitly given terms 1 and 2 by applying the described substitutions.

Now the structure of the Coulomb scattering integral is evident: The equal-time particle propagators $G^<$ (t', t'), i.e., the density matrices, all appear at the earlier time t', τ , or τ' because of the memory structure of the quantum kinetics. Due to the two-time-dependent effective Coulomb potential, the memory structure of the density matrices of the two interacting particles before and after the collision is considerably more involved than for the interaction with LO-phonons at least as long as the screening for this interaction is neglected. Later we will unify the treatment of both scattering processes by screening both the Coulomb interaction and the particle interaction caused by the exchange of phonons.

As discussed already for the phonon scattering kinetics, the diagonal elements of the factors $G^<$ give the probability that the initial states are populated, while those of $G^>$ yield the probabilities that the final states are unoccupied. In each of the four terms a product of a retarded and an advanced potential function appears, displaying the second order of the scattering integrals in the screened interaction explicitly. The time integrals over the particle spectral functions of the four involved states would give in the free-particle Markov limit the energy conservation. In general they contain important many-particle effects such as energy renormalization, excitonic and coherent field effects, if they are calculated in the mean-field approximation. Furthermore, also the damping of these functions may contain important physics as discussed in Chap. 16 in connection with the polaron formation.

These Coulomb scattering rates determine the one-time Coulomb quantum kinetics together with the self-consistently calculated retarded and advanced Coulomb potential which obeys according to (17.2) the following integral equation:

$$W_q^r(t, t') = V_q \delta(t, t') + \int_{t'}^t dt'' V_q L_q^r(t, t'') W_q^r(t'', t'), \quad (17.22)$$

where $L_q^r(t, t')$ is the RPA polarization which has been given already in (17.6) for the special value $q = 0$. Its general form is

$$\begin{aligned} L_q^r(t, t') &= \theta(t - t') (L_q^>(t, t') - L_q^<(t, t')) \\ &= -2i\theta(t - t') \sum_{k,\lambda,\lambda'} \left(G_{k-q,\lambda,\lambda'}^>(t, t') G_{k,\lambda',\lambda}^<(t', t) \right. \\ &\quad \left. - G_{k-q,\lambda,\lambda'}^<(t, t') G_{k,\lambda',\lambda}^>(t', t) \right) \end{aligned} \quad (17.23)$$

$$\begin{aligned}
&= -2i\theta(t, t') \sum_{k, \lambda, \lambda', \mu} G_{k-q, \lambda, \mu}^r(t, t') \left(G_{k-q, \mu, \lambda'}^>(t', t') G_{k, \lambda', \nu}^<(t', t') \right. \\
&\quad \left. - G_{k-q, \mu, \lambda'}^<(t', t') G_{k, \lambda', \nu}^>(t', t') \right) G_{k, \nu, \lambda}^a(t', t) = 0.
\end{aligned}$$

In this retarded formulation of the Coulomb quantum kinetics, we do not get a divergent result even in the initial time interval, where the Coulomb potential is still a bare one [72, 99] because in this interval there is also practically no energy conservation due to the time-energy uncertainty.

The total time development of the one-time density matrix, $\rho_{k, \lambda, \lambda'}(t) = -iG_{k, \lambda, \lambda'}^<(t, t)$, decomposed into the coherent evolution (15.7) and the mainly dissipative evolution due to the scattering integral (17.22), and the two-time effective potential $W_q^r(t, t')$ according to (17.22) together with the RPA polarization function (17.24) forms a closed system of equations, which be solved for special two-pulse femtosecond excitations. We will actually discuss in Chap. 18 first calculations for optical pump and THz probe experiments as they have been performed by Leitenstorfer et al. [160, 161] to measure directly the buildup of a correlated e-h plasma and of screening. After the studies of the two-time-dependent potential, we will apply the quantum kinetics of phonon and Coulomb scattering for various femtosecond FWM experiments carried out by Wegener et al. [159, 357]. Before we enter in the discussion of these self-consistent calculations, we want to develop a plasmon-pole approximation for the two-time-dependent screened Coulomb potential. The plasmon-pole approximation has been quite important in the development of the quasiequilibrium many-body theory of photoexcited semiconductors (see, e.g., Zimmermann [381] and Haug and Schmitt-Rink [142]).

17.4 Plasmon-Pole Approximation for the Two-Time-Dependent Potential

Today the self-consistent numerical solution of the RPA equation (17.24) of the screened Coulomb potential is not too complicated, but still it is worthwhile to get insight into this equation by developing with relatively simple approximations the so-called *plasmon-pole approximation*, for simplicity again for a single band.

For this purpose we take the spectral electron functions in the damped free-particle approximation:

$$\begin{aligned}
G_k^r(t, t') &= -i\theta(t - t') e^{(-ie_k - \gamma_k)(t - t')}, \\
G_k^a(t, t') &= i\theta(t' - t) e^{(-ie_k + \gamma_k)(t - t')},
\end{aligned} \tag{17.24}$$

where γ_k is some reasonable collision broadening. The polarization function will be approximated by its long-wavelength limit [100] as it is done in the quasiequilibrium theory [146].

Long-Wavelength Limit of the Polarization Function

We start by considering the long-wavelength limit of

$$\begin{aligned} \lim_{q \rightarrow 0} V_q L_q^r(t, t') &= \lim_{q \rightarrow 0} \frac{8\pi e^2}{\varepsilon_0 q^2} (-i)\theta(t-t') \\ &\times \sum_k G_{k-q}^r(t, t') G_k^a(t, t') [f_k(t') - f_{k+q}(t')]. \end{aligned} \quad (17.25)$$

With (17.24) we get the expression

$$\lim_{q \rightarrow 0} \frac{8\pi e^2}{\varepsilon_0 q^2} (-i)\theta(t-t') \sum_{\mathbf{k}} e^{[i(e_k - e_{k+q}) - 2\gamma](t-t')} [f_k(t') - f_{k+q}(t')]. \quad (17.26)$$

Using $e_k - e_{k+q} \simeq -\mathbf{k} \cdot \mathbf{q}/m$ and $f_{k+q} = f_k + \mathbf{q} \cdot \nabla f_k$, we find

$$\lim_{q \rightarrow 0} \frac{4\pi e^2}{\varepsilon_0 q^2} i\theta(t-t') 2 \sum_{\mathbf{k}} e^{[-i\mathbf{q} \cdot \mathbf{k}/m - 2\gamma](t-t')} \mathbf{q} \cdot \nabla f_k(t'). \quad (17.27)$$

A partial integration finally yields

$$\begin{aligned} \lim_{q \rightarrow 0} V_q L_q^r(t, t') &= -(t-t')\theta(t-t') e^{-2\gamma(t-t')} \frac{4\pi e^2}{\varepsilon_0 m} n(t') \\ &= -(t-t')\theta(t-t') e^{-2\gamma(t-t')} \omega_{\text{pl}}^2(t'). \end{aligned} \quad (17.28)$$

This result defines the plasma frequency $\omega_{\text{pl}}(t)$ in terms of the total density $n(t) = \sum_{\mathbf{k}} f_k(t)$ of any nonequilibrium distribution.

Next we rewrite the Dyson equation (17.22) for the retarded screened Coulomb potential by introducing a density–density correlation function $S_q(t, t')$ in the form

$$W_{s,q}^r(t, t') = V_q \left(\delta(t-t') + S_q(t, t') e^{-2\gamma(t-t')} \right). \quad (17.29)$$

The trivial damping constants γ from the damped free-particle Green functions are explicitly taken into account. For the screening described by the density–density correlation function, only the Landau damping contributes. A comparison of (17.22) and (17.29) yields

$$S_q(t, t') = V_q L_q^r(t, t') + V_q \int_{t'}^t dt'' L_q^r(t, t'') S_q(t_3, t'). \quad (17.30)$$

The polarization $L_q^r(t, t_3)$ has to be evaluated with $\gamma = 0$. For the long-wavelength limit of (17.30), we find with (17.28) the following differential equation

$$\frac{d^2 S_{q=0}(t, t')}{dt^2} = -\omega_{\text{pl}}^2(t) S_{q=0}(t, t'), \quad (17.31)$$

which shows that the long-wavelength limit density-density correlation function oscillates with the actual plasma frequency which may change parametrically with time t as the plasma density $n(t)$ changes. Furthermore, one finds the following initial conditions

$$S_{q=0}(t', t') = 0 \quad \text{and} \quad \left. \frac{dS_{q=0}(t, t')}{dt} \right|_{t=t'} = -\omega_{\text{pl}}^2(t'), \quad (17.32)$$

where we used $\lim_{t \rightarrow t'+} \theta(t - t') = 1$.

17.4.1 Parametric Plasma Oscillations

We solve (17.31) of a parametric oscillator with the ansatz

$$S_{q=0}(t, t') = \tilde{S}_0(t, t') \exp \left\{ -i \int_{t'}^t dt_3 \omega_{\text{pl}}(t_3) \right\}. \quad (17.33)$$

$\tilde{S}_0(t, t')$ obeys the following equation-of-motion in t

$$\ddot{s} - i\dot{\omega}_{\text{pl}} s - 2i\omega_{\text{pl}} \dot{s} = 0. \quad (17.34)$$

We assume that the parametric changes of $\omega_{\text{pl}}(t)$ are sufficiently small in an oscillation period, so that the second-order derivative of s can be neglected. The remaining equation can be solved by separation of variables. We find

$$\frac{ds}{s} = -\frac{1}{2} \frac{d\omega_{\text{pl}}}{\omega_{\text{pl}}}, \quad (17.35)$$

with the solution

$$s(t) = \tilde{S}_0(t, t') = S_0 \omega_{\text{pl}}^{-1/2}(t) \omega_{\text{pl}}^{1/2}(t'). \quad (17.36)$$

The first initial condition (17.32) yields

$$S_{q=0}(t, t') = -iS_0 \omega_{\text{pl}}^{-1/2}(t) \omega_{\text{pl}}^{1/2}(t') \sin \left[\int_{t'}^t dt_3 \omega_{\text{pl}}(t_3) \right]. \quad (17.37)$$

The second initial condition (17.34) at $t = t'$ determines S_0 . From

$$-iS_0 \omega_{\text{pl}}(t') = -\omega_{\text{pl}}^2(t'), \quad (17.38)$$

one gets $S_0 = -i\omega_{\text{pl}}(t')$.

The resulting long-wavelength limit of the time-dependent density-density correlation is in the plasmon-pole approximation [102]

$$S_{q=0}(t, t') = -\theta(t - t') \omega_{\text{pl}}^{3/2}(t') \omega_{\text{pl}}^{-1/2}(t) \sin \left[\int_{t'}^t dt'' \omega_{\text{pl}}(t'') \right]. \quad (17.39)$$

Before we can insert $S_q(t, t')$ into (17.29), we have to extend it to finite q values. This can be done by comparing the Fourier transform of the equilibrium density–density correlation $S_q^0(\omega)$ in the plasmon-pole approximation [142] with respect to the relative time coordinate $t - t'$ with (17.39). In equilibrium the time-dependent plasmon-pole approximation is [145]

$$\begin{aligned} S_q^0(t - t') &= \int_{-\infty}^{+\infty} \frac{d\omega}{2\pi} e^{-i\omega(t-t')} \frac{\omega_{pl}^2}{(\omega + i\delta)^2 - \omega_q^2} \\ &= -\theta(t - t') \frac{\omega_{pl}^2}{\omega_q^2} \sin[\omega_q(t - t')], \end{aligned} \quad (17.40)$$

with the dispersion of the effective plasmon pole:

$$\omega_q^2 = \omega_{pl}^2 \left(1 + \frac{q^2}{\kappa^2} \right) + Cq^4. \quad (17.41)$$

The inverse screening length κ can be expressed in a form which can also be used for nonequilibrium distributions

$$\kappa^2 = \frac{4\pi e^2}{\varepsilon_0} \int_0^\infty \frac{de_k}{e_k} \varrho(e_k) f_k, \quad (17.42)$$

assuming that the (nonequilibrium) distribution is isotropic, i.e., depends only on the energy e_k , $\varrho(e_k)$ is the third parabolic density of states. C is a numerical constant. The comparison between (17.39) and (17.40) shows that at finite q values one has to use the following nonequilibrium density–density correlation:

$$S_q(t, t') = -\theta(t - t') \frac{\omega_{pl}^2(t')}{\omega_q^{1/2}(t)\omega_q^{1/2}(t')} \sin \left(\int_{t'}^t dt'' \omega_q(t'') \right). \quad (17.43)$$

Naturally, the time-dependent frequencies $\omega_{pl}(t)$ and $\omega_q(t)$ have to be calculated from time-dependent $n(t)$, $\kappa(t)$, and $f_k(t)$. With this result the nonequilibrium damped plasmon-pole approximation for the retarded screened Coulomb potential [102] is obtained with (17.29) as

$$\begin{aligned} W_{s,q}^r(t, t') &= V_q \left\{ \delta(t - t') \right. \\ &\quad \left. - \theta(t - t') \frac{\omega_{pl}^2(t')}{\omega_q^{1/2}(t)\omega_q^{1/2}(t')} \sin \left(\int_{t'}^t dt'' \omega_q(t'') \right) e^{-2\gamma_q(t-t')} \right\}. \end{aligned} \quad (17.44)$$

The results hold also in 2D if the following 2D expressions [146] are used

$$V_q = \frac{2\pi e^2}{\varepsilon_0 L^2 q} \quad \text{and} \quad \omega_{pl}^2(t) = \frac{2\pi e^2 n(t) q}{m \varepsilon_0} \quad (17.45)$$

and

$$\omega_q^2(t) = \omega_{\text{pl}}^2(t) \left(1 + \frac{q}{\kappa(t)} \right) + Cq^4, \quad (17.46)$$

with

$$\kappa^2(t) = \frac{2e^2m}{\varepsilon_0} f_0(t). \quad (17.47)$$

17.4.2 Instantaneous Static Potential Approximation

In order to make contact with the Boltzmann limit on a longer timescale $t\omega_{\text{pl}} \gg 1$, we may use approximately a statically screened instantaneous potential [347]

$$W_{s,q}^r(t, t') = V_{s,q}(t') \delta(t - t'), \quad (17.48)$$

where $V_{s,q}$ is in the simplest approximation:

$$V_{s,q}(t) = V_q \frac{q^2}{q^2 + \kappa(t)^2}. \quad (17.49)$$

Consider now with (17.48) the first term of the quantum kinetic scattering integral again for one band only. Only the integral from t' to t contributes. With

$$\Delta e_{k,k',q} = e_k + e_{k'} - e_{k-q} - e_{k'+q}, \quad \Gamma_{k,k',q} = \gamma_k + \gamma_{k'} + \gamma_{k-q} + \gamma_{k'+q}, \quad (17.50)$$

the first term reduces with (17.24) to

$$\begin{aligned} & -2 \sum_{q,k'} \int_{-\infty}^t dt' V_{s,q}(t) V_{s,q}(t') e^{-i\Delta e_{k,k',q} - \Gamma_{k,k',q}(t-t')} \\ & \times f_k(t') f_{k'}(t') (1 - f_{k-q}(t')) (1 - f_{k'+q}(t')). \end{aligned} \quad (17.51)$$

The second term of (17.22) yields with an opposite sign the same result, only with the exchange of all occupied and empty states. Thus the sum of the first two terms is

$$\begin{aligned} & -2 \sum_{q,k'} \int_{-\infty}^t dt' V_{s,q}(t) V_{s,q}(t') e^{-i\Delta e_{k,k',q} - \Gamma_{k,k',q}(t-t')} \\ & \times \left\{ f_k(t') f_{k'}(t') (1 - f_{k-q}(t')) (1 - f_{k'+q}(t')) \right. \\ & \left. - (1 - f_k(t')) (1 - f_{k'}(t')) f_{k-q}(t') f_{k'+q}(t') \right\}. \end{aligned} \quad (17.52)$$

In the final contribution to (17.22), we have to exchange all k and $k - q$ variables as well as all k' and $k' + q$ variables. With this exchange $\Delta e_{k,k',q} \rightarrow -\Delta e_{k,k',q}$, while the population factors of the first and second terms are

interchanged. The oscillating exponential terms add up to a cosine. The final result is

$$\begin{aligned} \frac{\partial f_k(t)}{\partial t} = & -4 \sum_{q,k'} \int_{-\infty}^t dt' V_{s,q}(t) V_{s,q}(t') \cos[\Delta e_{k,k',q}(t-t')] e^{-\Gamma_{k,k',q}(t-t')} \\ & \times \left\{ f_k(t') f_{k'}(t') (1 - f_{k-q}(t')) (1 - f_{k'+q}(t')) \right. \\ & \left. - (1 - f_k(t')) (1 - f_{k'}(t')) f_{k-q}(t') f_{k'+q}(t') \right\}. \end{aligned} \quad (17.53)$$

Now all four distribution functions enter the collision rate at the same retarded time t' , while the statically screened potential enters at the times t and t' . Because we used an instantaneous statically screened potential, we consider consistently the limit of completed collisions, where all retardations of the distribution and of the screened potential are ignored. In this limit one gets the much simpler equation:

$$\begin{aligned} \frac{\partial f_k(t)}{\partial t} = & -2 \sum_{q,k'} V_{s,q}^2(t) 2\pi D(e_k + e_{k'} - e_{k-q} - e_{k'+q}) \\ & \times \left\{ f_k(t) f_{k'}(t) (1 - f_{k-q}(t)) (1 - f_{k'+q}(t)) \right. \\ & \left. - (1 - f_k(t)) (1 - f_{k'}(t)) f_{k-q}(t) f_{k'+q}(t) \right\}, \end{aligned} \quad (17.54)$$

where $D(\omega)$ is a broadened delta-function

$$2\pi D(\omega) = \frac{2}{\omega^2 + \Gamma^2} [\omega \sin(\omega t) e^{-\Gamma t} - \Gamma \cos(\omega t) e^{-\Gamma t} + \Gamma]. \quad (17.55)$$

The factor 2 in front of the transition rates stems from the two spin states of the second scattered electron. The only difference of the quantum kinetic equation in the completed-collision limit compared to a semiclassical Boltzmann equation is that the energy-conserving delta-function is replaced by a broadening function D , which takes into account the finite lifetime of a particle state in a plasma and the finite evolution time of the system. In Sect. 11.5 we showed, following the work of Reggiani et al. [291], that the quantum kinetic equation in the completed-collision approximation can be treated again by an extension of the Monte Carlo simulation method (at least for electron–phonon scattering).

However, the transition of the quantum kinetic regime to the Markovian Boltzmann regime is – particularly for Coulomb scattering – still not fully understood. The Wigner–Weisskopf approximation for the advanced and retarded Green functions and the introduction of the damping in the two-time-dependent screened Coulomb potential do not, in their present form, result in an asymptotic energy conservation. The Lorentzians, which replace the

energy-conserving delta-functions of the Boltzmann equation in the Markov limit of quantum kinetics, are spectrally too broad and cause the aforementioned problems. If one takes into account that the damping of the retarded Green function is not instantaneous, but has to be first built up, one finds [147] – instead of an exponential damping factor – a decay law which is inversely proportional to the hyperbolic cosine:

$$\exp[-\gamma(t - t')] \rightarrow \frac{1}{\cosh[\gamma(t - t')]} \quad (17.56)$$

This delayed decay at early times gives rise to an exponential fall-off of the resonance curve in frequency space. The resulting long-time limit of quantum kinetics conserves the total energy of the system much better – albeit still not exactly – in comparison with the Lorentzian spectral functions. For a stationary but frequency-dependent screened Coulomb potential, Mermin [264] showed how the damping has to be introduced in an energy-conserving approximation. A corresponding asymptotically energy-conserving introduction of the damping in the two-time-dependent screened Coulomb potential is still missing. Furthermore, in the optically studied multiband case, the exchange and correlation Coulomb self-energies give rise to large plasma-density-dependent band gap shrinkage. In II–VI compound semiconductors, this effect can be as large as 30 meV and is well studied in the nanosecond high excitation spectroscopy [146, 381]. Therefore, energy renormalizations should be included in a quantum kinetic description which will asymptotically result in a correct quasiparticle Boltzmann equation. However, as discussed before in the connection with phonon scattering, if one includes the real parts of the self-energy into the spectral functions, one runs into the problem of double counting. Thus, both the generalized Kadanoff–Baym ansatz, which introduces the spectral functions, and the approximations for the spectral functions have to be improved before one can successfully treat the transition from the delayed quantum kinetics to the generalized Boltzmann kinetics. An early attempt to describe this transition regime and to develop numerical solutions for it has been reported in Tran Thoai and Haug [348]. Because of the still unsolved problems, we will not describe this most difficult regime here in detail.

As far as the history of the ultrafast plasma kinetics is concerned, already in the 1980s high-intensity resonant femtosecond pump and probe experiments [34, 206, 242, 278] have been performed in order to study the fast relaxation kinetics in dense plasmas caused by carrier–carrier scattering. In earlier treatments of the carrier–carrier kinetics, semiclassical descriptions on the level of the Boltzmann equation have been applied. Monte Carlo simulations [14, 102, 126, 188, 277, 334] and direct numerical integrations [8, 43, 84, 85, 303] of the semiclassical Boltzmann equation have been used to describe the time development of the nonequilibrium electron distributions. As discussed in Part III, closely related studies of the nonequilibrium electron kinetics are required to describe the transport in semiconductor microstructures [109, 168]. The large electric fields in these small devices cause

large deviations from equilibrium distributions. All these earlier investigations disregarded the discussed two-time dependence of the screened Coulomb potential and are thus limited to timescales larger than an inverse plasma frequency.

As mentioned before we will in Chap. 18 discuss the formation of screening and more generally of a correlated dense electron–hole plasma and in a second part the action of screening on both the Coulomb interaction and the interaction caused by the exchange of an LO-phonon.

The Buildup of Screening

Summary. The two-time screened Coulomb potential, as it results from a self-consistent solution of the full Coulomb quantum kinetics after a femtosecond optical pulse, is described. The resulting potential is compared to femtosecond-resolved optical pump and THz-probe measurements including also the screening of the phonon-assisted carrier-carrier interaction. Excellent agreement between experiment and theory is found. Finally, the predictions of the Coulomb quantum kinetics for femtosecond four-wave mixing without and with coherent control are compared to corresponding experiments resulting in a density-dependent dephasing time and plasmon-phonon quantum beats.

18.1 Screening of the Coulomb Interaction

As discussed in the last chapter ultrafast carrier kinetics in femtosecond pulse excited semiconductors requires the introduction of a two-time-dependent effective interaction, because it takes a time of the order of an inverse plasma frequency before a correlated plasma is formed. In this correlated plasma, the charges are screened with a cloud of opposite charges so that the carrier-carrier interaction is reduced. At the same time as a correlated plasma evolves, a collective plasmon mode is formed. Fortunately these relatively new concepts about the ultrafast buildup of a correlated plasma can be tested directly by optical pump and THz probe spectroscopy, as shown by Leitenstorfer et al. [160]. The THz radiation can be generated by rectification of an optical femtosecond pulse in a nonlinear GaSe crystal. Using an optical 10 fs pulse, one obtains in this way a single-cycle THz pulse. This THz pulse has a broad spectrum which covers the whole midinfrared region and is resonant with the frequency of the collective oscillations in the e-h plasma which has been excited in GaAs by the same resonant optical pulse before. The transmission spectrum of the THz pulse as a function of the delay between pump and probe allows one

to study the dressing of the carriers and of the connected screening of their interactions.

Thus it is worthwhile to describe the calculation of the two-time-dependent carrier interaction. In a first attempt the integral equation for the retarded potential was solved together with semiconductor Bloch equations with the optical pump pulse, but without scattering [100]. It has been recognized that the resulting rapidly oscillating interaction $W_q^r(t, t')$ can only be analyzed in a meaningful way by taking an incomplete Fourier transformation with respect to the relative time coordinate. The resulting time- and frequency-dependent spectrum $W_q^r(\omega, t)$ clearly shows how the plasmon resonance builds up as a function of the time which has elapsed after the excitation by the pump pulse.

18.1.1 Calculations of the Two-Time-Dependent Screened Potential

A first self-consistent calculation has been obtained by Bányai et al. [22]. In this work the integral equation of the two-time-dependent potential has been solved together with the full semiconductor Bloch equation for the two-band density matrix containing a coherent femtosecond pump pulse and the self-consistent quantum kinetic scattering integrals. Because the scattering integrals expressed in terms of retarded and advanced potential functions contain a threefold time integration (17.22), it has been found to be time-saving for the numerical calculations to express the scattering integral only in terms of the kinetic components $W_q^>(t, t')$ and $W_q^<(t, t')$ (as in (17.13)) and calculate the scattering component $W_q^<(t, t')$ of the potential from the Dyson equation (17.7) for $W_q(t_1, t_2)$. From (17.8) we get explicitly

$$\begin{aligned} W_q^<(t, t') &= V_q \int_{-\infty}^t dt'' L_q^r(t, t'') W_q^<(t'', t') + V_q \int_{-\infty}^{t'} dt'' L_q^>(t, t'') W_q^a(t'', t') \\ &= V_q \int_{-\infty}^t dt'' L_q^r(t, t'') W_q^<(t'', t') + V_q L^<(t, t') V_q \\ &\quad + V_q \int_{-\infty}^{t'} dt'' L_q^>(t, t'') (W_q^<(t'', t') - W_q^>(t'', t')) . \end{aligned} \quad (18.1)$$

Together with the symmetry relation (17.14), i.e., $W_q^<(t, t') = W_{-q}^>(t', t) = W_q^>(t', t)$, one gets from (18.1) an integral equation for the scattering component $W_q^<$ alone. The resulting retarded potential obtained from the calculated $W^<$ and $W^>$ is as mentioned transformed into a frequency- and time-dependent function by the following incomplete Fourier transformation

$$\begin{aligned} W_q^r(\omega, t) &= \int_{-\infty}^t dt' e^{i\omega(t-t')} W_q^r(t, t') \\ &= \int_0^\infty d\tau e^{i\omega\tau} W_q^r(t, t-\tau) = \frac{V_q}{\varepsilon_q^r(\omega, t)} , \end{aligned} \quad (18.2)$$

where $\varepsilon_q^r(\omega, t) = \varepsilon_q(\omega, t)$ is the complex retarded dielectric function. The real and imaginary parts of the inverse dielectric function have been calculated in the described self-consistent way for bulk GaAs excited by a Gaussian coherent light pulse with a half-width of 15 fs and a field amplitude which corresponds to a 0.25π pulse. The excess energy with respect to the unrenormalized band edge was 50 meV. For computational reasons we could not calculate the complete long-wavelength limit of the dielectric function, which reflects the problems with the weak long-wavelength singularity discussed in Chap. 17. In order to get sufficient numerical accuracy we calculated $\varepsilon_q(\omega, t)$ for $qa_0 = 1$, where a_0 is the exciton Bohr radius.

Particularly from the imaginary part of the calculated inverse dielectric function shown in Fig. 18.1, one sees how the plasmon resonance evolves. The imaginary part of the inverse dielectric function is a measure of the energy loss of a charged particle propagating in the plasma. Before the pulse the imaginary part was 0, and the real part was 1. At 50 fs after the pulse a broad absorption develops which shows that at this stage a wide range of energies can be exchanged between the charged carriers. For successive times the broad spectrum sharpens to the fully developed plasmon resonance at about 250 fs. The period of the plasmon oscillation $T_{pl} = 2\pi/\omega_{pl} \simeq 100$ fs is of the same order of magnitude, showing that the plasmon period sets the timescale for the buildup of screening. The real part of the inverse dielectric function at least in the limit of a sharp plasmon resonance shows how the interaction is renormalized as a function of time and frequency. Below the plasmon resonance the interaction even changes sign due to the influence of

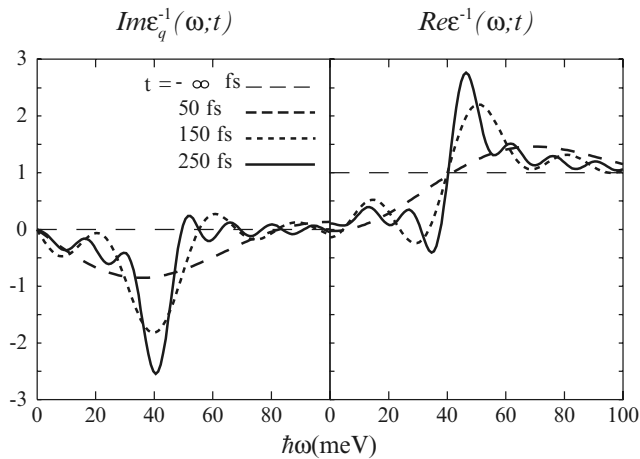


Fig. 18.1. Spectra of the imaginary (*left*) and real (*right*) parts of the inverse dielectric function calculated for a wavenumber $qa_0 = 1$ and various times t after the 15 fs pulse at $t = 0$. The plasma frequency of the excited carriers is about 31 meV, the corresponding plasma period is about 100 fs. According to Bányai et al. [22]

the screening cloud, as is well known from the equilibrium theory. The oscillations in the wings of the plasmon resonance are artifacts due to the limited accuracy of the Fourier transform.

18.1.2 Femtosecond Optical Pump and THz Probe Spectroscopy

We mentioned already at the beginning of the chapter that Leitenstorfer et al. [160] succeeded to measure the inverse dielectric function by a femtosecond optical pump and THz probe spectroscopy. They excited a GaAs crystal with a 10 fs pump pulse which had a central frequency of 1.55 eV. The photo-induced pair density was estimated to be $N = 2 \times 10^{18} \text{ cm}^{-3}$, which results in a plasma frequency $\omega_{pl}/2\pi \simeq 15 \text{ THz}$. The transverse THz field probes the transverse dielectric function, which however is degenerate with the longitudinal one in the long-wavelength limit. One can also argue that the strongly focused infrared beam is no longer purely transversal, but contains longitudinal components which are sensitive to the longitudinal plasma oscillations. The central frequency of the infrared beam was 28 THz, the half width of the pulse was 27 fs. The time delay t_D between the pump pulse and the single-cycle THz pulse varied between $t_D = -25 \text{ fs}$ and 175 fs. After the highest delay time of 175 fs, the spectra did no longer change in an appreciable way. The fit of the resonance with a damped plasmon pole-approximation (Drude formula) yielded a plasma frequency of $\omega_{pl}/2\pi = 14.4 \text{ THz}$ in good agreement with the frequency of 15 THz expected from the excited density. This experiment showed directly how long it takes until a bare charged particle obtains a cloud of opposite charges and forms a dressed quasiparticle, as illustrated on the r.h.s. of Fig. 18.2.

If we identify the time t after the pump pulse of the calculated spectra with the delay time t_D between pump and THz probe pulse, the calculated spectra of Fig. 18.1 are in a very good qualitative agreement with the measured spectra of Fig. 18.2. Thus the experiment fully supports the above developed concepts of the Coulomb quantum kinetics. The LO-phonon resonance is also seen in the unexcited crystal at $t_D = -25 \text{ fs}$. The limited resolution of the measured THz signal on the low-energy side however did not allow one to study the coupled plasmon–phonon resonance in the excited GaAs crystal. The study of the time-dependent interplay between the optical phonons and the plasmons remained an interesting problem of its own, which we will discuss in the next Sect. 18.2

18.2 Time-Dependent Screening of Phonon-Mediated and Coulomb Interactions

The interaction with LO-phonons provides in polar semiconductors the fastest mechanism for the cooling of the photoexcited e–h plasma toward the lattice temperature. In order to include this process in addition to the fast Coulomb

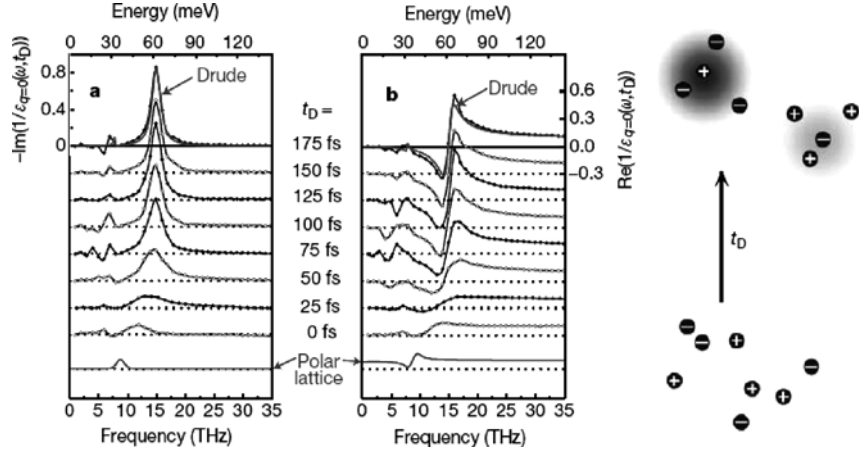


Fig. 18.2. Measured buildup of Coulomb screening and plasmon scattering according to Leitenstorfer et al. [160]. On the l.h.s. the negative imaginary part of the measured inverse dielectric function is shown for various delay times t_D . On the r.h.s. the corresponding dispersive spectra are shown. The curves at the longest delay time $t_D = 175 \text{ fs}$ have been fitted by a damped plasmon pole, i.e., by a Drude formula. On the right side of the figure the dressing of negative and positive carriers with an average screening cloud is illustrated

scattering it is important to treat both relaxation mechanisms on the same footing, particularly at intermediate carrier densities [356]. As is known from the RPA equilibrium theory of the simultaneous screening for the phonon-mediated and the Coulomb carrier–carrier interactions for doped semiconductors [255], one can generalize the RPA theory described in Sect. 18.1 by including the phonon GF $D_q(t_1, t_2)$ and the plasmon GF $W_q(t_1, t_2)$ in parallel: While the phonon propagator and the bare Coulomb potential can be included very easily in the frequency, momentum representation of the equilibrium theory, the two GFs have a rather different dependence in the two-time presentation of the nonequilibrium theory: While the bare Coulomb potential is instantaneous, i.e., $V_q(t_1, t_2) = \delta(t_1 - t_2)V_q$, the free phonon GF exhibits free oscillations. Another point which is worthwhile to state, is the fact that the Coulomb potential V_q and the Fröhlich coupling g_q^2 are both singular as $1/q^2$ in the long-wavelength limit. For the Keldysh contour-ordered GFs we get from Fig. 18.3 the following equation

$$W_q(1, 2) = V_q\delta(1, 2) + D_q(1, 2) + V_qL_q(1, 3)W_q(3, 2) + D_q(1, 3)L_q(3, 4)W_q(4, 2), \quad (18.3)$$

where again the matrix convention for the contour times is assumed. Langreth theorem (see Sect. 4.3) allows one to extract efficiently from contour time products their real time components. If $C(1, 2) = A(1, 3)B(3, 2)$ on the contour, one finds for real times $C^>(t, t') = A^r(t, t_2)B^>(t_2, t') + A^>(t, t_2)B^a(t_2, t')$,

Fig. 18.3. Screened interaction $W_q(t_1, t_2)$ for the Coulomb interaction and the interaction mediated by the exchange of LO-phonons. $\mathcal{D}_q(t_1, t_2)$ is the phonon propagator, g_q is the Fröhlich electron–LO phonon interaction matrix element, V_q is the bare Coulomb potential, and $L_q(t_1, t_2)$ is the intraband polarization function

where t_2 has to be integrated from $-\infty$ to $+\infty$. Similarly if on the contour $D = ABC$, one gets for real times $D^> = A^r B^r C^> + A^r B^> C^a + A^> B^a C^a$, where a matrix structure in the time arguments and integrations over repeated times are assumed. With these relations one gets for the effective scattering potential $W_q^>$ from (18.3) the following equation

$$W_q^> = \mathcal{D}_q^> + V_q(L_q^r W_q^> + L_q^> W_q^a) + \mathcal{D}_q^r L_q^r W_q^> + \mathcal{D}_q^r L_q^> W_q^a + \mathcal{D}_q^> L_q^a W_q^a. \quad (18.4)$$

In this formula V_q is a constant in time. All other quantities depend on two time arguments. The advanced potentials W_q^a can be represented as

$$W_q^a(t_1, t_2) = V_q \delta(t_1 - t_2) + \theta(t_2 - t_1)[W_q^<(t_1, t_2) - W_q^>(t_1, t_2)]. \quad (18.5)$$

With the symmetry relations $W_q^<(t_1, t_2)^* = -W_q^>(t_2, t_1)$ and $W_q^>(t_1, t_2) = W_q^<(t_2, t_1)$, the equation for the effective scattering potential $W_q^>(t, t')|_{t \geq t'} = w_q^>(t, t')$ becomes

$$\begin{aligned} w_q^>(t, t') &= \mathcal{D}_q^>(t, t') + V_q^2 L_q^>(t, t') + V_q \left(\int_{-\infty}^t dt_1 L_q^r(t, t_1) W_q^>(t_1, t') \right. \\ &\quad + 2 \int_{-\infty}^{t'} dt_1 L_q^>(t, t_1) \text{Re}[W_q^>(t', t_1)] + \int_{-\infty}^t dt_1 \mathcal{D}_q^r(t, t_1) L_q^>(t_1, t') \\ &\quad \left. + \int_{-\infty}^{t'} dt_1 \mathcal{D}_q^>(t, t_1) L_q^a(t_1, t') \right) + \int_{-\infty}^t dt_1 \mathcal{D}_q^r(t, t_1) \int_{-\infty}^{t_1} dt_2 L_q^r(t_1, t_2) W_q^>(t_2, t') \\ &\quad + 2 \int_{-\infty}^t dt_1 \mathcal{D}_q^r(t, t_1) \int_{-\infty}^{t'} dt_2 L_q^>(t_1, t_2) \text{Re}[W_q^>(t', t_2)] \\ &\quad + \int_{-\infty}^{t'} dt_1 \mathcal{D}_q^>(t, t_1) \int_{t_1}^{t'} dt_2 L_q^a(t_1, t_2) \text{Re}[W_q^>(t', t_2)]. \end{aligned} \quad (18.6)$$

After some rearrangement in order to get definite time order between the times t, t', t_1 and t_2 , one finds the following closed integral equation for the scattering potential

$$\begin{aligned}
w_q^>(t, t') = & \mathcal{D}_q^>(t, t') + V_q^2 L_q^>(t, t') + 2 \left[V_q \left\{ \int_{-\infty}^{t'} dt_1 \{ L_q^>(t, t_1) \text{Re}[w_q^>(t', t_1)] \right. \right. \\
& - \text{Re}[L_q^>(t, t_1)] w_q^>(t', t_1)^* \Big\} + \int_{t'}^t dt_1 \text{Re}[L_q^>(t, t_1)] w_q^>(t_1, t') \\
& + \int_{t'}^t dt_1 \text{Re}[\mathcal{D}_q^>(t, t_1)] L_q^>(t_1, t') + \int_{-\infty}^{t'} dt_1 \{ \mathcal{D}_q^>(t, t_1) \text{Re}[L_q^>(t', t_1)] \right. \\
& - \text{Re}[\mathcal{D}_q^>(t, t_1)] L_q^>(t', t_1)^* \Big\} + \int_{-\infty}^{t'} dt_1 \text{Re}[\mathcal{D}_q^>(t, t_1)] \\
& \times \{ M_{1,q}(t', t_1) + M_{5,q}(t', t_1) \} + \int_{t'}^t dt_1 \text{Re}[\mathcal{D}_q^>(t, t_1)] \\
& \times \{ M_{3,q}(t_1, t') + M_{2,q}(t_1, t') \} + \left. \int_{-\infty}^{t'} dt_1 \mathcal{D}_q^>(t, t_1) M_{4,q}(t', t_1) \right] \quad (18.7)
\end{aligned}$$

with

$$M_{1,q}(t', t_1)|_{t' \geq t_1} = \int_{-\infty}^{t_1} dt_2 \{ L_q^>(t_1, t_2) \text{Re}[w_q^>(t', t_2)] \quad (18.8)$$

$$- \text{Re}[L_q^>(t_1, t_2)] w_q^>(t', t_2)^* \},$$

$$M_{2,q}(t_1, t')|_{t_1 \geq t'} = \int_{-\infty}^{t'} dt_2 \{ L_q^>(t_1, t_2) \text{Re}[w_q^>(t', t_2)] \quad$$

$$- \text{Re}[L_q^>(t_1, t_2)] w_q^>(t', t_2)^* \},$$

$$M_{3,q}(t_1, t')|_{t_1 \geq t'} = \int_{t'}^{t_1} dt_2 \text{Re}[L_q^>(t_1, t_2)] w_q^>(t_2, t'),$$

$$M_{4,q}(t', t_1)|_{t' \geq t_1} = \int_{t_1}^{t'} dt_2 \text{Re}[L_q^>(t_2, t_1)] \text{Re}[w_q^>(t', t_2)],$$

$$M_{5,q}(t', t_1)|_{t' \geq t_1} = \int_{t_1}^{t'} dt_2 L_q^>(t_2, t_1)^* \text{Re}[w_q^>(t', t_2)]. \quad (18.9)$$

This integral equation for $W_q^>(t, t')$, together with the polarization function $L_q(t, t')$, the generalized Kadanoff–Baym ansatz, a mean-field equation for the retarded electron GF G_q^r with an additional polaron damping, and the one-time quantum kinetics for the reduced density matrix $\rho_q(t)$ with a coherent pump pulse and the scattering rates (17.13) form a closed set of equations and can now be solved simultaneously and self-consistently [357]. The calculations have been performed for GaAs excited by a 11 fs pulse in the shape of a hyperbolic secant $E(t) = E_0 / (\cosh(1.7627t/\delta t)) e^{-i\omega t}$. The excess energy of the laser excitation with respect to the unrenormalized band edge was

$\hbar\omega - E_g = 50$ meV. The propagators and spectral functions of the thermal phonon bath have been described in detail in Chap. 15. The phonon bath temperature has been assumed to be 300 K. Finally, the resulting effective interaction $W^r(t, t')$ which can be obtained from the scattering components $W^>$ and $W^<$ is

$$W_q^r(t, t') = V_q \delta(t, t') + \theta(t - t')(W_q^>(t, t') - W_q^<(t, t')) . \quad (18.10)$$

This two-time potential is analyzed as above in terms of an incomplete Fourier transform (18.3) resulting in an inverse longitudinal dielectric function. An example of the evolving spectra is shown for GaAs with an excitation density of $N = 1.1 \times 10^{18} \text{ cm}^{-3}$ in Fig. 18.4. One sees the LO-phonon resonance which was there, even before the crystal was excited. With increasing time a first broad and then sharpening plasmon resonance builds up which at the chosen excitation density was well above the phonon resonance. As the plasmon resonance builds up, the phonon resonance loses oscillator strength. One sees from the projection of the plasma peaks into the ω, q plane the quadratic dispersion of the plasmon in bulk material. We note critically that the numerical accuracy of the described numerical evaluation was not high enough to show clearly a shift of the phonon resonance as the plasmon peak forms.

Recently, similar calculations for low-dimensional systems [359] showed that for larger wavenumbers one gets for the two-component nonequilibrium e-h plasma not only a longitudinal optical plasmon mode, but also an acoustic plasmon mode. In 3D, however, the longitudinal plasmon mode has not enough spectral weight to show up appreciably. In the longitudinal optical plasmon mode the negative charges (*e*) oscillate against the positive charges (*h*), while in the longitudinal acoustic mode the two components oscillate in phase. In infrared absorption or transmission experiments, one only detects long-wavelength plasmons. For the study of plasmons with larger *q*-values scattering experiments have to be performed [377].

18.2.1 Buildup of the Phonon-Plasmon Mixed Modes

In GaAs the THz radiation with a central frequency of 28 THz did not allow to follow the optical phonon mode with a frequency of $\omega_{LO}/2\pi = 8.8$ THz. In InP, however, the situation is more favorable, because the LO-phonon frequency $\omega_{LO}/2\pi = 10.3$ THz is higher. Therefore we calculate the time- and frequency-dependent inverse dielectric function again self-consistently with the full LO-phonon-plasmon quantum kinetic scattering. In the process of comparing theory and experiment, we noticed that a higher accuracy can be obtained by calculating the retarded effective potential $W_q^r(t, t')$ not from the calculated scattering components $W^<$ and $W^>$, but directly from its Dyson equation

$$W_q^r(t, t') = W_q^0(t, t') + \int_{t'}^t dt'' \int_{t'}^{t''} dt''' W_q^0(t, t'') L_q^r(t'', t''') W_q^r(t''', t') \quad (18.11)$$

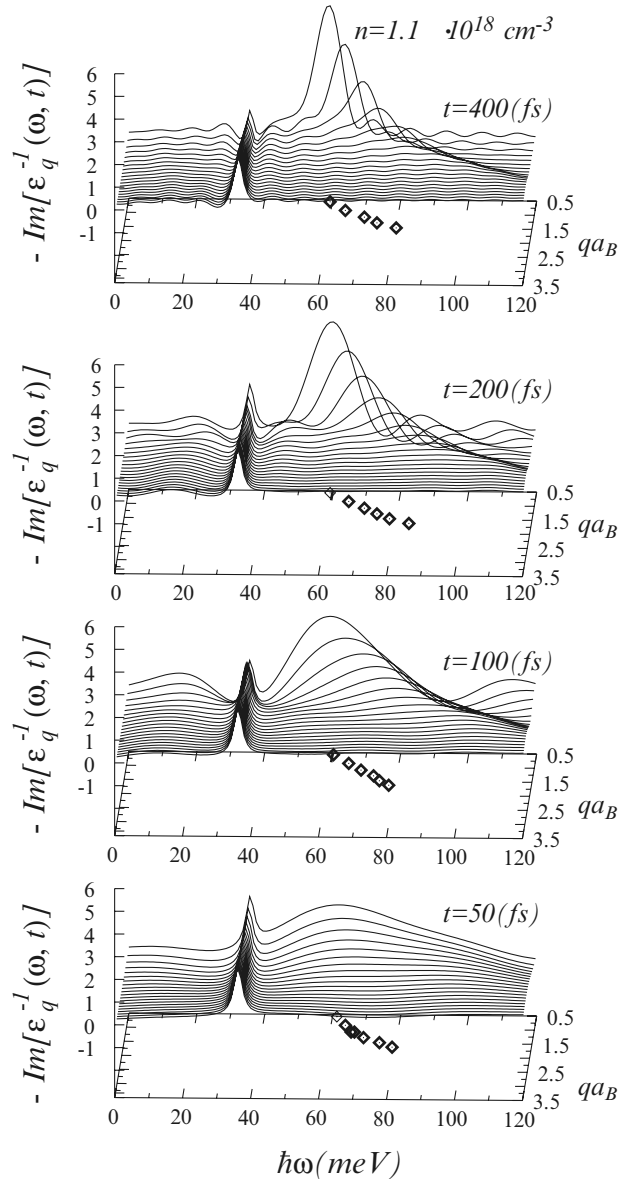


Fig. 18.4. Negative imaginary part of the inverse dielectric function vs. frequency and wavenumber in units of the exciton Bohr radius a_B for the times $t = 50, 100, 200, 400$ fs after a 11 fs pulse which excites 1.1×10^{18} e-h pairs per cm^3 . The projection of the plasmon resonance into the ω, q plane is indicated by symbols. According to Vu and Haug [357]

with

$$W_q^0(t, t') = g_q^2 \mathcal{D}_q^0(t, t') + V_q \delta(t - t') \quad (18.12)$$

and

$$L_q^r(t, t') = -2i\theta(t - t') \sum_k \left(G_{k-q}^>(t, t') G_k^<(t', t) - G_{k-q}^<(t, t') G_k^>(t', t) \right). \quad (18.13)$$

A further improvement of the theory is to take the strong polaron correlation for the spectral GF into account. Starting with an equilibrium polaron GF $\mathcal{G}_k^r(t - t')$, we put on top of it the mean-field dynamics by an approximate Dyson equation [121] of the form

$$G_k^r(t, t') = \mathcal{G}_k(t - t') + \int_{-\infty}^t dt'' \mathcal{G}_k(t - t'') \Sigma_k^{mf}(t'') G_k^r(t'', t'), \quad (18.14)$$

where $\Sigma_k^{mf}(t)$ is the self-energy (15.7) due to the mean-field Hamiltonian, which contains the HF Coulomb interaction and the interaction with the coherent light pulse. For InP we used the following material parameters [161]: The effective electron and hole masses of $m_e = 0.079 m_0$ and $m_h = 0.6 m_0$, and dielectric constants of $\epsilon_0 = 12.56$ and $\epsilon_\infty = 9.6$. The unrenormalized bandgap is $E_g = 1.34$ eV. We take $\alpha = 0.113$ for the Fröhlich coupling constant expressed in terms of the reduced e–h mass. Room temperature is assumed for the phonon bath ($T_L = 300$ K). The frequency of the pump is detuned only 50 meV above the bandgap in order to reduce the energy space over which one has to integrate. In Fig. 18.5a, b the calculated spectra of the imaginary part of the inverse dielectric function of InP are shown as a function of frequency for various delay times and for two excited carrier densities, $N = 1.25$ and 0.62×10^{18} cm $^{-3}$, respectively. The wave number times the excitation Bohr radius is taken to be $qa_B = 0.5$, because we cannot calculate the spectra with sufficient accuracy for longer wavelengths. In order to obtain a good Fourier transform we had to broaden the phonon resonance with $\gamma = 6$ meV/ \hbar . The most striking feature of these spectra is that the phonon resonance which is first at the LO frequency does not shift as the plasma builds up, as one would expect naïvely from an adiabatic picture of the avoided level crossing. Instead the phonon resonance vanishes at its original position (see the spectrum at 60 fs after the pump pulse) and reappears at lower frequencies. It approaches for larger times after the pulse the transverse optical (TO) frequency.

For comparison, the measured spectra in terms of the imaginary (a) and real (b) parts of the inverse dielectric function are shown in Fig. 18.6.

The calculated spectra of Fig. 18.5a qualitatively reproduce the key experimental findings: Starting from a bare phonon pole in the unexcited polar lattice, two branches of the coupled resonances arise and narrow down within approximately 160 fs. On the same timescale (the solid curves serve as guides

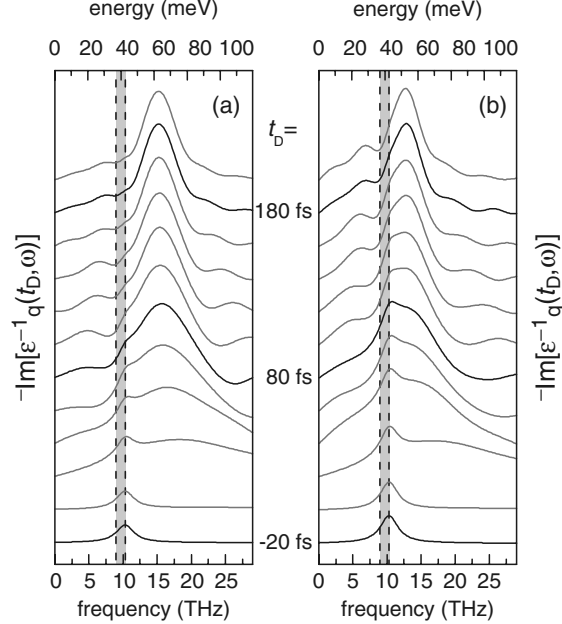


Fig. 18.5. Calculated spectra of the negative imaginary part of the inverse dielectric function for InP for two excitation densities: (a) $N = 1.25 \times 10^{18} \text{ cm}^{-3}$, (b) $N = 0.62 \times 10^{18} \text{ cm}^{-3}$. The spectra are depicted for times $-20 \text{ fs} \leq t_D \leq 200 \text{ fs}$ with a step width of 20 fs. The wavevector is set to $q = 0.5 a_B^{-1}$. The gray regions indicate the obtained Reststrahlen band between the TO and the LO frequency. According to Huber et al. [161]

to the eye), the bare LO phonon pole vanishes. In agreement with the calculations most of the oscillator strength is contained in the upper resonance. Quantitative differences between the calculated spectra and the experimental results may be primarily explained by the finite wave vector used in the simulation. The spectral positions of the two resonances at late delay times almost coincide with the calculated findings, although the excitation density of Fig. 18.5a is somewhat smaller than in Fig. 18.6. Both in theory and experiment, no resonance is found in the Reststrahlen region at any delay time.

For a lower excitation density of $N = 0.62 \times 10^{18} \text{ cm}^{-3}$ (see Fig. 18.5b), the plasma frequency is almost degenerate with the bare LO frequency. Therefore, mixing of the modes is particularly strong: The lower branch L_- appears with increased spectral weight. Its frequency ($\omega_-/2\pi = 6.9 \text{ THz}$) is strongly reduced with respect to $\omega_{\text{LO}}/2\pi$, due to anticrossing with the upper branch L_+ . The latter approaches the LO phonon frequency. Interestingly, the quasiequilibrium spectra are obtained slightly later than in Fig. 18.5a (see, e.g., the spectra corresponding to $t_D = 180 \text{ fs}$ and $t_D = 200 \text{ fs}$), indicating that the formation of phonon-plasmon coupling proceeds on the shortest characteristic

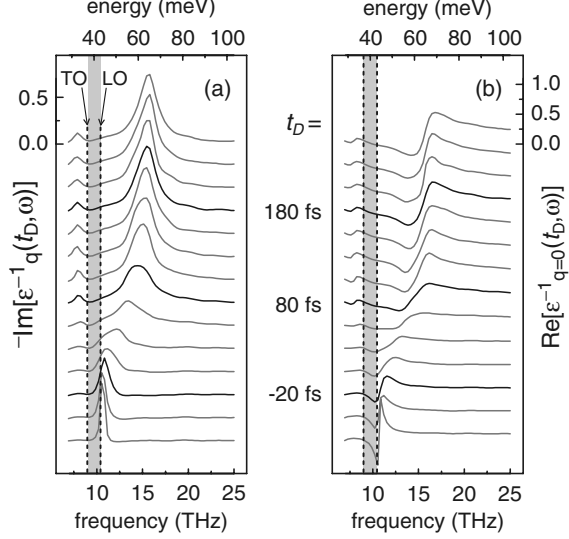


Fig. 18.6. Experiment: (a) imaginary and (b) real part of the long-wavelength limit of the inverse dielectric function of i-InP vs. frequency as extracted from the THz transmission for various delay times $-70 \text{ fs} \leq t_D \leq 255 \text{ fs}$ with a step width of 25 fs. The gray regions indicate the Reststrahlen band between $\omega_{\text{TO}}/2\pi = 9 \text{ THz}$ and $\omega_{\text{LO}}/2\pi = 10.3 \text{ THz}$. According to Huber et al. [161]

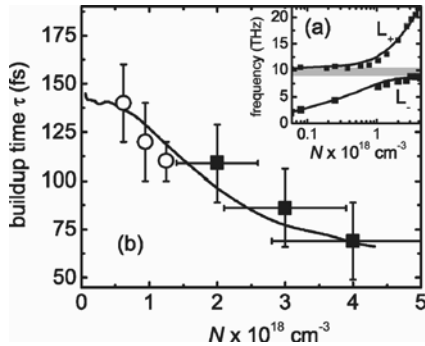


Fig. 18.7. Density dependence of the buildup time of the phonon–plasmon mixed modes. Open symbols: theory; filled symbols: experiment. The solid line is a multiple of the oscillation time of the upper branch: $1.6 \times 2\pi/\omega_+$. The inset shows the density dependence of the mixed modes L_- and L_+ measured after the buildup of correlations

timescale of the many-body system which is given by the inverse frequency of the upper branch L_+ .

Figure 18.7 shows the calculated and measured buildup times of the mixed-mode spectra. While the calculations are limited to the lower density range, the experiment becomes more accurate for higher densities. Both the calculated and measured points lie on a curve given by a multiple of the oscillation time of the upper branch, which is indeed the shortest characteristic timescale of the system. Asymptotically the phonon–plasmon mixed mode spectrum, well known from the equilibrium theory, is reached indeed as shown in the inset of Fig. 18.7.

Femtosecond Four-Wave Mixing with Dense Plasmas

Summary. The screened Coulomb-phonon quantum kinetics is applied to the two-pulse excitation of femtosecond four-wave mixing (FWM). The time-resolved FWM shows, both in theory and experiment, a characteristic photon echo structure. From the analysis of the theoretical and experimental time-integrated signal, a dephasing time is obtained which varies with the inverse cubic power of the plasma density. Finally, FWM with coherent control yields in theory and experiment coherent plasmon-phonon mixed mode quantum beats.

19.1 Time-Resolved Four-Wave Mixing

The question whether collective plasmon oscillations quantum beats similar to the LO-phonon quantum beats can be observed in high-density FWM experiments was one of the main motivations for the development of the Coulomb quantum kinetics. The delay in the buildup of the plasmon resonance, the plasmon dispersion, and density dependence made the task to observe these collective oscillations of the pulse-excited e–h plasma considerably more difficult. Before we present the results of ultrashort femtosecond FWM experiments, we want to remember that time-resolved FWM can display a photon-echo signal at the time which equals the time interval between the two pulses, i.e., the delay time. A necessary condition is that the system is inhomogeneously broadened (see the elementary discussion of the photon echo at the end of Sec. 14.2). According to the Bloch equations the polarization components induced by the first pulse rotate with different angular velocities given by their inhomogeneous detuning. The second pulse reverses the rotation after the delay time $\tau = t_{21}$, so that all polarization components align constructively after another time interval t_{21} and emit a photon echo. If however the system is homogeneously broadened, the polarization cannot be revived but it simply decays. A noninteracting e–h gas has a natural inhomogeneous broadening or rather inhomogeneous detuning with respect to the carrier frequency of the coherent pulses due to the dispersion of the pair energy with momentum.

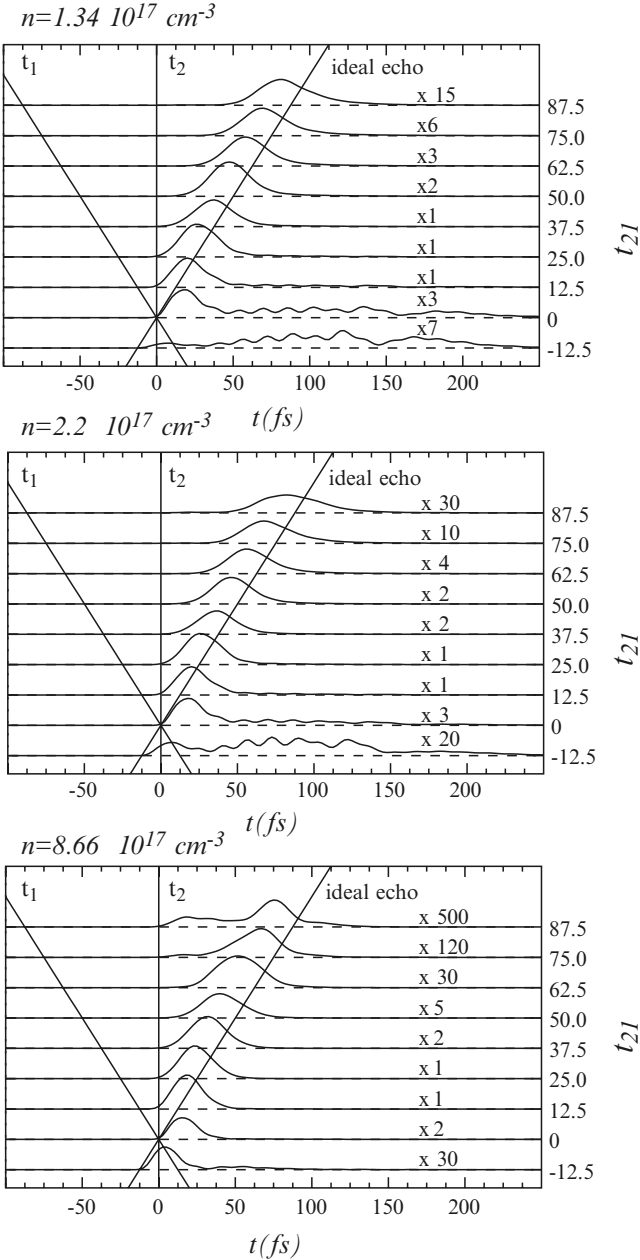


Fig. 19.1. Calculated time-resolved FWM signals for GaAs at 300 K for various delay times $\tau = t_{21}$ and three excitation densities. The *left and center line* mark the peaks of the two pulses, the *right line* is the ideal echo line according to Hügel et al. [159]

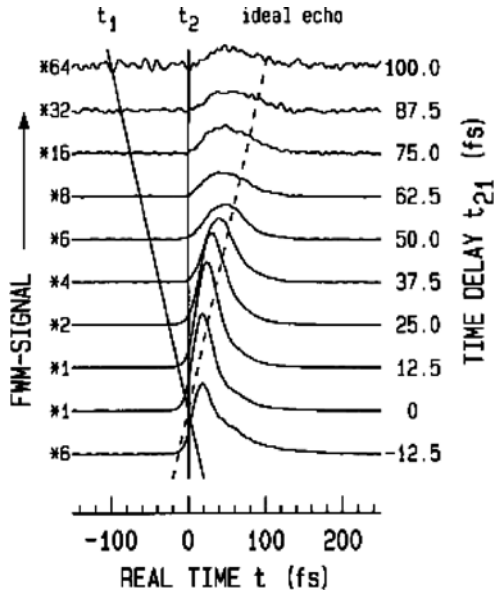


Fig. 19.2. Measured time-resolved FWM signals for GaAs at 300 K for various delay times $\tau = t_{21}$ and an excitation density of $n = 2 \times 10^{17} \text{ cm}^{-3}$. The left and center line mark the peaks of the two pulses, the right line is the ideal echo line according to Hügel et al. [159]

On the other hand, a strongly correlated plasmon reacts mostly collectively. Thus if these correlations had time to build up, the photon-echo signal is expected to decrease. The time-resolved FWM experiments have been performed by Wegener et al. [159] on a $0.6 \mu\text{m}$ GaAs layer embedded in higher bandgap layers of $\text{Al}_{0.3}\text{Ga}_{0.7}\text{As}$ in order to avoid free surface effects. In the experiments 11 fs $\text{sech}^2(t)$ -shaped pulses have been used, which excited resonantly at about 1.43 meV an e-h plasma with density n . The quoted densities are always the sum of the densities which would be excited by the two pulses individually, i.e., $n = n^{(1)} + n^{(2)}$ with $n^{(2)}/n^{(1)} = 5$. For the calculations GaAs parameters have been used. The pulses have been taken as in the experiment, assuming a detuning of 50 meV above the unrenormalized band edge. The results for the calculated time-resolved FWM signals are shown in Fig. 19.1 for three densities ranging from $n = 1.34 - 8.66 \times 10^{17} \text{ cm}^{-3}$. One sees that the calculated signal follows at smaller delay times and lower densities pretty well the positions $t = t_{21}$ of the ideal photon signal due to the inhomogeneous detuning of the free carriers. At later delay times and higher plasma densities the FWM signal occurs at earlier times and approaches the properties of a free induction decay due to the collective nature of the plasmon under these conditions.

Results of the time-resolved FWM experiments [159] for a plasma density of $n = 2 \times 10^{17} \text{ cm}^{-3}$ are shown in Fig. 19.2. Again photon-echo-like signals are seen for small delay times and even more pronounced than in theory a transition to a free induction decay at larger delay times is observed. The excellent qualitative agreement between the experimental time-resolved FWM signals and the signals calculated with the non-Markovian Coulomb quantum kinetics again gave evidence to the transition of the initially coherently excited individual carriers to a correlated plasma with screening and a collective plasmon mode. It is obvious that the observed time dependence of the FWM signals could not be described by a phenomenological T_2 time.

19.2 Time-Integrated Four-Wave Mixing

The time-integrated FWM signals as a function of the delay time have been measured in the same experiments (see Fig. 19.3) and yielded a

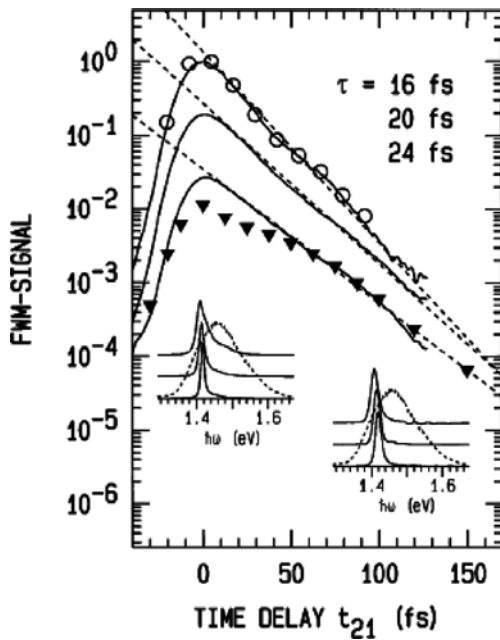


Fig. 19.3. Time-integrated FWM signals vs. delay time for three different optically excited carrier densities $n = 0.5, 1,$ and $2 \times 10^{17} \text{ cm}^{-3}$ according to Hügel et al. [159]. *Full triangles* are the result of quantum kinetic calculations with $n = 0.57 \times 10^{17} \text{ cm}^{-3}$. The *open circles* are the time-integrated data of Fig. 19.2 shifted by 8 fs. The decay time constants τ correspond to the *dashed straight lines*. The *left (right)* inset shows the vertically displaced and normalized FWM spectra (linear scale) for $t_{21} = 0$ ($t_{21} = 100$ fs) and the laser spectrum (*dashed*). Bulk GaAs, $T = 300$ K, excitation with 11 fs pulses centered 50 meV above the band edge

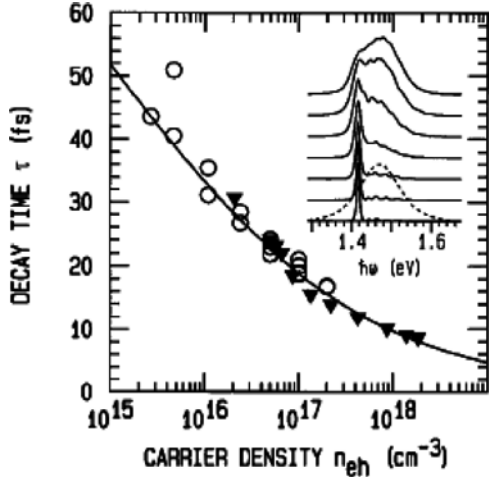


Fig. 19.4. Calculated (full triangles) and measured (open circles) dephasing times as a function of the excitation density according to Hügel et al. [159]. The inset shows the computed spectra at $t_{21} = 0$ for the carrier densities $n = 0.86, 1.34, 2.2, 4.2, 8.66, 13.9, 18.4 \times 10^{17} \text{ cm}^{-3}$. The dashed line is the laser spectrum

density-dependent dephasing as shown in Fig. 19.4. The calculated and measured dephasing time could be fitted with

$$\frac{1}{\tau} = \gamma_0 + an^{1/3}. \quad (19.1)$$

The same power-law dependence has already been found in a pioneering paper of Shank et al. [34]. Surprisingly we found that this law holds also for quasi-two-dimensional quantum wells [266]. If one argues that the mean distance between particles $d \propto n^{-1/3}$ in 3D and $d \propto n^{-1/2}$ in 2D determines the dephasing, one would expect a square-root dependence of the dephasing time, which earlier – but less accurate – experiments [41] suggested.

One sees from these results, shown in Fig. 19.4, that for high densities the dephasing times can get shorter than 10 fs. If experiments with resonant sub-ten femtosecond pulses are performed – the shortest optical pulses are presently around 4 fs – one never reaches the coherent limit in which the pulse duration is shorter than the dephasing time, because these short pulses are usually very intensive (see, e.g., Vu et al. [358]).

19.3 Four-Wave Mixing with Coherent Control

The accuracy of FWM experiments can be enhanced by applying the method of coherent control. Here the first pulse is split in a phase coherent doublet with a temporal distance $t_{1,1'}$ between them. It has been shown before that

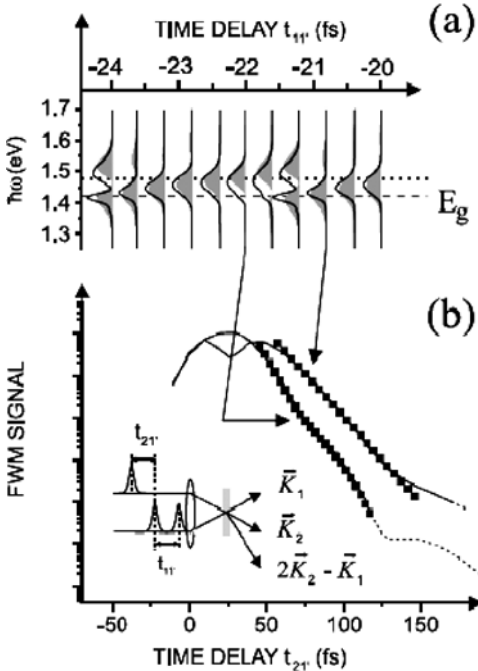


Fig. 19.5. Calculated FWM signal with coherent control for 11 fs pulses according to Vu et al. [357]. (a) The spectra (individually normalized) of the phase-locked pulse pair $11'$ (shaded) and the photon echo signal at $t_{21'} = 30 \text{ fs}$ and (b) two selected traces vs. delay time $t_{21'}$ for $t_{11'} = -20.8 \text{ fs}$ and $t_{11'} = -22.0 \text{ fs}$ plotted on the same scale. The symbols in (b) are the results of simple fits. For bulk GaAs at $T = 300 \text{ K}$ excited by 11 fs pulses with a density $n = 1 \times 10^{18} \text{ cm}^{-3}$. The oscillation period under these conditions is 60 fs. The inset illustrates the geometry

by tuning the coherent control time $t_{1,1'}$ the LO-phonon quantum beats can be switched on and off, which can be explained by the resulting spectral shape of the total first pulse. Therefore, Vu and Haug suggested and calculated the time-integrated signal of a resonant 11-fs FWM signal with coherent control. The calculations indeed suggested that the detection of collective plasmon beats, or rather mixed phonon-plasmon beats, should be possible (see Fig. 19.5). Here and in the following experiment, all three pulses have the same intensity and the density n is the sum of the excited densities by the three pulses individually. Encouraged by these calculations, Wegener et al. used 13-fs pulses with coherent control to look for the predicted phonon-plasmon-mixed mode oscillations. The result of these rather involved experiments is shown in Fig. 19.6 [357]. Except for the slightly longer pulse duration of 13 fs, all parameters are those assumed in the calculations. The values between the two phase-locked pulses are measured absolutely with a so-called “Pancharatnam screw” with attosecond accuracy. Besides some shift in the

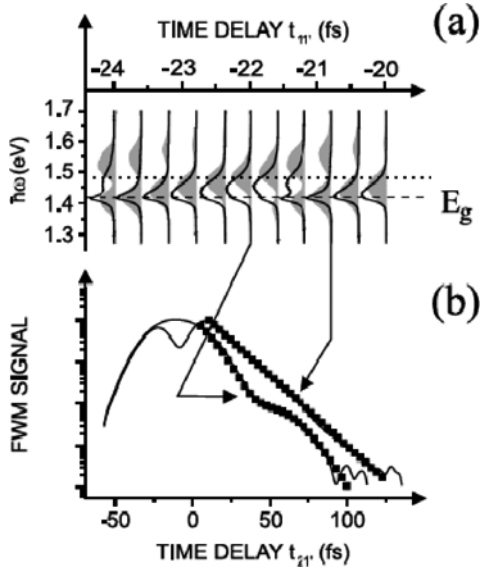


Fig. 19.6. Measured FWM signal with coherent control for 13 fs pulses according to Vu et al. [357] presented in the same way as in Fig. 19.5. (a) $t_{21'} = 0$ fs, the symbols in (b) are the result of simple fits. Bulk GaAs at $T = 300$ K excited by 13 fs pulses, $n = 5.3 \times 10^{17} \text{ cm}^{-3}$. The oscillation period under these conditions is 68 fs

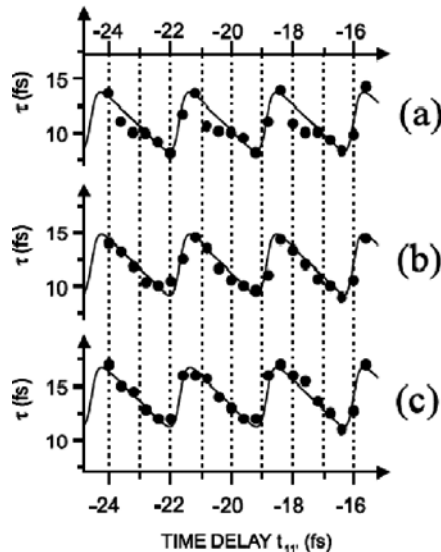


Fig. 19.7. Decay time τ of the photon echo signal vs. time delay $t_{11'}$ as determined from fits to the data (Fig. 19.5(b) and Fig. 19.6(b)). (a) theory, $n_{eh} = 1.0 \times 10^{18} \text{ cm}^{-3}$, (b) experiment, $n_{eh} = 1.0 \times 10^{18} \text{ cm}^{-3}$, (c) experiment, $n_{eh} = 5.4 \times 10^{17} \text{ cm}^{-3}$. According to Vu et al. [357]

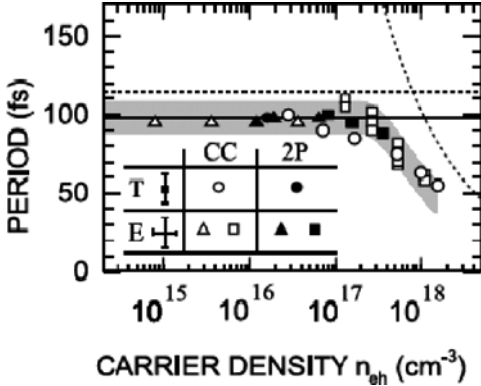


Fig. 19.8. Observed (*triangles and squares*) and calculated (*circles*) LO-phonon-plasmon oscillations in the resonant 11 fs FWM with coherent control (cc) according to Vu et al. [357]. Also shown are earlier results of two pulse experiments (*full symbols*). *Triangles* correspond to 77 K and *squares* to 300 K sample temperature. The shaded area is a guide to the eye. The two *dashed curves* correspond to the LO-phonon frequency and to the plasma frequency, while the *full line* represents $\omega_{\text{LO}}(1 + m_e/m_h)$

absolute position $t_{21'} = 0$, the agreement between theory and experiment is good. Figure 19.7 shows the decay time τ , which is obtained from the fits to data similar to those shown in Figs. 19.5 and 19.6. For those optical transitions, for which $t_{11'}$ corresponds to destructive interference, the carriers are excited by pulse 1 and coherently reemitted by pulse 1'. This leads to a modulation of the carrier density [149] vs. $t_{11'}$, which results in an obvious modulation of the carrier–carrier scattering time.

From this alone, one would expect a symmetric modulation of $\tau = \tau(t_{11'})$ and not the asymmetric saw-tooth shape shown in Fig. 19.7. This particular line shape is due to the fact that not only the carrier density but also the shape of the carrier distribution function is coherently modulated with time delay $t_{11'}$. Note that, again, theory (Fig. 19.7a) and experiment (Figs. 19.7b and c) agree quite well.

Figure 19.8 shows that the obtained beating oscillations belong to the upper branch of the mixed phonon–plasmon modes. Note that the quantum beats due to the exchange of a phonon or a plasmon in the conduction bands show up as frequencies enlarged by the factor $(1 + m_e/m_h)$ because of the finite curvature in the valence band, as discussed in detail with the LO-phonon quantum beats at low excitation intensities. Another factor which enlarges the plasmon frequency is the finite momentum value q of the exchanged plasmon. Therefore, the observed mode of oscillation is indeed the upper branch of the phonon–plasmon mixed mode. Historically, this was the first observation of the mixed LO-phonon–plasmon modes [357] in femtosecond excited semiconductors, before these mixed modes and their temporal buildup have been

observed rather directly with the optical pump and THz probe experiments of Huber et al. [161], already discussed in Chap. 18.

The observation and analysis of the coherent collective plasma oscillations as a function of the delay time superimposed on the rapidly dephased interband polarization caused by the same plasma was certainly among the highlights in the joint experimental and theoretical study of quantum kinetics.

References

1. M. Abramowitz, I. A. Stegun (eds.): *Handbook of Mathematical Functions* 9th edn. (Dover, New York, 1970)
2. A. A. Abrikosov, L. P. Gorkov, I. E. Dzyaloshinski: *Methods of Quantum Field Theory in Statistical Physics* (Dover, New York, 1975)
3. N. Agrait, C. Untiedt, G. Rubio-Bollinger, S. Vieira: Phys. Rev. Lett. **88**, 216803 (2002)
4. L. Allen, J. H. Eberly: *Optical Resonance and Two-Level Atoms* (Wiley, New York, 1975) reprinted with corrections (Dover, New York, 1987)
5. B. L. Altshuler, P. A. Lee, R. A. Webb (eds.): *Mesoscopic Phenomena in Solids* (Elsevier, Amsterdam, 1991)
6. E. V. Anda, F. Flores: J. Phys.: Condens. Matter **3**, 9087 (1991)
7. P. W. Anderson: Phys. Rev. **124**, 41 (1961)
8. M. Asche, O. G. Sarbei: Phys. Stat. Sol. B **141**, 487 (1987)
9. N. W. Ashcroft, N. D. Mermin: *Solid State Physics* (Holt, Rinehart and Winston, Philadelphia, 1976)
10. D. E. Aspnes: Phys. Rev. **147**, 554 (1966)
11. L. V. Atkinson, P. J. Harley, J. D. Hudson: *Numerical Methods in Fortran 77* (Addison-Wesley, New York, 1990)
12. V. M. Axt, A. Stahl: Z. Phys. B **93** (1994)
13. V. M. Axt, M. Herbst, T. Kuhn: Superlattices and Microstructures **26**, 117 (1999)
14. D. W. Bailey, M. A. Artaki, C. J. Stanton, K. Hess: J. Appl. Phys. **62**, 4638 (1987)
15. J. S. Bakos: Phys. Rep. **31C**, 209 (1977)
16. P. M. Bakshi, E. M. Gross: Annals of Phys. **49**, 513 (1968)
17. P. M. Bakshi, K. T. Mahanthappa: J. Mat. Phys. **4**, 1 (1963)
18. P. M. Bakshi, K. T. Mahanthappa: J. Mat. Phys. **4**, 12 (1963)
19. L. Bányai, T. Wicht, H. Haug: Z. Phys. B **77**, 343 (1989)
20. L. Bányai, D. B. Tran Thoai, R. Remling, H. Haug: Phys. Stat. Sol. B **173**, 149 (1992)
21. L. Bányai, D. B. Tran Thoai, E. Reitsamer, H. Haug, D. Steinbach, M. U. Wehner, M. Wegener, T. Marschner, W. Stolz: Phys. Rev. Lett. **75**, 2188 (1995)
22. L. Bányai, Q. T. Vu, B. Mieck, H. Haug: Phys. Rev. Lett. **81**, 882 (1998)
23. L. Bányai, H. Haug, P. Gartner: Europ. Phys. J. B **1**, 209 (1998)

24. U. Bockelmann, T. Egeler: Phys. Rev. B **46**, R15574 (1992)
25. H. U. Baranger, J. W. Wilkins: Phys. Rev. B **30**, 7349 (1984)
26. J. R. Barker: J. Phys C **5**, 1657 (1972)
27. J. R. Barker: J. Phys C **6**, 2663 (1973)
28. J. R. Barker: in *Handbook on Semiconductors*, ed. by T. S. Moss, W. Paul, (North-Holland, Amsterdam, 1982), Vol. 1
29. J. R. Barker, D. K. Ferry: Phys. Rev. Lett. **42**, 1779 (1979)
30. G. Bartels, A. Stahl, V.M. Axt, B. Haase, U. Neukirch, J. Gutowski: Phys. Rev. Lett. **81**, 5880 (1998)
31. G. Bastard: *Wave Mechanics Applied to Semiconductor Heterostructures* (Les Edition de Physique, Paris, 1988)
32. G. Baym, L. P. Kadanoff: Phys. Rev. **124**, 287 (1961)
33. G. Baym: Phys. Rev. **127**, 1391 (1962)
34. P. C. Becker, H. Fragnito, C. Brito-Cruz, R. L. Fork, J. E. Cunningham, J. E. Henry, C. V. Shank: Phys. Rev. Lett. **61**, 1647 (1988)
35. R. Bertoncini: Int. J. of Modern Physics **6**, 3441 (1992)
36. R. Bertoncini, A. P. Jauho: Phys. Rev. B **44**, 3655 (1991)
37. R. Bertoncini, A. P. Jauho: Phys. Rev. Lett. **68**, 2826 (1992)
38. R. Bertoncini, A. M. Kriman, D. K. Ferry: Phys. Rev. B **41**, 1390 (1990)
39. R. Bertoncini, A. M. Kriman, D. K. Ferry: J. Phys. Condens. Matter **2**, 5991 (1990)
40. M. Betz, G. Gröger, A. Leitenstorfer, A. Laubereau, P. Gartner, L. Bányai, H. Haug, K. Ortner, C. R. Becker, G. Böhm: Phys. Rev. Lett. **86**, 4684 (2001)
41. Y. Bigot, H. L. Fragito, C. H. Brito Cruz, R. L. Fork, J. E. Cunningham, C. V. Shank: Phys. Rev. Lett. **67**, 636 (1991)
42. K. Binder, M. H. Kalos: in *Monte Carlo Methods in Statistical Physics*, ed. by K. Binder (Springer, Berlin, Heidelberg, 1988) Chap.6
43. R. Binder, D. Scott, A. E. Paul, M. Lindberg, K. Henneberger, S. W. Koch: Phys. Rev. B **45**, 1107 (1992)
44. R. Binder, S. W. Koch: Prog. in Quant. Electr. **19**, 307 (1995)
45. R. Binder, H. S. Köhler, M. Bonitz: Phys. Rev. B **55**, 5110 (1997)
46. B. Birnir, B. Galdríkian, R. Grauer, M. Sherwin: Phys. Rev. B **47**, 6795 (1995).
47. Y. M. Blanter, M. Büttiker: Physics Reports **336**, 2 (2000).
48. A. Blandin, A. Nourtier, D. W. Hone: J. de Physique **37**, 369 (1976)
49. Ø. L. Bø and Y. Galperin: J. Phys. Condens. Matter **8**, 3033 (1996)
50. P. Bokes, H. Mera, R. W. Godby: Phys. Rev. B **72** 165425 (2005)
51. L. W. Boltzmann: Ber. Wien. Akad. **66**, 275 (1872)
52. L. L. Bonilla: J. Phys.: Condens. Matt. **14**, R341 (2002).
53. M. Bonitz, D. Kremp, D. C. Scott, R. Binder, W. D. Kräft, H. S. Köhler: J. Phys. Cond. Matter **8**, 6057 (1996)
54. M. Bonitz: *Quantum Kinetic Theory* (Teubner, Stuttgart, 1998)
55. M. Bonitz (Ed.): *Progress in nonequilibrium Green's functions* (World Scientific, Singapore, 2000)
56. M. Bonitz, D. Semkat (Eds.): *Progress in nonequilibrium Green's functions II* (World Scientific, Singapore, 2003)
57. M. Bonitz, A. Filinov (Eds.): *Progress in nonequilibrium Green's functions III*, Journal of Physics: Conference Series **35** (2006)
58. M. Brandbyge, J. L. Mozos, P. Ordejón, J. Taylor, K. Stokbro: Phys. Rev. B **65**, 165401 (2002)

59. S. Braig, K. Flensberg: Phys. Rev. B **68**, 205324 (2003)
60. G. A. Brooker, J. Sykes: Phys. Rev. Lett. **21**, 279 (1968)
61. E. R. Brown, J. R. Söderström, C. D. Parker, L. J. Mahoney, K. M. Molvar, T. C. McGill: Appl. Phys. Lett **58**, 2291 (1991)
62. C. Bruder, H. Schoeller: Phys. Rev. Lett. **72**, 1076 (1994)
63. R. Brunetti, C. Jacoboni, F. Rossi: Phys. Rev. **B39**, 10781 (1989)
64. V. V. Bryksin and P. Kleinert: J. Phys.: Condens. Matt. **9**, 15827 (1997)
65. M. Büttiker: J. Phys. Cond. Matt. **5**, 9361 (1993)
66. M. Büttiker, R. Landauer: Phys. Rev. Lett. **49**, 1739 (1982)
67. M. Büttiker, R. Landauer: Physica Scripta **32**, 429 (1985)
68. M. Büttiker, A. Prêtre, H. Thomas: Phys. Rev. Lett. **70**, 4114 (1993)
69. M. Büttiker, H. Thomas, A. Prêtre: Z. f. Physik B **94**, 133 (1994)
70. J. Bylander, T. Duty, P. Delsing: Nature **434**, 361 (2005)
71. J. Callaway: *Quantum Theory of the Solid State, Part A* (Academic, New York, 1974)
72. F. X. Camescasse, A. Alexandrou, D. Hulin, L. Bányai, D. B. Tran Thoai, H. Haug: Phys. Rev. Lett. **77**, 5429 (1996)
73. C. Caroli, R. Combescot, D. Lederer, P. Nozieres, D. Saint-James: J. Phys. C **4**, 2598 (1971)
74. C. Caroli, R. Combescot, P. Nozieres, D. Saint-James: J. Phys. C **4**, 916 (1971)
75. C. Caroli, R. Combescot, P. Nozieres, D. Saint-James: J. Phys. C **5**, 21 (1972)
76. C. Cercignani: *Theory and application of the Boltzmann equation* (Scottish Academic Press, Edinburgh, 1975)
77. J. Černe, A. G. Markelz, M. S. Sherwin, S. J. Allen, M. Sundaram, A. C. Gossard, P. C. van Son, D. Bimberg: Phys. Rev. B **51**, 5253 (1995)
78. L. Y. Chen, C. S. Ting: Phys. Rev. B **43**, 2097 (1991)
79. L. Y. Chen, C. S. Ting: Phys. Rev. B **43**, 4534 (1991)
80. K. C. Chou, Z. B. Su, B. L. Hao, L. Yu: Physics Reports **118**, 1 (1985)
81. P. Coleman: Phys. Rev. B **29**, 3035 (1984)
82. P. Coleman: Phys. Rev. B **35**, 5072 (1987)
83. P. Coleman, W. Mao: J. Phys. Cond. Matt. **16**, L263 (2004)
84. J. Collet, T. Ammand: J. Phys. Chem. Sol. **47**, 153 (1986)
85. J. Collet, T. Ammand, M. Pugnet: Phys. Lett. **A96**, 368 (1983)
86. R. Combescot: J. Phys. C **4**, 2611 (1971)
87. C. Comte, G. Mahler, Phys. Rev. B **34**, 7164 (1986)
88. E. M. Conwell: *High Field Transport in Semiconductors*, Solid State Physics: Advances and Applications (Academic, New York, London 1967)
89. N. E. Dahlen, R. van Leeuwen: Phys. Rev. Lett. **98**, 153004 (2007)
90. P. Danielewicz: Ann. Phys. (N.Y.) **152**, 239 (1984)
91. P. Danielewicz: Ann. Phys. (N.Y.) **152**, 305 (1984)
92. S. Datta: Phys. Rev. B **45**, 1347 (1992)
93. S. Datta: *Electronic Transport in Mesoscopic Systems* (Cambridge University Press, Cambridge, 1995)
94. J. H. Davies, J. W. Wilkins: Phys. Rev. B **38**, 1667 (1988)
95. J. H. Davies, S. Hershfield, P. Hyldgaard, J. W. Wilkins: Phys. Rev. B **47**, 4603 (1993)
96. S. Doniach, E. H. Sondheimer: *Green's Functions for Solid State Physicists* (Benjamin, Reading, 1974)
97. B. Doyon, N. Andrei: Phys. Rev. B **73**, 245326 (2006)

98. J. J. Duderstadt, W. R. Martin: *Transport Theory* (Wiley, New York, 1979)
99. K. El Sayed, L. Bányai, H. Haug: Phys. Rev. B **50**, 1541 (1994)
100. K. El Sayed, S. Schuster, H. Haug, F. Herzl, K. Henneberger: Phys. Rev. B **49**, 7337 (1994)
101. K. El Sayed, A. P. Jauho: (unpublished, 1994)
102. K. El Sayed, T. Wicht, H. Haug, L. Bányai: Z. Physik B **86**, 345 (1992)
103. V. F. Elesin: Sov. Phys. JETP **32**, 328 (1971)
104. R. J. Elliot, J. A. Krumhansl, P. L. Leath: Rev. Mod. Phys. **46**, 465 (1974)
105. C. P. Enz: *A Course on Many-Body Theory Applied to Solid-State Physics* (World Scientific, Singapore, 1992)
106. L. Esaki and R. Tsu: IBM J. Res. Develop. **14**, 61 (1970)
107. J. Faist, F. Capasso, D. L. Sivco, C. Sirtori, A. L. Hutchinson, and A. Y. Cho: Science **24**, 553 (1994)
108. U. Fano: Phys. Rev. **15**, 1866 (1961)
109. D. K. Ferry: *Semiconductors* (MacMillan, New York, 1991)
110. A. L. Fetter, J. D. Walecka: *Quantum Theory of Many-Particle Systems* (McGraw-Hill, New York, 1991)
111. B. F. Feuerbacher, J. Kuhl, R. Eccleston, K. Ploog: Sol. State Commun. **74**, 1279 (1990)
112. R. P. Feynman, A. R. Hibbs: *Quantum Mechanics and Path Integrals* (McGraw-Hill, New York, 1965)
113. T. Frederiksen: *Inelastic Electron Transport in Nanosystems*. MSc. Thesis, Technical University of Denmark (2004)
114. T. Frederiksen, M. Brandbyge, N. Lorente, A. P. Jauho: Phys. Rev. Lett. **93**, 256601 (2004)
115. T. Frederiksen, M. Paulsson, M. Brandbyge, A. P. Jauho: Phys. Rev. B **75**, 205413 (2007)
116. K. Flensberg: Phys. Rev. B **68**, 205323 (2004)
117. W. Franz, Z. Naturforsch. Teil A **13**, 484 (1958)
118. W. R. Frensley: Phys. Rev. B **36**, 1570 (1987)
119. Y. Fu, S. C. Dudley: Phys. Rev. Lett. **70**, 65 (1993)
120. C. Fürst, A. Leitenstorfer, A. Laubereau, R. Zimmermann: Phys. Rev. Lett. **78**, 3733 (1997)
121. P. Gartner, L. Bányai, H. Haug: Phys. Rev. B **60**, 14234 (1999)
122. P. Gartner, L. Bányai, H. Haug: in *Progress in Nonequilibrium Green's Functions*, ed. M. Bonitz (World Scientific, Singapore 2000), p. 485
123. P. Gartner, L. Bányai, H. Haug: Phys. Rev. B **62**, 7116 (2000)
124. S. M. Girvin, G. D. Mahan: Phys. Rev. B **20**, 4896 (1979)
125. V. J. Goldman, D. C. Tsui, J. E. Cunningham: Phys. Rev. B **36**, 7635 (1987)
126. S. M. Goodnick, P. Lugli: Phys. Rev. B **38**, 10135 (1988)
127. L. P. Gorkov, A. I. Larkin, D. Khmel'nitskii: JETP Lett. **30**, 228 (1979)
128. C. H. Grein, E. Runge, H. Ehrenreich: Phys. Rev. B **47**, 12590 (1993)
129. A. Groshev, T. Ivanov, V. Valtchinov: Phys. Rev. Lett. **66**, 1082 (1991)
130. P. S. S. Guimarães, B. J. Keay, J. P. Kaminski, S. J. Allen, P. F. Hopkins, A. C. Gossard, L. T. Florez, J. P. Harbison: Phys. Rev. Lett. **70**, 3792 (1993)
131. V. L. Gurevich, M. I. Muradov, D. A. Parshin: Europhys. Lett. **12**, 375 (1990)
132. F. Haake: *Springer Tracts Mod. Phys.* **66**, 98 (Springer, Berlin, Heidelberg, 1973)
133. J. E. Han, Phys. Rev. B **73**, 125319 (2006)

134. K. Hannewald, S. Glutsch, F. Bechstedt: Phys. Rev. B **58**, 15336 (1998)
135. K. Hannewald, S. Glutsch, F. Bechstedt: Phys. Rev. B **61**, 10792 (2000)
136. W. Hänsch, G. D. Mahan: Phys. Rev. B **28**, 1902 (1983)
137. M. Hartmann, W. Schäfer: Phys. Stat. Sol. B **173**, 165 (1992)
138. M. Hartmann, H. Stolz, R. Zimmermann: Phys. Stat. Sol. B **159**, 35 (1989)
139. H. Haug: in *Optical Nonlinearities and Instabilities in Semiconductors*, ed. by H. Haug, (Academic, New York, 1988) p. 53
140. H. Haug: Phys. Stat. Sol. B **173**, 139 (1992)
141. H. Haug: Nature, News and Views **414**, 261 (2001)
142. H. Haug, S. Schmitt-Rink: Prog. Quantum Electronics **9**, 3 (1984)
143. H. Haug, L. Bányai, J. Liebler, T. Wicht: Phys. Stat. Sol. B **159**, 309 (1990)
144. H. Haug, K. Henneberger: Z. Physik B **84**, 81 (1991)
145. H. Haug, C. Ell: Phys. Rev. B **46**, 2126 (1992)
146. H. Haug, S. W. Koch: *Quantum Theory of the Optical and Electronic Properties of Semiconductors* (World Scientific, Singapore, 2004 4th ed.)
147. H. Haug, L. Bányai: Solid St. Commun. **100**, 303 (1996)
148. A. P. Heberle, J. J. Baumberg, E. Binder, T. Kuhn, K. Köhler, K. H. Ploog: IEEE J. Select. Topics of QE **2**, 762 (1996)
149. A. P. Heberle, J. J. Baumberg: Phys. Rev. Lett. **75**, 2598 (1996)
150. K. Henneberger, S. W. Koch: Phys. Rev. Lett. **76**, 1820 (1996)
151. M. Herbst, V. M. Axt, T. Kuhn: Physica B **272**, 356 (1999)
152. M. Herbst, V. M. Axt, T. Kuhn: Phys. Stat. Sol. B **221**, 419 (2000)
153. S. Hershfield: Phys. Rev. Lett. **70**, 2135 (1993)
154. S. Hershfield, J. H. Davies, J. W. Wilkins: Phys. Rev. Lett. **67**, 3720 (1991)
155. S. Hershfield, J. H. Davies, J. W. Wilkins: Phys. Rev. B **46**, 7046 (1992)
156. M. H. Hettler, H. Schoeller: Phys. Rev. Lett. **74**, 4907 (1995)
157. T. Holstein: Ann. of Physics **29**, 410 (1964)
158. M. Holthaus, D.W. Hone: Phys. Rev. B **49**, 16605 (1994)
159. W. A. Hügel, M. F. Heinrich, M. Wegener, Q. T. Vu, L. Bányai, H. Haug: Phys. Rev. Lett. **83**, 3313 (1999)
160. R. Huber, F. Tauser, A. Brodschelm, M. Bichler, G. Abstreiter, A. Leitenstorfer: Nature **414**, 286 (2003)
161. R. Huber, C. Kübler, S. Tübel, A. Leitenstrofer, Q. T. Vu, H. Haug, F. Kohler, M. C. Amann: Phys. Rev. Lett. **94**, 027401 (2005)
162. K. M. Hung, G. Y. Wu: Phys. Rev. B **48**, 14687 (1993)
163. P. Hyldgaard, S. Hershfield, J. H. Davies, J. W. Wilkins: Ann. of Phys. N.Y. **236**, 1 (1994)
164. J. Iñarrea, G. Platero: Europys. Lett. **34**, 43 (1996)
165. R. C. Iotti, E. Ciancio, F. Rossi: Phys. Rev. B **72**, 125347 (2005)
166. T. Ivanov: Phys. Rev. B **52**, 2838 (1995)
167. T. Ivanov, D. Marvakov, V. Valtchinov, L. T. Wille: Phys. Rev. B **48**, 4679 (1993)
168. C. Jacoboni, L. Reggiani: Rev. Mod. Phys. **55**, 645 (1983)
169. C. Jacoboni, P. Lugli: *The Monte Carlo Method for Semiconductor Device Simulation.* (Topics in Computational Microelectronics) (Springer, Vienna, 1989)
170. A. P. Jauho: J. Phys. F: Met. Phys. **13**, L203 (1983)
171. A. P. Jauho: Phys. Rev. B **32**, 2248 (1985)
172. A. P. Jauho: Physica B **134**, 148 (1985)

173. A. P. Jauho: J. of Phys. A **20**, 2895 (1987)
174. A. P. Jauho: Solid-State Electron. **32**, 1265 (1989)
175. A. P. Jauho: in *Quantum Transport in Semiconductors*, ed. by D. K. Ferry, C. Jacoboni (Plenum, New York, 1991)
176. A. P. Jauho: in *Granular Nanoelectronics* eds. D. K. Ferry, J. R. Barker, C. Jacoboni, NATO ASI Series B: Physics **251** (Plenum, New York, 1991)
177. A. P. Jauho, K. Johnsen: Phys. Rev. Lett. **76**, 4576 (1996)
178. A. P. Jauho, J. W. Wilkins: Phys. Rev. Lett. **49**, 762 (1982)
179. A. P. Jauho, J. W. Wilkins: Phys. Rev. B **28**, 4628 (1983)
180. A. P. Jauho, J. W. Wilkins: Phys. Rev. B **29**, 1919 (1984)
181. A. P. Jauho, J. W. Wilkins, F. P. Esposito: J. Phys. Colloq. **42**, C7-301 (1981)
182. A. P. Jauho, N. S. Wingreen, Y. Meir: Phys. Rev. B **50**, 5528 (1994)
183. A. Jayannavar, N. Kumar: Phys. Rev. Lett. **48**, 553 (1982)
184. P. Jiang, H.-Z. Zheng (eds.): Proceedings of the 21st International Conference on the Physics of Semiconductors (World Scientific, Singapore, 1992)
185. K. Johnsen and A. P. Jauho: Phys. Rev. B **57**, 8860 (1998)
186. K. Johnsen and A. P. Jauho: Phys. Rev. Lett. **83**, 1207 (1999)
187. M. Jonson, A. Grincwajg: Appl. Phys. Lett. **51**, 1729 (1987)
188. R. P. Joshi, R. O. Grondin, D. K. Ferry: Phys. Rev. B **42**, 5685 (1990)
189. M. Joschko, M. Wörner, T. Elsässer, E. Binder, T. Kuhn, H. Kostial, K. Ploog: Phys. Rev. Lett. **78**, 737 (1997)
190. H. H. Jensen, H. Smith, J. W. Wilkins: Phys. Lett. **27A**, 532 (1968)
191. L. P. Kadanoff, G. Baym: *Quantum Statistical Mechanics* (Benjamin, New York, 1962)
192. A. Kalvová, B. Velický: Z. Physik B **94**, 273 (1994)
193. A. Kalvová, B. Velický: Phys. Stat. Sol. (b) **188**, 515 (1995)
194. A. Kalvová, B. Velický: Z. Phys. B **103**, 33 (1997)
195. B. J. Keay, S. J. Allen, J. Galán, J. P. Kaminski, K. L. Campman, A. C. Gossard, U. Bhattacharya, M. J. W. Rodwell: Phys. Rev. Lett. **75**, 4098 (1995)
196. R. Keiper, O. Ziep: Phys. Stat. Sol. B **131**, K91 (1985)
197. L. P. Keldysh: Sov. Phys. JETP **7**, 788 (1958)
198. L. P. Keldysh: Sov. Phys. JETP **20**, 1018 (1965)
199. F. Khan, J. H. Davies, J. W. Wilkins: Phys. Rev. B **36**, 2578 (1987)
200. V. A. Khlus: JEPT **93**, 2179 (1987)
201. M. Kira and S. W. Koch: Eur. Phys. J. D **36**, 143 (2005)
202. W. P. Kirk, M. A. Reed (eds.): *Nanostructures and Mesoscopic Systems* (Academic, San Diego, 1992)
203. C. Kittel: *Quantum Theory of Solids* (Wiley, New York, 1967)
204. H. Kishida, H. Tachibana, K. Sakurai, M. Matsumoto, S. Abe, Y. Tokura: Phys. Rev. B **54**, R14254 (1996)
205. N. C. Kluksdahl, A. M. Kriman, D. K. Ferry, C. Ringhofer: Phys. Rev. B **39**, 7720 (1989)
206. W. H. Knox, C. Hirlmann, D. A. B. Miller, J. Shah, D. S. Chemla, C. V. Shank: Phys. Rev. Lett. **56**, 1191 (1986)
207. S. W. Koch, N. Peyghambarian, M. Lindberg: J. Phys. C **21**, 5229 (1988)
208. S. Kohler, J. Lehmann, P. Hägggi: Phys. Rep. **406**, 379 (2005)
209. J. Kono, M. Y. Su, T. Inoshita, T. Noda, M. S. Sherwin, S. J. Allen, H. Sakaki: Phys. Rev. Lett. **79**, 1758 (1997)

210. B. Kramer (ed.): *Quantum Coherence in Mesoscopic Systems*, NATO ASI Series B, Physics **254** (1991)
211. T. Kuhn: *Ladungsträgerdynamik in Halbleitersystemen fern vom Gleichgewicht: Elektronisches Rauschen und Kohärente Prozesse*, Habilitation-Thesis, Universität Stuttgart (1994)
212. T. Kuhn: *Density matrix theory of coherent ultrafast dynamics* in: *Theory of Transport Properties of Semiconductor Nanostructures*, ed. E. Schöll (Chapmann and Hill, London, 1998) pp. 173 – 214
213. T. Kuhn, F. Rossi: Phys. Rev. Lett. **69**, 977 (1992)
214. T. Kuhn, V. M. Axt, M. Herbst, E. Binder: in *Coherent Control in Atoms, Molecules, and Semiconductors*, eds. W. Pötz and W. A. Schröder (Kluwer, Dordrecht 1999), p. 113
215. Yu. A. Kukharenko, S. G. Tikhodeev: Sov. Phys. JETP **56**, 831 (1982)
216. J. G. Kushmerick, J. Lazorcik, C. H. Patterson, R. Sahshidhar, D. S. Seferos, G. C. Bazan: Nano Lett. **4**, 639 (2004)
217. A. V. Kuznetsov: Phys. Rev. B **44**, 8721 (1991)
218. A. V. Kuznetsov: Phys. Rev. B **44**, 13381 (1991)
219. N. H. Kwong, M. Bonitz, R. Binder, H. S. Köhler: Phys. Stat. Sol. B **206**, 197 (1998)
220. N. H. Kwong, M. Bonitz: Phys. Rev. Lett. **84**, 882 (2000)
221. N. H. Kwong, R. Binder: Phys. Rev. B **61**, 8341 (2000)
222. C. Lacroix: J. Phys. F **11**, 2389 (1981)
223. R. Lake, S. Datta: Phys. Rev. B **45**, 6670 (1992)
224. R. Lake, G. Klimeck, M. P. Anantram, S. Datta: Phys. Rev. B **48**, 15132 (1993)
225. L. D. Landau, E. M. Lifshitz: *Course of Theoretical Physics: Quantum Mechanics* (Pergamon, Oxford, 1962) Vol. 3
226. L. D. Landau, E. M. Lifshitz: *Course of Theoretical Physics: Statistical Physics* (Pergamon, Oxford, 1980) Vol. 5
227. L. D. Landau, E. M. Lifshitz: *Course of Theoretical Physics: Kinetics* (Pergamon, Oxford, 1983) Vol. 10
228. R. Landauer: IBM J. Res. Dev. **1**, 233 (1957)
229. R. Landauer: Philos. Mag. **21**, 863 (1970)
230. R. Landauer: Physica Scr. **T42**, 110 (1992)
231. D. C. Langreth: in *Linear and Nonlinear Electron Transport in Solids*, ed. by J. T. Devreese, E. Van Doren (Plenum, New York, 1976)
232. D. C. Langreth, P. Nordlander: Phys. Rev. B **43**, 2541 (1991)
233. P. A. Lee, T. V. Ramakrishnan: Rev. Mod. Phys. **57**, 287 (1985)
234. S. C. Lee, A. Wacker: Phys. Rev. B **66** 245314 (2002)
235. R. van Leeuwen, N. E. Dahlen, A. Stan: Phys. Rev. B **74**, 195105 (2006)
236. X. L. Lei, N. J. M. Horing, and H. L. Cui: Phys. Rev. Lett. **66**, 3277 (1991)
237. M. Levanda, V. Fleurov: J. Phys. Cond. Matter **6**, 7889 (1994)
238. I. B. Levinson: Sov. Phys. JETP **30**, 362 (1970)
239. L. S. Levitov, G. B. Lesovik: JETP Letters **58**, 230 (1993)
240. X. Li, H. Chen, S.-X. Zhou: Phys. Rev. B **52**, 12202 (1995)
241. E. M. Lifshitz, L. P. Pitaevskii: *Physical Kinetics* (Pergamon, Oxford, 1981)
242. W. Z. Lin, J. G. Fujimoto, E. P. Ippen, R. A. Logan: Appl. Phys. Lett. **50**, 124 (1987)
243. P. Lipavský, F. S. Khan, F. Abdolsalami, J. W. Wilkins: Phys. Rev. B **43**, 4885 (1991)

244. P. Lipavský, F. S. Khan, A. Kalvova, J. W. Wilkins: Phys. Rev. B **43**, 6650 (1991)
245. P. Lipavský, F. S. Khan, J. W. Wilkins: Phys. Rev. B **43**, 6665 (1991)
246. P. Lipavský, V. Špička, B. Velicky: Phys. Rev. B **34**, 6933 (1986)
247. C. Liu, G. Niu: Phys. Rev. B **47**, 13031 (1993)
248. R. Lopez, R. Aguado, G. Platero, C. Tejedor: Phys. Rev. B **64**, 075319 (2001)
249. S. K. Lyo: Phys. Rev. B **43**, 7091 (1991)
250. O. Madelung: *Introduction to Solid State Theory*, Springer Ser. Solid-State Sci., Vol.2 (Springer, Berlin, 1978)
251. G. D. Mahan: *Many-Particle Physics* (Plenum, New York, 1981)
252. G. D. Mahan: Physics Reports **110**, 321 (1984)
253. G. D. Mahan: Physics Reports **145**, 253 (1984)
254. G. D. Mahan: *Many-Particle Physics*, 2nd edn. (Plenum, New York, 1990)
255. G. D. Mahan: *Many-Particle Physics* (Springer, Berlin, 2000)
256. J. Maciejko, J. Wang, H. Guo: Phys. Rev. B **74**, 085324 (2006)
257. B. A. Mason, K. Hess: Phys. Rev. B **39** 5051 (1989)
258. V. Meden, C. Wöhler, J. Fricke, K. Schönhammer: Phys. Rev. B **52**, 5624 (1995)
259. Y. Meir, N. S. Wingreen, P. A. Lee: Phys. Rev. Lett. **66**, 3048 (1991)
260. Y. Meir, N. S. Wingreen: Phys. Rev. Lett. **68**, 2512 (1992)
261. Y. Meir, N. S. Wingreen: Phys. Rev. B **49** 11040 (1994)
262. Y. Meir, N. S. Wingreen, P. A. Lee: Phys. Rev. Lett. **70**, 2601 (1993)
263. U. Meirav, M. A. Kastner, S. J. Wind: Phys. Rev. Lett. **65**, 771 (1990)
264. N. D. Mermin: Phys. Rev. B **1**, 2362 (1970)
265. P. Meystre, M. Sargent III: *Elements of Quantum Optics* (2nd edn.) (Springer, Berlin, 1991)
266. B. Mieck, H. Haug, W. A. Hügel, M. F. Heinrich, M. Wegener: Phys. Rev. B **62**, (2000)
267. A. B. Migdal: Sov. Phys. JETP **7**, 996 (1958)
268. A. Mitra, I. Aleiner, A. J. Millis: Phys. Rev. B **69**, 245302 (2004)
269. S. Mukamel: Annu. Rev. Phys. Chem **41**, 647 (1990)
270. D. Miller and B. Laikhtman: Phys. Rev. B **50**, 18426 (1994)
271. S. Mukamel: *Principles of Nonlinear Optical Spectroscopy* (Oxford Press, Oxford, 1995)
272. S. Nakajima: Prog. Theor. Phys. **20**, 948 (1958)
273. Y. V. Nazarov, D. A. Bagrets: Phys. Rev. Lett. **88**, 196801 (2002)
274. T. K. Ng: Phys. Rev. Lett. **76**, 487 (1996)
275. C. Niu, L. J. Liu, T. H. Lin: Phys. Rev. B **51**, 5130 (1995)
276. K. B. Nordstrom, K. Johnsen, S. J. Allen, A. P. Jauho, B. Birnir, J. Kono, T. Noda, H. Akiyama, and H. Sakaki: Physical Review Letters **81**, 457 (1998)
277. M. A. Osman, D. K. Ferry: Phys. Rev. B **36**, 6018 (1987)
278. J. L. Oudar, D. Hulin, A. Migus, A. Antonetti, F. Alexandre: Phys. Rev. Lett. **55**, 2074 (1985)
279. A. A. Ovchinnikov, N. S. Erikhman: Sov. Phys.-JETP **40**, 733 (1975)
280. O. A. Pankratov: Fiz. Tverd. Tela (Leningrad) **23**, 68 (1981) [Sov. Phys. – Solid State **23** (1981)]
281. H. M. Pastawski: Phys. Rev. B **46**, 4053 (1992)
282. S. Pilgram, A. N. Jordan, E. V. Sukhorukov, M. Büttiker: Phys. Rev. Lett. **90**, 206801 (2003)

283. G. Platero, R. Aguado: Phys. Rep. **395**, 1 (2004)
284. R. E. Prange, L. P. Kadanoff: Phys. Rev. **134**, A566 (1964)
285. J. Rammer: *Uligevægt i supraleddere*. MSc Thesis, University of Copenhagen (in Danish) (1981)
286. J. Rammer: Rev. Mod. Phys. **63**, 781 (1991)
287. J. Rammer, H. Smith: Rev. Mod. Phys. **58**, 323 (1986)
288. Yu. T. Rebane, Fiz. Tverd. Tela (Leningrad) **27**, 1364 (1985) [Sov. Phys. Solid State **27**, 824 (1985)]
289. B. Reulet, J. Senzer, D.E. Prober: Phys. Rev. Lett. **91**, 196601 (2003)
290. L. Reggiani (ed.): *Hot Electron Transport in Semiconductors*, Topics Appl. Phys. Vol. **58** (Springer, Berlin, 1985)
291. L. Reggiani, P. Lugli, A. P. Jauho: Phys. Rev. B **36** 6602 (1987)
292. L. Reggiani, P. Lugli, A. P. Jauho: Physica Scripta **38**, 117 (1988)
293. L. Reggiani, P. Lugli, A. P. Jauho: J. Appl. Physics **64**, 3072 (1988)
294. E. Reitsamer, L. Bányai, D. B. Tran Thoai, P. I. Tamborenea, H. Haug: in *Physics of Semiconductors*, ed. M. Scheffler, R. Zimmermann, (World Scientific, Singapore, 1996), p. 685
295. H. Risken: *The Fokker-Planck Equation* (Springer, Berlin, 1984)
296. B. Robertson: Phys. Rev. **144**, 151 (1966)
297. Yu. G. Rubo: Zh. Eksp. Teor. Fiz. **104**, 3536 (1993) [JETP **77**, 685 (1993)]
298. E. Runge, E. K. U. Gross: Phys. Rev. Lett. **52**, 997 (1984)
299. E. Runge, H. Ehrenreich: Annals of Physics **219**, 55 (1992)
300. E. Runge, H. Ehrenreich: Phys. Rev. B **45**, 9145 (1992)
301. E. Runge: Phys. Rev. **47**, 2003 (1993)
302. D. Sanchez-Portal, P. Ordejón, E. Artacho, J. M. Soler: Int. J. Quantum Chem. **65**, 453 (1999)
303. W. Schäfer: In *Festkörperprobleme* (Advances in Solid State Physics) (Vieweg, Braunschweig, 1988) Vol. **28**, p. 63
304. W. Schäfer, J. Treusch: Z. Phys. B **63**, 407 (1986)
305. W. Schäfer: J. Opt. Soc. Am. b **13**, 1291 (1996)
306. W. Schäfer, R. Loevenich, N. Frommer, D. S. Chemla: Phys. Stat. Sol. B **221**, 195 (2000)
307. W. Schäfer, M. Wegener: *Semiconductor Optics and Transport Phenomena* (Springer, Berlin, 2002)
308. J. Schilp, T. Kuhn, G. Mahler: Semicond. Sci. Technol. **9**, 439 (1994)
309. J. Schilp, T. Kuhn, G. Mahler: Phys. Rev. B **50**, 5435 (1994)
310. J. Schilp, T. Kuhn, G. Mahler: Phys. Stat. Sol. B **188**, 417 (1995)
311. J. Schlösser, C. H. Neumann, A. Stahl: J. Phys. Cond. Matter **4**, 121 (1992)
312. A. Schmenkel, L. Bányai, H. Haug: J. Luminesc. **76/77**, 134 (1998)
313. O. M. Schmitt, D. B. Tran Thoai, L. Bányai, P. Gartner, H. Haug: Phys. Rev. Lett. **68**, 2839 2000
314. S. Schmitt-Rink, D. Chemla, H. Haug: Phys. Rev. B **37**, 942 (1988)
315. H. Schoeller: Ann. of Phys. **229**, 320 (1993)
316. J. Schwinger: J. Math. Phys. **2**, 407 (1961)
317. D. C. Scott, R. Binder, S. W. Koch: Phys. Rev. Lett. **69**, 347 (1992)
318. J. Seebeck, T. R. Nielsen, P. Gartner, F. Jahnke: Phys. Rev. B **71** 125327 (2005)
319. V. P. Seminozhenko: Phys. Rep. **3**, 103 (1982)
320. J. Shah: Solid-State Electron. **32**, 1051 (1989)

321. J. Shah: *Ultrafast Spectroscopy of Semiconductors and Semiconductor Microstructures*, Springer Ser. in Solid-State Sci., Vol. 115 (Springer, Berlin, 1996)
322. W. Shockley: Bell System Tech. J. **30**, 990 (1950)
323. N. H. Shon, A. Ferraz: Sol. St. Commun. **86** 195 (1993)
324. C. Sieh, T. Meier, F. Jahnke, A. Knorr, S. W. Koch, P. Brick, M. Hübner, C. Ell, J. P. Prineas, G. Kitrova, H. M. Gibbs: Phys. Rev. Lett. **82**, 3112 (1999)
325. C. P. Slichter: *Principles of Magnetic Resonances*, 3rd edn., Springer Ser. Solid-State Sci., Vol.1 (Springer, Berlin, 1990)
326. R. H. M. Smit, C. Untiedt, J. M. van Ruitenbeek: Nanotechnology **15**, 472 (2004)
327. H. Smith, H. H. Jensen: *Transport Phenomena* (Clarendon, Oxford, 1989)
328. H. Smith, J. W. Wilkins: Phys. Rev. Lett. **24**, 221 (1970)
329. D. W. Snoke, W. W. Rühle, Y. C. Lu, E. Bauser: Phys. Rev. B **45**, 10979 (1992)
330. F. M. Souza, J. C. Egues, A. P. Jauho: Braz. J. Phys. **34**, 565 (2004). See also F. M. Souza: *Transporte quântico em spintrônica: corrente e shot noise via funções de Green de não-equilíbrio*, Ph. D. Thesis, University of São Paulo (2004)
331. V. Špička, P. Lipavský: Phys. Rev. Lett **73**, 3439 (1994)
332. V. Špička, P. Lipavský: Phys. Rev. B **52**, 14615 (1995)
333. C. Stafford , N. S. Wingreen: Phys. Rev. Lett. **76**, 1916 (1996)
334. C. J. Stanton, D. W. Bailey, K. Hess: IEEE-QE **24**, 1614 (1988)
335. A. Stahl, I. Balslev: *Electrodynamics of the Semiconductor Band Edge*, Springer Tracts in Modern Physics, Vol. 110 (Springer, Berlin, 1987)
336. G. Stefanucci, C. O. Almbladh: Phys. Rev. B **69**, 195318 (2004)
337. D. Steinbach, M. U. Wehner, M. Wegener, L. Bányai, E. Reitsamer, H. Haug: Chem. Phys. **210**, 49 (1996)
338. D. Steinbach, G. Kochschneidt, M. U. Wehner, H. Kalt, M. Wegener, K. Ohkawa, D. Hommel, V.M. Axt: Phys. Rev. B **60**, 12079 (1999)
339. M. Suhrke, S. Wilke: Phys. Rev. B **46**, 2400 (1992)
340. Q. F. Sun, J. Wang, T. H. Lin: Phys. Rev. B **58**, 13007 (1998)
341. T. Takemori, Y. Motomura, M. Inoue: J. Physics Condens. Matt. **7**, 4629 (1995)
342. K. K. Thornber: In *Path Integrals*, ed. G. J. Papadopoulos. (Plenum, New York, 1978)
343. K. K. Thornber: Solid State Electron. **21**, 259 (1978)
344. K. K. Thornber: In *Quantum Transport in Semiconductors*, ed. by D. K. Ferry, C. Jacoboni (Plenum, New Yor, 1991)
345. C. S. Ting (ed.): *Physics of Hot Electron Transport in Semiconductors* (World Scientific, Singapore, 1992)
346. D. B. Tran Thoai, H. Haug: Phys. Stat. Sol. B **173**, 159 (1992)
347. D. B. Tran Thoai, H. Haug: Phys. Rev. B **47**, 3574 (1993)
348. D. B. Tran Thoai, H. Haug: Z. Phys. B **91**, 199 (1993); Erratum *ibid.* B **3**, 532
349. D. B. Tran Thoai, L. Bányai, E. Reitsamer, H. Haug: Phys. Stat. Sol. B **188**, 387 (1995)
350. D. B. Tran Thoai, H. Haug: Unpublished (1995)
351. C. Toher, A. Filippetti, S. Sanvito, K. Burke: Phys. Rev. Lett. **95**, 146402 (2005)

352. Y. Toyozawa: Prog. Theoret. Phys. **20**, 53 (1958)
353. R. Tsu and G. Döhler: Phys. Rev. B **12**, 680 (1975)
354. G. Vignale, W. Kohn: Phys. Rev. Lett. **77**, 2037 (1996)
355. Q. T. Vu, L. Bányai, H. Haug, F. X. Camescasse, J. P. Likforman, A. Alexandrou: Phys. Rev. B **59**, 2760 (1999)
356. Q. T. Vu, H. Haug: Phys. Rev. B **62**, 7179 (2000)
357. Q. T. Vu, H. Haug, W. A. Hügel, S. Chatterjee, M. Wegener: Phys. Rev. Lett. **89**, 3508 (2000)
358. Q. T. Vu, H. Haug, O. Mücke, T. Tritschler, M. Wegener, G. Khitrova, H. M. Gibbs: Phys. Rev. Lett. **92**, 217403 (2004)
359. Q. T. Vu, H. Haug, S. W. Koch: Phys. Rev. B **73**, 205317 (2006)
360. A. Wacker and A. P. Jauho: Phys. Rev. Lett. **80**, 369 (1998)
361. A. Wacker, A. P. Jauho, S. Rott, A. Markus, P. Binder, and G. H. Döhler: Phys. Rev. Lett. **83**, 836 (1999)
362. A. Wacker: Phys. Rep. **357**, 1 (2002)
363. M. Wagner: Phys. Rev. B **44**, 6104 (1991)
364. M. Wagner: Phys. Rev. B **45**, 11595 (1992)
365. M. Wagner: Phys. Rev. B **45**, 11607 (1992)
366. M. Wagner: Phys. Rev. Lett. **76**, 4010 (1996)
367. W. Y. Wang, T. Lee, I. Kretzschmar, M. A. Reed: Nano Lett. **4**, 643 (2004)
368. M. Wegener, M. U. Wehner, D. Steinbach, L. Bányai, D. B. Tran Thoai, E. Reitsamer, H. Haug: in *Physics of Semiconductors*, M. Scheffler, R. Zimmermann, eds. (World Scientific, Singapore, 1996), p. 633
369. T. Weil, B. Vinter: Appl. Phys. Lett. **50**, 1281 (1987)
370. N. S. Wingreen: *Resonant Tunneling with Electron-phonon Interaction*, Ph. D. Thesis, Cornell University (1989)
371. N. S. Wingreen, K. W. Jacobsen, J. W. Wilkins: Phys. Rev. B **40**, 11834 (1989)
372. N. S. Wingreen, K. W. Jacobsen, J. W. Wilkins: Phys. Rev. Lett. **61**, 1396 (1988)
373. N. S. Wingreen, A. P. Jauho, Y. Meir: Phys. Rev. B **47**, 8487 (1993)
374. T. Wolterink, V. M. Axt, T. Kuhn: Phys. Rev. B **67**, 115311 (2003)
375. H. W. Wyld, B. D. Fried: Annals of Physics **23**, 374 (1963)
376. Y. Yacoby: Phys. Rev. **169**, 610 (1968)
377. P. Y. Yu, M. Cardona: *Fundamentals of Semiconductors* (Springer, Berlin, 1996)
378. Y. B. Yu, T. C. A. Yeung, W. Z. Shangguan, C. H. Kam: Phys. Rev. B **63**, 205314 (2001)
379. C. Zhang, M. L. F. Lerch, A. D. Martin, P. E. Simmonds, L. Eaves: Phys. Rev. Lett. **72**, 3396 (1994)
380. J. M. Ziman: *Electrons and Phonons* (Oxford University Press, Oxford, 1960)
381. R. Zimmermann: *Many-Particle Theory of Highly Excited Semiconductors* (Teubner, Leipzig, 1988)
382. R. Zimmermann: Phys. Stat. Sol. B **59**, 317 (1990)
383. R. Zimmermann: J. Luminesc. **53**, 187 (1992)
384. R. Zimmermann, J. Wauer, A. Leitenstorfer, C. Fürst: J. Luminesc. **76**, **34** (1998)
385. R. W. Zwanzig: J. Chem. Phys. **33**, 1338 (1960)
386. R. W. Zwanzig: *Lectures in Theoretical Physics*, Vol. 3 (Interscience, New York, 1961)

Index

- Accumulation region, 185
- Admittance
 - linear-response, 229
- Aharonov–Bohm effect, 183
- Analytic continuation, 59, 69, 97
 - weak localization self-energy, 112
- Anticommutator rule, 37, 91
- Balance equation approach, 130
- Barker–Ferry equation, 146
- Beam projection technique, 290
- Bethe–Salpeter equation, 159, 172
- Binomial coefficients, 22
- Bloch equations
 - optical, 251, 255
- Bloch oscillations, 199
- Bloch vector \mathbf{U}_k , 255
- Boltzmann equation
 - applied to $N^+N^-N^+$ -structure, 29
 - derivation of, 3, 5
 - eigenfunction expansion of, 8, 10, 11
 - elastic impurities, 21, 83, 126
 - integral form, 149
 - linearization of, 8, 10, 11
 - Monte Carlo solution of, 12
 - numerical integration of, 11
- Broadening
 - inhomogeneous, 256
- Buildup of quasi-particle dressing, 320
- Buildup time
 - phonon–plasmon mixed modes, 329
- Calculation of noise, 230
- Catch
- related to two-step process, 77
- Chemical potential, 194
- Coherent back-scattering, 111
- Coherent control, 335
- Coherent potential approximation (CPA), 135
- Collision broadening, 148–151
- Collision damping, 40
- Collision frequencies, 13
- Collision term
 - as an integral operator, 9
 - electron–phonon systems, 145
 - gauge-invariant, 90
 - Gaussian white noise model, 124
 - invariants of, 13
 - linearization of, 102
 - memory effects, 265
 - quantum, 77
 - non-Markovian nature, 265
 - resonant-level model, 143
- Commutator rule, 37
- Complex-time contour, 97
- Conductivity
 - electrical
 - Boltzmann result, 110
 - Drude, 114
 - linear d.c., 108
 - linear for elastic impurities, 101, 104–110
 - nonlinear, 154
- Conservation law
 - Boltzmann equation, 4
 - current, 191

- energy, 315
- momentum, 117
- Continuity equation
 - static, 30
 - time-dependent, 217
- Contour
 - deformation of, 70
- Correlation function
 - equation-of-motion, 76
 - retarded
 - current-current, 105
 - time-ordered
 - current-current, 105
- Correlation function $G^<$
 - approximate for Coulomb island, 207
 - Gaussian white noise model, 123
 - relation to observables, 93
- Coulomb island, 205
- Coulomb potential
 - screened, 12
 - static, 12
 - time-dependent screened, 318
 - two-dimensional Fourier transform, 12
- Coulomb quantum kinetics, 301
- Coupling
 - adiabatic, 70
- Current
 - density, 93
 - interacting model, 193
 - resonant-level model, 193
 - time-averaged, 217–218
 - for resonant-level model, 220
 - time-dependent, 216
 - linear-response, 227–229
- Current conservation, 106, 191
- Current standard, 213
- Current-voltage characteristic, 182
 - experimental, 196
 - resonant tunneling device, 194
- Damping
 - Markovian, 265
 - non-Markovian, 265
- Damping constants, 255
- Density functional theory, 185, 195
- Density matrix, 38
 - thermal equilibrium, 64
- Density matrix methods, 130
- Density of states
 - field-dependent
 - three dimensions, 163
 - two dimensions, 163
 - in terms of spectral function, 45
 - resonant-level model, 135
- Dephasing rate
 - density-dependent, 335
- Depletion region, 185
- Detailed balance, 14
- Detuning, 254
- Diagrams
 - crossed, 57, 111
 - disconnected, 49, 69
 - Feynman, 49, 69
 - ladder, 106
 - maximally crossed, 111
 - rainbow, 57
- Diamagnetic term, 107
- Dielectric breakdown, 129
- Dielectric function
 - time and frequency dependent, 320
- Dielectric susceptibility, 157
- Differential transmission spectroscopy, 287
- Diffusion
 - constant, 113
 - Gaussian white noise model, 127
- Dipole matrix element, 251
- Disorder averaging
 - Gaussian white noise model, 121
 - in external fields, 133
- Distribution function
 - Bose, 8
 - drifted Maxwellian, 33
 - Fermi, 8
 - generalized, 77
 - local equilibrium, 30
- Drift-velocity
 - quantum, 156
- Driving term
 - gauge-invariant, 88
 - with magnetic field, 89
 - generalized, 77
 - re-normalization of, 77
 - scalar potential gauge, 88
 - vector potential gauge, 88
- DTS, 287
- Dynamical Franz–Keldysh effect, 168

- Dyson equation
 - complex time, 78, 97
 - eigenfunction representation of, 153
 - elastic impurities, 107
 - electron-phonon systems, 53
 - for contour-ordered Green function, 70
 - for inter-band Green function, 252, 266
 - Gaussian white noise model, 122
 - nonequilibrium, 91, 98
 - resonant-level model, 192
 - concentration of impurities, 133
 - time-dependent, 218
 - retarded Coulomb potential, 304, 310
 - tight-binding representation, 200
- Eigenfunctions
 - for linearized collision term, 9, 16
 - norm, 9
 - scalar product, 9
- Eigenvalues
 - density of, 14
 - spectrum of, 14
- Einstein summation convention, 85
- Electron-phonon interaction, 186
- Electron-hole plasma, 301
- Energy relaxation
 - Gaussian white noise model, 127
- Energy renormalization, 46
- Envelope function, 250
- Equation-of-motion
 - for Bloch vector, 255
 - for nonequilibrium Green functions, 75
- Equation-of-motion technique, 69, 187
 - Coulomb island, 205
 - elastic impurity problem, 55
 - for reduced density matrix, 244
 - resonant-level model, 51, 132
- Fano model, 50, 51
- Fermi's golden rule, 4, 20
- Feynman diagrams
 - electron-phonon system, 52
 - for elastic impurity problem, 56
 - two-particle Green function, 54
- Feynman path integral method, 130
- Field operator, 38
- for quantum-well structure, 250
- in terms of Bloch waves, 250
- Floquet theory, 176
- Fluctuating energy-levels, 229–230
- Fluctuation-dissipation theorem, 102
 - derivation of, 45, 47
- Fluctuation-dissipation theorem, 206
- Fock space, 35
 - completeness relation of, 36
- Fokker-Planck equation, 11
- Formation of polarons, 295
- Four-wave mixing (FWM), 287
 - time-integrated, 334
 - time-resolved, 253, 333
 - with coherent control, 335
- Fractional quantum Hall effect, 52
- Fredholm iteration, 284
- Free electron laser, 158
- Free induction decay, 256
- Functional differentiation, 69
- FWM, 287
- Γ -point, 250
- Gauge
 - scalar potential, 87
 - vector potential, 87
- Gauge invariance, 85–92, 98
 - transformation of functions, 85
- Gauge transformation, 86
- Gaussian white noise model, GWN, 121
- Gell-Mann and Low theorem, 48
- Generalized Kadanoff-Baym ansatz,
 - 94–97, 145, 147, 245, 265, 295, 303
 - for multiple bands, 263
 - gauge invariant, 97
- GKBA, 94, 95, 97, 245, 246, 263–265, 295, 303
- Gradient expansion, 79–81, 85
 - derivation of, 80–81
- Gradient operator, 80
- Green function
 - advanced
 - definition of, 43, 68
 - elastic impurities, 57
 - for two bands, 264
 - non-interacting contacts, 216
 - antitime-ordered
 - definition of, 67
 - causal, 67, 105

- definition of, 41, 67
- contour-ordered, 63, 187
 - definition of, 67
 - perturbation expansion for, 69
- correlation function
 - definition of, 68
 - equilibrium theory of, 35, 59
 - finite temperature
 - definition of, 42
 - free-particle, 50
 - differential equation for, 42
 - gauge-invariant, 115, 119
 - greater
 - definition of, 43, 67
 - higher-order, 69
 - in scalar potential gauge, 87
 - in vector potential gauge, 87
 - inter-band
 - definition of, 252
 - lesser
 - definition of, 43, 67
 - non-interacting contacts, 216
 - perturbation expansion of, 47, 49
 - phonon
 - equilibrium, 73, 145
 - retarded
 - analytic structure, 119
 - approximate for Coulomb island, 206
 - definition of, 43, 68
 - disorder averaged for RLM, 133
 - elastic impurities, 57
 - field-dependent; scalar potential gauge, 115–118
 - field-dependent; vector potential gauge, 119
 - for two bands, 264
 - gauge-invariant, 91
 - Gaussian white noise model, 121–122
 - non-interacting contacts, 216
 - time-dependent resonant-level model, 219
 - time-ordered
 - definition of, 41, 67
 - two-particle, 53, 101, 105
 - causal impurity-averaged, 106
 - factorization of, 105
 - integral equation for, 107
 - H-function, 7
 - H-theorem, 5, 8
 - Hartree–Fock approximation, 208
 - High temperature superconductors, 52
 - Hilbert space, 9, 35
 - History
 - quantum kinetics and fs-spectroscopy, 249
 - Impurity averaging, 54, 58, 105
 - nonequilibrium, 133
 - prescription for, 54, 134
 - Induced polarizability, 157
 - Initial correlations, 70
 - Interaction
 - carrier - classical light field, 250
 - electron - classical light field
 - in rotating-wave approximation, 251
 - electron-phonon
 - in second quantization, 38
 - Fröhlich, 262
 - one-body
 - in second quantization, 37
 - two-particle
 - in second quantization, 37
 - Interband polarization, 253
 - Interband-polarization component, 254
 - Intra-collisional field-effect, 131, 148, 149, 151
 - Intracollisional field-effect, 126
 - Inversion, 255
 - Irreversibility
 - Boltzmann equation, 77
 - quantum kinetic equation, 77
 - IV-curves, 199, 201
 - Joint density of states, 161, 163
 - Joint spectral function, 161
 - Joule heating, 142
 - Kadanoff–Baym ansatz, 143, 264
 - Kadanoff–Baym equation, 77, 87, 98, 123
 - derivation of, 75–77
 - for inter-band Green function, 260
 - Keldysh equation, 96, 98, 123, 192, 206
 - derivation of, 77–78
 - for resonant-level model, 219
 - tight-binding representation, 200

- Kinetic energy
 - in terms of a Green function, 43
- Kinetic equations
 - numerical solution
 - stochastic, 20
- Kinetics
 - free-carrier, 251
 - linearized Coulomb, 12, 20
 - optical inter-band, 253
 - quantum
 - interband, 243
- Kondo phenomenon, 52, 186, 207
- Kondo temperature, 210
- Kubo formula, 101
 - Landau damping, 310
 - Landauer formula, 183, 190
 - for time-averaged current, 218
 - Langreth theorem, 70
 - Level-shift function, 194
 - Level-width
 - elastic, 194
 - inelastic, 194
 - total, 194
 - Level-width function, 189, 194
 - energy-dependence, 190
 - field-dependence, 132
 - generalized, 216
 - Light-induced gaps, 273, 274
 - Limit
 - Boltzmann, 79–83
 - completed collisions of, 149, 314
 - Markov, 284
 - wide-band (WBL), 217, 219
 - zero-field limit, 117
 - Lindhard formula, 306
 - Line shape
 - strong-coupling limit, 276
 - weak-coupling limit, 275
 - Liouville equation, 21
 - LO-phonon quantum beats, 292
 - Luttinger liquids, 52
 - Markov equations, 40
 - Mass-renormalization factor
 - nonequilibrium, 156
 - Master equation, 12, 20, 22, 23
 - Matsubara technique, 58
 - Maxwell’s equation, 157, 162
 - Mesoscopic phenomena, 55, 181
 - Mesoscopic transport, 183
 - Migdal theorem, 53
 - Miniband, 198
 - Miniband transport, 199
 - Mixed phonon-plasmon modes, 338
 - Modulation doping, 181
 - Molecular electronics, 182
 - Mollow triplet, two-band version, 274
 - Momentum distribution
 - Gaussian white noise model, 124
 - Monte Carlo simulations, 130, 148, 149, 151, 201
 - ensemble, 20, 29
 - random number generation, 23, 151
 - Negative differential resistance, 199, 229
 - NEGF, 75
 - Non-linear optical spectroscopy, 253
 - $N^+N^-N^+$ -structure, 29
 - Number density
 - relation to correlation function $G^<$, 94
 - Numerical solutions
 - for two-time-dependent GFs, 296
 - Operator
 - annihilation, 35, 36
 - contour-ordering, 65, 67
 - creation, 35
 - fermion, 35, 67
 - permutation, 36
 - time-ordering, 42, 65
 - Optical absorption
 - strong fields, 157
 - Parallel transport, 181
 - Particle density
 - in terms of a Green function, 43
 - Pauli principle, 4
 - Perpendicular transport, 181
 - Phase-braking length, 55
 - Phonon reaction time, 266
 - Phonon relaxation cascades, 291
 - Phonon resonance
 - longitudinal, transversal, 326
 - Phonon scattering, 200
 - Phonon sidebands, 282
 - Phonon-plasmon quantum beats, 336

- Photon echo, 256, 257, 331
 Photonic side-bands, 166, 221
 Picture
 Heisenberg, 47, 64, 67
 definition of, 42
 interaction, 44, 47
 Schrödinger, 47
 Plasma oscillations
 parametric, 311
 Plasmon-pole approximation
 time-dependent, 309, 313
 Poisson equation, 30
 Polarization, 253
 interband, 158
 Polaron constant, 263
 Polaron correlations
 in quantum kinetic relaxation, 300
 polaron GF, 278
 Ponderomotive energy, 165
 Projection operator techniques, 130
 Propagator
 hole, 44
 particle, 44
 phonon, 262

 Quantum Boltzmann equation, 101–104
 Quantum cascade lasers, 201
 Quantum coherence, 265
 Quantum kinetic equation
 elastic impurities, 109
 electron–phonon systems, 144–148
 gauge-invariant, 87–89
 Gaussian white noise model, 123–127
 inhomogeneous systems, 151
 interband, 259
 linear, 154
 resonant-level model, 141–144
 Quantum kinetics
 connection to Boltzmann equation, 83
 Markov limit, 315
 Quantum point contact, QPC, 182
 Quantum transport theory
 linear, 101
 nonlinear, 115–156
 Quantum unit of conductance, e^2/h , 183
 Quasibound state, 181
 Quasiclassical theory, 79

 Quasielastic regime, 150
 Quasienergy, 177
 Quasiparticle approximation, 81–82
 Quasiparticle dispersion, 120
 Quasiparticle weight, 120
 Rabi flop, 256
 Rabi frequency, 254
 Random number generation, 23
 Random phase approximation (RPA), 302
 Random walk
 one-dimensional chain, 21
 Relaxation frequencies, 10
 Relaxation kinetics
 Boltzmann, 10
 numerical studies, 23, 29
 Boltzmann equation, 17
 Relaxation time
 longitudinal (T_1), 254
 transversal (T_2), 254, 257
 Relaxation-time approximation, 10, 30, 153
 Representation
 interaction, 65
 Resonant tunneling, 186
 Resonant-level model, 50, 52, 192
 in high electric fields, 131–144
 time-dependent, 218–226
 Resonant-tunneling diode, RTD, 181
 high-frequency response, 229
 modeling of, 214
 Retarded Green function
 free-particle approximation, 266
 Gaussian damping, 276
 hyperbolic secant damping, 277
 mean-field approximation, 269
 Wigner–Weisskopf damping, 275
 Rotating-wave approximation, 251, 254
 Run-away
 field assisted, 151
 S-matrix, 48, 63
 Scattering rate
 elastic impurity, 21
 electron-electron, 23
 in Born approximation, 4
 electron-phonon, 5
 Screened Coulomb potential
 two-time-dependent, 318

- Screening
 - Coulomb and phonon-exchange mediated interaction, 323
 - equilibrium RPA, 306
 - in two-time GF formalism, 304
 - time-dependent RPA, 304
 - Screening length
 - Debye, 31
 - nonequilibrium, 312
 - Second quantization, 35, 38
 - Self-consistent Born approximation, 200
 - Self-energy, 52, 54
 - analytic continuation
 - resonant-level model, 140
 - Born approximation, 138, 145
 - electron-phonon systems, 52
 - equilibrium
 - imaginary part of, 76
 - greater
 - electron-phonon systems, 145
 - Hartree-Fock
 - time-dependent, 262
 - inter-band, 252
 - singular part of, 252
 - irreducible, 70
 - lesser
 - electron-phonon systems, 145
 - Gaussian white noise model, 123, 126
 - resonant-level model; impurity averaged, 141
 - nonequilibrium
 - imaginary part of, 76
 - retarded
 - for time-dependent resonant-level model, 219
 - Gaussian white noise model, 123
 - impurity-averaged for RLM, 135
 - self-consistent Born approximation, 138, 145
 - elastic impurities, 57, 82, 106
 - electron-phonon systems, 144
 - electron-phonon systems, 53
 - Gaussian white noise model, 121
 - tunneling, 191
 - weak localization, 111
 - nonequilibrium, 111
 - Self-scattering, 22
- Semiconductor
 - direct gap, 250
 - heterostructure, 181
 - two-band model for, 250
 - Semiconductor Bloch equations, 262
 - Semiconductor superlattice, 198
 - Sequential tunneling, 199
 - Single-electron pumps, 213
 - Slave-boson technique, 207
 - S*-matrix, 59
 - Spatial variation
 - adiabatic approximation, 289
 - Spectral function
 - definition of, 45
 - equilibrium, 76
 - Gaussian white noise model, 124
 - general structure, 120
 - interacting, 102
 - field-dependent, 119
 - free, 120
 - gauge-invariant
 - time-dependent fields, 164
 - in gradient approximation, 81
 - interacting
 - resonant-tunneling diode, 197
 - joint, 150, 151
 - nonequilibrium, 76
 - equation-of-motion, 77
 - resonant-level model, 193
 - sum rule, 45, 120, 140
 - Spectroscopy
 - optical pump and THz probe, 318
 - pump and probe, 12, 315
 - thin samples, 290
 - Split-gate geometry, 182
 - States
 - antisymmetric, 35
 - Streaming-motion regime, 150
 - Threshold
 - for one-LO-phonon emission, 278
 - THz spectroscopy, 318
 - Tight-binding representation, 199
 - Time-ordered Green function, 187
 - T*-matrix
 - functional of Green function, 135
 - resonant-level model, 52
 - field-dependent, 132
 - single-site, 134

- Total energy
 - in terms of a Green function, 43
- Transformation
 - similarity, 13
- Transient dynamics
 - Gaussian white noise model, 121
 - resonant-level model, 218–226
- Transitions
 - dipole-allowed, 250
- Transmission coefficient, 184, 190
 - elastic, 193
- Transport properties
 - Gaussian white noise model, 127–129
- semiconductors
 - high electric fields, 129–156
- Tunneling Hamiltonian, 185
- Tunneling problems, 184
- Two-branch time contour, 184
- Two-dimensional electron gas, 12, 182
- Two-pulse spectroscopy, 287
- Two-time-dependent GFs, 296
- Universal conductance fluctuations, 183
- Urbach absorption tail, 265
- Urbach tail, 265
- Variables
 - center-of-mass, 80, 86, 88, 91
 - difference, 80, 86, 91
- Vertex equation, 108
- Vertex function, 106
- Wannier–Stark hopping, 199
- Ward identities, 106
- Wave equation, 41
- Wavefunction renormalization, 46, 120
- Weak localization, 58, 106, 111–114, 183
- White-noise spectrum, 230
- Wick’s theorem, 49, 59, 63, 67, 68, 97, 105, 159, 207
- Wigner coordinates, 79, 80
- Wigner function, 93–94, 123
 - quantum kinetic equation, 89, 98, 123
 - electron–phonon systems, 146
 - nonlocal driving term, 152
- Zener effect, 159

Springer Series in SOLID-STATE SCIENCES

Series Editors:

M. Cardona P. Fulde K. von Klitzing R. Merlin H.-J. Queisser H. Störmer

- 90 **Earlier and Recent Aspects of Superconductivity**
Editor: J.G. Bednorz and K.A. Müller
- 91 **Electronic Properties and Conjugated Polymers III**
Editors: H. Kuzmany, M. Mehring, and S. Roth
- 92 **Physics and Engineering Applications of Magnetism**
Editors: Y. Ishikawa and N. Miura
- 93 **Quasicrystals**
Editor: T. Fujiwara and T. Ogawa
- 94 **Electronic Conduction in Oxides**
2nd Edition By N. Tsuda, K. Nasu, A. Fujimori, and K. Siratori
- 95 **Electronic Materials**
A New Era in MaterialsScience
Editors: J.R. Chelikowski and A. Franciosi
- 96 **Electron Liquids**
2nd Edition By A. Isihara
- 97 **Localization and Confinement of Electrons in Semiconductors**
Editors: F. Kuchar, H. Heinrich, and G. Bauer
- 98 **Magnetism and the Electronic Structure of Crystals**
By V.A. Gubanov, A.I. Liechtenstein, and A.V. Postnikov
- 99 **Electronic Properties of High-T_c Superconductors and Related Compounds**
Editors: H. Kuzmany, M. Mehring, and J. Fink
- 100 **Electron Correlations in Molecules and Solids**
3rd Edition By P. Fulde
- 101 **High Magnetic Fields in Semiconductor Physics III**
Quantum Hall Effect, Transport and Optics By G. Landwehr
- 102 **Conjugated Conducting Polymers**
Editor: H. Kiess
- 103 **Molecular Dynamics Simulations**
Editor: F. Yonezawa
- 104 **Products of Random Matrices in Statistical Physics** By A. Crisanti, G. Paladin, and A. Vulpiani
- 105 **Self-Trapped Excitons**
2nd Edition
By K.S. Song and R.T. Williams
- 106 **Physics of High-Temperature Superconductors**
Editors: S. Maekawa and M. Sato
- 107 **Electronic Properties of Polymers**
Orientation and Dimensionality of Conjugated Systems
Editors: H. Kuzmany, M. Mehring, and S. Roth
- 108 **Site Symmetry in Crystals**
Theory and Applications
2nd Edition
By R.A. Evarestov and V.P. Smirnov
- 109 **Transport Phenomena in Mesoscopic Systems**
Editors: H. Fukuyama and T. Ando
- 110 **Superlattices and Other Heterostructures**
Symmetry and Optical Phenomena
2nd Edition
By E.L. Ivchenko and G.E. Pikus
- 111 **Low-Dimensional Electronic Systems**
New Concepts
Editors: G. Bauer, F. Kuchar, and H. Heinrich
- 112 **Phonon Scattering in Condensed Matter VII**
Editors: M. Meissner and R.O. Pohl
- 113 **Electronic Properties of High-T_c Superconductors**
Editors: H. Kuzmany, M. Mehring, and J. Fink
-

Springer Series in SOLID-STATE SCIENCES

Series Editors:

M. Cardona P. Fulde K. von Klitzing R. Merlin H.-J. Queisser H. Störmer

- 114 **Interatomic Potential and Structural Stability**
Editors: K. Terakura and H. Akai
- 115 **Ultrafast Spectroscopy of Semiconductors and Semiconductor Nanostructures**
By J. Shah
- 116 **Electron Spectrum of Gapless Semiconductors**
By J.M. Tsidilkovski
- 117 **Electronic Properties of Fullerenes**
Editors: H. Kuzmany, J. Fink, M. Mehring, and S. Roth
- 118 **Correlation Effects in Low-Dimensional Electron Systems**
Editors: A. Okiji and N. Kawakami
- 119 **Spectroscopy of Mott Insulators and Correlated Metals**
Editors: A. Fujimori and Y. Tokura
- 120 **Optical Properties of III-V Semiconductors**
The Influence of Multi-Valley Band Structures By H. Kalt
- 121 **Elementary Processes in Excitations and Reactions on Solid Surfaces**
Editors: A. Okiji, H. Kasai, and K. Makoshi
- 122 **Theory of Magnetism**
By K. Yosida
- 123 **Quantum Kinetics in Transport and Optics of Semiconductors**
By H. Haug and A.-P. Jauho
- 124 **Relaxations of Excited States and Photo-Induced Structural Phase Transitions**
Editor: K. Nasu
- 125 **Physics and Chemistry of Transition-Metal Oxides**
Editors: H. Fukuyama and N. Nagaosa
- 126 **Physical Properties of Quasicrystals**
Editor: Z.M. Stadnik
- 127 **Positron Annihilation in Semiconductors**
Defect Studies
By R. Krause-Rehberg and H.S. Leipner
- 128 **Magneto-Optics**
Editors: S. Sugano and N. Kojima
- 129 **Computational Materials Science**
From Ab Initio to Monte Carlo Methods. By K. Ohno, K. Esfarjani, and Y. Kawazoe
- 130 **Contact, Adhesion and Rupture of Elastic Solids**
By D. Maugis
- 131 **Field Theories for Low-Dimensional Condensed Matter Systems**
Spin Systems and Strongly Correlated Electrons
By G. Morandi, P. Sodano, A. Tagliacozzo, and V. Tognetti
- 132 **Vortices in Unconventional Superconductors and Superfluids**
Editors: R.P. Huebener, N. Schopohl, and G.E. Volovik
- 133 **The Quantum Hall Effect**
By D. Yoshioka
- 134 **Magnetism in the Solid State**
By P. Mohn
- 135 **Electrodynamics of Magnetoactive Media**
By I. Vagner, B.I. Lembrikov, and P. Wyder
-